Seismic Hazard Analysis of the Hong Kong Region

GEO Report No. 311

ARUP

Geotechnical Engineering Office
Civil Engineering and Development Department
The Government of the Hong Kong
Special Administrative Region

Seismic Hazard Analysis of the Hong Kong Region

GEO Report No. 311

ARUP

This report was originally produced in February 2011 as Agreement No. CE49/2008(GE)

First published, May 2015

Prepared by:

Geotechnical Engineering Office,
Civil Engineering and Development Department,
Civil Engineering and Development Building,
101 Princess Margaret Road,
Homantin, Kowloon,
Hong Kong.

Preface

In keeping with our policy of releasing information which may be of general interest to the geotechnical profession and the public, we make available selected internal reports in a series of publications termed the GEO Report series. The GEO Reports can be downloaded from the website of the Civil Engineering and Development Department (http://www.cedd.gov.hk) on the Internet. Printed copies are also available for some GEO Reports. For printed copies, a charge is made to cover the cost of printing.

The Geotechnical Engineering Office also produces documents specifically for publication in print. These include guidance documents and results of comprehensive reviews. They can also be downloaded from the above website.

The publications and the printed GEO Reports may be obtained from the Government's Information Services Department. Information on how to purchase these documents is given on the second last page of this report.

H.N. Wong
Head, Geotechnical Engineering Office
June 2015

Forward

This GEO Report presents an updated seismic hazard assessment of Hong Kong by Arup, in collaboration with the GEO and the Guangdong Engineering Earthquake Resistance Research Institute (GEERRI) of the Earthquake Administration of Guangdong Province (EAGP). The assessment considered the extended latest records of earthquakes that occurred within a distance of about 500 km from Hong Kong, together with the regional seismo-tectonic setting and geological setting.

The GEO Report No. 65 on "Seismic Hazard Analysis of the Hong Kong Region" was published in 1998. It covered a region bounded by latitude 22°00' - 23°00' and longitudes 113°45' - 114°45', for seismic events up to 1995 with $M_L \geq 1.8$. Since then, more earthquake data within the region have been obtained by various earthquake monitoring agencies. These data are generally more accurate, as they have been recorded by advanced monitoring instruments. It is timely to update the seismic hazard assessment of Hong Kong with the available earthquake data and information.

This Report was prepared by a team led by Dr J.W. Pappin of Arup, in collaboration with GEO and GEERRI. The team members are Dr H. Jiang, Mr R.C.H. Koo, Mr Y.B. Yu, Dr P.L. Chen and Ms M.M.L. So. This work was coordinated by Dr J.S.H. Kwan and overseen by myself and Mr K.K.S. Ho. Draft versions of the Report were circulated to relevant Government departments and local academics for comment. The contributions of all parties are gratefully acknowledged.

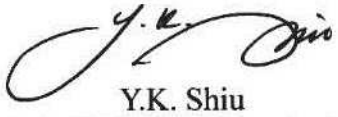

Y.K. Shiu

Chief Geotechnical Engineer/Standards and Testing

Table of Contents

Table of Contents

Table of Contents

Executive Summary

The Geotechnical Engineering Office (GEO) commissioned Arup as the lead consultant to undertake a Pilot Seismic Microzonation Study in the North-west New Territories and examine the potential effect of earthquake induced ground motion on natural terrain under Agreement No. CE 49/2008 (GE). The Guangdong Engineering Earthquake Resistance Research Institute, GEERRI (廣東省工程防震研究院), was engaged as a sub-consultant, to provide updated seismicity data, technical support and expertise pertaining to the Study.

This report covers the first stage of the Study which assesses the seismic hazard of the Hong Kong region based on an updated earthquake catalogue, provided by GEERRI within the Southeast China region. A new seismic source zone model which incorporates the seismicity of the region, geological and tectonic information, as well as the key information of the GEERRI's source zone model has been established for the hazard assessment. Field reconnaissance has been carried out by the experts from Arup and GEERRI to inspect selected major faults in Hong Kong and to assess their potential seismic activity. Several recent attenuation relationships have been applied in the assessment, and a sensitivity check has been carried out.

The results of the seismic hazard assessment are presented in terms of horizontal peak ground acceleration (PGA) and uniform hazard response spectra for structural periods up to 5 seconds for rock sites. The calculated PGA at the centre of the study area with 63%, 50%, 10% and 2% probabilities of being exceeded in the next 50 years are 0.026 g, 0.033 g, 0.092 g and 0.20 g, respectively. The PGA at the location of the Hong Kong Observatory has been also calculated in the seismic hazard model to allow direct comparison with previous assessments by other studies. It is noted that the PGA calculated in the present study is comparable with that determined by the previous GEO assessment as reported in GEO Report No. 65 (Lee et al, 1998).

The results of the previous seismic hazard study carried out by Arup for the Buildings Department (BD) in 2003 are also compared with this study. The comparison shows that the BD's study in 2003 gives response spectral values that are very consistent with those of this study for structural periods greater than 0.2 seconds. However the earlier study gives higher peak ground acceleration and spectral accelerations for structural periods of less than 0.2 seconds. The main reason for this difference is that, in the BD's study in 2003, a relatively higher attenuation relationship previously proposed by Atkinson & Boore (1997) was adapted and this relationship has been replaced by updated attenuation relationships in this study.

Contents

Page No.

List of Tables

List of Figures

1 Introduction

1.1 Background

The Geotechnical Engineering Office (GEO) of the Civil Engineering and Development Department (CEDD) has previously assessed the potential effects of earthquakes on the stability of man-made slopes and retaining walls in Hong Kong, but not on natural terrain. As the management of natural terrain landslide risk has become one of the focuses of the post-2010 Landslip Prevention and Mitigation Programme, there is a need to examine the responses and stability of Hong Kong's natural terrain under potential earthquake conditions.

On 1st April 2009, GEO commissioned Arup as the Consultant to undertake the Investigation Assignment of the Pilot Seismic Microzonation Study in North-west New Territories for the Study of Potential Effect of Earthquake on Natural Terrain under Agreement No. CE 49/2008 (GE). The Guangdong Engineering Earthquake Resistance Research Institute (GEERRI) was the sub-consultant of the project.

The study involved (i) an overall seismic hazard assessment of Hong Kong, (ii) an area-specific seismic microzonation assessment of the North-west New Territories area, and (iii) an evaluation of the potential effects of earthquakes on the natural terrain, account taken of local geology, topography and likely ground responses.

1.2 Scope of This Report

An overall probabilistic seismic hazard assessment of the Hong Kong region has been carried out in this study as described in Clause 6.2(b) of the Brief. The following sections describe the works that have been completed.

1.2.1 Fault Assessment

Potentially active faults, both in Hong Kong and in adjacent areas in Guangdong Province, have been assessed by a literature review. Joint field investigations between Arup and GEERRI were carried out on 13th and 14th July 2010 to inspect 5 potentially active fault sites in Hong Kong. They are Lung Kwu Sheung Tan, Tai Lam Chung Reservoir, Tong Yan San Tsuen, Butterfly Beach and Tai O. The findings of the literature review and field visits are presented in Section 2.

1.2.2 Earthquake Catalogue

All published historical and instrumental earthquake data available for Hong Kong and other areas that are pertinent to the overall seismic hazard assessment of Hong Kong have been collected and reviewed. The compiled earthquake catalogue includes major earthquake data of magnitude greater than 5.0 within 500 km of Hong Kong, and not just limited to 150 km as recommended in Mainland China. The review includes instrumental earthquake data obtained by world catalogues together with catalogues obtained from the Guangdong Seismic Network and the Hong Kong Observatory (HKO) Seismic Network. The sources and findings of the

earthquake catalogue compiled for Hong Kong is published in GEO Publication No. 1/2012 (GEO, 2012).

1.2.3 Seismic Source Zones

A seismic source zone is an area or a part of the earth's crust that has a likelihood of earthquake occurrence in the future. Such source zones can be active faults or area zones of diffused random seismicity. They are identified from studies of geological and seismological data. A comprehensive review has been carried out on the available geological information and the observed seismicity for the whole region of the southeast China. The seismic source model used by the Chinese National Seismic Code for Source Zonation in the Guangdong region (GB18306, 2001) has also been studied. The development of the seismic source zones is presented in Section 3 and the potential maximum earthquake magnitude for each seismic source zone is also presented.

1.2.4 Seismic Attenuation Relationships

Seismic attenuation relationships describe the reduction in earthquake induced ground-motion with distance away from a seismic source. They are dependent on the rock type in the region. For this study, attenuation relationships for response spectra at various structural periods are required. These have been derived by GEERRI and compared with empirical relationships from other regions of the world (notably the west and east coasts of North America) and with relationships developed theoretically based on the earthquake intensity records and seismological parameters in the region suggested by the University of Hong Kong. Suitable attenuation relationships are presented in Section 3.6.

1.2.5 Seismic Ground Motion at Rock Site

The seismic hazard assessment described in this report derived a series of response spectra of the anticipated seismic ground motions that will occur at rock sites in Hong Kong. The response spectra include peak ground acceleration and predictive ground motions that have probabilities of being exceeded of 63%, 50%, 10% and 2% in the next 50 years. The spectra are uniform hazard response spectra in that each point of the spectrum has the same probability of occurring. It must be emphasised that they do not represent the effects of a single future earthquake but rather the combined effect of many possible events. The hazard assessment has also derived the earthquakes most likely to give rise to the various probabilities of future ground motion. These events have been derived for a range of structural periods and show that, as expected, near field small magnitude events are most likely to cause high frequency motion that will affect low rise buildings, and progressively larger magnitude events at greater distance will be most likely to cause ground motion that will affect longer period structure e.g. mid-rise to high-rise buildings. The derived response spectra for rock site have also been compared to the current Chinese Seismic Code (GB50011, 2010). Section 4 presents the results of the seismic hazard assessment.

1.2.6 Comparison of Results with Previous Studies for Hong Kong

Various seismic hazard studies have been carried out by different parties in Hong Kong since the 1980's. The past major studies were by Pun & Ambraseys (1992), Lee et al (1998) as summarised in GEO Report No. 65 and Arup (2003) as discussed below.

Pun & Ambraseys (1992) described the results of a seismic hazard assessment for Hong Kong based on a seismic source model of 660 km x 600 km. The study by Lee et al (1998) was conducted under an agreement awarded by GEO to the University of Hong Kong (HKU), with the Guangdong Seismological Bureau (GSB) as a sub-consultant. The seismic belt in the model of Lee et al (1998) was divided into 13 inner zones characterised by low seismic activity, and 16 outer zones of relatively higher seismic activity. Both Pun & Ambraseys (1992) and Lee et al (1998) only calculated the horizontal peak ground acceleration and intensity for rock sites and no response spectra were reported, which are important for engineering applications. Arup (2003) carried out a seismic hazard study for Hong Kong as part of their hazard and risk study for the Buildings Department (BD) of Hong Kong in 2003. A detailed catalogue of historical and recent seismicity within the South China region up to year 2000 was compiled and attenuation models for different structural periods were adopted. Uniform hazard response spectra having 50%, 10% and 2% probabilities of being exceeded in the next 50 years were determined for rock sites.

In the present study, an updated earthquake catalogue has been used to determine the seismic source zone parameters. The seismic source zone model incorporates the seismicity of the region, geological and tectonic information and consideration of GEERRI's source zone boundaries. In addition, field reconnaissance had been carried out by the experts from Arup and GEERRI to inspect selected faults in the Hong Kong region and assess their potential seismic activity. The collected relevant information was considered in the seismic hazard assessment. Several updated attenuation relationships have been applied, with a sensitivity check carried out, in the assessment to establish the horizontal peak ground acceleration and uniform hazard response spectra for structural periods up to 5 seconds for rock sites. The present study, which is based on the updated earthquake information, is considered to be more comprehensive.

2 Geology and Tectonics of the Hong Kong Region

2.1 General

This section describes the geological setting of the region. Particular emphasis is given to the regional tectonic setting relevant to the development of seismic source models for the region.

2.2 Regional Tectonic Setting

It is now well established that the Earth's crust is divided into a mosaic of some 15 major tectonic plates, which move relative to each other (see Figure 2.1). Hong Kong is situated in Southeast China near the south-eastern margin of the Eurasian Plate about 700 km from the plate boundary with the Philippines Ocean Plate. The plate boundary between the Eurasian

and the Philippines Ocean Plate, which underlies Taiwan, trends south to the Philippines and northeast to Japan and is about 200 km to 700 km from the Southeast China coastline.

The paleogeography of Southeast China has been summarised by Sewell et al (2000) (see Figure 2.2). The tectonic evolution of the region is interpreted to have included major periods of tectonic activities ranging in age from the Mesoproterozoic (1100 Ma) to the present.

- From the Mesoproterozoic to early Palaeozoic (650 Ma), Southeast China was within a series of depositional environments resulting in thick sedimentary deposit. By the early Cambrian (650 Ma), the northeast-trending basin had been firmly established in Southeast China. Since then until the Early Permian (280 Ma), Southeast China migrated from alluvial floodplains, in intertidal deltas, to a shallow continental sea to a deep marine environment.

- Starting from the Triassic (about 250 Ma to 200 Ma), Southeast China was in a major period of uplift and erosion accompanied by intrusion of granites. Following these events, a shallow marine environment developed during the Early Jurassic (200 Ma to 180 Ma) followed by gentle uplift and the beginning of a major episode of volcanic-plutonic activity.

- Widespread volcanism and plutonism occurred throughout Southeast China from the Middle Jurassic (180 Ma) to the Early Cretaceous (about 100 Ma) associated with a SW to NE subduction zone about 200 km to the SE of Hong Kong.

- Since then to the Early Tertiary (60 Ma), the magmatic activity progressively deceased and the crustal activity since then has been relatively stable.

Most of the tectonic deformation that is evident in the geology of Hong Kong today is understood to have been caused by events that occurred during the Late Jurassic and Cretaceous periods (190 to 90 Ma) in what is referred to as the Yanshanian Orogeny. During this Orogeny period, an inferred subduction zone plate boundary was located to the south east of Hong Kong with regional faulting and folding, volcanism and intrusion of granitic magma into the crust taking place to the west of the subduction zone.

GEERRI has presented a regional tectonic setting for the Guangdong region and this is included in Section 2 of Appendix A. The Guangdong region has been divided into three main tectonic settings: basin (Mesoproterozic to Middle Triassic), continental margin (Middle Triassic to Early Tertiary) and stable continent (starting from Early Tertiary).

Workman (1983) describes the general tectonic features of the South China Sea (see Figure 2.3). Offshore data indicates that the continental shelf of this part of China comprises deep, fault-controlled, Tertiary age (65 million years to present) basins. The present day coastline of South China is not the boundary between continental type and oceanic type crust.

The continental crust thins from the Chinese mainland (approximately 30 km thick) to the central part of the South China Sea Basin (approximately 12 km thick) with typical continental type crust beneath the mainland and continental shelf, to a distance of approximately 200 km from the current coastline, and oceanic type crust in the South China Sea (see Figure 2.3). The continental crust beneath the continental shelf is referred to as a rifted margin.

Southeast China is interpreted to be composed of two major crustal blocks, the Yangtse Block to the north and the Cathaysia Block to the south (see Figure 2.4). The age of the basement rocks in these crustal blocks are commonly assumed to be Mesoproterozoic. Two major, regional northeast trending fault zones are interpreted to lie along the Southeast China coast. The Changle-Nanao Fault Zone, runs along the coast and is offshore east of Hong Kong. The Linhuashan Fault Zone, runs inland, parallel to the coast from Shanghai to Hong Kong (see Figure 2.4). Hong Kong is located within the Linhuashan Fault Zone, which is bounded by the Shenzhen Fault to the north and the Haifeng Fault to the south (Lai & Langford, 1996) (see Figure 2.5). The onshore northeast trending faults are commonly displaced by, or in places displace, shorter northwest trending faults. Pubellier & Chan (2006) showed a Morphotectonic Map of Cenozoic (65 Ma to present) structures of the South China-Northern Vietnam coastal region (Figure 2.6) showing superficial evidence of tectonic activity. This map covers both the onshore and offshore portions from eastern China to Vietnam. It was produced by compiling the existing geological, geographical and geophysical data in the region and critical locations were analysed with satellite imagery and field studies. The map summarises the geologic structure including active faults, Cenozoic faults, and earthquakes with focal mechanism, etc. Note that the "active" definition of faults described in the map does not necessarily imply evidence of historical motion record, but are considered representing activity in terms of a geological time scale.

2.3 Faults in Guangdong Province

The regional geologic and tectonic setting of Guangdong Province is described in the Geological Memoirs Series 1, Number 10, Regional Geology of Guangdong Province (Bureau of Geology and Mineral Resources of Guangdong Province (GMRGP), 1988). A collage of the geology and tectonic maps provided with the memoir are presented in Figures 2.7 and 2.8 respectively. GEERRI (2010) described the regional fault zones in detail and the faults in the Guangdong region are shown in Figure 2.9.

There are three main sets of faults identified:

(a) dominant northeast (NE) trending faults;

(b) east of northeast (ENE) trending faults; and

(c) northwest (NW) trending faults.

The NE trending faults, especially in the offshore region, are the most morphologically persistent with mapped and inferred faults that have shown to extend for several hundred kilometres. The NW trending faults appear to be less continuous and offset the northeast trending faults. Under the current regional tectonic stress regime, faults striking NE are more likely to be activated to create strike-slip moment. Due to the greater persistency of

east of NE trending faults, it is inferred that they have a higher potential to generate strong motion earthquakes upon reactivation. Earthquake records showed that large earthquakes occurred near Shantou and Nanao, where the NW striking faults intersect the ENE trending faults, namely the Binhai fault zone, to extend up to 200 ~ 600 km intermittently on the surface as shown in Figure 2.9. These faults represent deep structures extending more than 30 km into the crust. The active faults are coloured in red in Figure 2.9. The NW trending faults are relatively inactive as compared with the NE trending faults. It is evident that a number of strong earthquakes in Lingshan occurred at the intersection of NW and NE trending faults as shown in Figure 2.9. GEERRI (2010) suggested that the intersection of NE trending faults with the NNW-NW trending faults might also be a potential locus of future earthquakes. This has been deduced from strong earthquakes that have occurred in Yangjiang, Shantou, Jieyang and Chaozhou in Guangdong, a number of strong earthquakes in Lingshan in Guangxi's, Fujian Zhangzhou, and Changde in Hunan. The definition of “active” corresponds to fault activity in terms of a geological time scale from morphological features. Detailed descriptions of the major faults in Guangdong by GEERRI are included in Section 2 of Appendix A.

2.4 Geology of the Hong Kong Region

The geology of Hong Kong has been summarised by Sewell et al (2000) and Fyfe et al (2000). A detailed geological map of the Hong Kong region showing the distribution of geological units and geological structure is shown in Figure 2.10 (GEO, 2000). The geological map shows that more than three-quarters of the land area of Hong Kong is underlain by volcanic and plutonic rocks, predominantly Tuff and Granite, of Middle Jurassic to Early Cretaceous (180 to 140 Ma) age. Older (Late Paleozoic, 420 to 250 Ma sedimentary rocks) and younger (Late Mesozoic and Early Tertiary, 140 to 55 Ma sedimentary rocks) underlie the majority of the remaining land area. Superficial deposits, comprising Quaternary (less than 2.6 Ma) alluvium and other unconsolidated deposits are also present throughout the territory (see Figure 2.10).

2.5 Faults in Hong Kong

The structural evolution of Hong Kong has included events ranging in age probably from the Precambrian, and certainly from the late Palaeozoic, to the Recent (see Table 2.1). However, most deformation that is evident in the rocks of Hong Kong was caused by events that occurred during Jurassic and Cretaceous (Sewell et al, 2000).

The main faults in Hong Kong strike NE varying to NNE, and NW varying to NNW. There are also some E and a few N-striking faults (Figure 2.11). Detailed descriptions of the major faults in Hong Kong by GEERRI are included in Section 2 of Appendix A.

Figure 2.12 shows a Rosette plot presenting the striking density of certain and inferred faults shown in the published 1:20,000-scale geological maps. It should be noted that the faults presented are only in areas of solid geology and do not show their concealed traces beneath areas of superficial deposits, although these can often be inferred with reasonable confidence.

Table 2.1 Summary of Deformational Events That Have Affected Rocks in Hong Kong (Sewell et al, 2000)

Age			Orientation/Movement	Tectonic Setting
Mesozoic	Late Cretaceous		NE-sinistral S-directed thrust NW-dextral	Strike-slip, transtensional and transpressional basins
	Yanshanian	Early Cretaceous to Mid Jurassic	NNW varying to N and NW extension generated variable sinistral and dextral components on ENE-trending faults	extensional and variably transtentional convergent margin volcanic arc, becoming back-arc and eventually post-subduction
		Early Jurassic	?NNW-SSE	extensional basins (ENE)
	Indosinian		NE-dextral	Transpressional
Paleozoic (Caledonian)			NE	extensional basins (NE)
Precambrian			NE	terrane collision/amalgamation (NE)

2.6 Active Fault Assessment

For the purposes of this study, an active fault is defined as a fault which shows significant evidence of movement in association with recent earthquakes, during geologically recent time and has a potential for recurrence. An active fault should only be distinguishable from the surrounding faults if it can be demonstrated to be significantly more active than the general population of faults in the region. If any fault can be shown to be significantly more active than the general faults, a seismic hazard assessment will need to specifically model this feature to determine the increased seismic ground motion hazard in its vicinity. It will also have a significantly greater threat of ground rupture than the other faults in the region.

The concept of fault activity has been the topic of considerable discussion and controversy in the technical literature over the years (Kramer, 1996). In areas, such as Hong Kong, where earthquakes occur less often when compared to areas such as California or Japan, this issue of assessing fault activity becomes problematic.

To a large extent, the question of "activity" stems from the more general and controversial issue of defining what period to be considered when assessing recent fault activity with consideration to risk assessment. There is no consensus as to how fault activity should be evaluated. Slemmons & McKinney (1977), for example, found 31 different definitions of the term active fault. Most definitions were based on the time period since the most recent fault movement.

The California Bureau of Mines and Geology and the State of California, in legislation pertaining to the building of structures near fault lines, defines an active fault as one that has evidence of Holocene surface displacement, meaning displacement within about the past

10,000 years. The U.S. Army Corps of Engineers has used a time period of 35,000 years and the U.S. Bureau of Reclamation has used 100,000 years. The U.S. Nuclear Regulatory Commission has defined a "capable fault" as one that exhibits:

(a) movement at or near the surface at least once in 35,000 years or more than once in 500,000 years;

(b) historical or recent seismicity which is directly related with the fault; and

(c) a structural relationship to a capable fault such that movement on one could reasonably accompany movement on the other.

Eurocode 8: Part 5 states that an absence of movement in the late Quaternary (refer to 0.7 million years ago to present) can be considered as a non-active fault.

GEERRI and Lee et al (1998) recommend that a fault should be considered "active" where activity has been proven in the last 100,000 years.

2.6.1 Potential Fault Displacement in Hong Kong

For this study the likely amount of fault rupture offset that would be expected from the background seismicity observed from recent earthquake activity has been assessed. By combining observed fault displacement and rupture area to earthquake magnitude relationships with the observed rate of seismicity, an estimate of the general fault rupture offset that will be accumulated with time can be made. From the observed rate of seismicity explained in this report, it can be calculated that the larger earthquake events have a larger contribution to the expected fault rupture offset that is accumulated over time. By assuming an area for Hong Kong of about 2,300 km^2 that incorporates about 500 km of faulting and a fault rupture depth of 30 km, it is calculated that generally an offset of around 400 mm will be accumulated within a one million year time period. It follows that an offset in the whole Quaternary (2.6 Ma) of around 1 m could not be considered to be exceptional or to indicate a significantly higher fault slip rate than is generally assumed. An offset of greater than 40 mm in the Holocene (10,000 years) however would be exceptional as it is 10 times the average slip rate and could be used as a basis for assessing that a fault is particularly active. A similar study was done as a part of San Francisco Bay Area Hazard study by USGS in 2009.

2.6.2 Potential Evidence from Stratigraphy and Geomorphology

Sewell et al (2000) stated that there is no direct evidence of fault displacements in either the offshore or onshore Quaternary (less than 2.6 Ma) superficial deposits. In particular, they stated that no fault displacements have been identified from the many hundreds of kilometres of offshore seismic lines of Quaternary offshore alluvial and marine sequences.

A number of investigations, including those of Liu (1985) and the Hong Kong Geological Survey (Langford et al, 1989) identified recent raised terraces and beach features in

some coastal areas of Hong Kong. A plausible mechanism for the development of these raised terraces is active faulting rather than caused by faulting. Whittaker et al (1992) attributed these features to the oceanward tilting of the region during the late Quaternary or the general increase in the rock head level from north to south of Hong Kong.

2.6.3 Potential Evidence from Dating

In recent years the thermo-luminescence (TL) dating technique has been used to estimate the timing of fault movement by dating both fault gouge and alluvial sediments that overlie the faults in Southeast China (Ding & Lai, 1997).

(a) Dating of fault gouge

In Hong Kong, the northeast trending and northwest trending faults have been given TL dates of between 278,700 ± 23,100 and 33,300 ± 2,700 years BP with possible peaks in activity at 270,000, 190,000 and 100,000 years BP. Lee et al (1998) stated that from TL dating, the last major fault activity in Hong Kong can be interpreted to have occurred between 80,000 to 100,000 years ago. Figure 2.13 shows the relationship between the TL dating results and the fault systems in Hong Kong.

(b) Dating of sediments

TL dating of sediments that overlie a fault can be used to estimate the timing of fault displacements in the following three circumstances:

(i) where the sediments are themselves faulted, the depositional age of the sediments constrains the maximum possible age of fault movement when the sediments are themselves faulted;

(ii) TL dating of colluvial deposits which are formed adjacent to fault scarps may yield the age of vertical fault displacement; and

(iii) where sediments unconformably overlie a fault zone, but are themselves undisturbed, a minimum age of movement can be determined.

To the south of Yuen Long, at Sha Ha Tsuen, a major northwest trending fault within the Lau Fau Shan- East Lamma Channel Fault Zone is overlain by a sequence of alluvial deposits. Duller & Whistle (1996) employed OSL testing gave the oldest alluvial layer an age of 81,000 ± 14,000 years. Ding & Lai (1997) concluded that this age is the minimum age of fault movement. While not explicitly stated, this implies they also have evidence that the alluvial sequence is not disturbed above the fault.

Northwest of Tai Po, the Lam Tsuen River abruptly alters its course from northeast to southwest. The cause of the river capture is not certain. However, Lai & Langford (1996) and Ding & Lai (1997) proposed that it is due to damming of the old river course along a southeast trending fault. They suggested that this event occurred between the deposition of the

youngest alluvial deposits that have a TL age of 84,700 ± 16,300 years and the overlying organic lake deposits that have a ^{14}C age of 24,000 ± 5,300 years.

(c) ^{40}Ar-^{39}Ar dating

^{40}Ar-^{39}Ar has been used to date the more common minerals present in Hong Kong's faulted rock such as schist and mylonite. Fault movement is estimated by the following two approaches:

(i) to indirectly constrain the age of faulting by dating hydrothermal mineralization in the faulted rocks, using the concept that permeable pathways for fluids are often created during active crustal deformation; and

(ii) to directly constrain the silicate minerals of faulted rocks which were supposed to be formed by extremely small heating events in the fault movement.

Sewell et al (2000) noted that ^{40}Ar-^{39}Ar dating of whole rock specimens from the Tolo Channel Fault and the Rambler Channel Fault indicated that the main phase of activity occurred between 60 to 80 Ma.

A study from Campbell & Sewell (2007) indirectly constrained the age of faulting by dating hydrothermal mineralization in the faulted rocks, using the concept that permeable pathways for fluids were created during active crustal deformation. The hydrothermal mineralization dating results yielded ages older than 30 Ma. However there were four samples from the faults (see Figure 2.14) that showed mineralisation events around 60 Ma to 90 Ma and 34 Ma. Two out of the four samples showed evidence for events at 10 Ma and 3 to 4 Ma. In the low temperature portions of the samples, where the diffusion of Ar could be neglected, the results showed near-zero age but they only account for less than 2% of the total sample ^{39}Ar volume (Figure 2.14), which might suggest late Pleistocene to Holocene fault activity.

2.6.4 Potential Evidence from Natural Terrain Landslides

Recently, GEO (Tang et al, 2009; Wong & Ding, 2010; Tang et al, 2010 and Wong et al, 2010) carried out studies to examine possible neotectonic movement of major faults (earthquakes) in Hong Kong which might trigger landslides. The reports contained geomorphological assessment, field observations, ground investigation and dating of superficial deposits to investigate the extent of possible neotectonic fault movement on major faults in Hong Kong and their potential correlation with natural terrain landslides. Four study areas were investigated, namely Ho Lek Pui area, Wong Chuk Yeung, Tung Chung East, and Nam Shan and Pui O area (Figure 2.15) :

(a) Ho Lek Pui Area

Tang et al (2009) examined evidence for possible neotectonic movement from the inferred apparent rupture of superficial deposits and displacement of drainage and ridgelines

across the NW-trending fault in Tai Po Kau - Ho Lek Pui area. Also, "Mega" boulders (up to 5 m diameter) clustered along both sides of the fault which may have been dislodged by the associated seismic activity.

Detailed field observations and ground investigation showed that the deformation features such as silicified fault breccia and quartz veins could be found in the weathered volcanic rock along the axis of the upper valley and this would probably be associated with an "ancient" period of fault movement. There is no evidence showing that superficial deposits have been displaced by the NW trending fault. However, two prominent NW trending fault scarps are still recognisable in the aerial photograph interpretation. As an upper age limit for the recognition in the landscape by aerial photo is about 50,000 years (Tang et al, 2009), it is postulated that the last movement on the NW trending fault at Ho Lek Pui occurred between 20,000 and 100,000 years ago. However, no evidence has been found to confirm that the superficial deposits have been deformed by this faulting.

(b) Wong Chuk Yeung Village

Wong & Ding (2010) recognised two groups of large landslide features near Wong Chuk Yeung Village, 1.4 km to the southwest of Ho Lek Pui. The two features are located seperately in the western and eastern catchments of the village. The western feature is a large colluvial lobe approximately 250 m wide and 200 m long at the toe of a hillslope. The eastern feature is an assemblage of extensive sporadic rock outcrops and associated boulders, colluvial deposits in the middle and upper parts of the adjacent hillslope.

The study investigated the stratigraphy and age of the colluvial lobe in the western feature, and the ages of the rock scarps and very large boulders in the colluvium in the eastern feature, with the objective of establishing the age correlation, if any, between the western and eastern features. In the western features, the colluvial lobe contained many boulders as revealed in the trial pits and drillholes but the lack of stratigraphical variation suggested that they might be deposited in a single large landslide event with a volume of approximately 1 Mm^3. It was revealed that the lobe was probably formed round 49,200 ± 3,900 years ago. For the eastern feature, surface exposure dating and the geomorphological assessment suggested that the feature was an accumulation of multiple landslide events (11,400 ± 1,100, 28,500 ± 4,700, 79,200 ± 5,300 and 115,900 ± 7,600).

There is no clear evidence to confirm this is an earthquake-induced landslide.

(c) Tung Chung East

Tang et al (2010) investigated large landslide features which may represent an earthquake-induced event near Yu Tung Road and North Lantau Highway, Lantau Island. This study involved the investigation of geomorphology and dating of the debris fan on the hillsides to assess the likelihood of a seismic origin for the relict debris fans. The geomorphological assessment verified there are five large relict debris fans in which the size ranges between 0.12 Mm^3 to 1.07 Mm^3. Luminescence ages of colluvial deposits from these four relict debris fans confirm they occurred at four events (67,500 years ago, 25,000 to 30,000 years ago, 10,000 to 14,000 years ago and 3000 to 4000 years ago). There is insufficient evidence from the Study Area to distinguish between a rainstorm or seismic triggered mechanism for the deposition of the large relict debris lobes.

(d) Nam Shan and Pui O area

Wong et al (2010) investigated two large arcuate scarps with associated debris lobes located on the southern hillslopes below Yi Tung Shan and Lin Fa Shan near Nam Shan and Pui O respectively.

Ground investigation including surface exposure dating and OSL dating of rock scarps and debris of the Nam Shan debris lobe suggested that were at least two major landslide events occurring between 57,300 to 49,700 years ago and 37,700 to 34,700 years ago. The Pui O debris lobe composed dominantly of one thick debris avalanche deposit. Dating of rock scarps and debris showed that event occurred between 67,000 to 51,000 years ago. It is not possible to determine confidently whether the landslide events were due to rainstorm or earthquake. However, the overlapping landslide age of both areas (57,300 to 49,700 years ago in Nam Shan Area and 67,000 to 51,000 years ago in Pui O Area) cannot rule out the possibility that seismic events about 55,000 years ago induced these landslides.

2.7 Active Faults Proposed by GEERRI

GEERRI defines a fault as active if it shows evidence of movement in the past 100,000 years and a related tectonic map is shown in Figure 2.11. Using this definition, GEERRI has classified two faults as active in their draft seismic hazard report submitted in October 2010, they are the Lau Fau Shan - East Lamma Channel Fault Zone (F19 in Figure 2.11) and the Shek Pik - Tung Chung Fault (F10 in Figure 2.11). Details of the GEERRI study are shown in Figure 3.2-0 in Appendix A.

The Lau Fau Shan - East Lamma Channel Fault Zone is regarded as being active based on the borehole information from Tsing Ma Bridge. For example, two boreholes which are about 150 m apart show about 6 m thickness difference in marine deposits. GEERRI regarded this variation is probably due to fault movement in Holocene. However, there are alternate interpretations such as disturbance from maintenance of the navigation channel or possibly the natural morphology (e.g. channel scour) of the marine deposits. Recent tectonic activity of this fault cannot therefore be confirmed.

The Shek Pik - Tung Chung Fault is regarded as active in the seismic hazard assessment of Hong Kong-Zhuhai-Macau Link by the Institute of Crustal Dynamics, China (ICD, 2004). Their report stated that the fault breccias and mylonite presented in this fault zone at Wong Nai Uk area in Tung Chung showed that movement occurred about 98,300 ± 6,300 and 82,000 ± 6,800 years ago, implying there was fault movement within the past 100,000 years.

2.8 Field Reconnaissance on Indentified Possible Faults in Hong Kong

Field reconnaissance to examine indications of recent fault activity was carried out with GEERRI on 13th and 14th July 2010. Five faults (Lung Kwu Sheung Tan, Tai Lam Chung Reservoir, Tong Yan San Tsuen, Butterfly Beach and Tai O in Figure 2.16) were visited based on recommendations from GEERRI.

Additional field reconnaissance to investigate Shek Pik - Tung Chung Fault was carried out on 6th and 7th December 2010. This fault was regarded as active by GEERRI in their draft seismic hazard report submitted in October 2010. Three locations on Lantau Island were visited as shown by the red circles in Figure 2.16.

The following sections summarise the site observations and findings by GEERRI on any evidence of recent fault movement on superficial deposits. It must be noted that it was not intended to carry out detailed geological mapping or fault investigation. The visits served to provide an opportunity for GEERRI to evaluate their interpretation on these particular faults.

2.8.1 Lung Kwu Sheung Tan

This EW-ENE trending fault is about 5.4 km long as shown in Geological Map of Hong Kong (GEO, 2000) and is terminated at its eastern end by a NNW fault.

The site is underlain by medium grained granite. A photo-lineament is noted at the site based on the 1:20,000 solid and superficial geological map sheet 5 (GEO, 1988a) (see Figure 2.17). As observed in the field the lineament has geomorphic expression as a valley (Figure 2.18). In the axis of the valley, breccias are observed as subvertical and dipping to north (see Figure 2.19).

No evidence was found to show movement has occurred in the Quaternary Period.

2.8.2 Tai Lam Chung Reservoir

A NW trending fault zone namely Lau Fau Shan - East Lamma Channel Fault Zone, is located in Lau Fau Shan, Sham Tseng and Lamma Island with length about 50 km consisting of a series of parallel faults. TL dating of the fault materials suggested the fault movement can be as early as 33,300 ± 2,700 years B.P. (see Figure 2.12). GEERRI regarded that this fault could be active as presented in Figure 2.11 and may possibly pass through the Tai Lam Chung Reservoir.

The site is underlain by fined grained granite and a series of NW trending faults and some NE trending faults are noted to pass through the site (Figure 2.20). The granite has been metamorphosed based on 1:20,000 solid and superficial geological map Sheet 6 (GEO, 1988b).

The NW trending fault is represented by brecciated rock juxtaposed against non-brecciated rock (Figure 2.21). The matrix of the breccia is quartz implying mineralization of the breccias had a hydrothermal origin of high temperature and most likely depth (Figure 2.22). A recent fault rupture would not be expected to be mineralised with hydrothermal quartz.

An exposed surface with slickensides was also observed that is trending about 330° and dipping 62° to the northeast (see Figure 2.23). It is uncertain whether the features are directly related to Lau Fau Shan - East Lamma Channel Fault Zone, but the field observations suggest that the activity is old, related to the tectonic development of Hong Kong.

2.8.3 Tong Yan San Tsuen

The Lau Fau Shan - East Lamma Channel Fault Zone described above is a NW fault zone which also passes through Tong Yan San Tsuen. Based on the 1:20,000 solid and superficial geological map sheet 6 (GEO, 1988b), the site is underlain by fine to medium grained granite which has been metamorphosed. A thick alluvium deposit is covering the granite around that site and obscuring the fault expression as seen on the geologic map (see Figure 2.24).

GEERRI observed some stepped features on the slope (Figure 2.25) and proposed that these may have been caused by movement of the fault in the Quaternary Period. Conversely, it may be also caused by the nature of the rock outcrop topography.

Quaternary strata exposed at the side of a deep channel found near the site, showed no offset (Figure 2.26). The findings from the site visit showed there was no clear fault-formed features observable in current surface expression.

2.8.4 Butterfly Beach

Based on the 1:20,000 solid and superficial geological map Sheet 5 (GEO, 1988a), there is a rock outcrop located at the boundary between fine grained granite and tuff and andesite from the Tum Mun Formation (Figure 2.27). This boundary is defined by a thrust fault (Tsing Shan Fault) in which the Tsing Shan Pluton was thrust from the west over volcanic rocks of Tuen Mun Formation at the east. No apparent fault features were found in this location (Figure 2.28).

2.8.5 Tai O

An NNW fault with a length of about 5.4 km as shown in Geological Map of Hong Kong (GEO, 2000) stretching just to the east of Tai O (see Figure 2.10) was visited at the suggestion of Professor Ding of GEERRI. This fault is the same as that shown in Figure 2.13 to have been dated by TL at 278,700 ± 23,100 years (Sample 13).

Based on the 1:20,000 solid and superficial geological map sheet 9 (GEO, 1994), the site is covered with cobbles and boulders of beach deposit. Eutaxite from Lantau Formation or metasiltstone/metasandstone from Lok Ma Chau Formation underlies the Quaternary deposits. The fault is not shown on the geological map but is inferred to pass through the site (Figure 2.29).

At the site, there is about 3 m thick of cobbles and boulders deposits overlying the bedrock. The uppermost 1 m is covered with top soil (Figure 2.30). There was an offset of the bedrock observed in the site (Location A in Figures 2.30 & 2.31) representing an apparent drop in the bedrock surface of ~1 m. Gravel appears to be down-dropped and lies against the rock in footwall of the fault. The field expression is representative of a normal fault and the juxtaposition of gravels against the bedrock surface implies timing after the deposition of the gravels.

However, the Quaternary cobbles and boulders stratum do not show any sign of fault disturbance through the gravel layers above the bedrock as the size of cobbles and boulders maintains a consistent stratigraphic size sorting across the surface projection of the fault. If the Quaternary deposits had been offset by the active fault, the displacement of the same stratum (similar size of cobbles and boulders) should be apparent.

It is plausible that the bedrock fault is a much older feature. The current river and valley are located on the fault they represent weaker and erodible rock. During the Quaternary, fluvial processes eroded and deposited gravel on top of the faulted surface.

In Figure 2.32, it seems that there are two lineaments dipping about 40° across the cobble and boulder stratum which may represent a fault cutting across the Quaternary stratum. However, the dimension of the cobbles and boulders does not change much in the horizontal direction which implies the stratum is unlikely to have been offset.

GEERRI suggested that if the cobbles and boulders were deposited after the offset of bedrock (which means after the fault movement), they should be orientated parallel to the offset surface of the bedrock (see Figure 2.33). However, the orientation of the deposit is considered to be controlled by a variable deposition environment.

This limited field evidence suggests that fault movement in the rock may have occurred before the deposition of the gravels in the Quaternary.

2.8.6 Lantau Island

A NE trending fault, Shek Pik - Tung Chung Fault, with length of about 9 km noted in Geological Map of Hong Kong (GEO, 2000). Sewell et al (2000) described that this fault transects Lantau Island, where it appears to split into two main segments, one passing just to the south of Tung Chung and continuing to Shek Pik, the other crossing the eastern part of the island between Tin Tsui Tau and Pui O. The sinistral offset along fault is about 3 to 3.5 km.

Based on the 1:20,000 solid and superficial geological map Sheet 9 (GEO, 1994), the fault is mainly in rhyolite lava and tuff with some localised debris on slope and terraced alluvium overlain the fault (Figure 2.34). A photolineament can be observed in the aerial photo (Figure 2.34).

Three locations which are closed to the Shek Pik - Tung Chung Fault noted in the map have been visited, at (a) the Wisdom Path at Ngong Ping, (b) the helicopter park near Tai Long Wan, and (c) a rock cut slope adjacent to North Lantau Highway (Figures 2.16 & 2.34).

(a) East to the Wisdom Path in Ngong Ping, closely spaced joints, striking NE-SW direction, can be observed (Figure 2.35). At Ngong Ping the rock is silicified and some broken quartz veins are noted (Figure 2.36). Some angular fragments embedded in the boulders were found (Figure 2.37);

(b) At the helicopter park near Tai Long Wan, some discontinuous minor quartz veins can be observed

(Figure 2.38) and these maybe the result of fault movement after the quartz crystallisation; and

(c) At the rock slope adjacent to North Lantau Highway, a series of minor NE trending shear zones can be observed that are general dipping to SE at 75° (Figure 2.39). They are closely spaced shear zones about 10 to 30 cm in width. Slickensides exposed on the surface were observed (Figure 2.40). At the micro scale the shear surface is observed to be undulating, however it becomes quite linear at the macro-scale.

The fault features exposed at these sites were all in pre-Quaternary materials and therefore no evidence of more recent movements can be deduced.

2.9 Summary of Fault Assessment

Faults in the Hong Kong study area have been assessed for their recent activity by a review of published literature and mapping at selected locations by subsequent field reconnaissance.

Activity of the recent faulting have been assessed from reported evidence of offset stratigraphic units, age-dating of minerals created from faulting and age dating of landslides interpreted to be related to large earthquakes.

2.9.1 Stratigraphic Offset Evidence

A number of studies examine stratigraphy both onshore and offshore in Hong Kong. No evidence has been found that Quaternary units are offset by faulting.

2.9.2 Age Dating of Fault Derived Materials

A series of TL age dating on fault related materials has produced dates varying from 33,000 to 300,000 years ago, with the majority of the samples showing dates between 100,000 to 270,000 years ago. The youngest TL date obtained (33,300 ± 2,700 years ago) from a NW trending fault may indicate a relatively recent period of fault movement, however more dating data are required to confirm this activity. TL ages from sediment overlying fault zones at one location suggest a younger age between 24,000 to 100,000 years ago, but a direct link to fault movement has not been proven. Therefore, the age provided may not reflect the real time of fault movement.

^{40}Ar-^{39}Ar dating of hydrothermal mineralisation in faults zones shows events around 34 Ma, 10 Ma and 3 to 4 Ma. Although the results of low temperature portions of some samples show near-zero age which may suggest a more recent fault activity, the effect of this activity on the minerals in those samples are too weak to constrain temporally at this point.

2.9.3 Age Dating of Possible Large Scale Landslides

Studies of four large natural terrain landslides revealed that a number of the landslides occurred in single event. Other large landslides occurred in separate events within about the last 116,000 years. The occurrence of multiple large landslides triggered by a single event is suggestive of an earthquake trigger, although direct evidence is lacking.

2.9.4 Field Reconnaissance

Field reconnaissance at five sites in the Hong Kong area did not show any evidence of fault movement in Quaternary Period. At a site in Tai O, the juxtaposition of Quaternary gravels against faulted bedrock is suggestive of a young fault; however there was no observation of a faulted offset of the Quaternary deposit over the projection of the fault implying the fault is older than the Quaternary.

2.9.5 Conclusions

For the purposes of this study it has been concluded that there are no active faults in Hong Kong that should be specifically modelled when assessing the hazard from seismically induced ground motion. While any of the numerous faults in Hong Kong could potentially experience rupture in the event of a near surface large magnitude event, no clear evidence has been found to associate this risk with any particular fault.

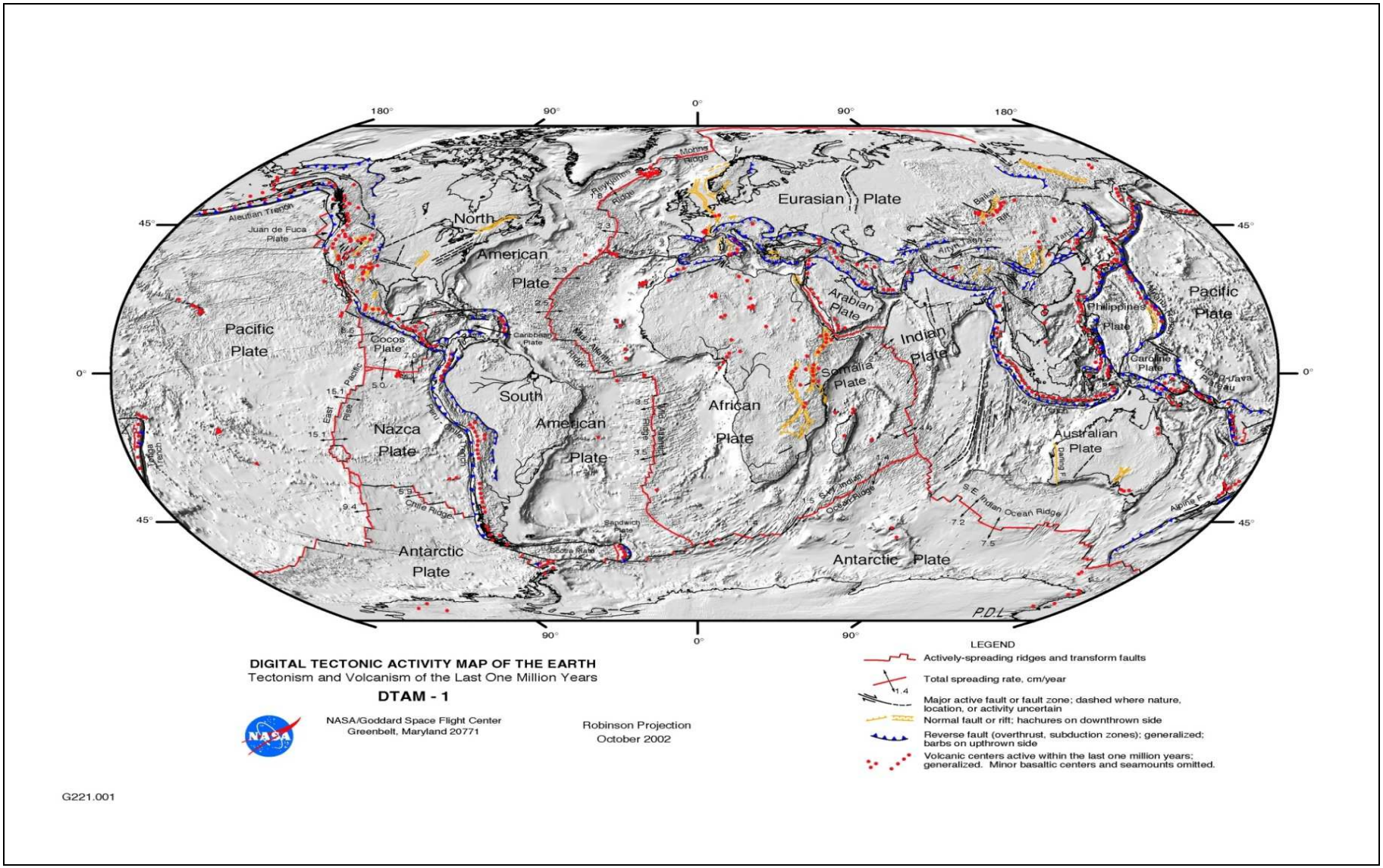

Figure 2.1 Tectonic Map of the Earth Showing Tectonic Plate Boundaries (from NASA, 2003)

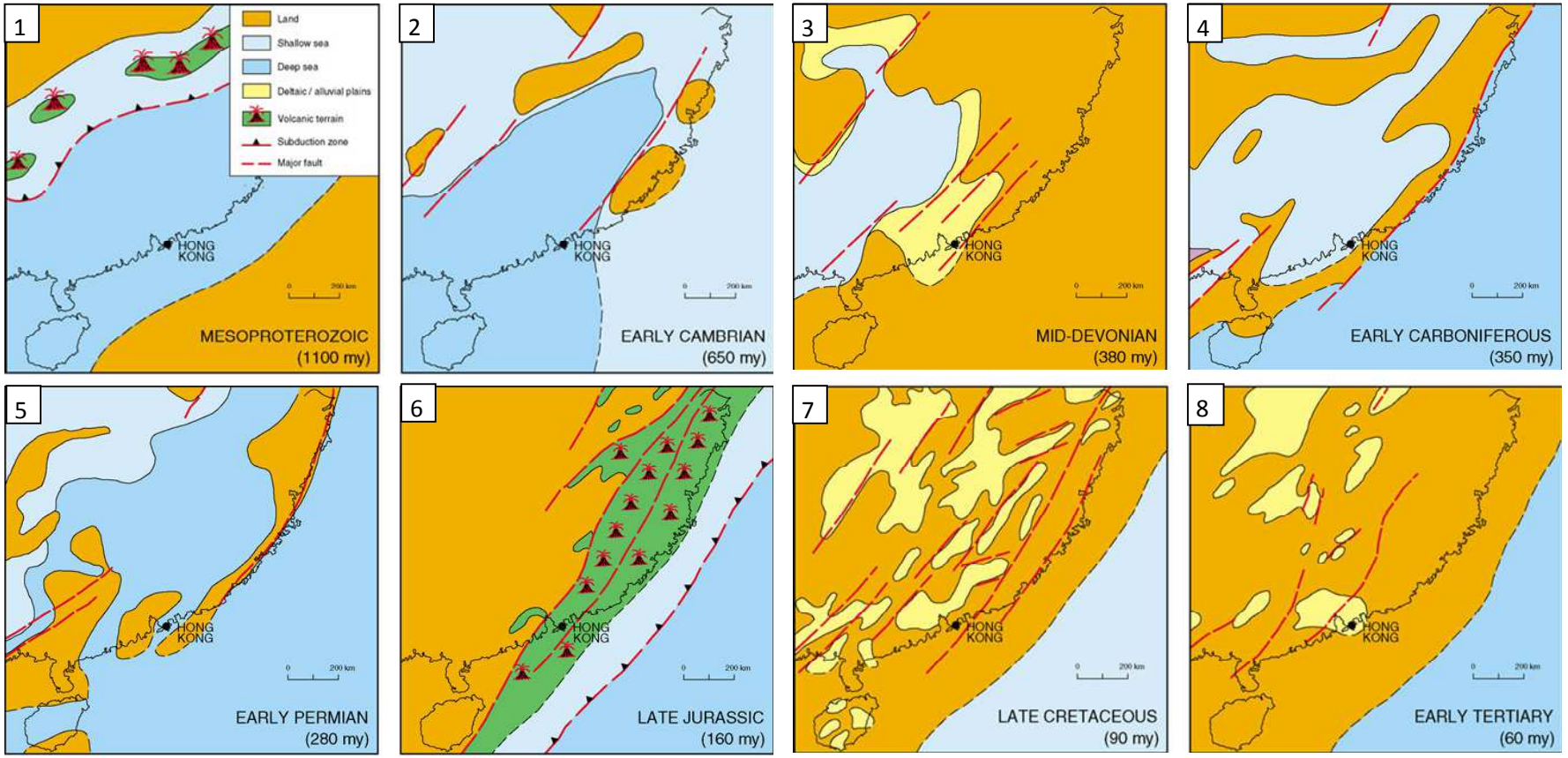

Figure 2.2 Paleogeographic Reconstructions of Southeast China (from Sewell et al, 2000)

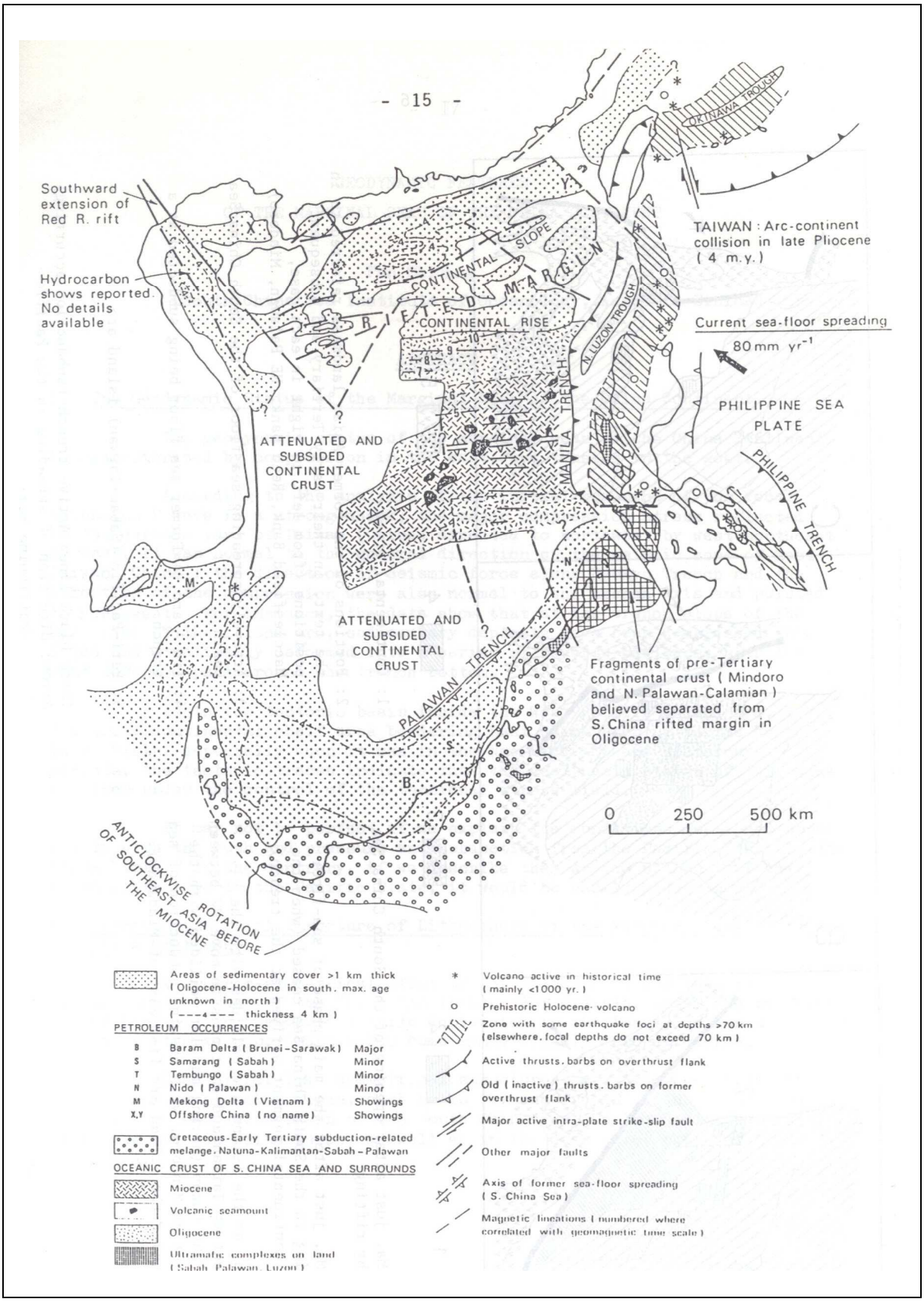

Figure 2.3 General Tectonic Elements of South China Sea Region (from Workman, 1983)

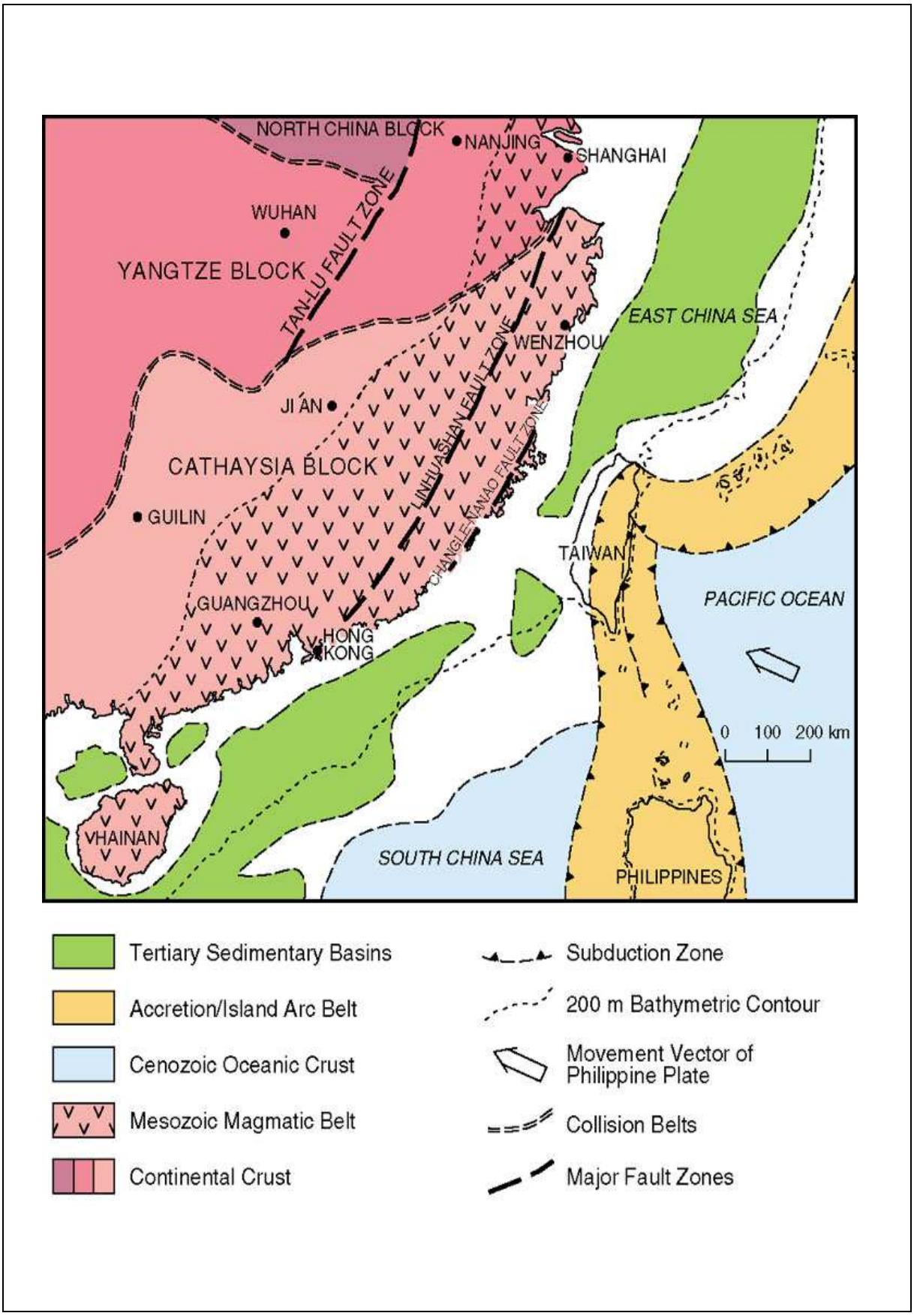

Figure 2.4 Regional Tectonic Elements of Southeast China (from Sewell et al, 2000)

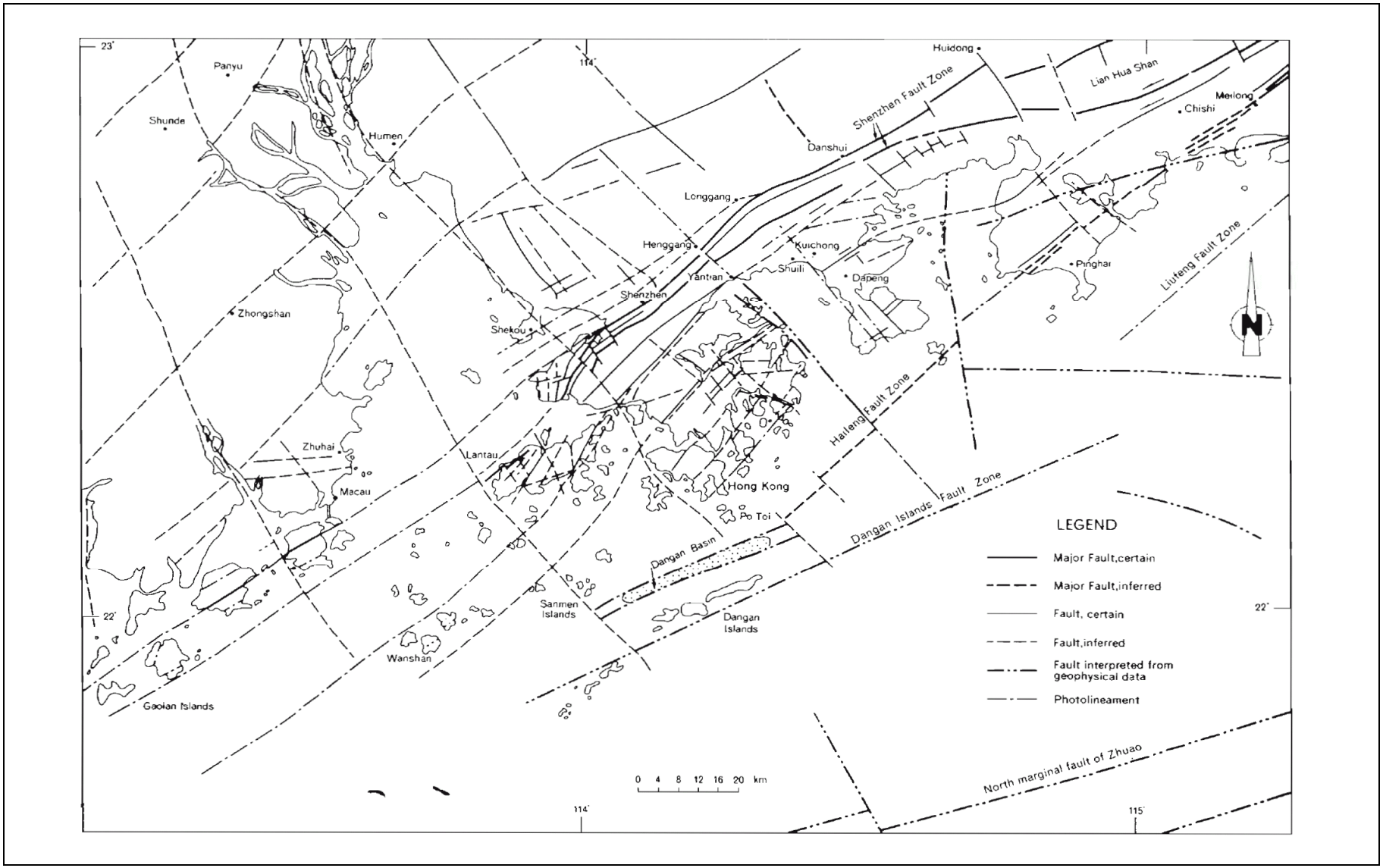

Figure 2.5 Fault System of Hong Kong and Adjacent Areas (from Lai & Langford, 1996)

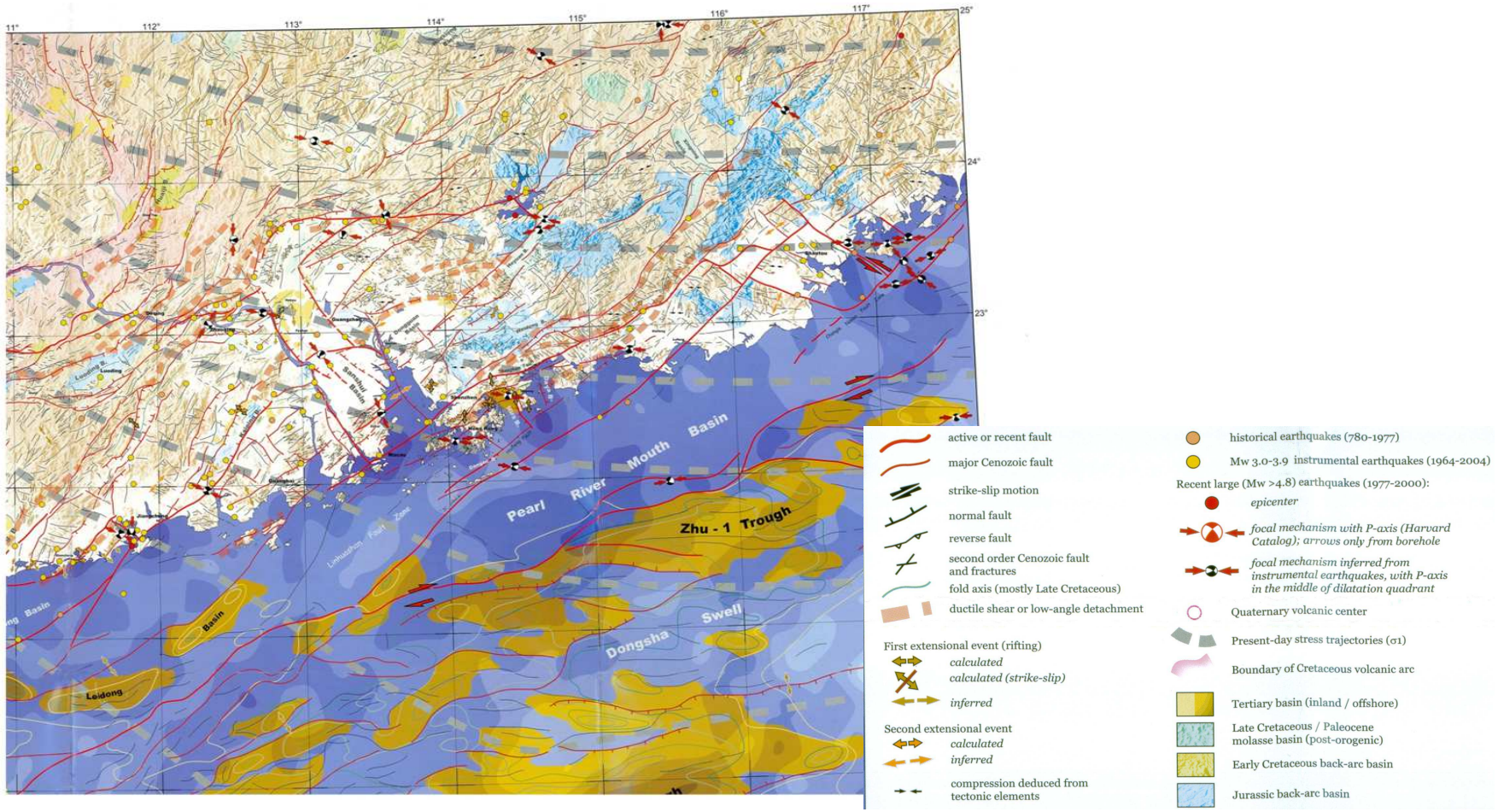

Figure 2.6 Morphotectonic Map of Cenozoic Structures of the South China-Northern Vietnam Coastal Region (from Pubellier & Chan, 2006)

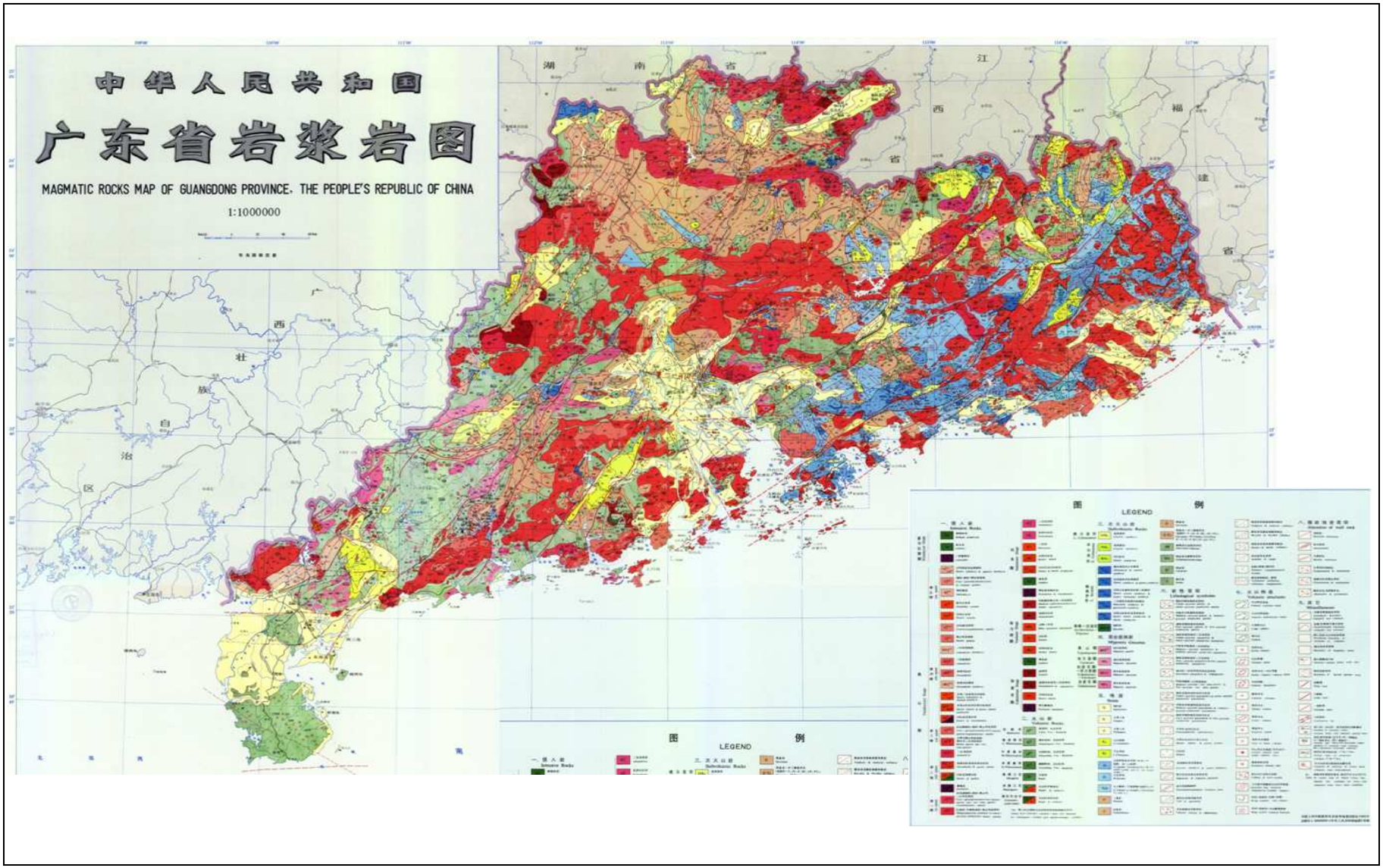

Figure 2.7 Geology Map of Guangdong Province (from Bureau of Geology and Mineral Resources of Guangdong Province, 1988)

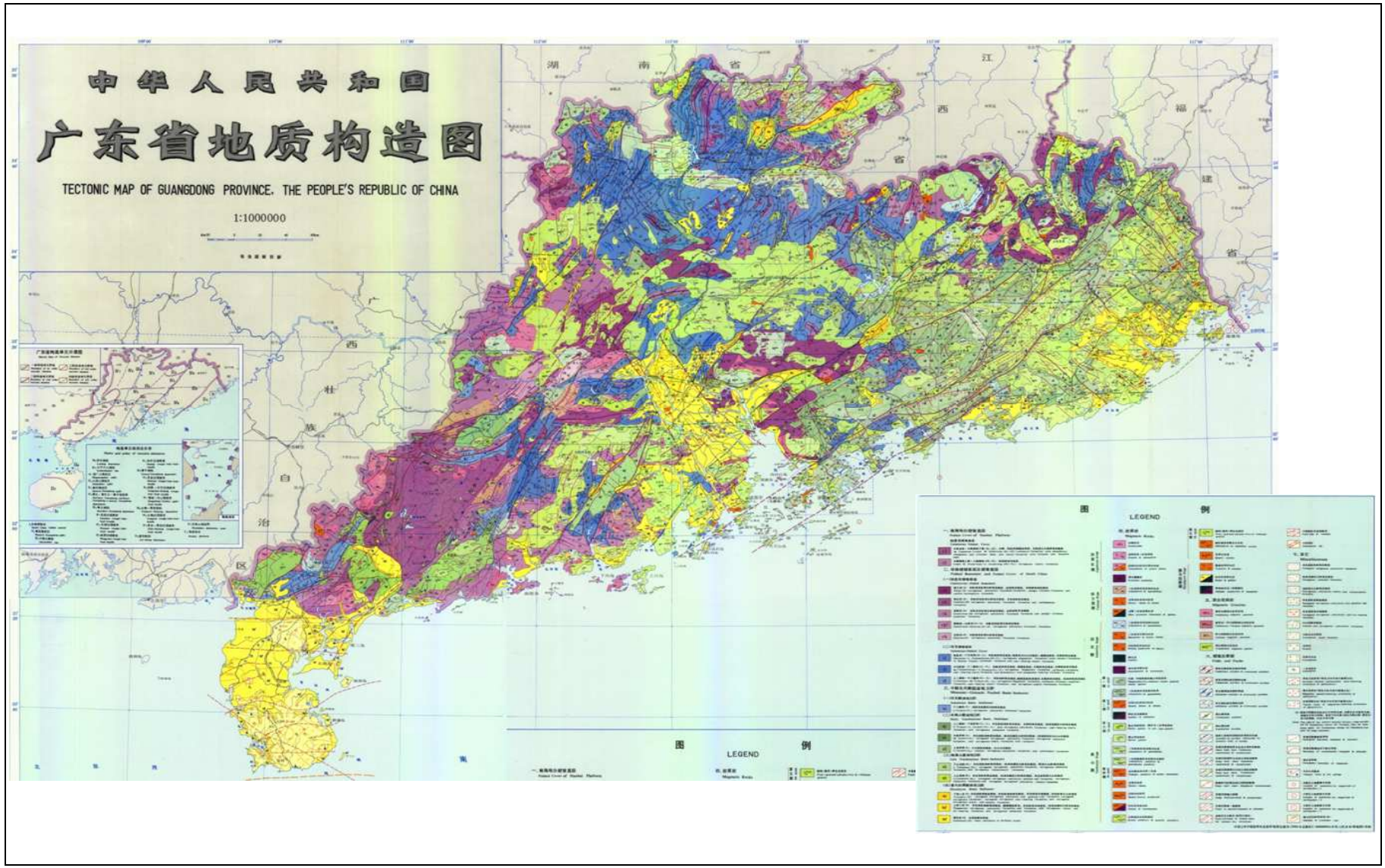

Figure 2.8 Tectonic Map of Guangdong Province (from Bureau of Geology and Mineral Resources of Guangdong Province, 1988)

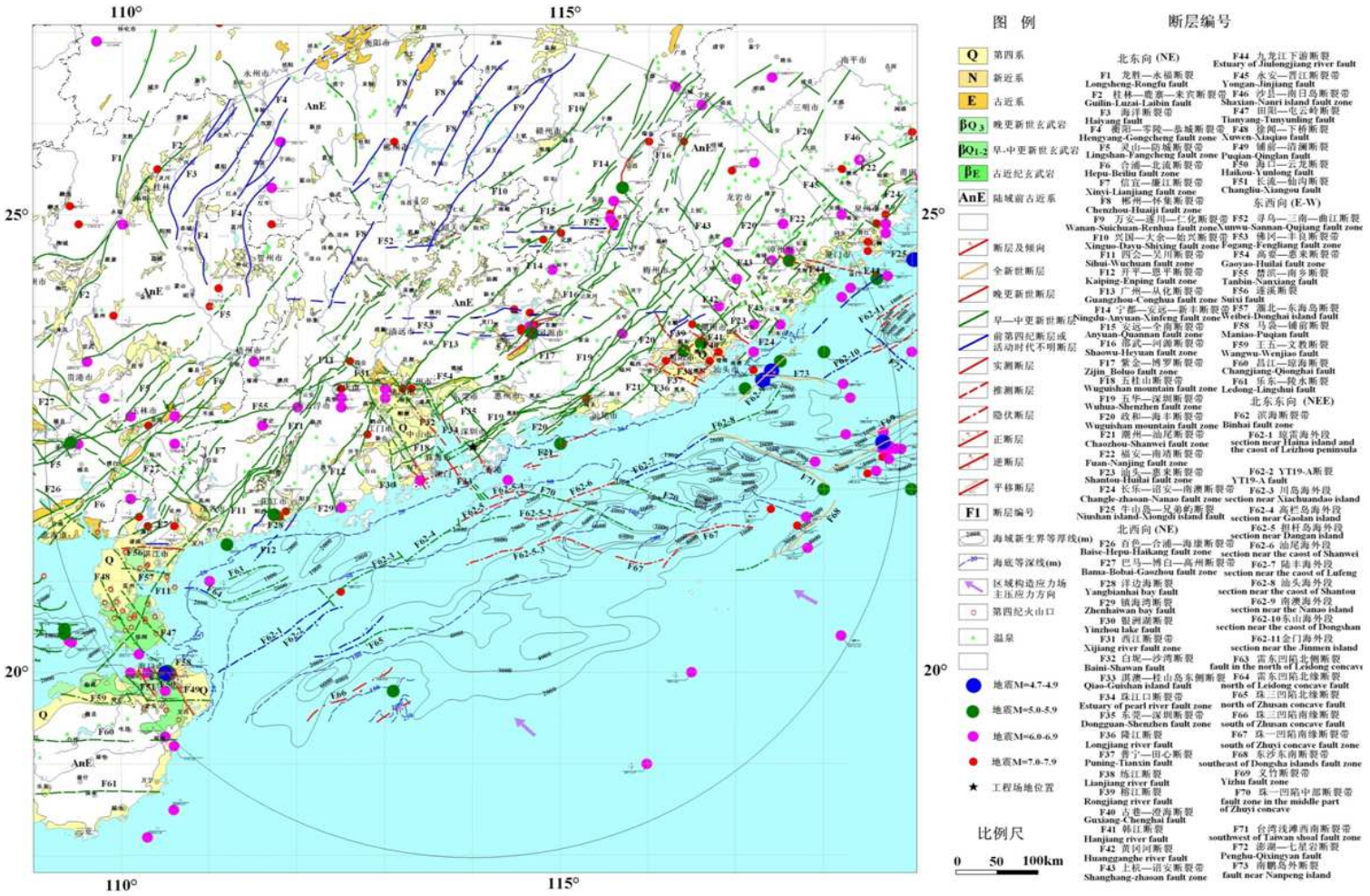

Figure 2.9 Tectonic Structure of Guangdong Region (from GEERRI, 2010)

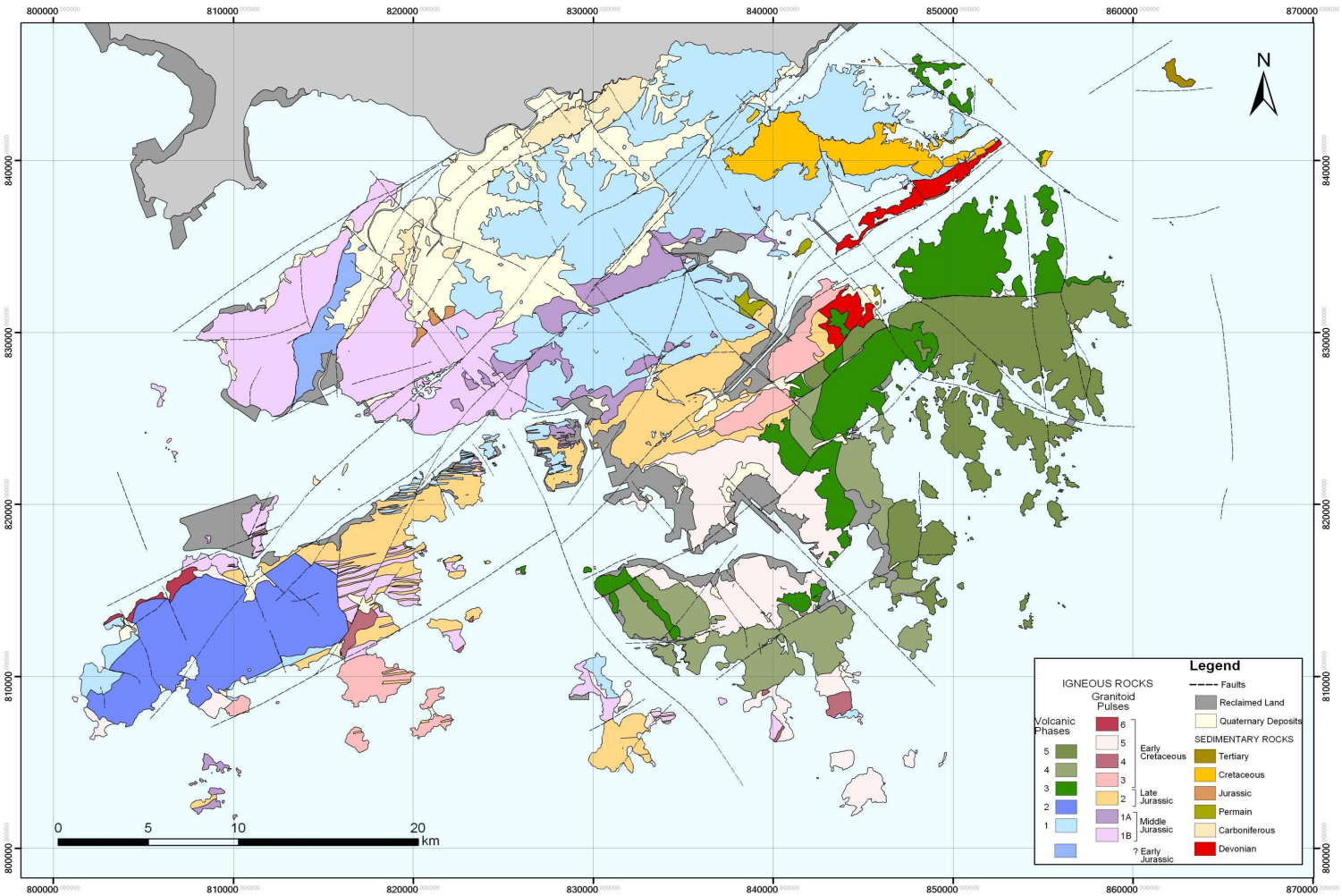

Figure 2.10 Geology Map of Hong Kong (from GEO, 2000)

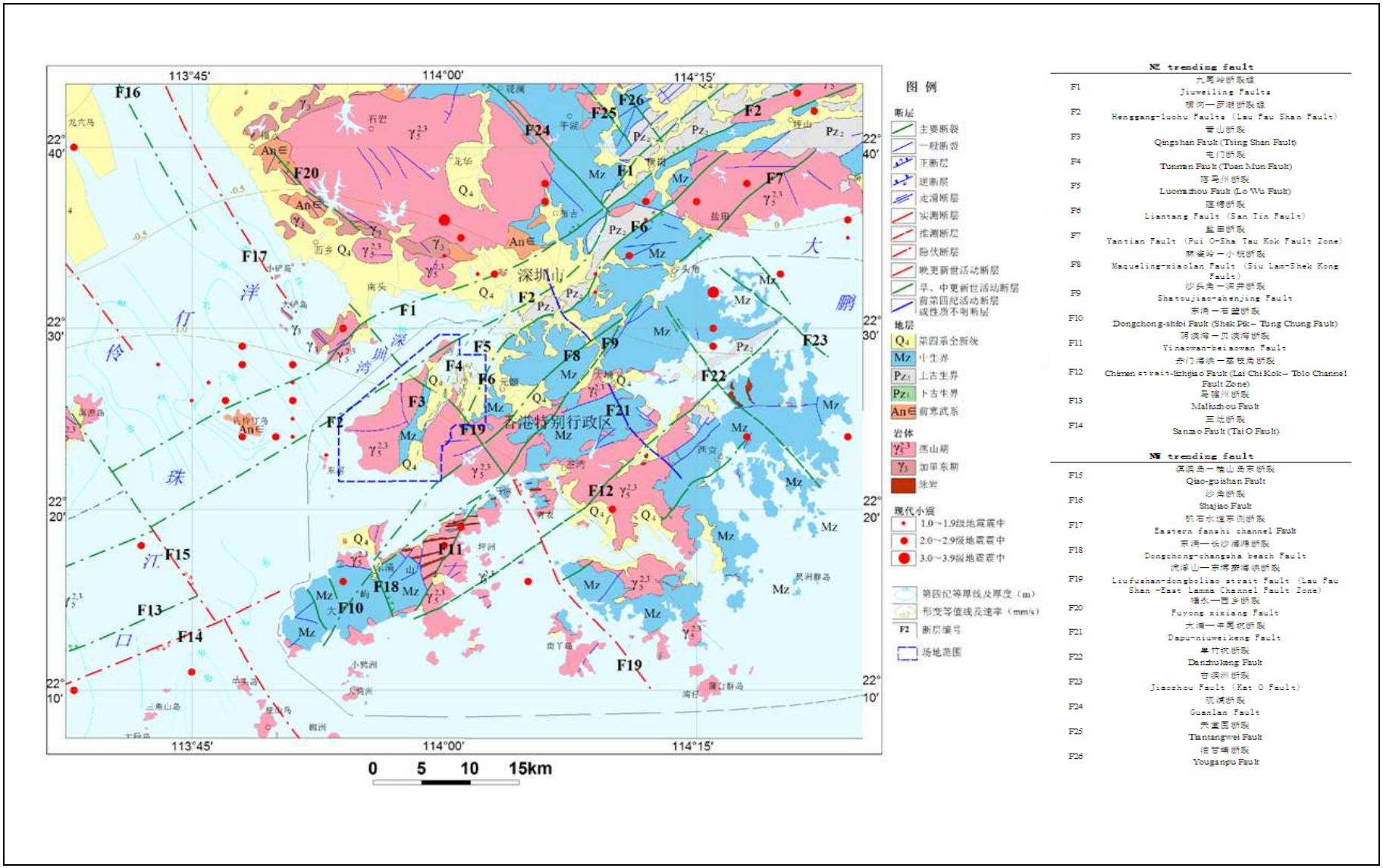

Figure 2.11 Tectonic Structures around Hong Kong Region (from GEERRI, 2010)

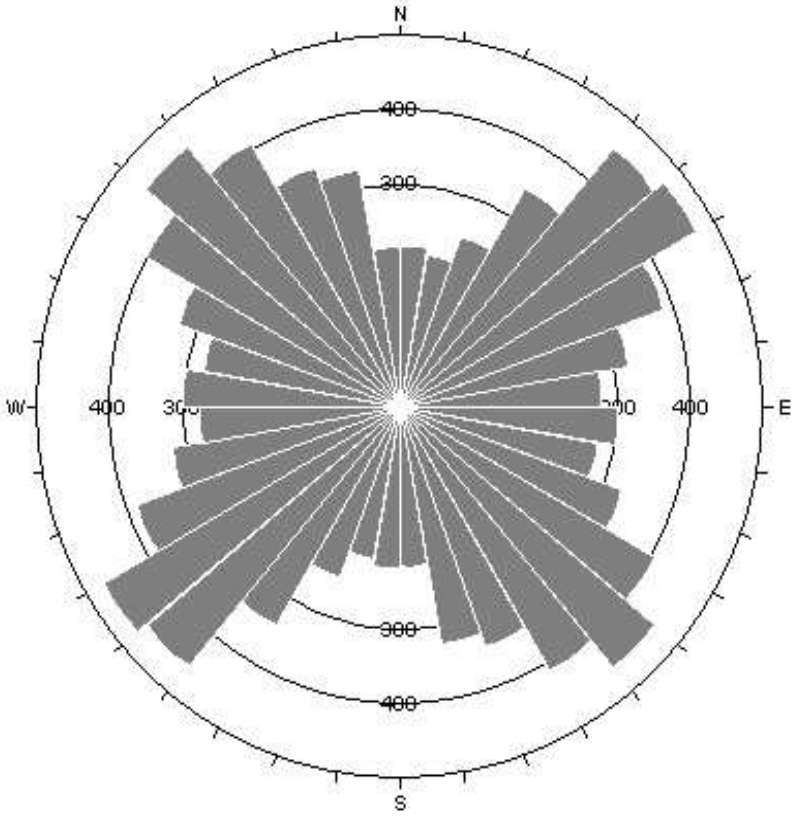

Figure 2.12 A Rosette Plot Showing the Strike Density of Certain and Inferred Faults Presented in 1:20,000 Geological Map in Hong Kong

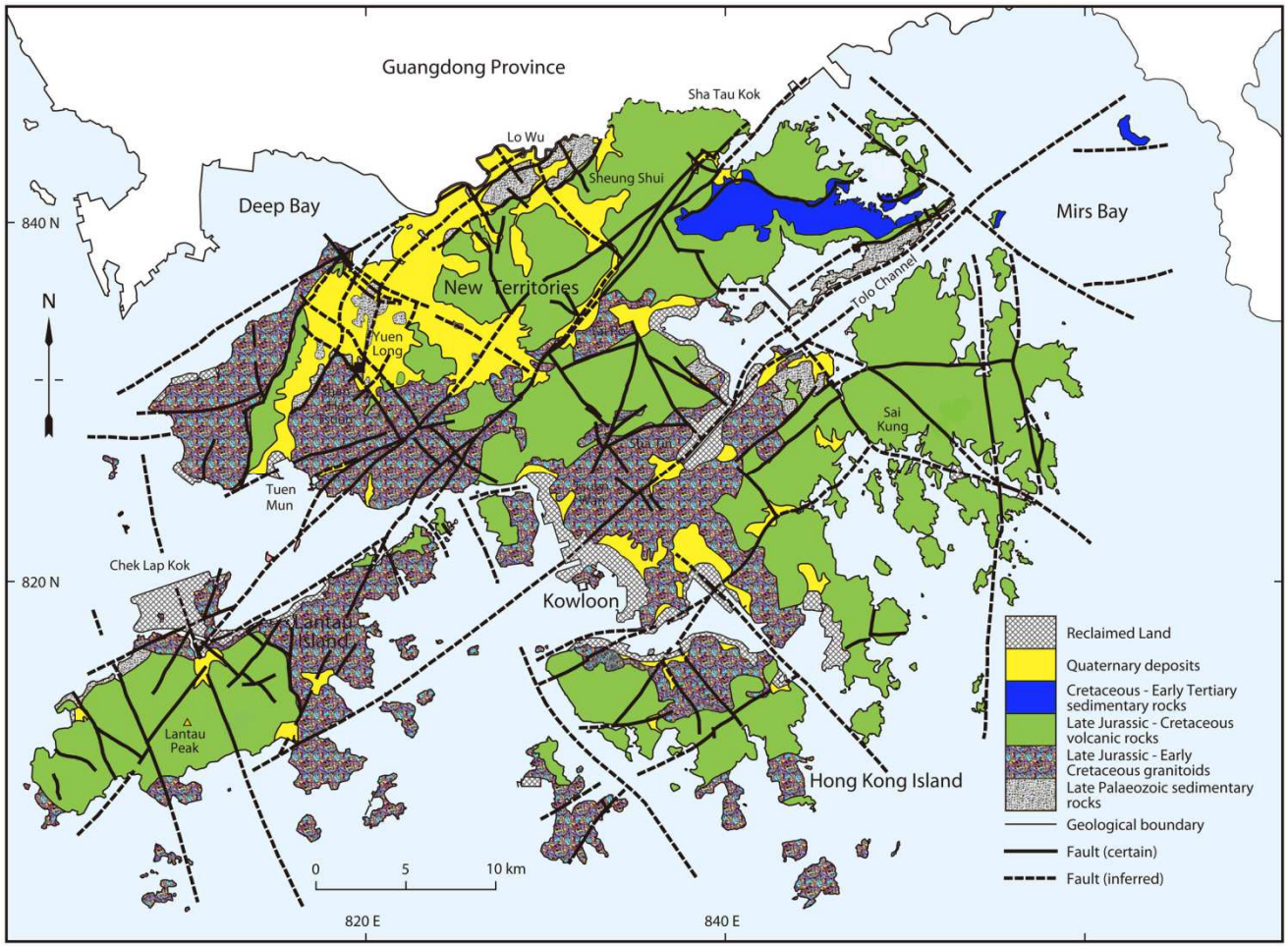

Sample	TL age
1	265,500 ± 21,000
2	177,700 ± 15,100
3	105,100 ± 8,700
4	94,700 ± 8,100
5	91,100 ± 7,500
6	93,900 ± 7,900
7	101,000 ± 8,600
8	222,260 ± 17,800
9	196,100 ± 16,900
10	33,300 ± 2,700
11	82,000 ± 6,800
12	147,500 ± 11,800
13	278,700 ± 23,100
14a	190,600 ± 15,800
14b	201,800 ± 16,100
14c	177,500 ± 13,300
15	254,500 ± 20,400
16	118,700 ± 9,700
17	196,800 ± 16,300
18	188,500 ± 15,400
19	126,200 ± 10,300

Figure 2.13 TL Dating Data for Main Fault Systems in Hong Kong (Figure from GEO, 2000 and TL Age from Ding & Lai, 1997)

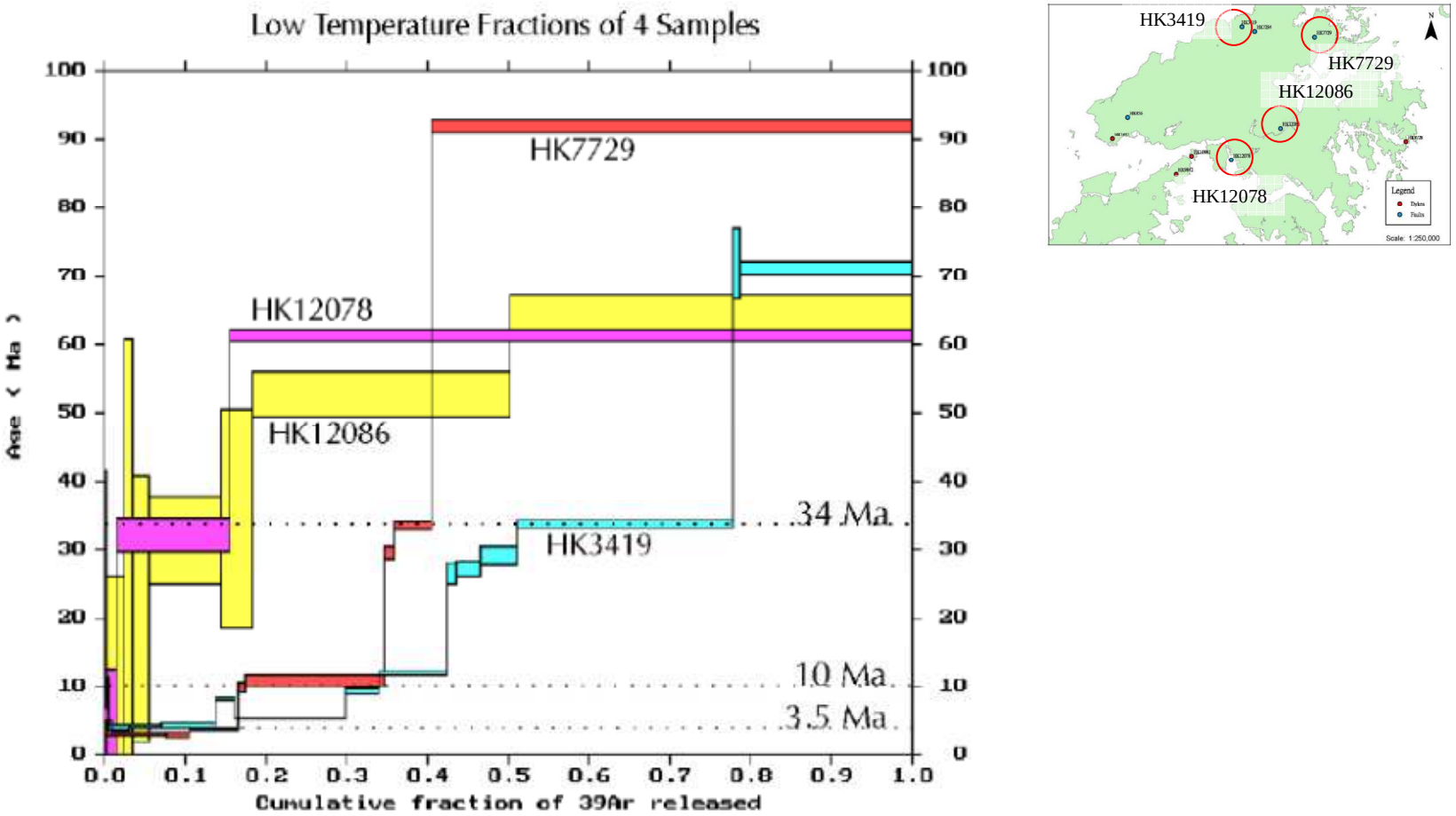

Figure 2.14 The Result of Low Temperature Fractions of Fault Rocks Samples Used in ^{40}Ar-^{39}Ar Dating and their Corresponding Locations (from Campbell & Sewell, 2007)

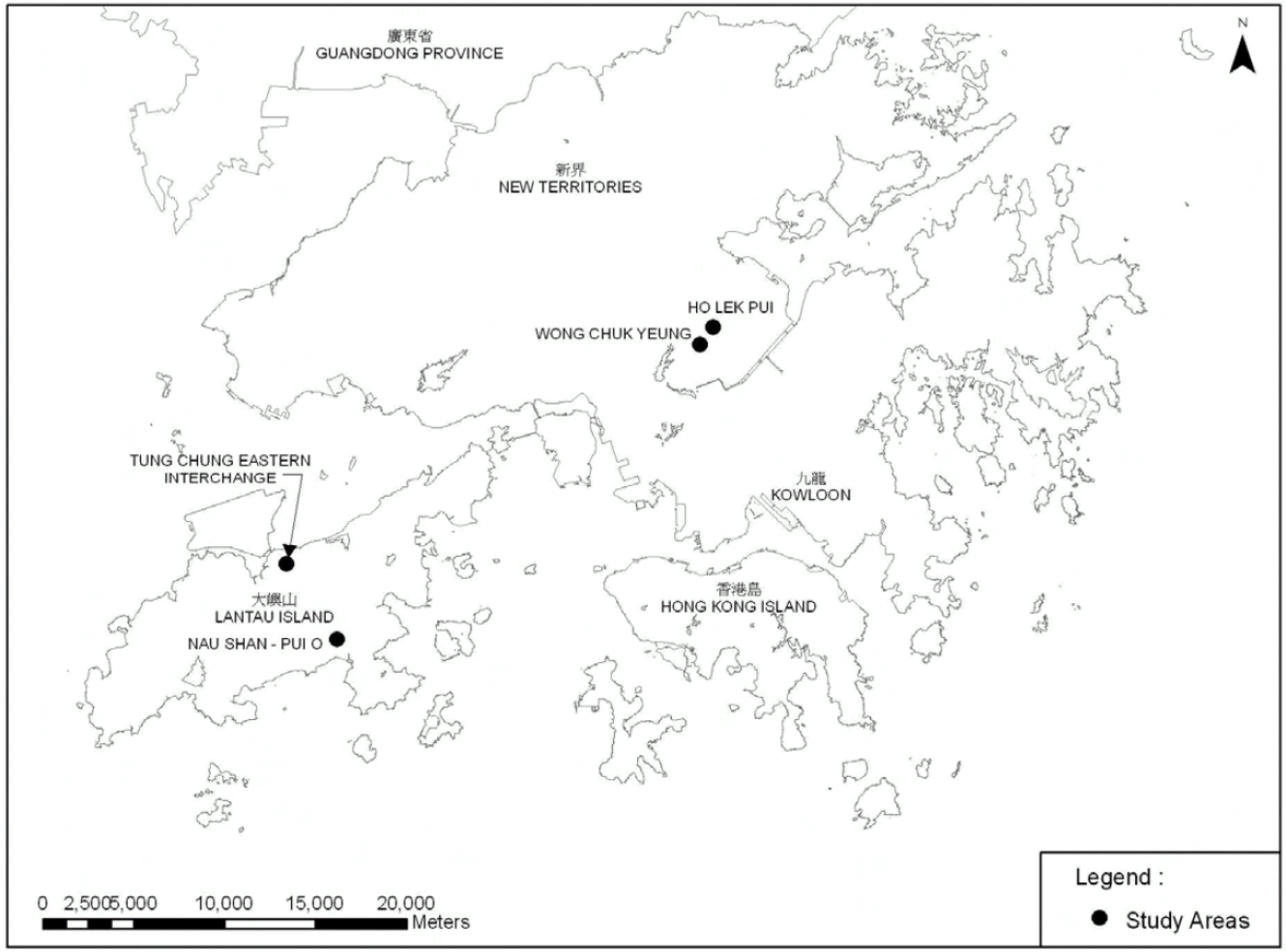

Figure 2.15 Location Plan for Four Areas in the Study (from Wong & Ding, 2010)

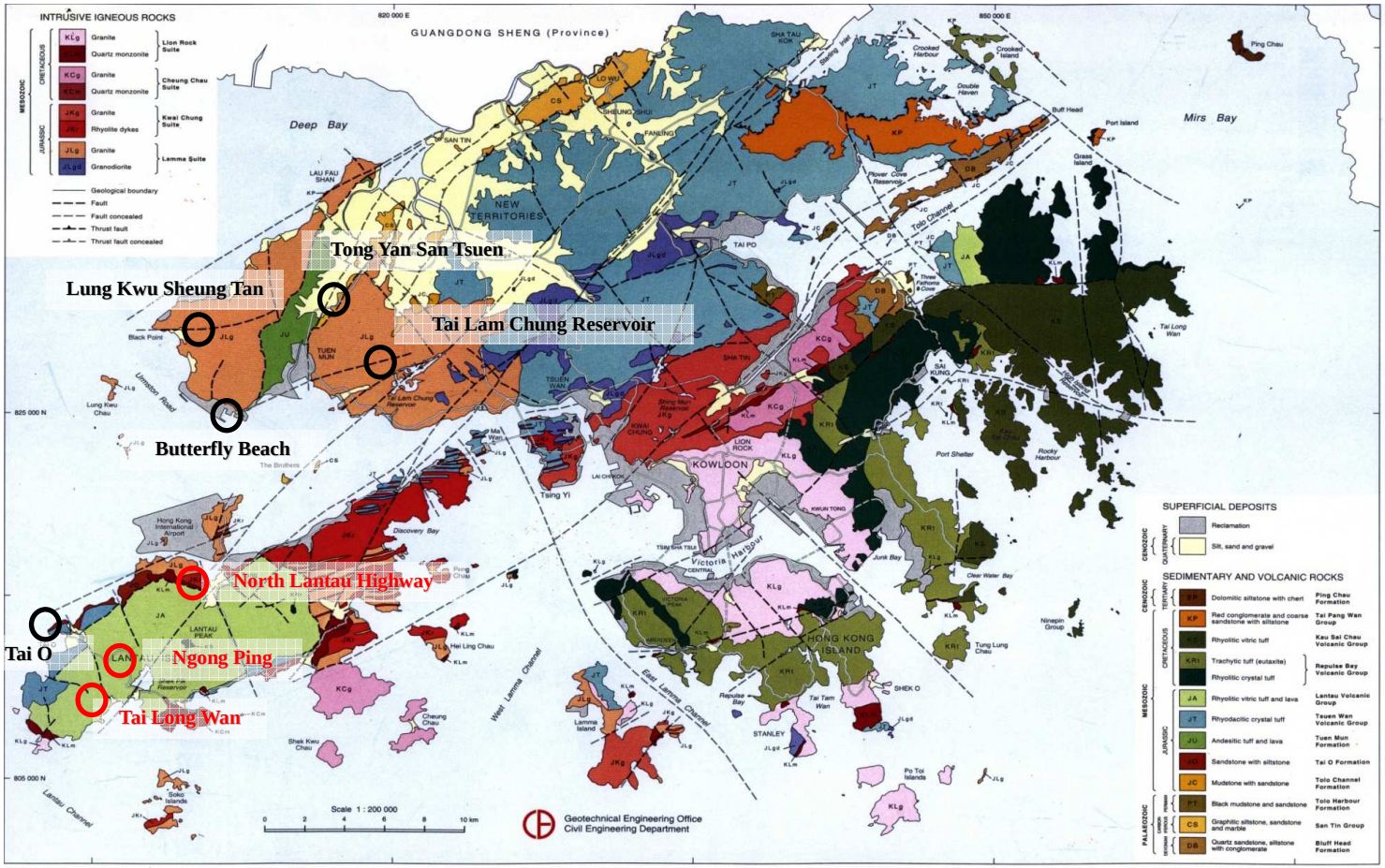

Note: The black circles represent the site visits on 13th and 14th of July 2010 and the red circles represent the site visits on 6th and 7th December 2010.

Figure 2.16 Location Plan for Locations in the Two Site Visits (Geology Map from GEO, 2000)

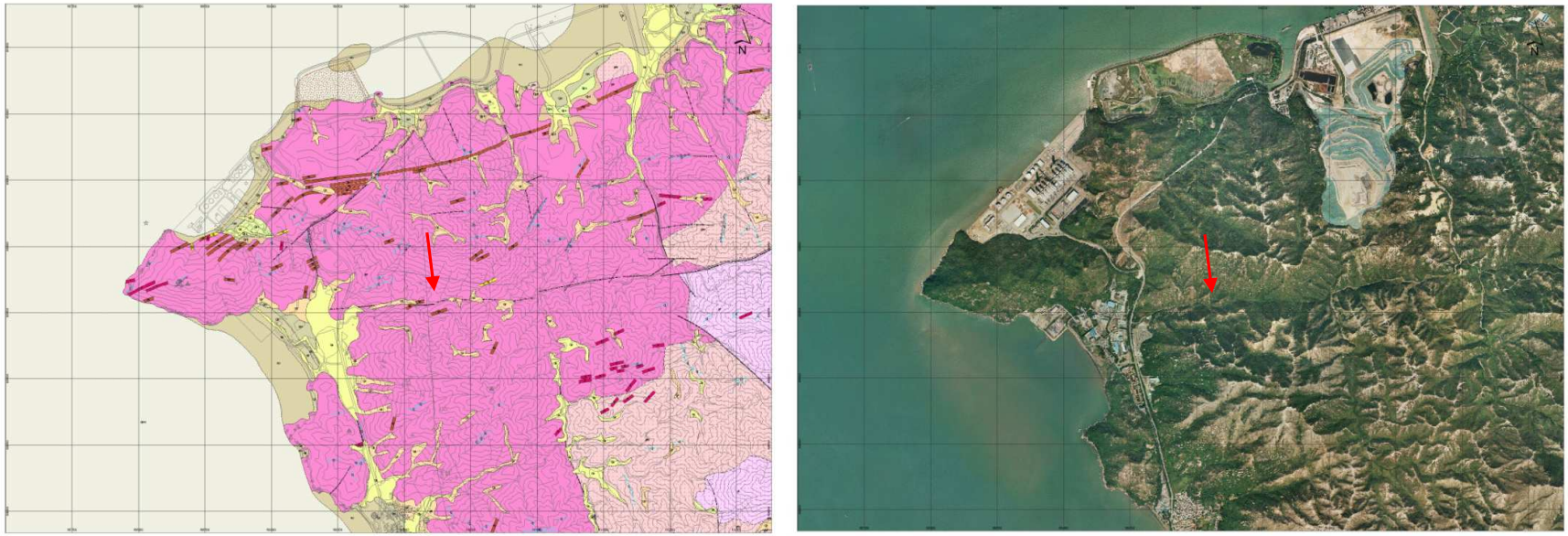

Figure 2.17 Geological Map and Aerial Photo of Location of Lung Kwu Sheung Tan

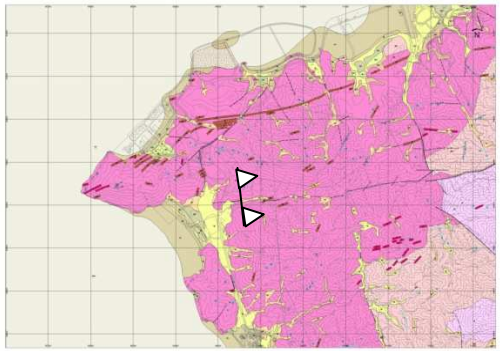

Figure 2.18 Valley in Lung Kwu Tan

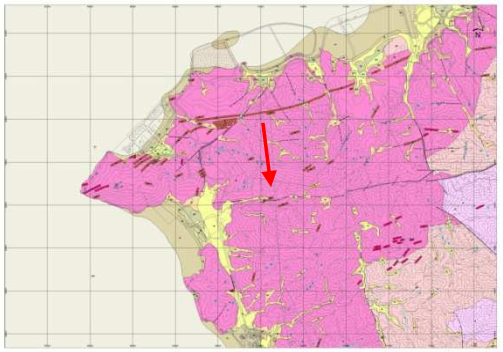

Figure 2.19 Valley in Lung Kwu Tan

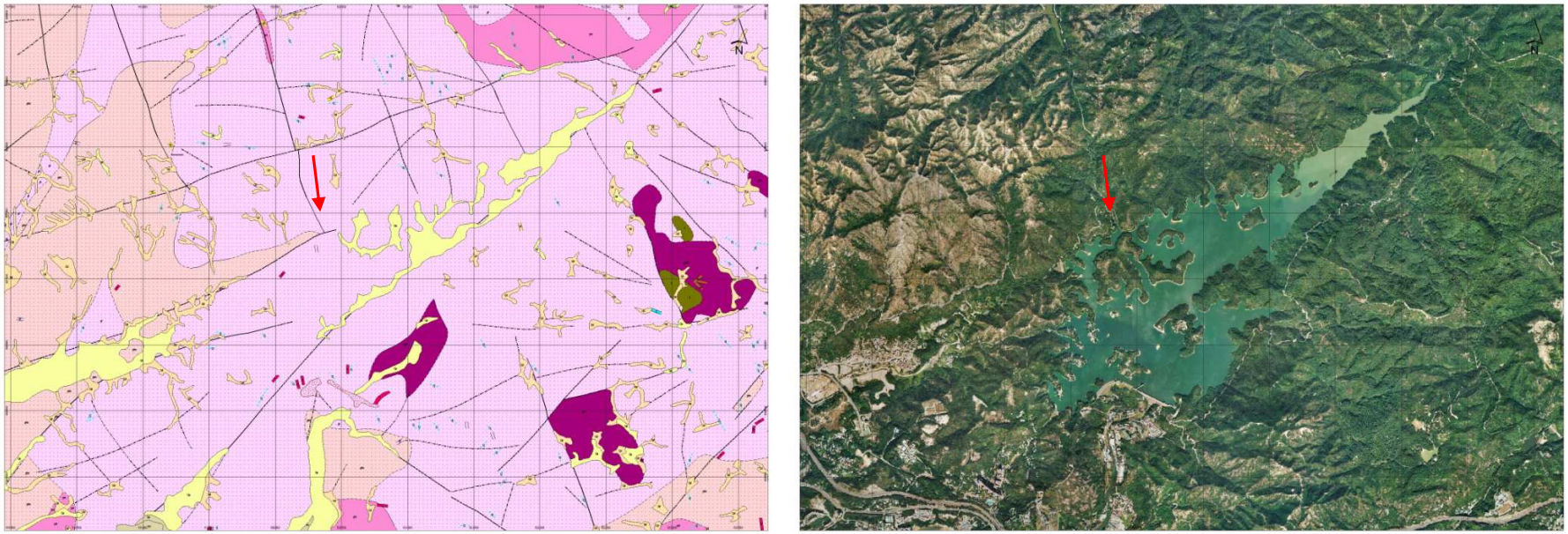

Figure 2.20 Geological Map and Aerial Photo of Location of Tai Lam Chung Reservoir

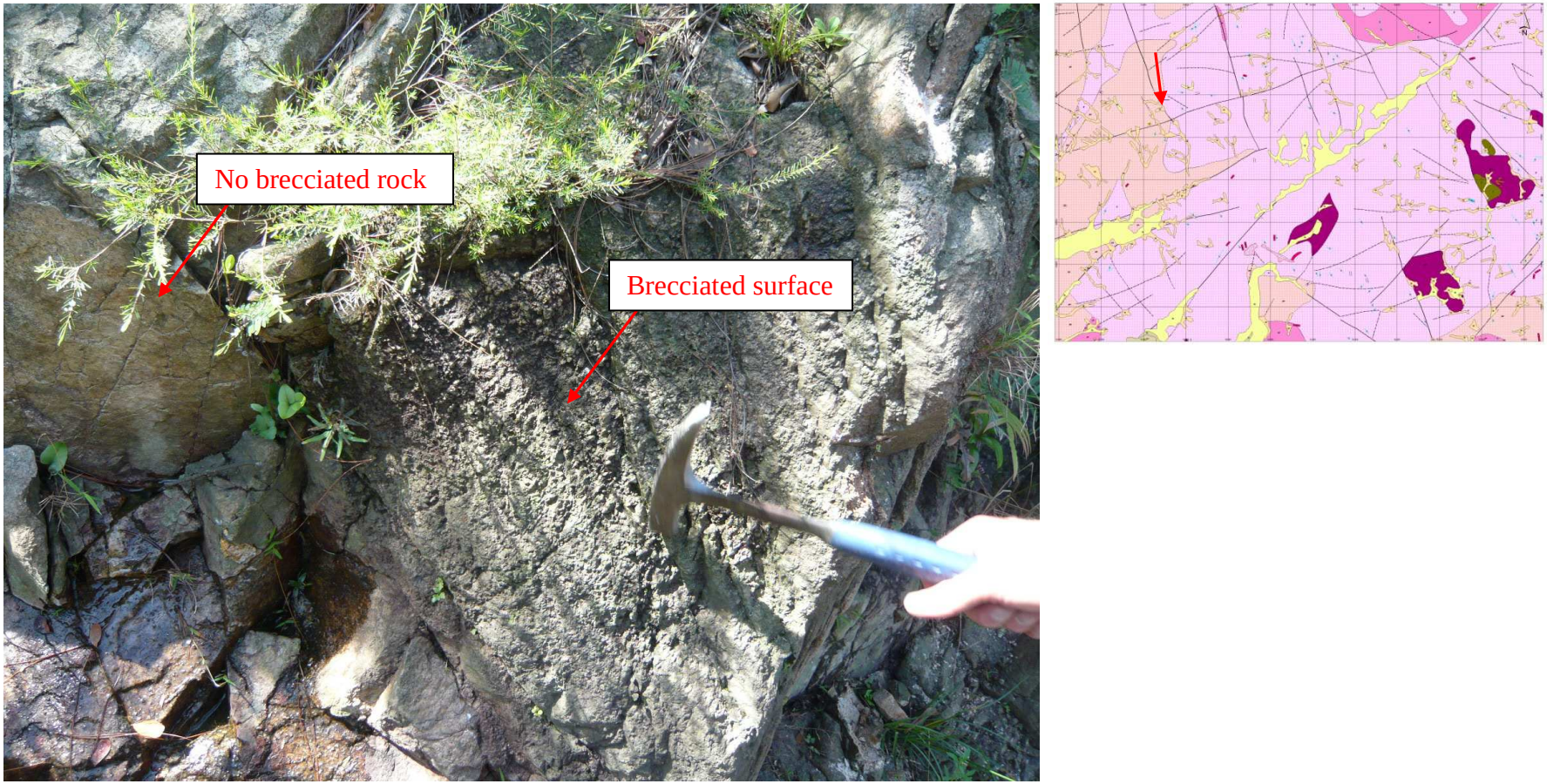

Figure 2.21 Brecciated Rock Compared with Better Rock of Tai Lam Chung Reservoir

Figure 2.22 Breccias Exposed at the Surface at Tai Lam Chung Reservoir

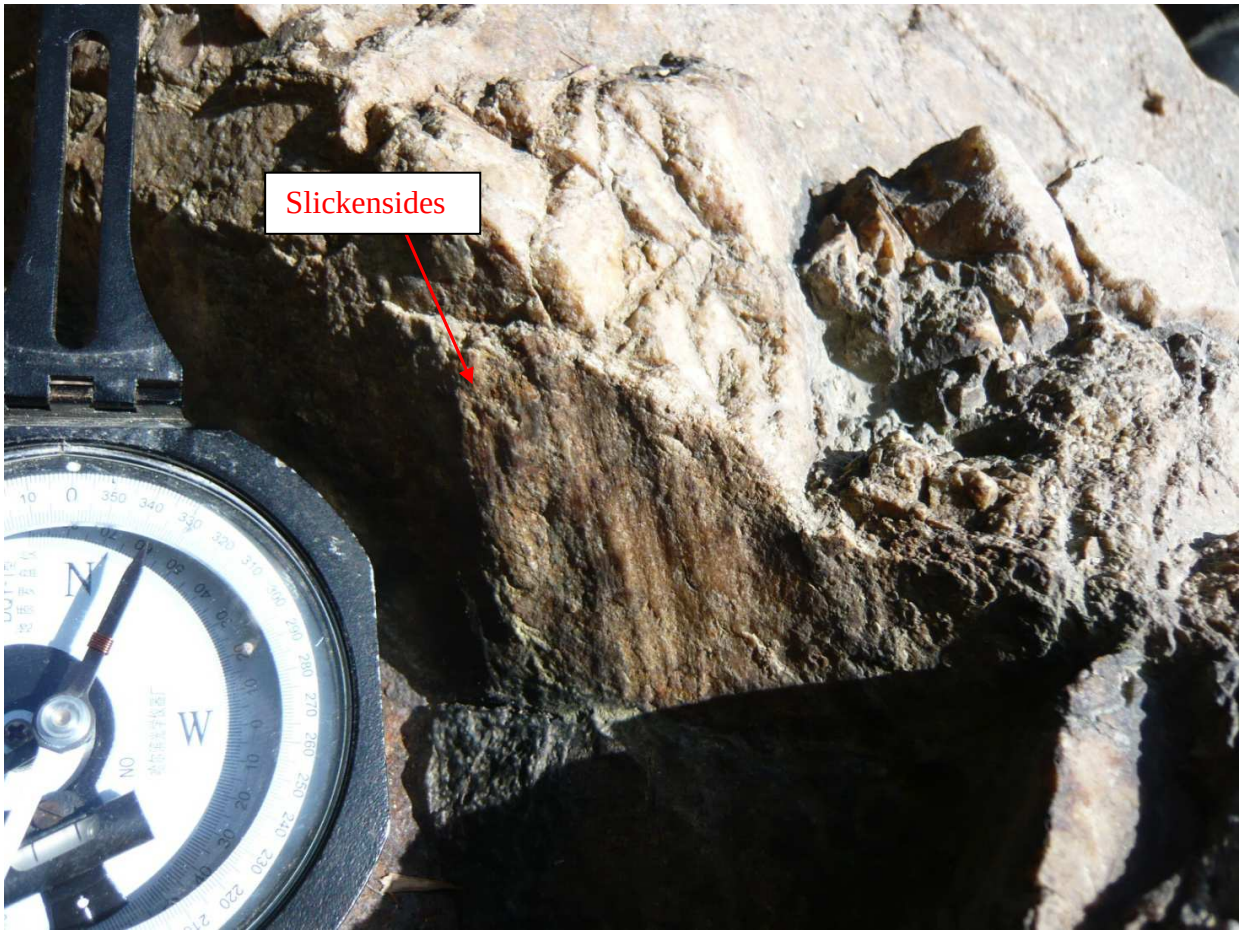

Figure 2.23 Slickensides Exposed at Tai Lam Chung Reservoir

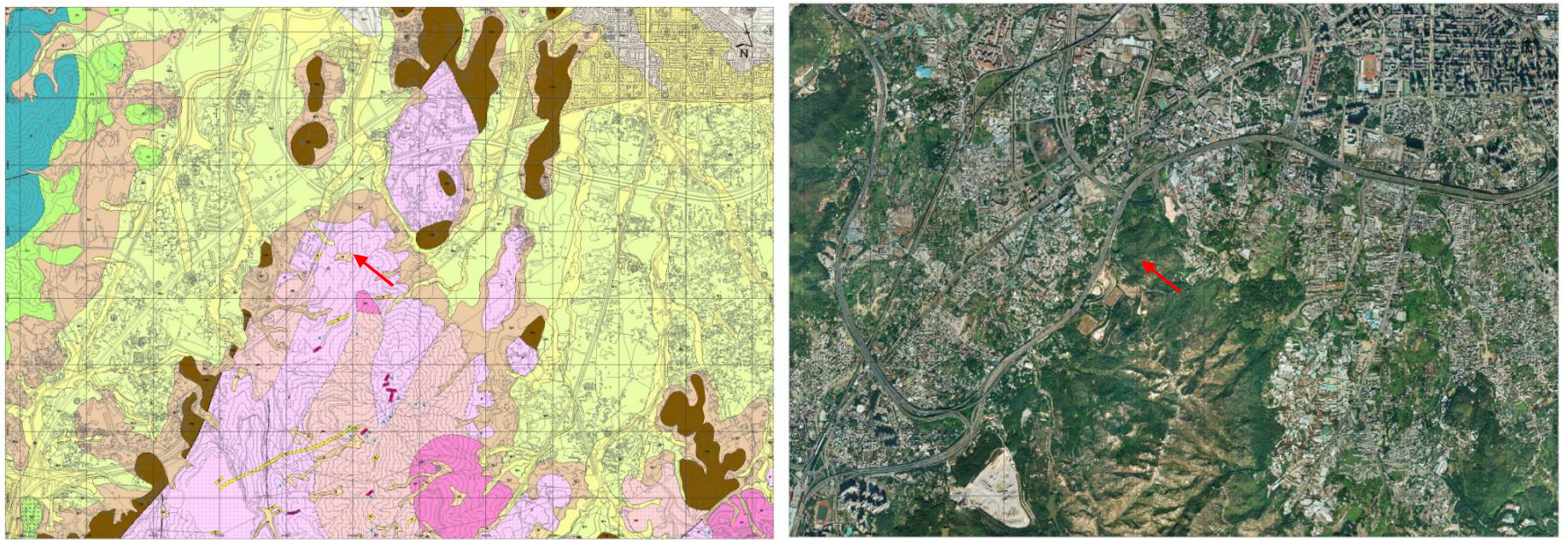

Figure 2.24 Geological Map and Aerial Photo of Location of Tung Yan San Tsuen

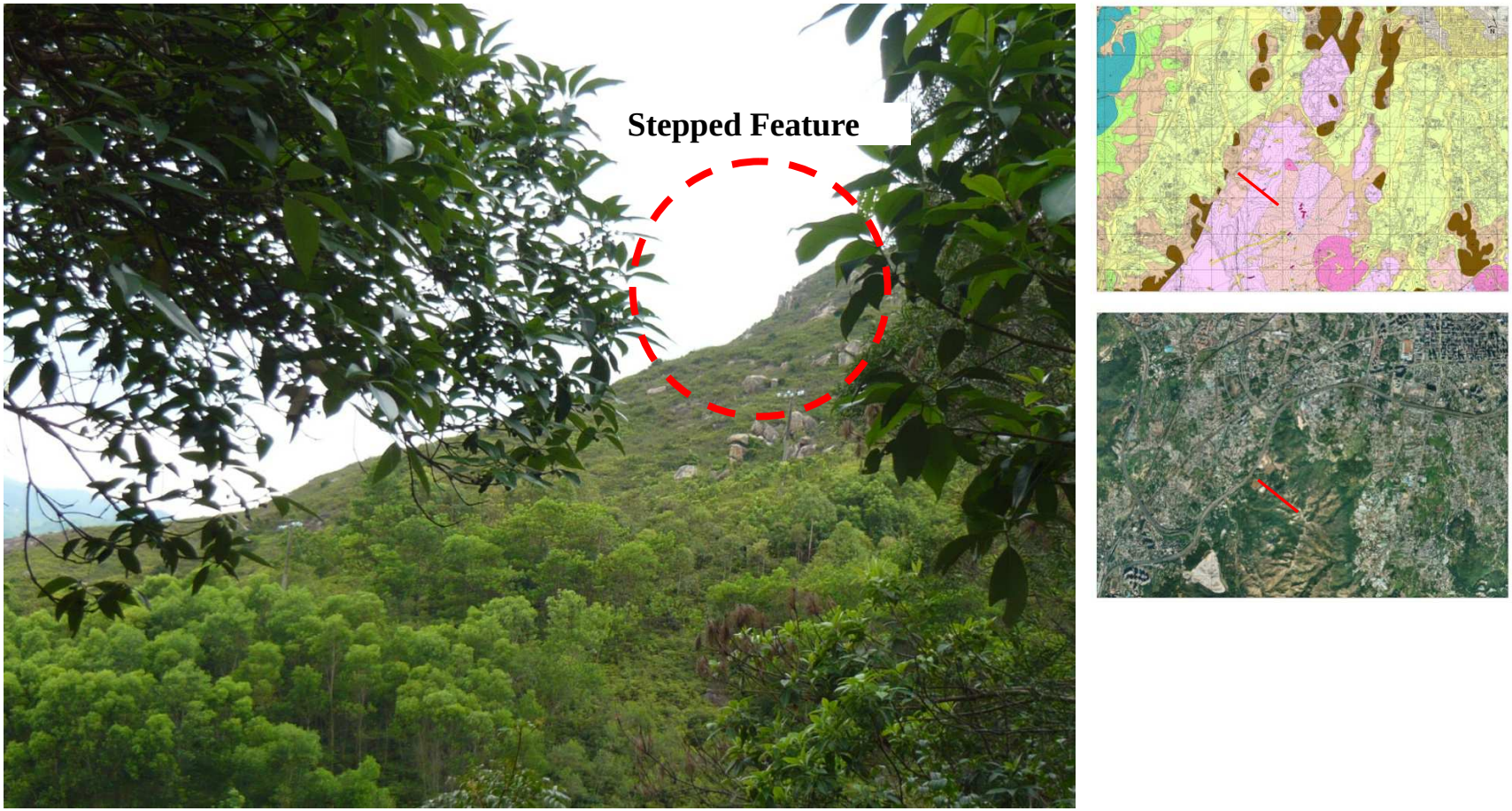

Figure 2.25 Stepped Features in a Slope near Tung Yan San Tsuen

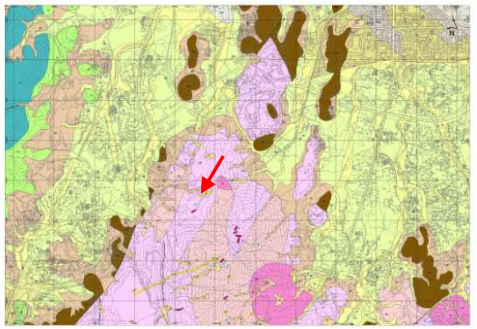

Figure 2.26 Quaternary Strata Exposed near Tung Yan San Tsuen

Figure 2.27 Geological Map and Aerial Photo of Location of Butterfly Beach

Figure 2.28 Rock Outcrop of Location of Butterfly Beach

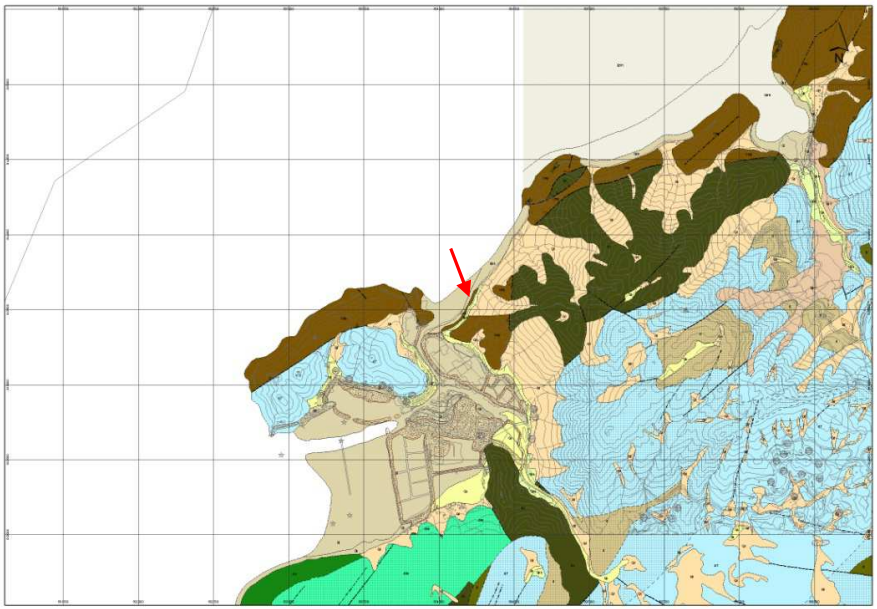

Figure 2.29 Geological Map and Aerial Photo of Location of Tai O

Figure 2.30 Rock Outcrop of Location of Tai O

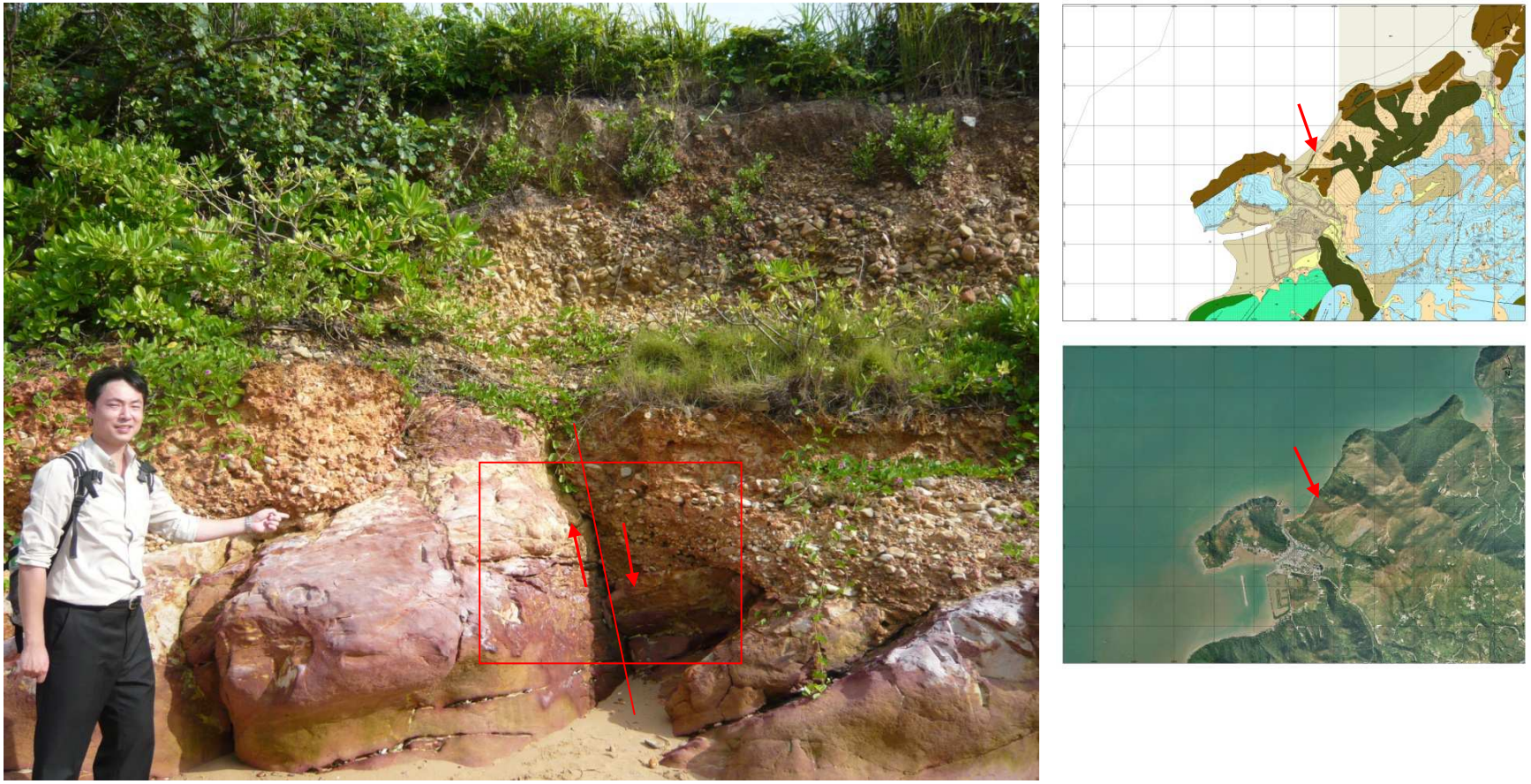

Figure 2.31 Rock Outcrop in Location A in Figure 2.29

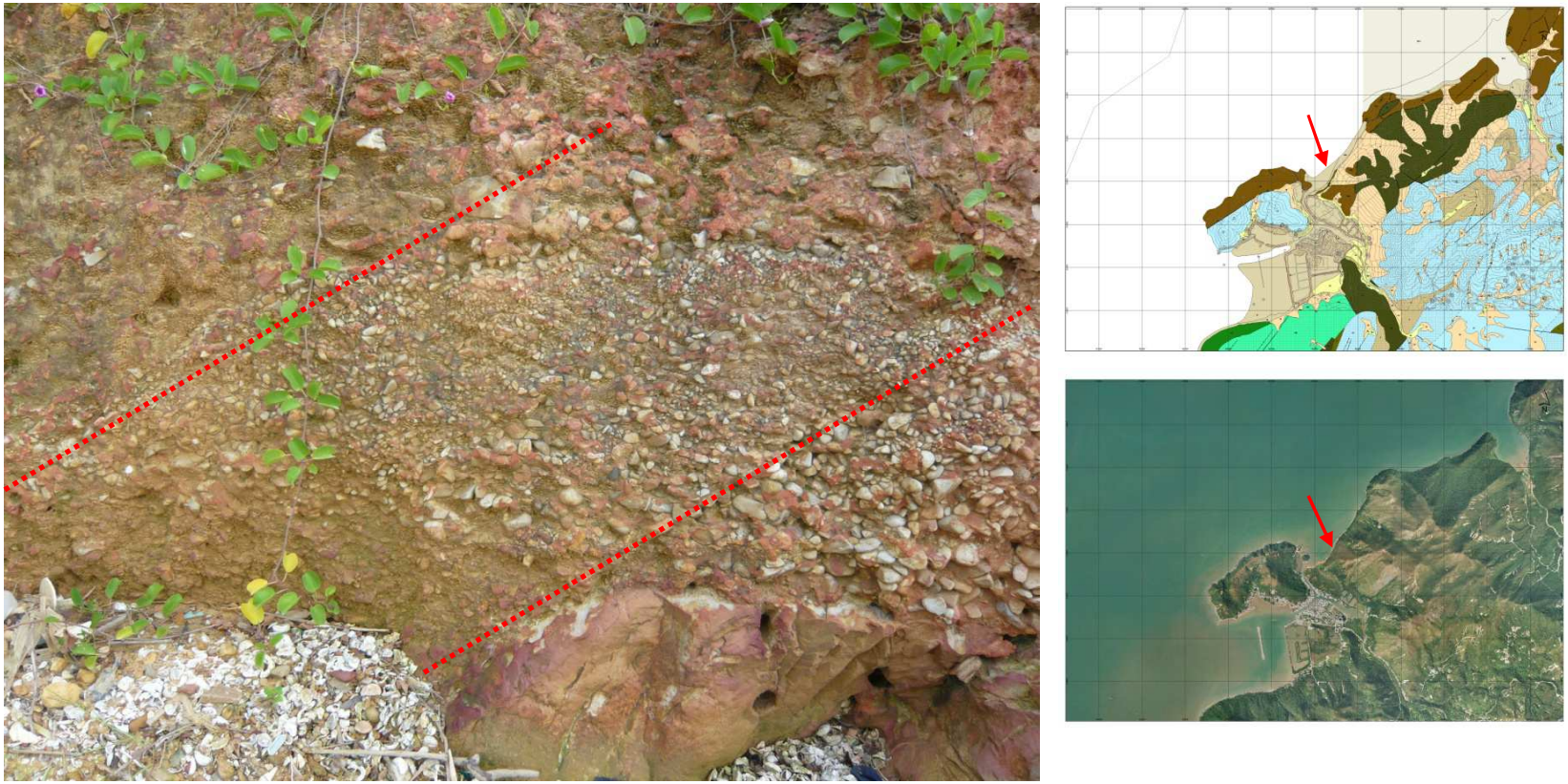

Figure 2.32 Rock Outcrop in Location B in Figure 2.29. The Dotted Lines Represent the Two Lineaments

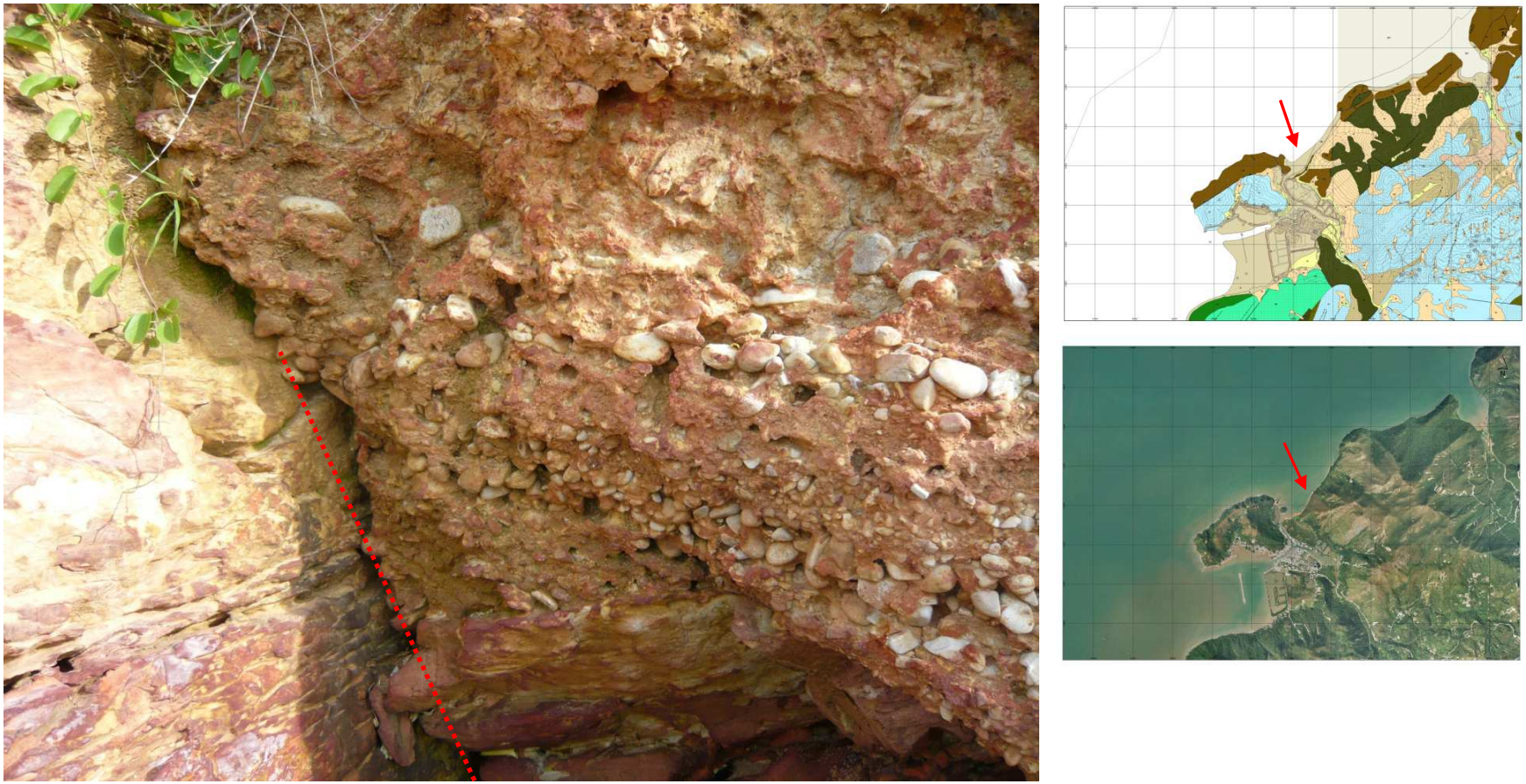

Figure 2.33 Close-up of Red Rectangular Boundary in Figure 2.31. The Implication of Cobbles and Boulders along the Offset Surface Do Not Show Any Changes

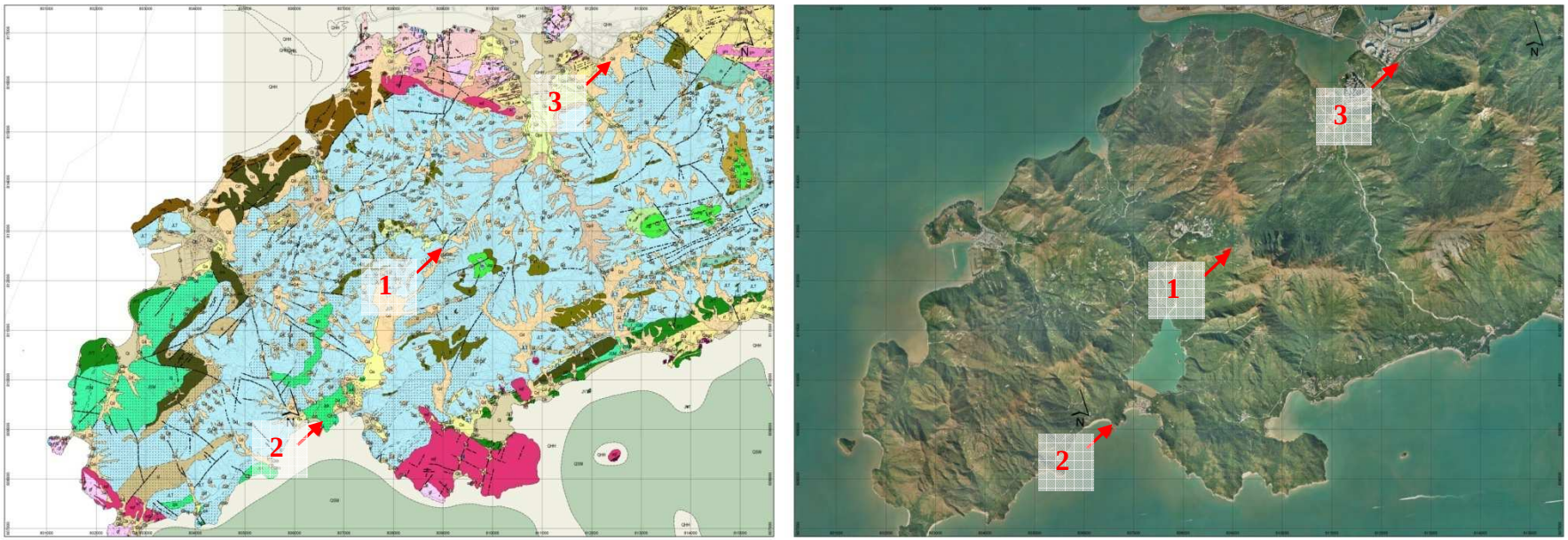

Figure 2.34 Geological Map and Aerial Photo of Three Locations Site Visit on 6th and 7th December 2010

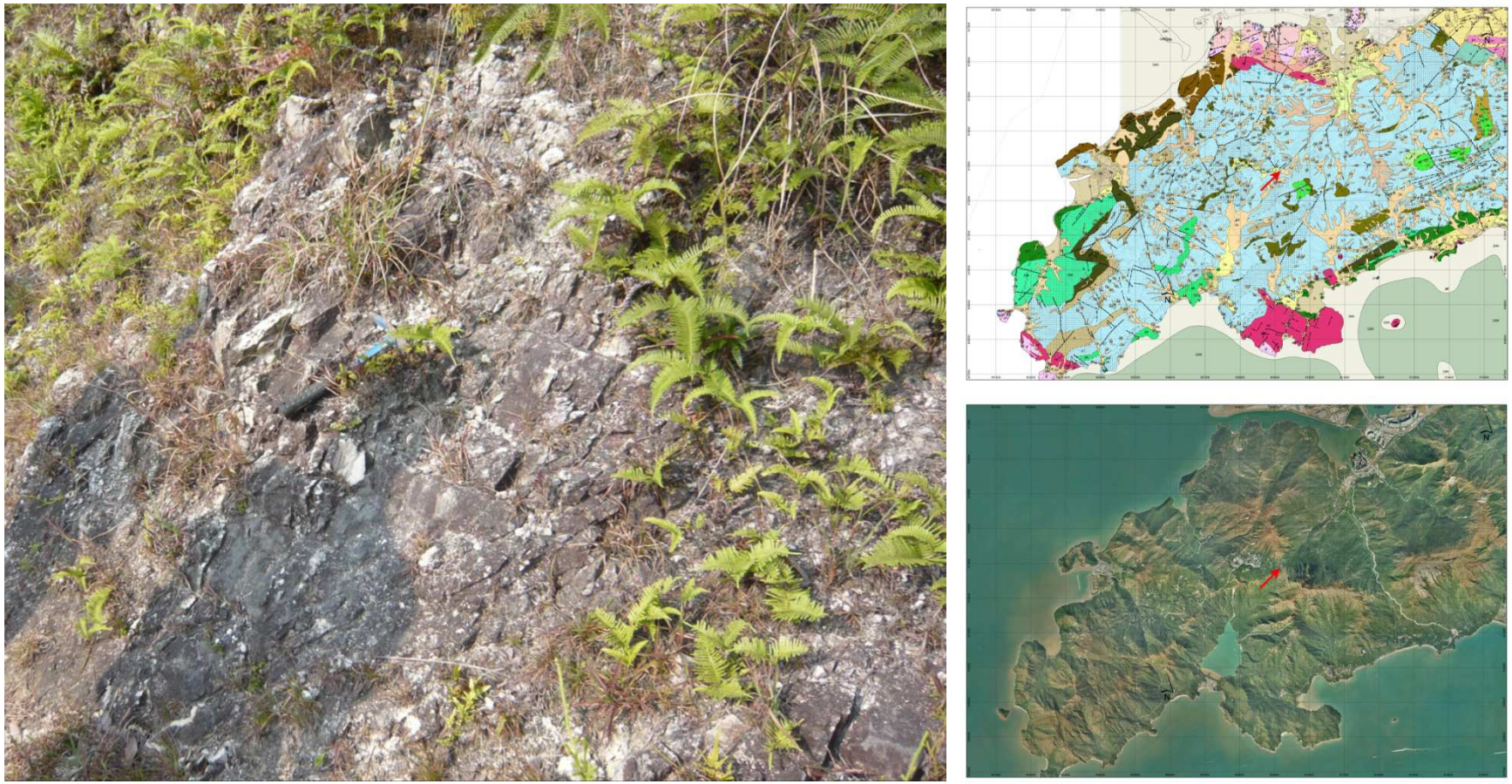

Figure 2.35 Closely Spaced Joints were Well Developed Striking NE-SW Direction Observed in Ngong Ping

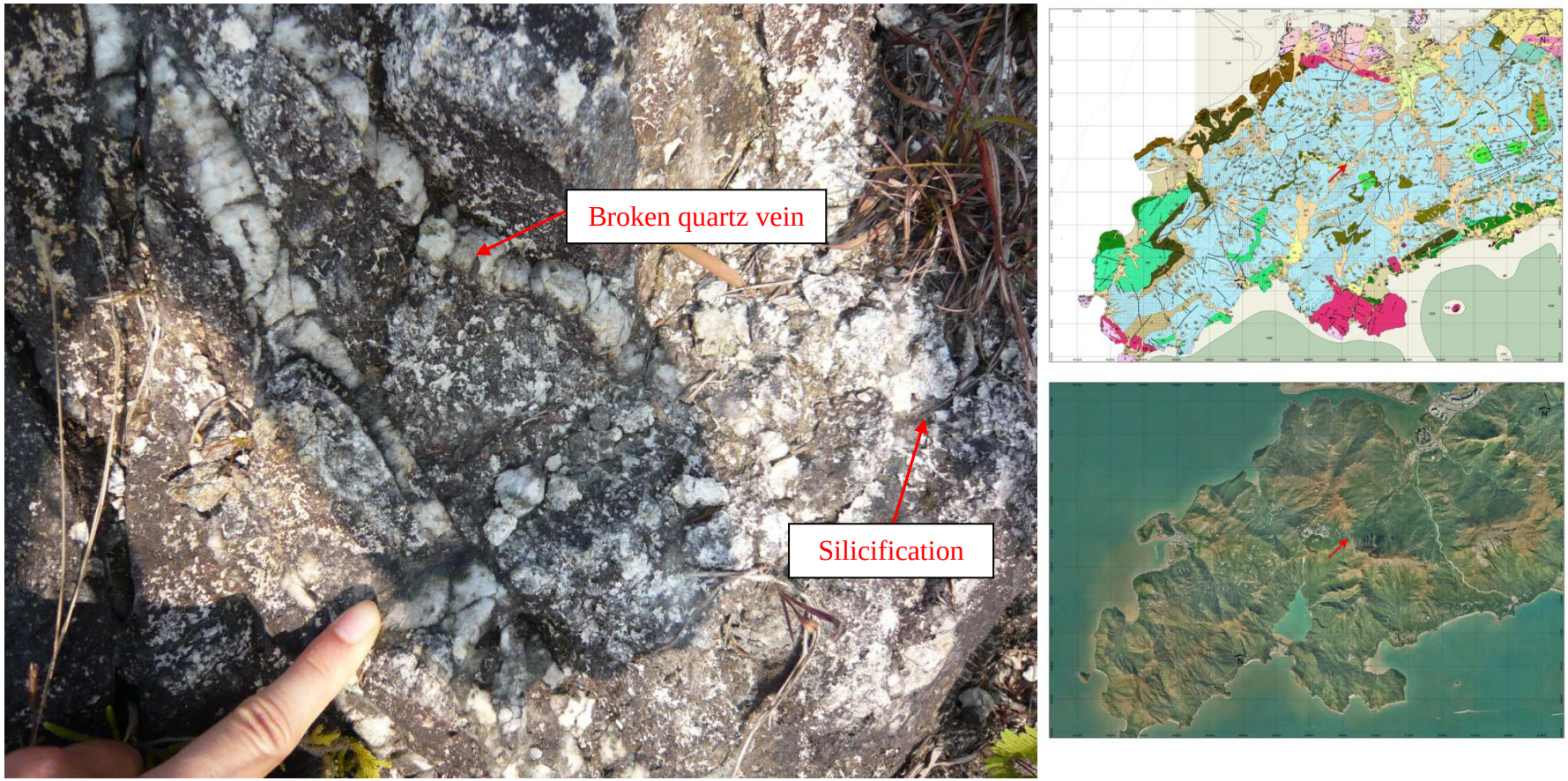

Figure 2.36 Silicification and Broken Quartz Veins are Noted on the Rock Outcrop in Ngong Ping

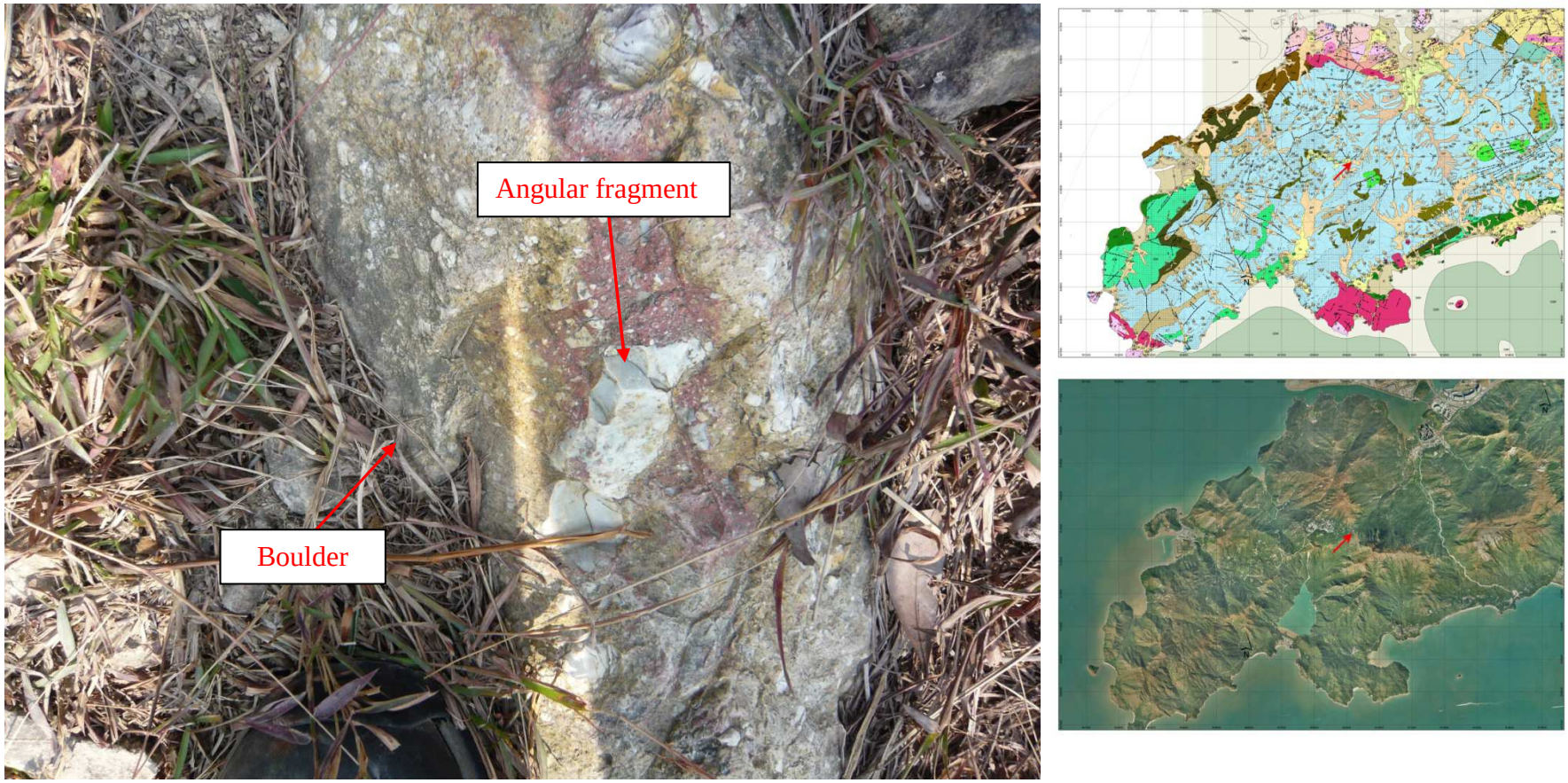

Figure 2.37 Some Angular Fragments Embedded in the Boulders Found in Ngong Ping

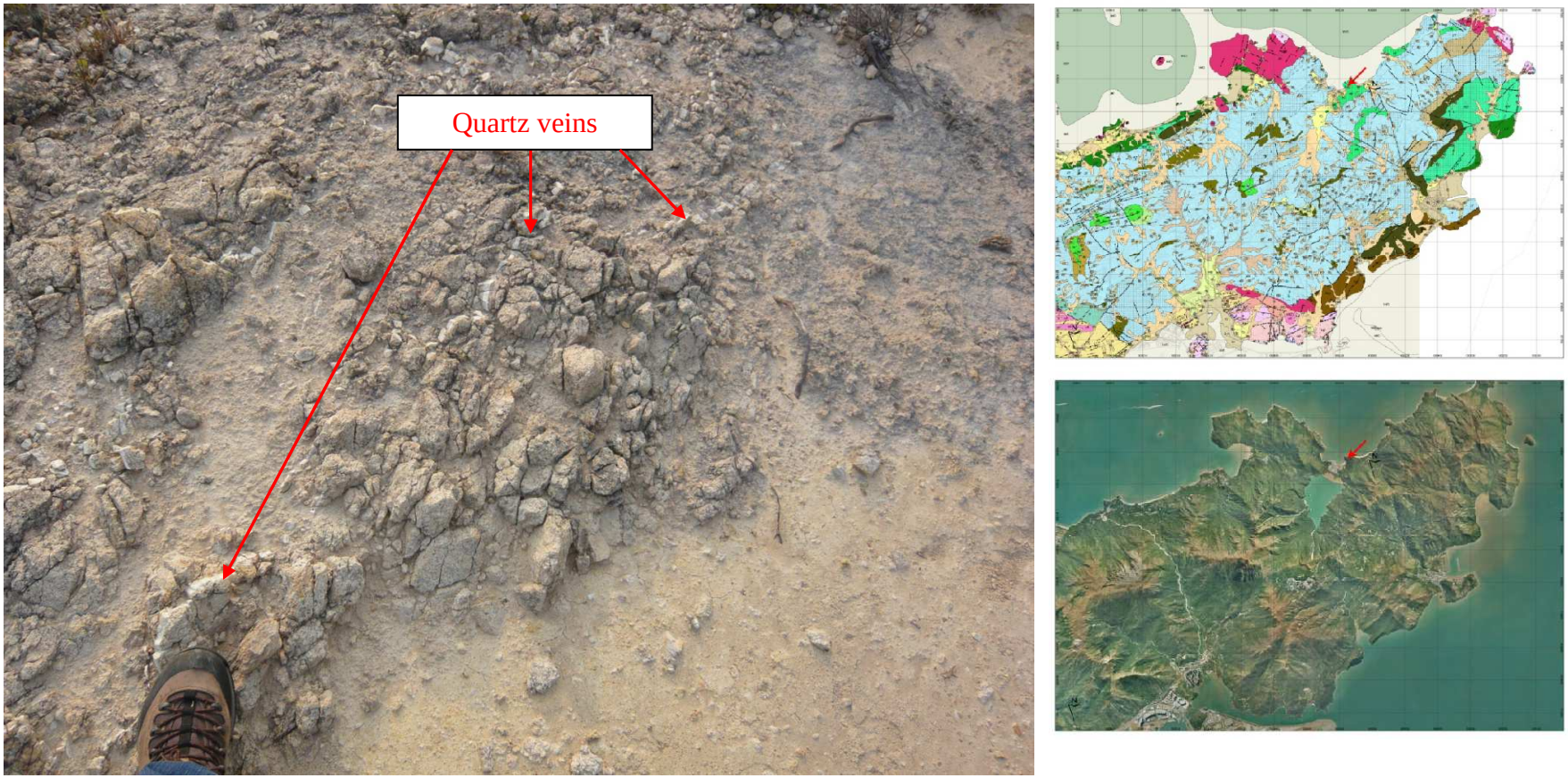

Figure 2.38 Some Discontinuous Minor Quartz Veins Can Be Observed at the Helicopter Park near Tai Long Wan

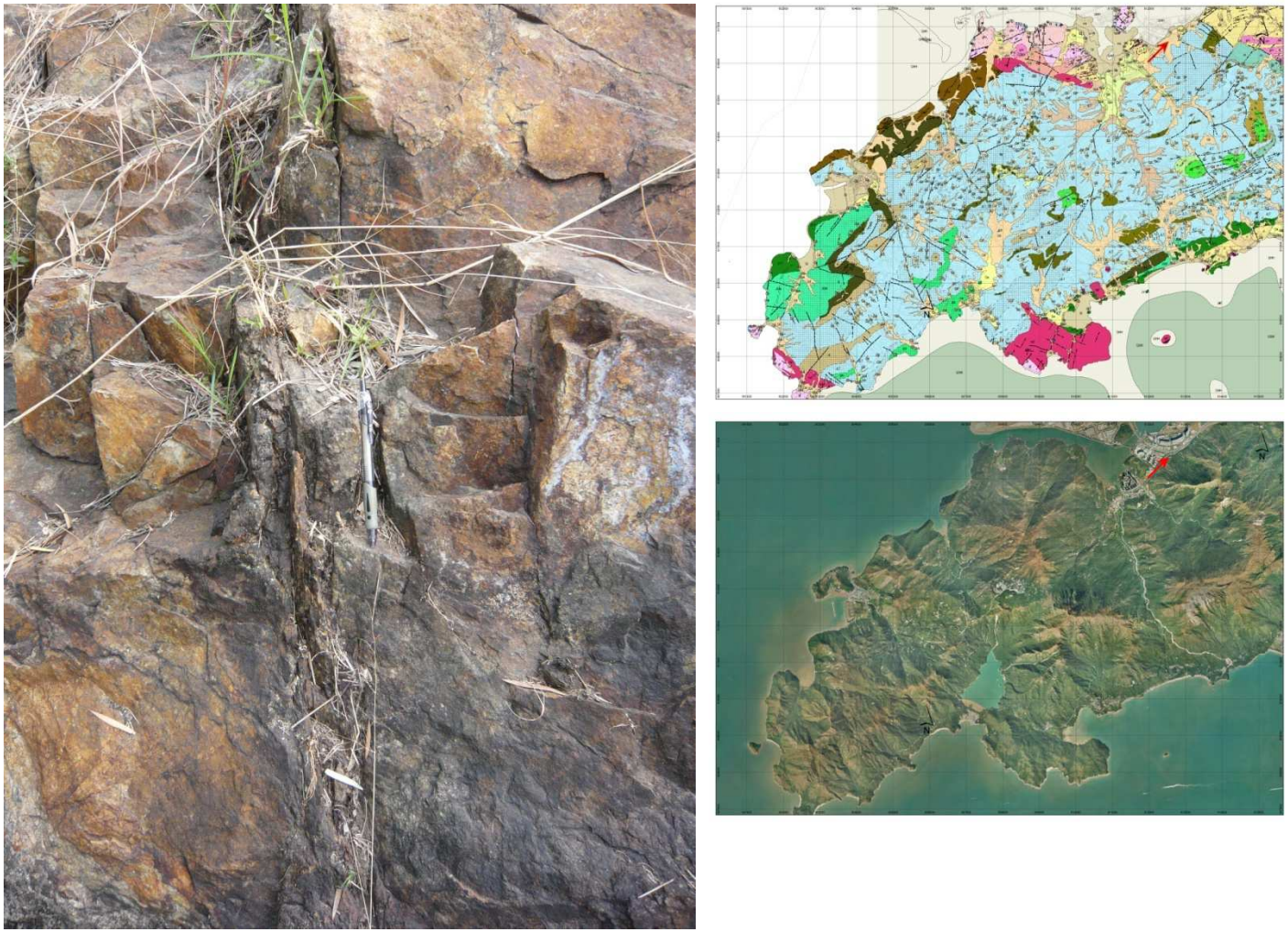

Figure 2.39 Minor NE Trending Shear Zones Were Observed with General Dipping to SE at 75°

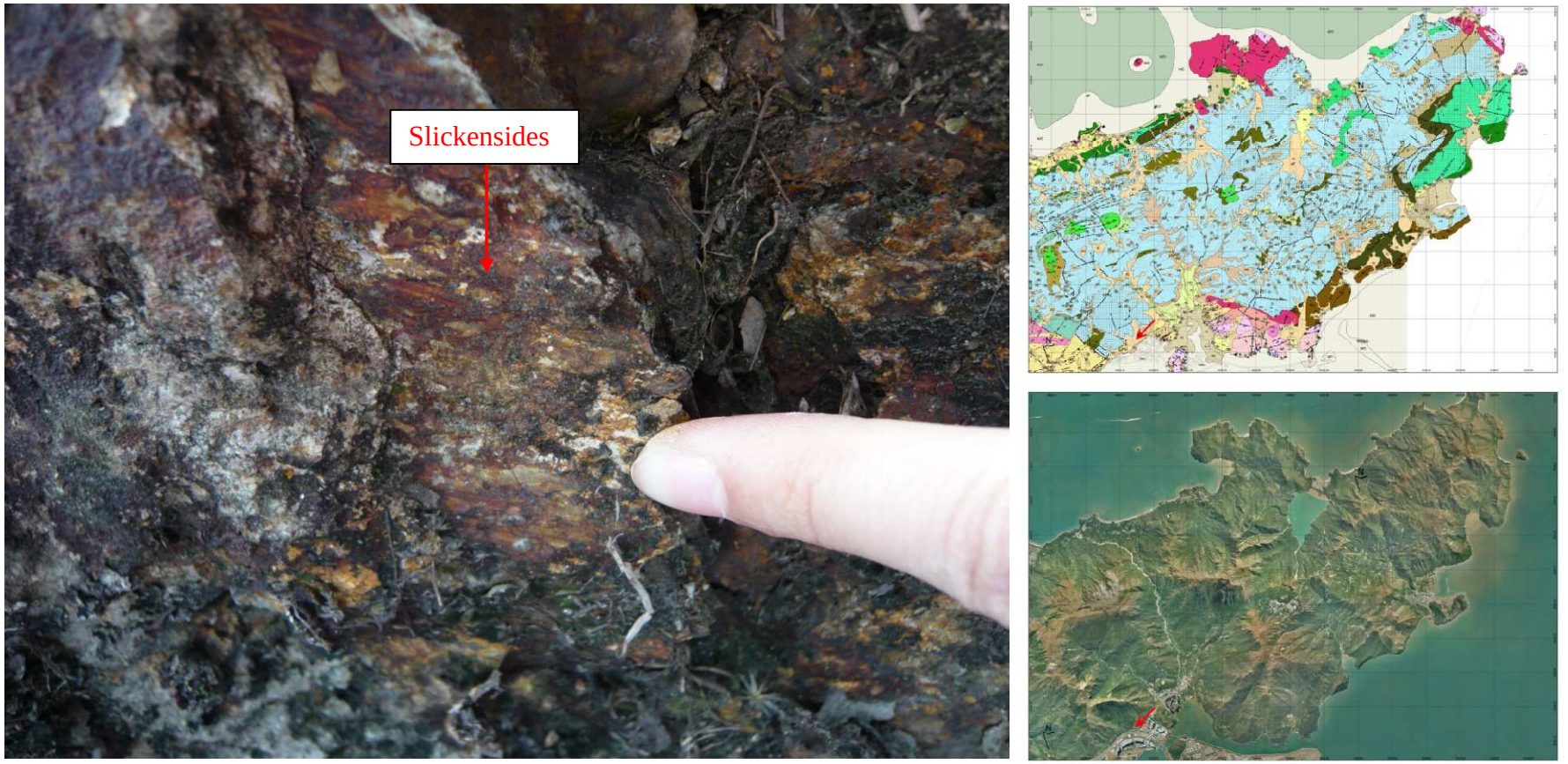

Figure 2.40 Slickensides Exposed on the Surface Which Is Dipping to SE Were Observed

3 Seismic Hazard Assessment Methodology

3.1 General

This section of the report describes the methodology used for the seismic hazard assessment and describes how the input parameters for the seismic hazard assessment were determined. The principles and input requirements of a probabilistic hazard assessment are discussed. The earthquake data for the seismic hazard of Hong Kong Region can be found in the GEO Publication No. 1/2012 (GEO, 2012). GEERRI have previously carried out a seismic hazard assessment using the Mainland China methodology and their model is described in this section. Arup have then taken that model and adapted it to develop a model that is compatible with methods used conventionally by other international practitioners.

3.2 Assessment Methodology

3.2.1 Probabilistic Seismic Hazard Assessment (PSHA)

The PSHA method incorporates the following stages (see Figure 3.1):

(a) define the potential seismic sources;

(b) define for each source, a magnitude recurrence relationship and estimate of the maximum possible earthquake magnitude;

(c) use attenuation relationships are used to calculate the likelihood of a certain ground motion level being exceeded from an earthquake in a certain magnitude range occurring at a certain distance from the site;

(d) combine the likelihood of a certain ground motion level being exceeded is combined with the frequency of earthquakes in that magnitude range at that distance in each source to determine the annual frequency of this particular ground motion level arising from that magnitude range and distance; and

(e) determine the overall frequency of a particular ground motion level being exceeded, by summing up the annual frequencies from all distance ranges and for all magnitude ranges.

The three key elements of the PSHA method are:

Seismic source zones - A seismic source is defined as an area (or volume) of the Earth's crust that has a relatively uniform likelihood of earthquake occurrence in the future. In regions of the earth where active faults exist, the faults are usually treated as seismic source zones and modelled as plane sources with generally large earthquakes. In less active stable continental intraplate regions, such as Hong Kong, seismic activity is diffuse and seismic

sources are generally modelled as area zones. Within each area an understanding of the frequency of recurrence of earthquakes of various magnitudes is required and is determined from observed seismicity. The depth distribution of the earthquakes is also required and is based on observed seismicity.

Source zone activity - The frequency of earthquake occurrence is required and is usually described in terms of magnitude recurrence relationships that define the annual number of earthquakes to occur within each source zone for each magnitude range. It is often defined in terms of the 'Gutenberg-Richter' relationship which is defined later in Section 3.2.3.

Ground motion attenuation - The ground motion attenuation relationship describes the degradation of seismic wave energy along the path from the earthquake source to the site being evaluated. The attenuation of ground motion for rock site is dependent on the tectonic environment. It has been found that motions for rock sites generally attenuate more rapidly in plate boundary regions such as Western USA and the Philippines than in stable continental intraplate regions such as Eastern North America or Southeast China. Attenuation relationships are expressed as a function of earthquake magnitude and distance from the earthquake source. Such relationships have been developed for various ground motion parameters including intensity, peak ground acceleration and response spectral values at various frequencies.

The ground motions measured at equal distances from the earthquake source will vary from location to location. It has been found that this variation in ground motions can be represented by a log normal distribution (Cornell, 1968). Most published attenuation relationships now contain a measure of the standard deviation of the log normal distribution and this value is incorporated explicitly in the hazard assessment.

In this study, PSHA was carried out using an Arup in-house program *Oasys* SISMIC. GEERRI also carried out PSHA with the program ESE. Both programs have the same methodology and an independent check by using the same input seismic parameters by GEERRI into *Oasys* SISMIC has been carried out in this study. The output results between these two programs are comparable. Details of this comparison are presented in Section 4.

3.2.2 Maximum Magnitude

There are many approaches adopted to define the upper bound earthquake magnitude to be used in a hazard assessment. In this study, the upper bound earthquake is considered to be the maximum earthquake that is capable of occurring under the known tectonic framework. Terms such as maximum credible earthquake or maximum probable earthquake are not used. This is consistent with the recommendations of the Committee on Seismic Risk (1984).

The estimation of maximum magnitude that a stable continental intraplate region seismic source is capable of generating is difficult because of the short period of observation relative to the recurrence interval for the largest earthquakes. A study for the Electrical Power Research Institute (EPRI) in the United States has developed approaches for estimating maximum earthquakes within stable continental intraplate seismic source zones (Coppersmith et al, 1987). The EPRI study developed a database of all earthquakes magnitude greater than

M_S = 5 that have been observed in stable continental intraplate regions worldwide (Johnston, 1995a & 1995b). It has been observed that large magnitude earthquakes with magnitude *M* greater than 7.5 in stable continental regions are very rare worldwide. Johnston et al (1994) divided stable continental intraplate regions into two main types, namely cratonic regions (i.e. the oldest and most stable crust) and extended continental crust (i.e. geologically younger stable crust that has been subjected to rifting in the geological past). No earthquake magnitude greater than 6.5 has been reported for a cratonic region. Earthquakes with magnitudes greater than 7.5, though these are very rare, have been reported for regions of extended continental crust.

Lee et al (1998) have estimated maximum magnitude values for their outer and inner zones according to the characteristics of the seismic activity and regional geological structures. Lee et al (1998) stated that their outer zone was characterised by relatively stronger seismic activity and historically several earthquakes of magnitude greater than 7 occurred. They stated that their inner zone was characterised by relatively lower seismic activity and there was no record of events with magnitude greater than 7. Lee et al (1998) used the source zones identified in the Southeast Coastal Belt of China during the development of the Intensity Zoning Map of China (1990). The source zones were slightly modified and maximum magnitudes defined on the basis of historical seismicity and geological structures. In this way, maximum magnitude values were defined for 25 source zones around Hong Kong. In their model, the Dangan Islands source zone south of Hong Kong has a maximum magnitude of M_S = 7. Other zones around Hong Kong have maximum magnitudes of M_S = 5.5 to 6.5.

The earthquake catalogue compiled for this study for Southeast China includes three earthquakes with assigned magnitudes greater than M_S = 7. Earthquakes with assigned magnitudes of M_S = 7.5 occurred in 1604 and 1605 and an earthquake with magnitude M_S = 7.3 in 1918. An earthquake with a magnitude M_S = 7 is likely to be associated with a surface rupture length in the order of 45 km, and a magnitude M_S = 7.5 with a surface rupture in the order of 125 km (Wells & Coppersmith, 1994). There are a large number of certain and inferred faults in the Southeast China Region. The inferred lengths of these faults are typically in the order of 40 to 50 km although greater lengths on less well defined faults are also evident (GEO, 2012).

3.2.3 Source Zone Parameters

The rate of occurrence of earthquakes within each source zone is often described in terms of a magnitude-recurrence, 'Gutenberg-Richter' relationship.

$$\log_{10} N = a - b\,M \quad \text{..... (3.1)}$$

where *N* is the annual frequency of earthquakes greater than *M*, *M* is moment magnitude, and *a* and *b* are constants.

The Gutenberg-Richter relationship may also be expressed as:

$$\lambda_m = 10^{(a-bM)} = \exp^{(\alpha - \beta M)} \quad \text{..... (3.2)}$$

where λ_m is the annual frequency of earthquakes greater than M, $\alpha = 2.303a$ and $\beta = 2.303b$.

The standard Gutenberg-Richter relationship covers an infinite range of magnitudes. For engineering purposes, a lower threshold magnitude m_o is defined. If earthquakes smaller than m_o are eliminated, the mean annual rate of being exceeded is determined using the revised relationship for the activity of events where $M > m_o$:

$$\lambda_m = \nu \exp [- \beta (M - m_o)] \quad \text{..... (3.3)}$$

where $\nu = \exp (\alpha - \beta m_o)$.

Each source zone will be limited by the maximum magnitude, m_{max}. By taking this into account the mean annual rate of being exceeded can then be expressed using the following relationship for $m_o \leq M \leq m_{max}$:

$$\lambda_m = \nu \frac{\exp[- \beta (M - m_o)] - \exp [- \beta (m_{max} - m_o)]}{1 - \exp [- \beta (m_{max} - m_o)]} \quad \text{..... (3.4)}$$

The earthquake catalogue has been plotted in this form for the onshore and near-shore region as shown in Figure 3.2. The best estimate line corresponds to a b value of 0.88. Figure 3.3 shows the equivalent plot for the offshore region and the best estimate line corresponds to a b value of 0.86.

3.2.4 Uniform Hazard Response Spectra

A response spectrum is defined as a graphical relationship of the maximum response of a range of single degree of freedom elastic oscillators, with or without damping, to dynamic motion (Housner, 1959). These spectra are very useful for engineering purpose as they give a direct indication of the peak distortion of a structure provided that its fundamental period (corresponding to the first or fundamental mode) is known or can be estimated. For high rise structures over about 10 storeys, the response of their higher modes also need to be considered.

In the past, for seismic hazard assessment studies, it was common practice to calculate peak ground acceleration with a desired annual frequency of being exceeded and then using this acceleration to scale a standard response spectral shape to obtain spectral values at higher fundamental periods. Now, best practice is to calculate response spectral values at a range of fundamental periods so that at each period the spectral value has the same annual frequency of being exceeded. Response spectra produced in this way are referred to as Uniform Hazard Response Spectra and have been generated as part of this study.

3.3 GEERRI Model

The GEERRI seismic source zone model is presented in Figure 3.4. This model has been developed by the expert panel of the Chinese National Seismic Code Committee in China. The zonation of seismic source zone is based on the location and magnitude of the earthquake records, and the characteristic and pattern of recent large earthquake activity and

medium to small earthquake activity. It is assumed that locations having a history of large earthquakes are likely to have similar earthquakes in future.

Details of the principles used by GEERRI in their source zone demarcation are described in Appendix A. The following points have been considered:

(a) If an area has significantly high neotectonic activity especially in Late Quaternary, the potential seismic source zone of the area will be assigned with slightly higher earthquake magnitude.

(b) If there is an obvious offset of the fault in early to middle Pleistocene strata in the area, the potential seismic source zone of the area would be assigned with medium earthquake magnitude.

(c) If only dating of fault materials shows that the fault movement occurred in early Pleistocene or before without evidence of offset of the corresponding strata and earthquake activity, then the area is not considered as no potential seismic source zone. If the dating of fault materials shows that fault movement occurred in middle Pleistocene, as well as the scale is large, the potential seismic source zone of the area would be assigned with a slightly lower earthquake magnitude.

(d) If distributions of small and medium earthquake activities have developed as a belt, the activity in the deep structure could be considered different. Although medium to strong earthquakes have not occurred in that area, the seismic source zone of the area will be considered to be with a slightly lower estimate of the earthquake magnitude.

(e) The boundary and orientation of the seismic source zone are mainly based on the fault trending direction, the fault scale and the distribution of the medium and small earthquakes. Also, the fault segmentation and the faults intersection would be considered.

The morphotectonic map provided by Prof. Chan of the University of Hong Kong (Pubellier & Chan, 2006 as discussed previously in Section 2) is superimposed on the GEERRI source zones as shown in Figure 3.5. It indicates that the extent and orientation of the GEERRI source zones generally follow the major fault zones. Figures 3.6 and 3.7 show the GEERRI source zones with the full and complete earthquake catalogues respectively. It can be seen that there is earthquake activity that is not within the GEERRI source zones. This is especially noticeable for the offshore area well southeast of Hong Kong but it is accepted that this will have limited impact on the hazard assessment for Hong Kong. It also raises question as to why GEERRI have derived such small zones often with areas of no activity within them. Again this will have limited effect on the hazard assessment however

provided that there is still about the same amount of overall seismicity within each part of the overall model.

GEERRI has defined the maximum magnitude for each seismic source zone based on the relationship between regional earthquakes and the geological structure as well as the criteria for earthquake with different magnitudes to occur, together with the principle and method to determine seismic source zones. According to GEERRI, the maximum magnitudes of the seismic source zones were determined as follows:

(a) the maximum earthquake magnitude of seismic source zone would be generally controlled by the capable potential maximum earthquake magnitude generated by any major fault system in regional scale;

(b) the maximum earthquake magnitude of the seismic source zone should be greater than or equal to the maximum magnitude of the recorded earthquake within the zone;

(c) if there is no evidence of tectonic activity in late Quaternary in the neotectonic structure, the maximum magnitude should be assigned as same as the maximum magnitude in seismic source zone with the similar tectonic setting;

(d) if fault offsets in late Pleistocene or Holocene strata are observed at the ground surface, the maximum magnitude of the seismic source zones should be assigned as 6.5 or above. In this case, the fault movement amplitude and fault activity should be considered;

(e) if there are fault offsets in early to middle Pleistocene, the maximum magnitude of 6 or above should be assigned for that potential source zone; and

(f) if the fault zone is large with dating of fault gouge showing there is fault movement in Pleistocene, as well as lineament expressed geomorphologically, the potential seismic source zone would be assigned with smaller earthquake magnitude for maximum earthquake magnitude like magnitude 5.5.

Figure 3.8 shows the GEERRI zonation map for the maximum earthquake magnitudes assigned for each 156 source zones. It can be seen that the maximum value of 8 is assigned to the Shantou area where the magnitude 7.3 event occurred in 1918. Nearer to Hong Kong it is seen that the Dangan Islands source zone is assigned a maximum magnitude of 7.5 and in other adjacent areas magnitude 7. The Pearl River delta area is assigned magnitude 6.5. Interestingly many other areas are assigned only magnitude 5.5. However, all areas that are known to contain faults are capable of producing an earthquake of 6.0. Also, it is important to note that the uncoloured areas are assumed to have no seismicity that affects the seismic hazard.

The overall occurrence rate of earthquakes is described by GEERRI based on a 'Gutenberg-Richter' relationship. Their recurrence curve for Southeast China earthquake data is shown in Figure 3.9. Their activity rate *a* and *b* values correspond to their earthquake catalogue between 1900 and 2005.

GEERRI assigned different contribution factors to each source zone based on their judgement on the observed seismicity and their available geological information. The contribution frequencies of all the 156 source zones at each range of earthquake magnitude sum to 1. Figure 3.10 shows the corresponding annual frequency recurrence plots for all of the GEERRI source zones. The annual activity rate for each of the GEERRI source zones is also presented in a graphical format in Figure 3.11 to Figure 3.16 for various earthquake magnitudes. The blank colour represents where no activity has been assigned in that source zone. The activity rate of each zone is also divided by the zone area to show a relative activity density of each source zone area in Figure 3.17 to Figure 3.22.

Of particular interest to this study is the high activity rate assigned to the larger earthquakes in the Dangan Islands. This is highlighted in Figure 3.10 and is also seen in Figures 3.13, 3.14, 3.18, 3.19 and 3.20. It is considered that the assigned activity rates of Dangan Islands for magnitude 6 and 6.5 are significantly higher than the observed seismicity. GEERRI estimates that the return periods for magnitude 6 and 6.5 events are 170 years and 200 years, respectively.

3.4 Arup Model

Although GEERRI has developed a comprehensive source zone model, it is considered that there is no strong evidence to differentiate some of the GEERRI adjacent zones with similar tectonic setting and observed seismicity. Also, ideally the size of source zones should be sufficiently large such that a reasonable amount of earthquake data is available within each zone to derive the earthquake recurrence relationship.

In order to take as much from the GEERRI model as practically possible, Arup has prepared a revised seismic source zone model for this study. It incorporates the seismicity in the region, the geological and tectonic information and many of the GEERRI source zone boundaries. The Arup model with the zone numbers identified is shown in Figure 3.23. In the Arup source model, the trend and the boundaries of the 20 source zones generally follow the GEERRI source models to take into account of their detailed study of the geological and tectonic information (see Figure 3.24). The Morphotectonic Map (Pubellier & Chan, 2006) which contained the information of recent fault and Cenozoic fault location was also considered to correlate with the orientation of the main geologic and tectonic structures (see Figure 3.25). The distribution of historical and recent seismicity in the region was also reviewed to develop the Arup source model (see Figures 3.26 & 3.27). The Arup 20 source zones are divided into offshore and onshore regions below:

- Zone 1 to Zone 4 - Offshore south to southwest of Hong Kong.
- Zone 5 to Zone 20 - Onshore surrounding Hong Kong and offshore coast.

The observed seismicity and tectonic setting of these 20 source zones are generally described as follows:

(a) Zone 1 is an offshore source zone with a region of relatively low seismic activity and is identified mainly on this basis. This zone is not included in the GEERRI offshore model. However, it is considered that this offshore boundary should be extended to incorporate the main geologic and tectonic structures shown in Figure 3.25 and the full and complete earthquake catalogues are shown in Figures 3.26 and 3.27 respectively. It should be noted that due to the different completeness levels the relative observed seismicity in the offshore areas as compared to the onshore areas will be greater than shown.

(b) Zone 2 is a region of relatively low to moderate seismic activity and is identified by the main geologic and tectonic structures. The northwest and southeast boundaries have been oriented parallel to one of the dominant geologic structure orientations. Also, this zone combines the major GEERRI offshore source zones at the south.

(c) Zone 3 is a region of very low seismic activity. Only a few earthquake events with magnitude less than 4 have been reported in the zone. This zone is also not considered in the GEERRI model.

(d) Zone 4 is a region of relatively high seismic activity near Taiwan. The increased seismicity may be related to the proximity to the tectonic plate boundary to the east and the intersections of northeast and northwest oriented faults in this region.

(e) Zone 5 is a region of low to moderate seismic activity. This source zone is within the Hainan region.

(f) Zone 6 is a region of low to moderate seismic activity. The northwest and southeast boundaries have been oriented parallel to one of the dominant NE trending geologic structure orientations.

(g) Zone 7 is a region of moderate seismic activity. The Dangan Islands are also inside this zone in which an earthquake magnitude 5.7 occurred in 1874. The complex intersection between northeast and northwest oriented faults within the zone may be capable of producing a larger earthquake magnitude.

(h) Zone 8 is a region of low to moderate seismic activity similar to Zone 6. The northwest and southeast boundaries have been oriented parallel to one of the dominant NE trending geologic structure orientations. It should be noted that the 1911 magnitude 6 earthquake is the closest known event of this magnitude to Hong Kong.

(i) Zone 9 is a region of relatively high seismic activity and is identified mainly on this basis. The increased seismicity may be related to the proximity to the tectonic plate boundary to the east and the intersections of northeast and northwest oriented faults identified in this region.

(j) Zone 10 is a region of high seismic activity at Shantou. The 1918 magnitude 7.3 earthquake that has caused the largest amount of known damage to Hong Kong occurred in this zone. The increased seismicity may be related to the proximity to the tectonic plate boundary to the east and the intersections of northeast and northwest oriented faults identified in this region.

(k) Zone 11 is a region of moderate to high seismic activity similar to Zone 9. The increased seismicity may be related to the nearby tectonic plate boundary to the east and the intersections of northeast and northwest oriented faults identified in this region.

(l) Zone 12 is a region of low to moderate seismic activity located north of Hainan with several historical earthquakes associated with the major faults.

(m) Zone 13 and Zone 15 are regions with low to moderate seismic activity and similar tectonic setting along the coastal line.

(n) Zone 14 is a region of low to moderate seismic activity at the Pearl Delta area. The northwest and southeast boundaries have been oriented parallel to one of the dominant NW trending geologic structure orientations.

(o) Zone 16 is a region with very high seismic activity in Heyuan. Since the Xinfengjiang Reservoir built in 1962, there were induced earthquakes. Several earthquakes greater than 5 have occurred in the last 20 years in this region. Also, tectonic findings suggest that the Heyuan fault is relatively active.

(p) Zone 17 and Zone 18 are regions of moderate seismic activity with observed historical earthquakes between

magnitude 5 and 6. It is considered that the NW trending geologic structure orientations control the seismic activity.

(q) Zone 19 and Zone 20 are regions of low to moderate seismic activity with only a few observed small earthquakes.

Maximum magnitudes have been assigned to each of the source zones as shown in Figure 3.28 and summarised in Table 3.1. For the Shantou zone the maximum value of 8 recommended by GEERRI has been used. For the adjacent offshore and near onshore areas down to the Dangan Islands and for Hainan a maximum magnitude of 7.5 has been used. A value of 7 has been used for areas near to Hainan and offshore and for Zone 17 Northwest of Shantou. For other onshore zones a value of 6.5 has been used.

Table 3.1 Maximum Magnitudes

Arup Model Source Zones	Maximum Magnitude
10	8.0
4, 5, 7, 8, 9, 11	7.5
1, 2, 6, 12, 17	7.0
13, 14, 15, 16, 18, 19, 20	6.5

The earthquake recurrence curves for each Arup source zones have been derived from the observed seismicity as shown in Figures 3.29 to 3.48 based on the 'Gutenberg-Richter' relationship. The observed seismicity indicates that the *b* value is related to the tectonic activity. Zones with higher activities of larger earthquake magnitude imply lower *b* values. Table 3.2 summarises the design *b* value for different regions as a function of maximum earthquake magnitudes.

Table 3.2 Design *b*-values

b-value	Maximum Magnitude
0.85	6.5
0.75	7
0.65	7.5
0.55	8

The best estimate recurrence curves for each Arup source zones are presented in Figures 3.29 to 3.48. The corresponding activity rates used in the seismic hazard analysis are given in Table 3.3. The annual earthquake activity rate plots for the Arup model are

provided in Figures 3.49 to 3.55 for different earthquake magnitudes. When differing maximum magnitudes M_{max} are used, the b value needs to be reduced for those with higher M_{max} to preserve the total overall activity for the whole region as shown in Figure 3.56. In addition, the curves tend to fit the reliable complete data of earthquake magnitudes 5.0 to 7.0, especially in those offshore areas without complete data record of small earthquake events.

Table 3.3 Best Estimate Activity Rates for the Arup Model

Source	Location	Area (km^2)	Annual Activity $M_W > 4$	
			Number	Density (per 10^6 km^2)
Zone 1	Offshore-south	157,683	0.30	1.9
Zone 2	Offshore-east of Hainan	58,377	0.15	2.6
Zone 3	Offshore-south of Dangan	67,481	0.01	-
Zone 4	Offshore-southwest of Taiwan	35,638	1.10	31
Zone 5	Onshore-northeast Hainan	17,446	0.07	4.0
Zone 6	Offshore-northeast of Hainan	25,519	0.10	3.9
Zone 7	Offshore-Dangan Island	10,496	0.10	9.5
Zone 8	Offshore-northeast of Dangan	30,133	0.12	4.0
Zone 9	Offshore-west of Taiwan	18,052	0.30	17
Zone 10	Onshore-Shantou	10,216	0.43	42
Zone 11	Onshore-northeast of Shantou	23,586	0.30	13
Zone 12	Onshore-north of Hainan	54,258	0.35	6.5
Zone 13	Onshore-west of Hong Kong	64,987	0.60	9.2
Zone 14	Onshore-Pearl River delta	21,830	0.12	5.5
Zone 15	Onshore-northeast of Hong Kong	46,199	0.32	6.9
Zone 16	Onshore-Heyuan	2,839	0.48	170
Zone 17	Onshore-northwest of Shantou	22,553	0.20	8.9
Zone 18	Onshore-north of Shantou	34,801	0.25	7.2
Zone 19	Onshore-northwest of Pearl River	38,048	0.15	3.9
Zone 20	Onshore-north	10,999	0.13	1.2

To compare the design recurrence curve between Arup and GEERRI in particular for the major zones that contribute most of the hazard to Hong Kong, the activity rate of each magnitude for the Pearl Delta region (Arup Zone 14 and GEERRI Zones 83 & 84) and the Dangan Islands region (Arup Zone 7 and GEERRI Zone 29) has been normalised by their zone areas. Figures 3.57 and 3.58 show the comparison of the normalised recurrence curves for the Pearl River Delta zones and the annual recurrence curves for the Dangan Island zone, respectively. The comparisons show the GEERRI model generally estimates higher activity rates at higher magnitudes and correspondingly lower *b*-values for larger magnitudes than the Arup model. It is considered that the GEERRI *b*-values for these two regions are relatively too low and the higher magnitude recurrence values too high.

3.5 Minimum Magnitude

The calculation of seismic hazard by the probabilistic method requires a lower-bound earthquake magnitude value to be specified. Based on a broad range of engineering research, experience, and application of probabilistic seismic hazard results, as well as observation of the lack of damage associated with smaller magnitude events, a moment magnitude value $M_W = 5$ has typically been considered a reasonable lower bound value for seismic hazard probabilistic computations. Studies indicate that earthquakes smaller than $M_W = 5$ have negligible potential for causing damage to engineered structures (Jack R. Benjamin & Associates, 1989).

A minimum magnitude value, $m_b = 5$, was used in the development of the United States Seismic-Hazard Maps (Frankel et al, 1996) and a minimum magnitude value, $M_S = 4.75$, was used in the development of the Seismic Hazard Maps of Canada (Adams et al, 1999).

Lee et al (1998) report that a minimum magnitude, $M_S = 4$ was used in their study. A minimum magnitude of $M_S = 4$ was also used by Scott et al (1994). This value was selected in both studies because the likelihood of an earthquake with a magnitude $M_S = 4$ causing damage to engineered structures was considered to be small. The moment magnitude scale has been used in the current study and therefore an equivalent minimum moment magnitude has been determined using the correlation between surface wave magnitude, M_S and moment magnitude, M_W proposed by Johnston (1996b). The equivalent moment magnitude is $M_W = 4.9$.

Based upon the information described above a minimum magnitude value of $M_W = 5$ has been selected for this study.

3.6 Attenuation Relationships

3.6.1 General

Attenuation relationships describe the change in earthquake ground-motion with distance. In interplate regions, such as California, Japan, New Zealand or Southern Europe, where a large number of earthquake strong-motion records have been recorded, the attenuation relationships are derived based on an analysis of the records available for the specific region. However, in stable continental intraplate regions, such as Southeast China, where very few strong-motion records have been recorded it is not possible to derive similar

attenuation relationships. In stable continental intraplate regions, alternative methods are required to determine suitable attenuation relationships for use in the hazard assessment. The alternative methods used can be classified into three categories:

(a) Attenuation relationships based on data from other regions with or without adjustment;

(b) Attenuation relationships derived by correlation between Intensity and a ground-motion parameter such as acceleration; and

(c) Theoretical relationships.

There are currently no ground-motion attenuation relationships for the Southeast China Region that have been consistently derived for peak ground acceleration and response spectral ordinates from empirical data for 5% structural damping. A number of researchers are investigating ground motion attenuation in Southeast China and these relationships are discussed below.

3.6.2 Attenuation of Macroseimic Intensity

Relationships derived for the attenuation of macroseismic intensity have been used to provide an indication of the differences in rates of attenuation of ground motion amplitude between Western and Eastern North America and Southeast China. Published relationships for magnitude versus isoseismal area for Western and Eastern North America have been compared with the isoseismal areas determined for individual earthquakes reported in GCO Publication No. 1/91 (see Figure 3.59) (GCO, 1991). These plots indicate that, in general, the isoseismal areas determined for Southeast China earthquakes are less than those for Eastern North America and larger than those for Western North America. This result would suggest that the attenuation of ground motion amplitude in Southeast China would generally also be expected to be greater than that in Eastern North America but would generally be expected to be less than that in Western North America. Based upon this observation, it is recommended that attenuation relationships for both Eastern and Western North America be adopted in the probabilistic seismic hazard assessment and the resulting mean hazard level used.

3.6.3 Eastern North America Attenuation Relationships

Atkinson & Boore (1997) investigated ground motion relationships for stable continental intraplate areas based on a stochastic point source model and these were developed for Eastern North America (ENA). Atkinson & Boore (1997) note that the quadratic equations developed did not adequately match the results of more accurate stochastic simulations for small to moderate events ($M_W < 5$) resulting in over-prediction at distances greater than 30 km. They considered that these small to moderate events at larger distances were unlikely to contribute significantly to the hazard. Furthermore, they derived the simple quadratic form for the convenient use in hazard analysis and they considered they were sufficiently accurate in the magnitude distance ranges that were being considered to be most significant. The attenuation relationships developed by Atkinson & Boore were based

on a stochastic model calibrated with data from earthquake records from stations at distances up to approximately 1000 km from the earthquake source.

In 2006, Atkinson & Boore re-developed their attenuation relationships for stable continental intraplate areas by using a stochastic finite-fault model. The model also incorporates new information obtained from ENA seismographic data gathered over the past 10 years, including three-component broadband data that provided new information on ENA source and path effects. These new prediction equations were similar to those that were previously developed based on a stochastic point-source model (Atkinson & Boore, 1997). The main difference was that high-frequency amplitude events ($f \geq 5$ Hz) were less than previously predicted (by about a factor of 1.6 within 100 km), because of a slightly lower average stress parameter (140 bars versus 180 bars) and a steeper near-source attenuation. At frequencies less than 5 Hz, the predicted ground motions from the new equations were generally within 25% of those predicted by Atkinson & Boore (1997). The Atkinson & Boore (2006) attenuation relationships are used in this study.

3.6.4 NGA Relationships for Western North America

Next Generation Attenuation (NGA) relationships have recently been developed from Western North America (WNA) and worldwide data for rock sites in shallow crust for earthquake magnitudes between 5 and 8. They were developed as part of the PEER Next Generation Attenuation of Ground Motion (NGA) Project. The common database of worldwide strong motion recordings was used to determine relationship formulations with appropriate predictor variables. The predictors were derived using different regression analyses to determine the attenuation relationships with calculated uncertainties. The available NGA attenuation relationships used in this study are listed below:

(a) Abrahamson & Silva (2007),

(b) Boore & Atkinson (2007),

(c) Campbell & Bozorgnia (2007), and

(d) Chiou & Youngs (2007).

These NGA attenuation relationships contain ground motion predictive equations for a particular measure of horizontal-component ground motions as a function of earthquake mechanism, distance from source to site, local average shear-wave velocity, and fault type. The equations are for peak ground acceleration (PGA), peak ground velocity (PGV), and 5%-damped pseudo-absolute-acceleration spectra (PSA) at structural periods between 0.01 and 10 seconds. The equations were derived by empirical regression of the PEER NGA strong motion database and the averages of the above relationships have been adopted in this study to represent the NGA model.

3.6.5 GEERRI Attenuation Relationships

GEERRI adopted an attenuation model by Yu (2005) which compared the attenuation

models derived from the Southeast China macroseismic intensity records to those observed in WNA. The reduced attenuation in Southeast China (as shown in Figure 3.59 for example) was then used to scale response spectral attenuation relationships developed in the WNA (e.g. Boore & Joyner, 1993) to produce response spectral attenuation relationships for Southeast China. The Yu (2005) model contained two sets of equations, one for the short axis and one for the long axis of an earthquake. This was assumed that larger earthquakes occurred over a length of a fault and were not just point sources. The long axis was applicable to the ground motion at a distance from the epicentre. At locations along the fault, the short axis represented ground motion at locations normal to the fault direction. North American relationships generally got around this same issue by defining the distance term as the distance from the fault rupture rather than from the epicentre or hypocentre. The directivity effects for choosing the long and short axis of the attenuation relationships for the source model have been considered in this study. The directivity motions of each of the GEERRI source zones are presented in Figure 3.60.

While the Yu (2005) methodology may be appropriate for short period ground motions it is questionable for long period motion. This is because intensity data, especially for higher levels of damage, is usually obtained from damage observations from low rise buildings up to about 3 storeys, and these buildings are sensitive to short period ground motion. Figures 3.61 to 3.64 show comparisons of the response spectra between the Yu (2005) model and the WNA relationships (Boore & Joyner, 1993) and the NGA relationships (Abrahamson & Silva, 2007; Boore & Atkinson, 2007; Campbell & Bozorgnia, 2007; Chiou & Youngs, 2007) for earthquakes with magnitude 6 and 7 at distances of 20 km and 100 km. While the long period shapes between these two models are similar, the GEERRI model is significantly higher than the WNA relationships for magnitude 7. The Yu (2005) relationships for peak ground acceleration and acceleration response spectral ordinates at 0.2-, 1- and 5-second periods from earthquake magnitudes 6 and 7 are also shown in Figures 3.65 to 3.72. Ground motions for ENA predicted by Atkinson & Boore (2006) and the NGA relationships for WNA are shown on these figures. It can be seen that for peak ground acceleration, the Yu (2005) predictions are similar to Arup-HKU but higher than WNA and ENA until distance greater than 100 km (see Figures 3.65 & 3.66). At 0.2-second period, the comparison between the Yu predictions and the others are similar to PGA as shown in Figures 3.67 and 3.68. However, at 1-second, the Yu (2005) predictions are significantly higher than all the other relationships especially at distances less than about 200 km (see Figures 3.69 & 3.70). The 5-second ground motion prediction show a similar comparison to the 1-second values of the other relationships as shown in Figures 3.71 and 3.72. Therefore, it is recommended not to use Yu (2005) predictions after 0.2-second to avoid an unrealistic conservative high values in long periods.

For the purposes of a probabilistic seismic hazard assessment, it is necessary to estimate the variability associated with the ground motions from these relationships. It is conventional practice for these to be represented by a log-normal distribution of the ground motion. Yu (2005) followed this practice and used standard deviations very similar to those recommended by Boore & Joyner (1993) for WNA.

3.6.6 Ground Motion for Southeastern China Based on the Research of the University of Hong Kong and the University of Melbourne

A considerable amount of research has been undertaken by Prof. Chandler and his team at the Centre for Earthquake Engineering Research at University of Hong Kong to investigate the attenuation of earthquake ground motion in the Southeastern China region. A theoretical, "Component Attenuation Model" for attenuation has been derived, which combines a seismic source component and a travel path component based upon the results of the synthetic earthquake accelerograms generated using program GENQKE developed by Dr Lam at the University of Melbourne. Details of program GENQKE can be found in Lam et al (2000b).

The Component Attenuation Model (CAM) is defined as follows:

CAM = α(source) G (path, crust) β(path, crust) γ(crust)

The output from the model is in terms of maximum spectral acceleration, maximum spectral velocity and maximum spectral displacement. These three values can be combined on a tripartite plot to provide a simplified, and generally conservative, design response spectrum.

Table 3.4 summarises the seismological parameters for Southern China used in the analyses undertaken by the study of the University of Hong Kong.

Recently, in collaboration with the University of Hong Kong and the University of Melbourne, Arup used the program GENQKE to develop a suite of synthetic acceleration time-histories for a range of magnitude and distance combinations. Mean peak horizontal ground acceleration values have been derived from the synthetic time-histories and mean response spectral ordinates have been derived from the response spectra determined from the synthetic time-histories. The relationships for peak ground acceleration and acceleration response spectral ordinates at 0.2-, 1- and 5-second period for earthquake magnitude 6 and 7 are shown in Figures 3.65 to 3.72. As can be seen it is quite similar to Yu (2005) for peak ground acceleration and 0.2-second period motion but then reduces to be consistent with the Western North America at long periods.

To allow for the known variability of the ground motion, a standard deviation of the natural logarithm from the mean value of 0.55 has been assumed, i.e. a similar standard deviation from the mean value to that in the relationships of Atkinson & Boore for stable continental regions. This assumption is considered appropriate, as the underlying stochastic methodology for the determination of the relationships is the same in both cases.

3.6.7 Weighting of Attenuation Relationships

The weighting factors for the different relationships used in this study are summarised in Table 3.5 to consider the variability of the ground motions derived from different sources. The long period attenuation relationships proposed by GEERRI are considered to be too conservative without justifications. It is recommended not to use it for structural periods greater than 0.2-second. Further sensitivity analyses with different weightings for long period motion are discussed in Section 4.3.

Table 3.4 Coefficients for GENQKE Ground Motion Assessment for the South China Region

Seismological Parameters		Input Value
Source Model		Atkinson (1993) CENA model.
Geometrical Spreading		$30 / R$ ($R \leq 45$ km) 0.667 (45 km < $R \leq 75$ km) $5.77 / R^{0.5}$ ($R > 75$ km) where R is hypocentral distance in km. (Lam et al, 2000a)
Anelastic Attenuation		$Q = 256f^{0.7}$ for $R < 200$ km $Q = 348f^{0.54}$ for $200 < R < 500$ km $Q = 384f^{0.51}$ for $R > 500$ km where Q is the wave transmission quality factor and f is frequency. (Tsang, 2006)
Crustal Effect	Mid-crust	$\beta = 3.5$ km/s where β is the average shear wave velocity at mid-crust. (~10 km depth) (Lam et al, 2000a)
Source Model		Atkinson (1993) CENA model.
Crustal Effect	Upper-crust	$\kappa = 0.03$ where κ is the kappa value that represents the upper crust attenuation, which represent the upper crust amplification. (Chandler et al, 2006a & 2006b)

Table 3.5 Weighting Factors of Attenuation Relationships

Attenuation Relationships	Weighting Factor	
	PGA, 0.1 to 0.2 sec	0.2 to 5.0 sec
Arup-HKU (2006)	0.25	0.50
NGA-WNA (2007)	0.25	0.25
Atkinson & Boore (2006)-ENA	0.25	0.25
Yu-GEERRI (2005)	0.25	0

3.7 Focal Depths

The available data on focal depth of earthquakes in the Hong Kong region is limited. The distribution in focal depth of earthquakes is shown in Figure 3.73. The earthquakes typically have focal depths in the range 5 to 25 km. The distribution factors used in this study are summarised in Table 3.6.

Table 3.6 Distribution Factors of Depth Contribution

Focal Depth	Distribution Factor
5	0.25
10	0.4
15	0.2
20	0.1
25	0.05

The NGA ground motion attenuation relationships used in the hazard assessment for this study included earthquake focal depth as a variable and therefore the observed variation in depth was not used for the calculations using their relationships. The relationships of Yu (2005), Atkinson & Boore (2006) and the Arup-HKU GENQKE derived models use hypocentral distance and as such the focal depth is included in the calculation. It is noted that GEERRI only considered a constant focal depth of 10 km in their seismic hazard study.

3.8 Analysis Software

The probabilistic seismic hazard calculations, incorporating the logic tree methodology, have been carried out using the program *Oasys* SISMIC. This program, developed by Arup, is based on the methodology developed by Cornell (1968) and McGuire (1993). The program has been used for projects worldwide, including seismic hazard assessments for nuclear power facilities where review by international expert panels has been carried out.

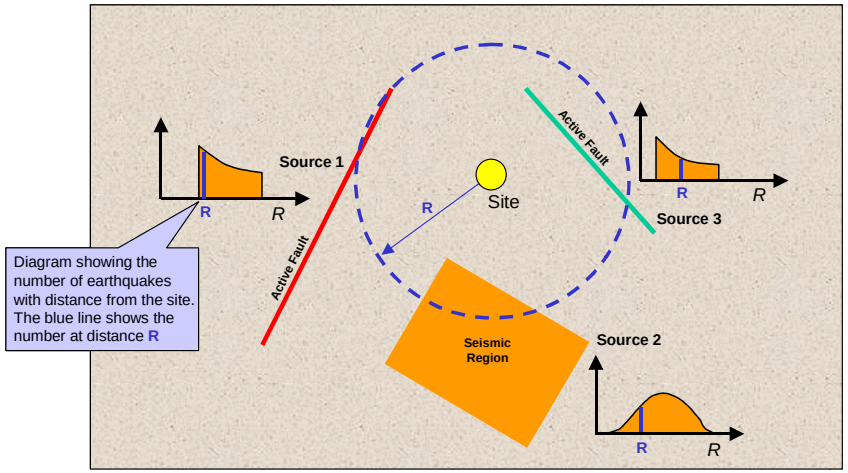

STEP 1 - source model

This is a plan representing the observed seismicity in the region of the site. The designer must select fault (Source 1 and 3) and area sources (Source 2). The annual number of earthquakes within each Source must also be decided.

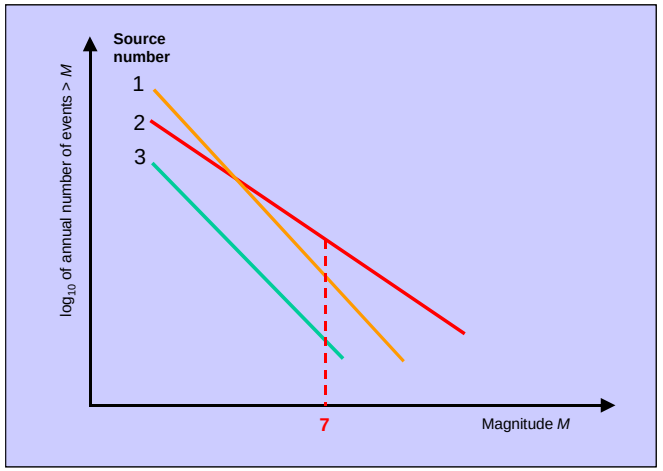

STEP 2 - earthquake recurrence

For each source zone the distribution of earthquake size (or magnitude) within that source must be determined. It is conventional to describe this using the Gutenberg Richter as above. The slope of the line is referred to as the b value and is often taken to be a constant within a particular region.

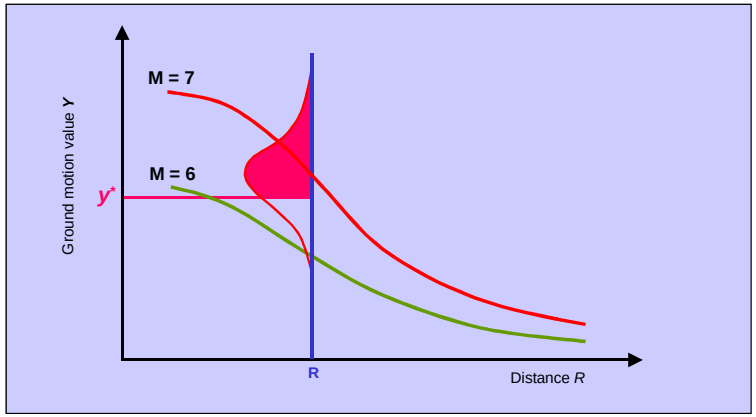

STEP 3 - attenuation relationship

The attenuation relationship defines the level of ground motion (whether it be acceleration or velocity etc.) that is likely to occur at a certain distance from an earthquake of known magnitude. There is an observed variability associated with this value. Here it is shown that at distance R a magnitude 7 earthquake has a 60% chance of exceeding the target ground motion y^*.

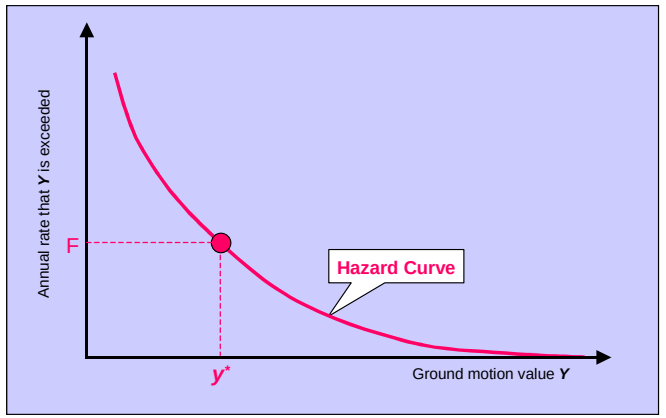

STEP 4 - sum results and repeat

From Steps 1, 2 and 3 we know the rate at which y* is exceeded due to magnitude 7 earthquakes at distance R [= 0.6 times annual rate of events]. By adding the result from all magnitudes at all distances we obtain the annual rate y* is exceeded [= F]. By repeating this whole calculation at a range of y* values the above hazard curve is derived.

Figure 3.1 Seismic Hazard Assessment Methodology

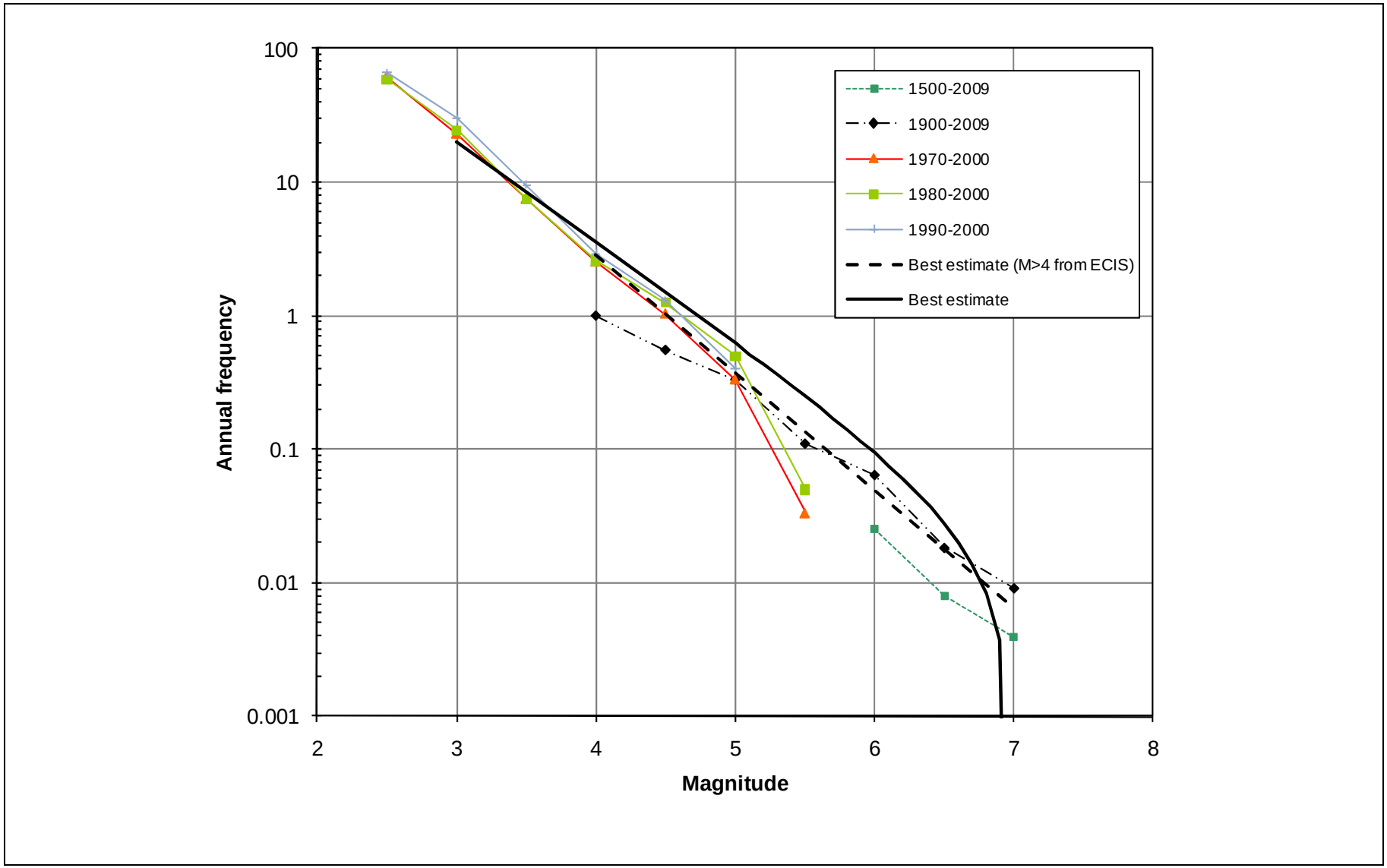

Figure 3.2 Earthquake Recurrence Plot for the Onshore and Near-shore Region

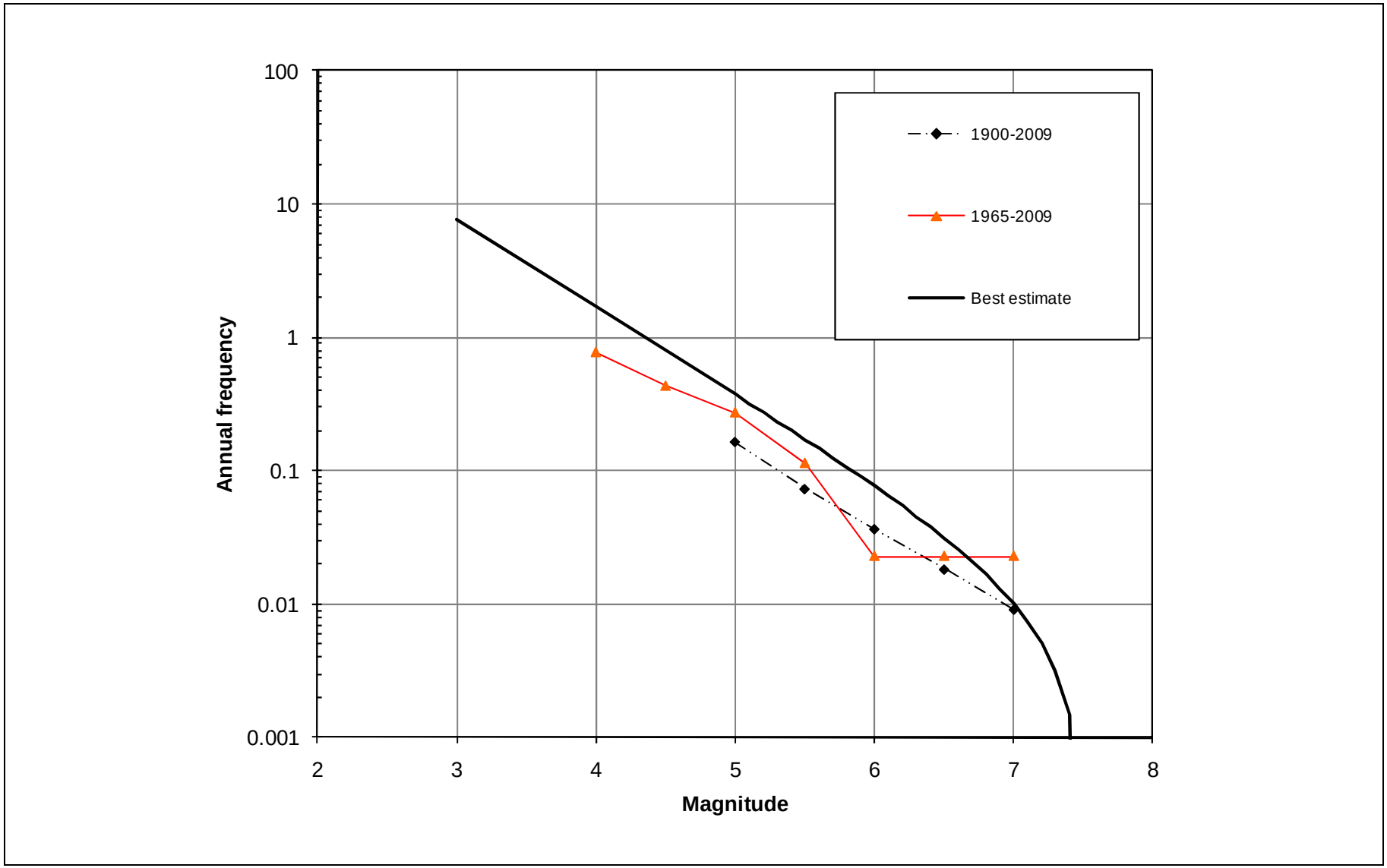

Figure 3.3 Earthquake Recurrence Plot for the Offshore Region

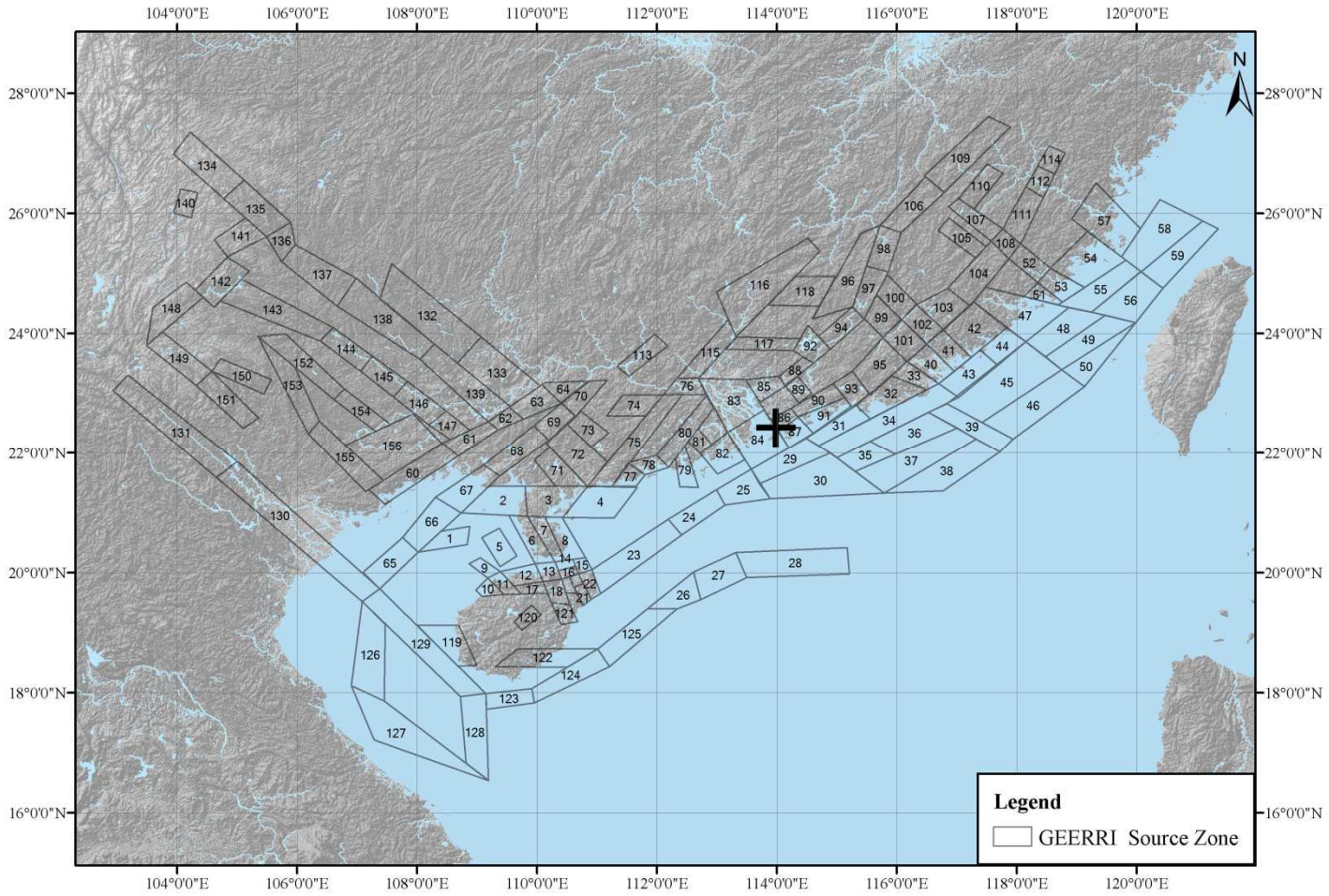

Figure 3.4 GEERRI Source Model

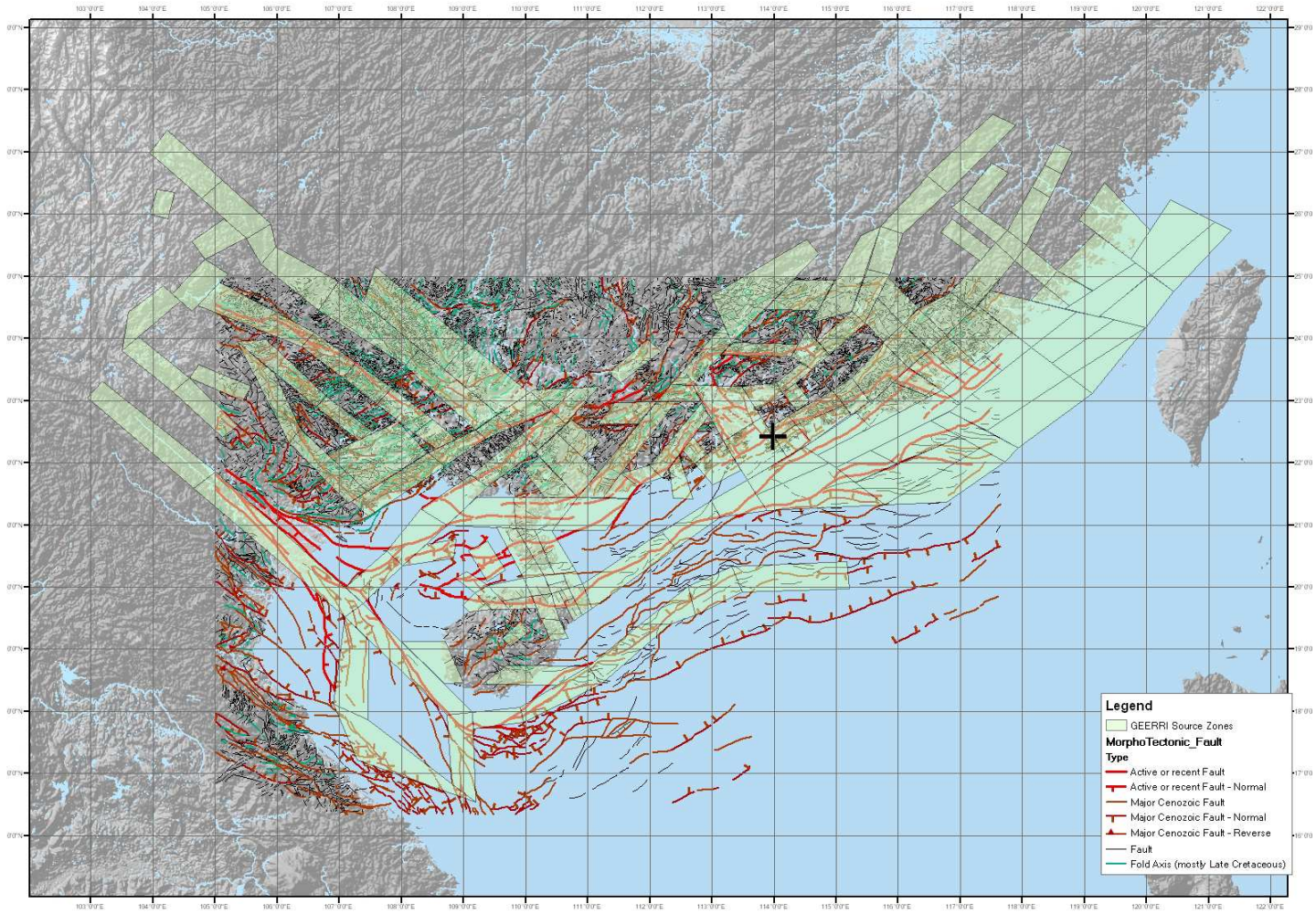

Figure 3.5 The GEERRI Source Model Superimposed on the Morphotectonic Map by Pubellier & Chan (2006)

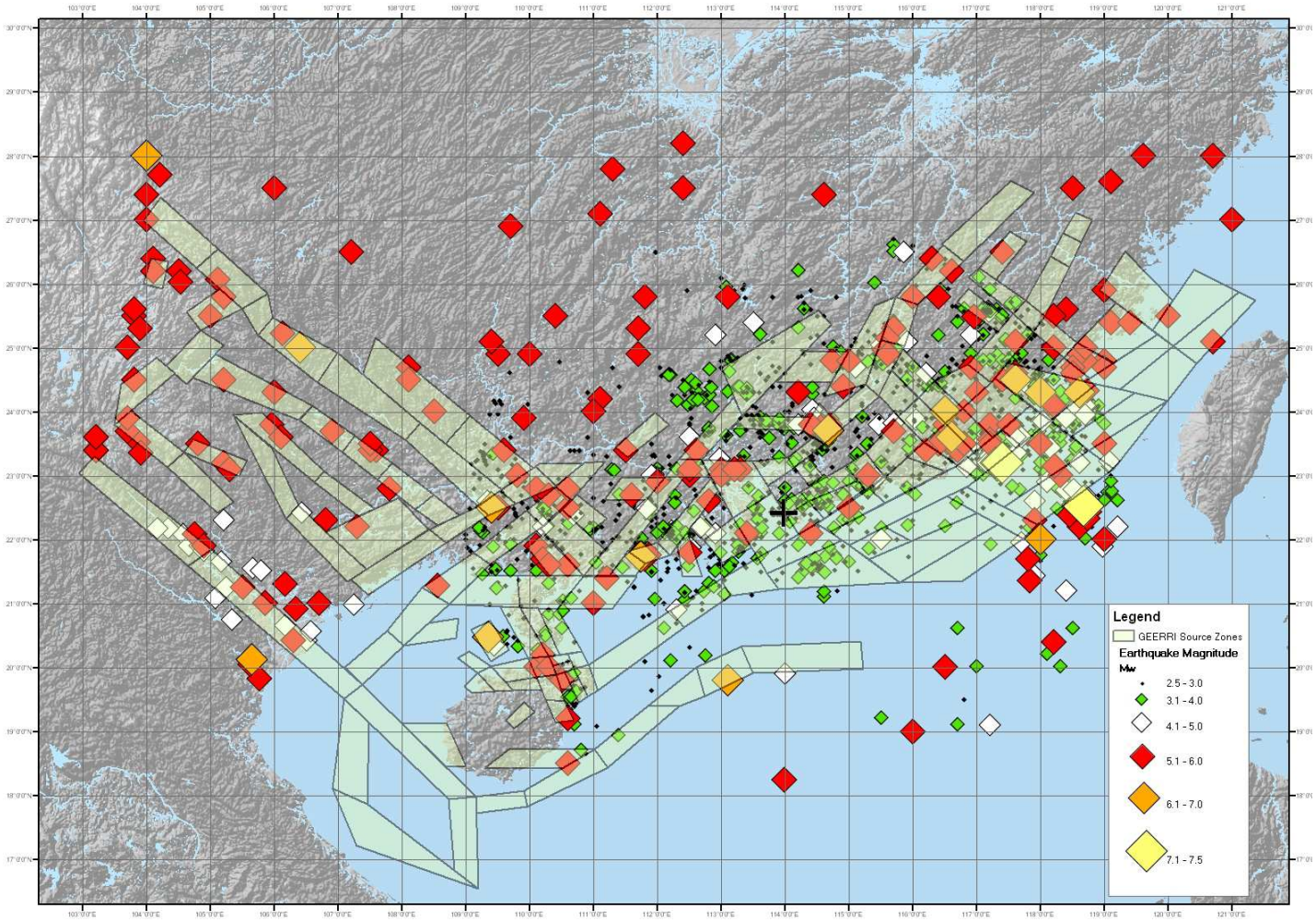

Figure 3.6 The GEERRI Source Model and the Full Earthquake Catalogue

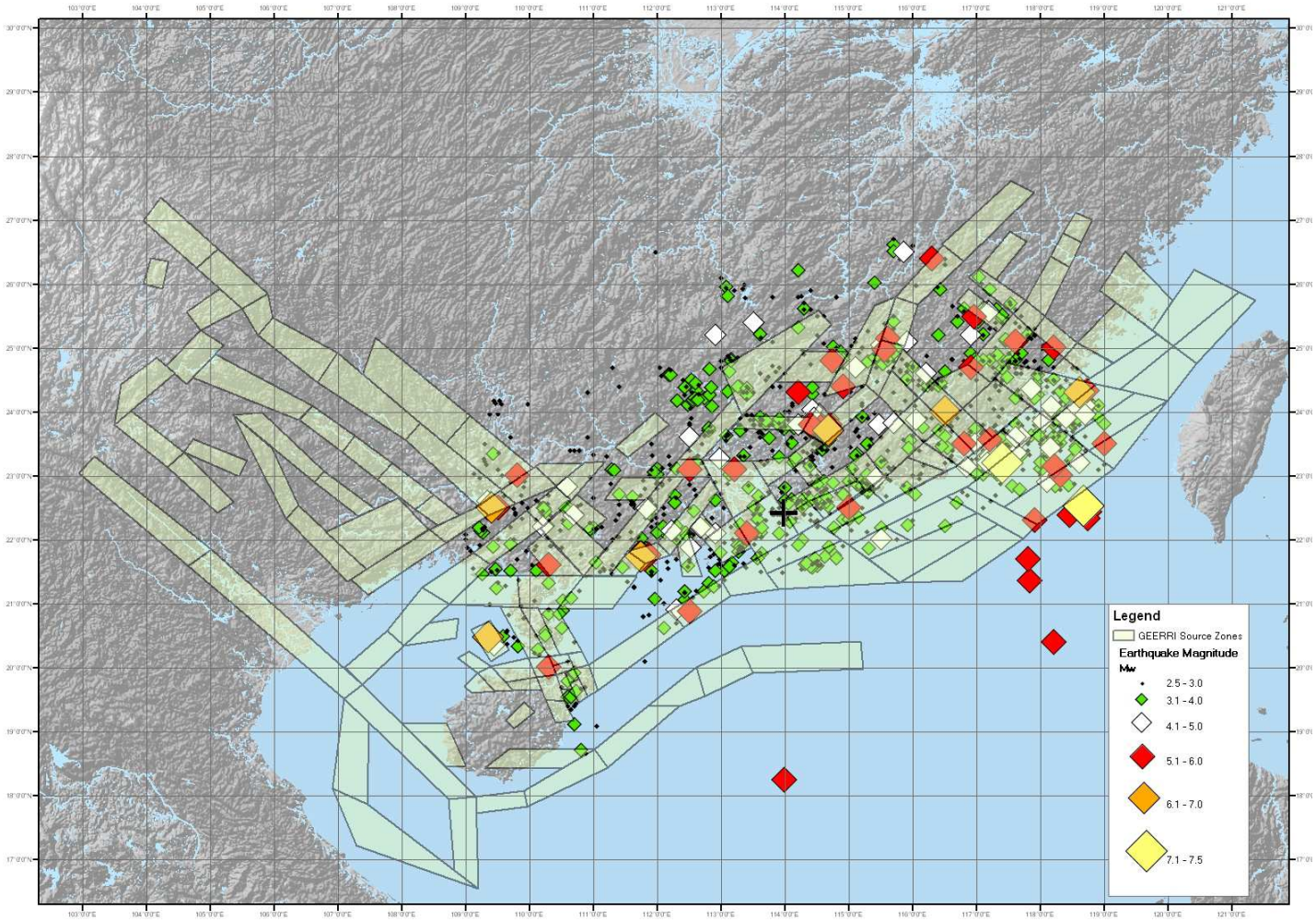

Figure 3.7 The GEERRI Source Model and the Complete Earthquake Catalogue

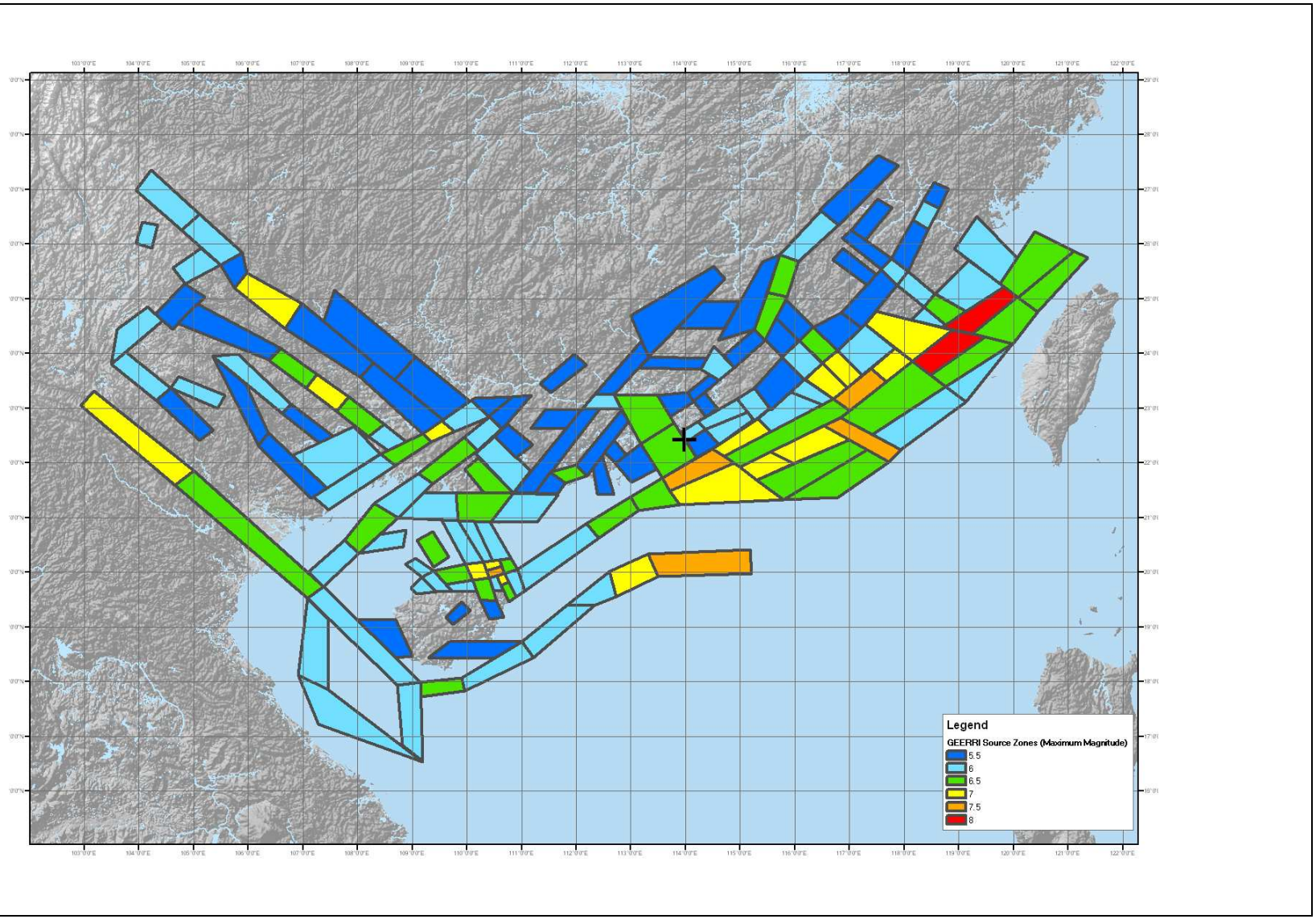

Figure 3.8 Maximum Magnitude Distribution of the GEERRI Source Model

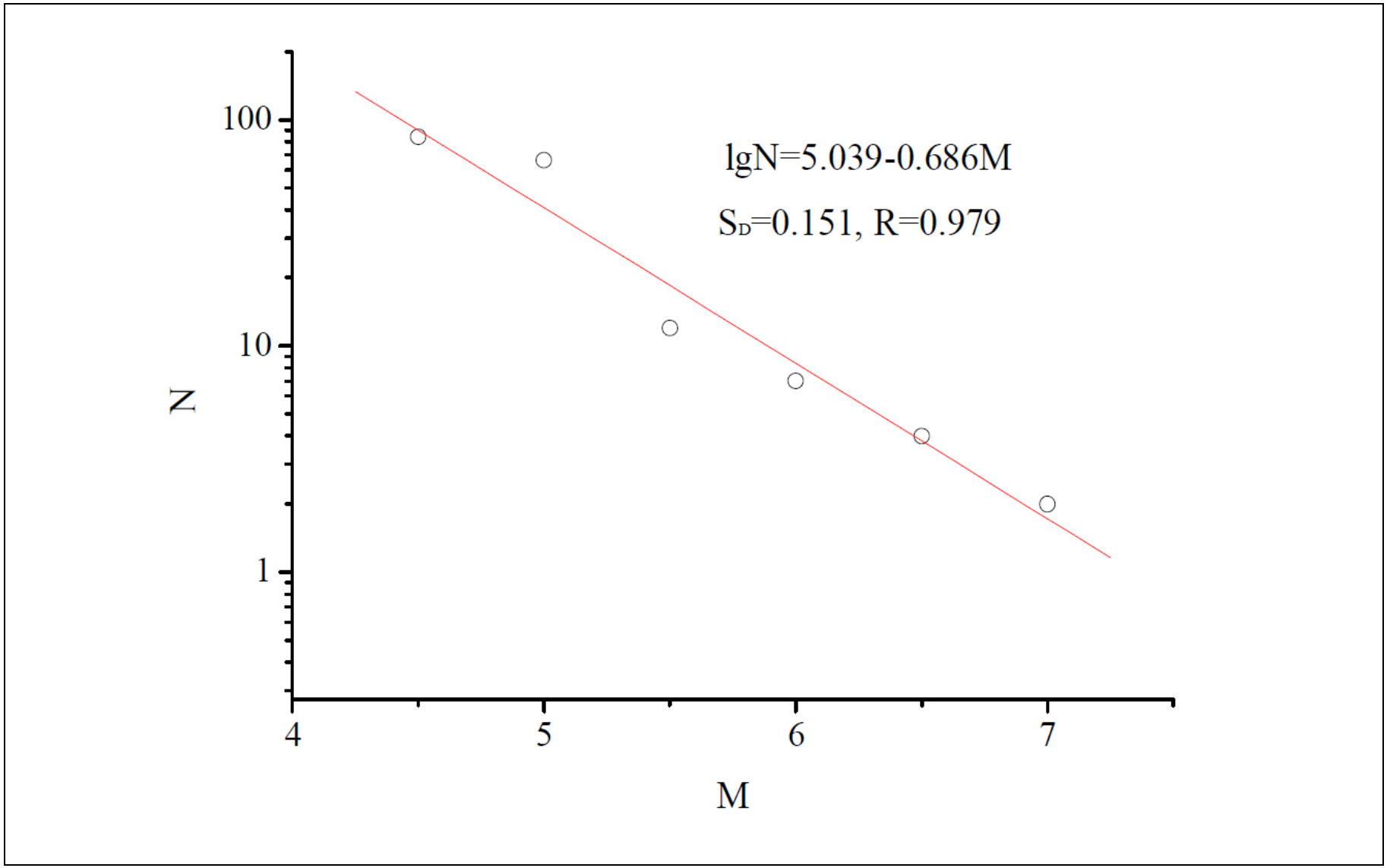

Figure 3.9 GEERRI Earthquake Recurrence Curve for the Whole Southeast China

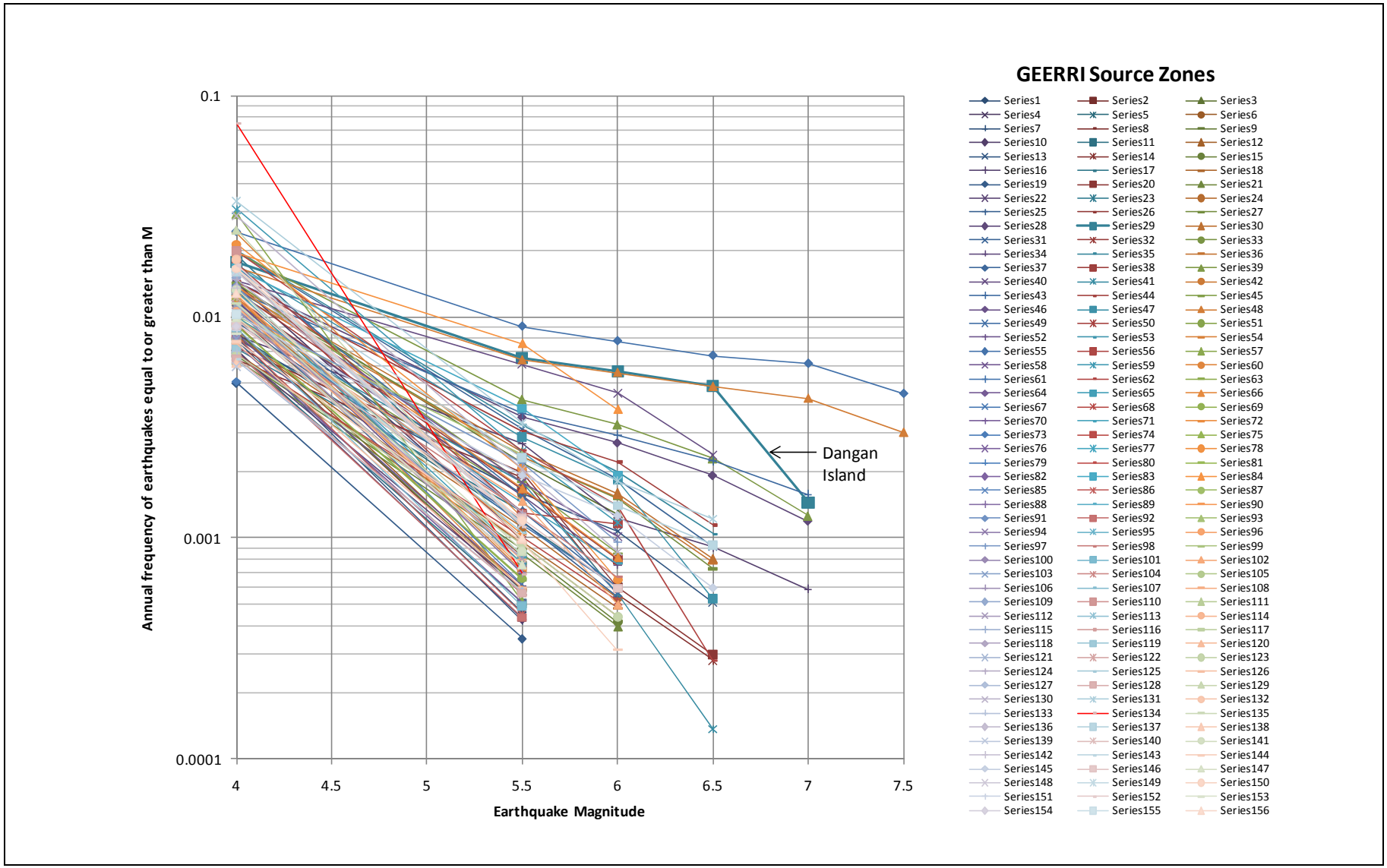

Figure 3.10 GEERRI Source Zone Recurrence Plots

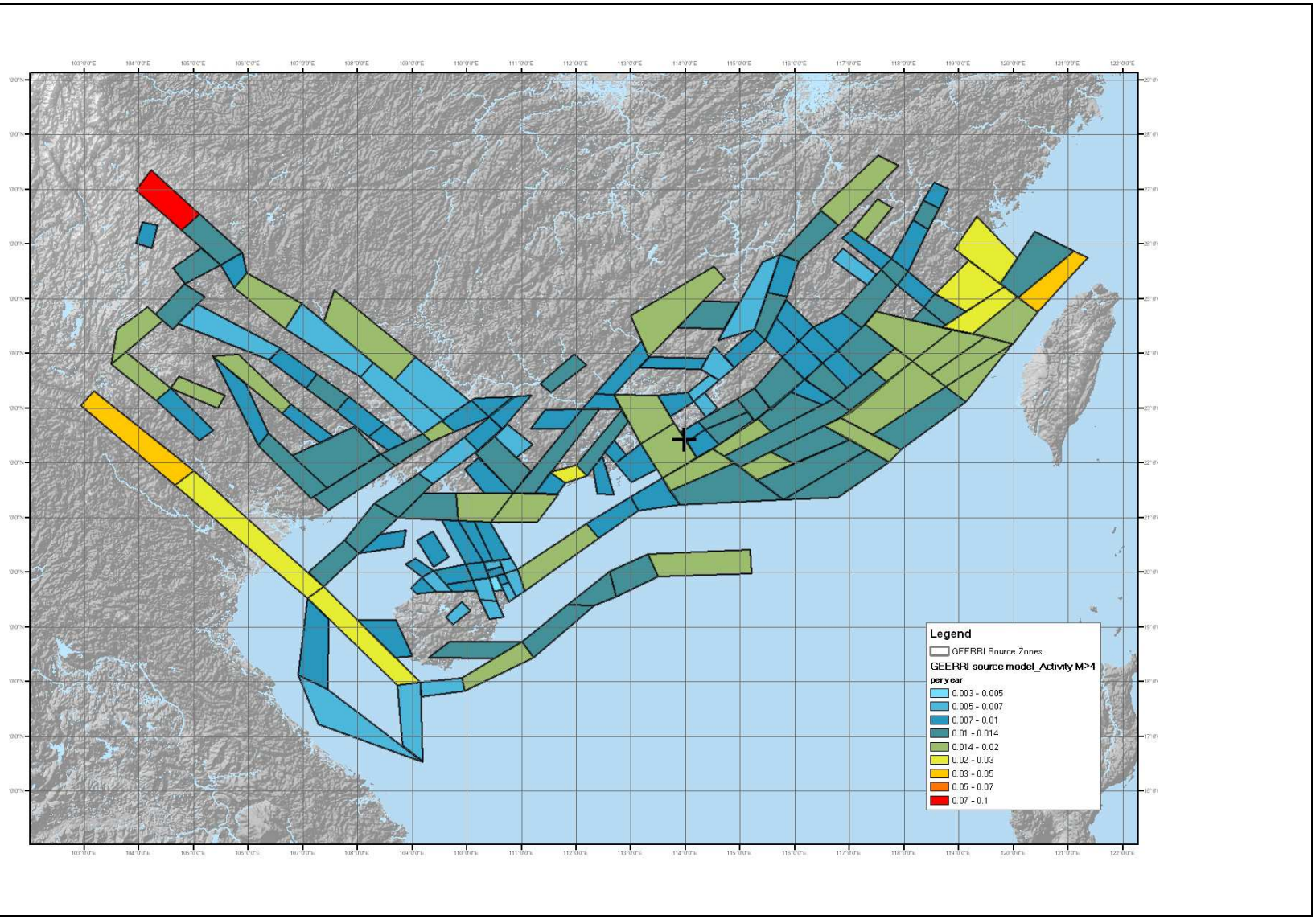

Figure 3.11 GEERRI Annual Activity Rate for Earthquake Magnitude Greater than 4

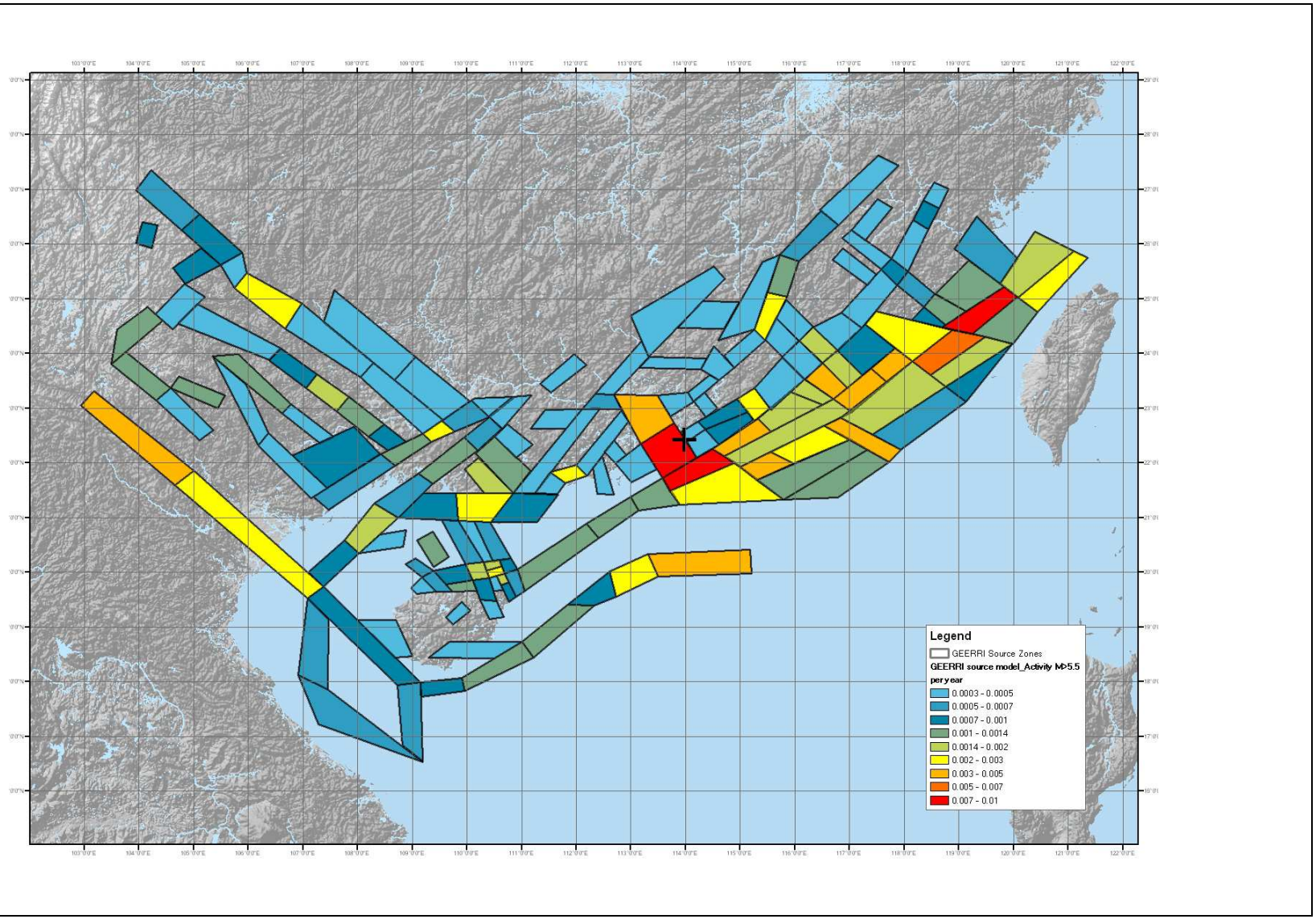

Figure 3.12 GEERRI Annual Activity Rate for Earthquake Magnitude Greater than 5.5

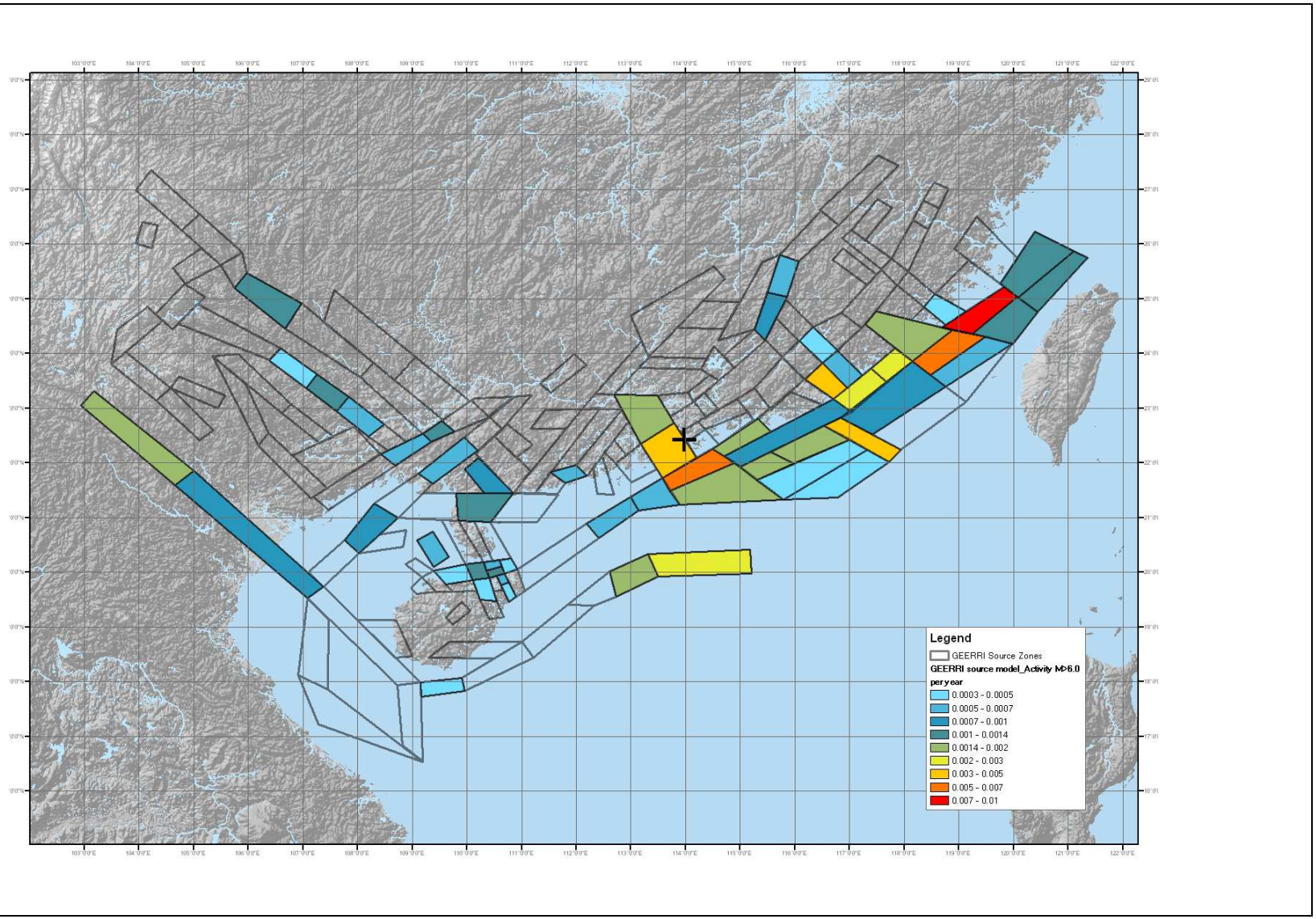

Figure 3.13 GEERRI Annual Activity Rate for Earthquake Magnitude Greater than 6

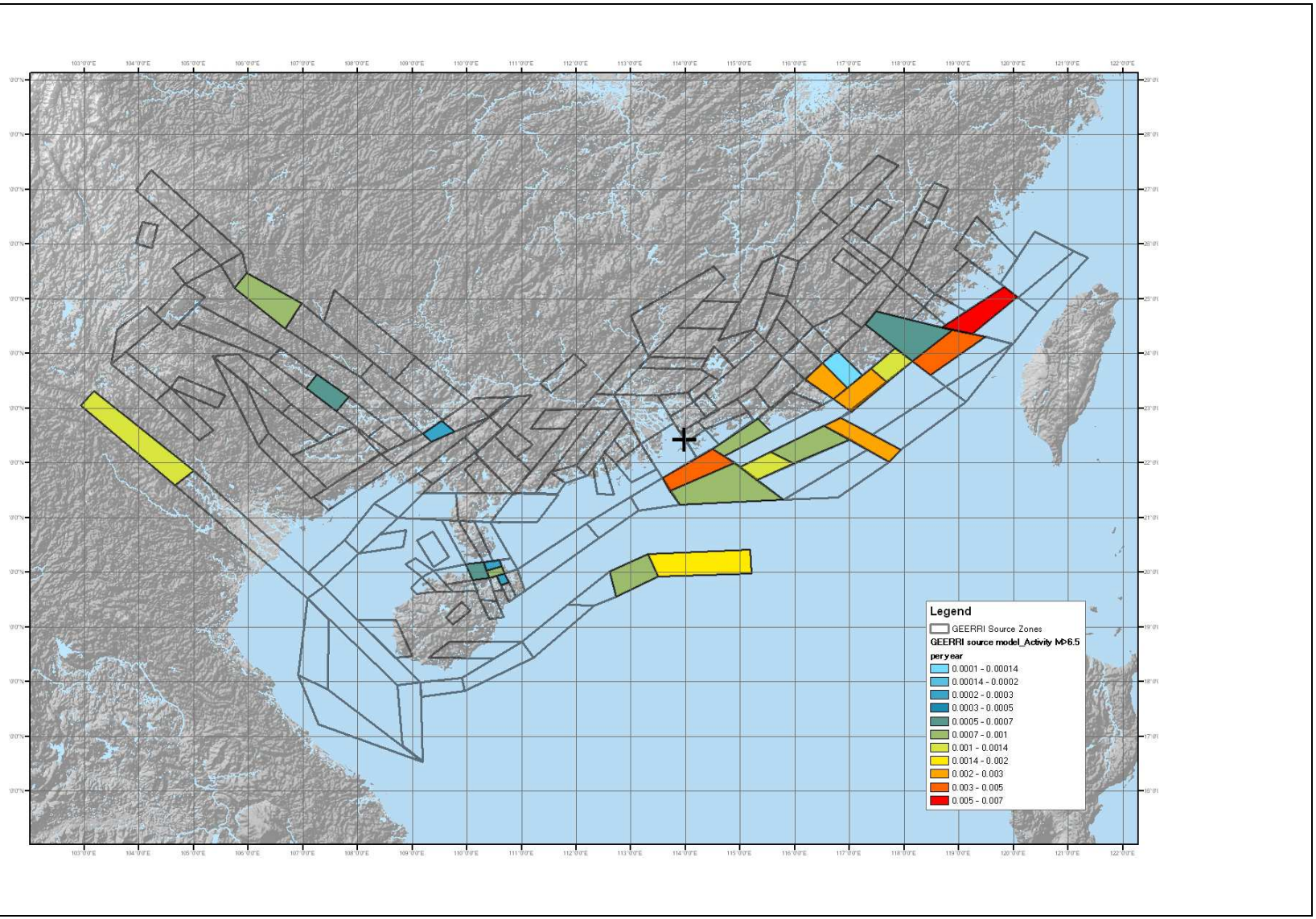

Figure 3.14 GEERRI Annual Activity Rate for Earthquake Magnitude Greater than 6.5

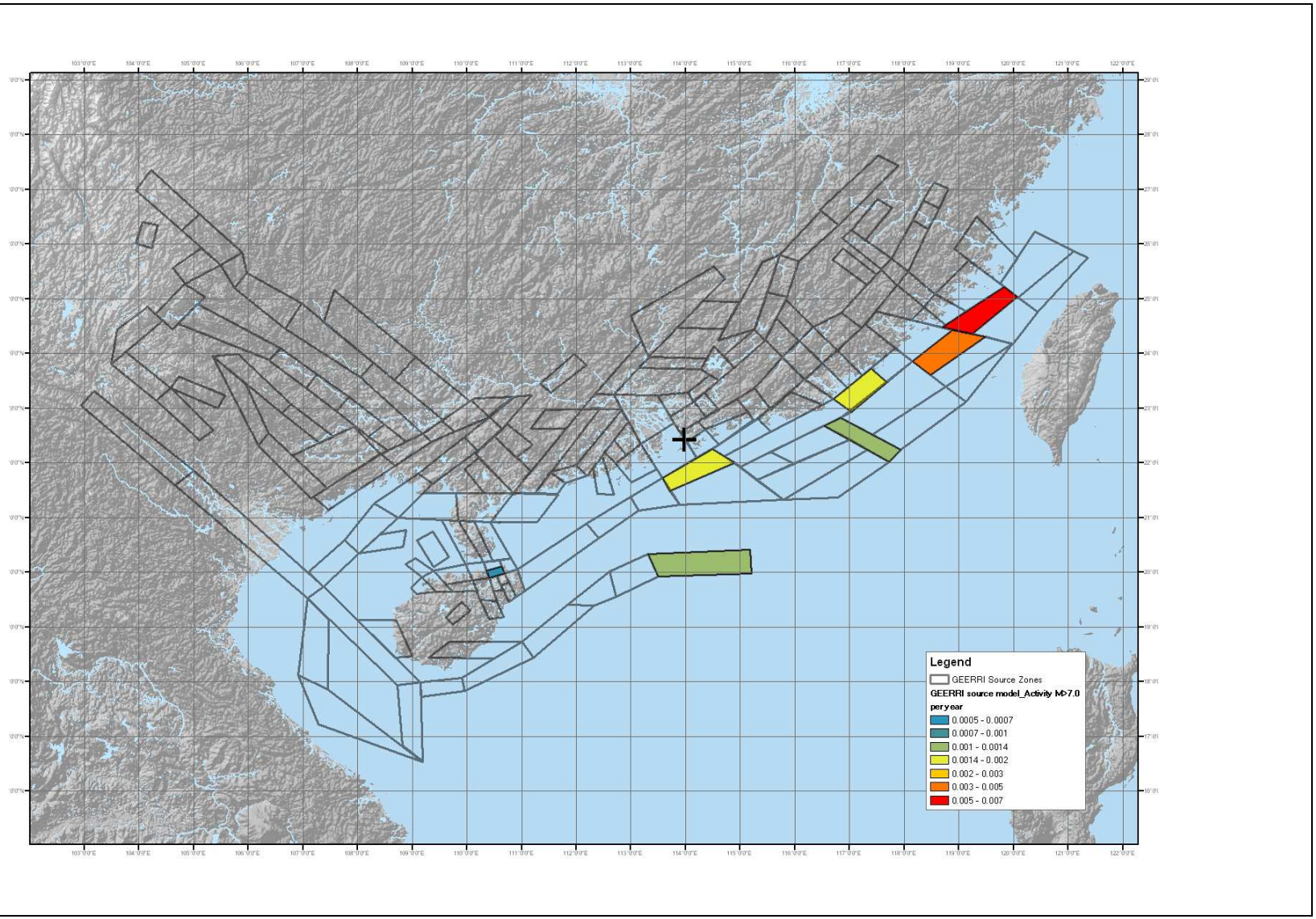

Figure 3.15 GEERRI Annual Activity Rate for Earthquake Magnitude Greater than 7

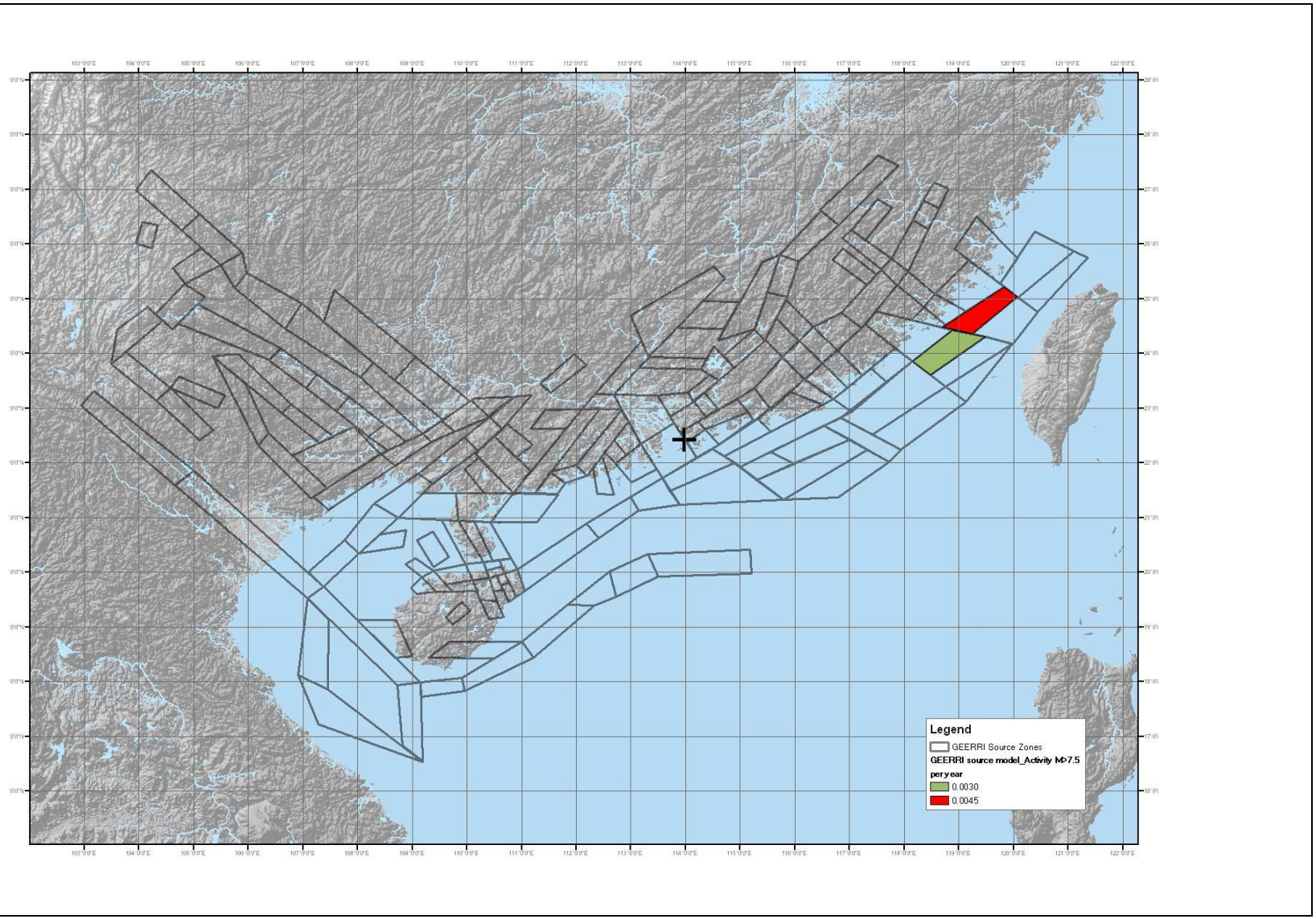

Figure 3.16 GEERRI Annual Activity Rate for Earthquake Magnitude Greater than 7.5

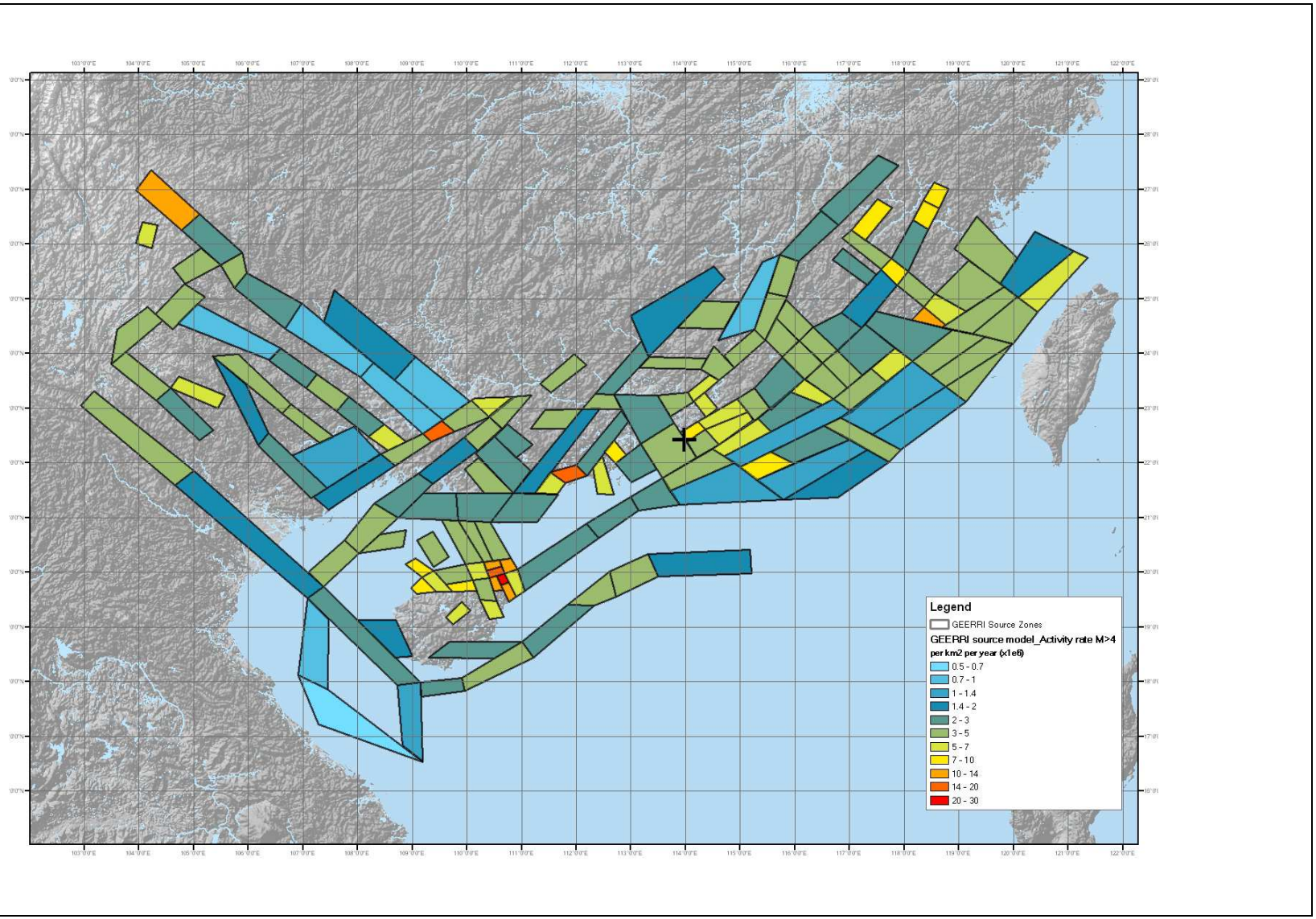

Figure 3.17 GEERRI Annual Activity Rate Divided by Zone Area for Earthquake Magnitude Greater than 4

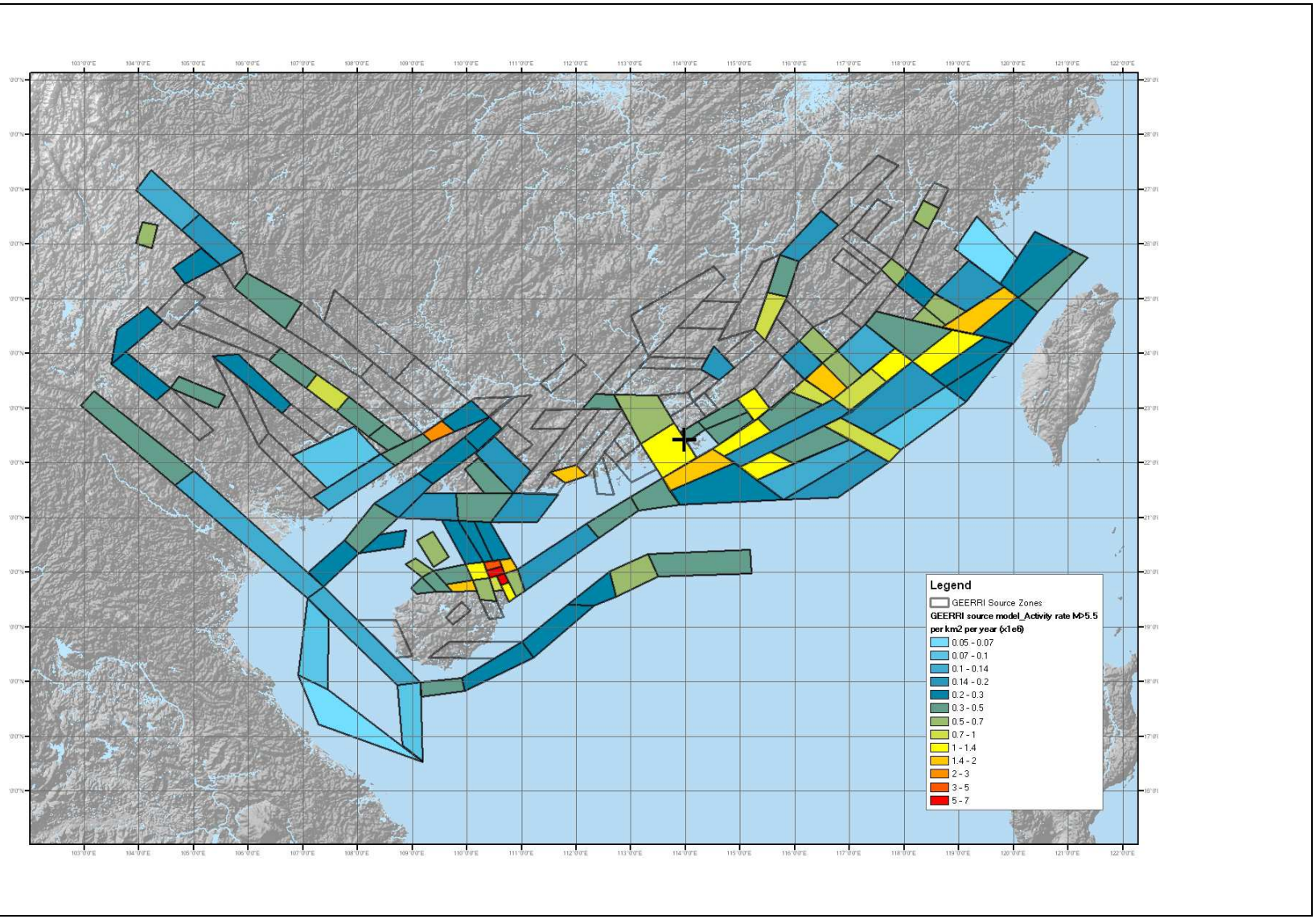

Figure 3.18 GEERRI Annual Activity Rate Divided by Zone Area for Earthquake Magnitude Greater than 5.5

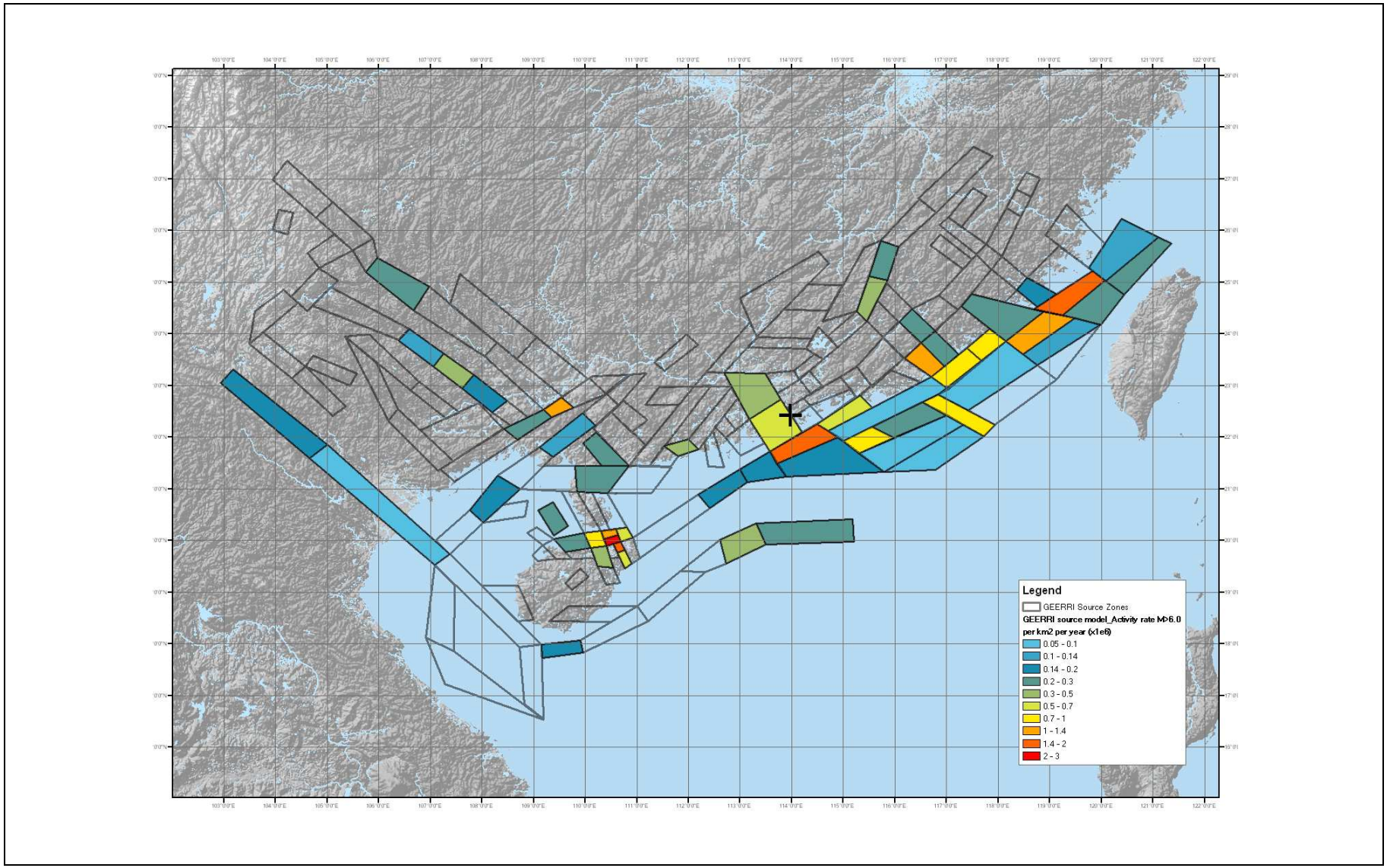

Figure 3.19 GEERRI Annual Activity Rate Divided by Zone Area for Earthquake Magnitude Greater than 6

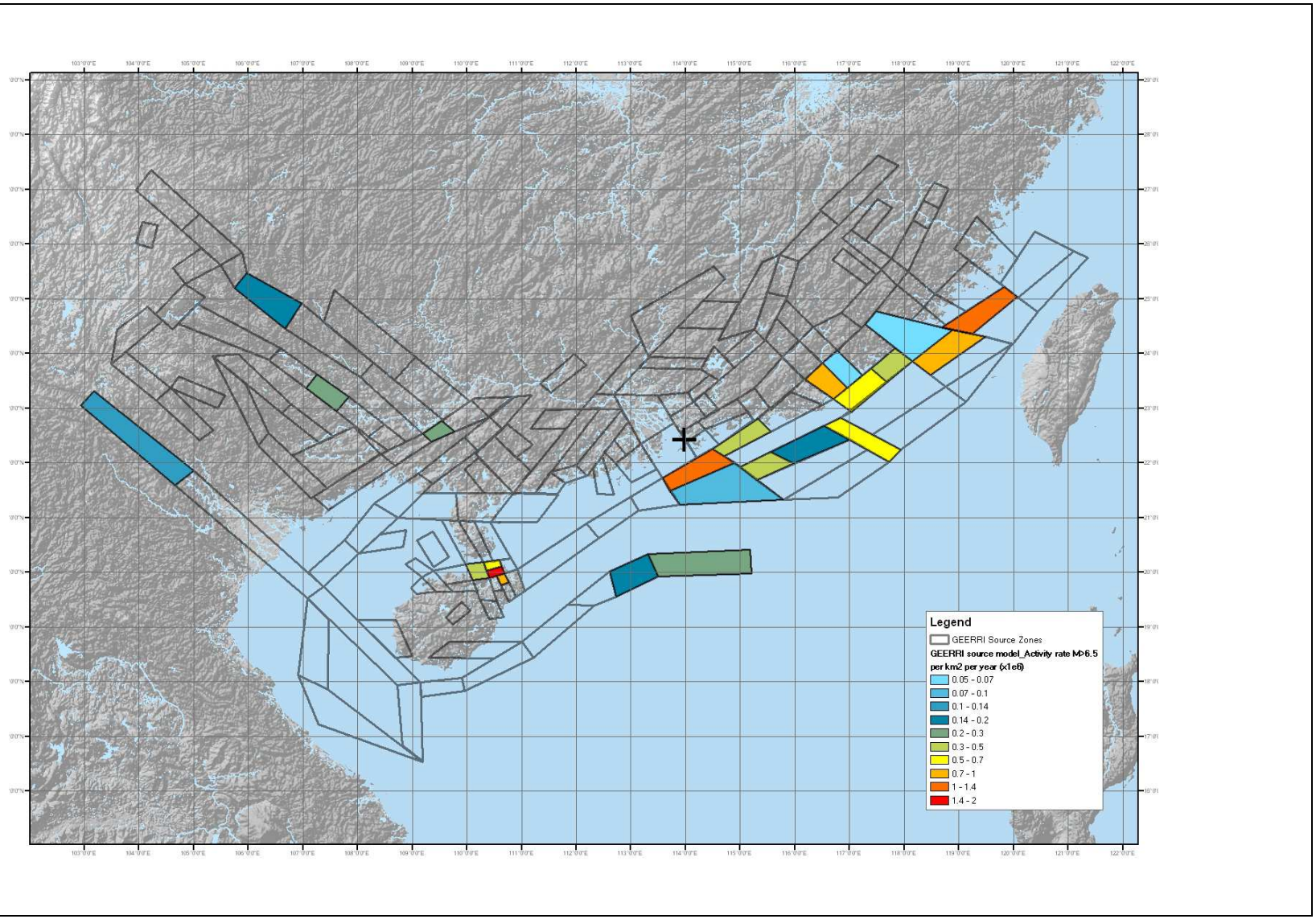

Figure 3.20 GEERRI Annual Activity Rate Divided by Zone Area for Earthquake Magnitude Greater than 6.5

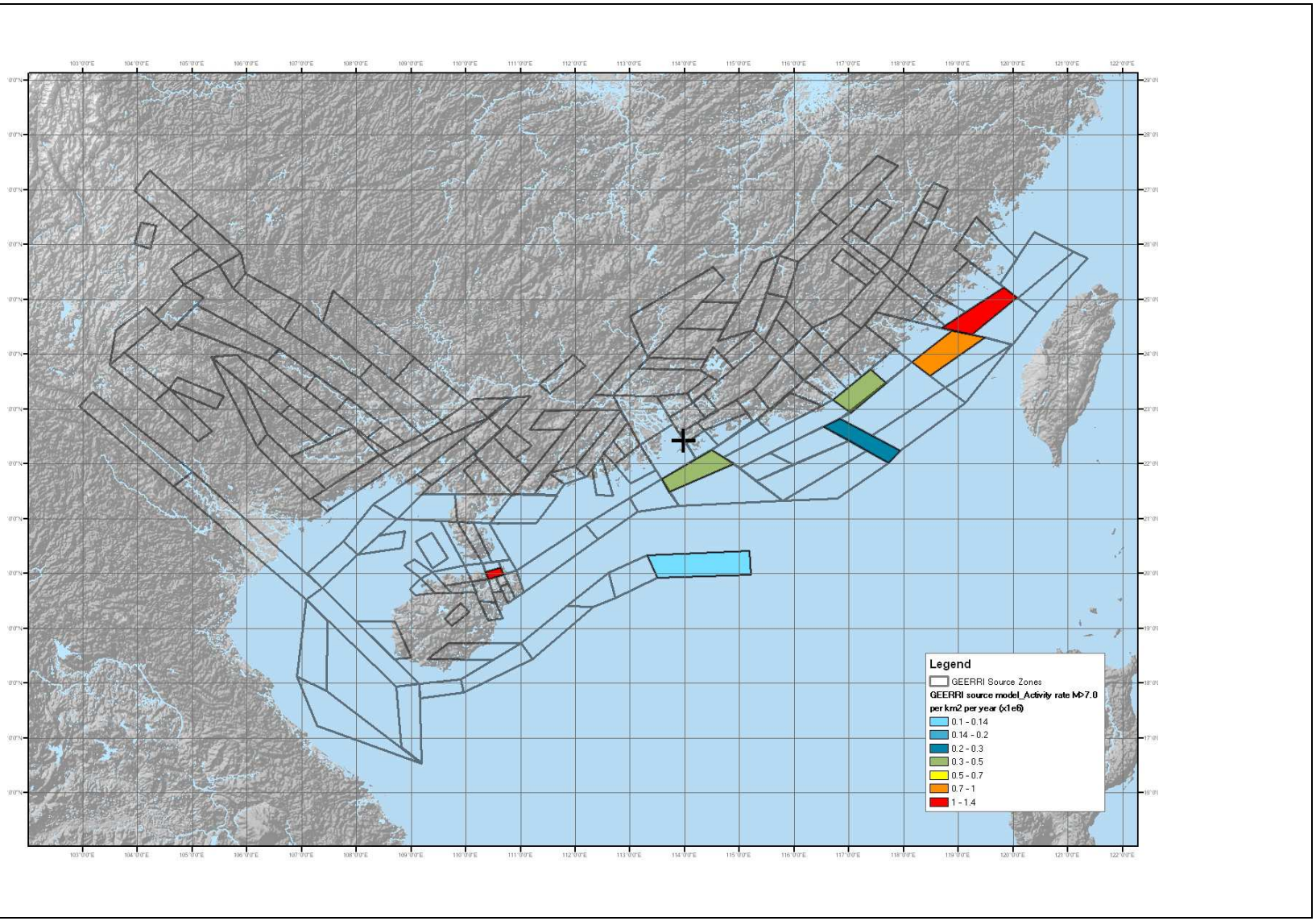

Figure 3.21 GEERRI Annual Activity Rate Divided by Zone Area for Earthquake Magnitude Greater than 7

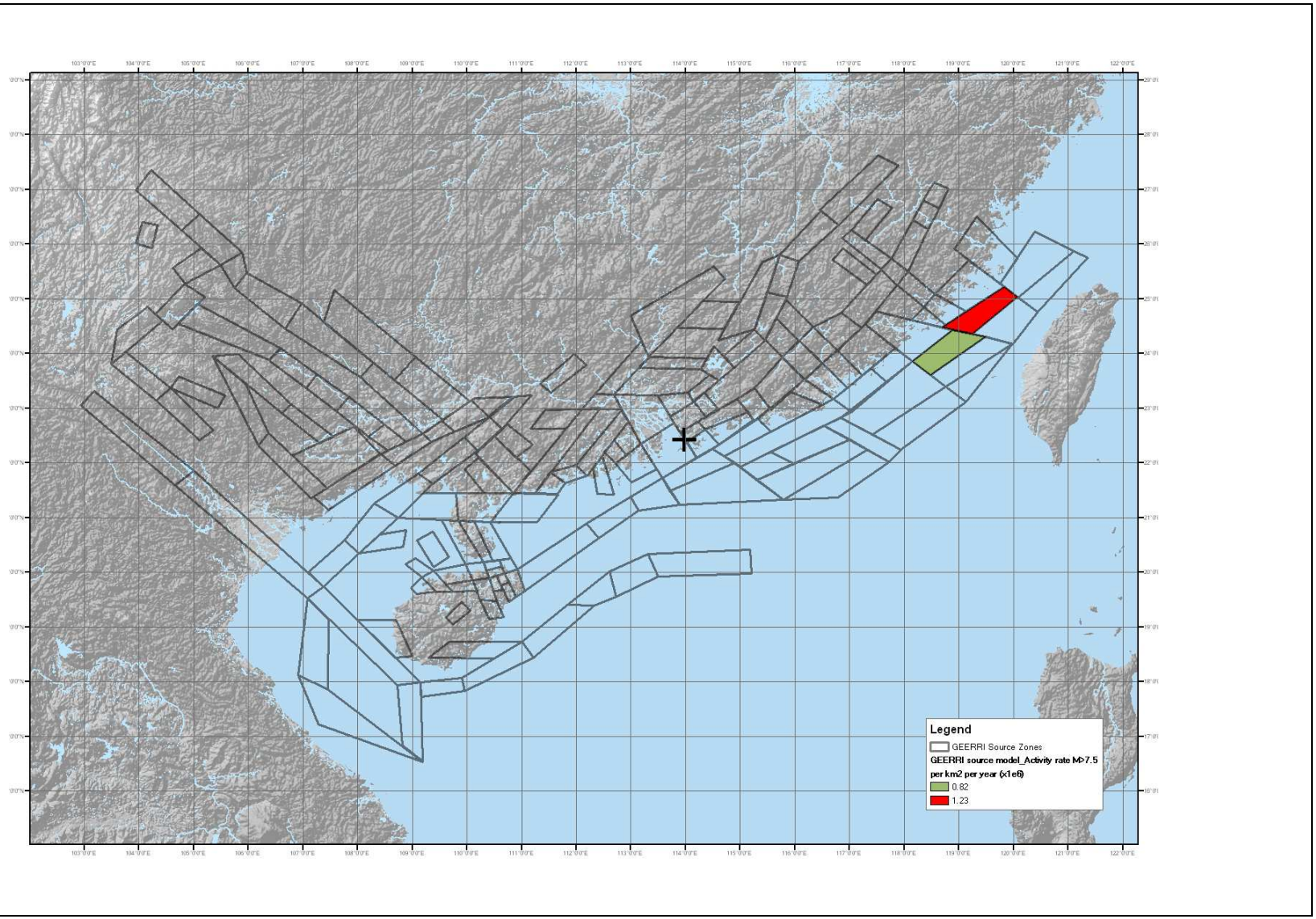

Figure 3.22 GEERRI Annual Activity Rate Divided by Zone Area for Earthquake Magnitude Greater than 7.5

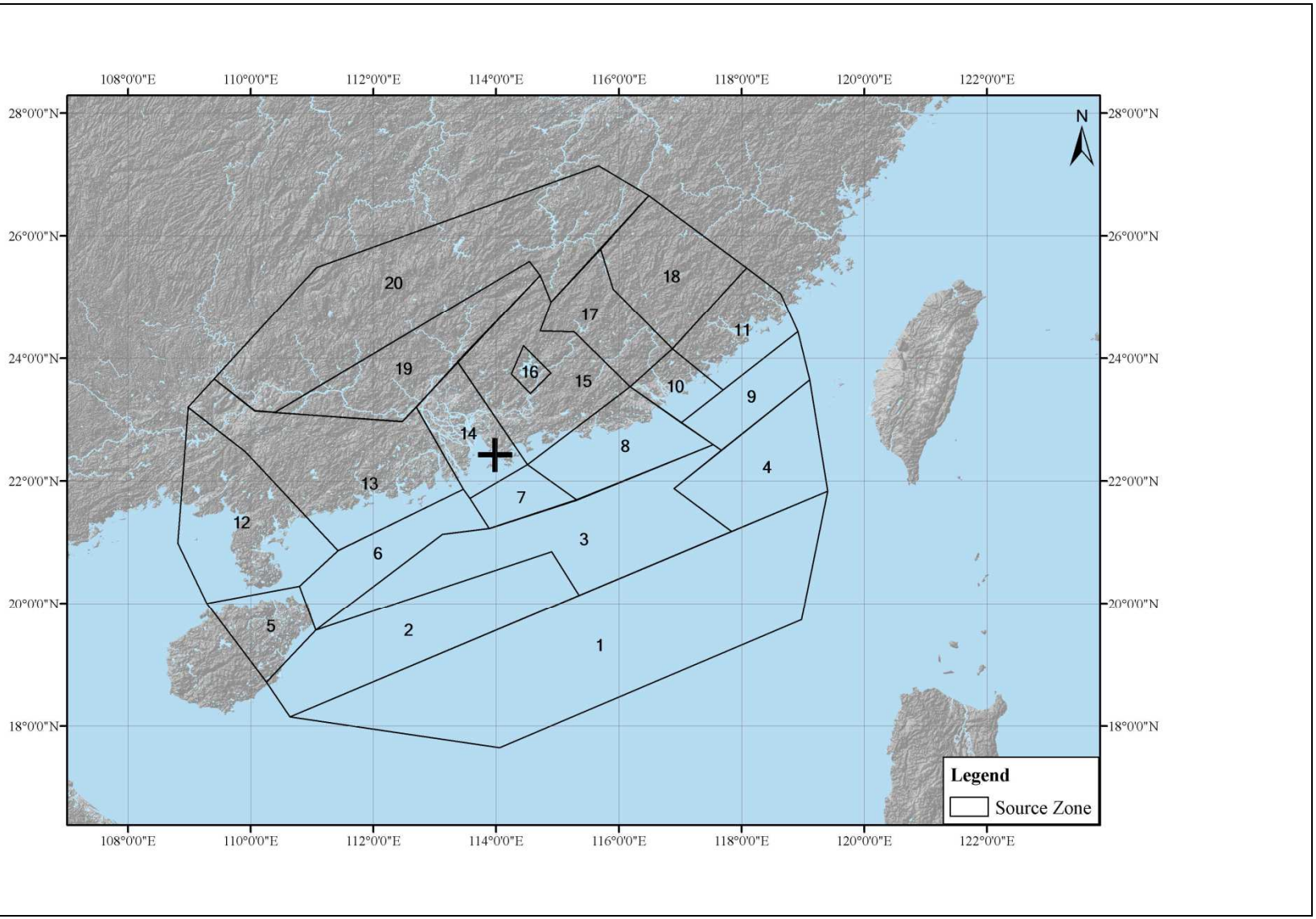

Figure 3.23 Arup Source Zone Model

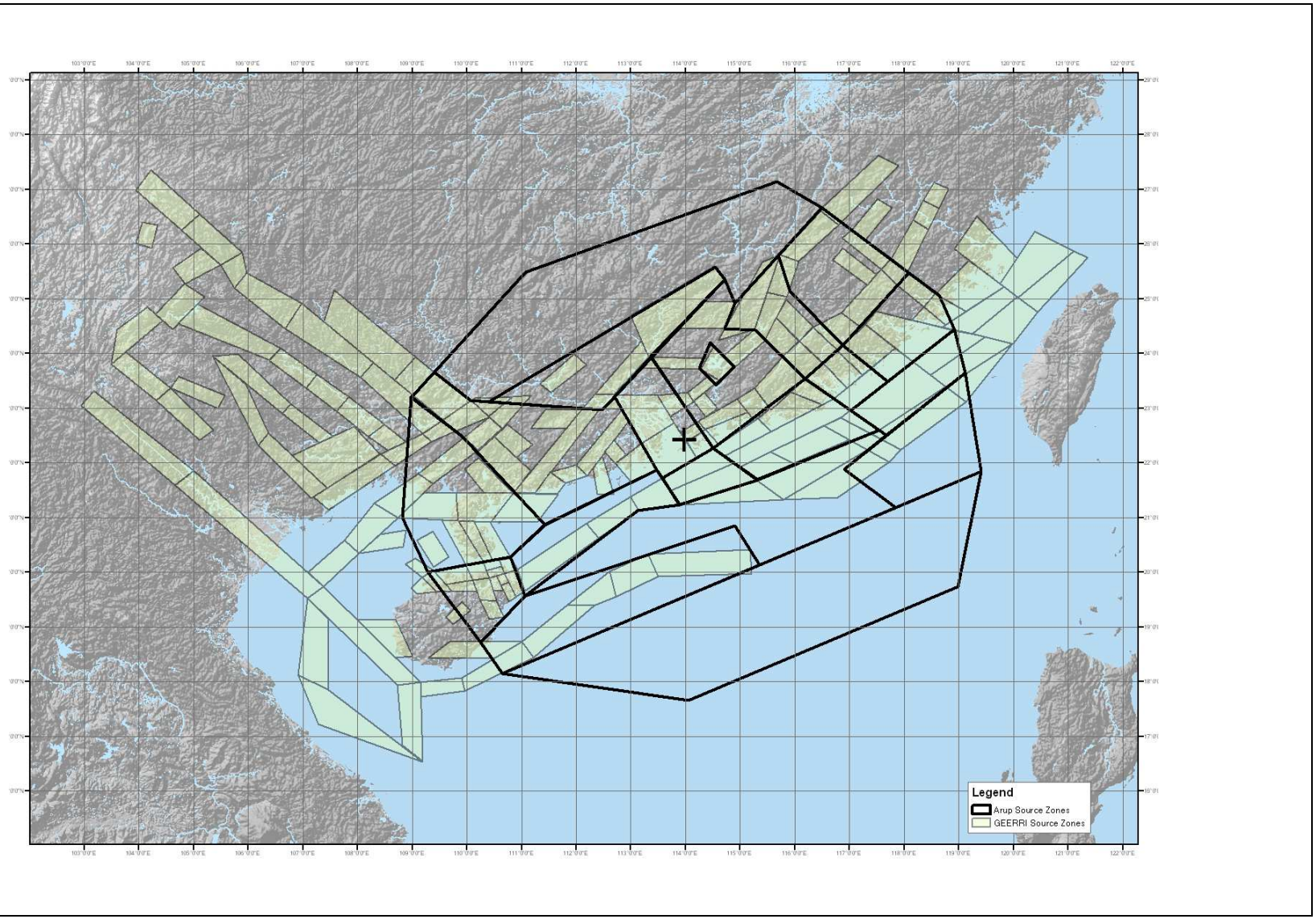

Figure 3.24 Comparison between Arup and GEERRI Source Zone Model

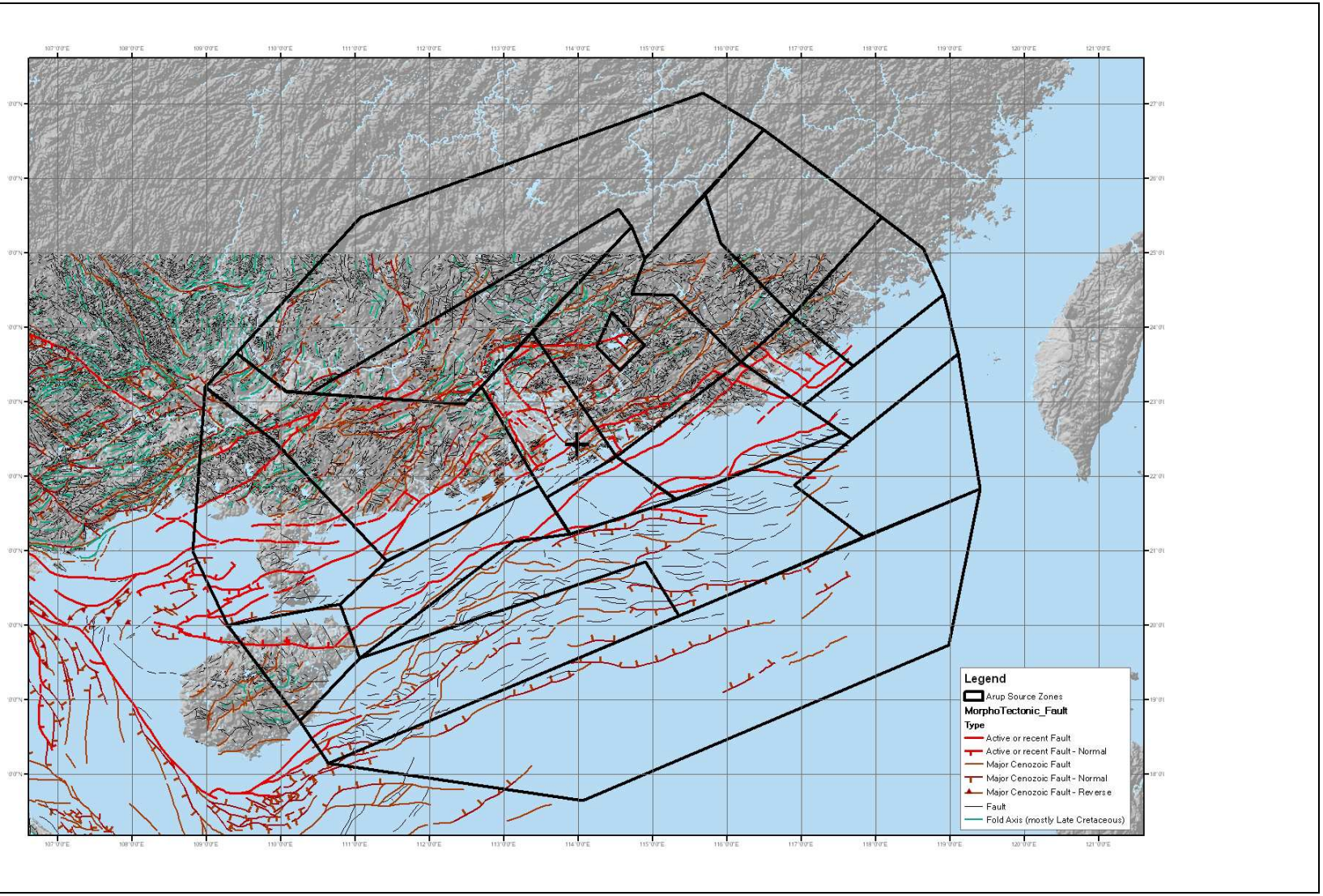

Figure 3.25 Arup Source Zone Model with Geological Information Provided by the University of Hong Kong (Pubellier & Chan, 2006)

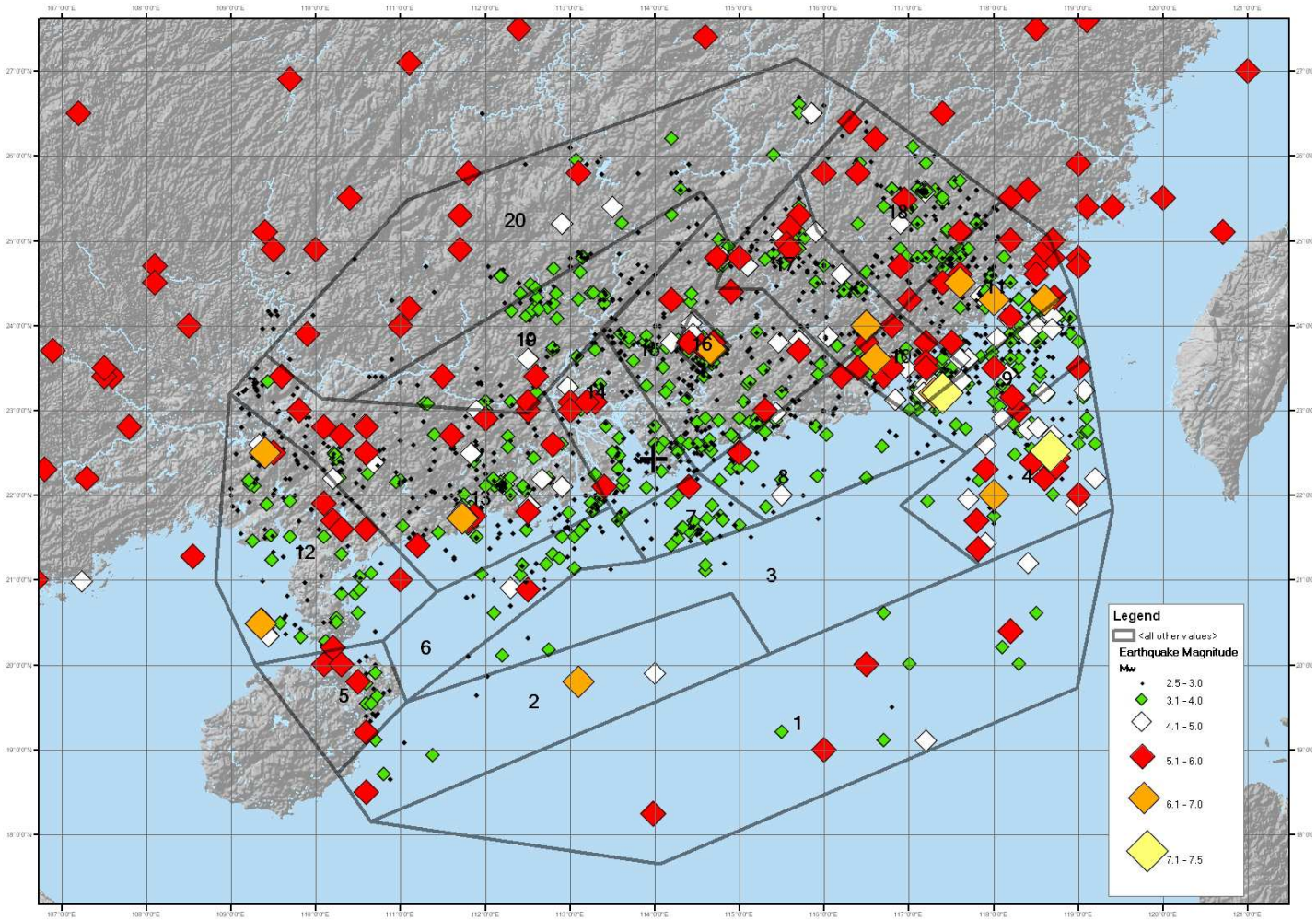

Figure 3.26 Arup Source Zone Model with Full Earthquake Catalogue

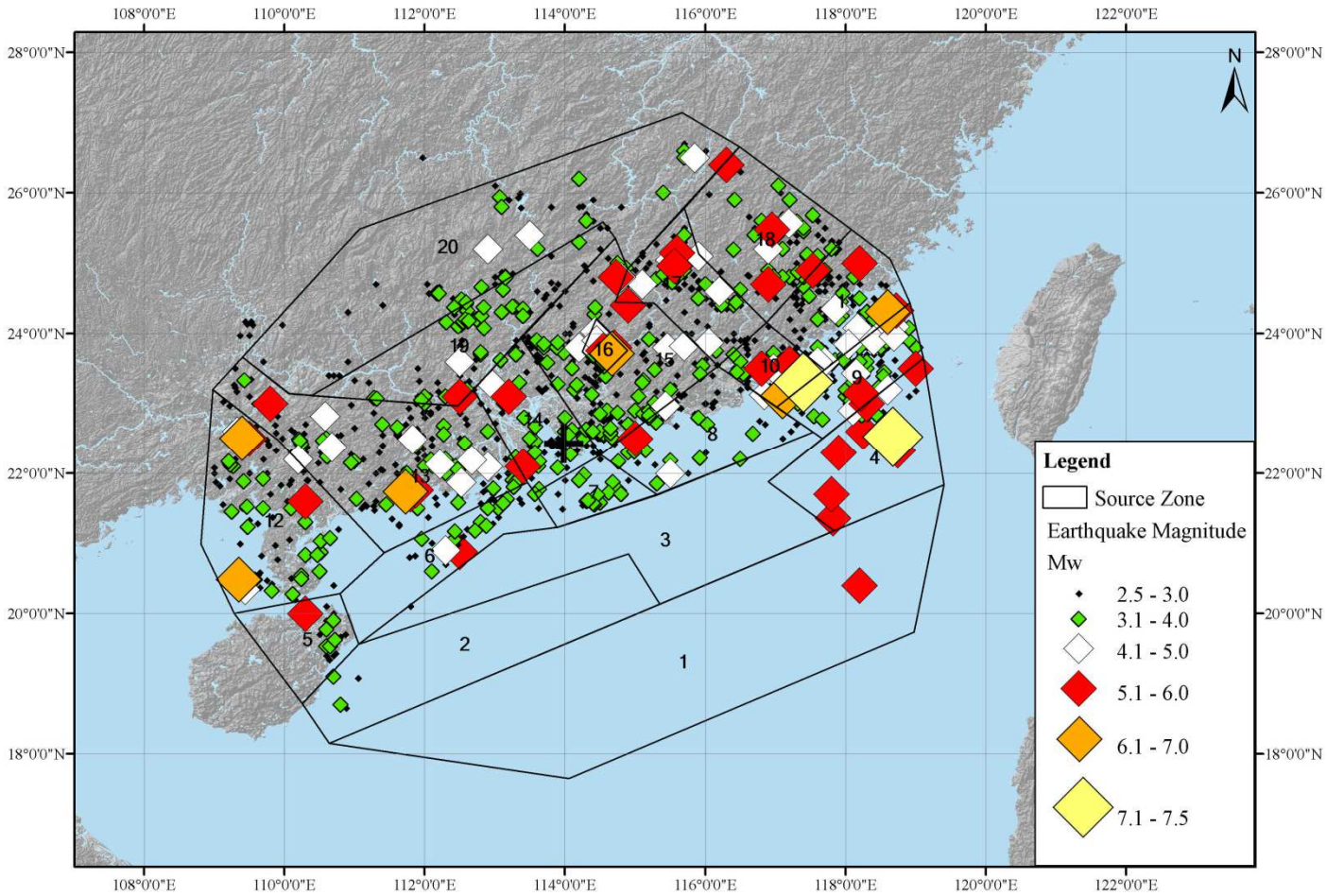

Figure 3.27 Arup Source Zone Model with Complete Earthquake Catalogue

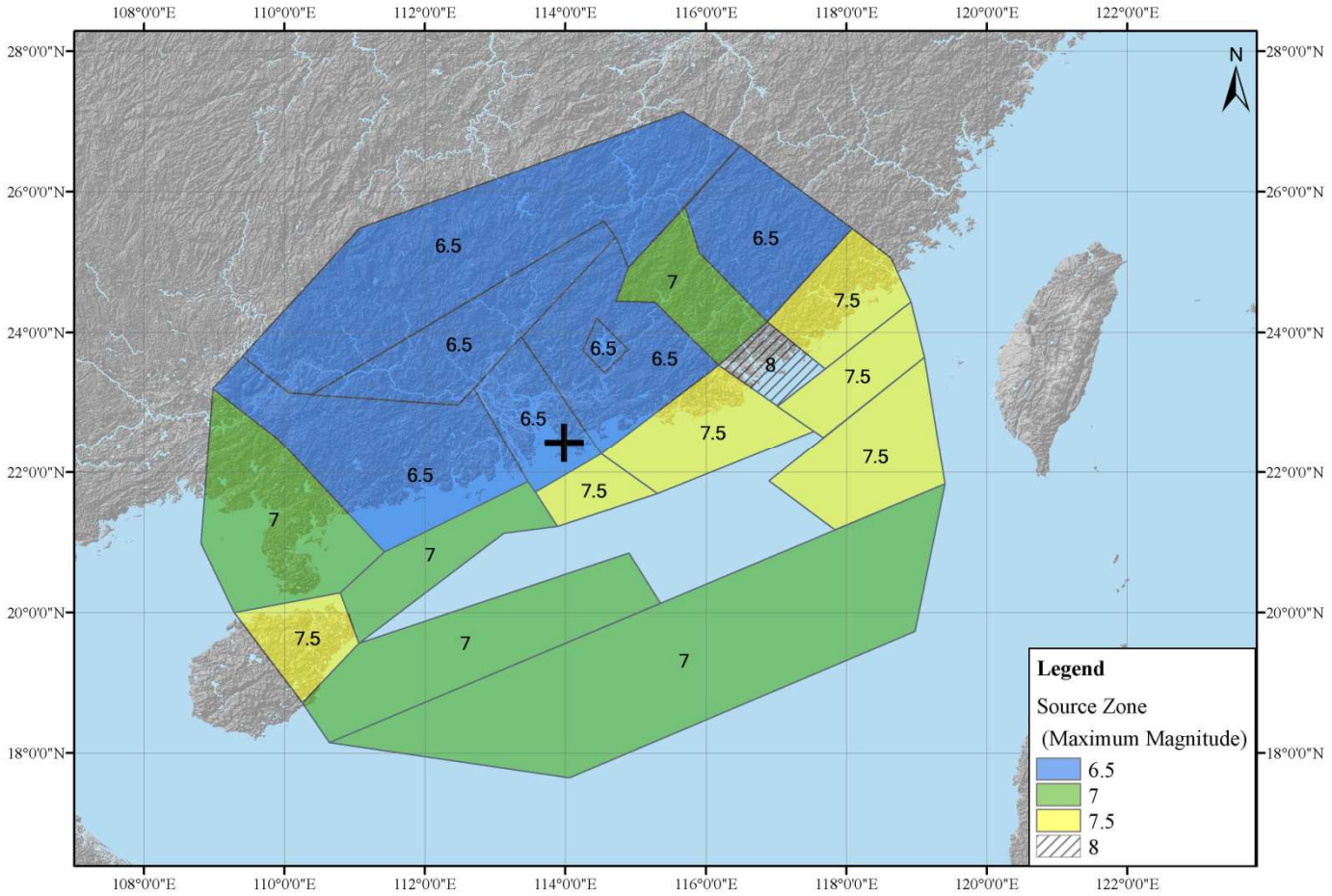

Figure 3.28 Arup Zonation Map for Maximum Earthquake Magnitude

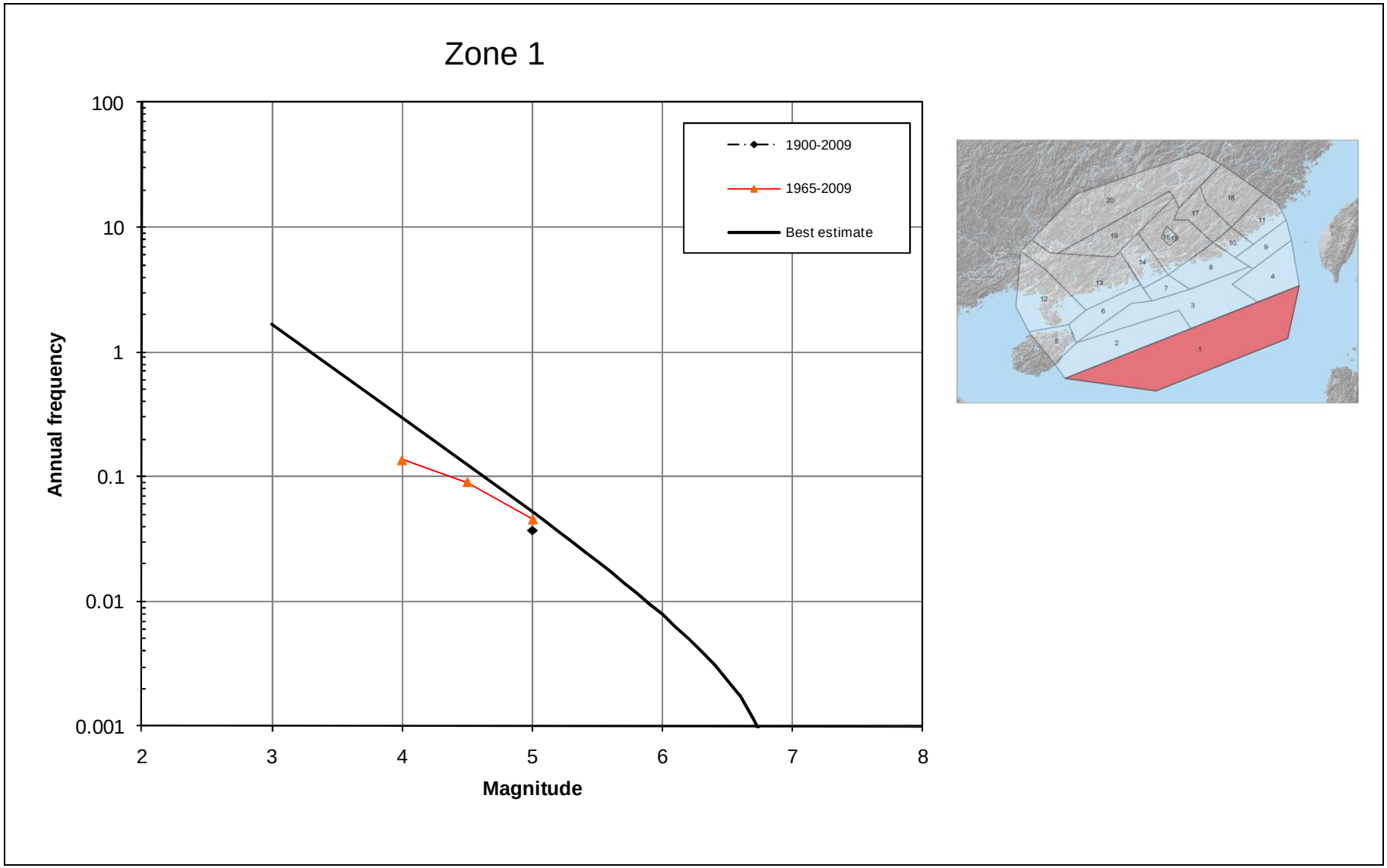

Figure 3.29 Arup Earthquake Recurrence Plot for Zone 1

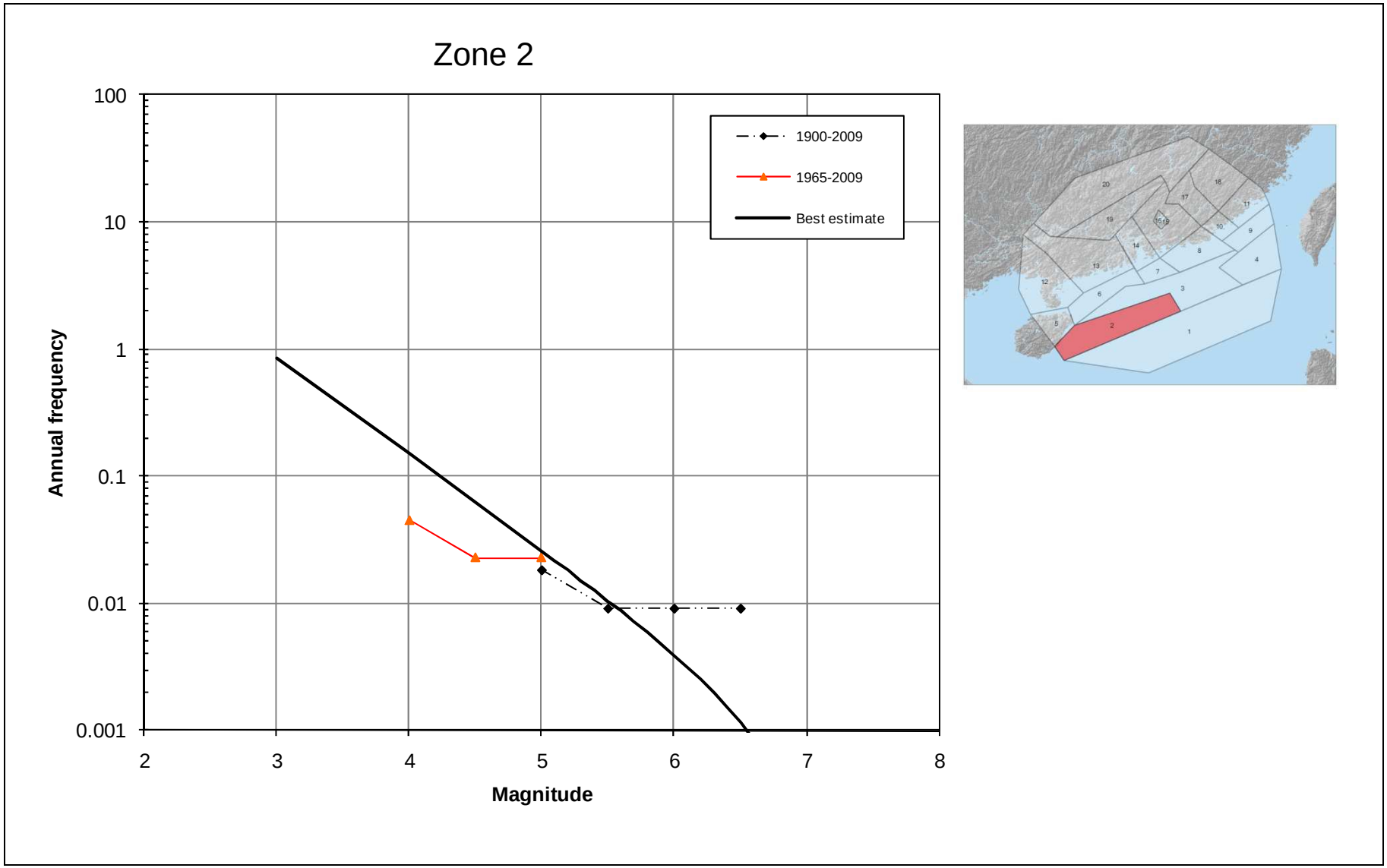

Figure 3.30 Arup Earthquake Recurrence Plot for Zone 2

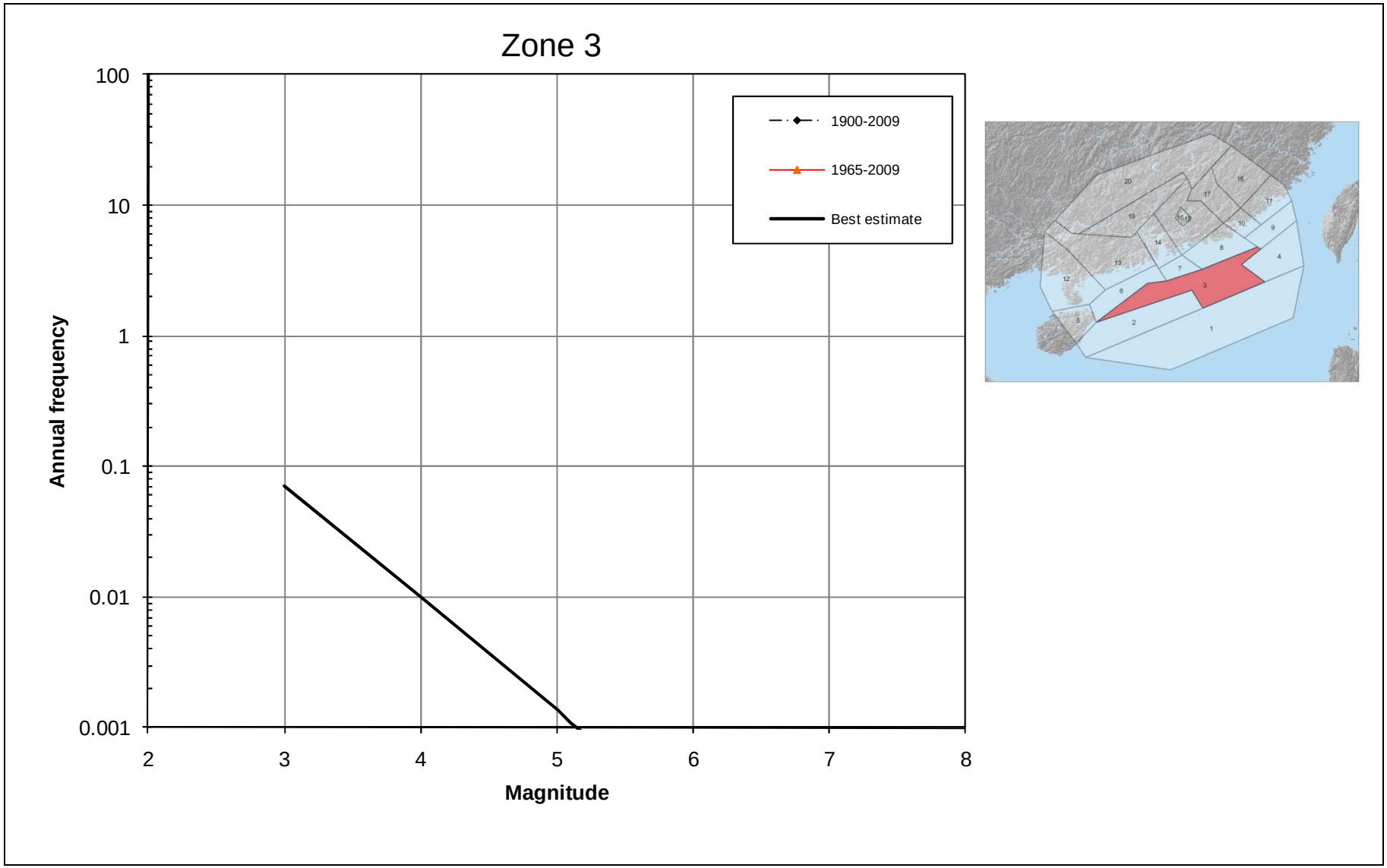

Figure 3.31 Arup Earthquake Recurrence Plot for Zone 3

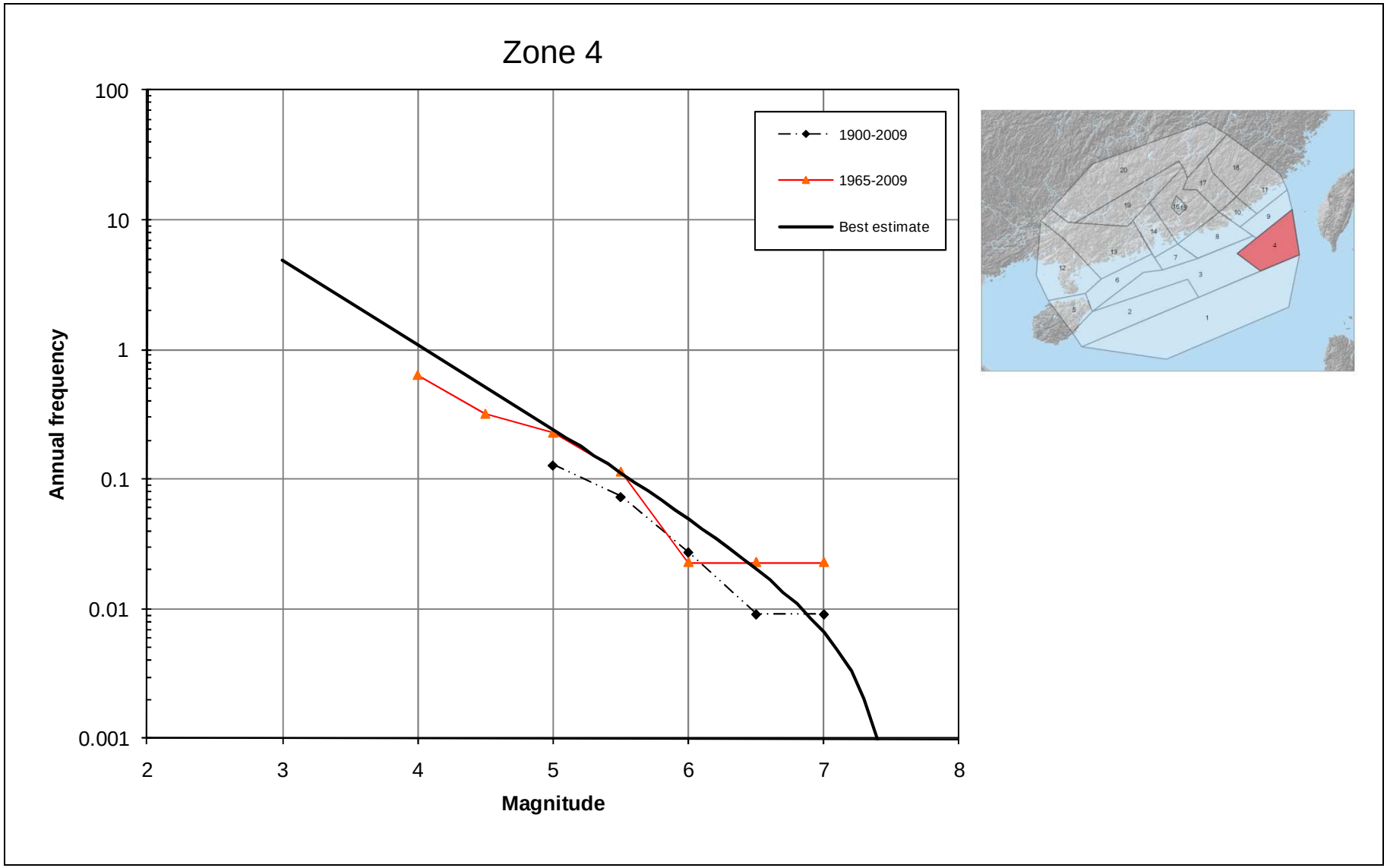

Figure 3.32 Arup Earthquake Recurrence Plot for Zone 4

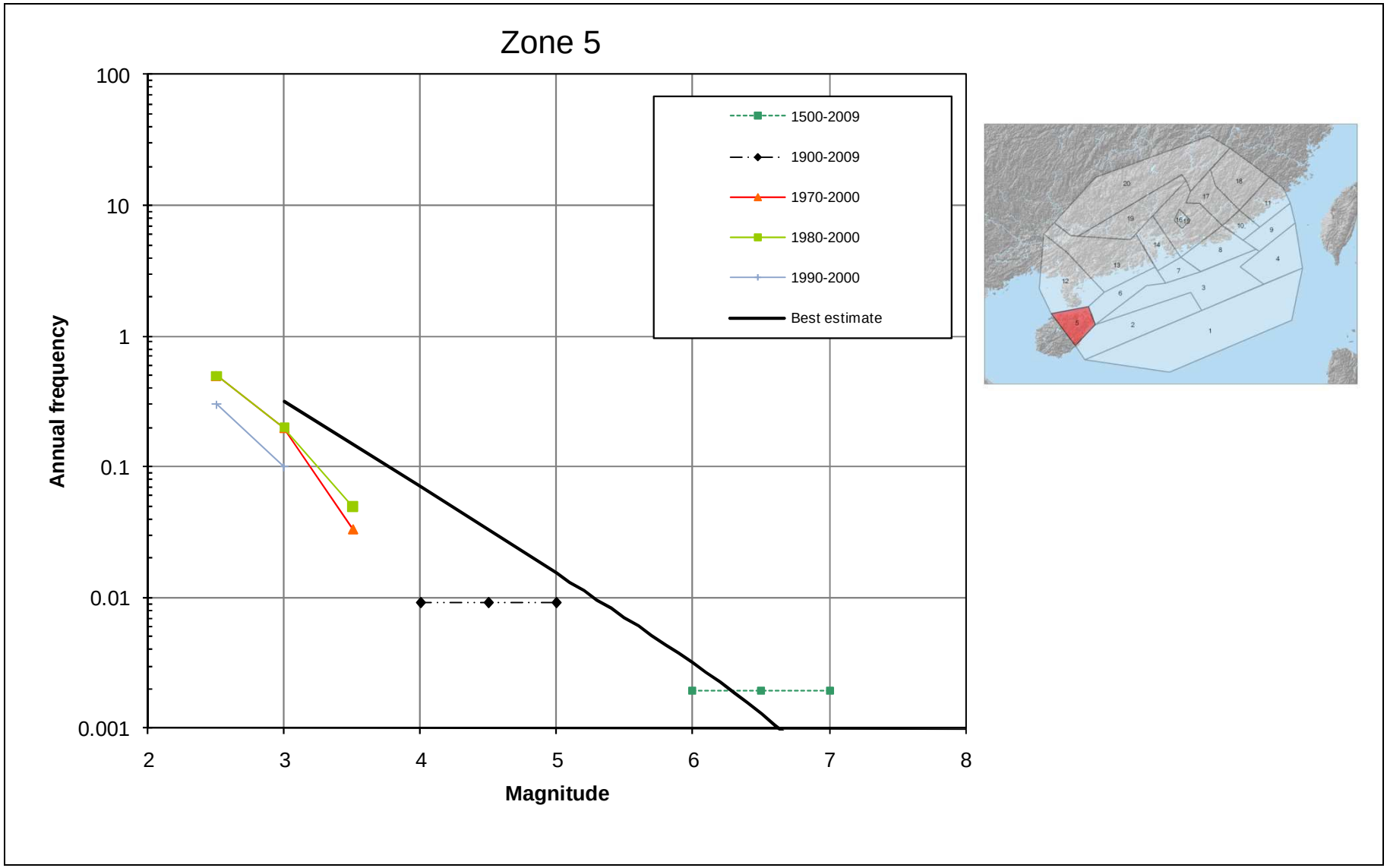

Figure 3.33 Arup Earthquake Recurrence Plot for Zone 5

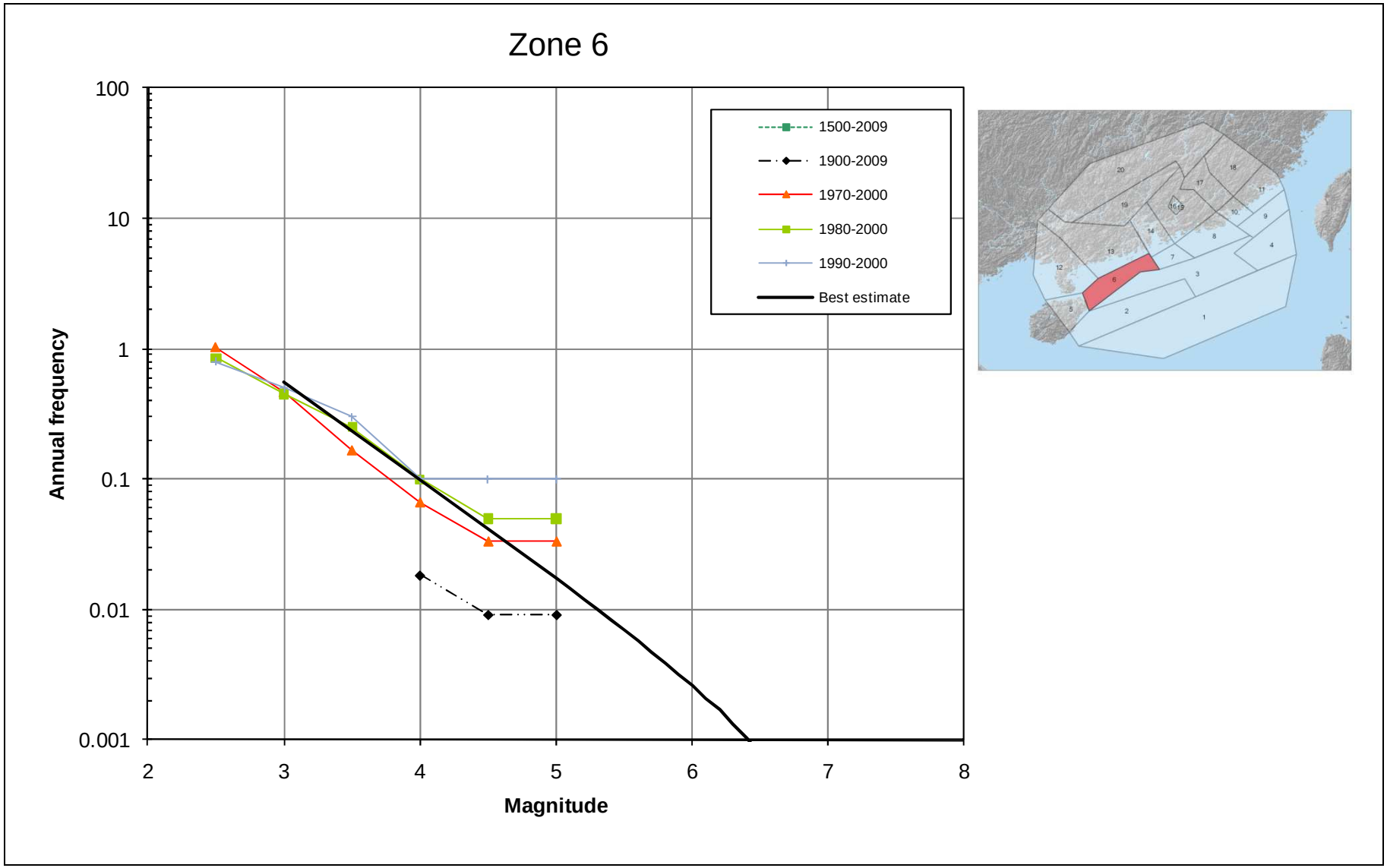

Figure 3.34 Arup Earthquake Recurrence Plot for Zone 6

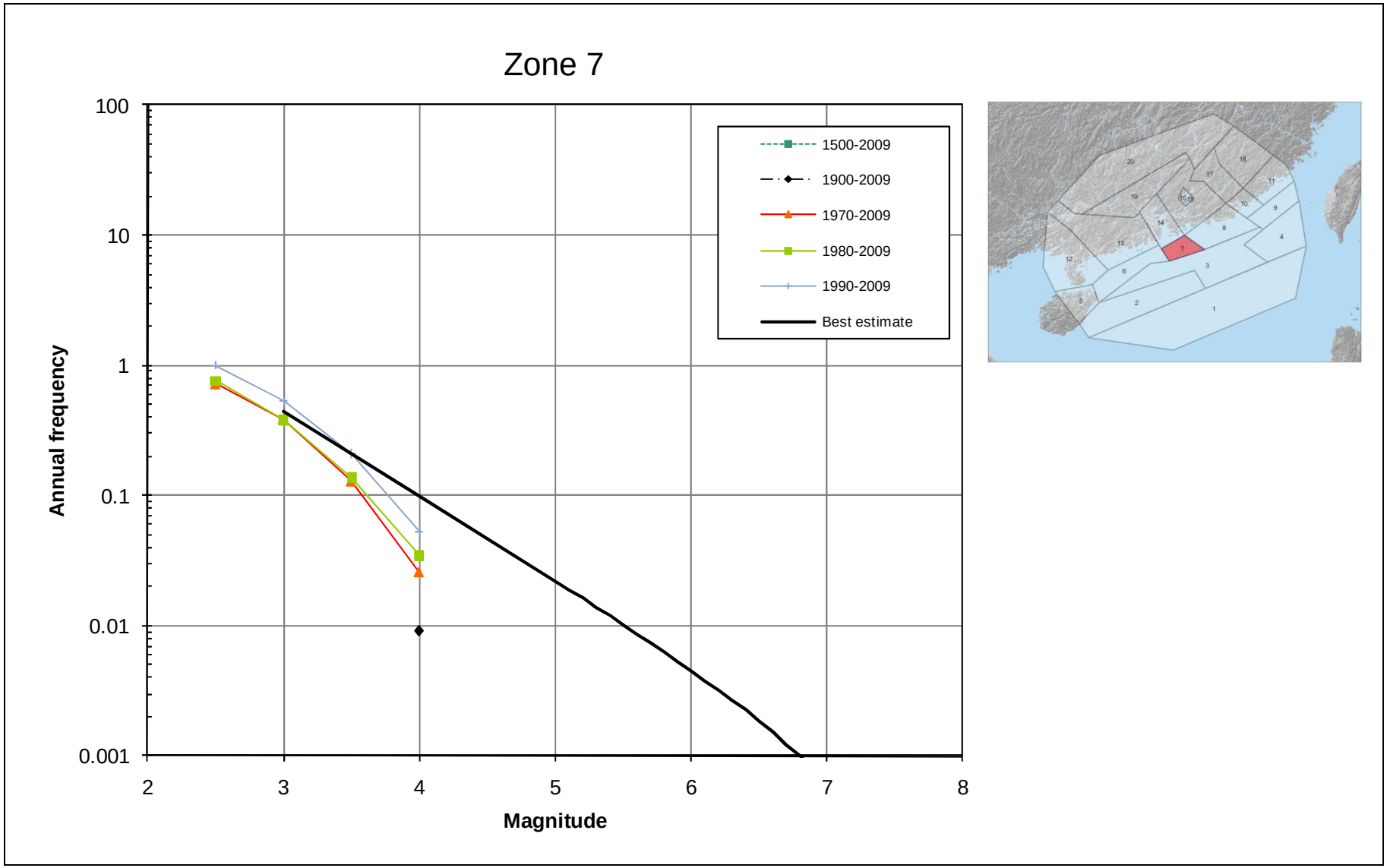

Figure 3.35 Arup Earthquake Recurrence Plot for Zone 7

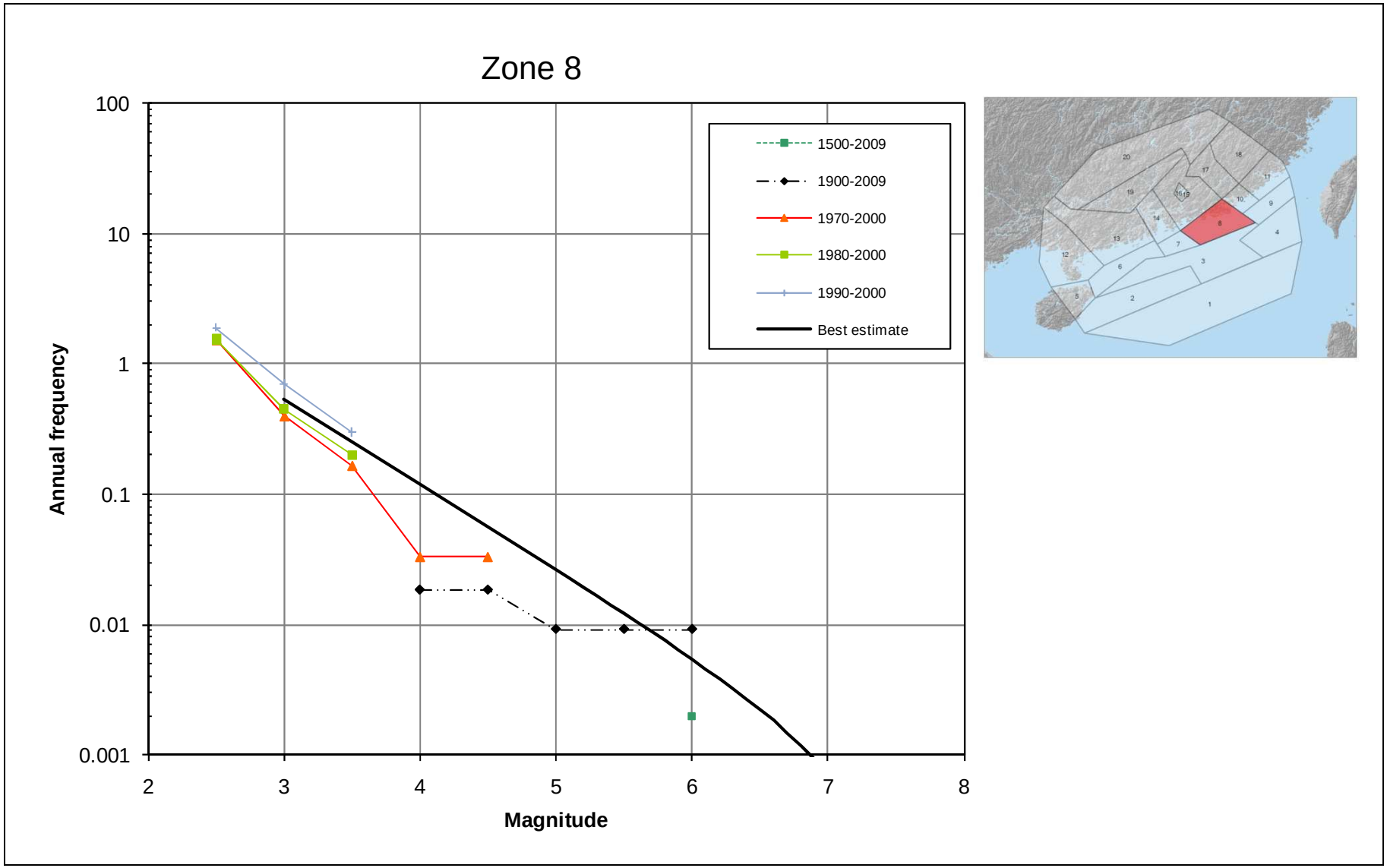

Figure 3.36 Arup Earthquake Recurrence Plot for Zone 8

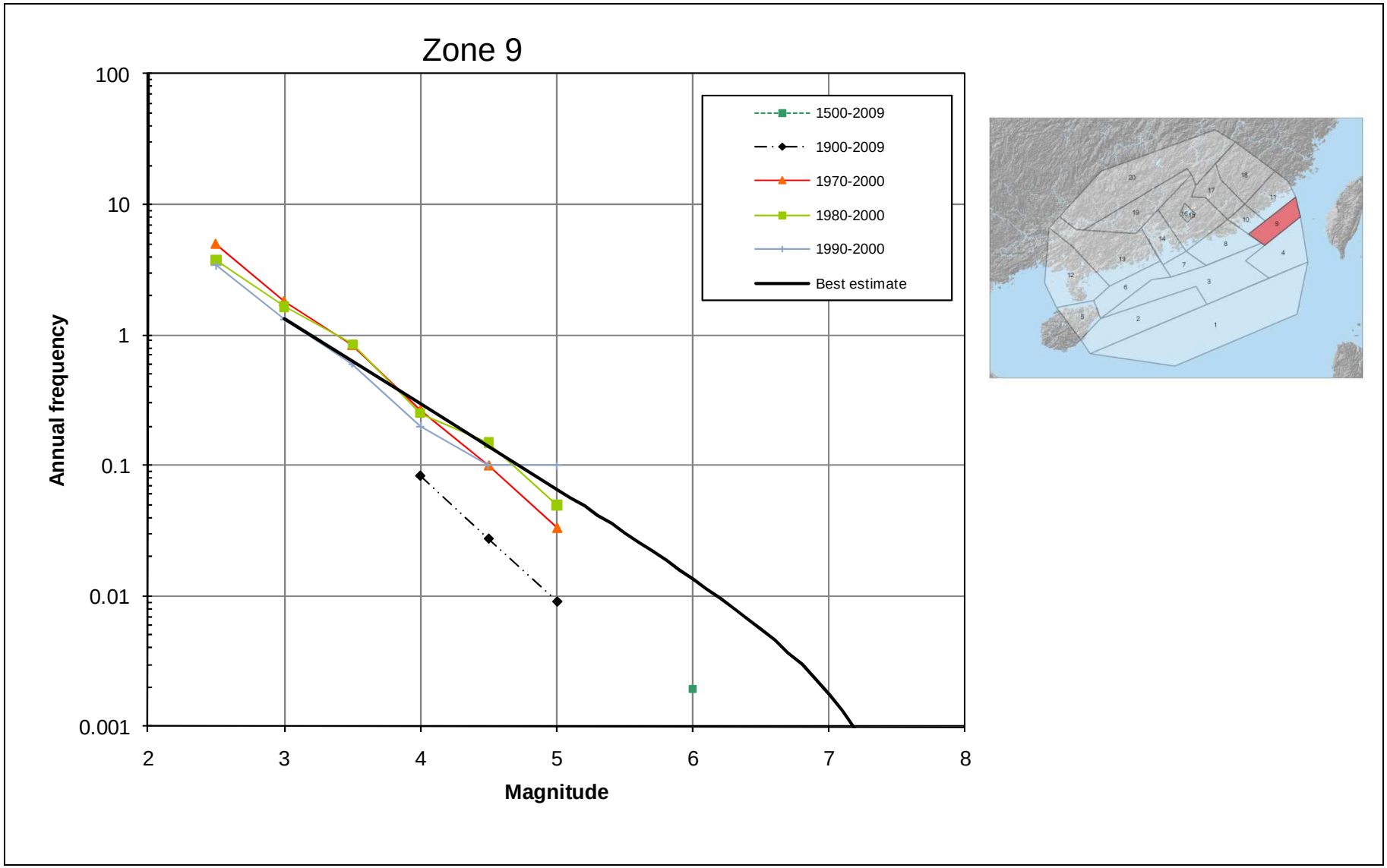

Figure 3.37 Arup Earthquake Recurrence Plot for Zone 9

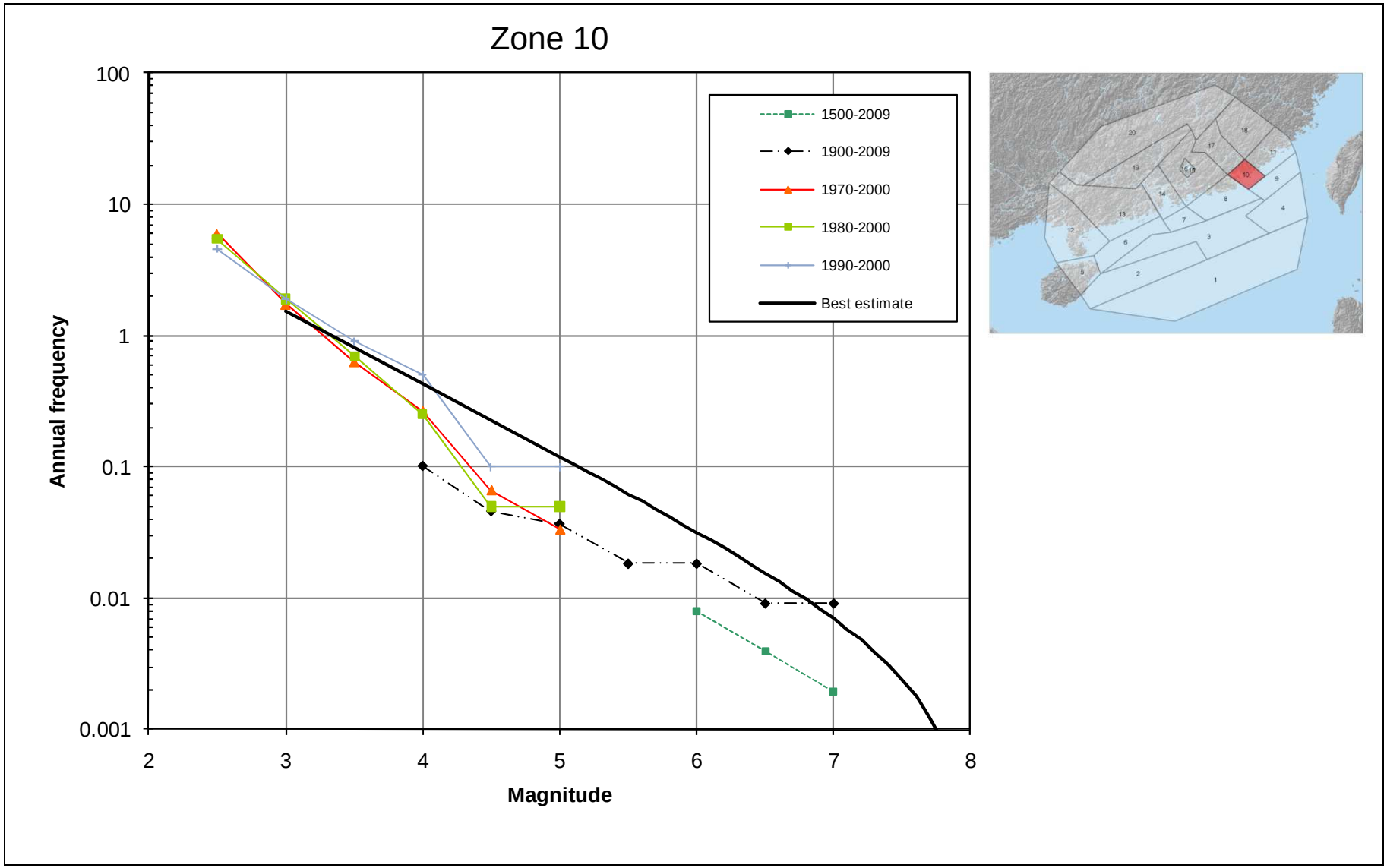

Figure 3.38 Arup Earthquake Recurrence Plot for Zone 10

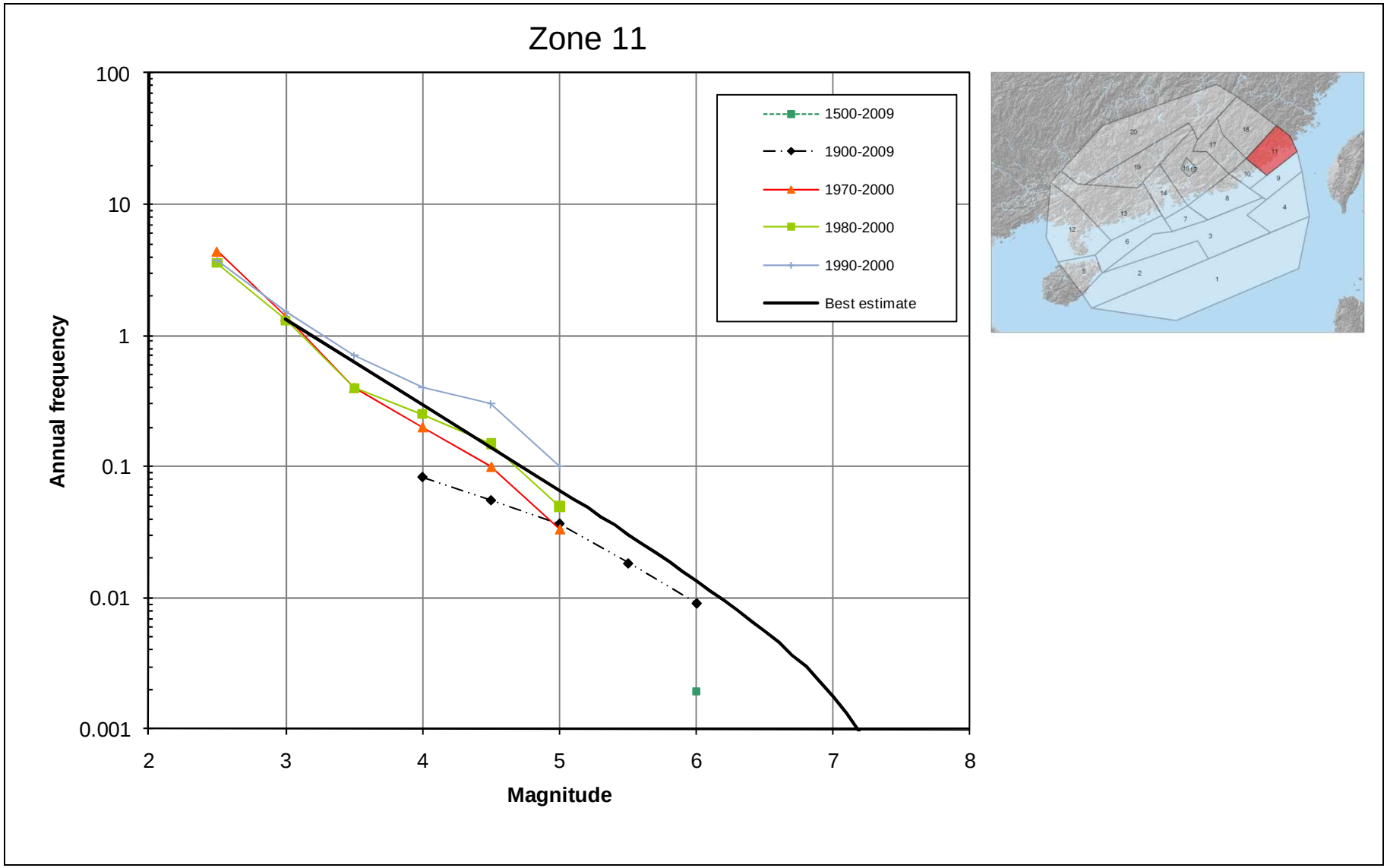

Figure 3.39 Arup Earthquake Recurrence Plot for Zone 11

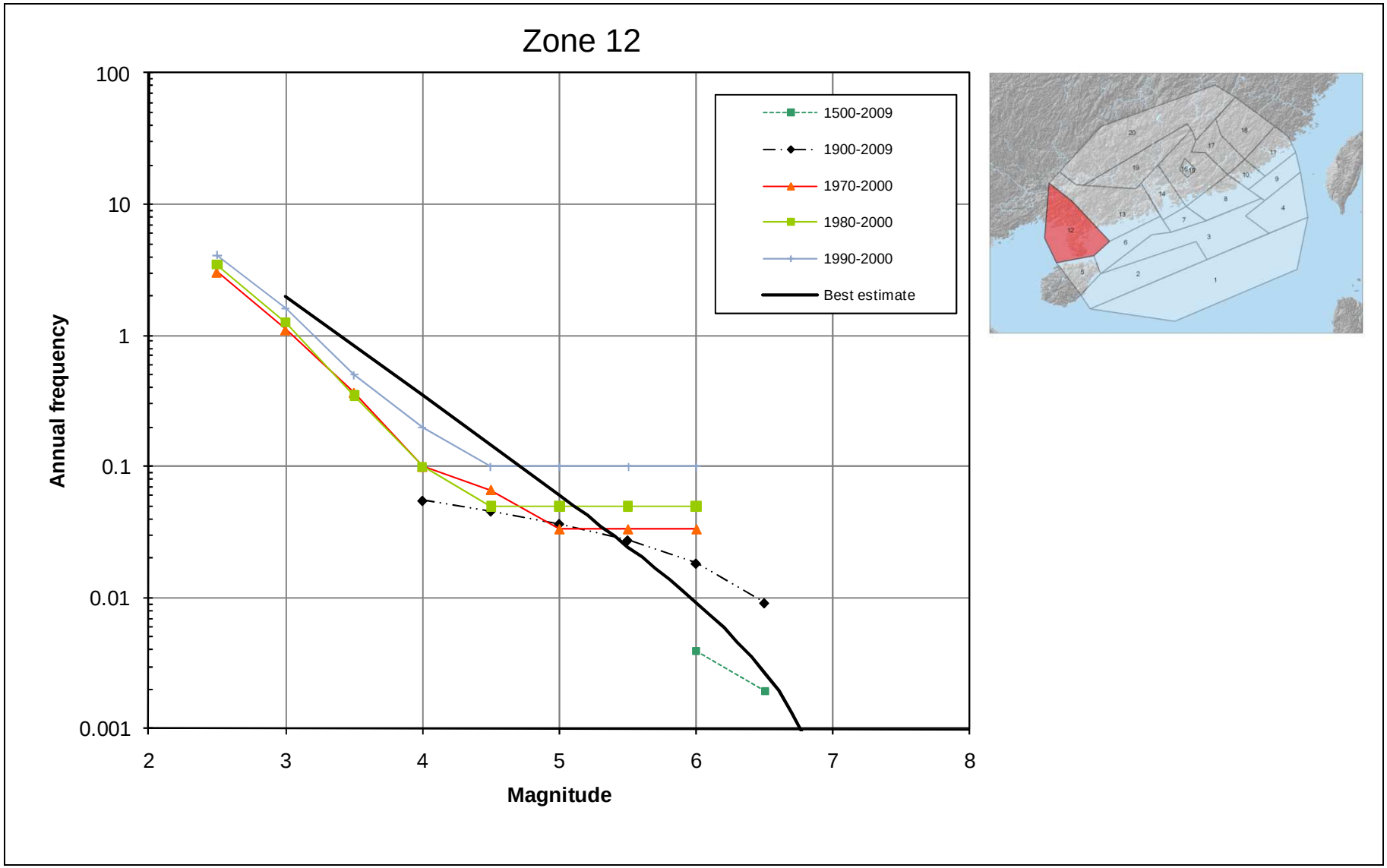

Figure 3.40 Arup Earthquake Recurrence Plot for Zone 12

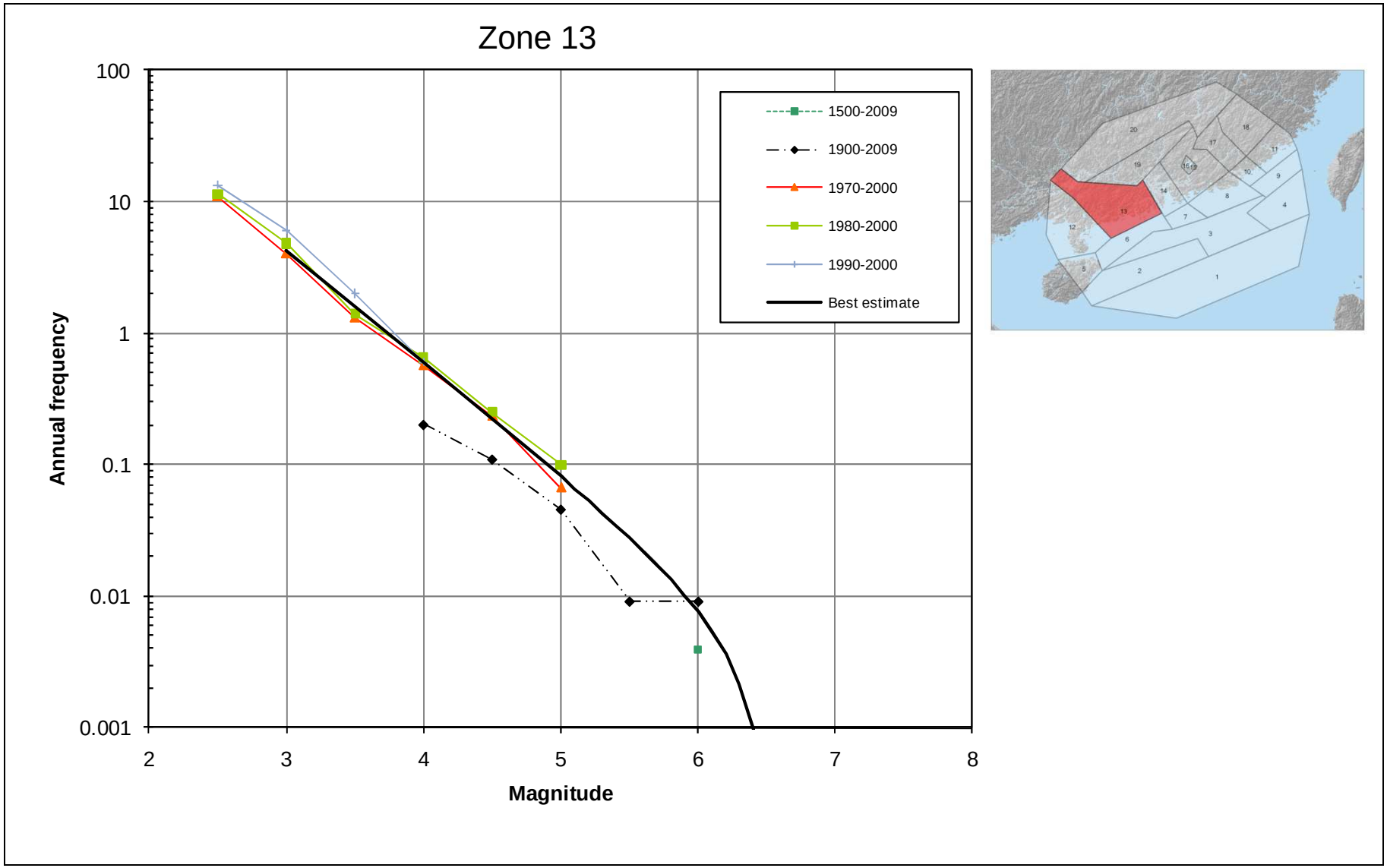

Figure 3.41 Arup Earthquake Recurrence Plot for Zone 13

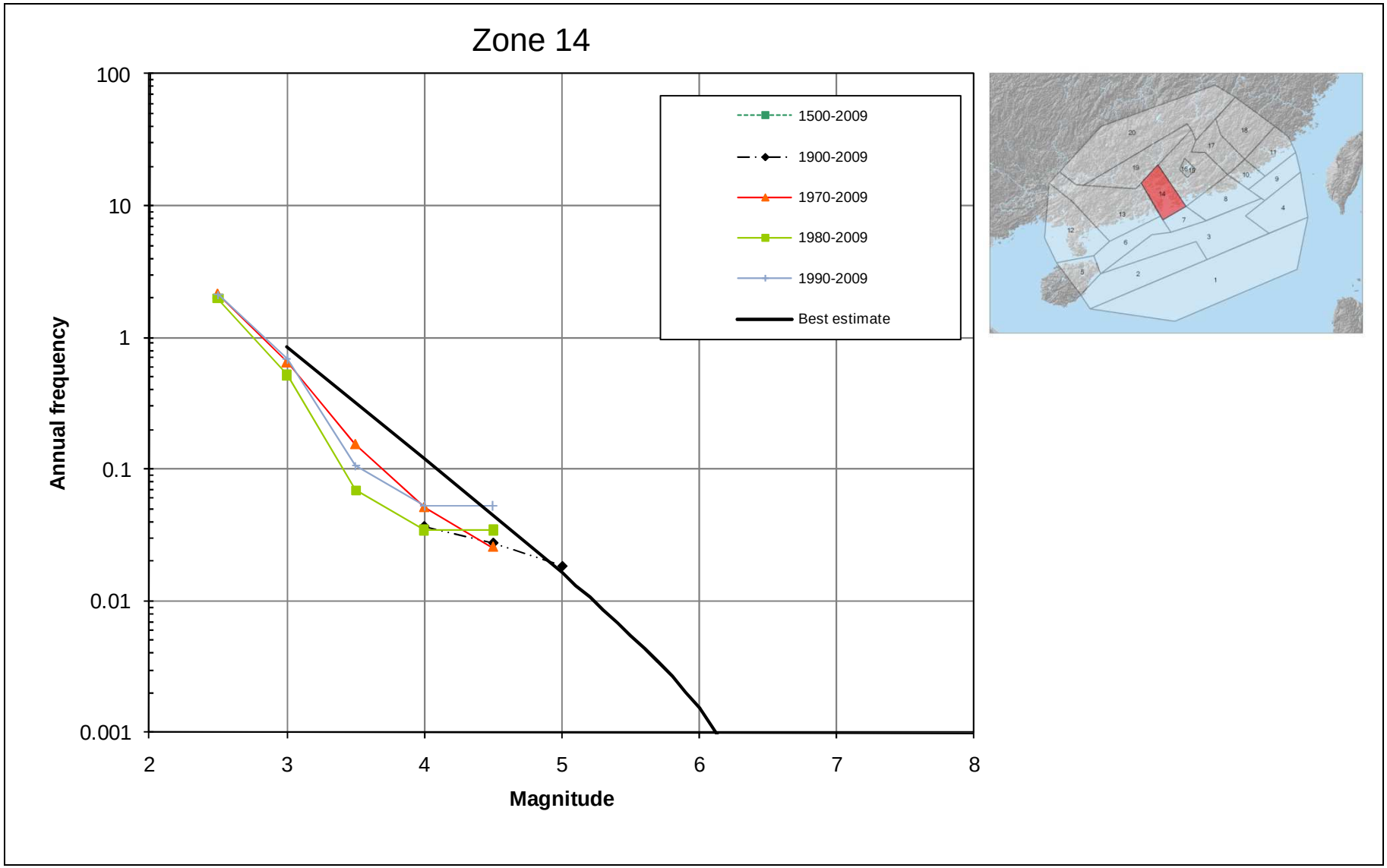

Figure 3.42 Arup Earthquake Recurrence Plot for Zone 14

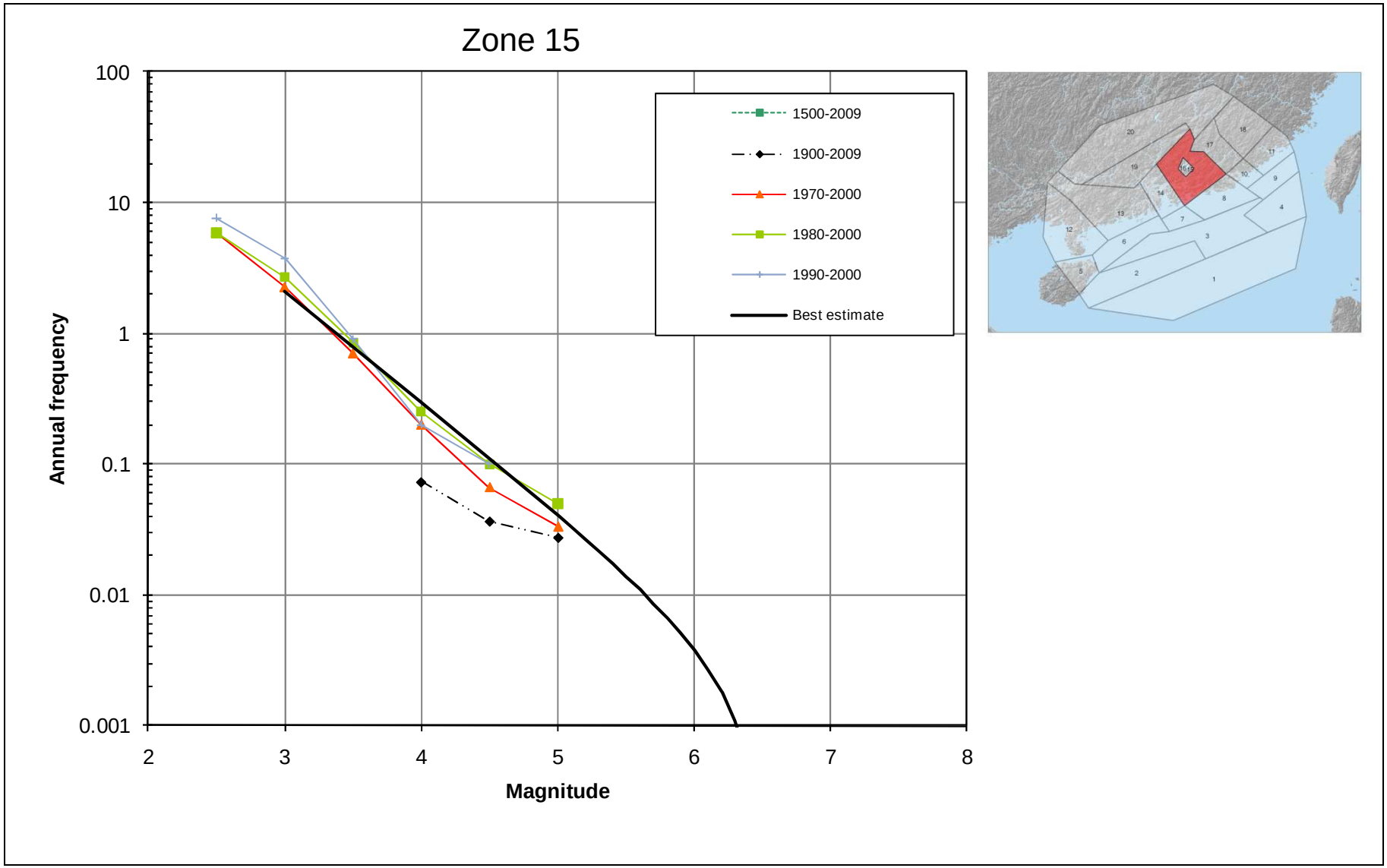

Figure 3.43 Arup Earthquake Recurrence Plot for Zone 15

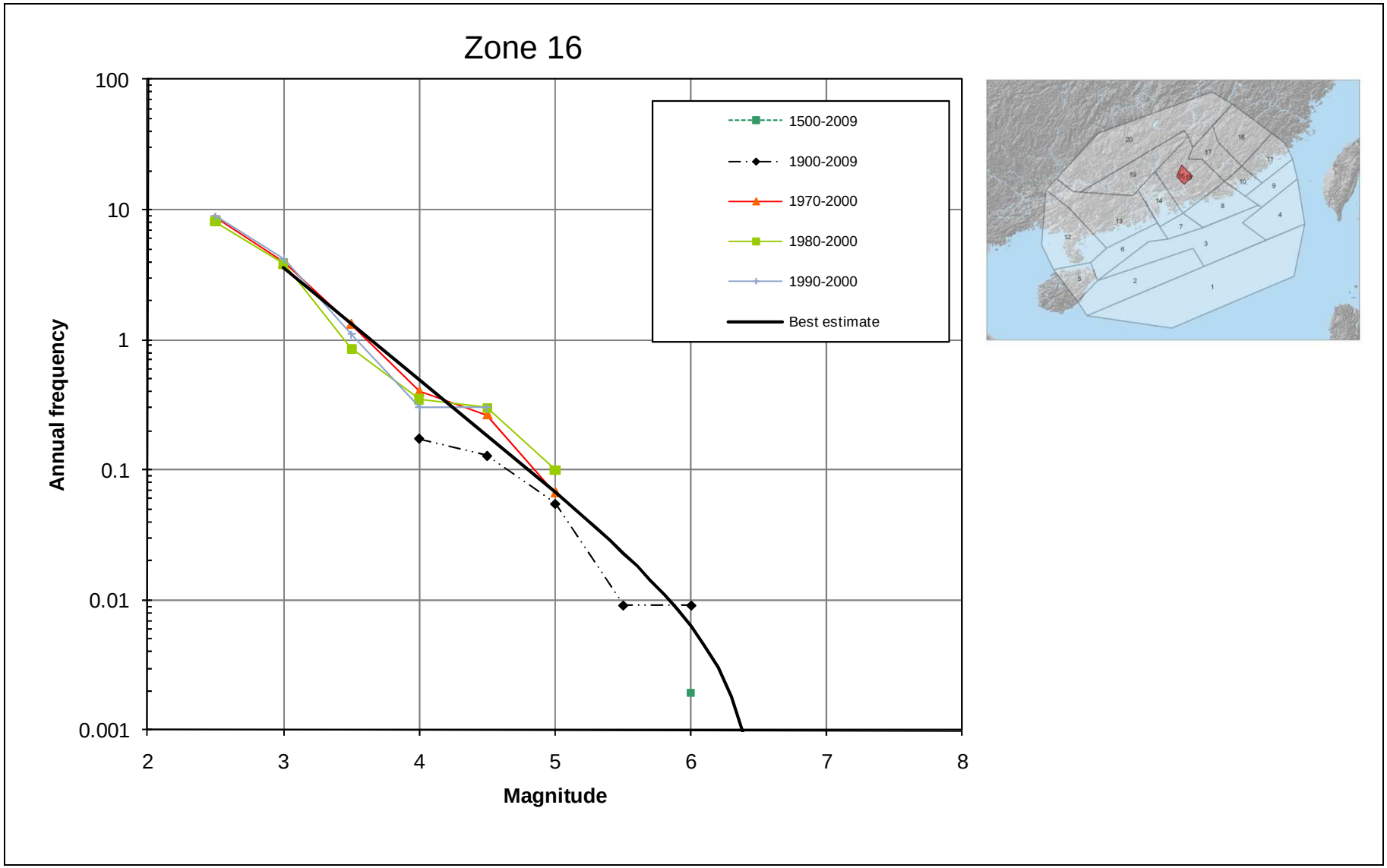

Figure 3.44 Arup Earthquake Recurrence Plot for Zone 16

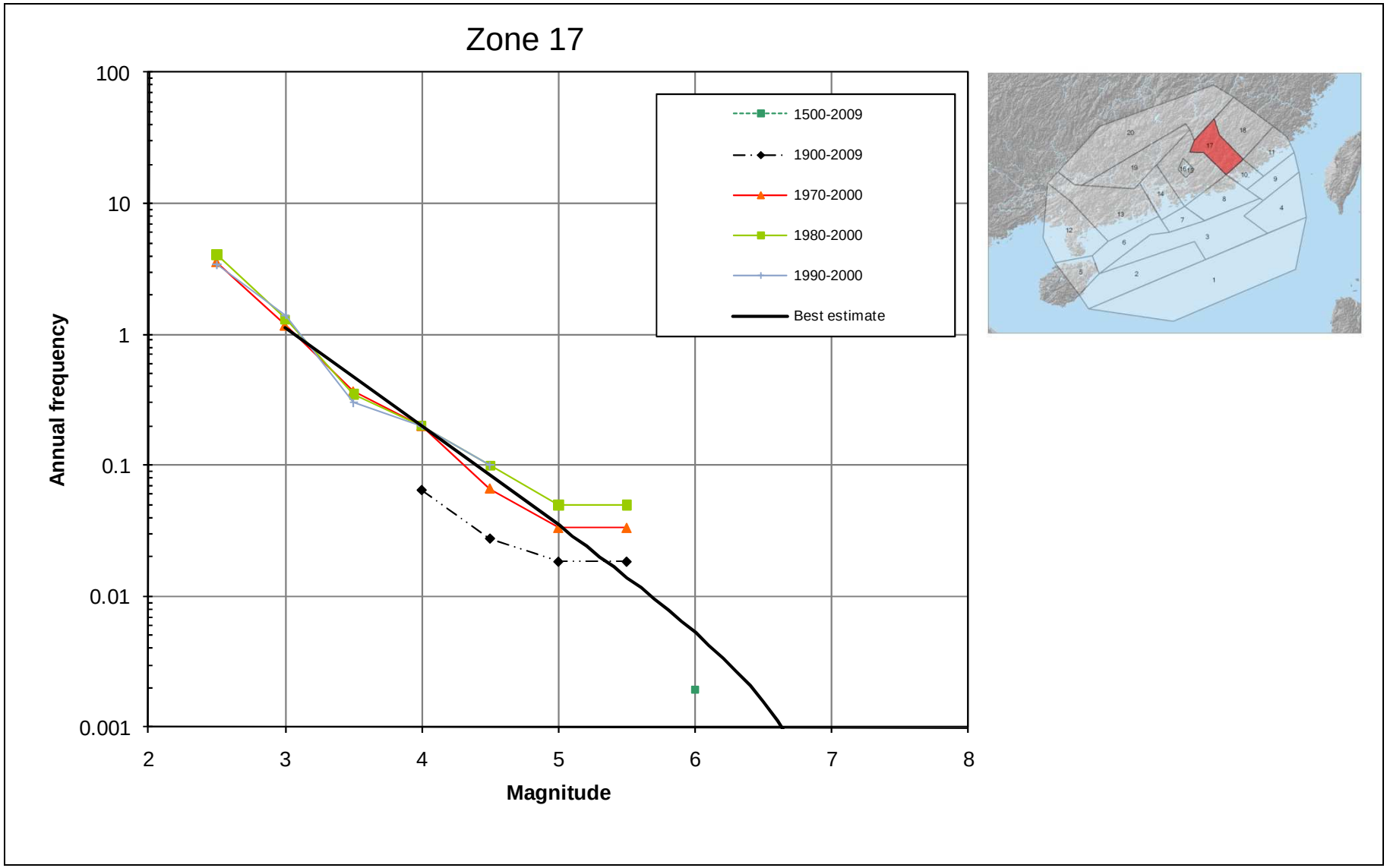

Figure 3.45 Arup Earthquake Recurrence Plot for Zone 17

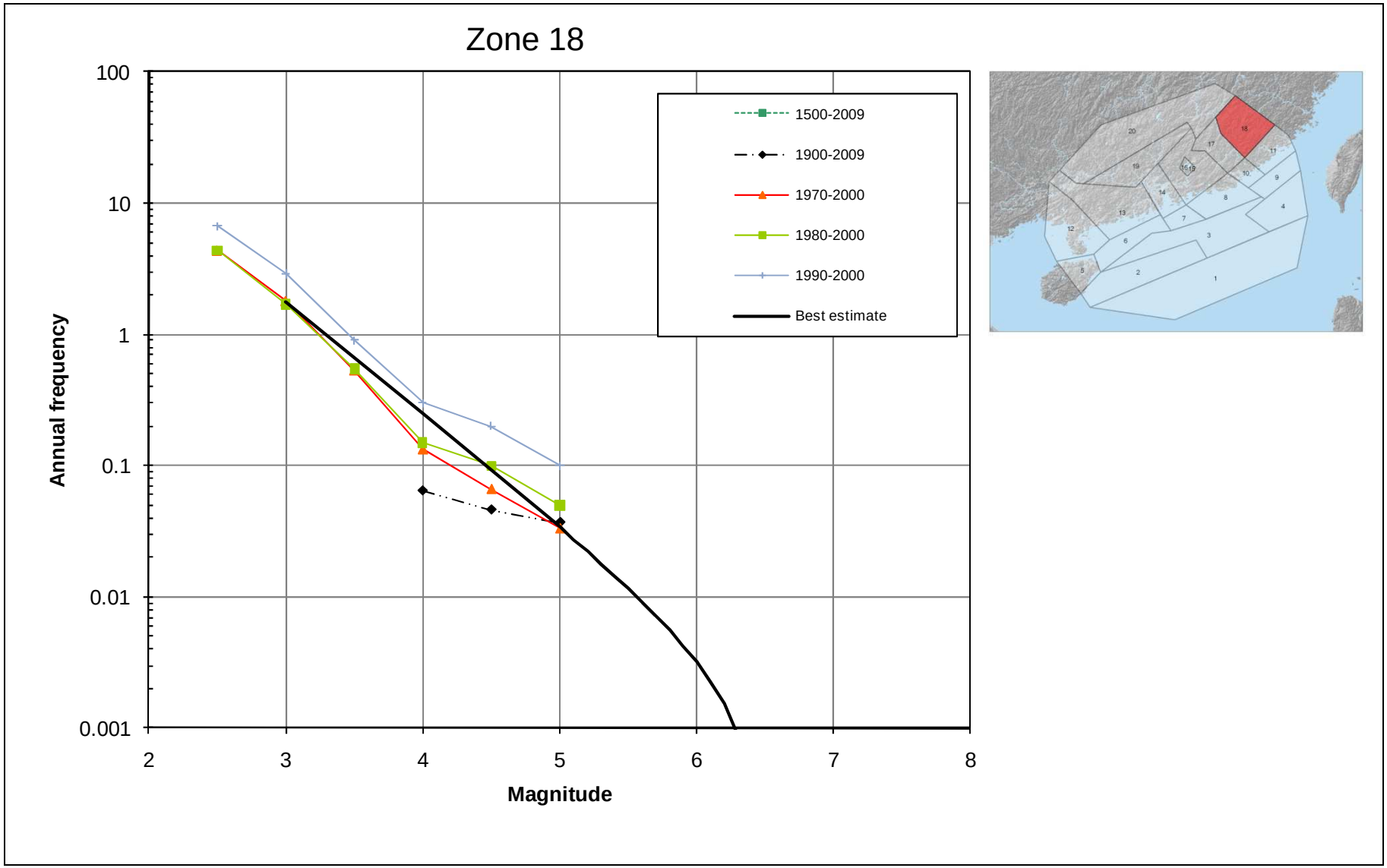

Figure 3.46 Arup Earthquake Recurrence Plot for Zone 18

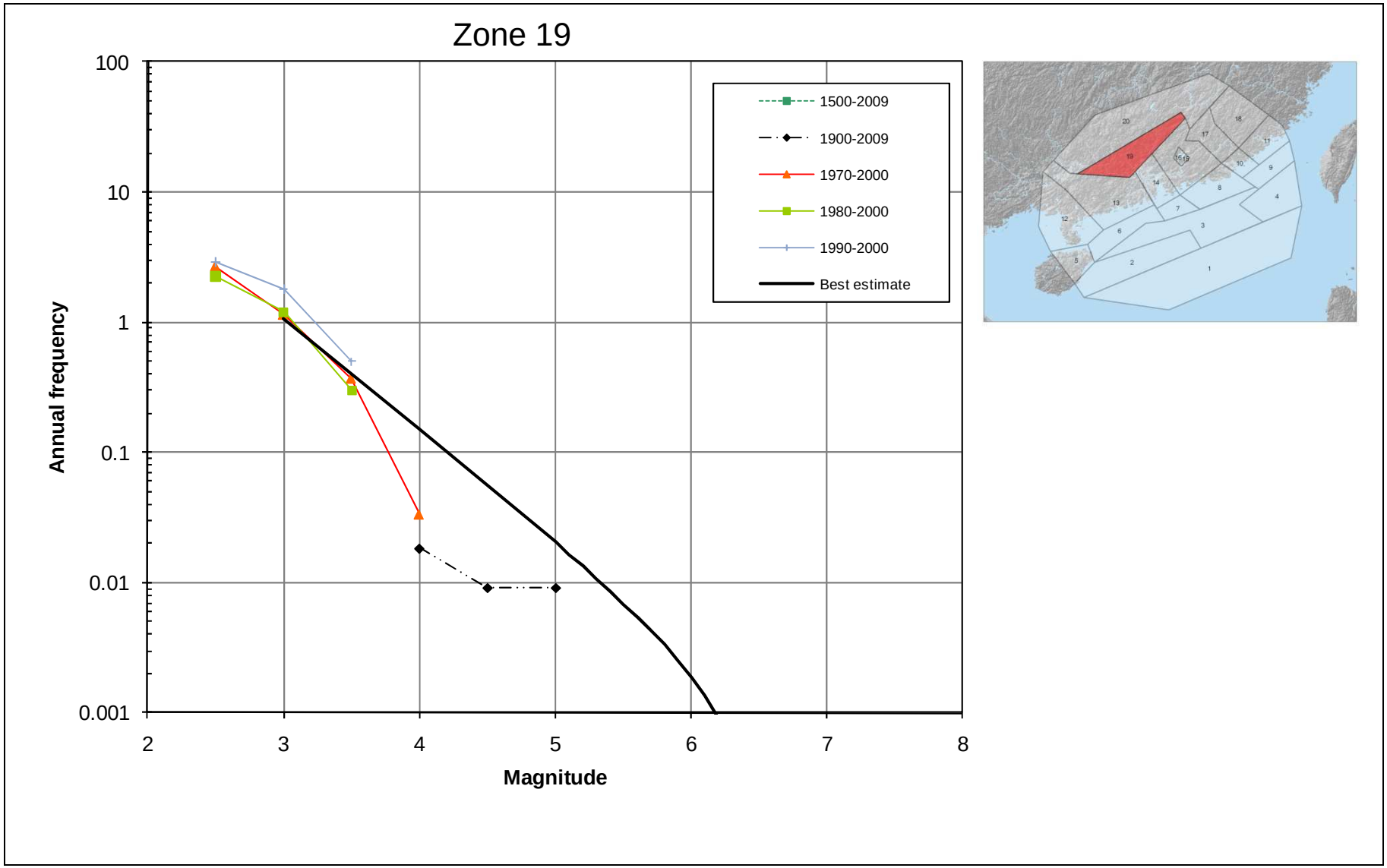

Figure 3.47 Arup Earthquake Recurrence Plot for Zone 19

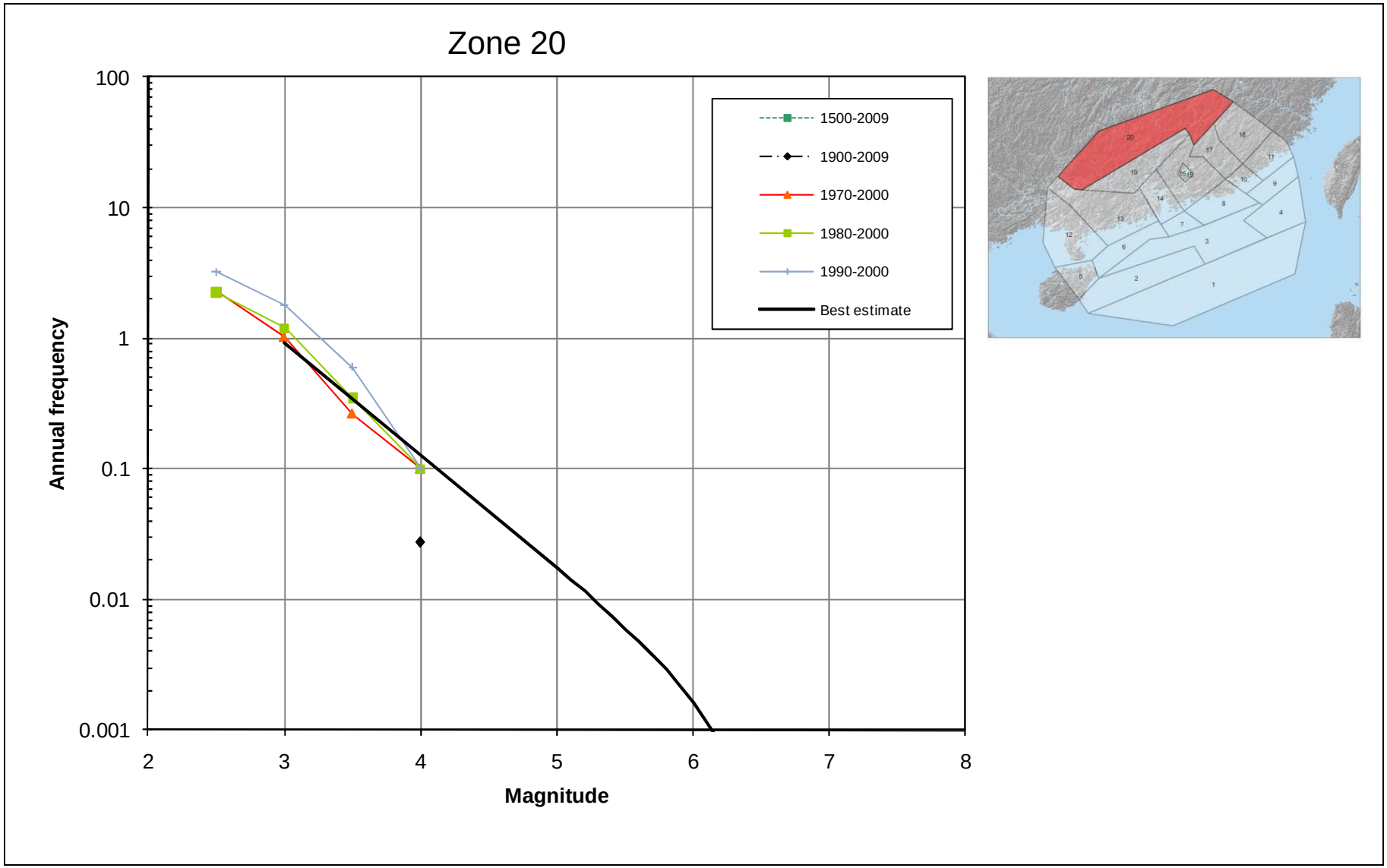

Figure 3.48 Arup Earthquake Recurrence Plot for Zone 20

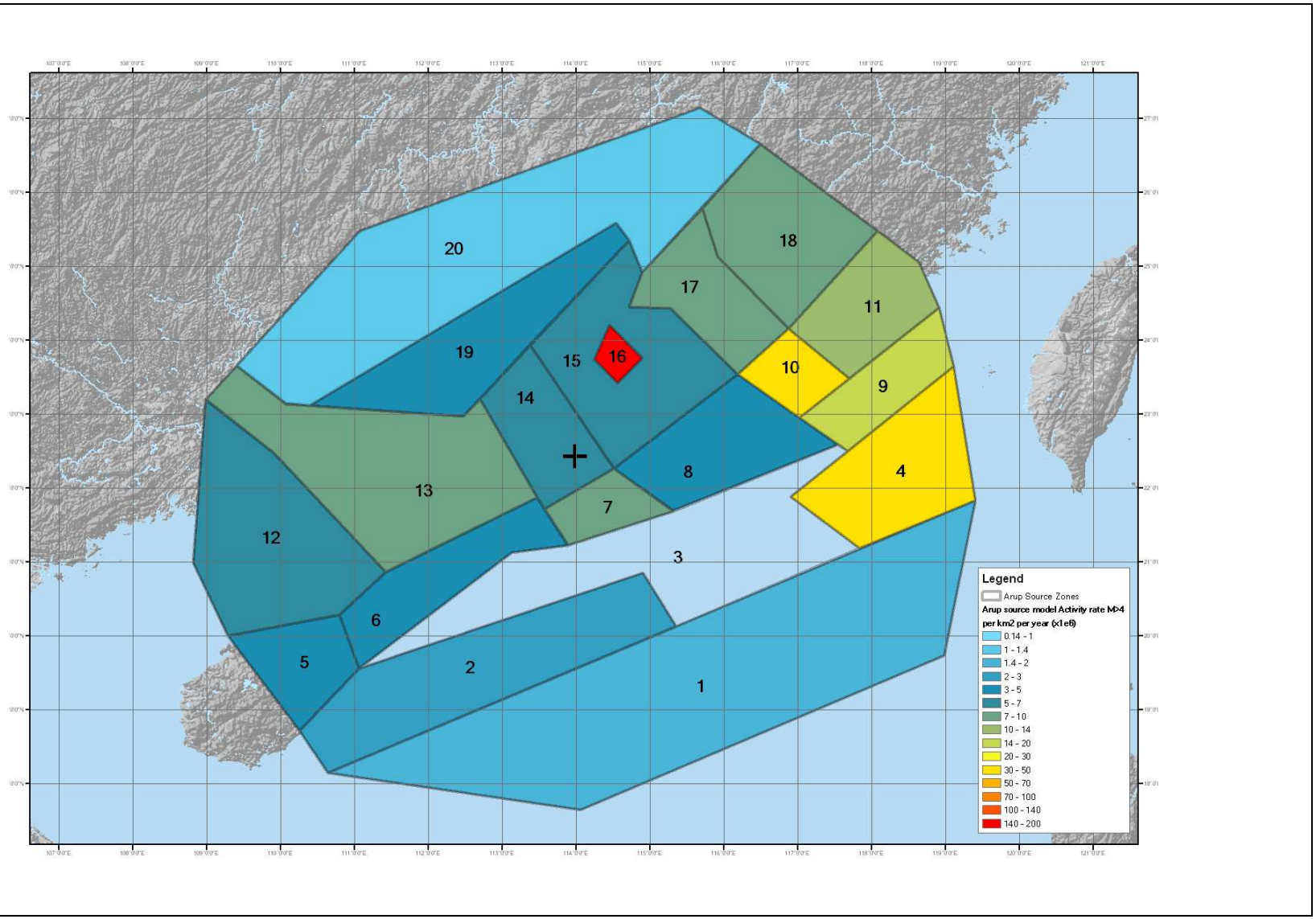

Figure 3.49 Arup Annual Activity Rate Divided by Zone Area for Earthquake Magnitude Greater than 4

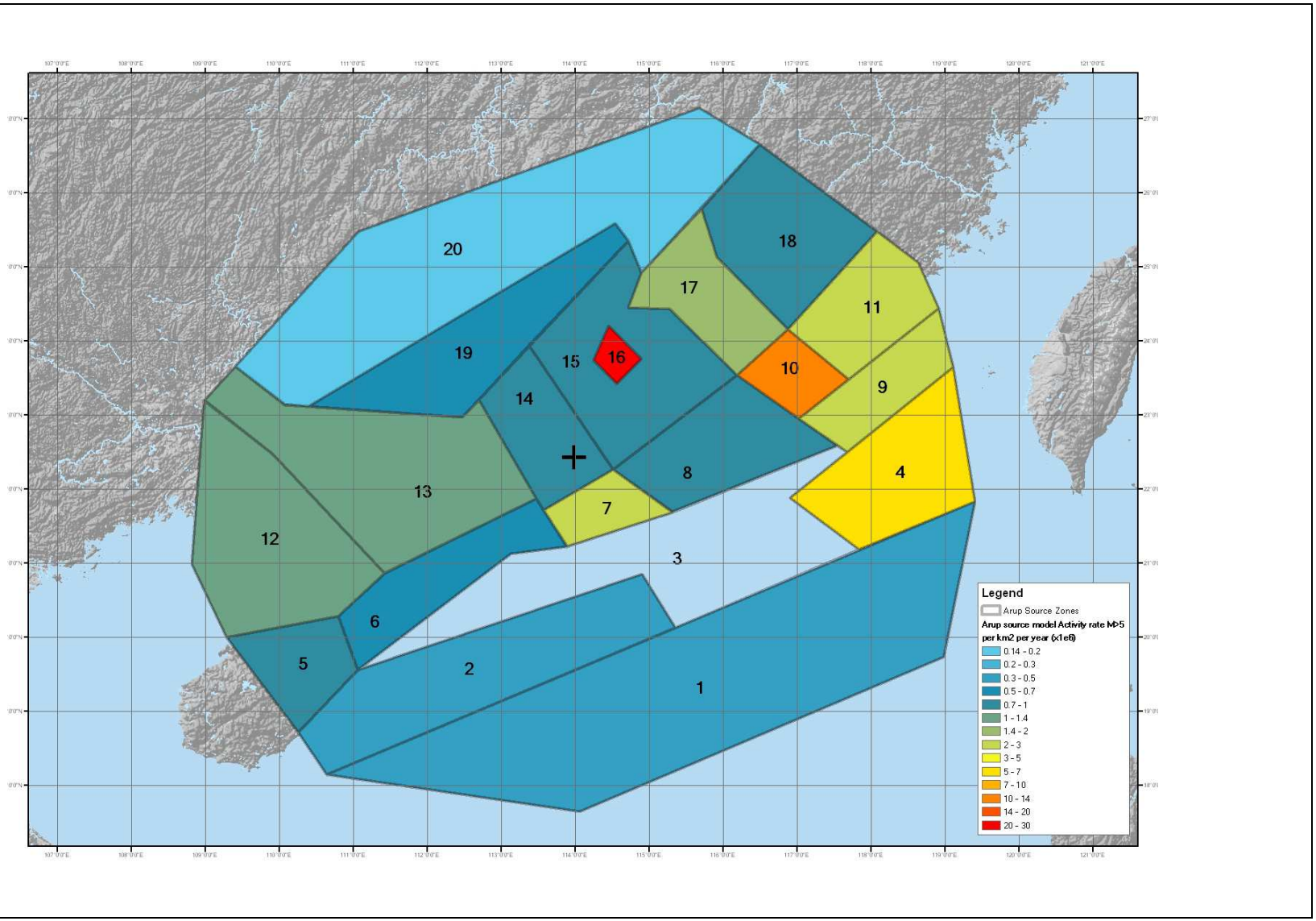

Figure 3.50 Arup Annual Activity Rate Divided by Zone Area for Earthquake Magnitude Greater than 5

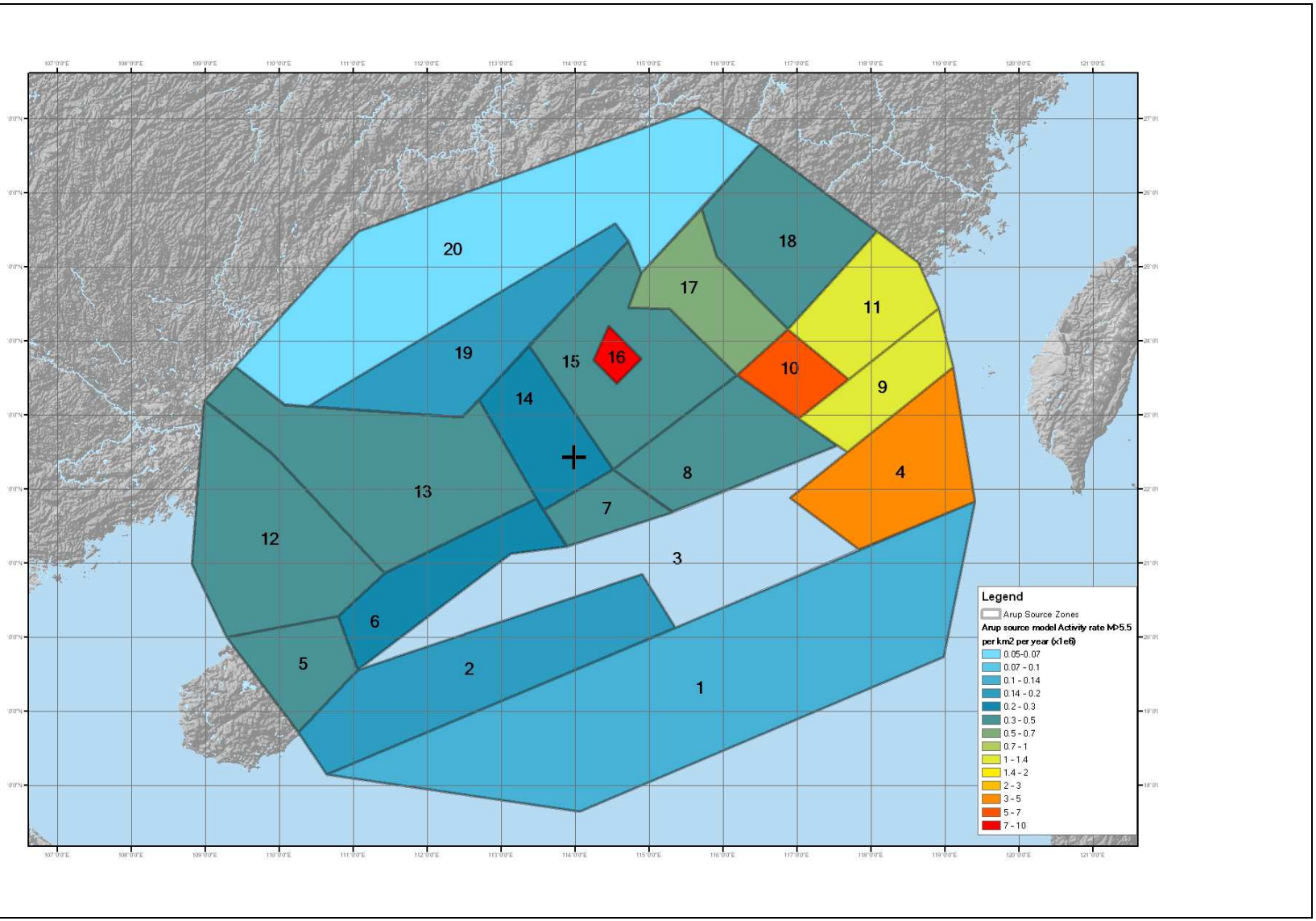

Figure 3.51 Arup Annual Activity Rate Divided by Zone Area for Earthquake Magnitude Greater than 5.5

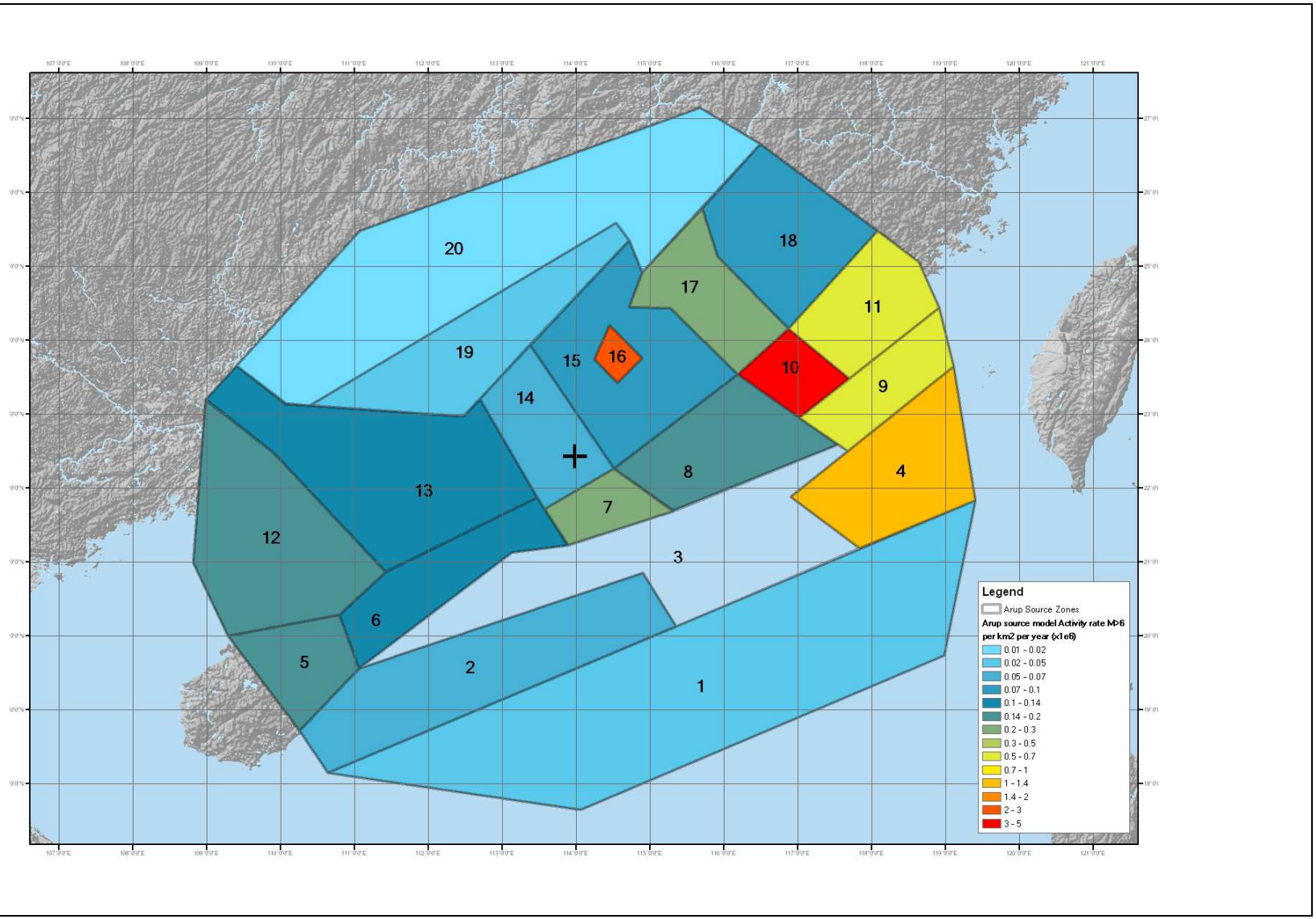

Figure 3.52 Arup Annual Activity Rate Divided by Zone Area for Earthquake Magnitude Greater than 6

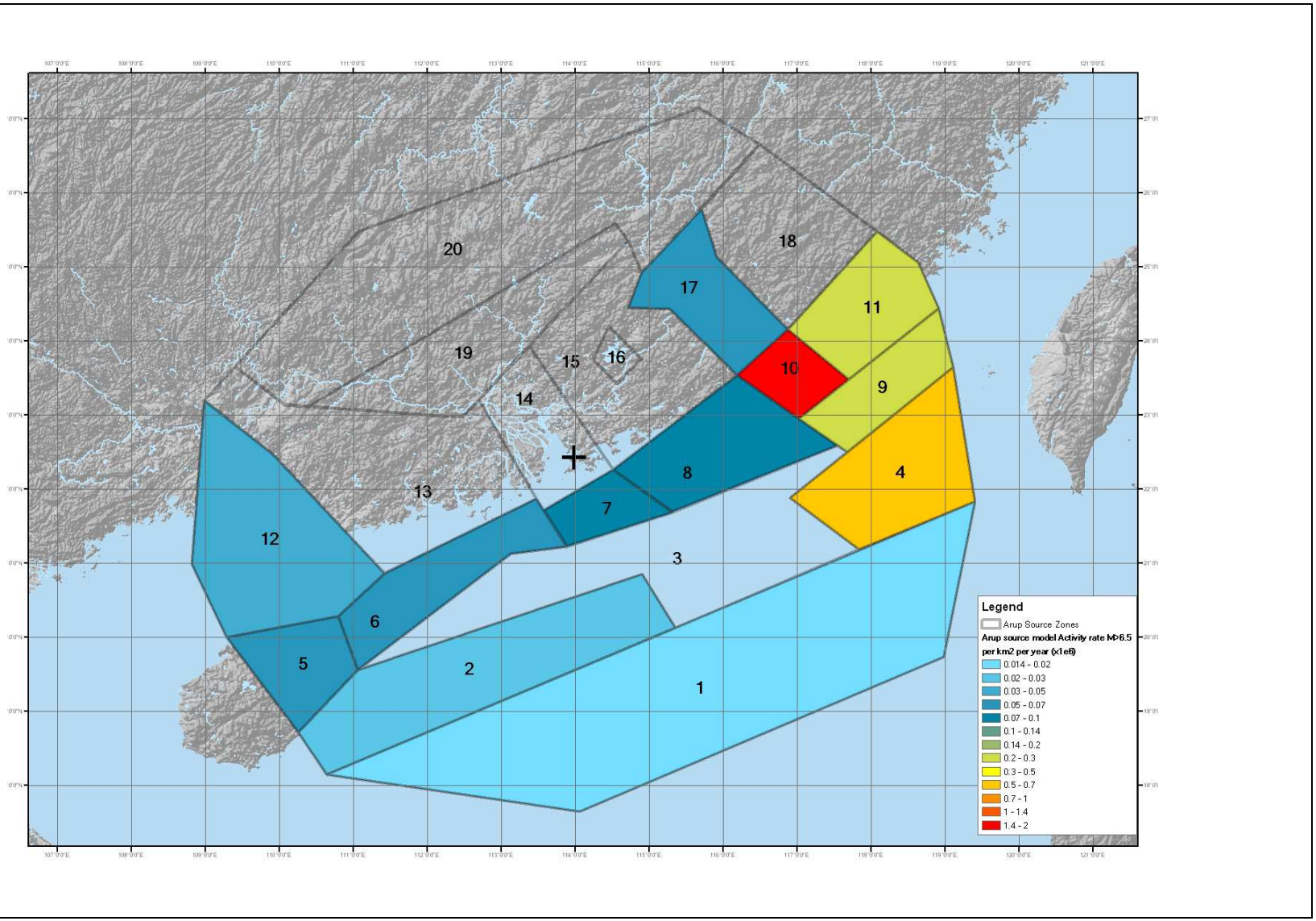

Figure 3.53 Arup Annual Activity Rate Divided by Zone Area for Earthquake Magnitude Greater than 6.5

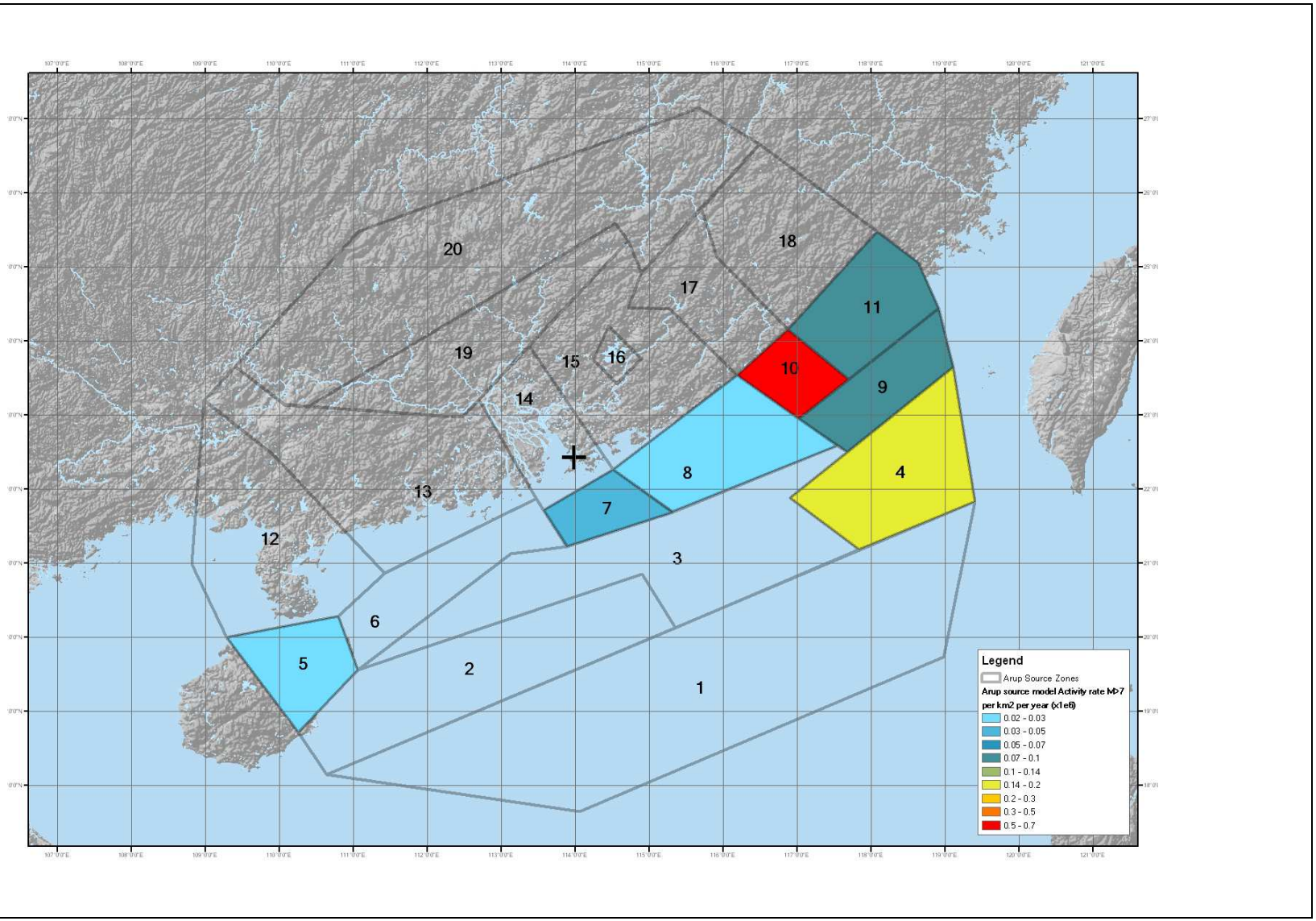

Figure 3.54 Arup Annual Activity Rate Divided by Zone Area for Earthquake Magnitude Greater than 7

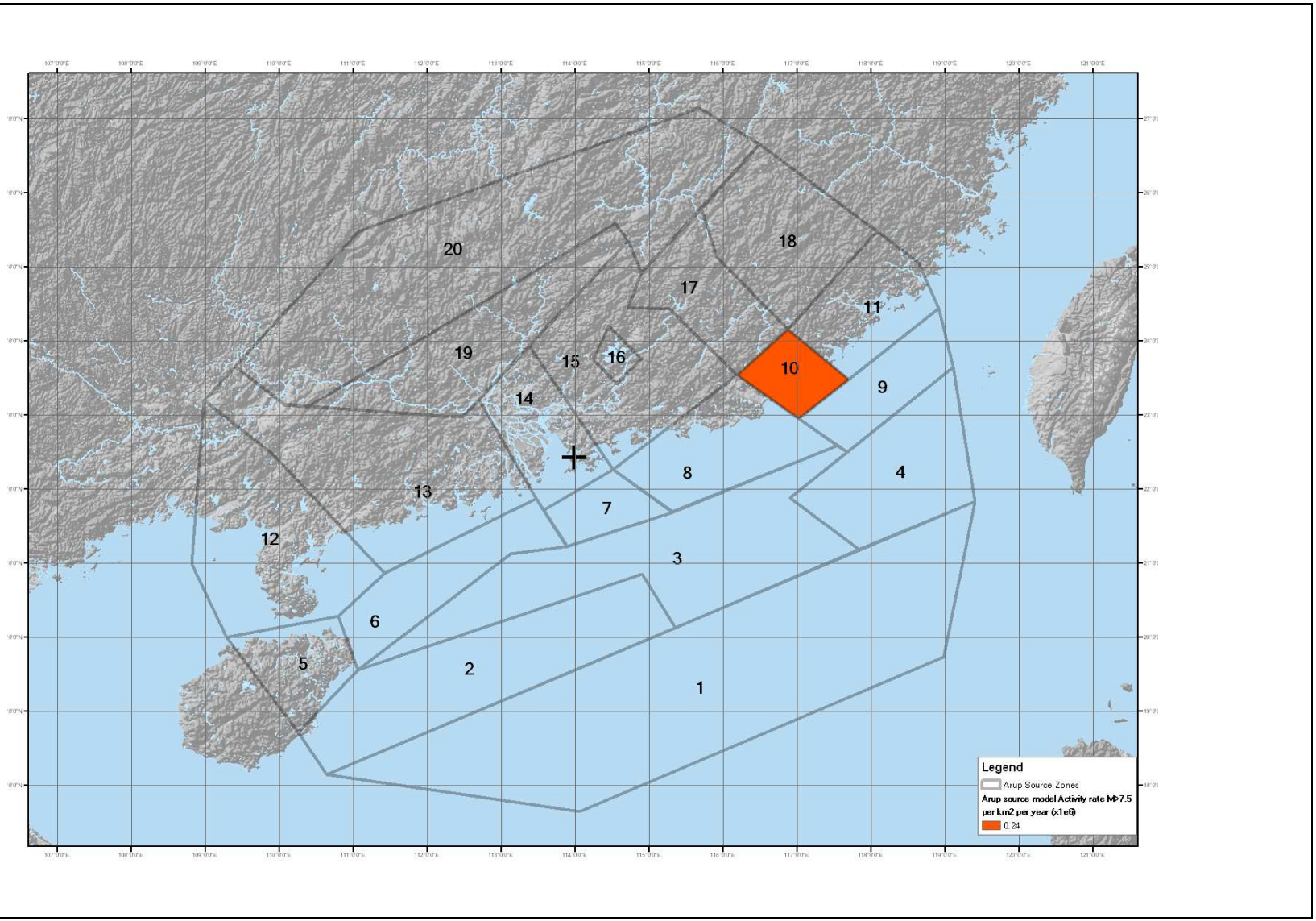

Figure 3.55 Arup Annual Activity Rate Divided by Zone Area for Earthquake Magnitude Greater than 7.5

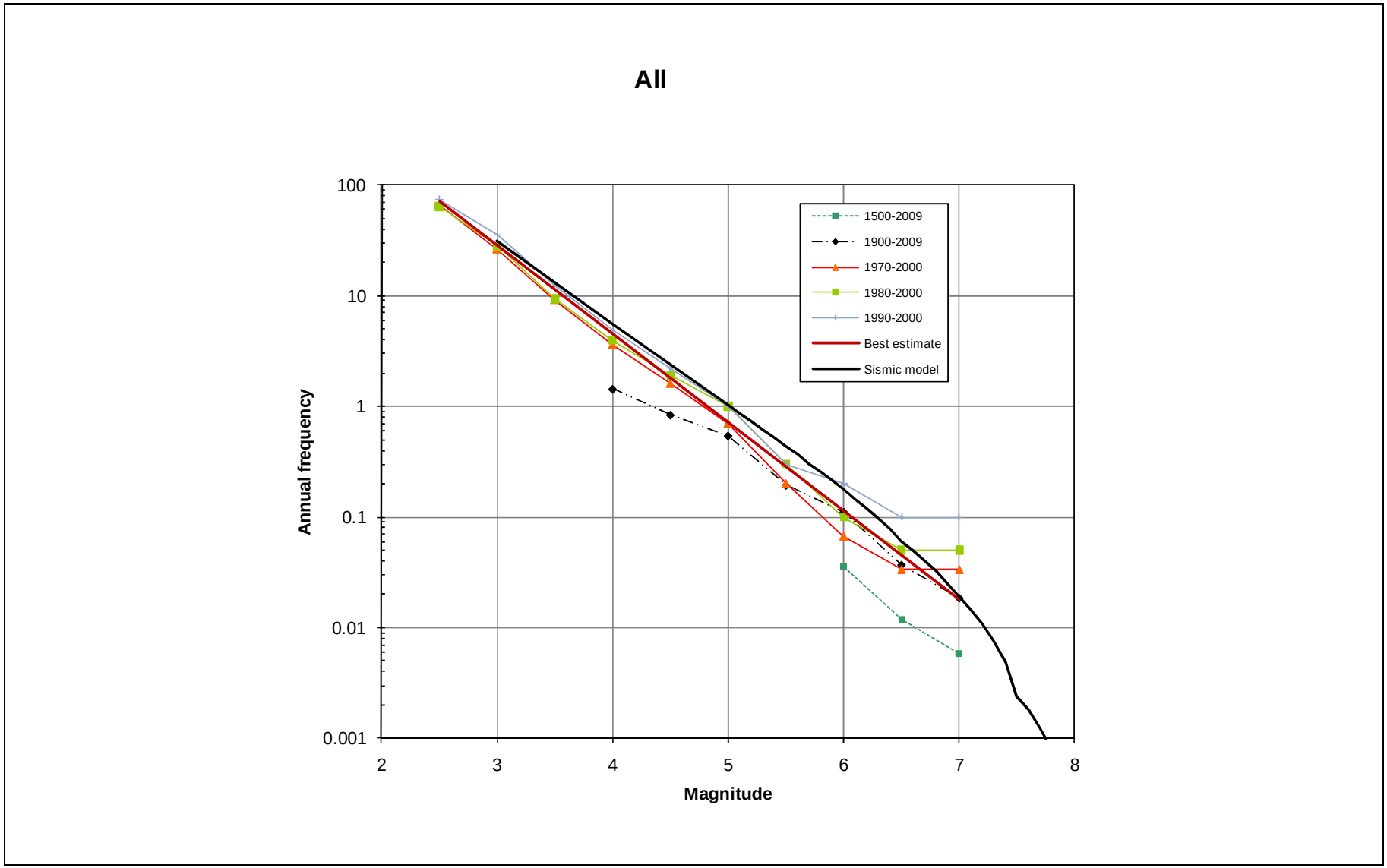

Figure 3.56 Recurrence Curves Showing Overall Activity for the Whole Region

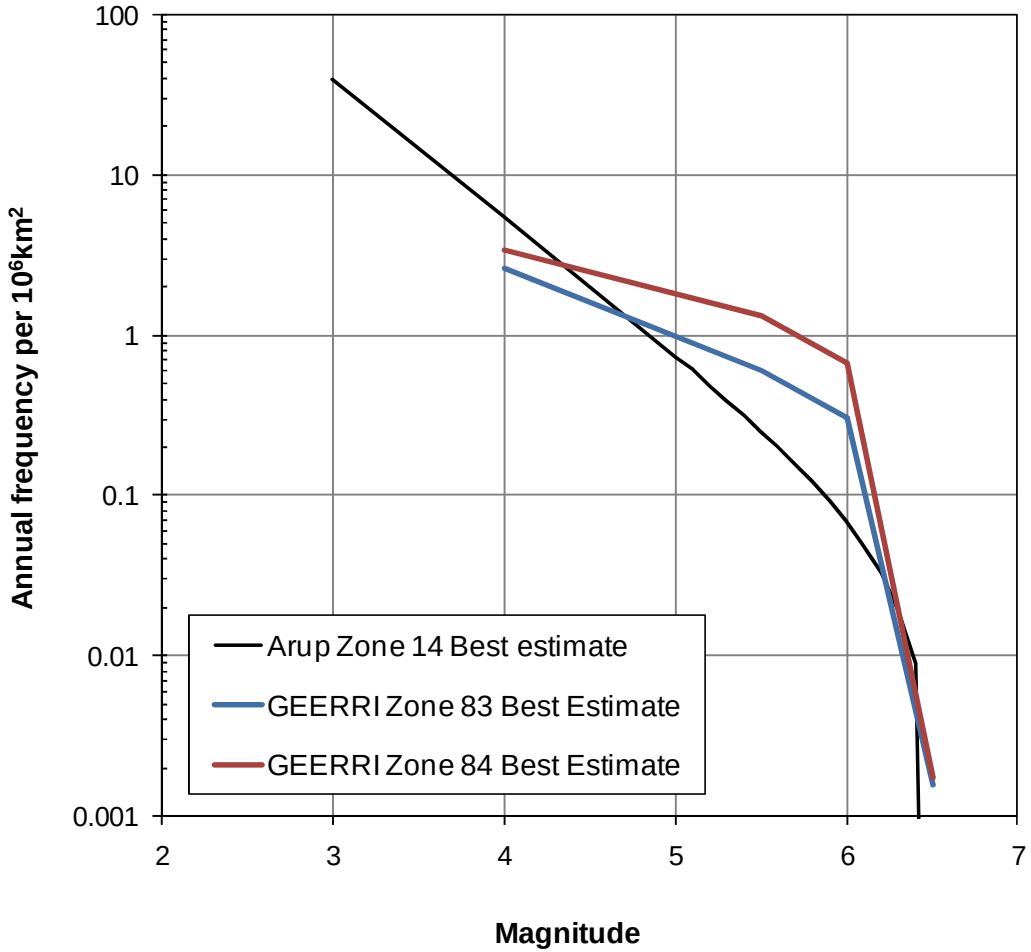

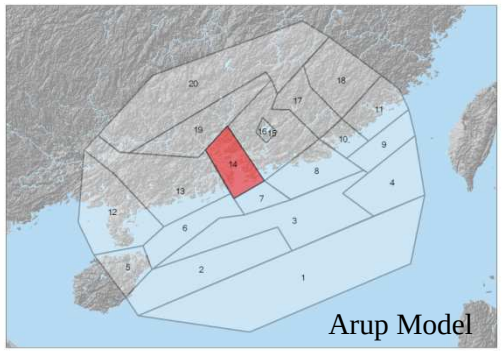

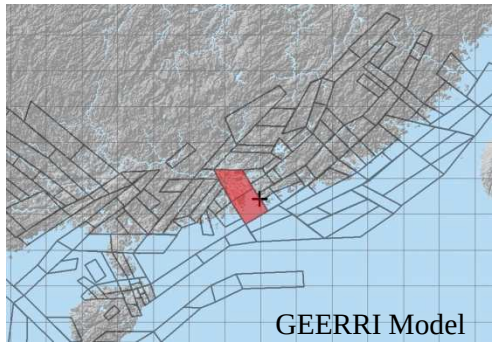

Figure 3.57 Comparison of Earthquake Recurrence Curve between Arup and GEERRI Models for Pearl Delta Region

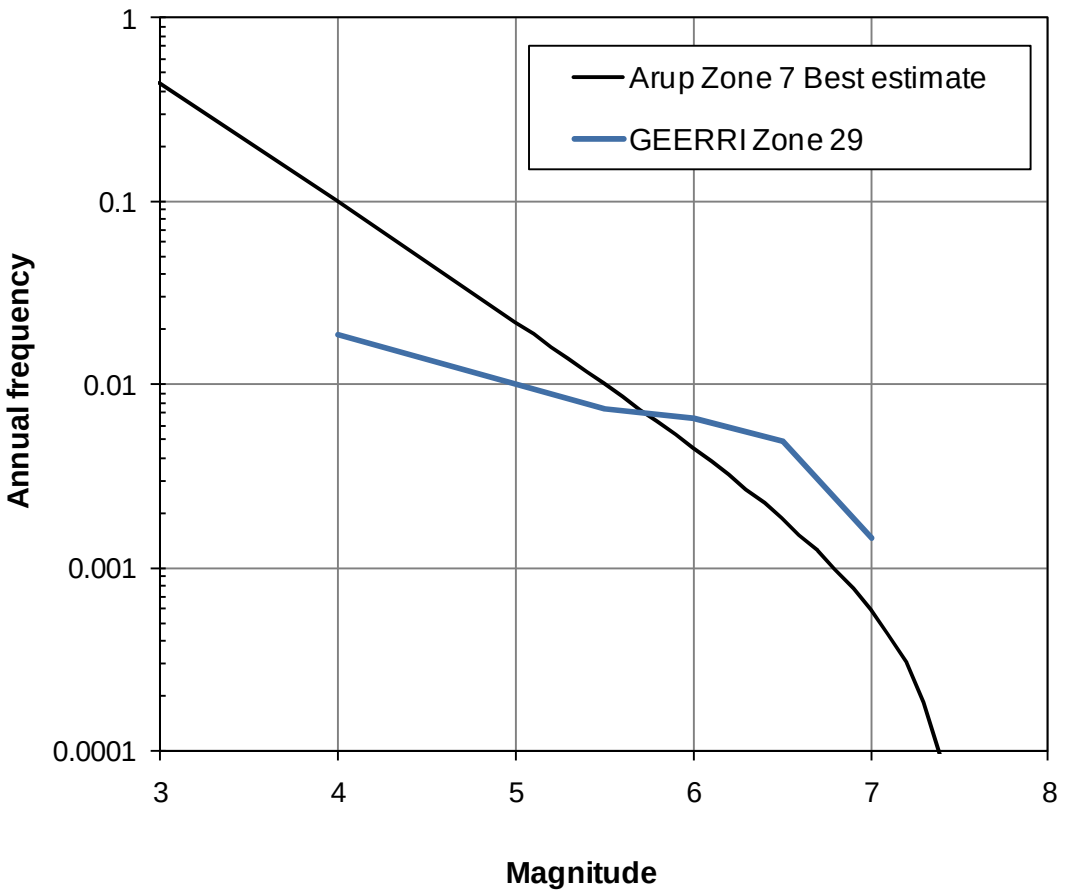

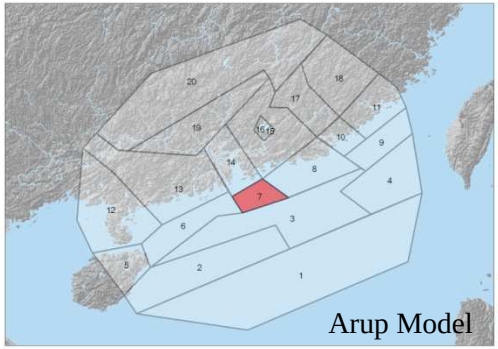

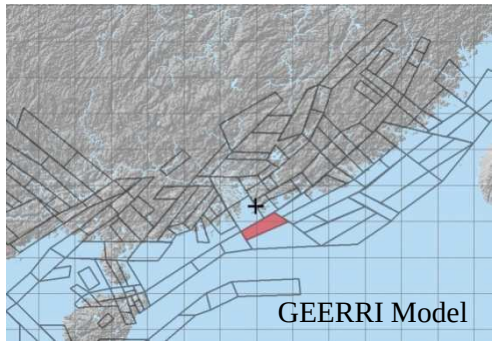

Figure 3.58 Comparison of Earthquake Recurrence Curve between Arup and GEERRI Models for Dangan Islands Region

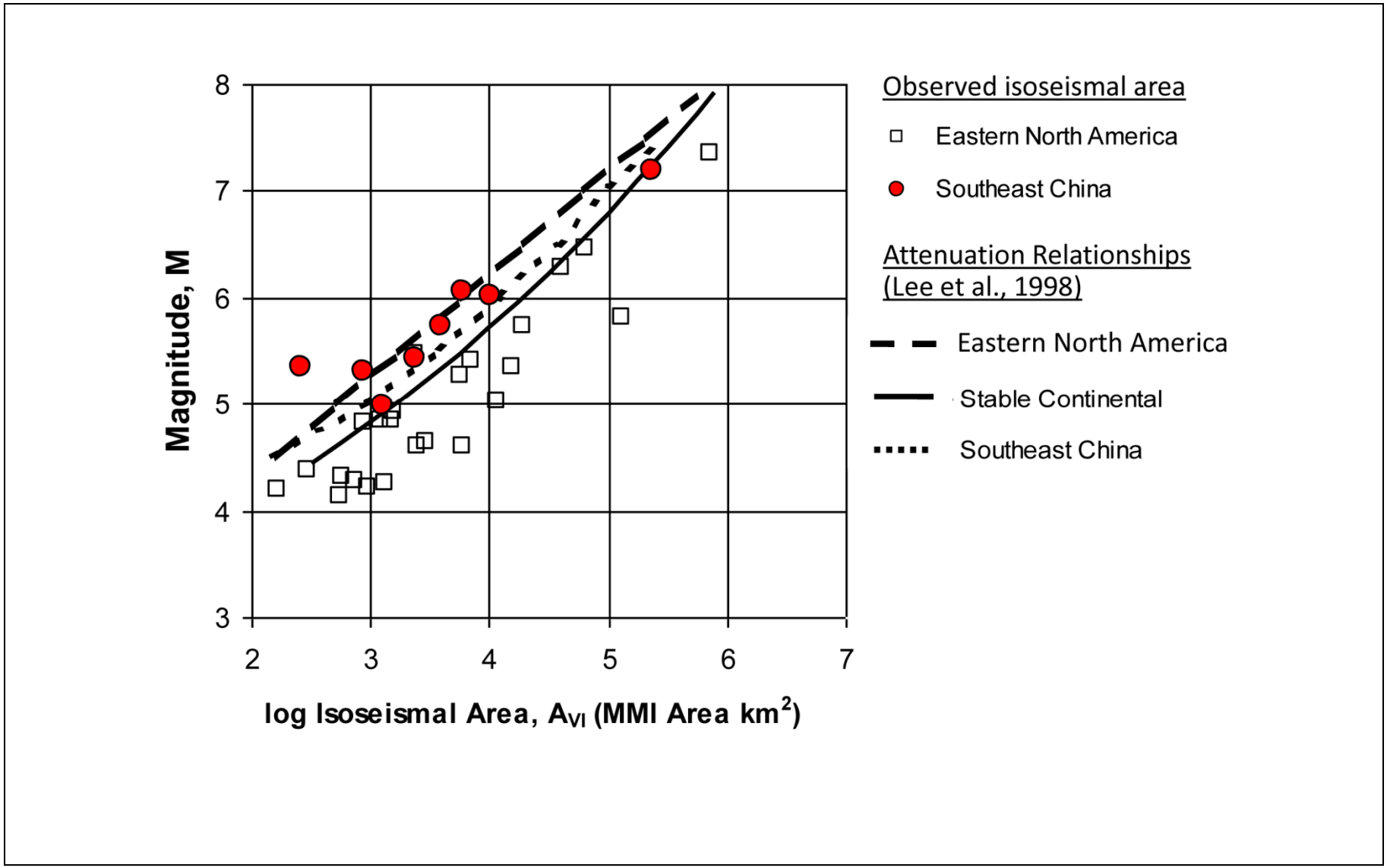

Figure 3.59 Comparison of Isoseismal Areas in the United States and Southeast China

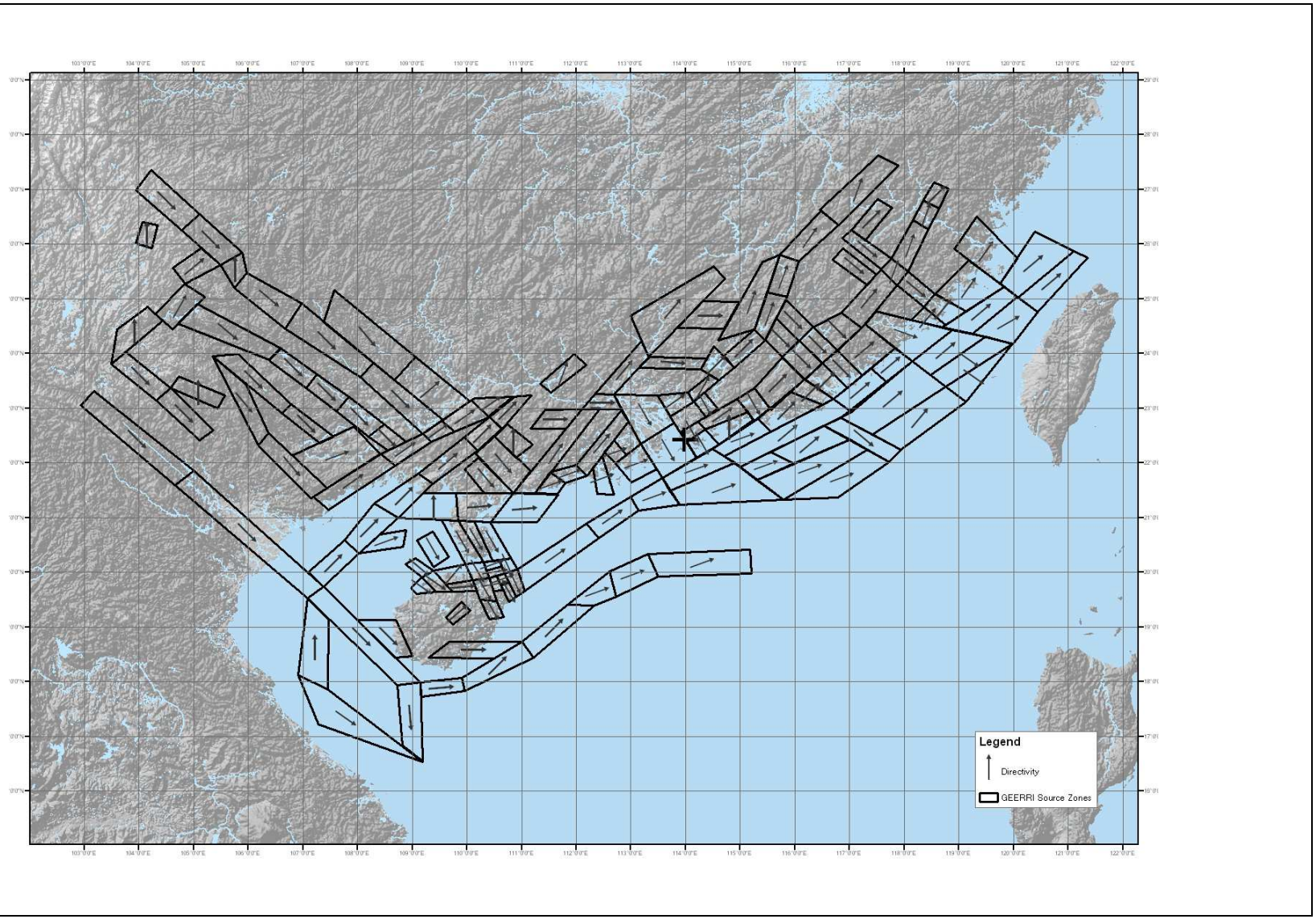

Figure 3.60 Directivity Motions of Each GEERRI Source Zones (Long and Short Axis)

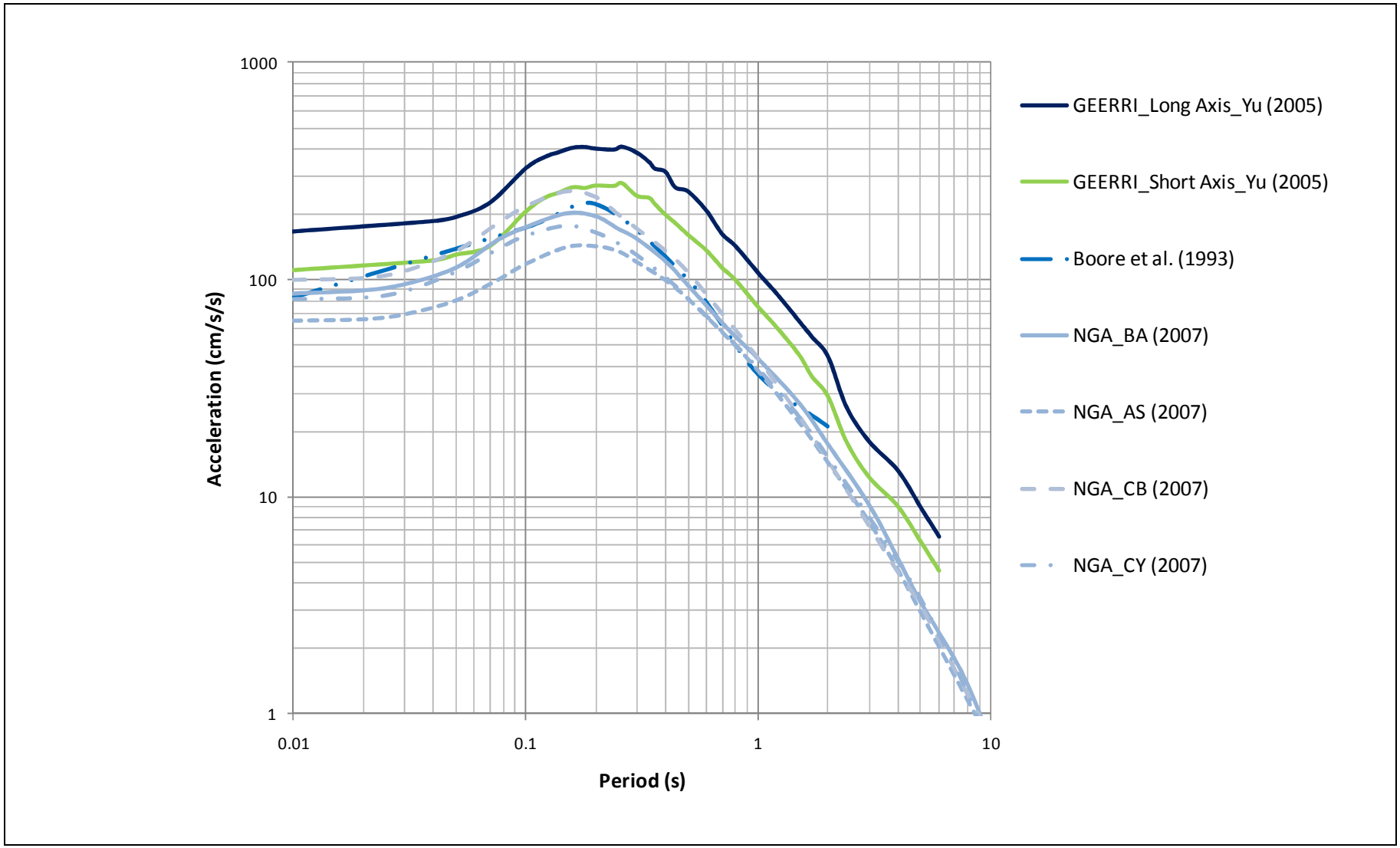

Figure 3.61 Comparison of Response Spectra between GEERRI and California Attenuation Models (with Magnitude 6 at Source Distance 20 km)

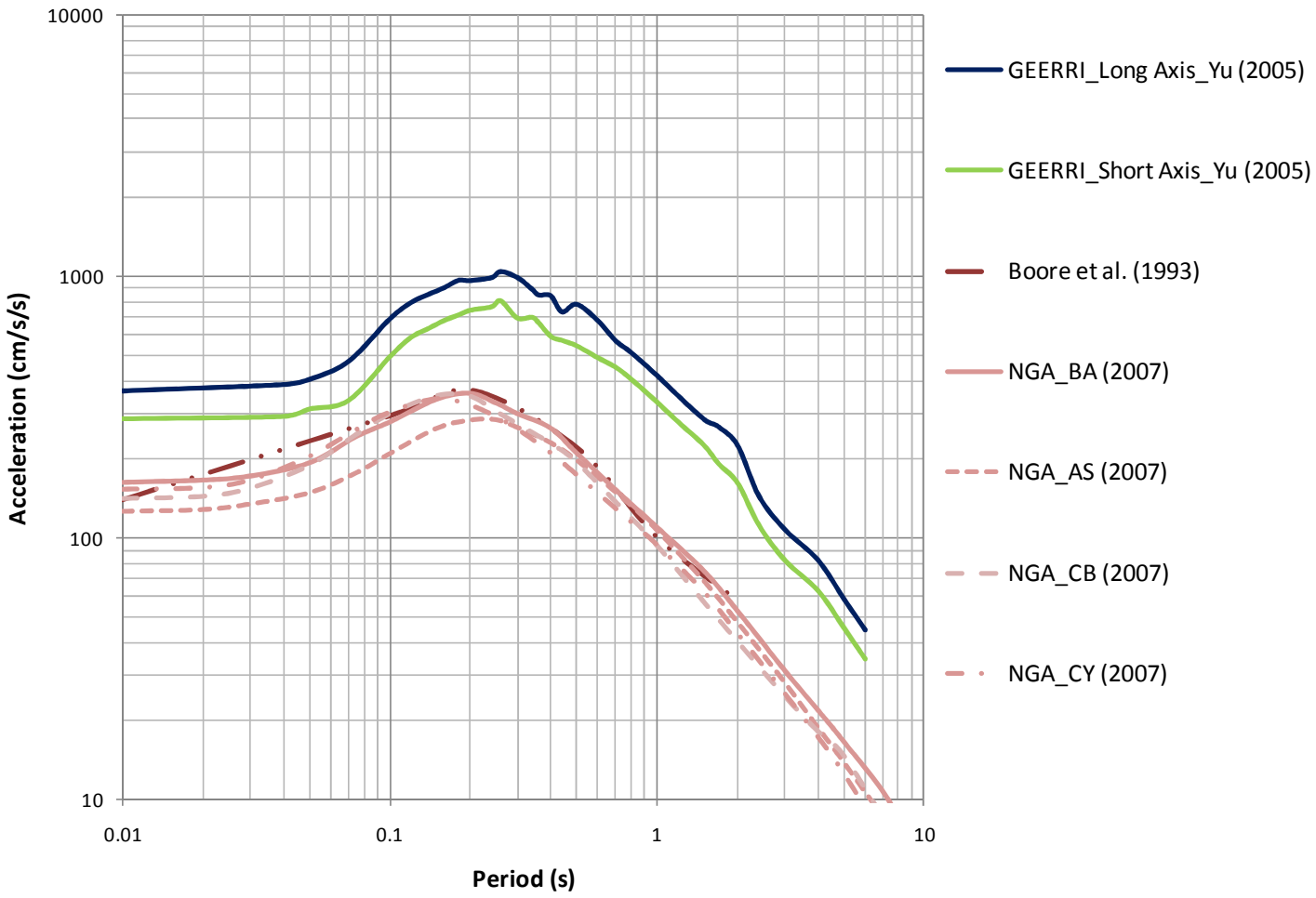

Figure 3.62 Comparison of Response Spectra between GEERRI and California Attenuation Models (with Magnitude 7 at Source Distance 20 km)

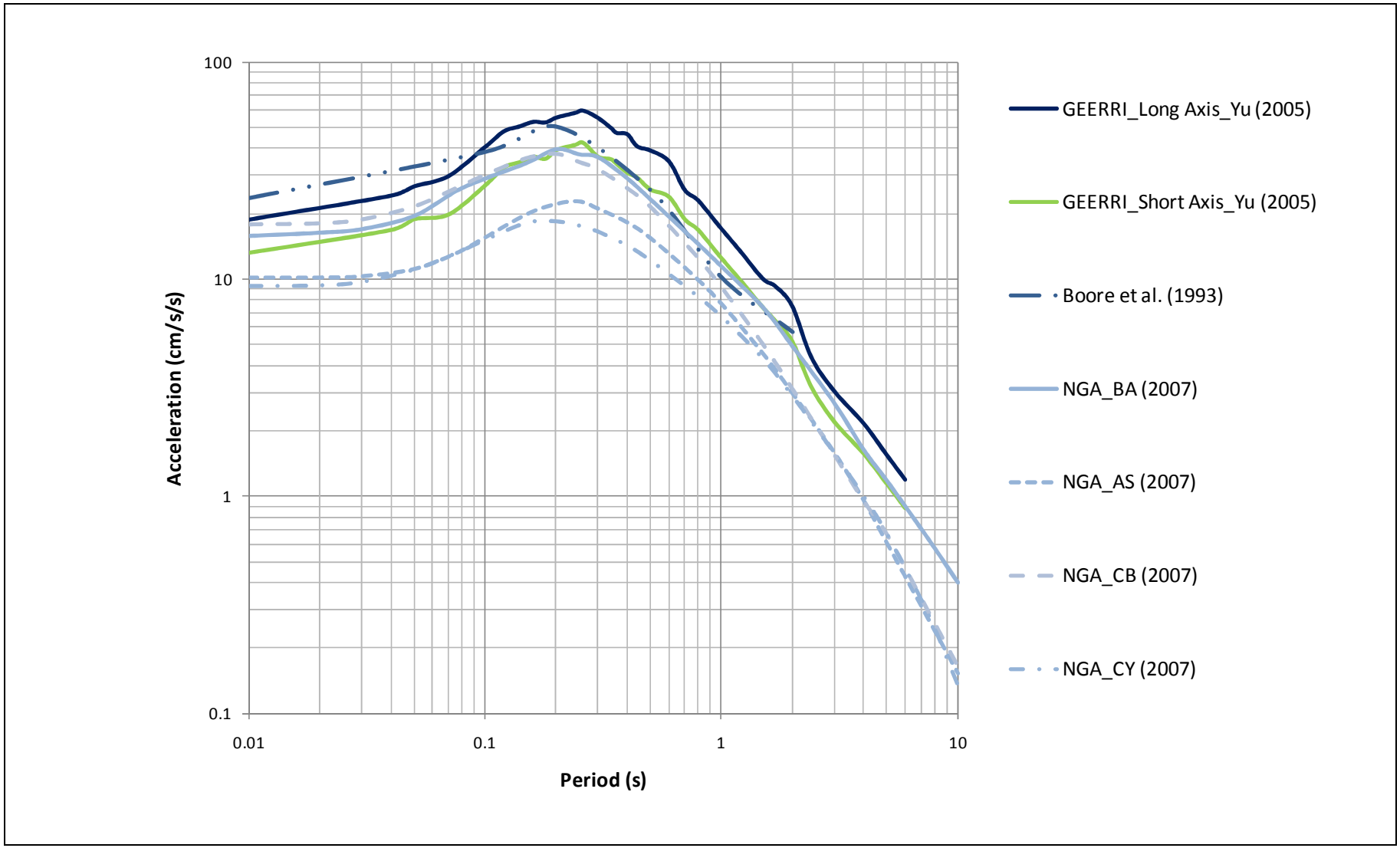

Figure 3.63 Comparison of Response Spectra between Yu (2005) and California Attenuation Models (with Magnitude 6 at Source Distance 100 km)

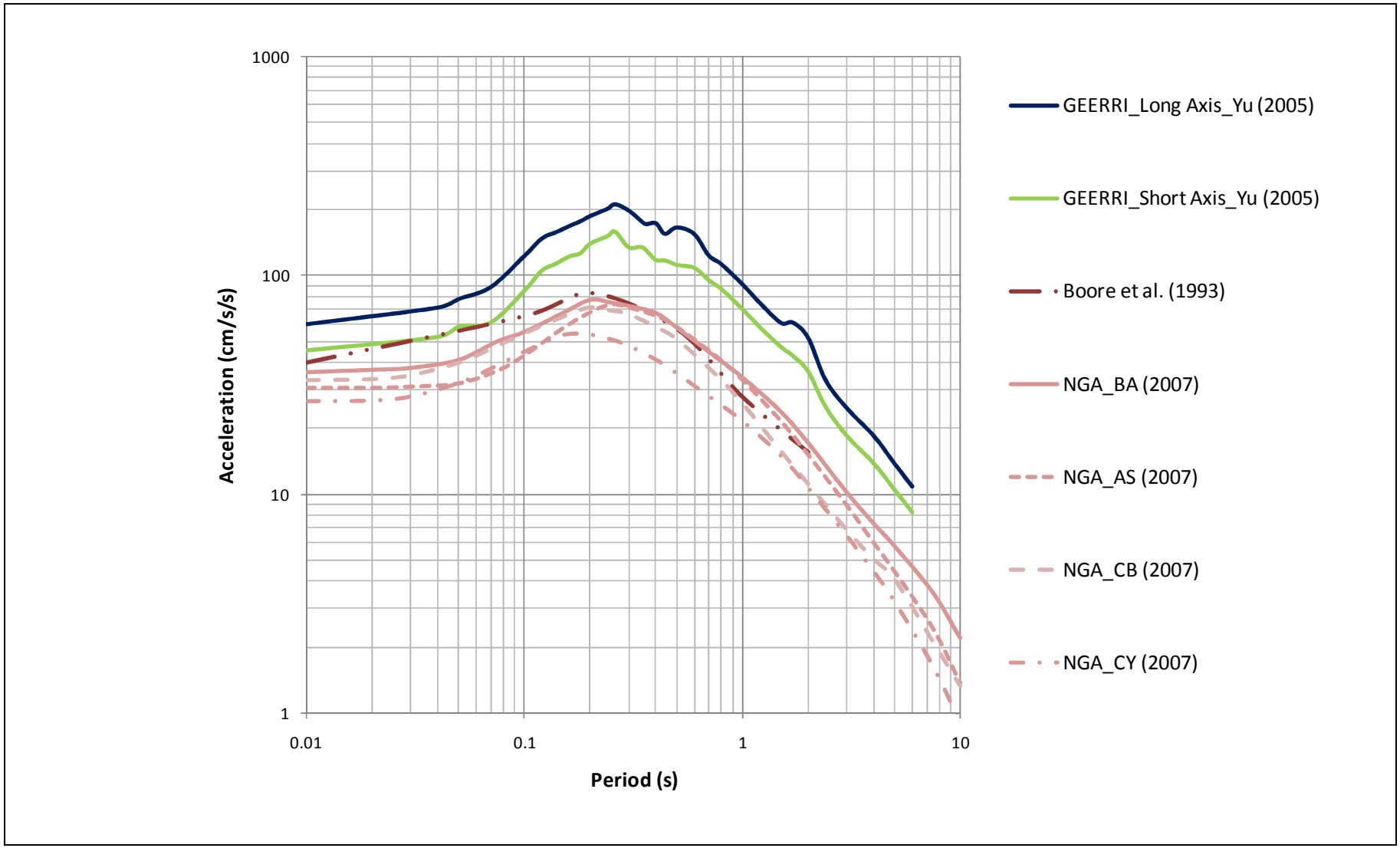

Figure 3.64 Comparison of Response Spectra between Yu (2005) and California Attenuation Models (with Magnitude 7 at Source Distance 100 km)

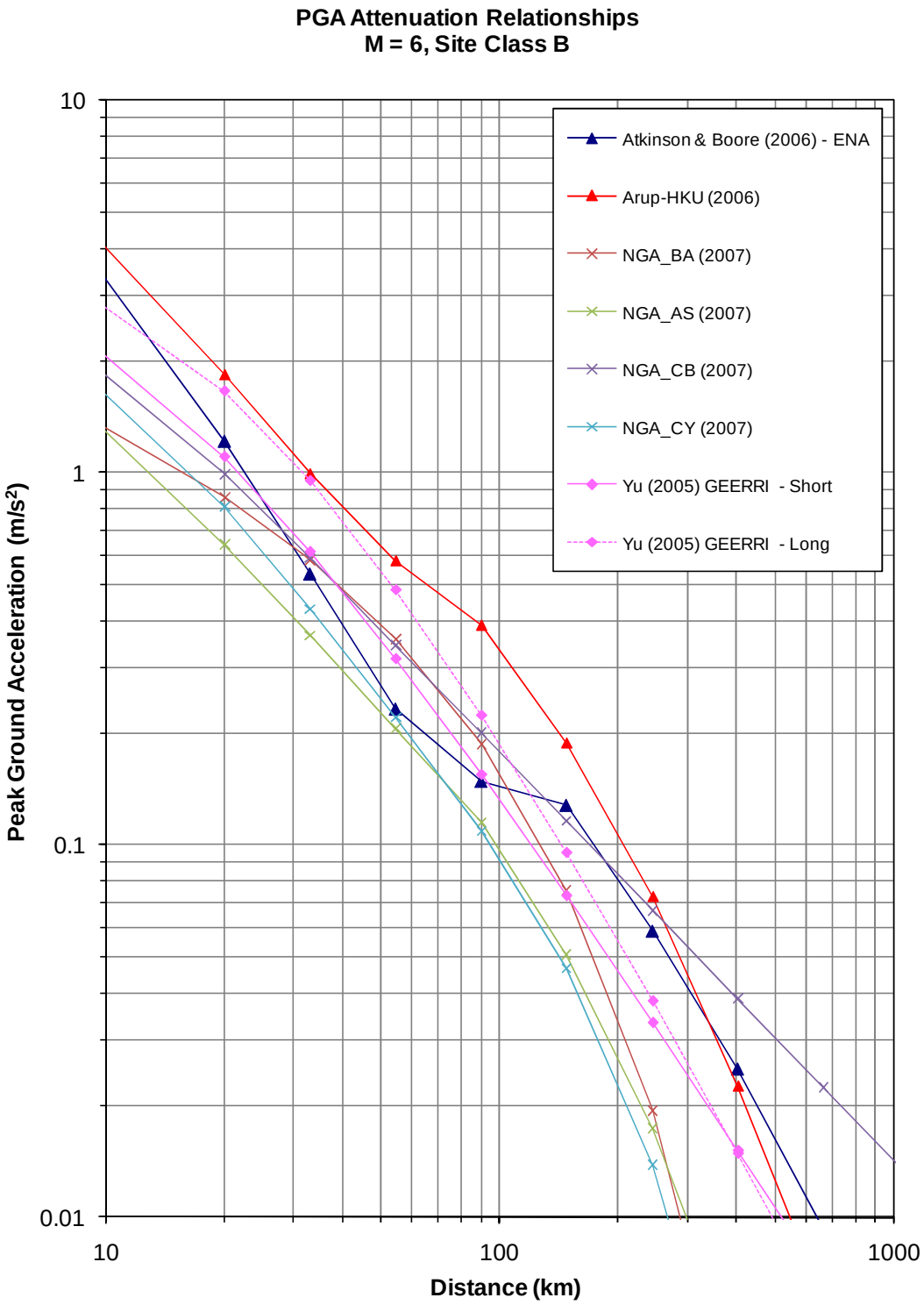

Notes:
(1) NGA_BA (2007) refers to Boore & Atkinson (2007).
(2) NGA_AS (2007) refers to Abrahamson & Silva (2007).
(3) NGA_CB (2007) refers to Campbell & Bozorgnia (2007).
(4) NGA_CY (2007) refers to Chiou & Youngs (2007).

Figure 3.65 Attenuation Relationships for Peak Ground Acceleration (Magnitude 6)

Table of Contents
Table of Contents
Table of Contents
Table of Contents

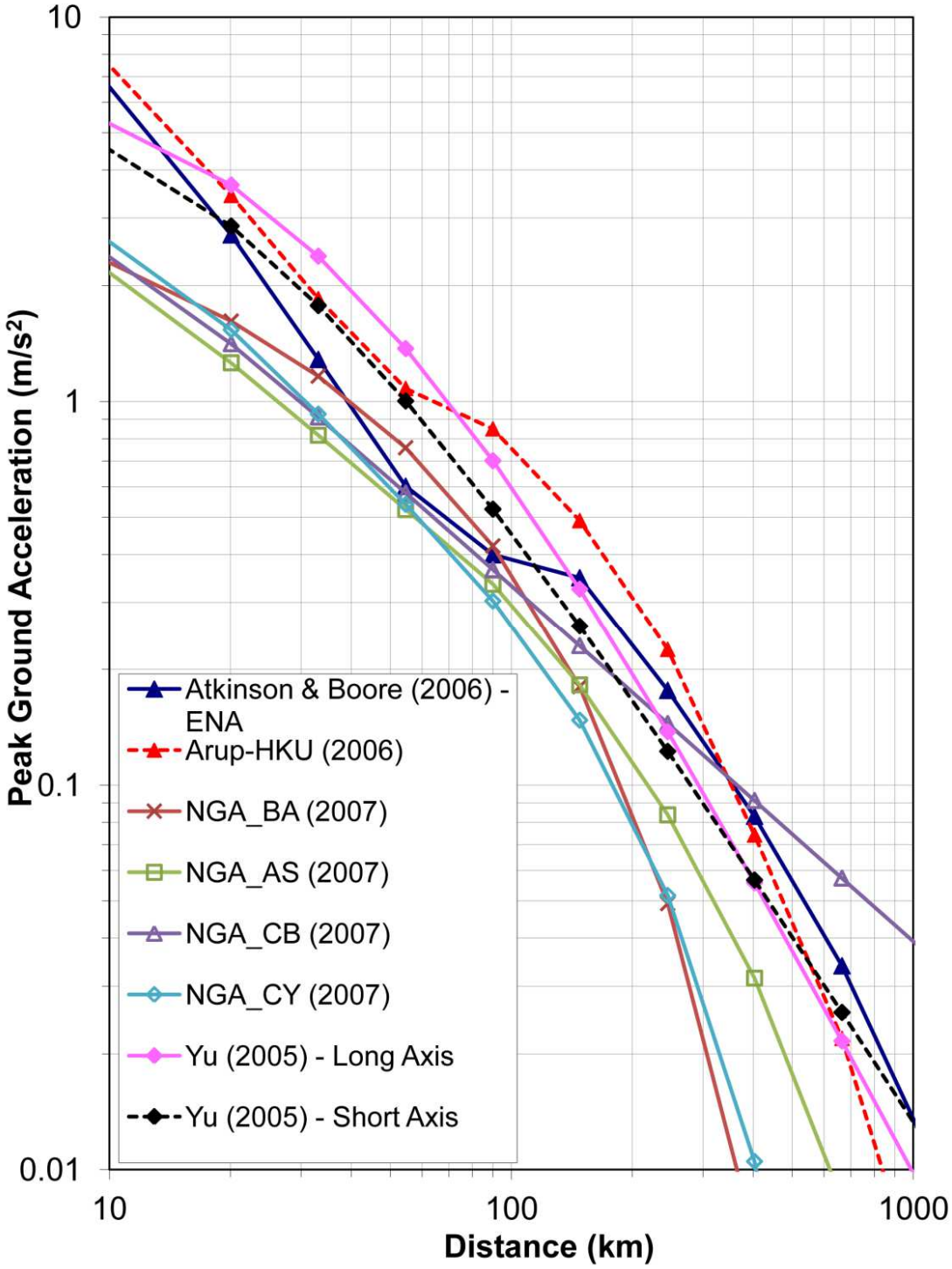

Note: Refers to Figure 3.65 for the denotations of NGA_BA (2007), NGA_AS (2007), NGA_CB (2007) and NGA_CY (2007).

Figure 3.66 Attenuation Relationships for Peak Ground Acceleration (Magnitude 7)

Table of Contents
Table of Contents
Table of Contents
Table of Contents

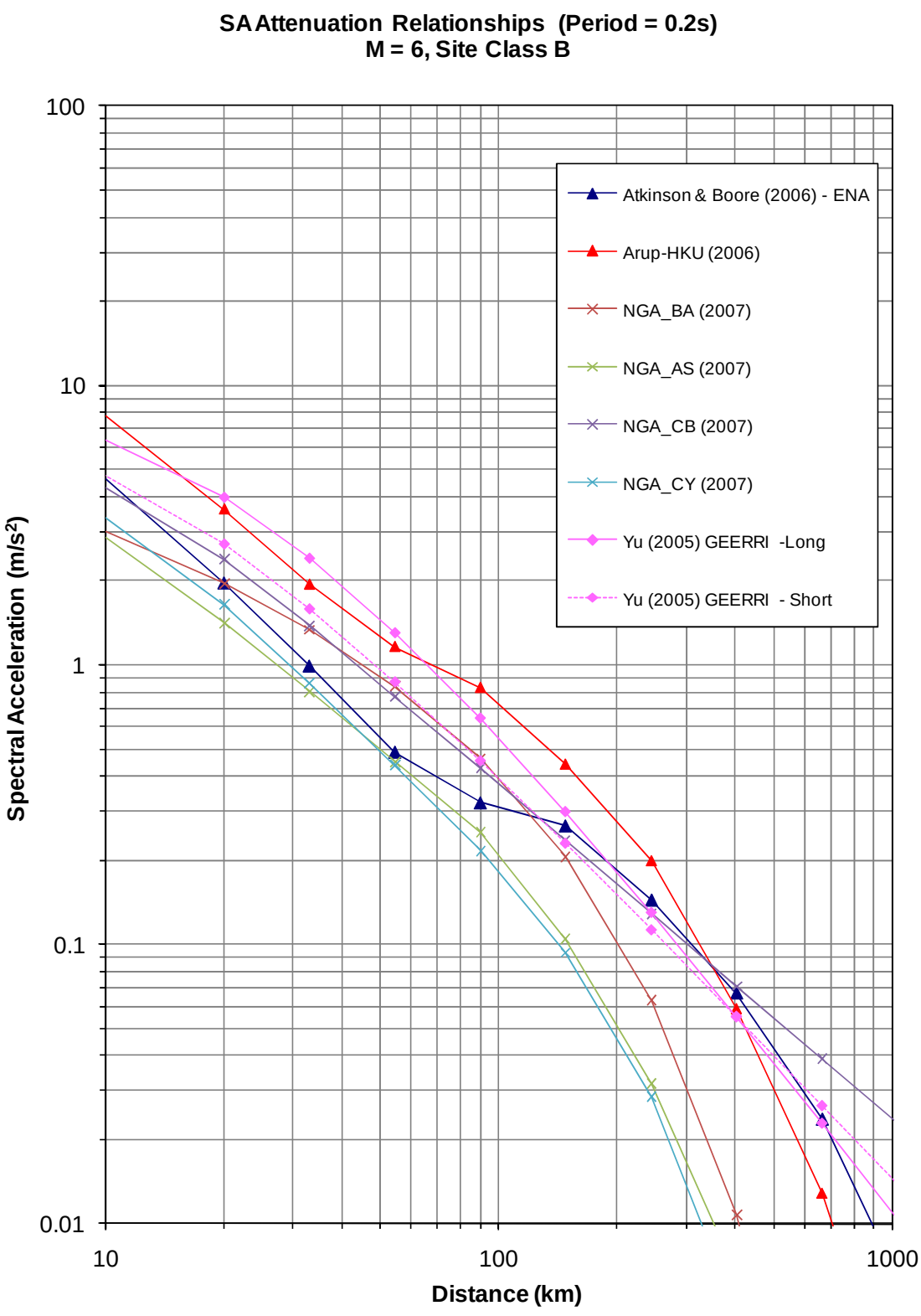

Note: Refers to Figure 3.65 for the denotations of NGA_BA (2007), NGA_AS (2007), NGA_CB (2007) and NGA_CY (2007).

Figure 3.67 Attenuation Relationships for 0.2 Seconds Period Acceleration (Magnitude 6)

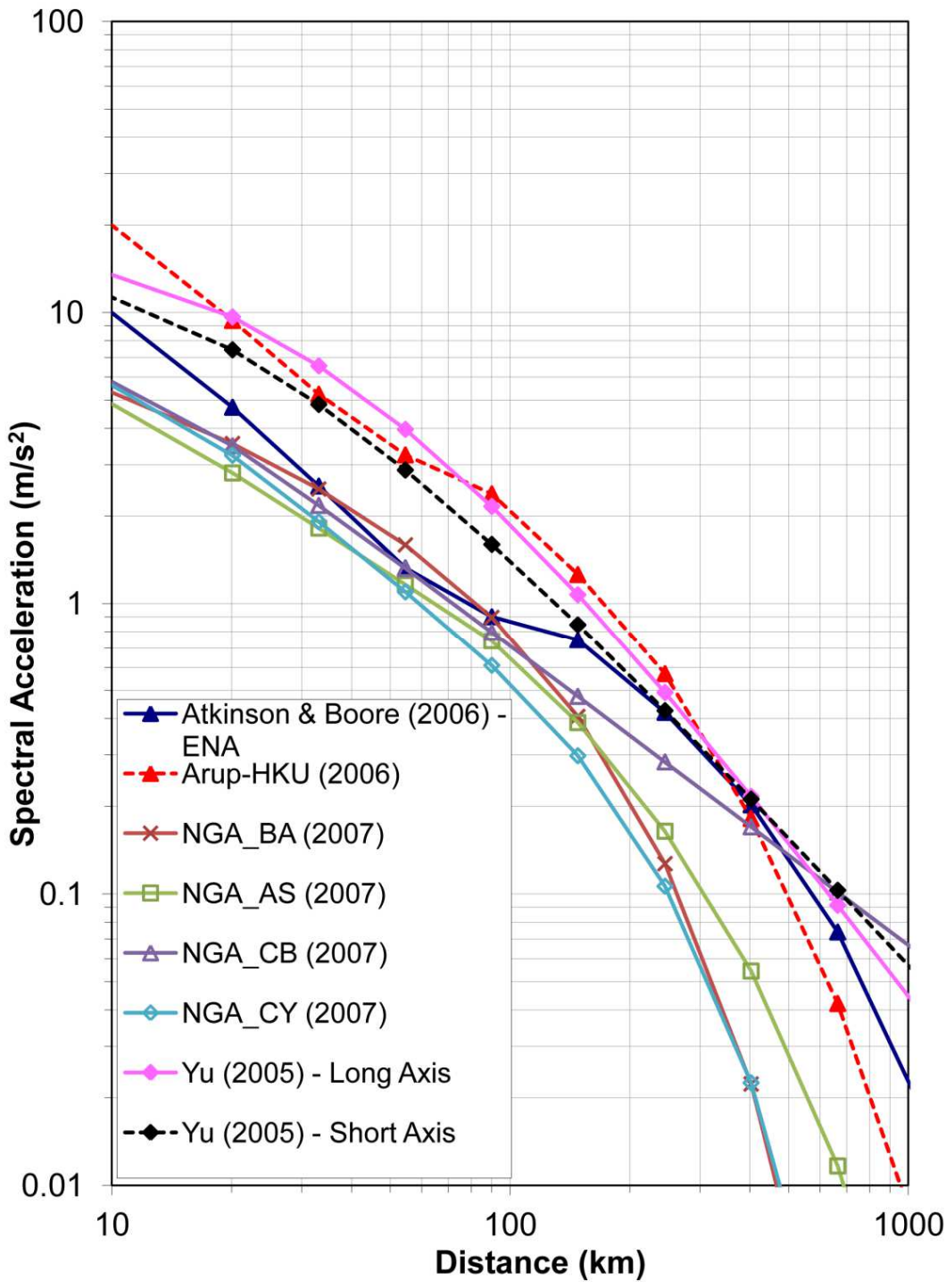

Note: Refers to Figure 3.65 for the denotations of NGA_BA (2007), NGA_AS (2007), NGA_CB (2007) and NGA_CY (2007).

Figure 3.68 Attenuation Relationships for 0.2 Seconds Period Acceleration (Magnitude 7)

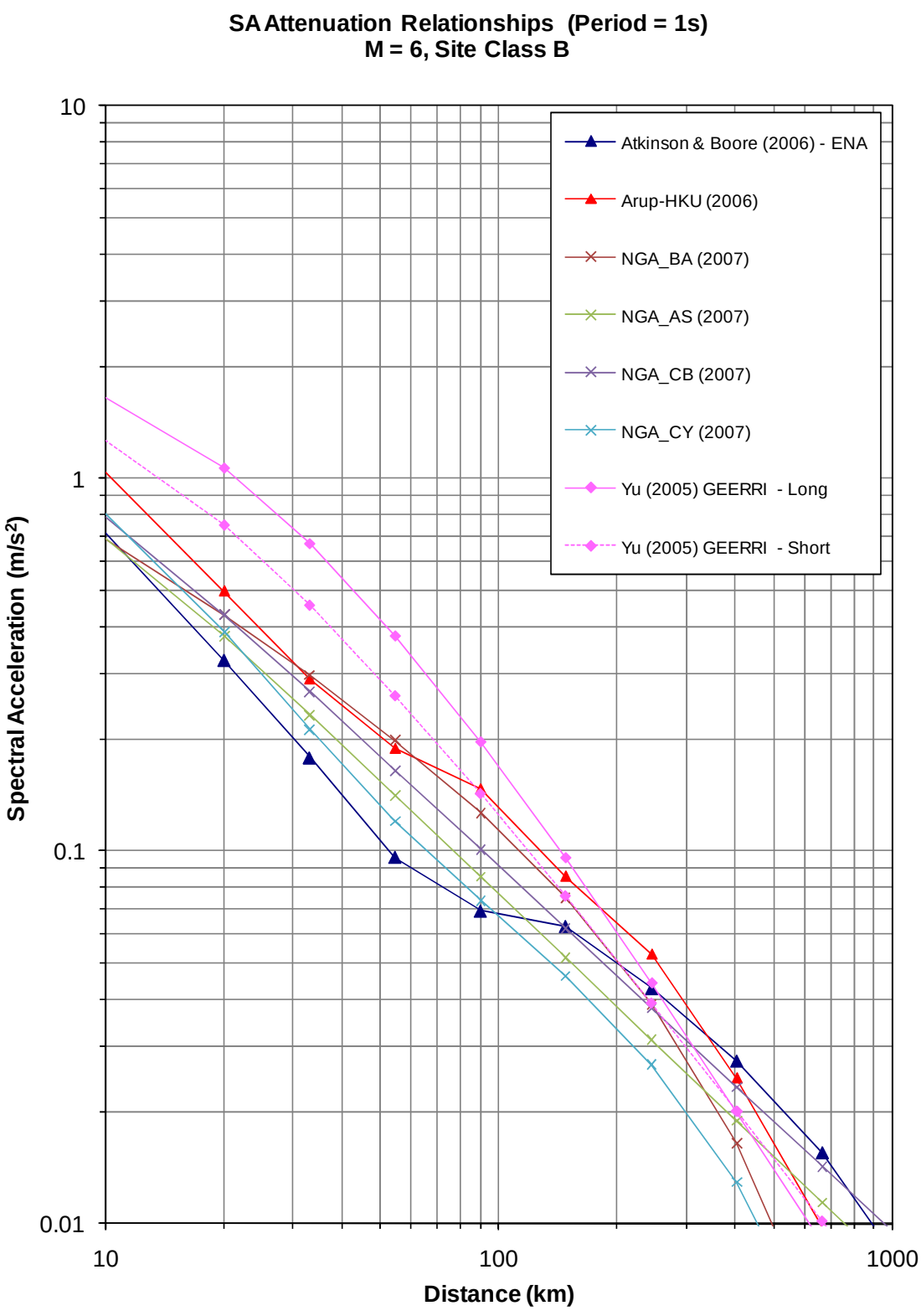

Note: Refers to Figure 3.65 for the denotations of NGA_BA (2007), NGA_AS (2007), NGA_CB (2007) and NGA_CY (2007).

Figure 3.69 Attenuation Relationships for 1 Second Period Acceleration (Magnitude 6)

Table of Contents
Table of Contents
Table of Contents
Table of Contents

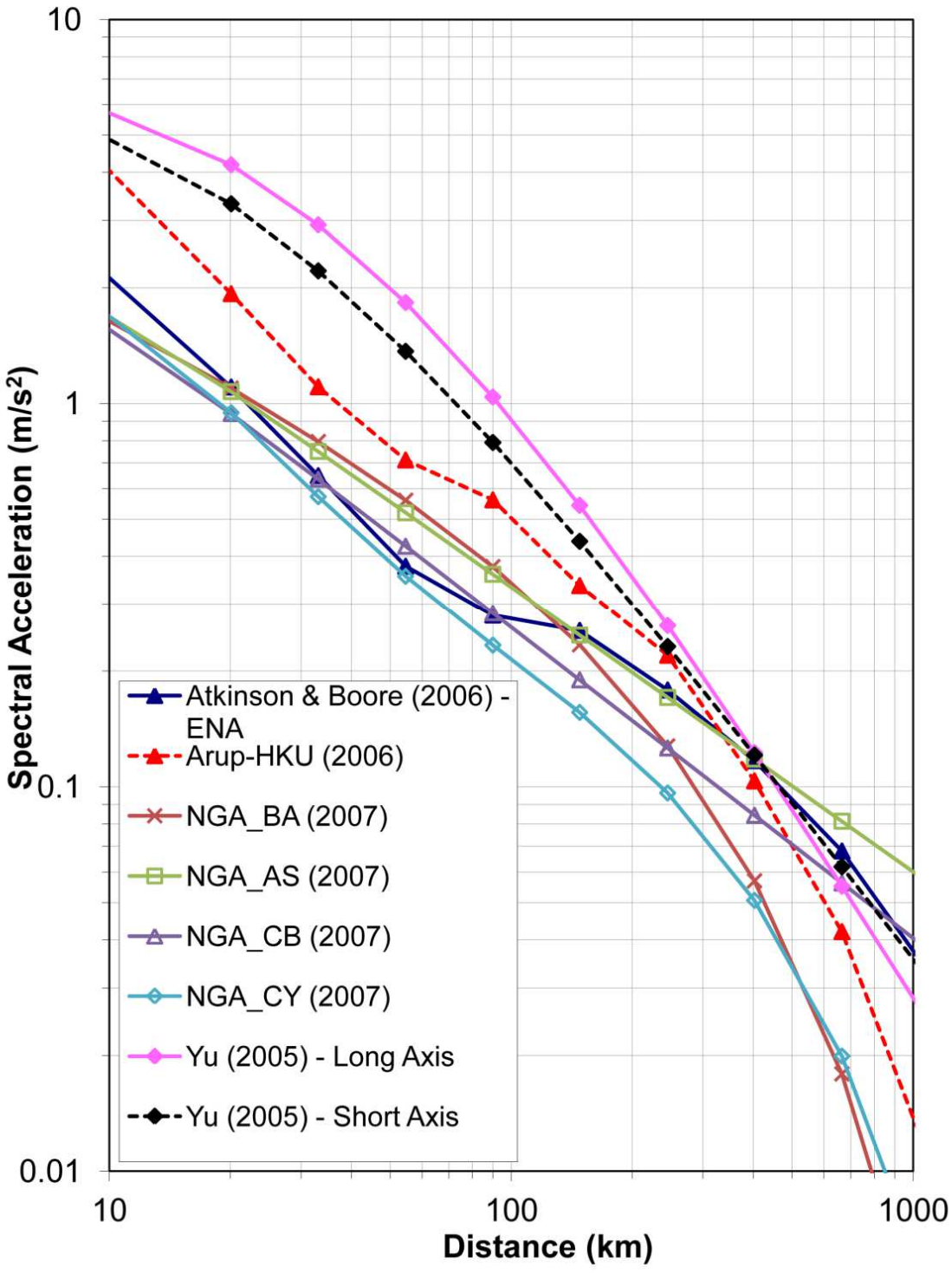

Note: Refers to Figure 3.65 for the denotations of NGA_BA (2007), NGA_AS (2007), NGA_CB (2007) and NGA_CY (2007).

Figure 3.70 Attenuation Relationships for 1 Second Period Acceleration (Magnitude 7)

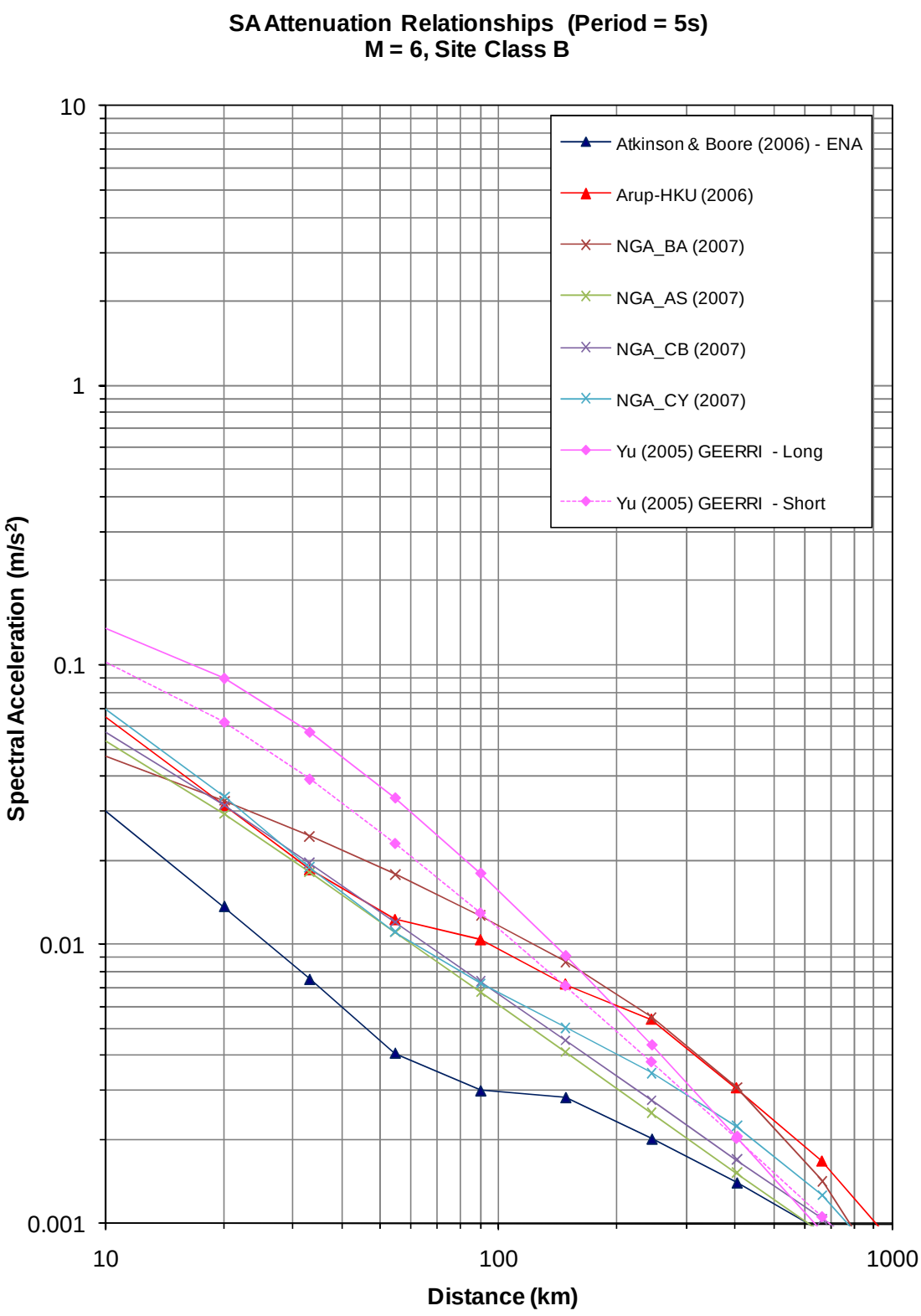

Note: Refers to Figure 3.65 for the denotations of NGA_BA (2007), NGA_AS (2007), NGA_CB (2007) and NGA_CY (2007).

Figure 3.71 Attenuation Relationships for 5 Seconds Period Acceleration (Magnitude 6)

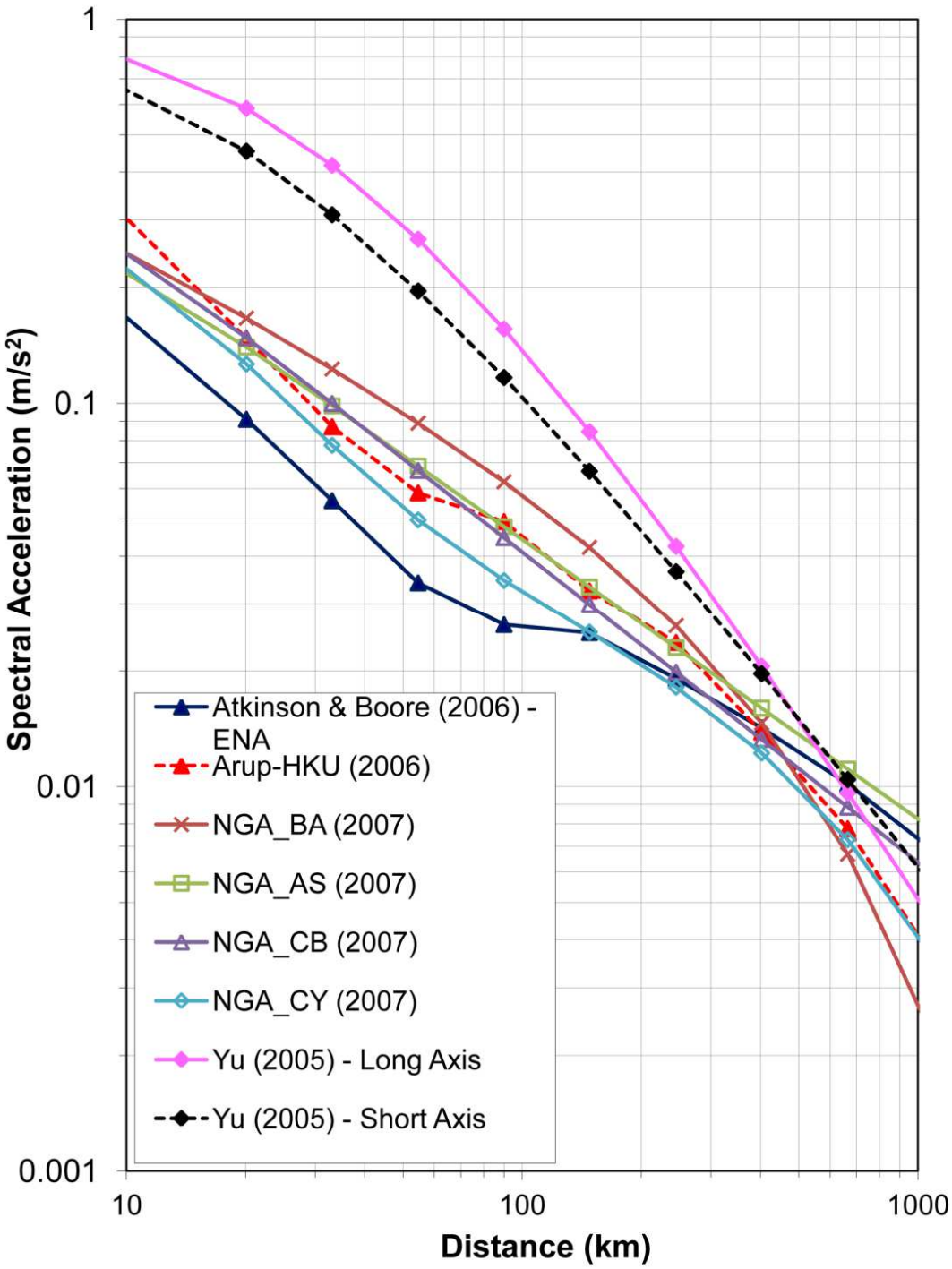

Note: Refers to Figure 3.65 for the denotations of NGA_BA (2007), NGA_AS (2007), NGA_CB (2007) and NGA_CY (2007).

Figure 3.72 Attenuation Relationships for 5 Seconds Period Acceleration (Magnitude 7)

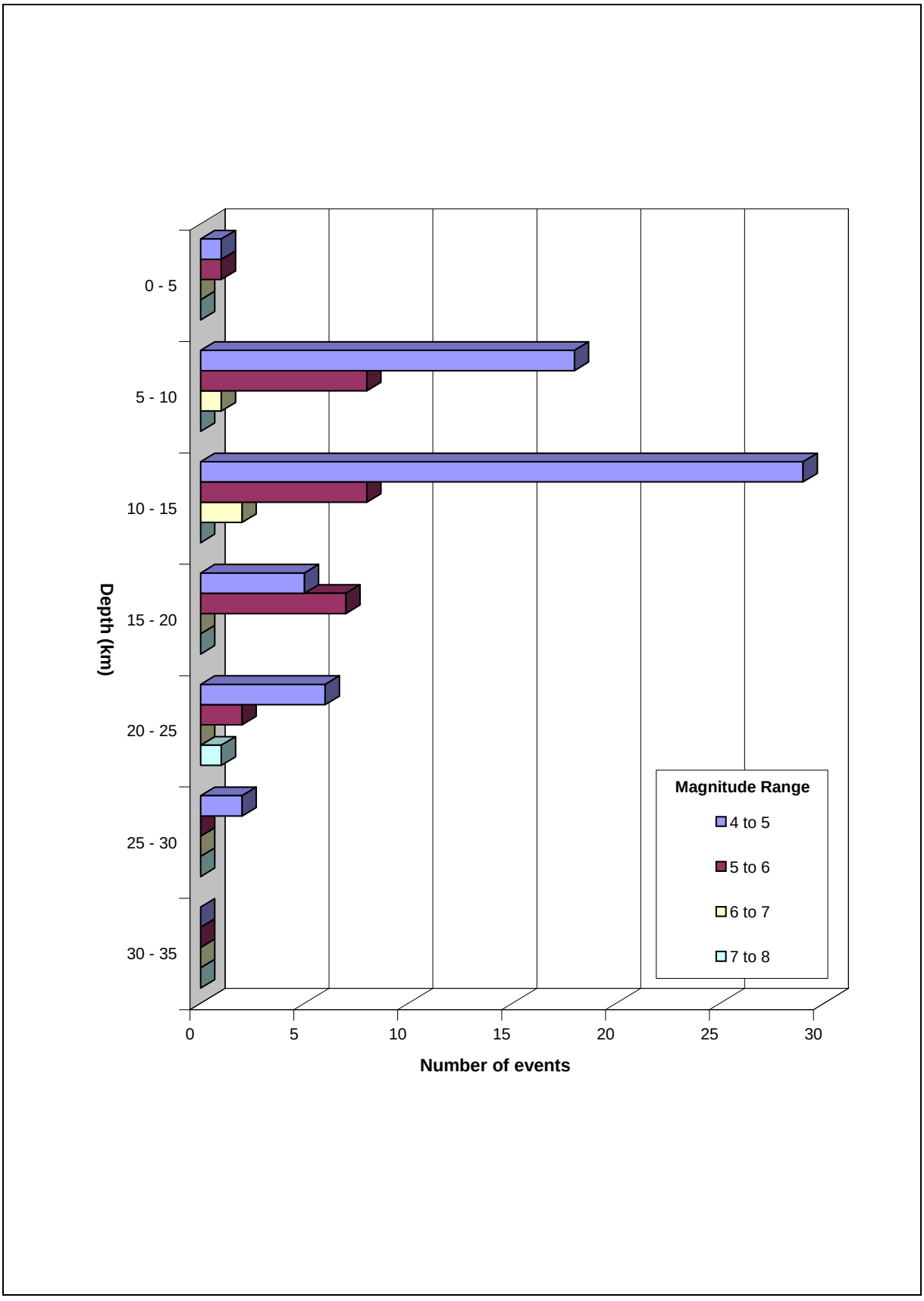

Figure 3.73 Earthquake Focal Depth Distribution for Events in Region within 500 km from Hong Kong

Table of Contents
Table of Contents
Table of Contents
Table of Contents

4 Seismic Hazard Assessment Results

4.1 General

The results of the seismic hazard assessment using the Arup source model are presented in terms of horizontal peak ground acceleration and uniform hazard response spectra for rock site ground conditions. A rock site in this study is defined as shear wave velocity greater than 760 m/s as defined as rock in Soil Class B of IBC2009 and 800 m/s as defined as rock in Soil Type 1 of the Chinese Seismic Code GB50011-2010. The results are presented for four earthquake probabilities:

(a) 63% probability of being exceeded in the next 50 years (50-year return period),

(b) 50% probability of being exceeded in the next 50 years (72-year return period),

(c) 10% probability of being exceeded in the next 50 years (475-year return period), and

(d) 2% probability of being exceeded in the next 50 years (2,475-year return period).

The detailed hazard results are presented as hazard curves, which show ground-motion hazard level (peak ground acceleration or spectral acceleration) plotted against annual frequency of being exceeded.

The seismic hazard assessment results have been de-aggregated to investigate the distribution of the potential earthquake occurrences, in terms of magnitude and distance, which have contributed to the ground-motion hazard.

4.2 Peak Horizontal Ground Acceleration on Rock

The hazard levels at the centre of this study area (i.e. latitude 22.426 degrees and longitude 113.988 degrees) and the location of Hong Kong Observatory, in terms of peak horizontal acceleration on rock, for each return period, are summarised in Table 4.1.

A plot of peak horizontal acceleration and spectral accelerations for structural periods of 0.2, 1, 2 and 5 seconds on a rock site versus return period at the centre of the study area is shown in Figure 4.1.

Table 4.1 Peak Horizontal Acceleration on a Rock Site

Probability of Being Exceeded	Peak Horizontal Acceleration (m/s²)	
	Centre of this study area (NW Hong Kong)	Hong Kong Observatory
63% in 50 years	0.26	0.28
50% in 50 years	0.32	0.34
10% in 50 years	0.90	1.00
2% in 50 years	1.96	2.18

4.3 Uniform Hazard Horizontal Response Spectra for Rock Site

The hazard levels, in terms of horizontal response spectral acceleration (for 5% structural damping) on rock at the centre of this study area and the location of Hong Kong Observatory, for each probability, are summarised in Table 4.2 and Table 4.3 respectively. The assessment has been undertaken for structural periods of 0.1, 0.2, 0.5, 1, 2 and 5 seconds.

Table 4.2 Uniform Hazard Horizontal Response Spectral Ordinates (at the Centre of this Study Area)

Probability of Being Exceeded	Spectral Acceleration (m/s²)					
	Structural Period (seconds)					
	0.1	0.2	0.5	1.0	2.0	5.0
63% in 50 years	0.550	0.639	0.368	0.178	0.069	0.018
50% in 50 years	0.688	0.786	0.445	0.215	0.085	0.022
10% in 50 years	1.962	2.125	1.073	0.514	0.210	0.060
2% in 50 years	4.238	4.482	2.073	0.953	0.386	0.115

Figure 4.1 shows the PGA, and response spectral values for structural periods of 0.2, 1, 2 and 5 seconds against return period. It can be seen that the increase with return period is quite similar to that of the peak ground acceleration. Figures 4.2 to 4.4 show the uniform hazard response spectra for a rock site for this study at the centre of the NW New Territories. The uniform hazard response spectra have been plotted in terms of spectral acceleration, velocity and displacement respectively.

Table 4.3 Uniform Hazard Horizontal Response Spectral Ordinates (at the Hong Kong Observatory)

Probability of Being Exceeded	Spectral Acceleration (m/s²)					
	Structural Period (seconds)					
	0.1	0.2	0.5	1.0	2.0	5.0
63% in 50 years	0.570	0.661	0.379	0.182	0.071	0.019
50% in 50 years	0.721	0.823	0.461	0.225	0.088	0.023
10% in 50 years	2.153	2.323	1.166	0.556	0.225	0.063
2% in 50 years	4.708	4.951	2.341	1.068	0.422	0.125

To illustrate the sensitivity of the results to the input parameters, the contribution to the uniform hazard response spectrum from the different attenuation relationships used in the analysis is shown in Figure 4.5 for a probability of being exceeded of 10% in 50 years. It can be seen from Figure 4.5 that the contribution to the hazard level from the relationship by Yu (2005) is significantly higher than the others at long periods after 0.2-second and that the Arup-HKU relationship gives similar results with this study that considers Yu (2005), Arup-HKU, ENA and WNA with reasonable weighting factors as shown in Table 3.5. Hence, the predictions of Yu (2005) are significantly higher than the others at the long period, sensitivity analyses with different weighting of Yu (2005) after 0.2-second have been studied. Figures 4.6 to 4.8 show the results of the acceleration, velocity and displacement response spectra respectively for 10% and 2% chance of being exceeded in 50 years. It can be seen that the spectral values are increased by about double at 5-second from the use of 0% to 25% weighting of Yu (2005).

Figure 4.9 shows that the GEERRI source model gives similar results to those using the Arup source model by using the same attenuation relationship of Yu (2005). This shows that the effects of the choice between these two source models are actually quite small. This is an encouraging conclusion and demonstrates that there is a relatively similar total seismic activity rate between the two models in the Hong Kong region.

4.4 Uniform Hazard Vertical Response Spectra for Rock Site

Attenuation equations specific for vertical motions are relatively few. Consequently, the vertical response spectra have been developed using period dependent vertical to horizontal ratios (V/H). A review of appropriate V/H ratio is presented below.

- Chinese Code (GB 50011-2010) suggests $V/H = 0.65$ for all periods.
- The European Seismic Code (EN1998-1:2004) recommends $V/H = 1.1$ for short periods and $V/H = 0.4$ for long periods.

- Bozorgnia & Campbell (2004) determined the horizontal and vertical components for PGA and a wide range of frequency (0.25 - 20 Hz) for shallow crustal earthquakes. They also propose simple procedures for developing a preliminary vertical design spectrum.

As it is generally considered that the *V*/*H* ratio is dependent on the structural period, the mean curve of *V*/*H* ratio of EN1998-1:2004 and Bozorgnia & Campbell (2004) were used in this study as a basis to develop the vertical target response spectra (Figure 4.10). The *V*/*H* ratio from GB 50011-2010 is also plotted in Figure 4.10 for reference and its constant ratio is approximately the mean value of the derived mean curve for the whole spectrum. The resulting vertical target response spectra are illustrated in Figure 4.11.

4.5 De-aggregation of Hazard

One of the primary advantages of the probabilistic seismic hazard assessment methodology is that all possible earthquake occurrences that may contribute to a particular level of the ground-motion hazard are accounted for. When this approach is applied for each period of the response spectra, a uniform hazard response spectrum is obtained. In addition, multiple hypotheses on input assumptions, reflecting relative credibility and engineering judgement, are applied in a transparent manner.

One disadvantage of the PSHA methodology is that the concept of a design earthquake is lost, i.e. there is no single event, in terms of magnitude and distance, which is likely to give rise to a ground motion that will match the uniform hazard spectrum at all structural periods. This perceived disadvantage can be overcome by de-aggregating all the possible earthquake occurrences that contribute to the ground-motion hazard value at any particular period. This enables the relative likelihood of any individual earthquake event giving rise to the ground motion at that period to be determined. The most likely event can then be derived and a more reasonable response spectrum centred on that period can be determined.

The PSHA results of this study have been de-aggregated, in terms of magnitude and distance, to investigate earthquake occurrences that have contributed the most to resulting ground-motion hazard. When carrying this de-aggregation, earthquake magnitude and distance pairs that give rise to the target ground motion hazard value are determined in accordance with the procedures recommended by McGuire (1995). Bazzurro & Cornell (1999) discussed various methods to carry out de-aggregation including the method proposed by McGuire together with the de-aggregation of earthquake events that lead to ground motions equal to or greater than the target ground motion. They also discussed how to determine the relative contribution at various distances, the log of the distance or the linear distance.

De-aggregation has been carried out for the PGA and the 0.2-, 1- and 5-second response spectral ordinates. Three annual probabilities have been investigated and the results of the de-aggregation are shown on a linear distance scale in Figures 4.12 to 4.15.

The de-aggregation of the 0.2-second response spectral ordinate results indicates that the possible earthquakes at relatively close distance are contributing most to the hazard level. Possible earthquakes at distances greater than 150 km make relatively little contribution and

as the ground motion level increases, i.e. the probability reduces, the relative contribution increases from earthquakes occurring at nearer distances. The de-aggregation in terms of magnitude indicates that the contribution from moderate to larger magnitudes increases with increasing ground motion.

The de-aggregation of the 1-second and 5-second response spectral ordinate results indicates that the contribution from earthquakes at large distances (greater than 250 km), is increased significantly. However, for the less probable ground motions, i.e. 2% in 50 years, the contribution from large distance earthquakes (i.e. 250 to 400 km) becomes larger.

The most likely scenario event to represent the short period ground motion for a relatively likely ground motion having a 50% chance of being exceeded in the next 50 years is about a magnitude M_W = 5.75 at 60 km and a magnitude M_W = 6.75 at 150 km for longer period ground motion. For less probable, extreme ground motions having a 2% chance of being exceeded in the next 50 years, a magnitude M_W = 5.5 very close to the site is appropriate for short period ground motion and from a magnitude M_W = 7 at 60 km to a magnitude M_W = 7.75 event at 300 km for long period ground motions.

4.6 Comparison of Results with Previous Studies for Hong Kong

4.6.1 Peak Ground Acceleration

Various seismic hazard studies for Hong Kong have been carried out by different researchers since the 1980s. The past major studies were Pun & Ambraseys (1992), Lee et al (1998), Chandler & Lam (2002), Free et al (2004) and Tsang & Chandler (2006). Pun & Ambraseys (1992) describe the results of a seismic hazard assessment for Hong Kong based on a seismic source model covering an area of 660 km x 600 km. A seismic catalogue with surface-wave magnitude, M_S > 4.7 and instrumental magnitude 4.0 between 1067 and 1989 was presented. The attenuation relationships of PGA developed for Western USA were used. Uncertainty in the attenuation relationships was not directly incorporated into the calculation and the predicted mean PGA for Hong Kong having a 10% probability of being exceeded in the next 50 years for rock sites is 0.08 g assuming no uncertainty and 0.15 g if one standard deviation from the mean is used. Lee et al (1998) divided the south-eastern coastal seismic belt of about 300 km x 400 km into 13 inner zones characterised by low seismic activity, and 16 outer zones of relatively higher seismic activity. Data of the historical earthquakes and microseismicity records between 1800 and 1995 provided by the Guangdong Seismic Bureau (now called, Earthquake Administration of Guangdong Province) were adopted in their study. The attenuation relationships used for PGA were based upon correlation between PGA and intensity for southeast China. The calculated PGA and seismic intensity of Hong Kong for a ground motion having a 10% chance of being exceeded in the next 50 years were between 0.076 g and 0.115 g and 6.9 and 7.3 respectively for rock sites, using the conventional probability seismic hazard assessment method (Cornell, 1968). However, both Pun & Ambraseys (1992) and Lee et al (1998) only calculated PGA and intensity, and no ground motion response spectra were established.

The attenuation relationships for PGA and intensity are quite well developed for the South China region including Hong Kong (Lee et al, 1998). The intensity relationships are based on long historical intensity data in China to reflect the response of low rise buildings

having periods up to about 0.2-second. However, long period attenuation (greater than 0.5 seconds) ground motion is more uncertain than short period, due to the lack of strong motion instrumental earthquake data to derive the whole response spectrum. Chandler & Lam (2002) developed a theoretically based seismological attenuation model for the Hong Kong region based on the available research data on the crustal and rock properties in South China. They also found that the shallow crustal shear wave velocity profile of Hong Kong could be between rock conditions of Eastern North America (ENA) and Western North America (WNA).

According to the study by Free et al (2004), on the basis of intensity attenuation observed in China and the USA, also recommended equal weighting of attenuation relationships of ENA and WNA to represent the Hong Kong rock sites in their seismic hazard assessment. The ENA and WNA attention relationships provide spectral accelerations for different structural periods. Based on these relationships, Free et al (2004) developed uniform hazard response spectra for rock sites in Hong Kong having 50%, 10% and 2% probabilities of being exceeded in the next 50 years. The calculated PGA values were 0.075 g, 0.15 g and 0.32 g respectively for the above probabilities. The results, as shown in Figure 4.16, gave higher PGA than this study. The main reason is the use of relatively higher PGA attenuation relationships for Atkinson & Boore (1997) in Free et al (2004) which gives about 30% higher than the current use of attenuation relationships in this study.

The PGA values varied from 0.10 g to 0.15 g defined for the Hong Kong region in the Mainland China Seismic Ground Motion Parameter Zonation map GB 18306 (2001) are shown in Figure 4.17. It can be seen from Figure 4.16 that the PGA at the centre of Hong Kong (HKO), i.e., PGA about 0.1 g, is comparable to the Chinese code at both the 475-year and 2475-year return periods.

4.6.2 Horizontal Response Spectra

4.6.2.1 GEERRI Study (2010)

The horizontal response spectral values determined in this study are compared with the results from GEERRI study in the Appendix A. The response spectra for 10%, 50% and 2% chance probability being exceeded in next 50 years are compared in Figure 4.18. It can be seen that while the response spectrum values from this study are smaller than those determined by GEERRI at long periods they agree well at shorter periods. This is consistent with the observations from the Yu (2005) attenuation model in the GEERRI study as discussed above.

In addition, the validation between Arup seismic hazard program *Oasys* SISMIC and GEERRI program ESE have been carried out by using the same GEERRI source model and Yu (2005) attenuation model for the 10% in 50-year ground motion. The focus depth in this program comparison is assumed to be a constant of 10 km in order to follow the same assumption of the GEERRI model. Figure 4.19 shows that the results of the comparison between these two computer models are very consistent.

4.6.2.2 Arup Study for BD (2003)

Arup carried out a seismic hazard study (Free et al, 2004) for Hong Kong as part of their hazard and risk study for the Buildings Department (BD) in 2003. Results from the current study are compared with the BD's study (Figure 4.20). The comparison shows that the response spectral values from the current study are smaller than those in the BD study at short periods. As explained previously, the short period attenuation relationships used in the BD study were higher than the more recent attenuation models used in the current study. Response spectral values for the long periods are agreed well with the BD's study.

4.6.2.3 Chinese Code GB50011-2010

The acceleration response spectra from the current study are compared with the spectra determined using the Chinese Seismic Code for Buildings coefficients in Figure 4.21. The Chinese Code values have been derived using the coefficients listed in the code for Hong Kong. The Chinese code shows two values of PGA for the 10% in 50 year (475-year return period) values for Hong Kong, namely 0.10 g and 0.15 g.

The spectrum with PGA of 0.10 g presented by the Chinese Code agrees well with the spectrum of the current study up to a structural period of 1 second. It is quite apparent that the Chinese Seismic Code for Buildings design spectra are very conservative at longer periods. However, the spectrum produced by the GEERRI study exceeds even the spectral upper range of the Chinese Code at periods greater than 0.2-second.

4.7 Comparison with Other Regions

4.7.1 Comparison of Seismicity

The seismicity of the Hong Kong region, in terms of the average recurrence relationship, is compared with recurrence relationships published for other regions of the world in Figure 4.22. It can be seen that the seismicity of the Hong Kong region is very similar to Eastern North America and about 40 times less than that in highly seismic areas such as California, Japan, Taiwan or the Philippines.

4.7.2 Comparison for New York, USA

The 2% in 50 years ground motion response spectra determined in this study are compared with the 0.2-second and the 1.0-second spectral values defined in the International Building Code (IBC) for New York City (IBC, 2009) in Figure 4.23. It can be seen that these values for New York are similar to those of the current study for the NW New Territories of Hong Kong. The results of the recent study for the New York City Department of Transport by Weidlinger Associates (2000) also show similar results at all structural periods (see Figure 4.23).

4.7.3 IBC2009

The acceleration response spectra of the current study are compared with the spectra determined using the 2009 International Building Code (IBC) Provisions coefficients in Figures 4.24. These curves are created by using formulae anchored to the short period 0.2-second (S_S) and long period 1-second (S_1) values by the current study. Therefore, there must be perfect agreement at these two periods. This comparison shows that the spectra from the current study are compatible with the IBC formulae.

4.8 Seismic Hazard Contour Plots for Hong Kong

Figures 4.25 to 4.30 show calculated PGA and spectral acceleration for periods of 0.2-second and 1-second for rock site contoured across the Hong Kong region. The contours give the values for ground motions having a 10% and 2% probability of being exceeded in the next 50 years.

The contours were developed by running the hazard model at 25 locations evenly spaced across the Hong Kong region. It is interesting to note that the variation (expressed as a ratio) across the region is somewhat slightly greater for the PGA ground motion (1.78 for the 2% in 50 year) than that for the 0.2-second and 1-second ground motion (1.67 and 1.65 respectively for the 2% in 50 year).

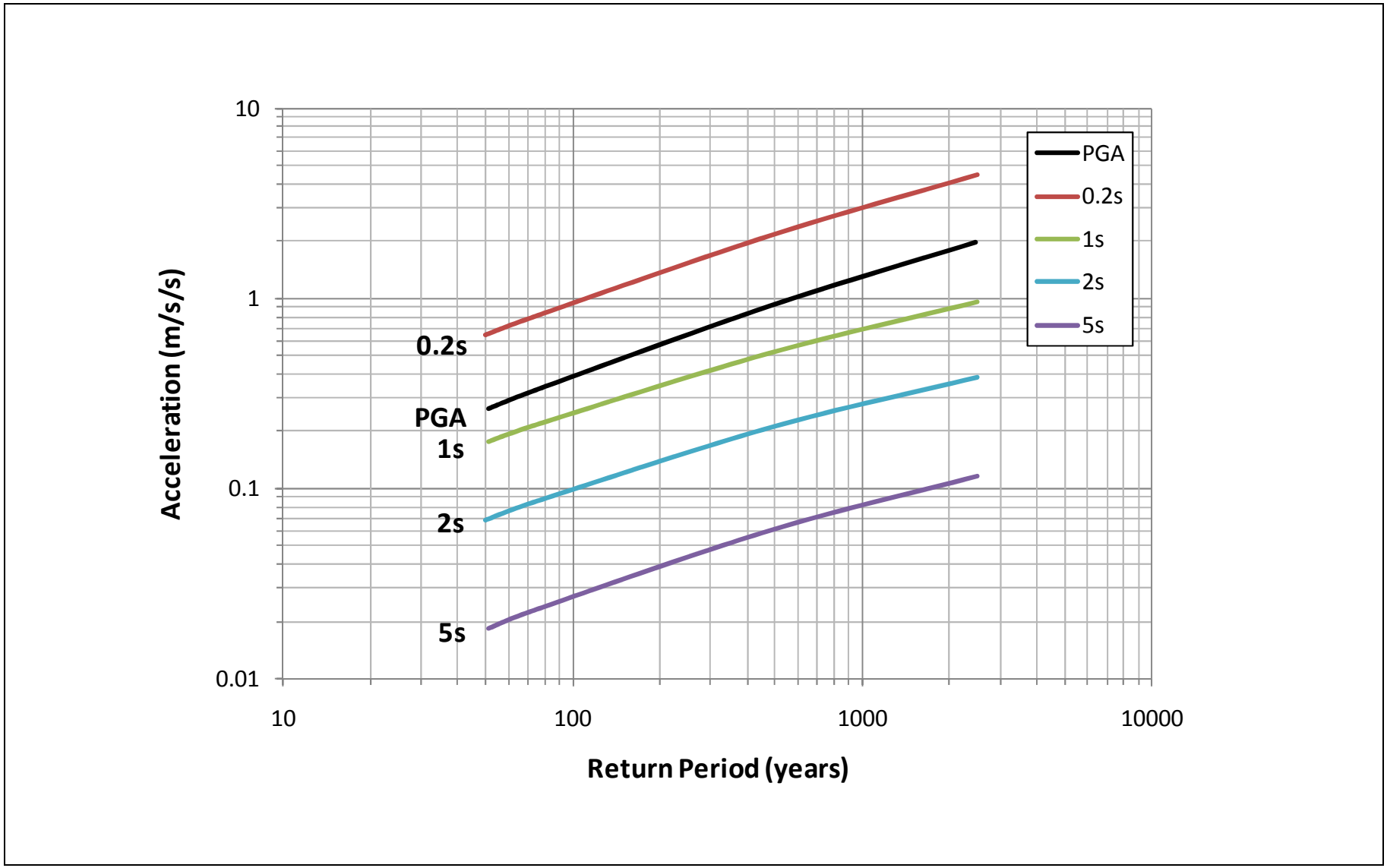

Figure 4.1 Hazard Curve for Peak Horizontal Acceleration for Rock Site

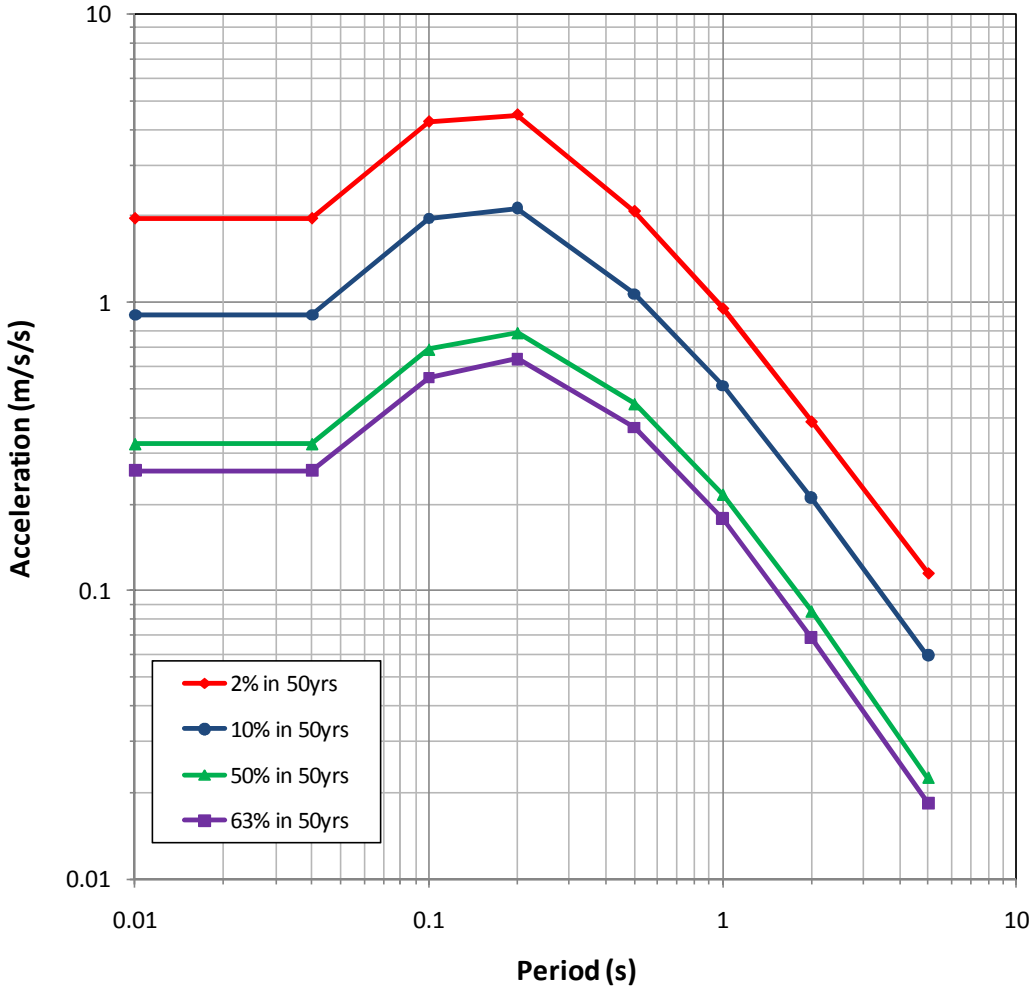

Figure 4.2 Uniform Hazard Horizontal Acceleration Response Spectra

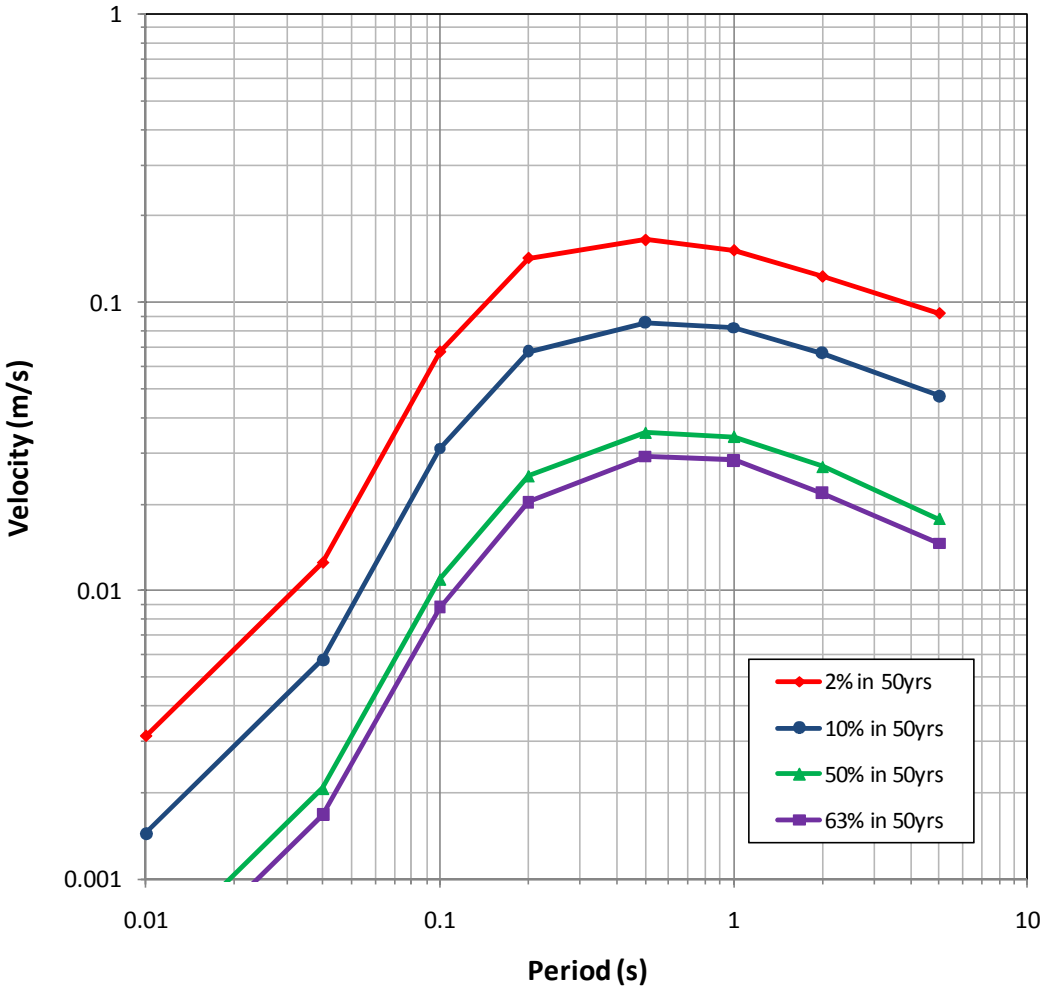

Figure 4.3 Uniform Hazard Horizontal Velocity Response Spectra

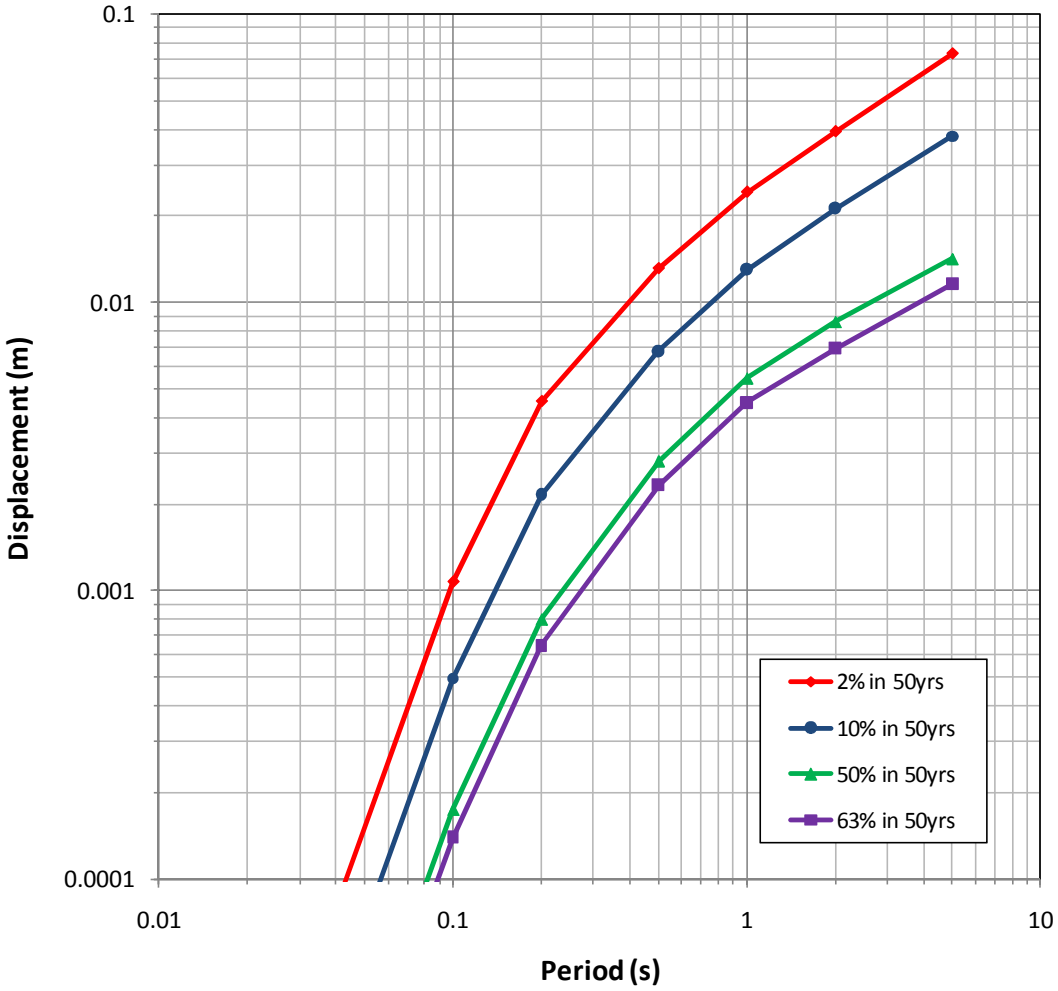

Figure 4.4 Uniform Hazard Horizontal Displacement Response Spectra

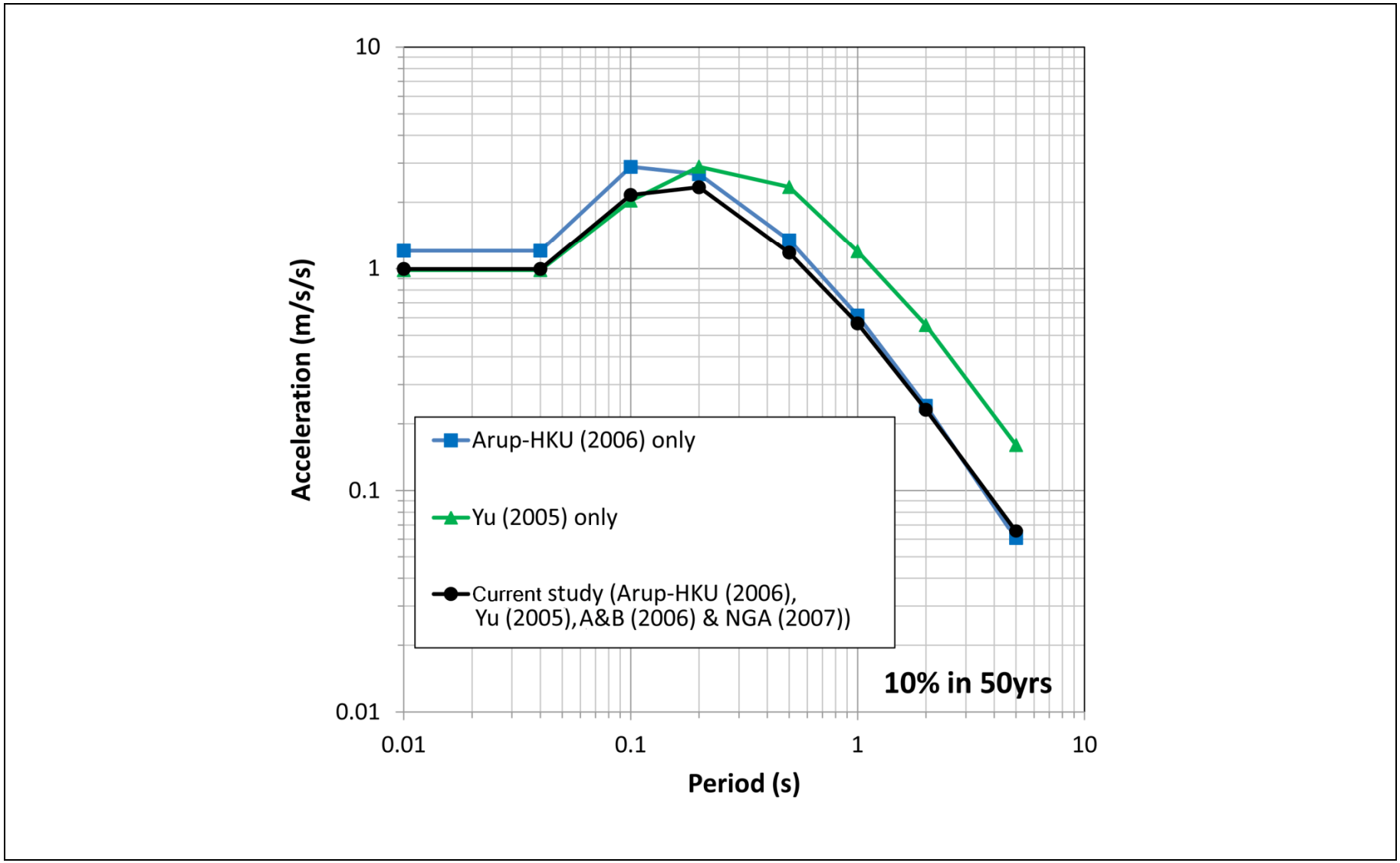

Figure 4.5 Comparison of Response Spectrum of Different Attenuation Relationships (Location at the Hong Kong Observatory)

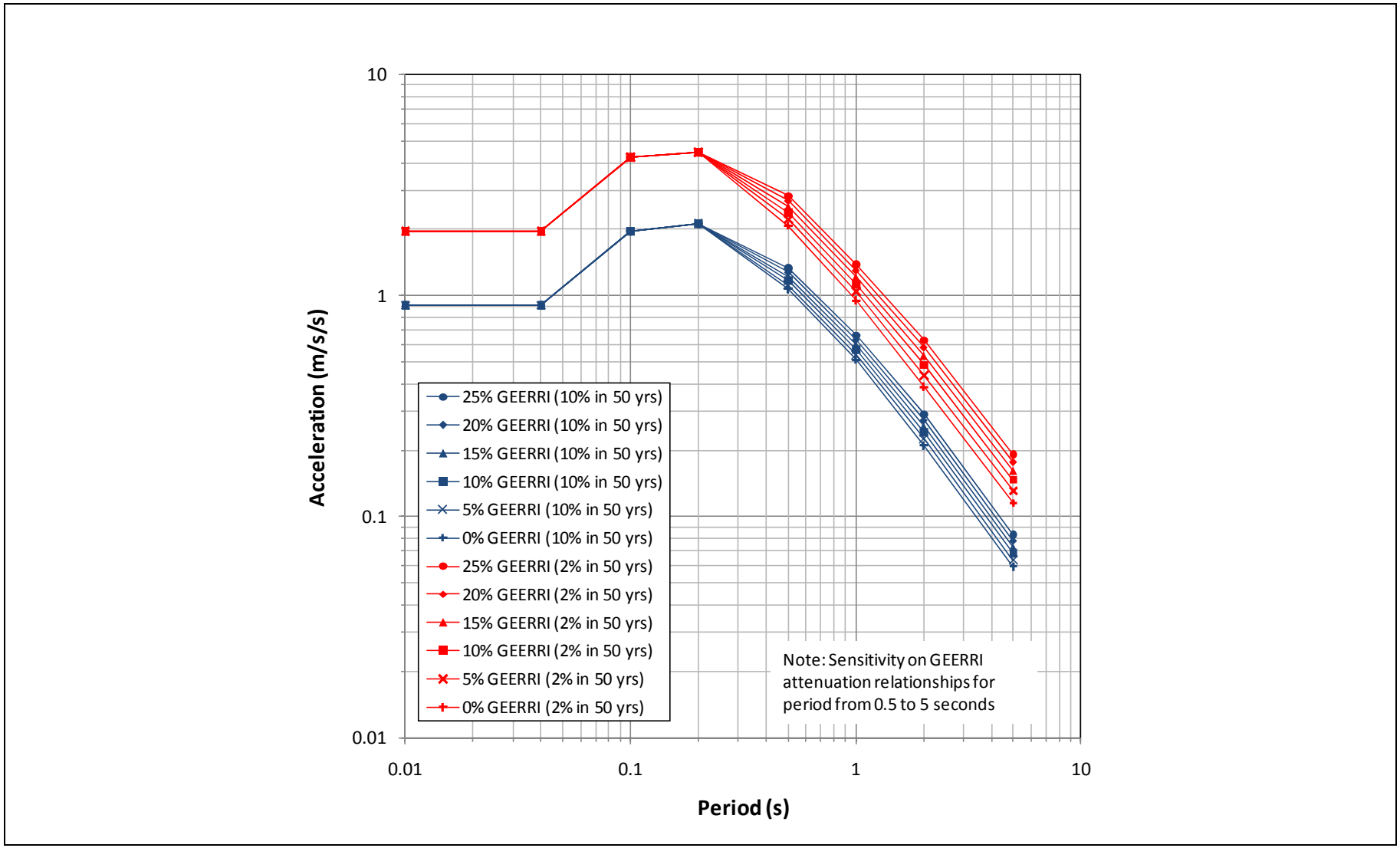

Figure 4.6 Comparison of Uniform Hazard Horizontal Acceleration Response Spectra with Different Weighting of Yu (2005) after 0.2 Seconds

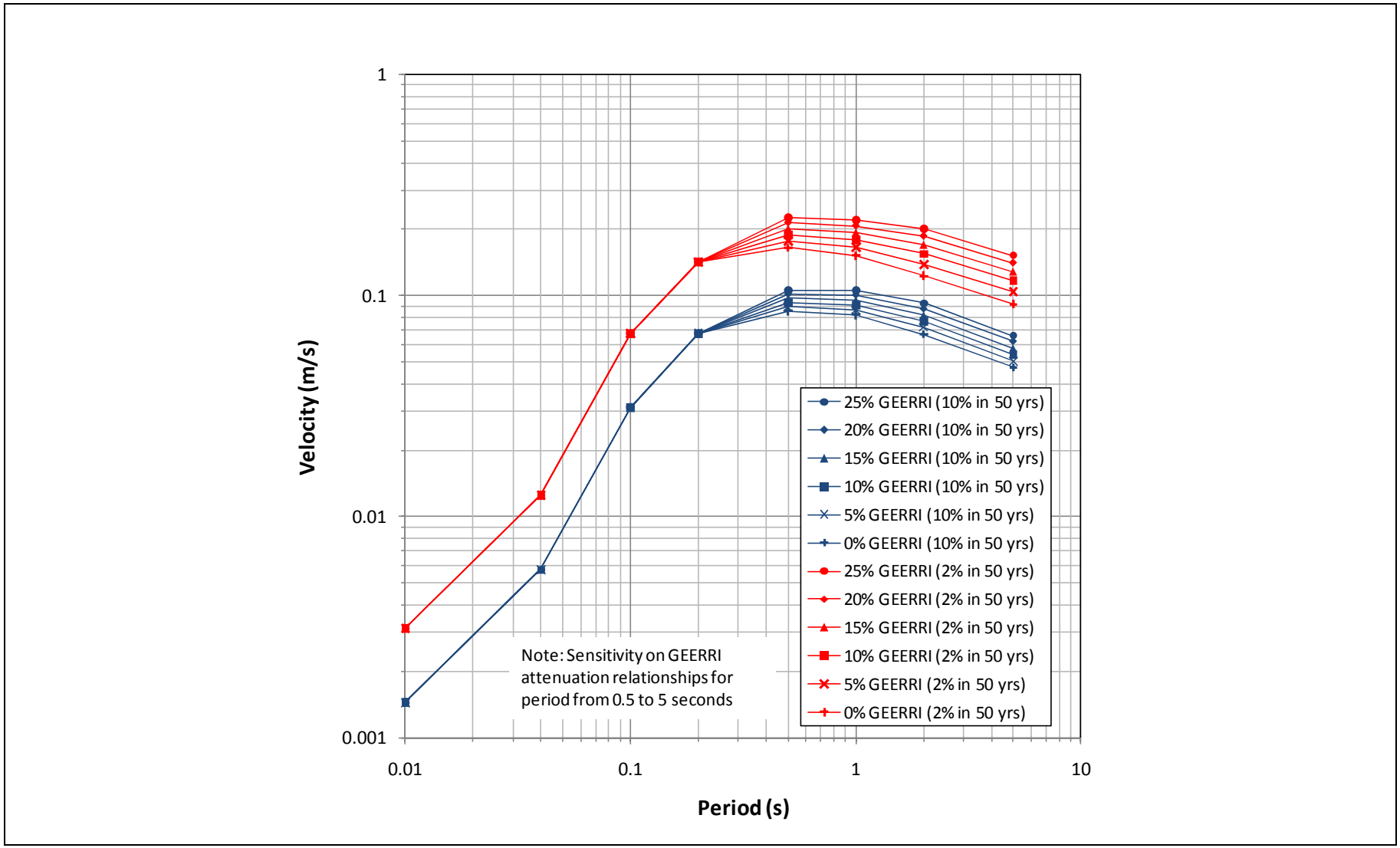

Figure 4.7 Comparison of Uniform Hazard Horizontal Velocity Response Spectra with Different Weighting of Yu (2005) after 0.2 Seconds

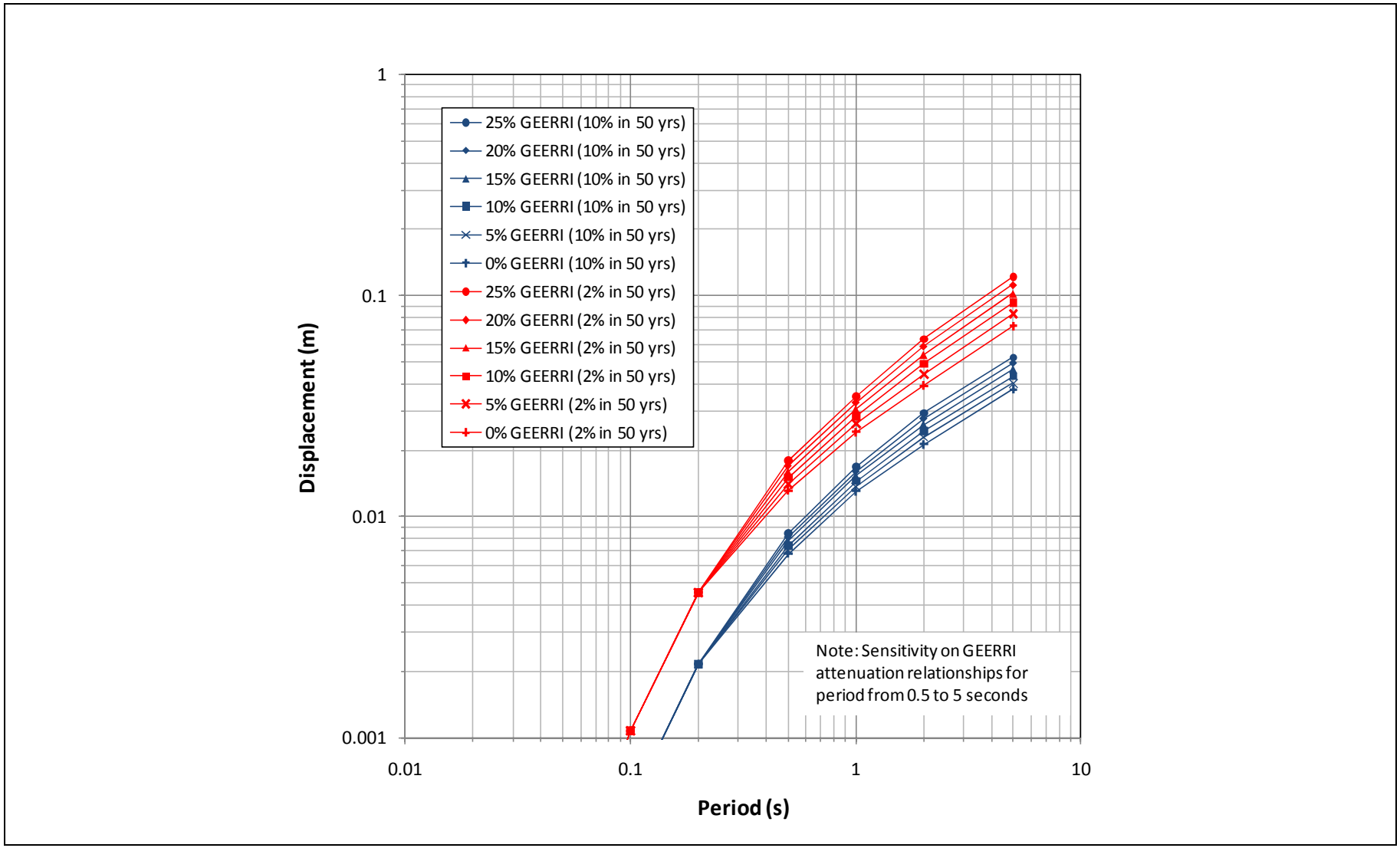

Figure 4.8 Comparison of Uniform Hazard Horizontal Displacement Response Spectra with Different Weighting of Yu (2005) after 0.2 Seconds

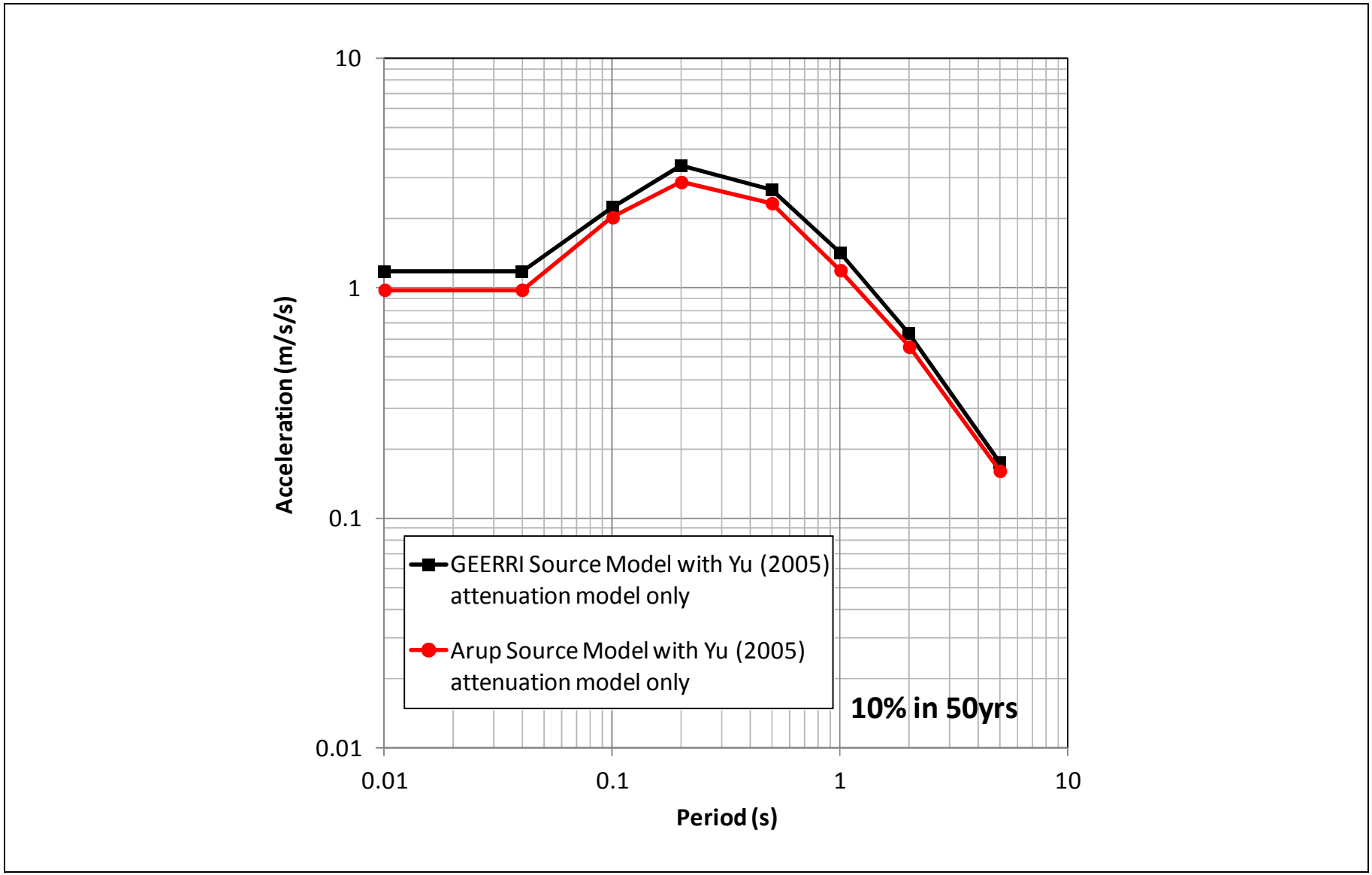

Figure 4.9 Comparison of Response Spectrum between Arup and GEERRI Source Models

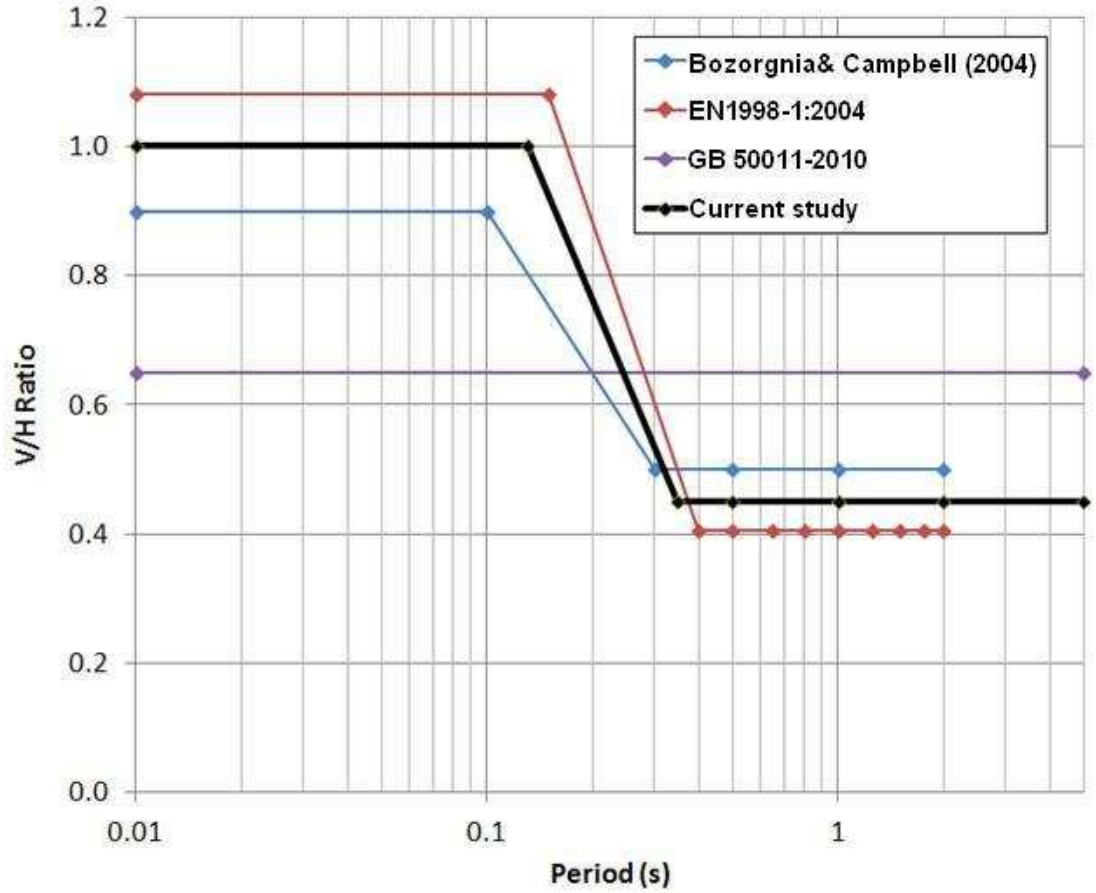

Figure 4.10 Comparison of Vertical to Horizontal (*V*/*H*) Ratios

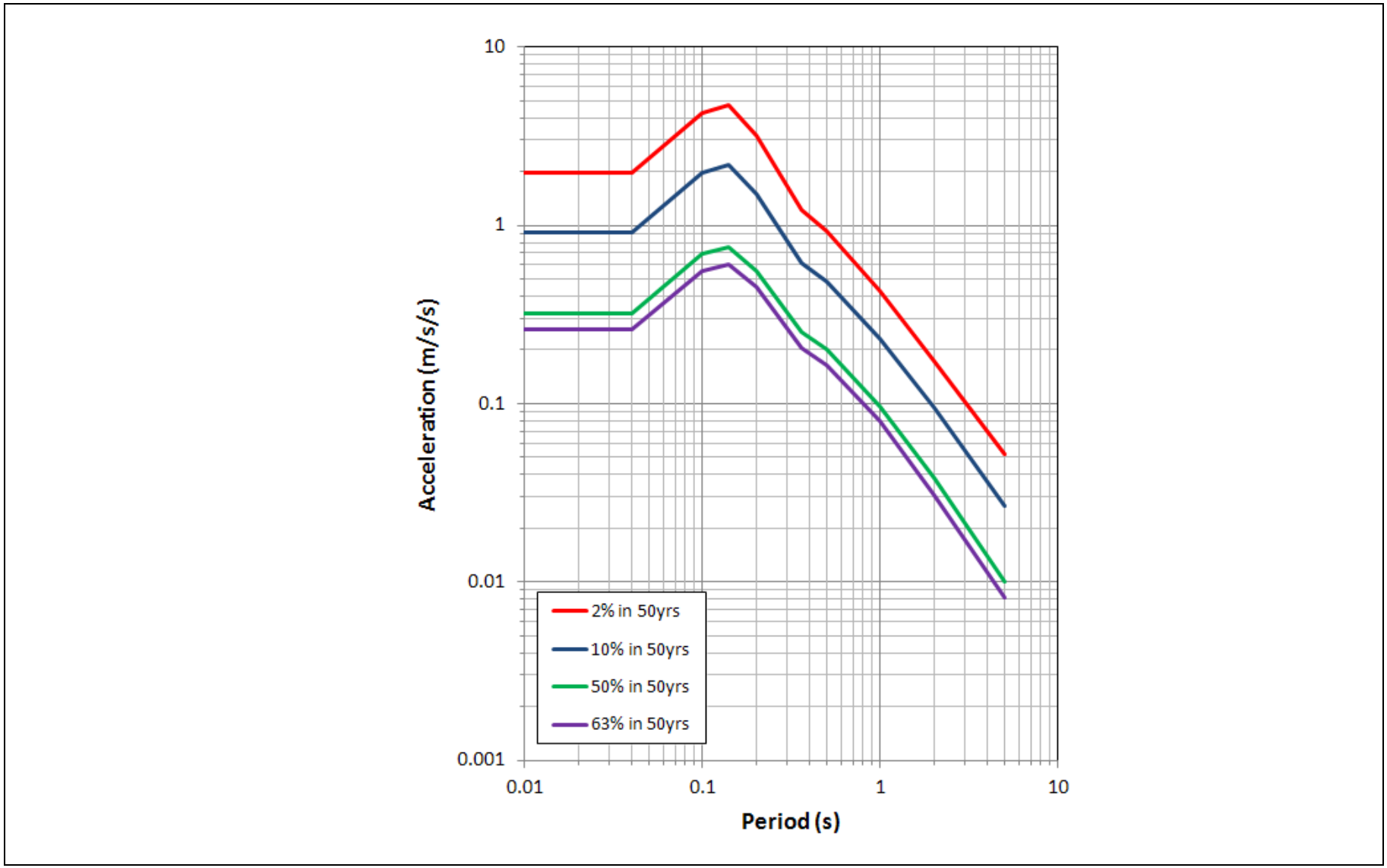

Figure 4.11 Derived Vertical Acceleration Response Spectra

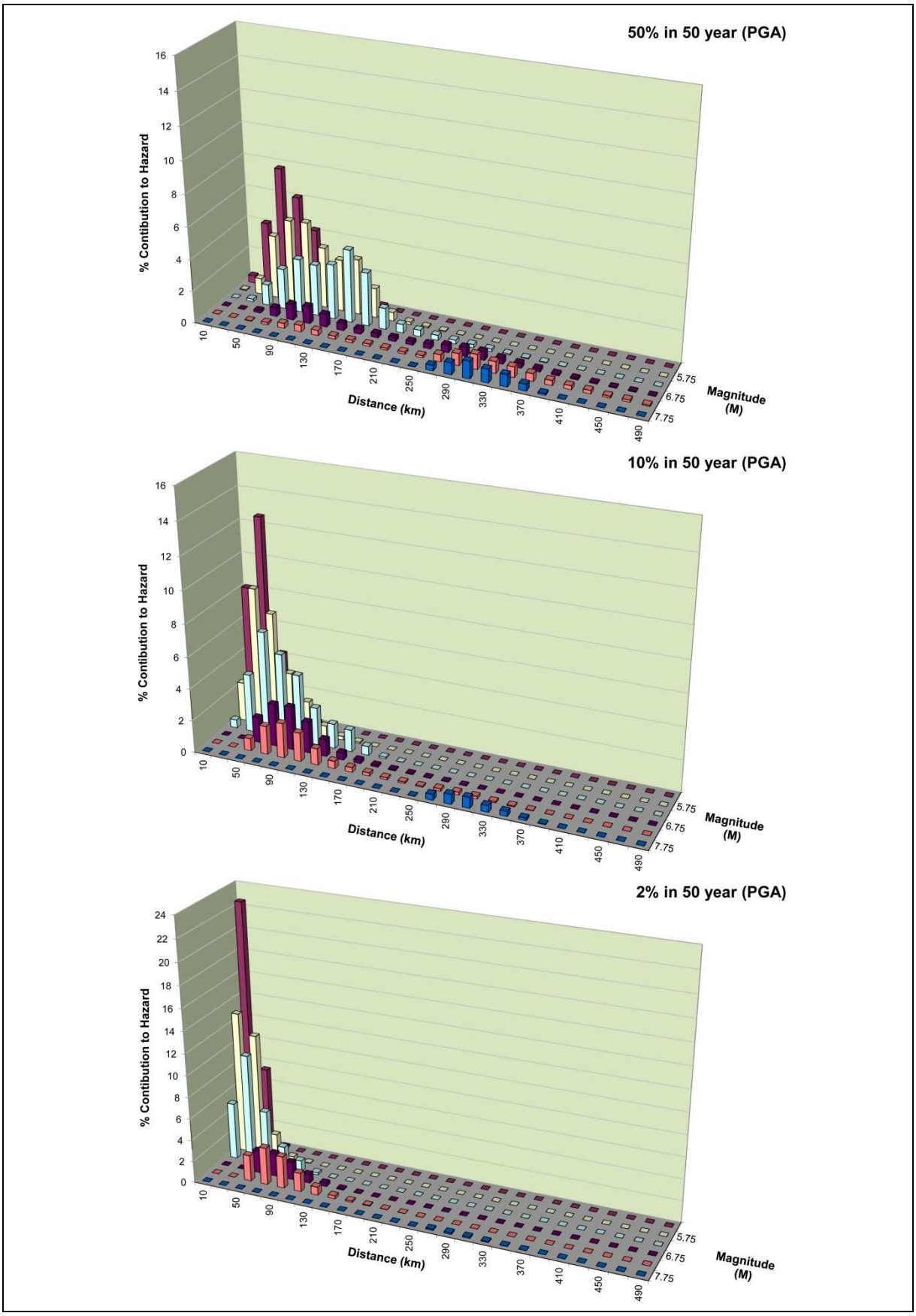

Figure 4.12 De-aggregation Plot for PGA

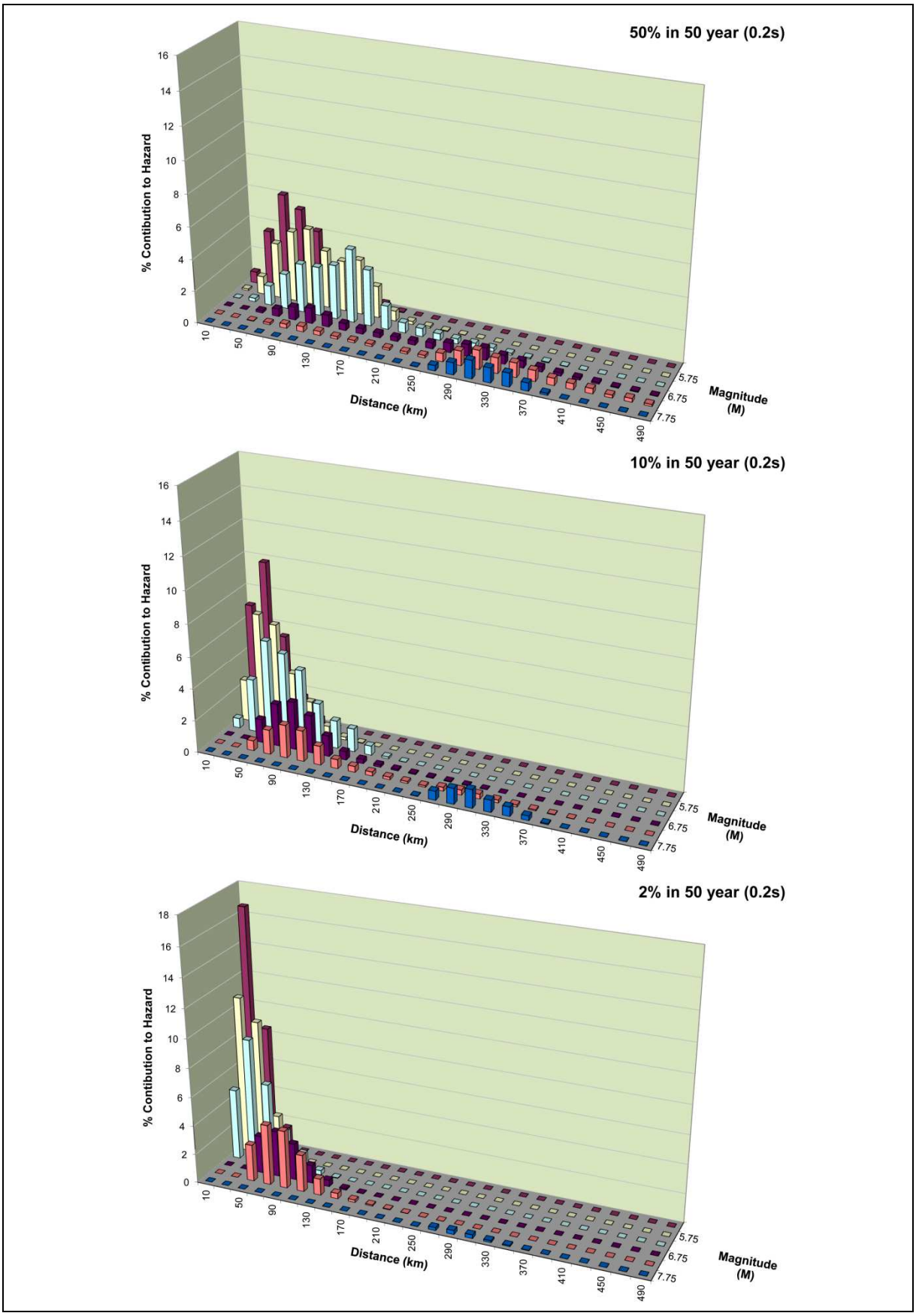

Figure 4.13 De-aggregation Plot for 0.2 Seconds Ground Motion

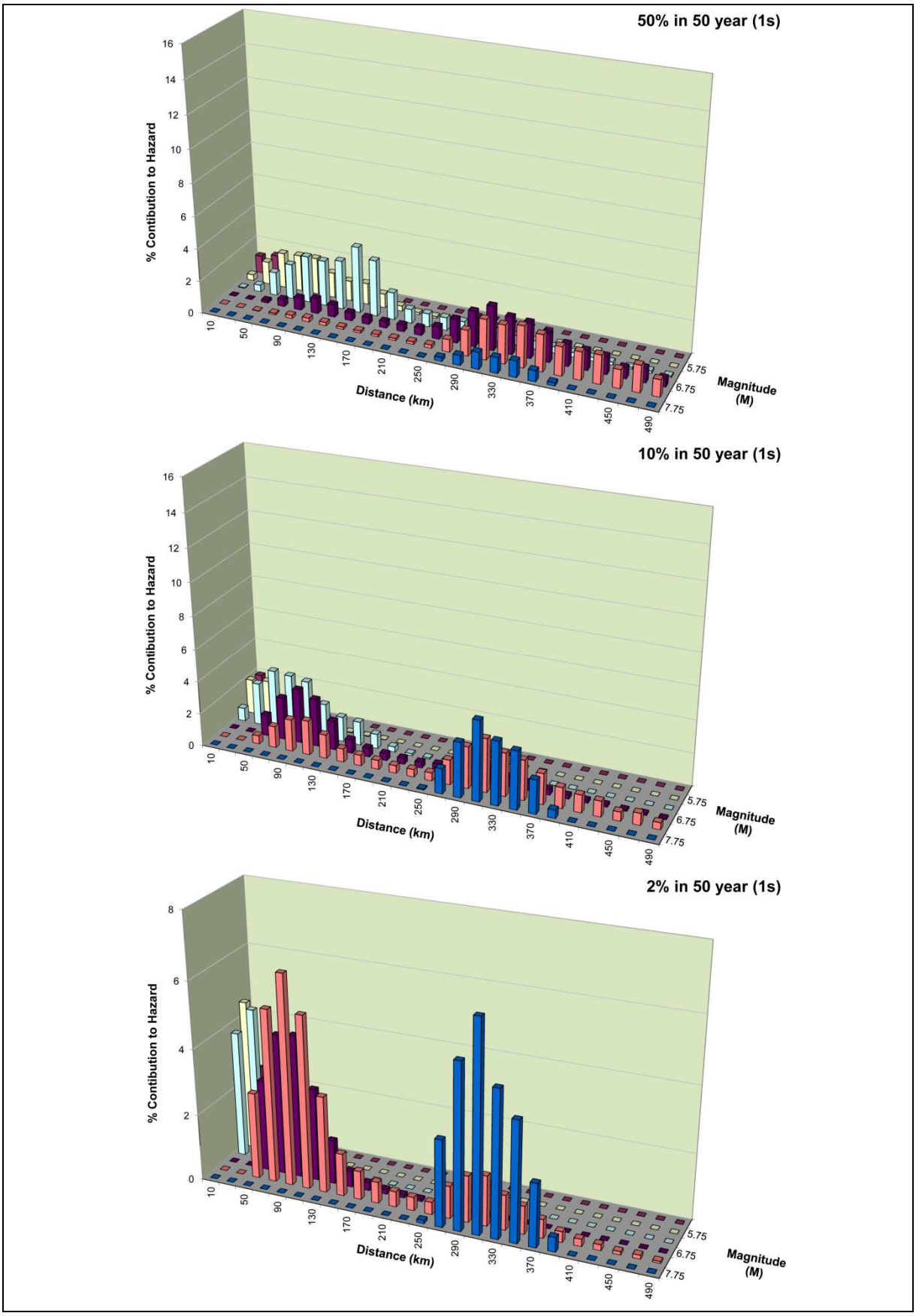

Figure 4.14 De-aggregation Plot for 1 Second Ground Motion

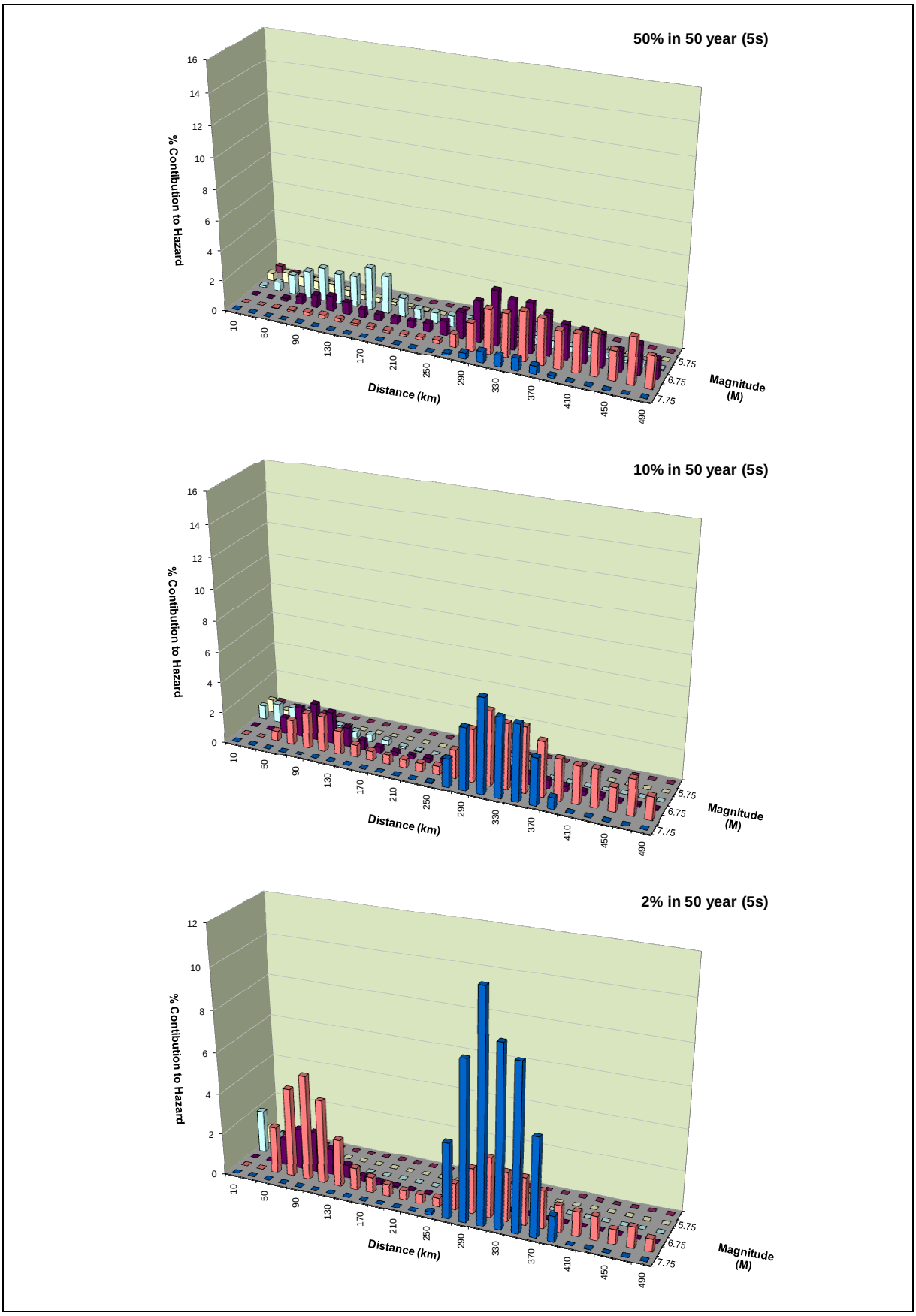

Figure 4.15 De-aggregation Plot for 5 Seconds Ground Motion

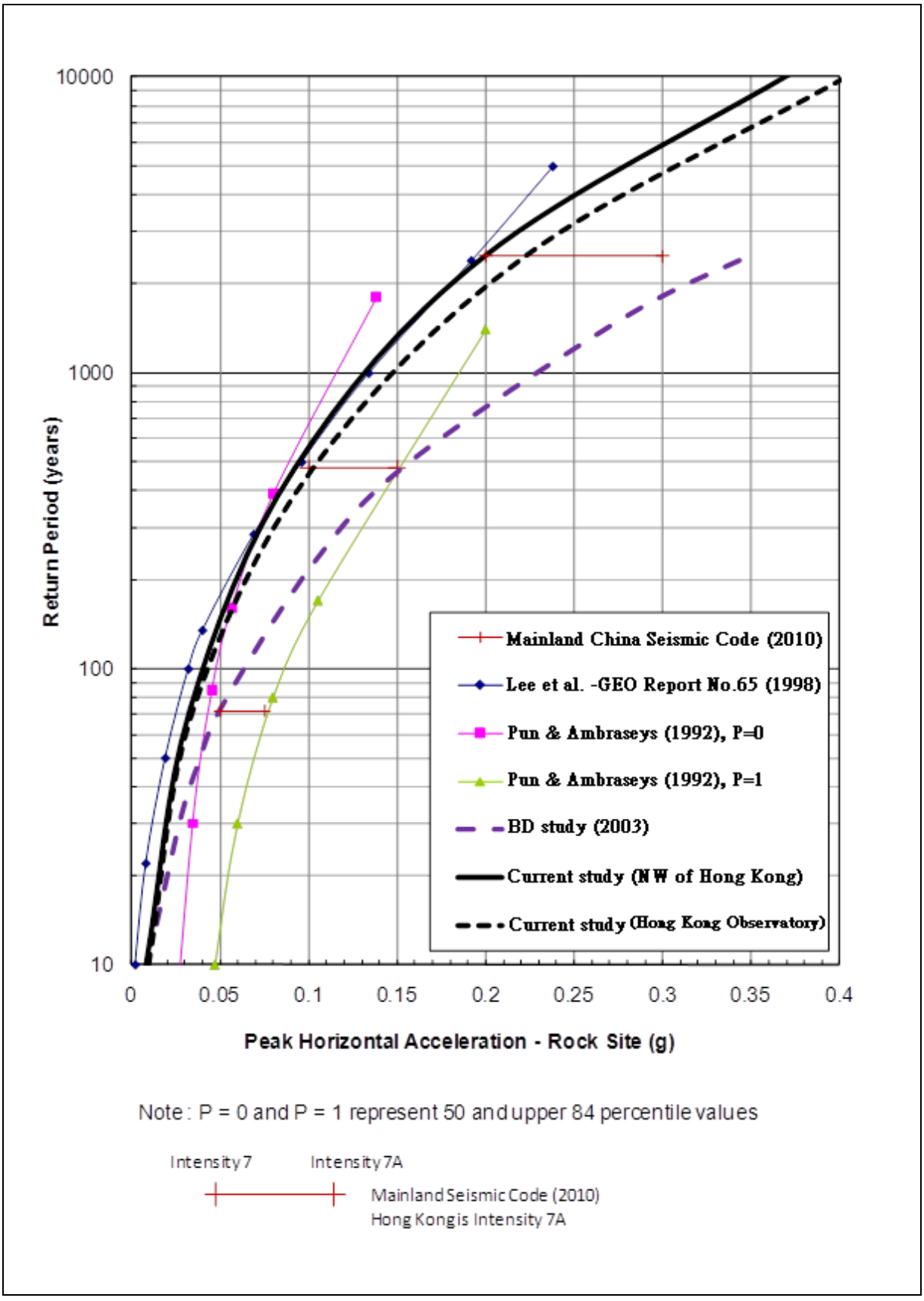

Figure 4.16 Comparison of Peak Horizontal Acceleration for Rock Site with Previous Studies by Others

Table of Contents
Table of Contents
Table of Contents
Table of Contents

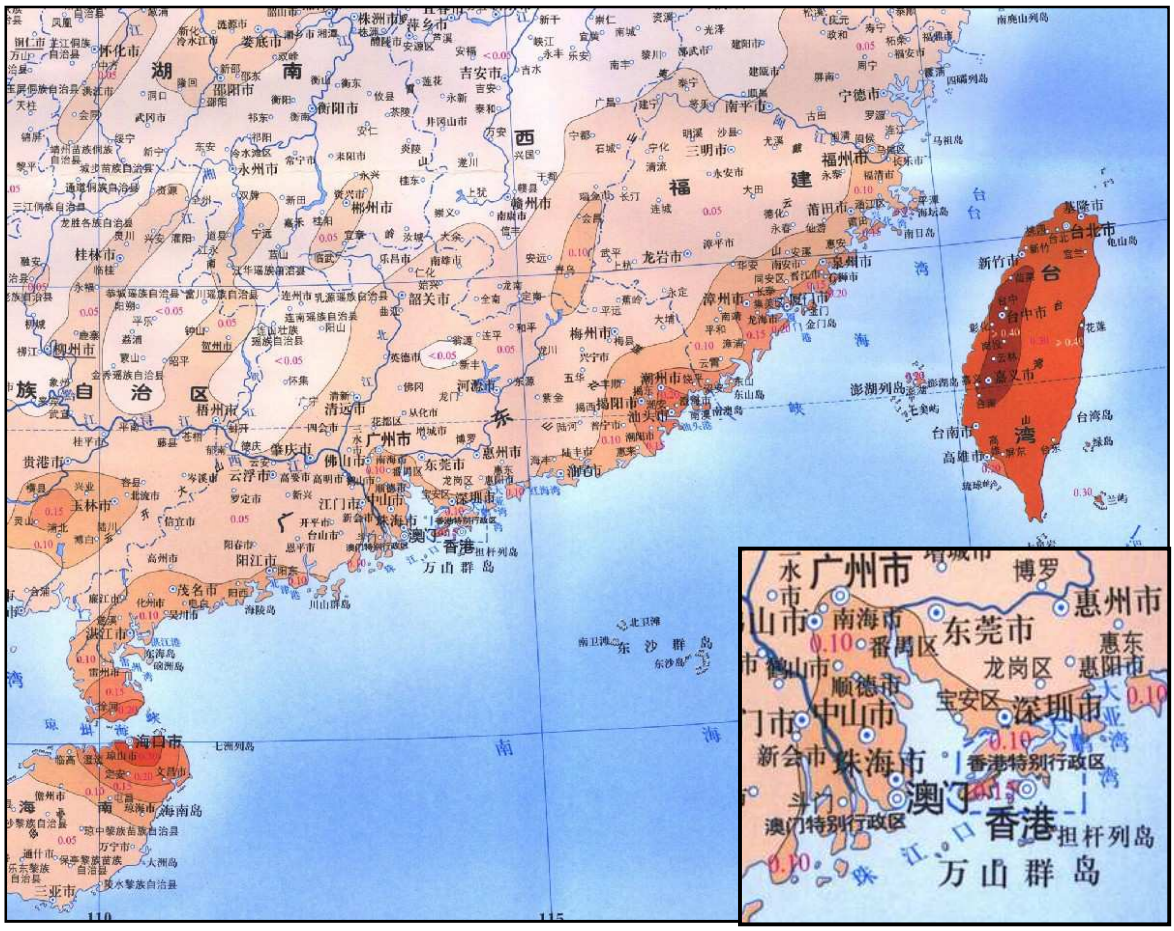

Note: The values in red on the map are the peak ground acceleration values, in units of g, having a 10% chance of being exceeded in the next 50 years

Figure 4.17 Chinese Seismic Design Code, Acceleration Zoning Map of China (GB18306-2001)

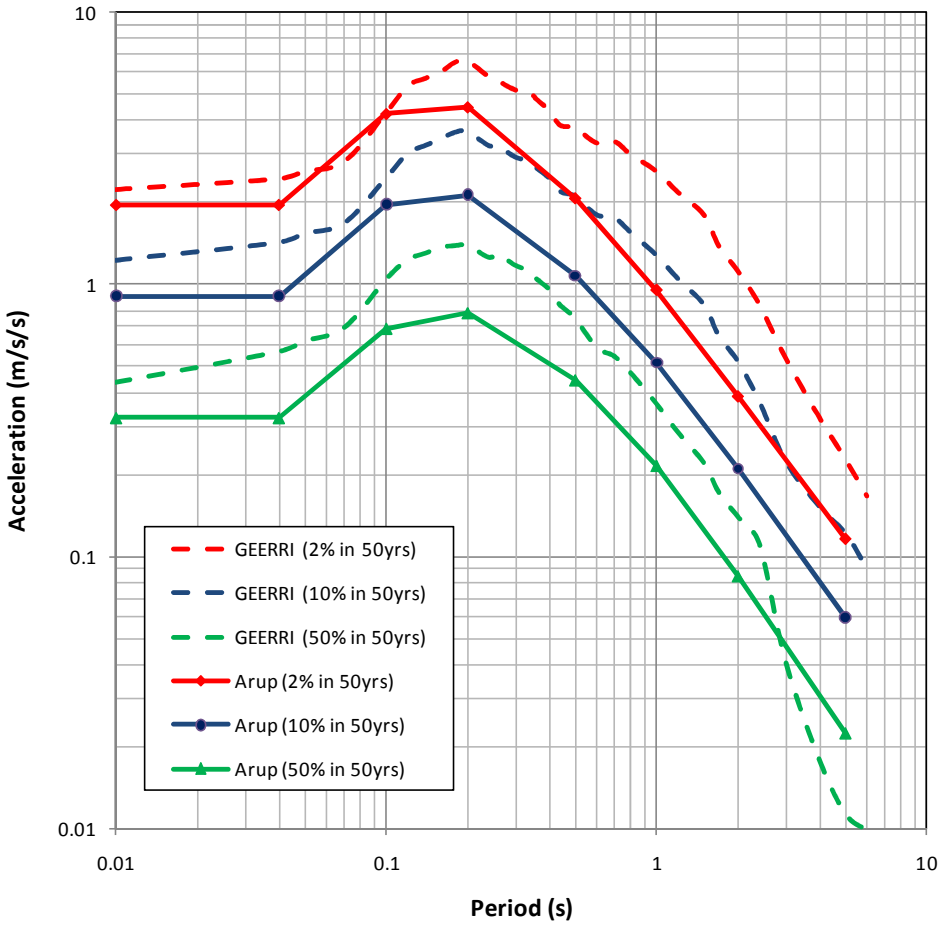

Figure 4.18 Comparison of Acceleration Response Spectra between Arup and GEERRI

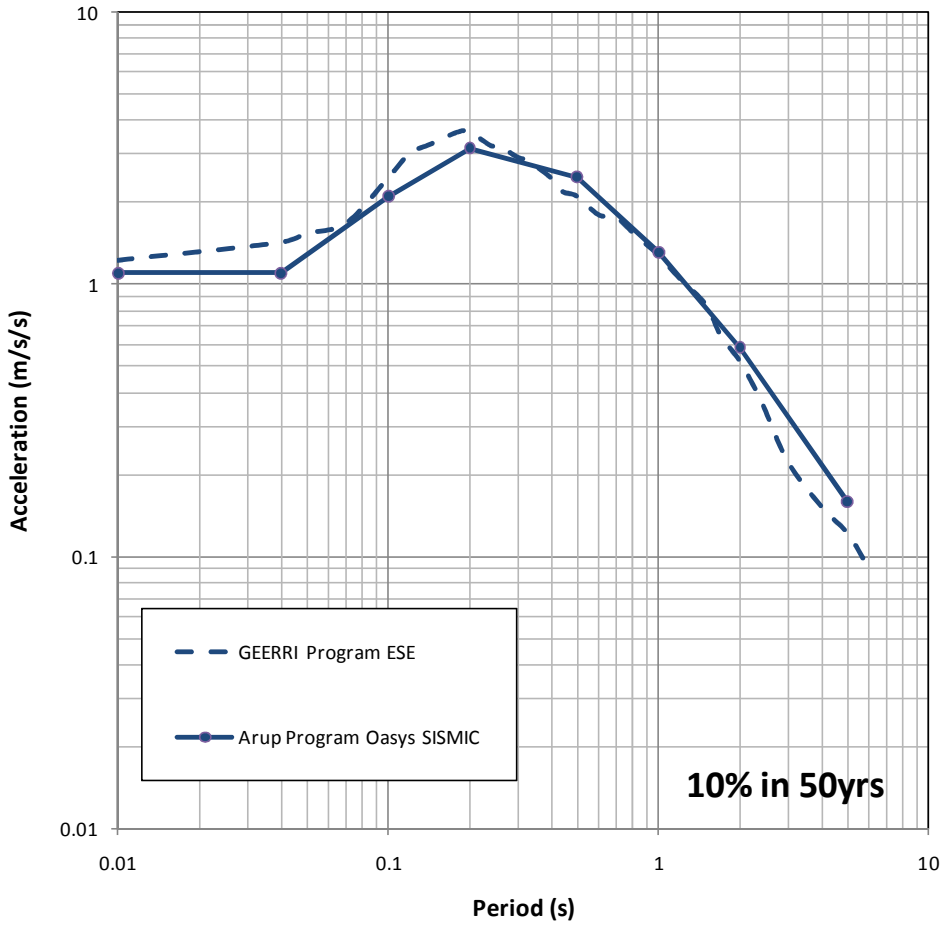

Figure 4.19 Comparison of Acceleration Response Spectra between Arup Program *Oasys* SISMIC and GEERRI Program ESE

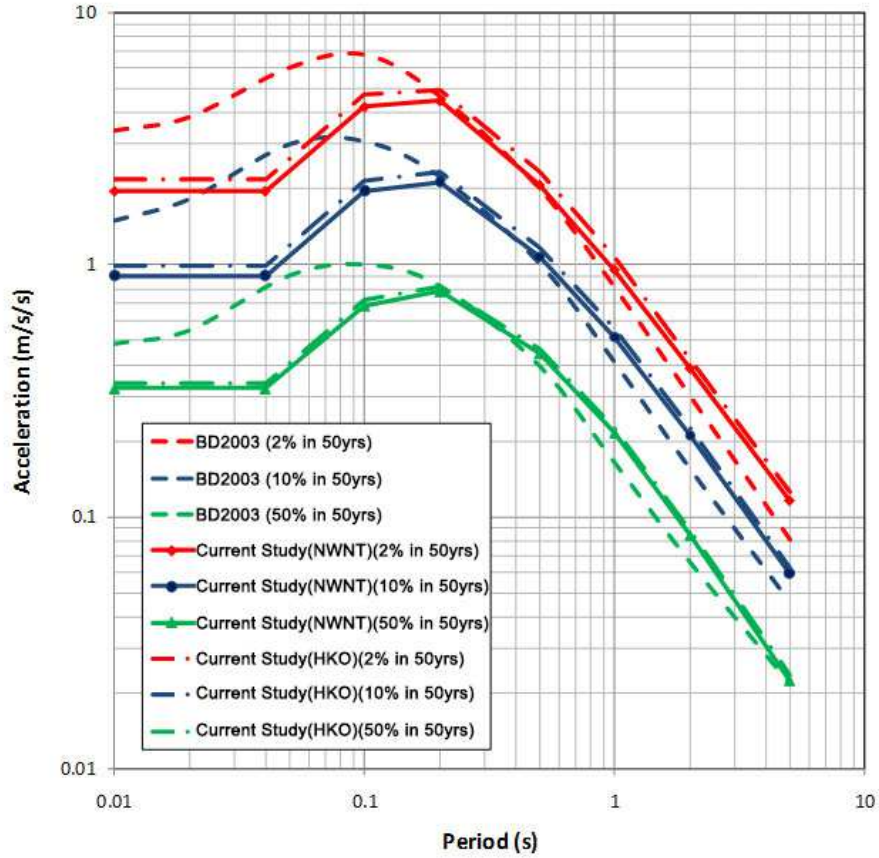

Figure 4.20 Comparison of Horizontal Response Spectra between the current Study and the 2003 BD Study by Arup

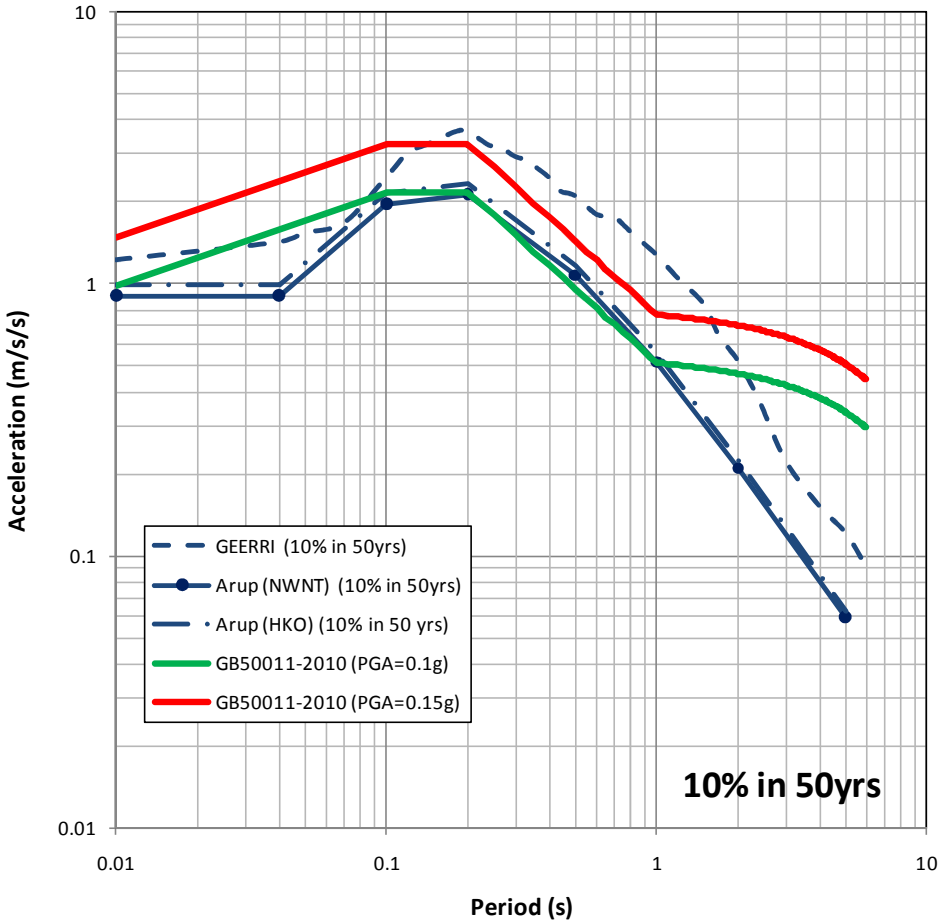

Figure 4.21 Comparison of Horizontal Response Spectra between the current Study and the Chinese Seismic Code GB50011-2010

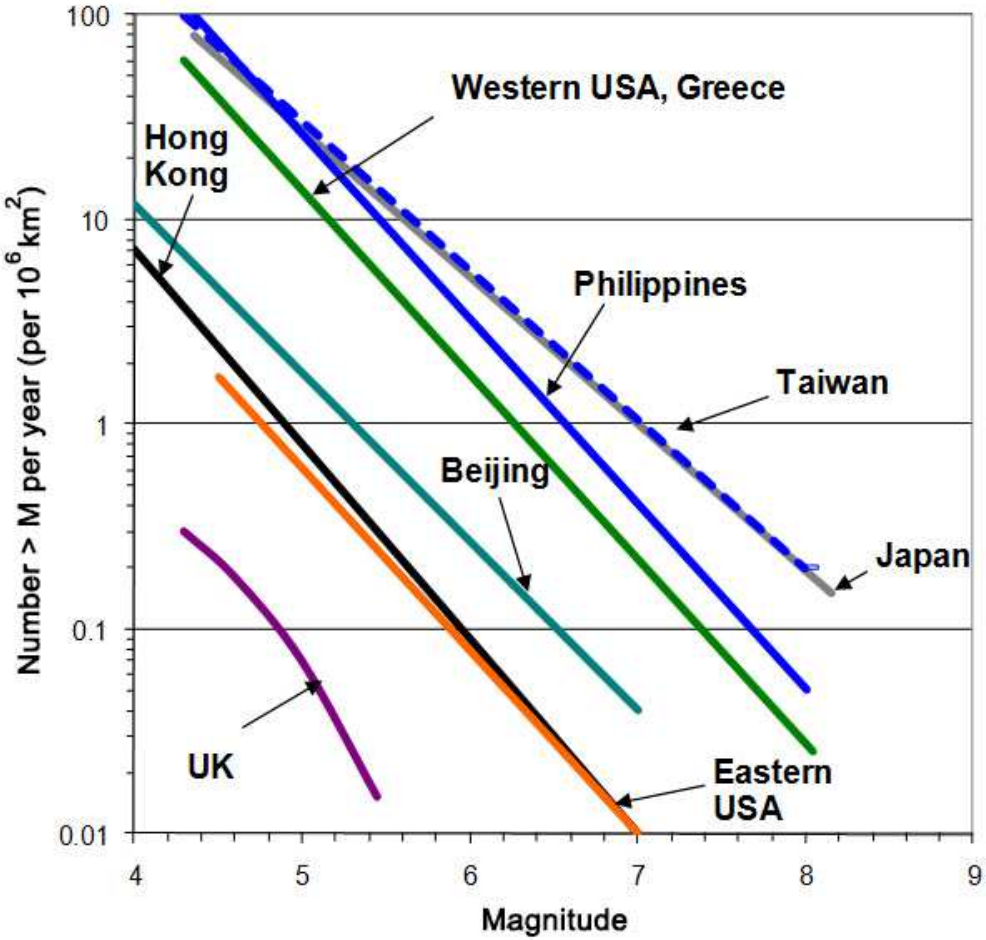

Sources:
UK: Ove Arup & Partners (1993)
Eastern USA: Atkinson (1989)
Western USA: Atkinson (1989)
Philippines: Ove Arup & Partners (1990)
Japan: Tsapanos (1988)
Greece: Tsapanos (1988)
Beijing: Ove Arup & Partners - unpublished

Figure 4.22 Comparison of Seismicity of the Hong Kong Region with Other Regions

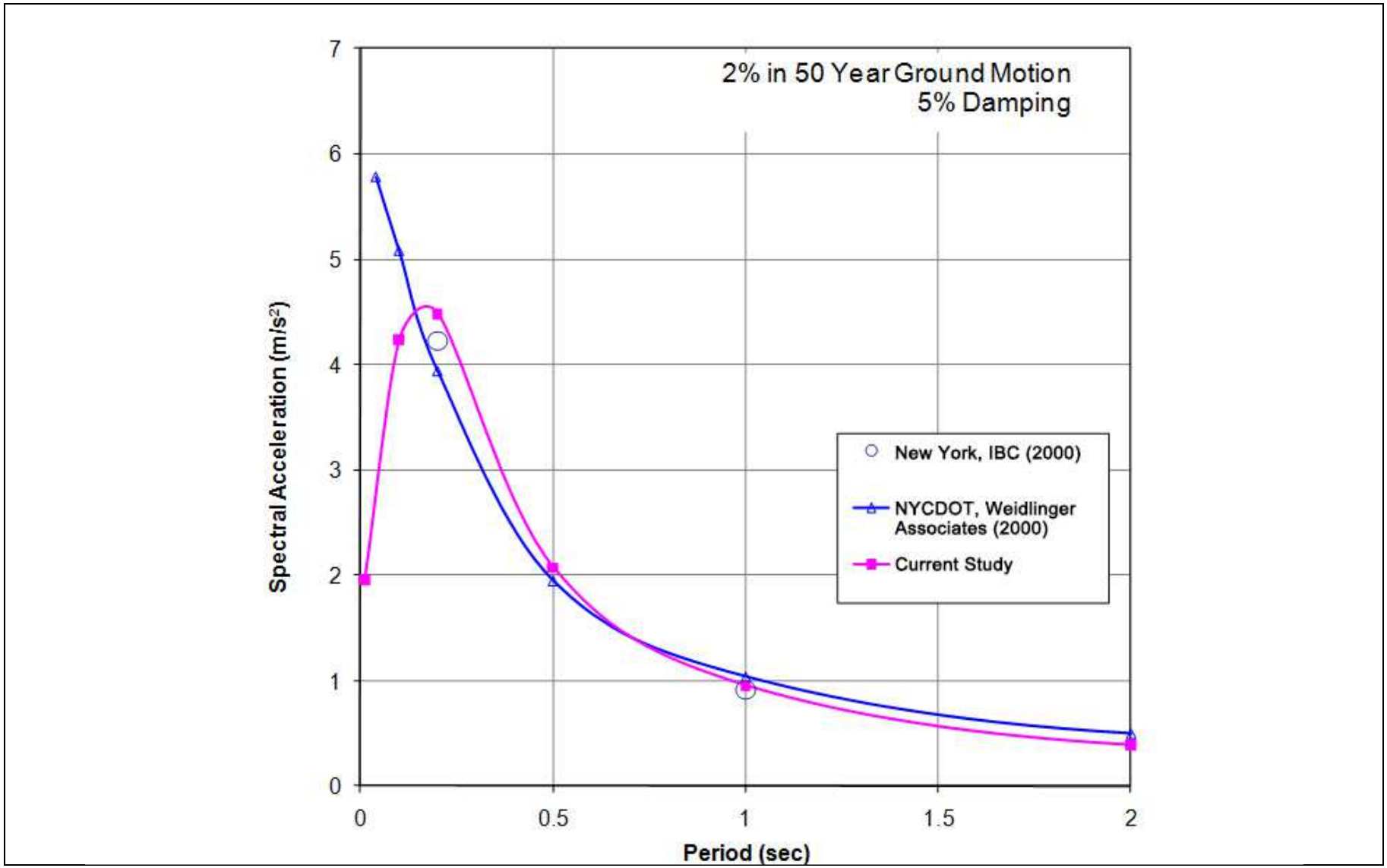

Figure 4.23 Comparison of Response Spectra Values with IBC 2000 and NYCDOT, Weidlinger Associates (2000) for New York

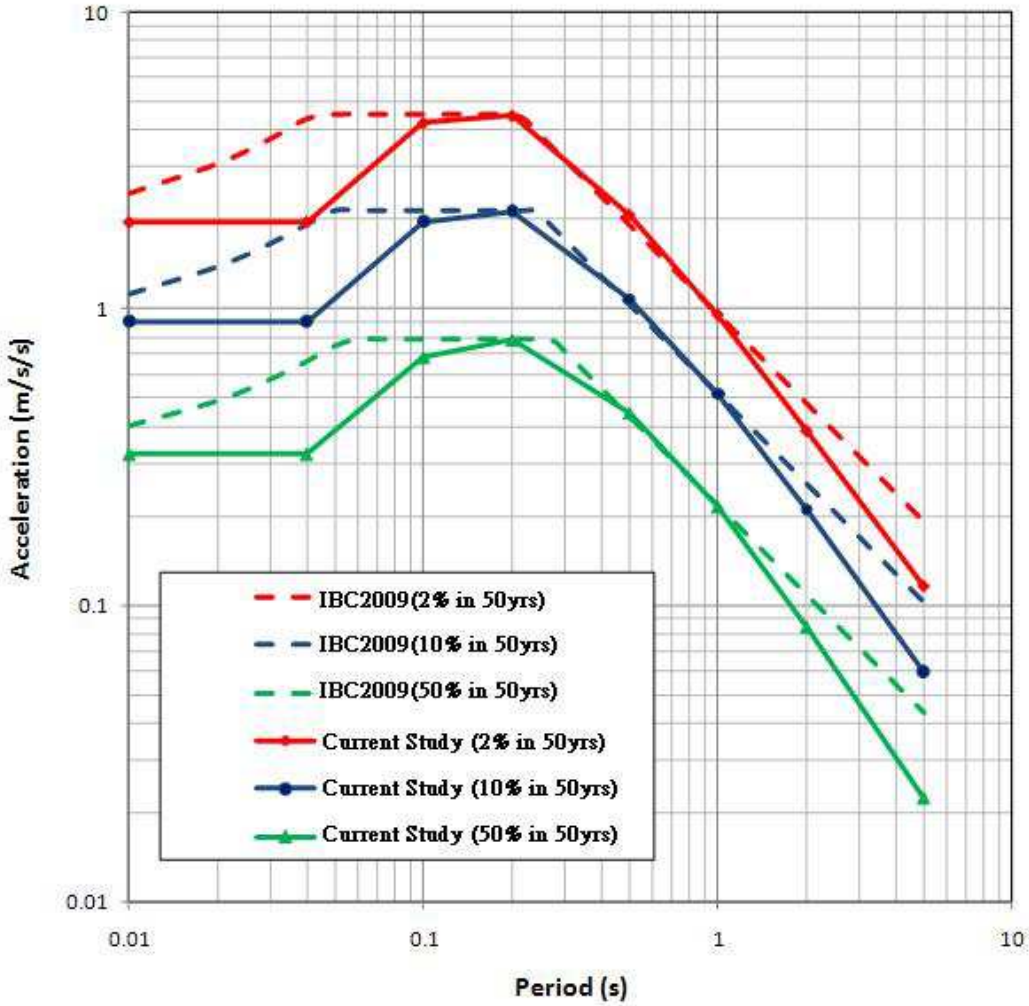

Figure 4.24 Comparison of Response Spectra Values with the current Study and IBC2009

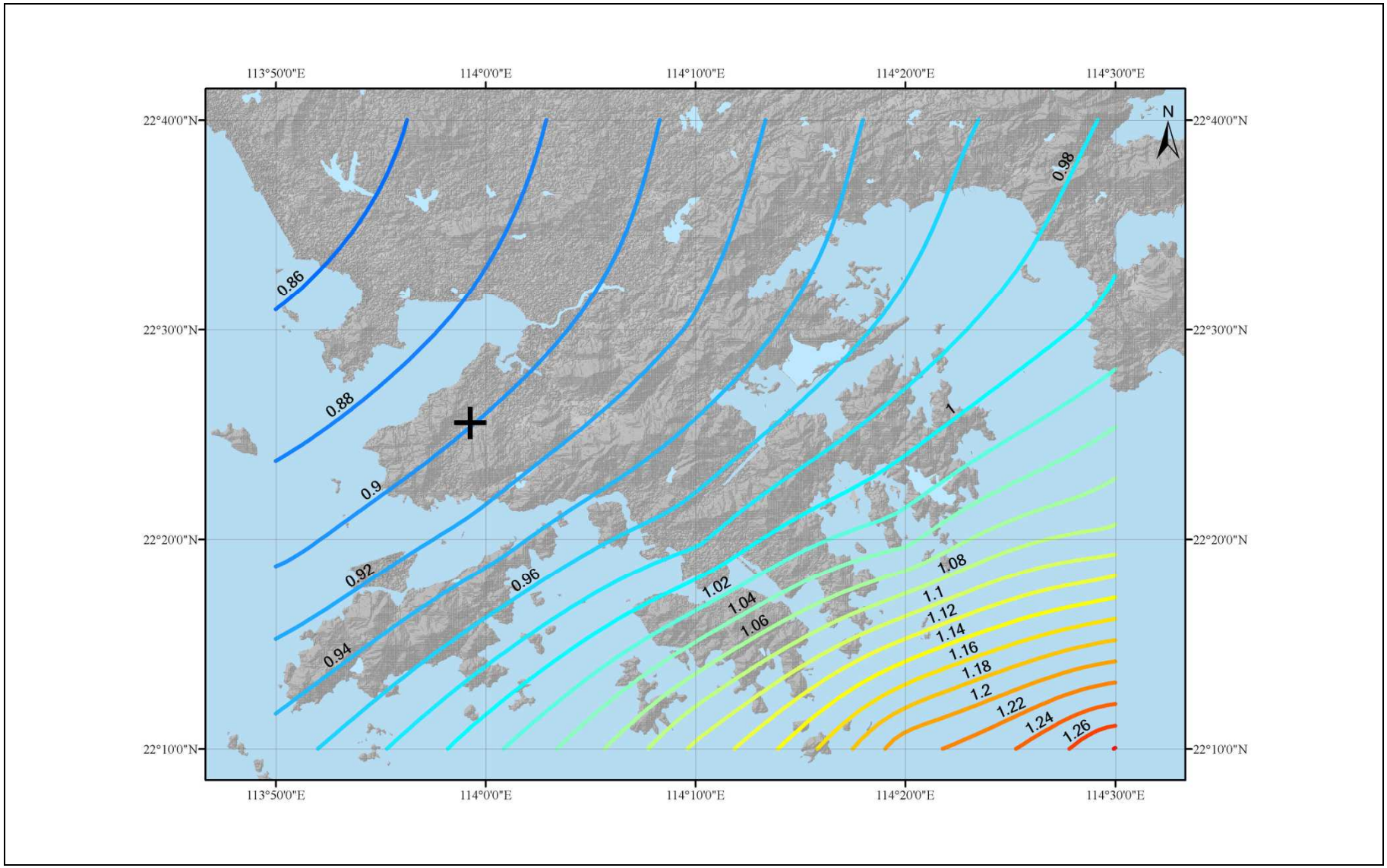

Figure 4.25 Contour Plot for PGA (m/s^2) for a 10% Probability of Being Exceeded in the Next 50 Years

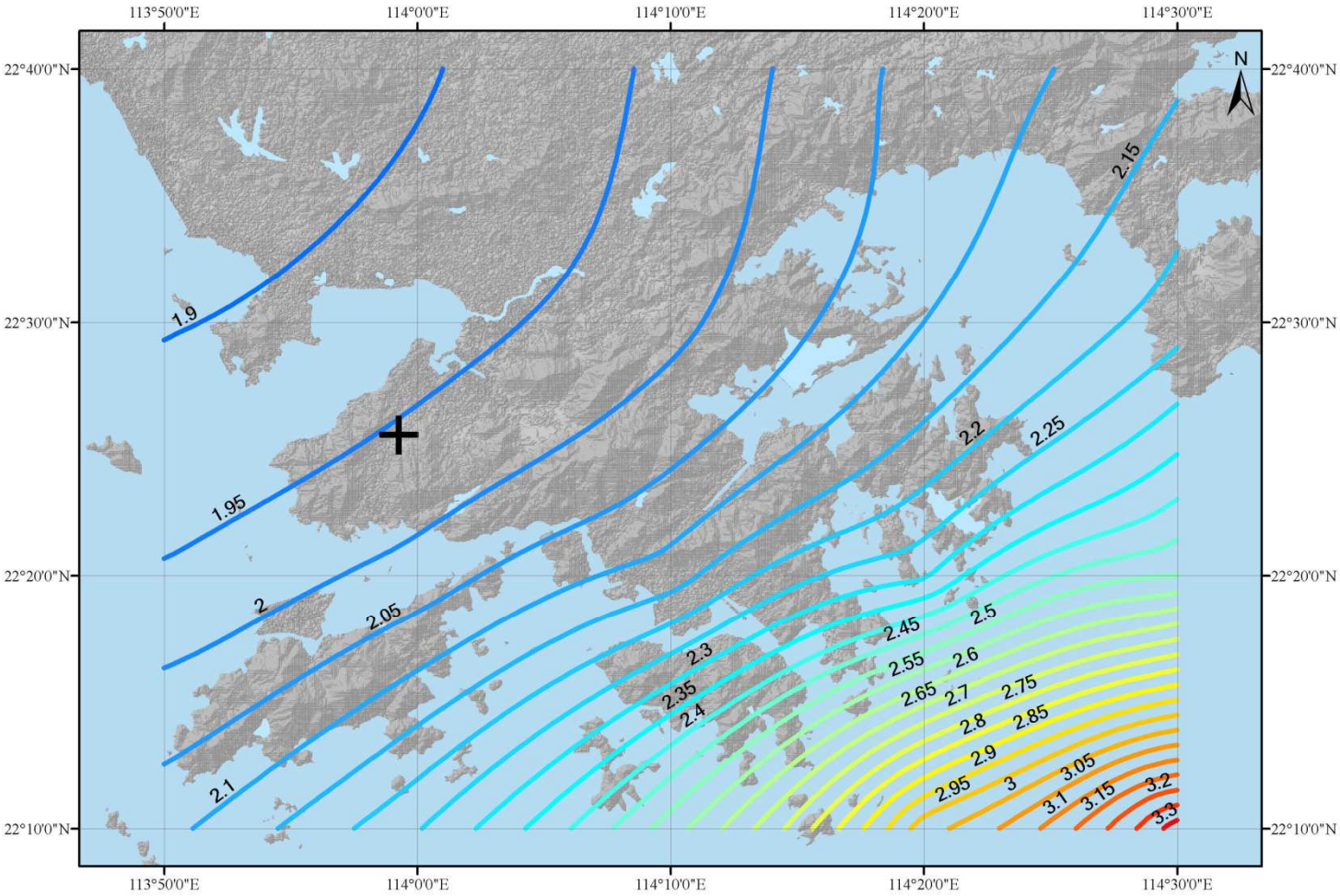

Figure 4.26 Contour Plot for PGA (m/s^2) for a 2% Probability of Being Exceeded in the Next 50 Years

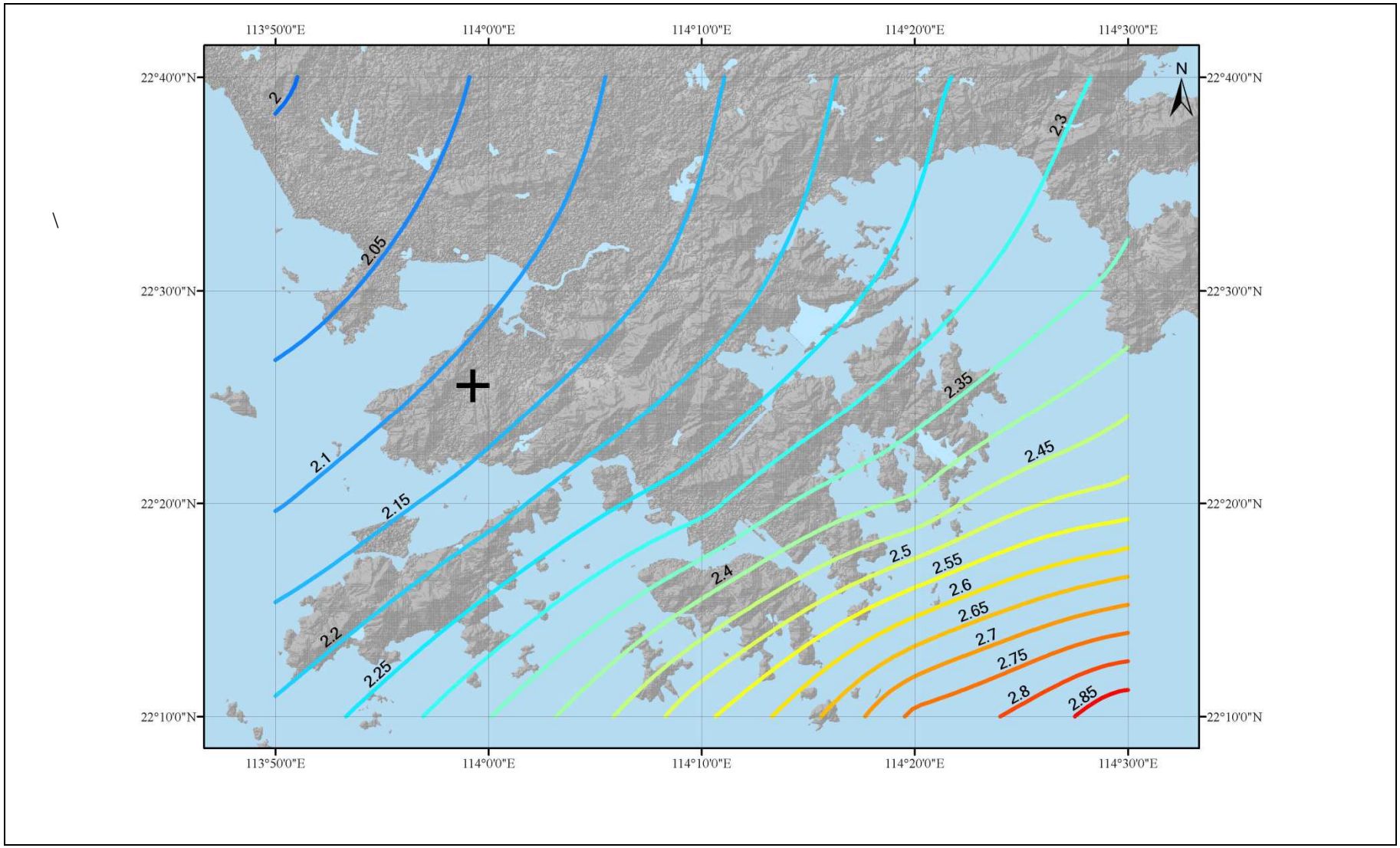

Figure 4.27 Contour Plot for Spectral Acceleration (m/s^2) at 0.2 Seconds Period for a 10% Probability of Being Exceeded in the Next 50 Years

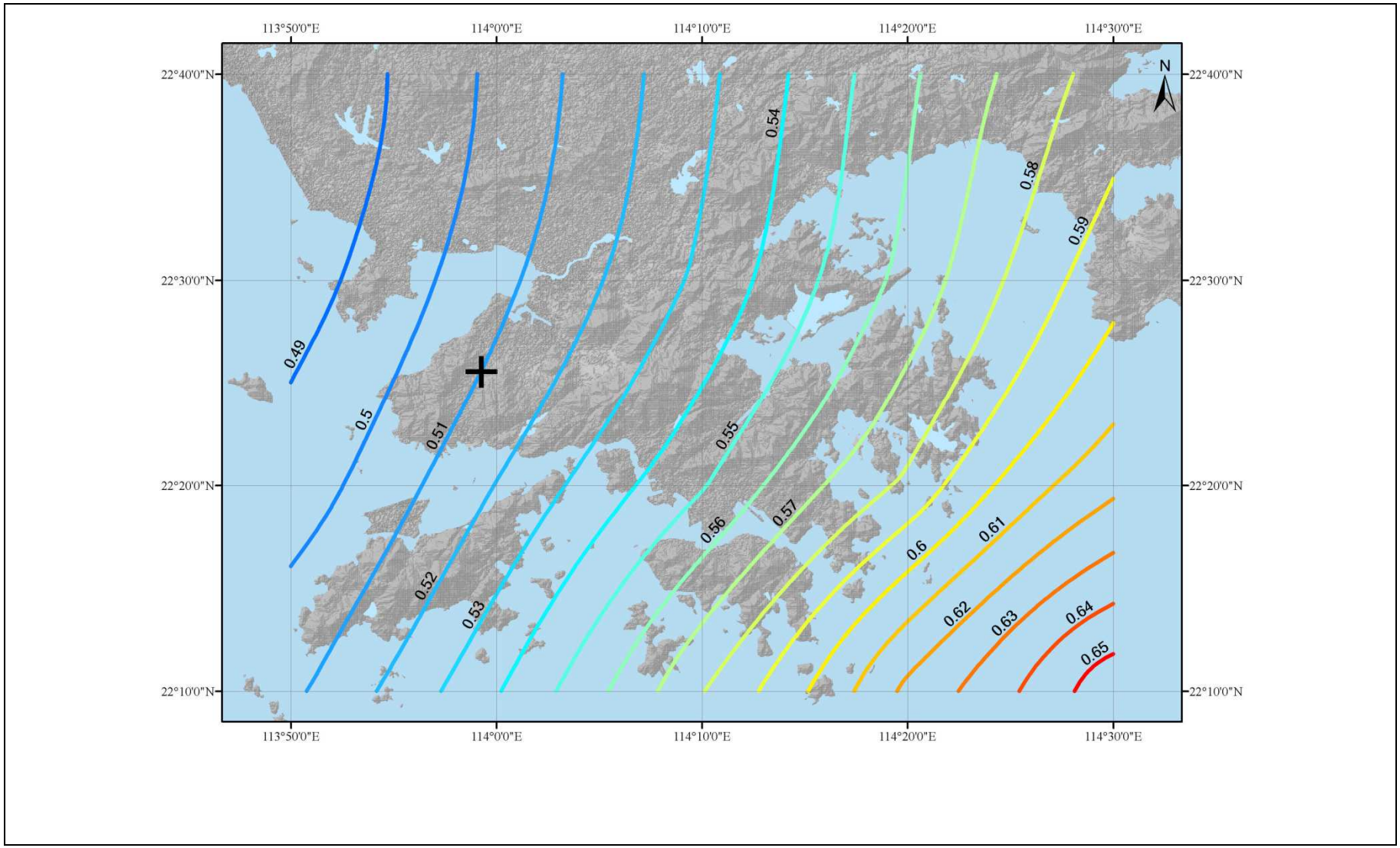

Figure 4.28 Contour Plot for Spectral Acceleration (m/s^2) at 1 Second Period for a 10% Probability of Being Exceeded in the Next 50 Years

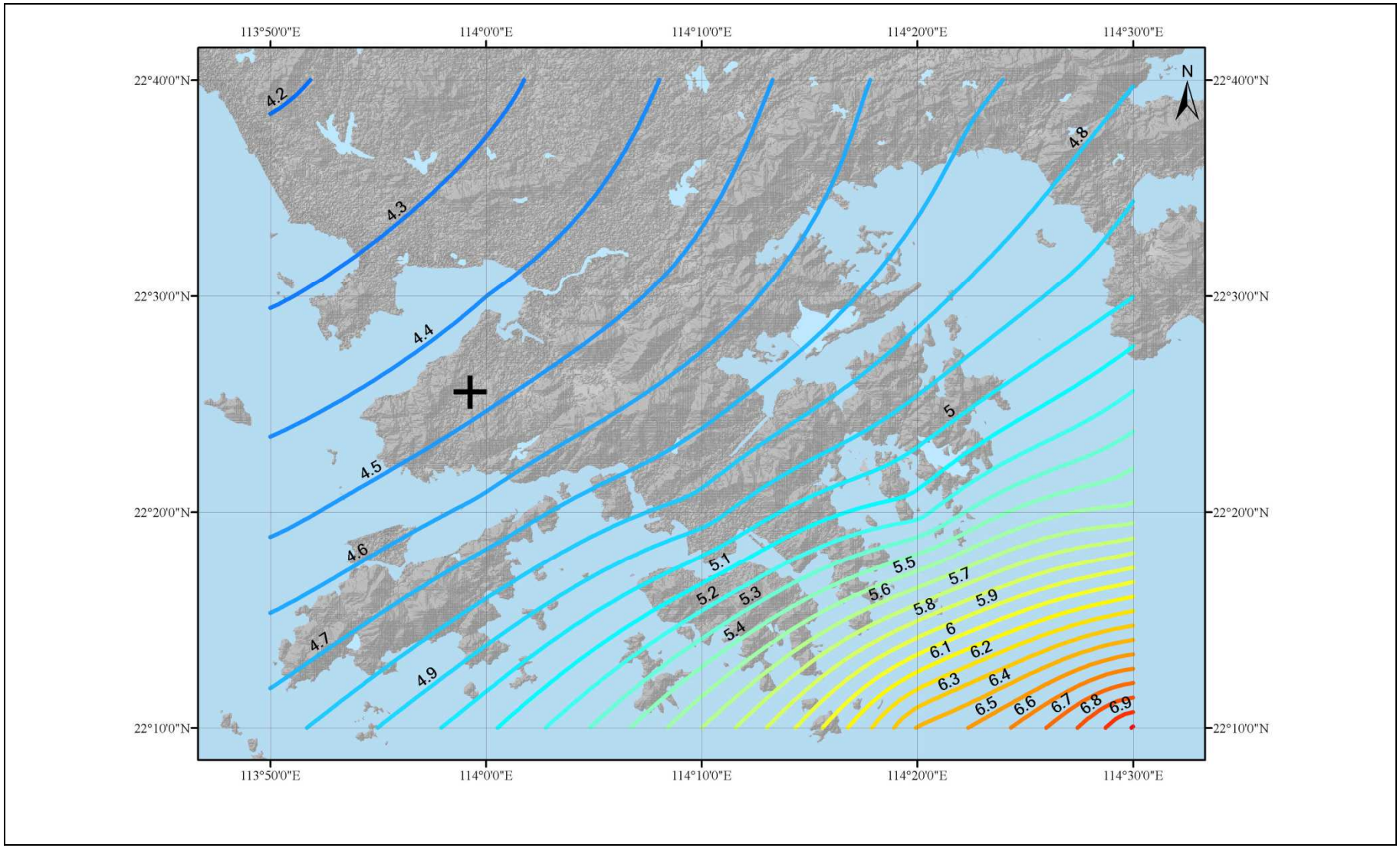

Figure 4.29 Contour Plot for Spectral Acceleration (m/s^2) at 0.2 Seconds Period for a 2% Probability of Being Exceeded in the Next 50 Years

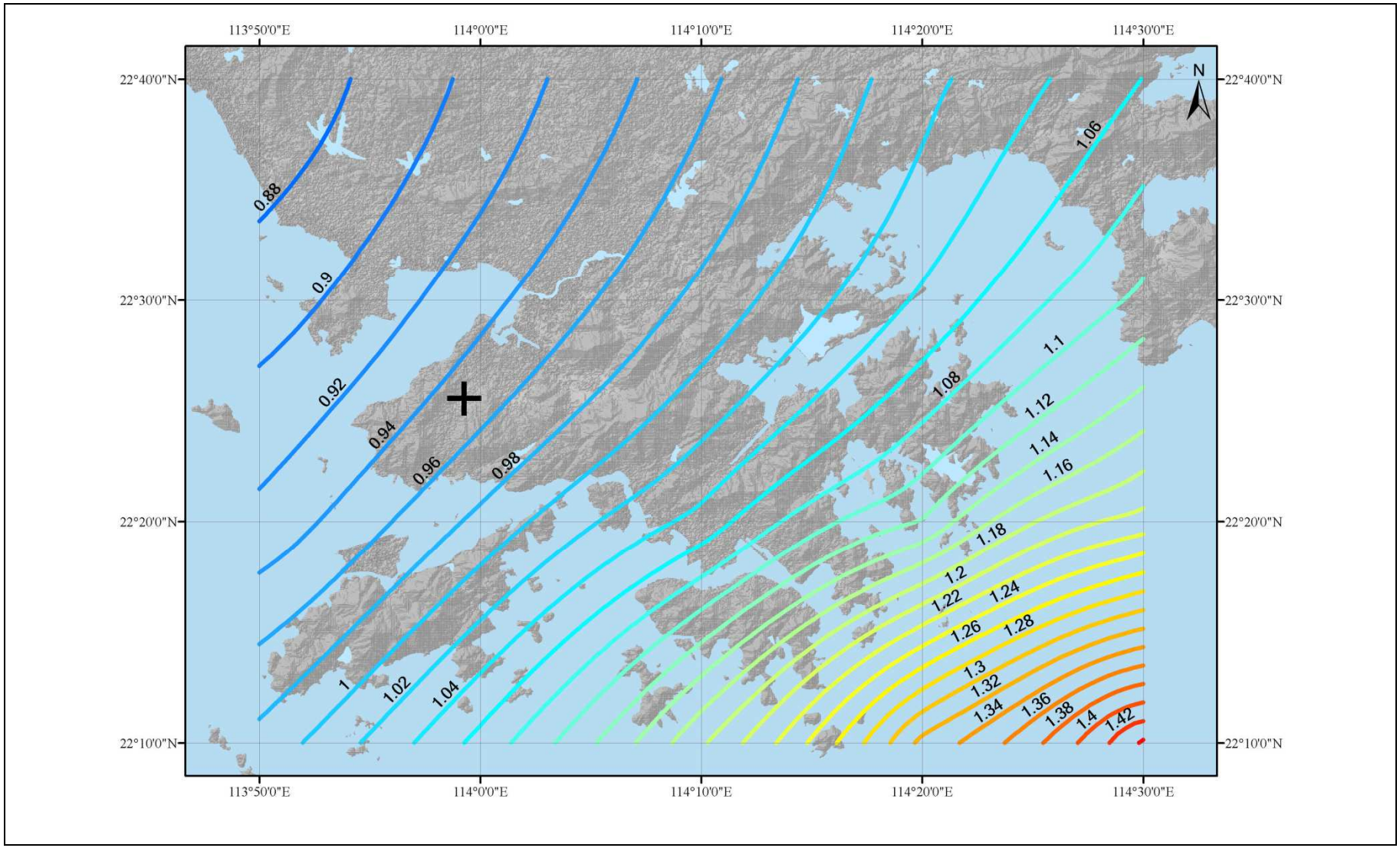

Figure 4.30 Contour Plot for Spectral Acceleration (m/s^2) at 1 Second Period for a 2% Probability of Being Exceeded in the Next 50 Years

5 Conclusions

A literature review has been carried out for documents relating to seismic hazard assessments for the Hong Kong region and the key findings have been summarised.

Available seismicity data within the region have also been assembled and statistically analysed. Data have been compiled for the region of the Southeast China. Full details are contained within this report together with other input required for the evaluation of the seismic hazard. The earthquake catalogue has been used to determine the seismic source zone parameters to use in the seismic hazard assessment.

No strong evidence of active fault displacements was found in the Hong Kong region by this study in either the offshore or onshore Quaternary superficial deposits that can give rise to ground surface rupture hazard.

A probabilistic seismic hazard assessment has been carried out for the Hong Kong region. The results of the seismic hazard assessment are presented in terms of horizontal peak ground acceleration and uniform hazard response spectra for structural periods up to 5 seconds for rock site ground conditions. A rock site in this study is defined as IBC2009 Site class B with V_S greater than 760 m/s and Chinese Code GB50011-2010 Soil Type 1 with V_S greater than 800 m/s. The results are presented for ground motions having the following probabilities:

(a) 63% probability of being exceeded in the next 50 years,

(b) 50% probability of being exceeded in the next 50 years,

(c) 10% probability of being exceeded in the next 50 years, and

(d) 2% probability of being exceeded in the next 50 years.

This report presents the details of the seismic hazard calculations used to evaluate the ground motion. The Arup seismic source zone model incorporates the seismicity in the region, the geological and tectonic information and the GEERRI source zone boundaries. To capture uncertainty in the results, the calculation input includes several different attenuation relationships.

The response spectra for 63%, 50%, 10% and 2% probabilities of being exceeded in the next 50 years are compared with the GEERRI study for a site located in the centre of the study area. It can be seen that while the response spectrum values from this study are smaller than those determined by the GEERRI at long periods, they agree well at shorter periods. The differences are mainly caused by the use of a conservative long period attenuation model of Yu (2005) in the GEERRI study. This attenuation model was developed by scaling up attenuation relationships from Western North American studies and based on a comparison of the attenuation of macroseismic intensity observed in China as compared to that observed in Western North America. This procedure is only reliable however for structural periods up to about 0.2-second as the macroseismic intensity is largely established based on damage to low-rise buildings of less than 3 storeys. Comparisons with other attenuation relationships developed for Eastern North America and other parts of the world and also with theoretical

models developed for South China show that the Yu (2005) relationships become very conservative at long structural periods. As a result, Yu's model has only been adopted for structural periods up to 0.2-second. It is also noted that the GEERRI estimates of activity rates for regions of the Pearl River Delta and the Dangan Islands are higher than the observed seismicity. However, both the Arup and GEERRI source models give a similar overall seismic hazard level.

Contour plots have been prepared for the whole of the Hong Kong SAR for PGA, and spectral accelerations for structural periods of 0.2-second and 1-second for ground motions having respectively 10% and 2% probabilities of being exceeded in the next 50 years. The hazard values at the Hong Kong Observatory are about 10% higher than those at the study area in the North-west New Territories.

The seismicity in the Hong Kong region shows that the seismic activity is similar to that observed in the Eastern North America and about 40 times less than that in highly seismic areas such as California, Japan, Taiwan or the Philippines.

The seismic hazard has been de-aggregated to determine scenario earthquakes for the three design levels (ground motion levels with 50%, 10% and 2% probability of being exceeded in the next 50 years). The most likely scenario event to represent the short period ground motion for a relatively likely ground motion having a 50% chance of being exceeded in the next 50 years will be about a magnitude M_W = 5.75 at 60 km and a magnitude M_W = 6.75 at 150 km for longer period ground motion. For less probable, extreme ground motions having a 2% chance of being exceeded in the next 50 years, a magnitude M_W = 5.5 very close to the site is appropriate for short period ground motion and from a magnitude M_W = 7 at 60 km to a magnitude M_W = 7.75 event at 300 km for long period ground motions.

6 References

Abrahamson, N. & Silva, W. (2007). *Abrahamson & Silva New Generation Attenuation (NGA) Ground Motion Relations for the Geometric Mean Horizontal Component of Peak and Spectral Ground Motion Parameters.* Pacific Earthquake Engineering Research Center, USA.

Adams, J., Weichert, D.H. & Halchuk, S. (1999). *Trial Seismic Hazard Maps of Canada - 1999: 2%/50 Year Values for Selected Canadian Cities.* Geological Survey of Canada, Open File Report 3724, Natural Resources, Canada, 114 p.

Arup (2003). *Seismic Hazard Effects on Buildings in Hong Kong*. Final report prepared for the Buildings Department, Hong Kong.

Atkinson, G.M. (1993). Source spectra for earthquakes in Eastern North America. *Bulletin of the Seismological Society of America*, vol. 83, pp 1778-1798.

Atkinson, G.M. & Boore, D.M. (1997). Model of Strong Motions from Earthquakes in Central and Eastern North America: Best estimates and Uncertainties. *Seismological Research Letters*, vol. 68, no. 1, pp 41-57.

Atkinson, G.M. & Boore, D.M. (2006). Earthquake Ground-Motion Prediction Equations for Eastern North America. *Bulletin of the Seismological Society of America*, vol. 96, no. 6, pp 2181-2205.

Bazzurro, P. & Cornell, C.A. (1999). Disaggregation of Seismic Hazard. *Bulletin of the Seismological Society of America*, vol. 89, no. 2, pp 501-520.

Boore, D.M. & Atkinson, G.M. (2007). *Boore-Atkinson New Generation Attenuation (NGA) Ground Motion Relations for the Geometric Mean Horizontal Component of Peak and Spectral Ground Motion Parameters.* Pacific Earthquake Engineering Research Center, USA.

Boore, D.M. & Joyner, W. (1993). *Estimation of Response Spectra and Peak Accelerations from Western North American Earthquakes: An Interim Report*. Open File Report 93-509, United States Geological Survey.

Bozorgnia, Y. & Campbell, K.W. (2004). *Engineering Characterization of Ground Motion.* In Earthquake Engineering: From Engineering Seismology to Performance-Based Engineering, Bororgnia, Y., and Bertero V.V. (eds.). CRC Press, Boca Ration, Florida, Chapt. 5, pp 1-74.

Bureau of Geology and Mineral Resources of Guangdong Province (1988). Regional geology of Guangdong Province. *Geological Memoirs Series*, vol. 1, 941 p.

Campbell, K.W. & Bozorgnia, Y. (2007). *Campbell-Bozorgnia New Generation Attenuation (NGA) Ground Motion Relations for the Geometric Mean Horizontal Component of Peak and Spectral Ground Motion Parameters.* Pacific Earthquake Engineering Research Center, USA.

Campbell, S.D.G. & Sewell, R.J. (2007). *^{40}Ar-^{39}Ar Laser Microprobe Dating of Mafic Dykes and Fault Rocks in Hong Kong, GEO Report No. 206.* Geotechnical Engineering Office, Hong Kong, 78 p.

Chandler, A.M. & Lam, N.T.K. (2002). Scenario predictions for potential near-field and far-field earthquakes affecting Hong Kong. *Soil Dynamics and Earthquake Engineering*, vol. 22, pp 29-46.

Chandler, A.M., Lam, N.T.K. & Tsang, H.H. (2006a). Near-surface Attenuation Modelling based on Rock Shear-Wave Velocity Profile. *Soil Dynamics and Earthquake Eng.*, vol. 26, no. 11, pp 1004-1014.

Chandler, A.M., Lam, N.T.K. & Tsang, H.H. (2006b). Regional and Local Factors in Attenuation Modelling: Hong Kong Case Study. *J. Asian Earth Sciences*, vol. 27, no. 6, pp 892-906.

Chiou, S.S.-J. & Youngs, R.R. (2007). *Chiou & Youngs New Generation Attenuation (NGA) Ground Motion Relations for the Geometric Mean Horizontal Component of Peak and Spectral Ground Motion Parameters.* Pacific Earthquake Engineering Research Centre, USA.

Committee on Seismic Risk (1984). Glossary of terms for probabilistic seismic-risk and hazard analysis. *Earthquake Spectra*, vol. 1, no. 1, pp 33-40.

Coppersmith, K.J., Johnston, A.C. & Arabasz, W.J. (1987). *Estimating Maximum Earthquakes in Central and Eastern United States: A Progress Report. Proc. Symp. on Seismic Hazards, Ground Motions, Soil Liquefaction and Engineering Practice in Eastern North America*, Technical Report, NCEER 87-0025.

Cornell, C.A. (1968). Engineering seismic risk analysis. *Bulletin of the Seismological Society of America*, vol. 58, pp 1583-1606.

Ding, Y.Z. & Lai, K.W. (1997). Neotectonic fault activity in Hong Kong: evidence from seismic events and thermoluminescence dating of fault gouge. *Jn. of the Geological Society*, London, vol. 154, pp 1001-1007.

Duller, G.A.T. & Whintle, A.G. (1996). *Luminescence Dating of Alluvial and Colluvial Deposits in Hong Kong*. Report for the Geotechnical Engineering Office, Hong Kong, 30 p (not seen).

Free, M., Pappin, J.W., Koo, R.C.H. (2004). Seismic hazard assessment in a moderate seismicity region, Hong Kong. *Proc. 13th World Conf. on Earthquake Engineering*, Vancouver, Canada, Paper number 1659, 10 p.

Fyfe, J.A., Shaw, R., Campbell, S.D.G., Lai, K.W. & Kirk, P.A. (2000). *The Quaternary Geology of Hong Kong, Hong Kong Geological Survey.* Geotechnical Engineering Office, Hong Kong, 210 p.

GB 18306 (2001). *Seismic Ground Motion Parameter Zonation*, Peoples Republic of China.

GB 50011 (2010). *Seismic Design Code for Buildings*, Peoples Republic of China.

GCO (1991). *Review of Earthquake Data for the Hong Kong Region*, GCO Publication No. 1/91. Geotechnical Control Office, Hong Kong, 115 p.

GEERRI (Guangdong Engineer Earthquake Resistance Research Institute) (2010). *Seismic Hazard Assessment Report.* Guangdong (included in this report as Appendix A).

GEO (1988a). *Tsing Shan (Castle Peak) Hong Kong Geological Survey Sheet 5, Solid and Superficial Geology, 1:20,000 Series HGM20.* Geotechnical Engineering Office, Hong Kong.

GEO (1988b). *Yuen Long. Hong Kong Geological Survey Sheet 6, Solid and Superficial Geology, 1:20,000 Series HGM20.* Geotechnical Engineering Office, Hong Kong.

GEO (1994). *Tung Chung. Hong Kong Geological Survey Sheet 9, Solid and Superficial Geology, 1:20,000 Series HGM20.* Geotechnical Engineering Office, Hong Kong.

GEO (2000). *Geological Map of Hong Kong - Millenium Edition.* Geotechnical Engineering Office, Hong Kong.

GEO (2012). *Review of Earthquake Data for the Hong Kong Region,* GEO Publication No. 1/2012. Geotechnical Engineering Office, Hong Kong, 153 p.

Housner, G.W. (1959). Spectrum intensities of strong motion earthquakes. *Proc. Sym. Earthquakes and Blast Effects on Structures*, EERI, Berkeley, CA, pp 20-36.

IBC (2009). *International Building Code*. International Code Council, California, USA.

ICD (2004). *Seismic Hazard Assessment of Hong Kong-Zhuhai-Macau Link.* The Institute of Crustal Dynamics, Beijing, China. (港珠澳大橋工程場地- 地震安全性評價專題研究報告).

Jack R. Benjamin & Associates (1989). *Lower-bound Magnitude for Probabilistic Seismic Hazard Assessment.* Report Summary, EPRI NP-6496 Research Project 2556-25.

Johnston, A.C. (1996a). Seismic moment assessment of earthquakes in stable continental regions, part 1: instrumental seismicity. *Geophysical Journal International*, vol. 124, issue 2, pp 381-414.

Johnston, A.C. (1996b). Seismic moment assessment of earthquakes in stable continental regions, part 2: historical seismicity. *Geophysical Journal International*, vol. 125, issue 3, pp 639-678.

Johnston, A.C., Coppersmith, K.J., Kanter, L.R. & Cornell, C.A. (1994). *The Earthquakes of Stable Continental Regions: Volume 1: Assessment of Large Earthquake Potential*. Report for Electric Power Research Institute.

Kramer, S.L. (1996). *Geotechnical Earthquake Engineering*. Prentice Hall, 653 p.

Lai, K.W. & Langford, R.L. (1996). Spatial and temporal characteristics of major faults in Hong Kong. In: Owen, R. B., Neller, R. J. & Lee, K. W. (eds) Seismicity in East Asia, *Geological Society of Hong Kong Bull*., no. 5, pp 72-84.

Lam, N.T.K., Wilson, J.L., Chandler, A.M. & Hutchinson, G.L. (2000a). Response spectral relationships for rock sites derived from the component attenuation model. *Earthquake Engineering & Structural Dynamics*, vol. 29, pp 1457-1489.

Lam, N.T.K., Wilson, J.L. & Hutchinson, G.L. (2000b). Generation of synthetic earthquake accelerograms using seismological modelling: a review. *J. Earthquake Eng*., vol. 4(3), pp 321-354.

Langford, R.L., Lai, K.W., Arthurton, R.S. & Shaw, R. (1989). *Geology of the North-West New Territories, Memoir No. 6, Geological Survey of Hong Kong.* Geotechnical Control Office, Hong Kong.

Lee, C.F., Ding, Y.Z., Huang, R.H., Yu, Y.B., Guo, G.A., Chen, P.L. & Huang, X.H. (1998). *Seismic Hazard Analysis of the Hong Kong Region,* GEO Report No. 65. Geotechnical Engineering Office, Hong Kong, 145 p.

Liu, Y.X. (1985). Active faults along the coast from Pearl River to Hanghai Bay. *Proc. Seminar on the Marine Geology of Hong Kong and the Pearl River Mouth.* Geol. Soc. of Hong Kong, pp 21-28.

McGuire, R.K. (1993). *Computations of Seismic Hazard*. In Giardini, D., and Basham, P.W. (eds), Global Seismic Hazard Assessment Program, Annali di Geofisica, vol. 34, pp 181-200.

McGuire, R.K. (1995). Probabilistic seismic hazard analysis and design earthquakes: closing the loop. *Bulletin of the Seismological Society of America*, vol. 85, no. 5, pp 1275-1284.

NASA (2003). *Digital Tectonic Activity Map* (http://denali.gsfc.nasa.gov/dtam/).

Pubellier, M. & Chan, L.S. (2006). *Morphotectonic Map of Cenozoic Structures of South China-Northern Vietnam Coastal Region (with CD-ROM and explanatory text).* Hong Kong University, Dept. Earth Sc., 16 p. with map.

Pun, W.K. & Ambraseys, N.N. (1992). Earthquake Data Review and Seismic Hazard Analysis for the Hong Kong Region. *Earthquake Eng. and Structural Dynamics*, vol. 21, pp 433-443.

Scott, D.M., Pappin, J.W. & Kwok, M.K.Y. (1994). Seismic design of buildings in Hong Kong. *Transactions Hong Kong Institution of Eng*., vol. 1, no. 2, pp 37-50.

Sewell, R.J., Campbell, S.D.G., Fletcher, C.J.N., Lai, K.W. & Kirk, P.A. (2000). *The Pre-Quaternary Geology of Hong Kong,* Hong Kong Geological Survey. Geotechnical Engineering Office, Hong Kong, 181 p.

Slemmons, D.B. & McKinney, R. (1977). *Definition of Active Fault.* Miscellaneous Paper S-77-8, U.S. Army Corps of Engineers Experiment Station, Vicksburg, Mississippi.

Tang, D.L.K., Ding, Y.Z., Lee, C.W., Wong, J.C.F. & Sewell, R.J. (2009). *Study of the Potential Evidence for Neotectonic Fault Movement and Correlation with Natural Terrain Landslides in Hong Kong (Part 1: Ho Lek Pui Area),* Hong Kong Geological Survey. Geotechnical Engineering Office, Hong Kong.

Tang, D.L.K., Sewell, R.J., Wong, J.C.F. & Ding, Y.Z. (2010). *Study of the Potential Evidence for Neotectonic Fault Movement and Correlation with Natural Terrain Landslides in Hong Kong (Part 3: Tung Chung East),* Hong Kong Geological Survey. Geotechnical Engineering Office, Hong Kong.

Tsang, H.H. (2006). *Probabilistic Seismic Hazard Assessment: Direct Amplitude-Based Approach.* PhD Thesis, Department of Civil Engineering, University of Hong Kong.

Tsang, H.H. & Chandler, A.M. (2006). Site-specific probabilistic seismic-hazard assessment: direct amplitude-based approach. *Bull. Seismol. Soc. Am.*, vol. 96, no. 2, pp 392-403.

Weidlinger Associates (2000). *New York City Seismic Hazard Study*, prepared for the New York City Department of Transport. (www.wai.com)

Wells, D.L. & Coppersmith, K.J. (1994). New empirical relationships among magnitude, rupture length, rupture width, rupture area, and surface displacement. *Bulletin of the Seismological Society of America*, vol. 84, no. 4, pp 974-1002.

Whittaker, A., Musson, R.M.W., Brereton, N.R., Busby, J.P., Evans, C.D.R. & Evans, C.J. (1992). *A Review of the Crustal Structure and Seismotectonics Pertinent to Hong Kong. Technical Report WC/92/17*, International Geology Series, British Geological Survey, Nottingham, UK.

Wong, J.C.F. & Ding, Y.Z. (2010). *Study of the Potential Evidence for Neotectonic Fault Movement and Correlation with Natural Terrain Landslides in Hong Kong (Part 2: Wong Chuk Yeung Area).*

Wong, J.C.F., Tang, D.L.K., Sewell, R.J. & Lee, C.W. (2010). *Study of the Potential Evidence for Neotectonic Fault Movement and Correlation with Natural Terrain Landslides in Hong Kong (Part 4: Nam Shan and Pui O Areas).*

Workman, D.R. (1983). Structures of the South China Sea Basin. *Geol. Soc. Hong Kong Newsletter*, vol. 1, no. 6, pp 1-4.

Yu, Y.X. (2005). *The Study of Seismic Hazard Assessment for Structural Seismic Design-Attenuation Relationship Study.* The Institute of Geophysics, China Earthquake Administration. (地震安全性評價研究與結構抗震研究：地震動參數衰減關係研究).

Appendix A

GEERRI Seismic Hazard Assessment Report

附錄 A

地震危險性分析報告

香港新界西北

廣東省工程防震研究院

廣東省地震局

目　錄

第一章 區域地震活動特徵

根據中華人民共和國《工程場地地震安全性評價》（GB17741-2005）（國家技術品質監督局，2005）的有關規定，本報告以香港元朗—屯門地區滑坡與地震影響小區劃為中心，不小於工程場地外延 150 公里作為環境地震的研究範圍。本專案選取工程場地外延 500 公里作為環境地震（M_L≥5.0）的研究範圍，大致在東經 109.10° - 118.90°，北緯 18.00° - 27.00°的區域。由於香港地處華南沿海地震帶，考慮到地震活動性參數 *b* 值計算的需要，環境地震（M_L≥5.0）的研究範圍還包括整個華南沿海地震帶；M_L≥2.0 級地震的研究範圍，則選取工程場地外延 150 公里，即大致在東經 112.42° - 115.57°，北緯 21.03° - 23.91°的區域。

研究區域地震活動性，利用了我國豐富的歷史地震資料和 1970 年 1 月至今的近期地震觀測資料。

1.1 區域地震資料

1.1.1 區域地震目錄和地震震中分佈圖編制

1．編目原則

全面收集區域內已有的各種地震資料，並確定以下幾條主要地震目錄編制原則：

(1) 對以往工作中已經進行過詳細調查並獲得評審通過的歷史地震，直接引用其地震參數的調查結論。

(2) 以正式出版的地震目錄為準，對有不同認識的一些地震條目，根據不同版本目錄編目資料的可靠性和工作深度，確定其取捨，綜合編制專案使用的目錄，並在目錄中註明取捨原因。

2．所用地震資料

國家地震局震害防禦司編 1995 年《中國歷史強震目錄》（西元前 23 世紀至西元 1911 年）；

國家地震局震害防禦司編 1999 年《中國近代地震目錄》（西元 1912 年至 1990 年 Ms≥4.7）；

國家地震局地球物理研究所編《中國地震年報》（1991 年至 2000 年）；

國家地震局地球物理研究所編《中國數位地震台網觀測報告》（2001 年至 2008 年）；

中國地震局分析預報中心彙編《中國地震詳目》（1970 年 1 月至 2009 年 2 月 $M_L \geq 1.0$）；

廣東省地震局監測中心 1970 年 1 月- 2010 年 2 月的地震記錄資料；

美國地質調查局（USGS）網站查詢的震中初步測定（PDE）地震目錄（1982 - 2010 年 2 月）；

中國地震局“中震防函[2005] 44 號”中的福建省若干歷史地震覆核結果；

中國地震局地球物理研究所編 2006 年《島嶼核電地震安全性評價》；及

雲南省地震局編 2009 年《中越紅河斷裂活動性研究》。

3．地震目錄編制說明

(1) 編目的時、空、強範圍

本次地震目錄編制的區域範圍、時間段及震級範圍如表 1.1-1 所列。

表 1.1-1　地震編目的時、空、強範圍

區域範圍	華南沿海地震帶	香港元朗為中心 半徑 505 公里	香港元朗為中心， 長 300 公里 x 寬 300 公里
時間段	西元 963 年 - 2010 年 2 月	西元 1067 年 - 2010 年 2 月	西元 1970 年 - 2010 年 2 月
震級範圍	$M_L \geq 5.0$（$M_S \geq 4.7$）	$M_L \geq 5.0$（$M_S \geq 4.7$）	$2.0 \leq M_L \leq 4.9$

(2) 地震震級的確定

歷史地震震級採用的是 M_S，這部分地震為 $M_S \geq 4.7$ 級地震。其中，無儀器記錄的地震，其震級的確定均由史料記載評定其震中烈度，再按震級（M_S）與震中烈度的經驗關係換算出，然後採用《地震工作手冊》中的轉換公式：$M_S = 1.13M_L - 1.08$ 將 M_S 換算為 M_L，與近代小震採用的 M_L 震級相統一。凡有儀器記錄的地震，其震級以儀器測定的為準。

本專案的小震與強震震級統一採用 M_L，而南海海域部分地震採用美國地質調查局（USGS）所提供的體波震級 M_b，將在綜合目錄中作出說明，不再另行震級換算。

(3) 地震震中位置和震源深度（h）的選取

凡同時具有儀器震中與宏觀震中位置的地震，均取宏觀震中位置。為與地震動衰減關係確定及地震活動性參數估計一致，這裡只使用淺源地震（$h \leq 70$ 公里）。

對於發生於國內陸地和近海區的地震主要採用了國內的地震目錄資料，其震中位置也以國內目錄的經緯度為準。臺灣海峽與南海北部海域地震的震中位置則主要根據美國地質調查局和國內目錄資料進行綜合對比取捨。

震源深度按原始地震目錄中提供的深度資料直接選取，原始地震目錄中（尤其是 1985 年以前的地震）沒有列出震源深度的地震，按國際地震目錄處理慣例，其預設設為 33 公里。

2.0≤M_L≤4.9 的地震參數主要採用中國大陸地震目錄特別是廣東省地震台網 1970 年 1 月 1 日以來的地震目錄資料。由於 2000 年後廣東建立了數位地震台網，因此小震震源深度資料從當時起才比較齊全。

4・區域地震目錄和地震震中分佈圖編制

根據上述資料，編制研究區（包括整個華南沿海地震帶和東經 114.00°北緯 22.47°為中心半徑 505 公里）範圍內具破壞性地震目錄（M_L≥5.0，西元 963 年 - 2010 年 2 月）。另外還編制了以香港元朗為中心，長 300 公里 x 寬 300 公里範圍（北緯 21°01' - 23°55'，東經 112°25' - 115°34'）的近代小震（2.0≤M_L≤4.9）（西元 1970 年 - 2010 年 6 月）目錄，該目錄所選地震全部來自廣東省地震台網，共收錄 2.0≤M_L≤4.9 地震。考慮到河源新豐江地區的地震為水庫誘發震群，故未將其列入該目錄中。

根據這兩部分地震目錄的參數，繪製出區域（505 公里）具破壞性地震震中分佈圖（圖 1.1-1）和區域（150 公里）近代小震震中分佈圖（圖 1.1-2）。

上述編制的地震目錄資料已收錄在土力工程處刊物系列第 1/2012 號 “Review of Earthquake Data for the Hong Kong Region” （GEO, 2012）。

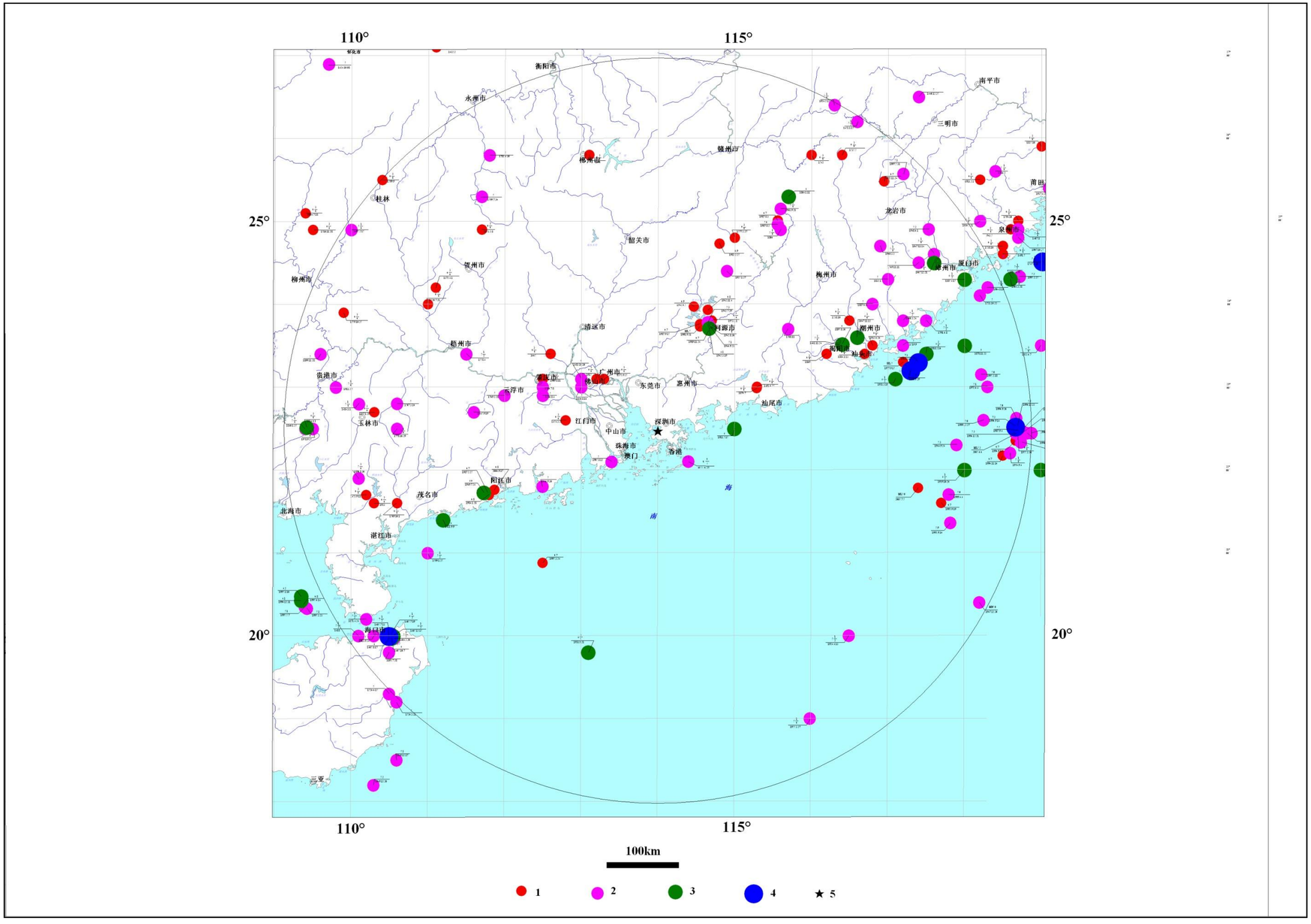

圖 1.1-1　區域歷史強震震中分佈圖（地震資料自西元 963 年—2010 年 2 月，工程場地外延 505 公里，　M_L≥5.0（M_S≥4.7））

1. M_S4.7-4.9；　2. M_S（M_L）5.0-5.9；　3. M_S（M_L）6.0-6.9；　4. M_S（M_L）7.0-7.9　　5. 工程場地位置

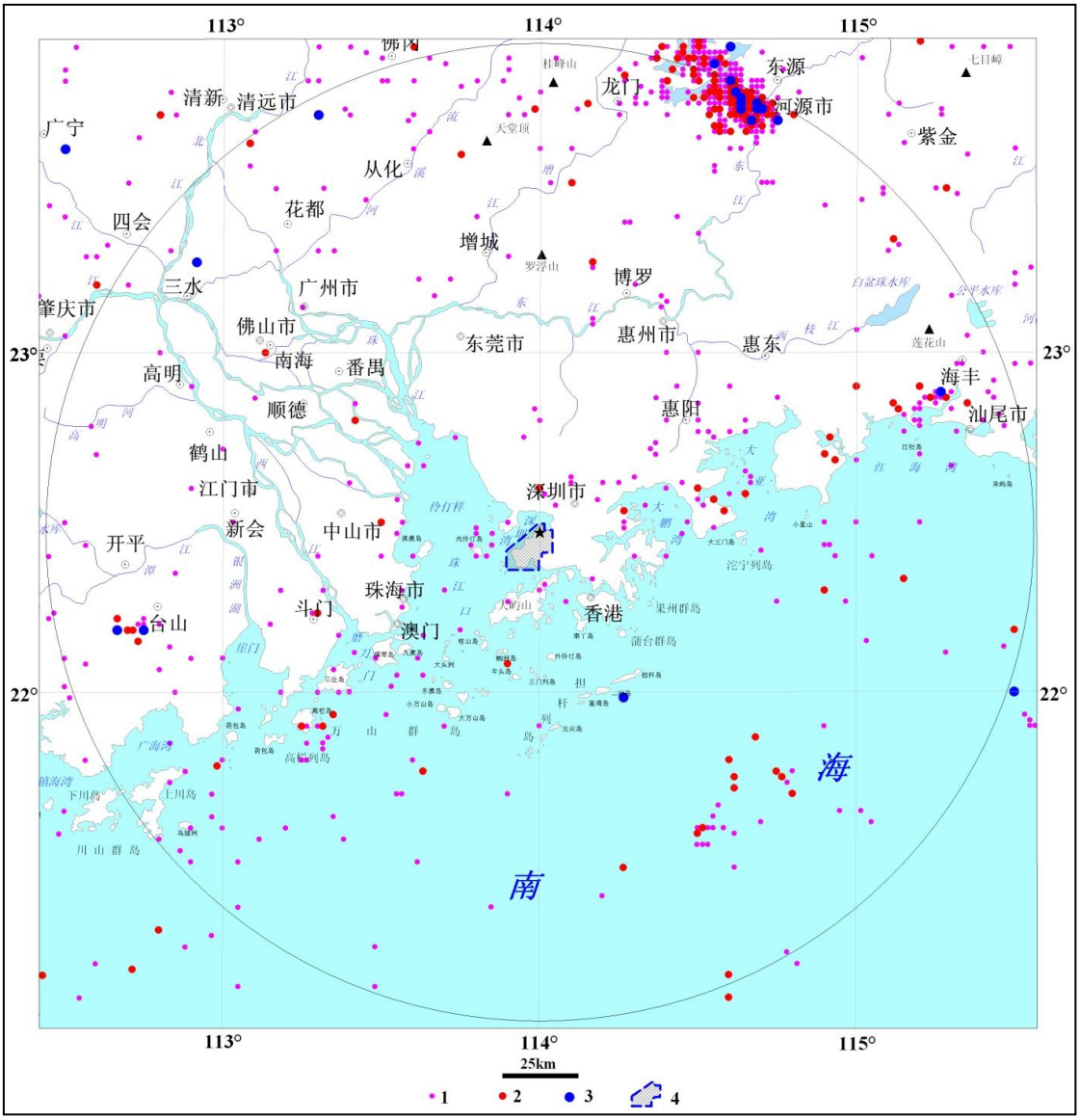

圖 1.1-2　區域近代小震震中分佈圖（1970 年－2010 年 6 月，工程場地外延 150 公里，2.5≤M_L≤4.9）

1. M_L 2.0-2.9；　2. M_L 3.0-3.9；　3. M_L 4.0-4.9；　4. 工程場地範圍

1.2 區域地震空間分佈特徵

1.2.1 區域地震震中分佈特徵

研究區範圍內 M_S≥4.7 級地震在陸域呈北東方向分佈的條帶比較明顯（圖 1.1-1），表明地震活動主要受北東向斷裂構造所控制，尤以泉州－汕頭、邵武－河源斷裂帶最為顯著。該帶範圍內的從化－陽江、吳川－四會斷裂帶均顯示出地震活動與北東向構造的密切相關性。值得注意的是，6 級以上強震大都發生在北西向

構造發育並與北東方向斷裂交匯的地區。如福建的泉州、漳州、廈門，廣東的潮州、汕頭等地區。

從整體來看，研究區範圍陸域大體上呈現出從沿海一帶起，由東南向西北逐漸減弱的趨勢。為了從整體空間分佈圖像中找出較具體而有意義的地震活動特點，在綜合考慮地震空間分佈和地質構造界限之後，可將東南沿海地震帶劃分為內帶和外帶。兩帶的分界線為:北以蓮花山斷裂為界,南延至珠江口外,接珠江口外坳陷北緣斷裂帶，往西沿著近東西向的遂溪斷裂進入北部灣。這樣分帶呈現出如下的特點：從歷史強震的空間分佈來看，外帶地震活動的強度遠大於內帶。7 級以上的地震均發生在外帶，內帶的強震一般都小於 7 級。

在南海中部和北部海域以及臺灣海峽一帶，M_S≥4.7 級地震局部相對集中，但條帶狀規律不明顯。

從近代小震分佈圖顯示，以場地為中心，半徑 150 公里範圍內地震活動表現了繼承性，即近代小震的活躍地區，也是歷史上強震的發生地，如南部沿海和南海北部海域的局部等地帶。其中，河源地區的地震主要為水庫誘發地震。

1.2.2 場地周圍地震隨距離的分佈

由表 1.2-1 可以看出，場地周圍 150 公里範圍內具破壞性地震不多，只有 16 次 M_S≥4.7 級的地震，M_S≥6.0 級的地震只有 2 次，分別為 1911 年的海豐外海域 M_S = 6.0 級和 1962 年 3 月 19 日的河源 M_S = 6.1 級水庫誘發地震，沒有 7 級地震。在 150 - 300 公里範圍內，各檔次的強震有所增加，主要集中在廣東陽江和江西尋烏一帶，但仍然沒有 7 級以上地震。而在 300 - 505 公里的區域，具破壞性地震活動頻密，M_S = 6.0 - 6.9 級地震 13 次，7 級以上地震共有 4 次，集中在瓊北、南澳和臺灣海峽等地。

表 1.2-1　研究區 M_S≥4.7 的地震隨距離的分佈

（統計自西元 963 - 2010 年 2 月，以次數計，括弧內為不含河源水庫誘發地震的數值）

場地距離 / 震級（M_S）	150 公里以內	150-300 公里	300-505 公里	合計（次）
4.7 - 4.9	9（5）	14（12）	22	45（39）
5.0 - 5.9	5（4）	11（10）	55	71（69）
6.0 - 6.9	2（1）	4（4）	13	19（18）
7.0 - 7.9	0	0	4	4（4）
合計（次）	16（10）	29（26）	94	139（130）

區域 4.9≥M_L≥2.5 的地震隨距離的分佈見表 1.2-2 和圖 1.1-2 所示，場地 100 公里範圍內小震活動較弱，大於 100 公里在河源、海豐、臺山和南海北部海域，其中，河源地區水庫誘發地震頻次較高，佔區內小震的 90%。

表 1.2-2　區域 4.9≥M_L≥2.5 的地震隨距離的分佈

（統計自 970 - 2010 年 6 月，括弧內為不含河源水庫誘發地震的數值）

距離 / 震級（M_L）	25 公里以內	25-50 公里	50-100 公里	100-150 公里	150 公里以外	合計
2.0 - 2.9	20（20）	31（31）	99（98）	2159（371）	613（161）	2922（681）
3.0 - 3.9	1（1）	2（2）	20（19）	255（55）	80（22）	358（99）
4.0 - 4.9	0（0）	0（0）	1（1）	15（6）	5（2）	21（9）
合計	21（21）	33（33）	120（118）	2429（432）	698（185）	3301（789）

1.2.3 地震震源深度分佈特徵

一般只有儀器記錄才可能測定出震源深度參數，歷史地震記載沒有給出震源深度，其預設值設為 33 公里。區域內及其附近的中強地震震源深度一般為 5 - 33 公里，河源地區地震深度多數為 4 - 8 公里，江西尋烏、龍南地震深度為 9 - 23 公里，1962 年河源 6.1 級和 1969 年陽江 6.4 級，地震宏觀深度均為 5 公里，總之，本區地震均屬發生於地殼內的淺震。

1.3 地震時間分佈特徵和未來活動趨勢

1.3.1 地震帶的劃分

由於地震活動和地質構造有密切的關係,且中國地震活動具有明顯的成帶性，劃分地震帶是為了區分構造活動性和地震活動性的區域性差異，它是分析地震時間分佈特徵、估計未來百年地震活動趨勢及地震危險性分析中地震活動性參數估計的基本統計單元。

在中國的地震區劃研究工作中，對中國地震區、地震帶的劃分已進行過相當系統的研究。在本工作中，將採用《中國地震動參數區劃圖》（GB18306-2001）（國家技術品質監督局，2001）編制中所使用的地震區、帶劃分方案（見圖 1.3-1），

華南沿海地震帶為圖 1.3-1 中的“V”字形條帶。工程場地處在華南地震區的華南沿海地震帶的中段，該地震帶北側為同一地震區的長江中游地震帶，南側為南海地震區，東側為臺灣地震區，各地震區和地震帶均具有不同地震活動特徵和不同的地震構造背景。

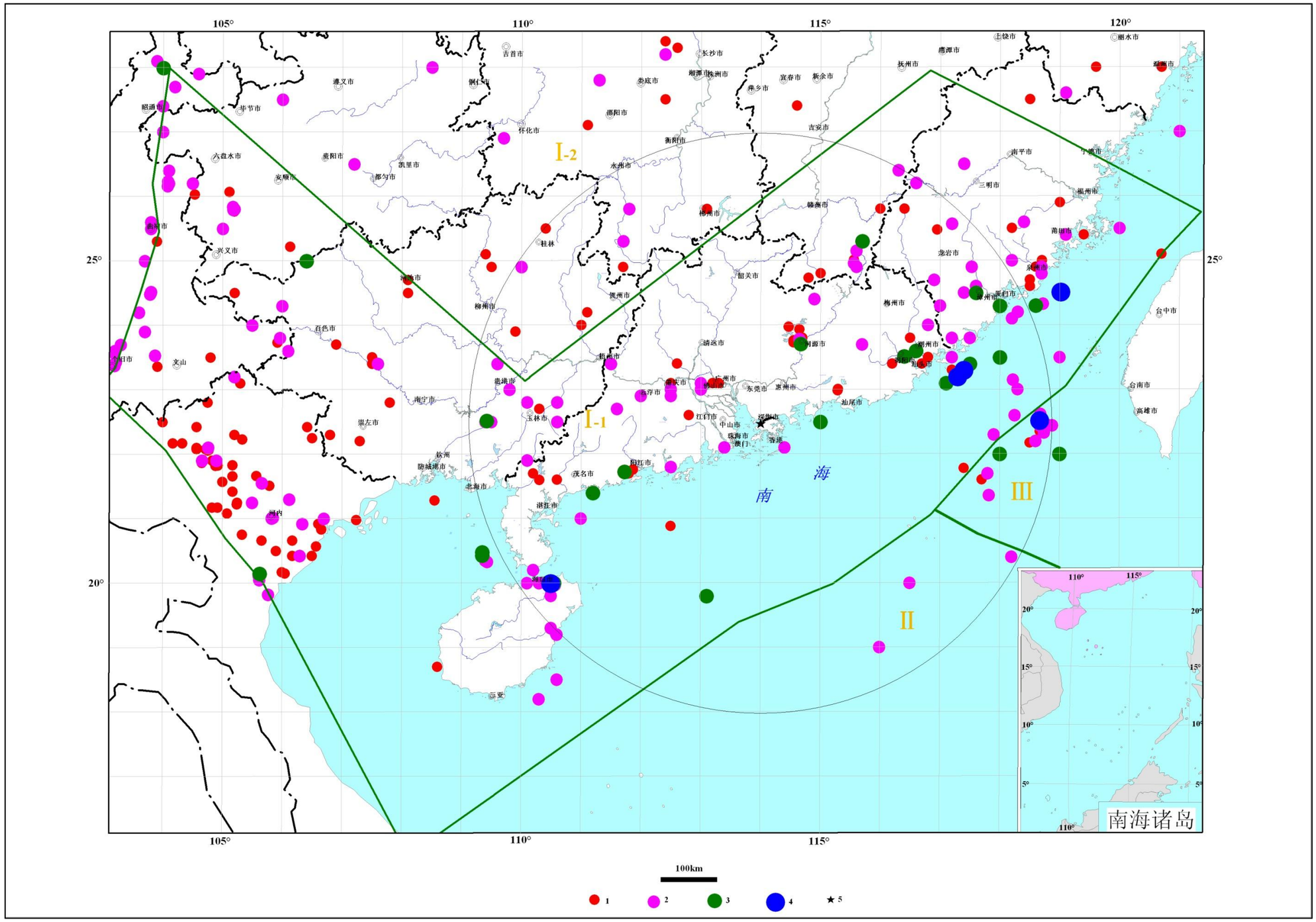

圖 1.3-1　區域及周圍地區地震帶劃分圖（地震資料自西元 963 年—2010 年 2 月，M_L≥5.0（M_S≥4.7））

1. M_S 4.7-4.9；　2. M_S（M_L）5.0-5.9；　3. M_S（M_L）6.0-6.9；　4. M_S（M_L）7.0-7.9；　5. 工程場地位置　Ⅰ-1. 華南地震區-華南沿海地震帶；　Ⅰ-2. 華南地震區-長江中游地震帶；　Ⅱ. 南海地震區；　Ⅲ. 臺灣地震區

1.3.2 華南沿海地震帶地震活動時間分佈特徵

華南沿海地震帶 M_S≥4.7 級地震序列圖表明（圖 1.3-2），本帶的地震活動在時間上具有明顯的週期性，即以低潮和高潮期交替出現為其主要特徵。從序列分佈來看，自 1400 年以來明顯存在著兩個活動週期，即 1400 - 1710 年為第一活動週期，1711 年至今為第二活動週期。進一步研究自 1400 年來兩個地震活動週期地震序列隨時間的發展過程可以看出：每一活動週期都可以明顯地劃分成四個階段，即平靜階段、加速階段、大釋放階段和剩餘釋放階段。各段經歷的時間分別約為 80、120、10、50 年。以元朗為中心，半徑 505 公里的區域範圍地震活動的週期性和階段性特徵非常相似（圖 1.3-3）。

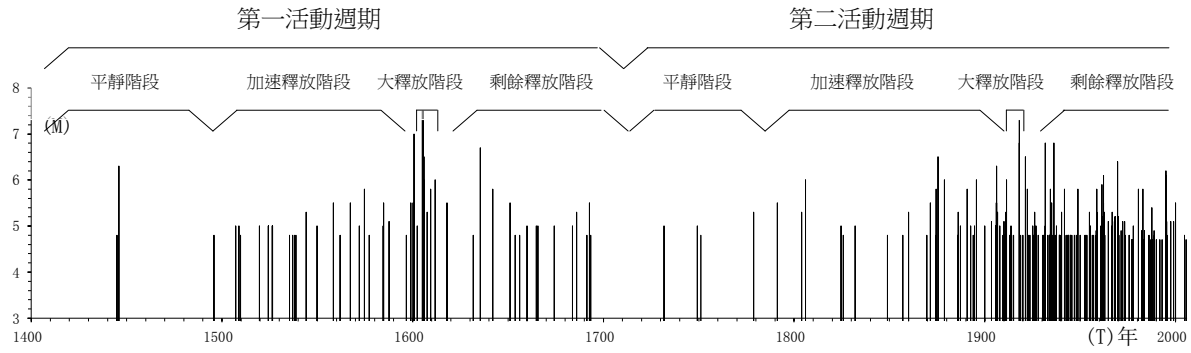

圖 1.3-2　華南沿海地震帶 M-T 圖（西元 1400 年至今，*Ms*≥4.7）

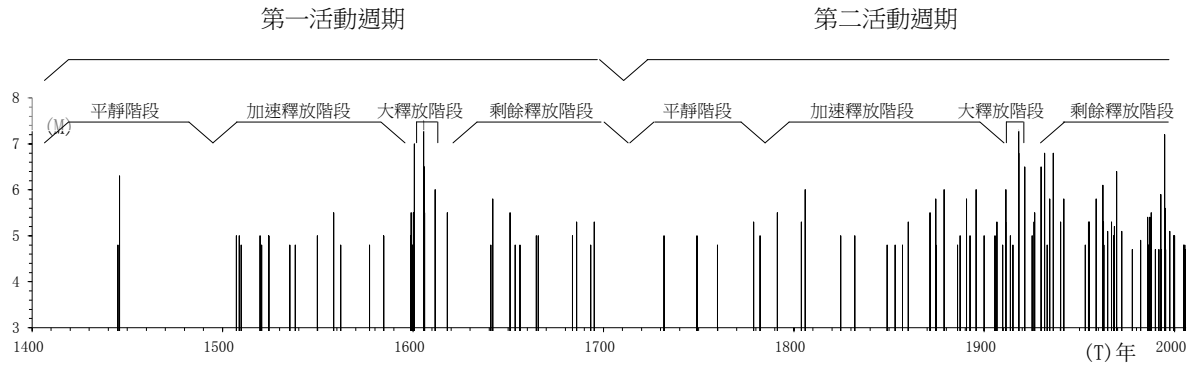

圖 1.3-3　區域（505 公里）範圍 M-T 圖（西元 1400 年至今，*Ms*≥4.7）

第一活動週期的地震序列，明顯展現了本帶一個典型的完整週期過程，第二活動週期則尚未完結。且地震活動在空間分佈上較分散，釋放能量只及第一週期的三分之一，但記錄的地震次數卻遠超過前一週期，這是兩個地震週期之差異。對比兩個活動週期的過程，考察其序列的時間分佈和能量釋放的情況得知：1600 - 1605 年和 1918 - 1921 年分別是兩個活動週期的高潮期，即大釋放階段，兩者相距的時間與完整的第一活動週期所經歷的時間相當一致，大約為 310 - 320 年。

為了更嚴格和更確切地認識上述地震活動的週期性，對本帶地震序列採用富裡埃分析和最大熵譜分析方法進行數值分析。從而得到華南沿海地震帶地震活動的最顯著週期為 300 - 320 年，這進一步證明華南沿海地震帶的地震序列的確存在 300 多年的活動週期。目前，華南沿海地震帶尚處於活動週期的剩餘釋放階段，估計在本世紀最初 20 - 30 年才能轉入到第三活動週期的平靜階段。認識這一點，對估計本帶未來的地震發展趨勢，無疑是十分重要的。

在目前的剩餘釋放階段，華南沿海地震帶自 1925 年以後地震活動有三個時段顯示相對活躍的活動幕與相對平靜的平靜幕交替出現。即 1925 - 1941 年為第一活動幕，以 1931 年文昌東海域 $6\frac{3}{4}$ 級和 1936 年廣西靈山 $6\frac{3}{4}$ 級為釋放高潮。1953 - 1969 年為第二活動幕，1969 年陽江發生 6.4 級地震。1981 至 1997 年為第三活動幕，在這一活動幕裡 1987 年發生江西尋烏中強地震的震群活動，1994、1995 年北部灣發生了 6.1、6.2 級強震。至本世紀初，第三活動幕已經歷 16 年(即 1994 至 2010 年)，估計將進入平靜幕。

1.4 區域地震震源機制及現代構造應力場

1.4.1 震源應力場

本報告收集了反映華南沿海地區現代構造應力場的 60 次地震的震源機制解(圖 1.5-1)。從圖可看出，華南沿海地區的主壓應力的主導方向為 NW—SE 向，也有地震的震源機制解反映為 NNW、近 SN 或近 SE 向。最大主壓應力 P 軸與主張應力 T 軸的傾角大多數小於 30°。

中國地震研究人員曾經利用地震台網記錄到的數百個地震 $\overline{P}$ 、 $\overline{S}$ 波振幅比法資料，得到了華南地區和諧、統一的震源應力場結果（表1.5-1、圖1.5-2和圖1.5-3），它具有三個較為明顯的特徵。

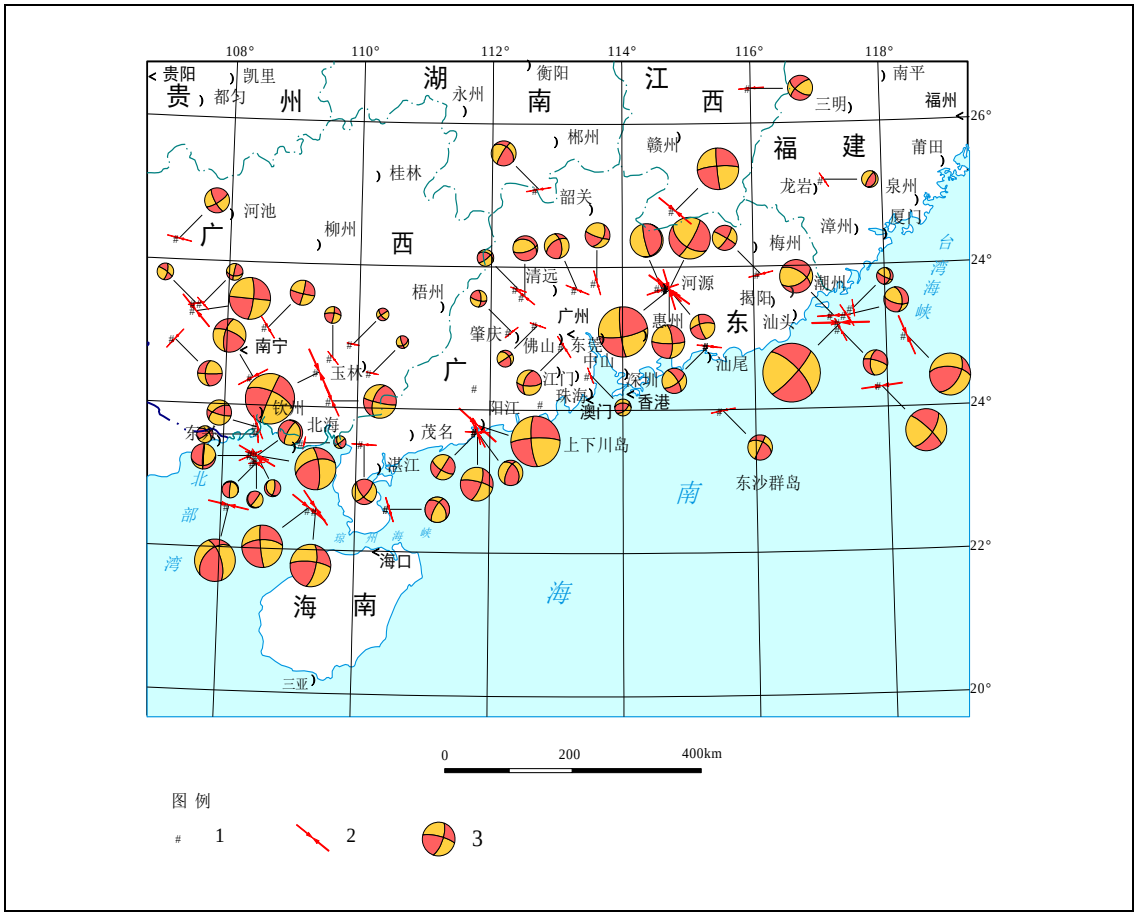

圖 1.5-1　華南地區震源機制解圖

1. 地震震中　2. 主壓應力 P 軸方向　3. 震源機制解

表1.5-1　華南地區各分區主應力軸統計結果

區名	Ⅰ區	Ⅱ區	Ⅲ區	Ⅳ區	Ⅴ區	Ⅵ區	Ⅶ區	Ⅷ區	Ⅸ區
P軸方位角	327°	365°	348°	312°	296°	292°	280°	334°	312°
T軸方位角	235°	282°	255°	222°	208°	203°	186°	242°	217°

（1）震源應力場普遍近於水平，主壓應力軸和主張應力軸的仰角都比較小，前者平均為31°，後者平均為29°，震源錯動面較陡，節面仰角平均62°。

（2）從該區的西部到東部，主壓應力軸的方向由北北西、經西北向過度到北西西方向，顯示出華南地區主壓應力軸方向的扇形結構分佈特徵。

（3）沿著海岸線，從廣西到福建主張應力軸的方向由北西西、經北東東逐步過渡到北北東方向，顯示出華南地區主張應力軸方向的弧形結構分佈特徵。

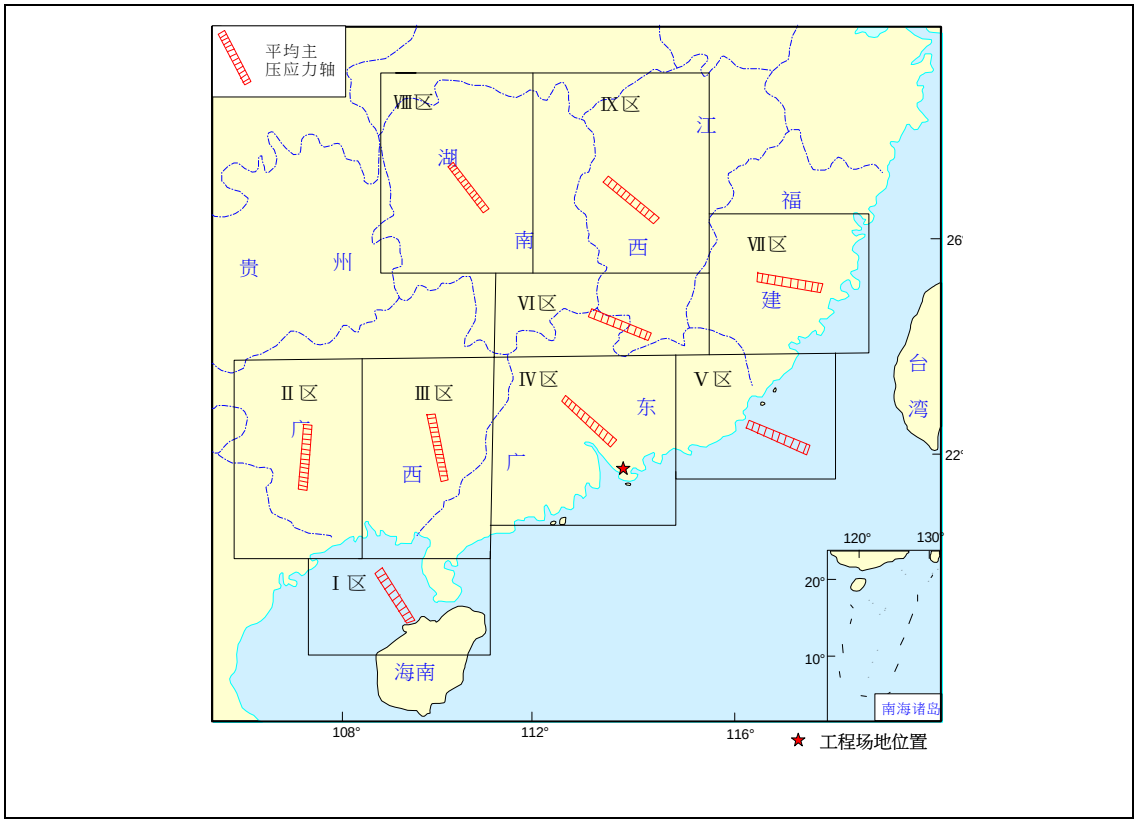

圖 1.5-2　華南地區平均主壓應力軸分佈圖

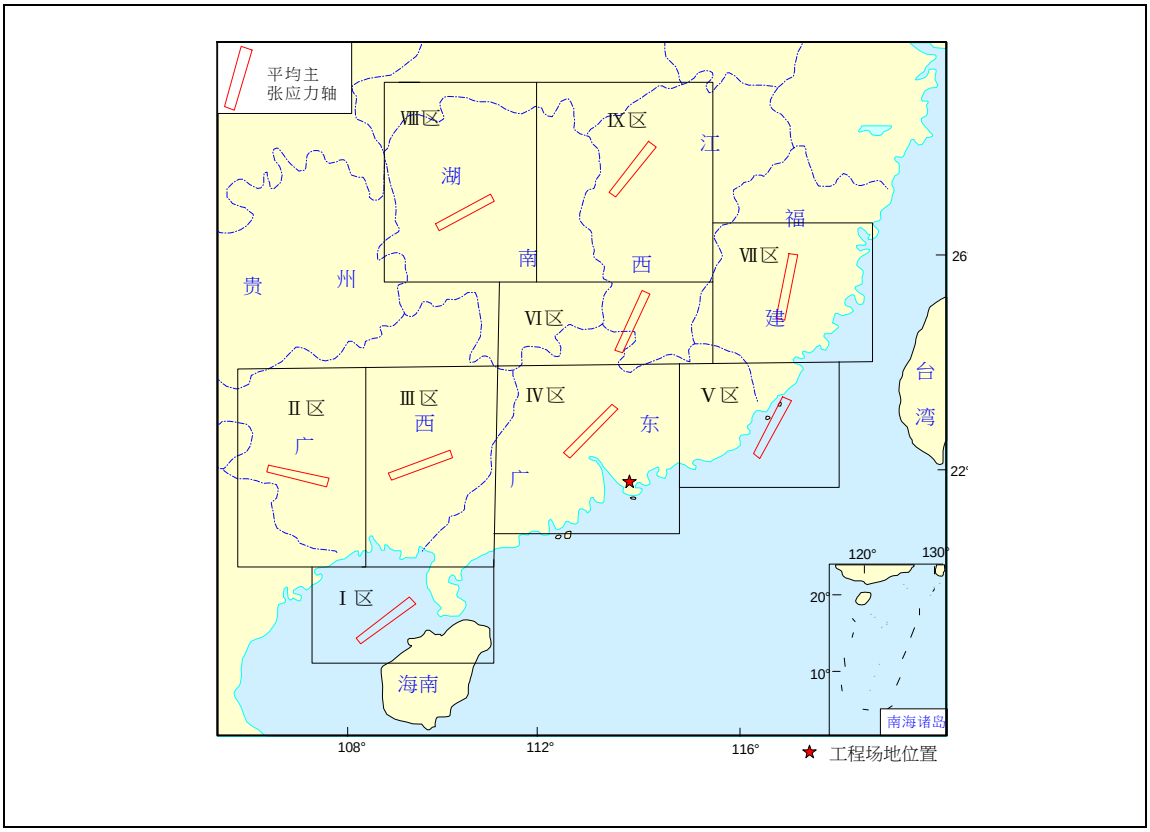

圖 1.5-3　華南地區平均主張應力軸分佈圖

為了滿足工程報告的需要，收集了 1972 - 2005 年三十多年間附近地區可定位的地震的初動，求出廣州、新會、深圳、珠海、從化 5 個台站的小震綜合解（表 1.5-2），結合附近地區的震源機制解進行應力張量反演，得到的區域構造應力場主壓應力方向仍為 NWW 向。

表 1.5-2　小震綜合面解

台站名	台站位置		P 軸		T 軸		矛盾比
	經度	緯度	走向	傾角	走向	傾角	
廣州（石榴崗）	113.3439°	23.0869°	130°	14°	34°	20°	0.06
新會	113.0294°	22.5522°	308°	33°	198°	27°	0.04
深圳	114.1333°	22.5333°	344°	48°	212°	31°	0.06
珠海	113.5667°	22.2667°	299°	50°	204°	4°	0.00
從化	113.65°	23.65°	274°	54°	52°	28°	0.07

香港屯門—元朗地震影響小區劃工程場地所處區域主要受到主壓應力軸為 300°左右和主張應力軸為 210°左右的構造應力場作用，區域發育的北西向和北東向構造在此構造應力場作用下容易發生剪切錯動，區域近東西向至北東東向的斷裂面上可見大量近水平方向擦痕，左旋及右旋均有，其中以右旋較明顯、新鮮，並具傾滑分量，如長寧西南石麟圩出露的瘦狗嶺－羅浮山斷裂，發現大量走滑擦痕與階步。北西向的觀瀾－溫塘斷裂帶左旋切錯北東向斷裂構造，說明它有較明顯的左旋走滑性質。區域的北東向斷裂構造，從其大量斷裂物質分析，顯示以擠壓為其特徵。1969 年 6.4 級陽江地震區內，北北西向斷裂發生左旋斷錯水系。博羅－紫金斷裂帶中段的義容－秀嶺斷層在由北東折向北東東走向的地段內，斷裂有右旋斷錯水系。河源斷裂的南段，在斷裂由近南北向向南轉為北東走向段內，亦有多處右旋斷錯水系。據前人的研究考察，1936 年桂東南靈山發生的 $6\frac{3}{4}$ 級地震中心區內，沿 NW330°/NE∠70°斷裂破碎帶發生左旋斷錯，形成窗櫺脊構造，左旋錯斷了與斷裂近於直交的山脊線與溝谷線，造成一系列明顯的窗櫺脊構造地貌景觀。

綜上所述，本區東至梅州，西至恩平的陸地及近海域區內，區域構造擠壓應力場的方位（北西西－南東東）是可信的。

由於現階段構造應力場的擠壓應力場方位穩定在北西西－南東東向，且以水平方向擠壓為主，主要源於菲律賓海板塊向西俯衝、推擠歐亞大陸板塊的結果。

這對分析不同斷裂運動方向，錯動的難易提供了重要的科學依據。

在北西西—南東東向水平構造應力場的作用下，區域內的北東向斷裂多表現為逆衝兼走滑性質，而北西向斷裂多表現為左旋走滑兼傾滑的活動特性。

第二章 區域地震構造綜合評價

本章將重點討論區域大地構造環境的滋生及其演化簡史、新構造運動基本特徵、地球物理場與地殼結構、主要斷裂帶的基本特徵與活動性，最後對區域地震構造環境的總貌作出評價，其目的在於為潛在震源區的劃分提供地質學依據和深部構造背景。按照中華人民共和國國家標準《工程場地地震安全性評價》（GB17741-2005）（國家技術品質監督局，2005）中對區域範圍的要求，將區域範圍確定為東經 112.08° - 116.16°，北緯 20.80° - 24.30°的區域。

2.1 區域大地構造環境與新構造運動

香港屯門—元朗地震影響小區劃所在區域在大地構造上屬於華南地槽褶皺系的一部分，位於增城－臺山隆斷束內。區域內各時代地層發育較齊全，沉積建造類型複雜，並經歷了多個構造階段發展演化歷史，形成了較複雜的地質構造格局（圖 2.1-1）。

自震旦紀以來，本區經歷了由地槽－準地台－大陸邊緣活動帶三個發展階段。震旦紀－志留紀為地槽發展階段，沉積了約 12,000 公尺的碎屑岩，志留紀末的加里東運動結束了地槽沉積，使沉積物形成了以北東東向為主的緊密線性褶皺和斷裂。泥盆紀—中三疊世，本區進入相對平穩的準地台發展階段，沉積了 5,000 - 6,000 公尺的碎屑岩和炭酸岩，中三疊世末的印支運動使這些岩層形成開闊的褶皺。其後，本區進入大陸邊緣活動構造帶發展階段，沉積了 4,000 - 5,000 公尺的陸相碎屑岩。強烈的燕山運動使本區發生強烈的地殼運動，並出現大面積的中酸性岩漿侵入和噴發，奠定了本區地質構造格局的基本輪廓。新生代沿斷裂帶形成新生代盆地，構造運動以間歇式斷塊差異運動為主，但活動強度明顯減弱。

本區經歷三個大地構造發展階段，發育了從震旦紀至第四紀各個時代的地層，發生強烈的酸性到基性的各類岩漿侵入和噴發活動，以及廣泛的區域變質和動熱

變質作用，造就了眾多的深、大斷裂帶，形成了東西向、北東向、北西向斷裂相互交匯和斷陷盆地、斷隆山地相間排列的地質構造背景。

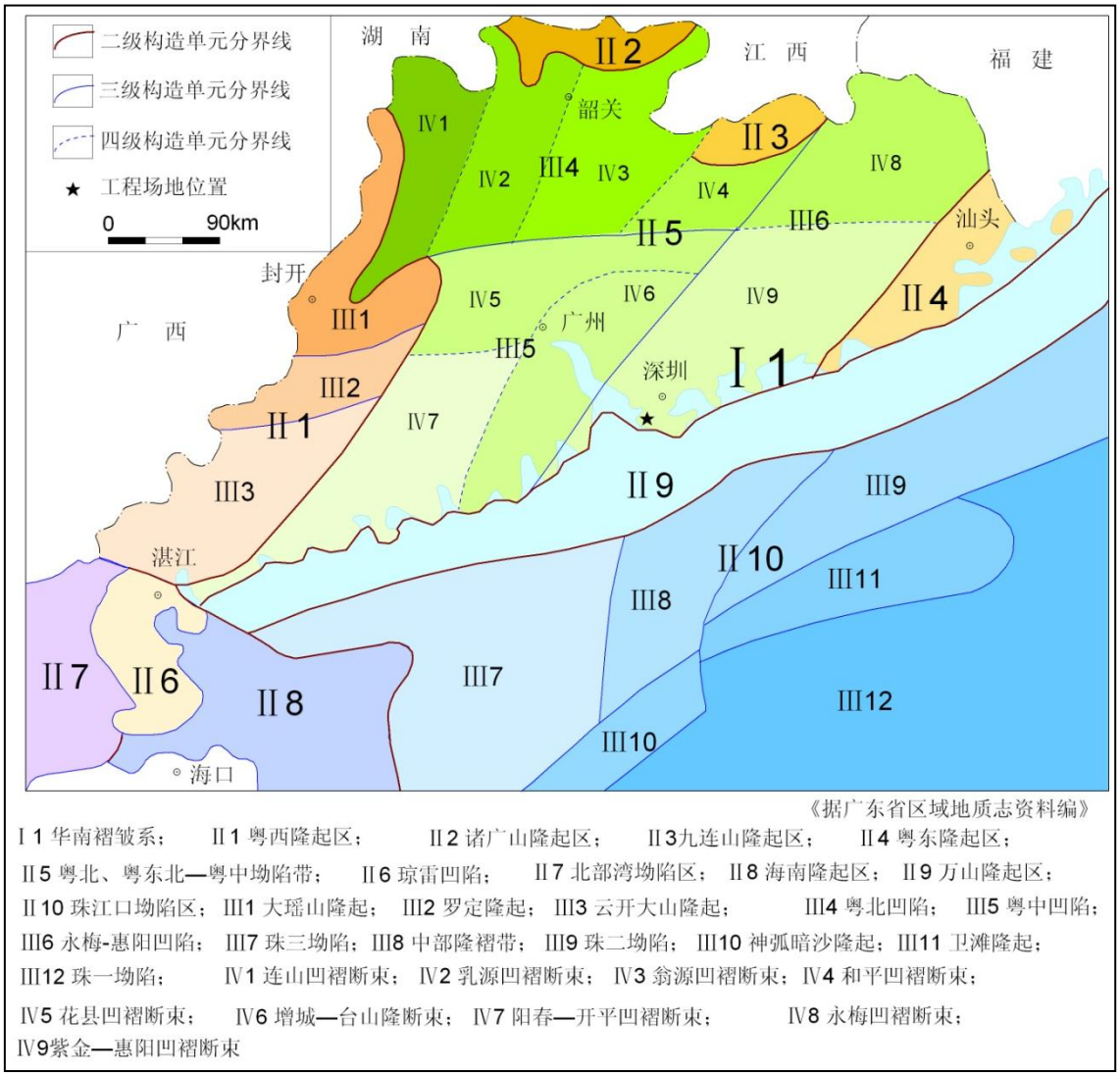

圖 2.1-1　區域大地構造位置及區域圖

2.2 區域新構造運動的基本特徵

本區新構造運動相當活躍，以斷裂的繼承性活動和斷塊差異運動為基本特徵，表現出既有頻繁的升降運動，又有水平的擠壓和走滑活動；既有大規模的火山噴發活動，又有眾多的溫泉湧出。由於活動的繼承性和新生性，時間上的間歇性和空間上的差異性，構成了山地、丘陵、盆地相間排列的地貌景觀。

Table of Contents (Chinese)
Table of Contents (Chinese)
Table of Contents (Chinese)
Table of Contents (Chinese)

2.2.1 沉積建造

區內新構造期以來的主要活動為晚第三紀及第四紀的沉積建造，晚第三紀含油碎屑岩建造主要分佈在南海海域，第四系主要分佈於河流兩岸、三角洲和濱海一帶，以沖洪積相、河海相粘土、砂礫等鬆散沉物積為主。

2.2.2 斷裂活動和斷塊差異運動

斷裂，特別是深、大斷裂，控制了區域地質發展史，成為大地構造和新構造單元的分界線。斷裂活動的繼承性和新生性主要表現在斷陷盆地的繼承性和新生性。如濱海斷裂帶控制珠江口外盆地厚達數千公尺的上第三系和第四系，而在斷裂北側的萬山群島則見 180 公尺高程的海蝕遺跡，這充分反映出斷塊（斷陷與斷隆）的差異性運動。

2.2.3 大面積、間歇性的升降運動

本區上升的標誌表現為多級夷平面、多層溶洞、多級臺地和階地。下降的標誌則見於平原中的埋藏風化殼，埋藏溶洞、貝丘遺址、泥炭層和腐木層。

區內近代垂直形變主要表現在中部大面積下沉、西北部強烈上升和東部和緩上升（圖 2.2-1）。垂直等值線既有北東向也有北西向穿插。區內西北部的懷集、廣寧和英德一帶上升幅度較大，上升速率為每年 2.0 - 3.5 毫米。珠江三角洲地區是廣東沿海地區大面積的沉降區，平均每年的下沉速率是-1.8 毫米，範圍大致包括惠州、廣州、佛山、鶴山、開平、中山、珠海和深圳等地，最大平均降幅約-3 毫米。總的形態從南向北傾斜，從東向西至三水、開平到南端海岸一帶迅速轉緩向粵西抬升。

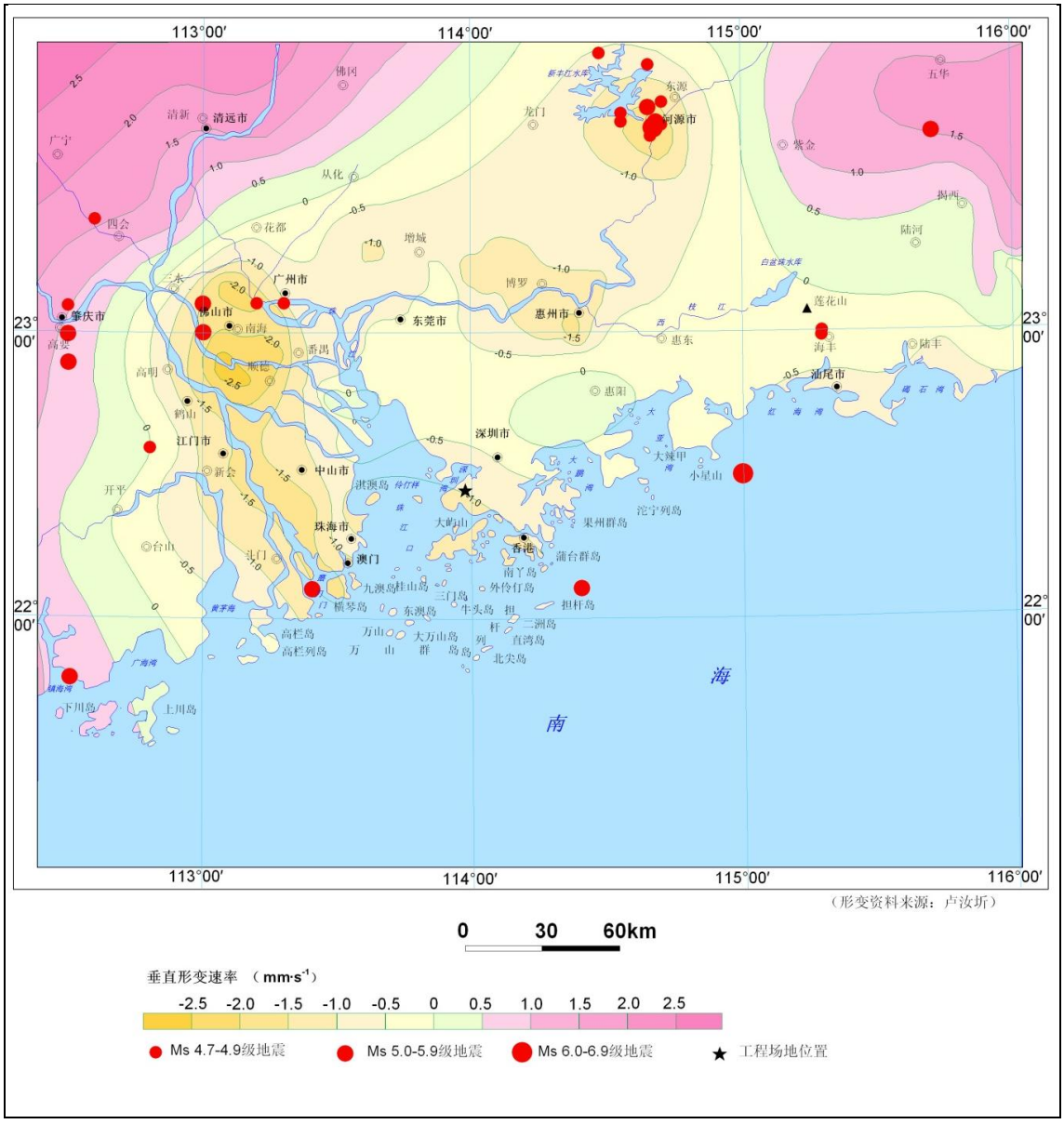

圖 2.2-1 區域陸地地殼垂直形變速率與強震關係圖

2.2.4 火山活動

區內大陸區新生代火山活動主要分佈在三水盆地及西樵山地區，火山活動開始於早第三紀早期，早第三紀末基本結束。火山盆地明顯受區域大斷裂控制，表現為多期次間歇性噴發活動，可劃分四個火山噴發旋回，其中以始新世火山活動最為強烈，岩性以粗面岩、玄武岩、凝灰岩為主，總厚 1,000 公尺以上，分佈面積 320 平方公里。

南海海域在第四紀時期內，有大面積玄武岩岩流溢出活動。

2.2.5 新構造分區

根據新構造運動的發展歷史、繼承性和新生性，斷塊構造特點以及各類動態指標，將研究區由北而南分為 3 個Ⅰ級新構造單元（I_1、I_2、I_3），其中I_2又可細分為 12 個Ⅱ級單元（圖 2.2-2）。

1. 粵北大面積間歇性隆起區I_1

位於佛崗－豐良斷裂和新豐－連平斷裂一線以北的粵北地區。構造線方向主要為北東－北北東向及東西向。區內在新構造時期以來一直處於隆升狀態，白堊紀至早第三紀的紅色盆地普遍抬升，自晚第三紀以來均未接受沉積。斷塊差異運動不明顯，發育多級夷平面，未發現喜山期岩漿活動，新構造運動上升的總幅度最大可達 1,800 公尺，為相對穩定區。區內僅發生少數 5 級左右地震，屬中弱震區，即相對安全區。

2. 華南沿海斷塊差異隆起區I_2

位於粵北大面積間歇性上升區以南至海岸線。構造線方向主要為北東向，其次為北西向。區內大部分地區自晚古生代以來為相對隆起區，中生代強烈活動，以斷裂活動和斷塊運動為特徵。沿斷裂帶有大規模的中酸性岩漿侵人和噴發活動以及強烈的動熱變質作用，形成頗具規模的斷裂變質帶，在局部斷裂下陷地區形成斷陷盆地，沉積了白堊系－下第三系紅色岩層，新構造運動在總體上繼承了斷裂和斷塊運動特徵，大部分的白堊紀－早第三紀紅色盆地已經抬升，僅在少數紅層盆地內繼續接受上第三系和/或第四系沉積，並出現新的第四紀盆地。本區地震活動頻繁，是東南沿海地震帶的主要組成部分。區內又可分出 12 個Ⅱ級單元：

(1) 帽峰山—羅浮山隆起區II_1

位於瘦狗嶺—羅浮山斷裂帶北，東西長超過 100 公里，南北寬 30 - 50 公里。該區為走向北東東至近東西的古隆起，隆起的軸部為燕山期多幕次侵入的花崗岩體，該隆起是一繼承性極為強烈持久的隆起區，歷經晚古生代、中生代直至新生代均以剝蝕隆起為主。新構造時期以來，完全保留著地史時期其自身的固有特徵，即隆起為主，目前拱曲隆起最強烈的地方在東段的羅浮山地區，其次是西部的帽峰山地區。隆起的幅度和強度從中心地帶向兩側降低，內部斷裂不發育，僅南側與西北江、東江三角洲斷陷區發育了東西向的瘦狗嶺—羅浮山斷裂帶，新構造時期以來，沿斷裂帶以低丘臺地為主，由此向北，以持續上升為主為其特徵。

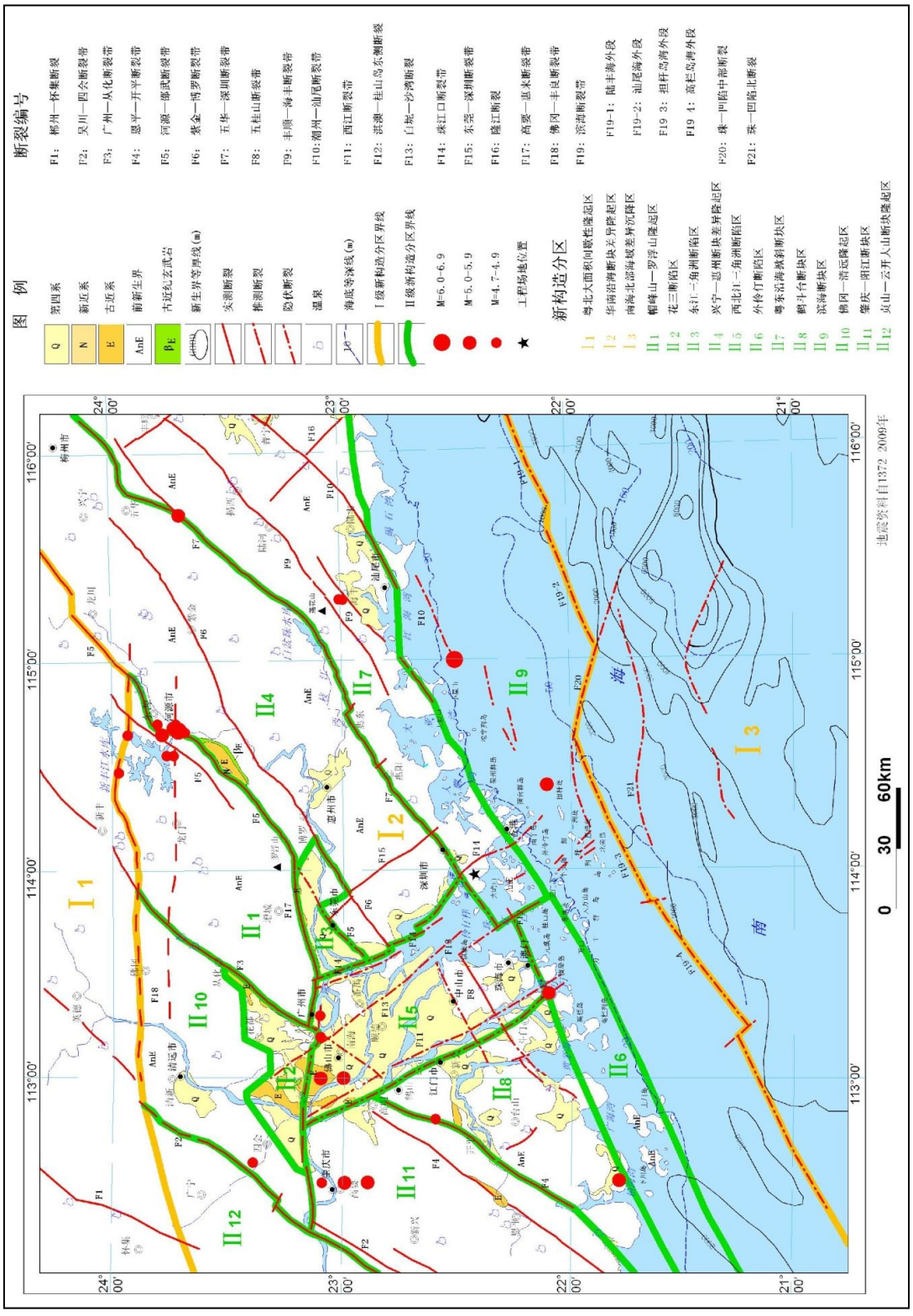

圖 2.2-2 區域新構造分區圖

(2) 花（都）三（水）斷陷區Ⅱ$_2$

位於三水至花都一帶，東與帽峰山—羅浮山隆起區為鄰，西北面與佛岡—清遠隆起區相接，南以廣三斷裂為界與南側的西北江三角洲斷陷區分開。花三斷陷區第四紀主要為沖積平原區，包括廣（州）花（都）平原與北江平原，堆積了晚更新世至全新世的河流沖積層系，沿白雲山西麓一帶，伴有沖洪積層系。第四系厚度不大，一般 10 至 20 公尺。平原面高程由北往南和緩下降，到達南部邊界一帶與西北江三角洲相堆積交織一起，平原面高程也降至 1 公尺以下，花三斷陷區沖積平原內含多處剝蝕殘山與星羅棋佈的侵蝕剝蝕臺地。

(3) 東江三角洲斷陷區Ⅱ$_3$

北以羅浮山斷裂、東北以長寧—龍溪斷裂為界與帽峰山—羅浮山隆起區分開，西以珠江口東側斷裂為界與西北江斷陷下沉區為鄰，東南受河源—邵武斷裂西南段（石龍—厚街斷裂）、觀瀾—溫塘斷裂和紫金—博羅斷裂西南段（南坑—虎門斷裂）的控制而與虎門—樟木頭斷塊差異隆起區相交接。斷陷的基底為上白堊統，古近系，局部為白堊統，由此可見斷陷盆地最新始於早白堊世，晚白堊世時，盆地範圍急劇擴展，可能遍及全區，古近紀時，由於羅浮山斷裂的強烈正斷活動，續延了斷陷盆地的歷史。新構造時期以來，新近紀—中更新世全區處於上升狀態，以侵蝕為主，但相對於上白堊—古近系沉積盆地周邊蝕源區而言，仍屬相對下沉的區域，以準平原地貌為其特徵，晚更新世—全新世原古紅盆地所屬範圍開始下沉，遂有上更新統—全新統沖積和三角洲相沉積物的形成。

(4) 興寧—惠州斷塊差異隆起區Ⅱ$_4$

西及西北分別與西北江和東江兩個斷陷下沉區為鄰。區內斷裂發育：珠江口斷裂、河源—邵武斷裂，觀瀾—溫塘斷裂北段及南坑—虎門斷裂東北段構成了本區的西界與北界，深圳—五華斷裂帶成為南界。區內為元古界變質岩基底發育區。震旦紀後，地槽隆起，晚古生界至中三疊世，區內地殼處在地台區期，晚三疊世開始地台活化，白堊紀開始，區內地窪沉積結束，全區上隆遭受剝蝕，但在晚白堊世時，由於斷裂特別是邊界性斷裂間的差異活動，本區成為西及西北兩個斷陷紅盆的主要蝕源區。古近紀至第四紀，區域仍以侵蝕上升為主且持續至今，而發育於邊界及其內在的斷裂構造仍然有一定的活動性。

(5) 西北江三角洲斷陷區Ⅱ$_5$

西北江三角洲斷陷區四周均有斷裂作為邊界，北界是廣三斷裂帶與瘦狗嶺斷裂，東界是珠江口東側斷裂帶，西界是西江斷裂帶，南界是五華—深圳斷裂帶及橫琴島—下川島斷裂帶。斷陷區元古界基底淺，部分已暴露至地表，燕山運動期，有大量花崗岩類侵入，早白堊世開始裂陷形成早白堊世沉積盆地，晚白堊世—古近紀階段開始坳斷下陷，接受盆地沉積，在古近紀時，西北江三角洲斷陷區之西

北江三角洲斷陷帶內基本上為 K_1 - E 地層所覆蓋。新近紀一早更新世，全區和緩上升以侵蝕夷平為主，但相對於四周隆起區應屬低平的準平原地貌，中更新世時，局部地段沉積了沖積相砂礫岩系。晚更新世以來，除區內某些次級隆起繼續遭受剝蝕侵蝕外，全區和緩下沉，出現沖積一海積的三角洲相沉積，並且一直續延至今，晚更新世一全新世沉積厚度一般為 25 公尺左右，較淺地段＜20 公尺，較深地段 30 - 40 公尺，最深處在燈龍沙地區，厚達 63.6 公尺。

(6) 外伶仃斷陷區Ⅱ$_6$

位於西北江三角洲斷陷區與鶴（山）斗（門）台（山）隆起區之南，其間有五華一深圳斷裂帶與橫琴島一下川島斷裂帶，斷陷區南界在珠一北緣斷裂帶，斷陷區西北一東南寬約 100 公里，東側以珠江口斷裂帶與平海一深圳斷塊隆起區為鄰，估計在下川島南側一帶，北東一南西長超過 160 公里。斷陷區普遍為海水所淹，但島嶼星羅棋佈，基岩主要為元古界、寒武系及燕山期花崗岩體。斷陷區水域水層厚度表明，西北邊界一帶普遍為約 10 公尺，向東南漸漸增大，到南側珠一北緣斷裂帶時，水層厚度普遍達 50 - 60 公尺。在珠江三角洲外海域，一般以水深 50 - 60 公尺處為界，劃分出內陸架與外陸架，內陸架表層為近代陸源碎屑層所覆蓋，普遍可見兩級水下堆積階地，高程分別為水下 15 - 25 公尺、35 - 50 公尺左右。

(7) 粵東沿海掀斜斷塊區Ⅱ$_7$

斷塊區呈北東一南西走向，西北界為五華一深圳斷裂帶，東南界為政和一海豐斷裂帶，西南以珠江口斷裂為界。由五華一深圳斷裂帶與政和一海豐斷裂帶所夾持的斷塊相對於南北兩側而言是一個較強烈上升的大型地壘構造，粵境內自東北而西南有多座 1,000 公尺以上山峰，顯示以中一低山構造地貌為其特徵。平海一深圳掀斜斷塊區是蓮花山地壘構造向西南的傾伏部份，上升強度自東北向西南減弱，區域僅是其西南端部，地形地貌上顯示以低山丘陵為主及山間海灣凹地等為其特徵。

(8) 鶴（山）斗（門）台（山）斷塊區Ⅱ$_8$

東北邊有西江斷裂帶，西北邊有鶴城一金雞斷裂帶，南界有橫琴島一下川島斷裂帶，區內出露基岩主要是印支一燕山期花崗岩類，其次是寒武系，此外還有少量泥盆系、白堊系及古近系。沿潭江與西江右岸一帶是第四系覆蓋區。沿鶴斗台斷塊區周邊地震活動較明顯，歷史上於鶴城及磨刀門外海先後有過中強地震。

(9) 濱海斷塊區Ⅱ$_9$

位於海豐斷裂帶與濱海斷裂帶之間的海域地帶，是華南大陸在海上的延伸部分。從地貌上來看，該區北接半島海灣帶，為沿海島鏈帶。從構造上來看，該區南鄰南海北部斷階帶，為相對隆起帶。新構造時期以來，該區以斷裂差異運動為特徵，地震活動頻繁，是大陸東南沿海地震帶的主要組成部分。

(10) 佛岡—清遠隆起區Ⅱ$_{10}$

東段南與帽峰山—羅浮山隆起區為鄰，西段與貞山—雲開大山斷塊隆起區接壤，北以佛岡—豐良斷裂為界與粵北大面積間歇性隆起區相接。隆起區主要是近東西向的巨型燕山期花崗岩體分佈區，部份可見上古生界頂蓋圍岩，以近東西向基底斷裂發育為其主要特徵，在地球物理場上是為向北傾斜的康氏面莫氏面的斜坡地帶。新生代來，區域一直處於隆起狀態，缺失古近紀與新近世的盆地沉積，第四紀以來，亦以侵蝕剝蝕為主，缺失較大面積的第四系分佈區，僅有小型第四系槽地發育。地貌上全區以丘陵山地為主，低至中山地形地貌分佈面積較廣。區域以整體上升為主，斷裂差異活動不明顯，地震活動以中小地震為主。

(11) 肇慶—陽江斷塊區Ⅱ$_{11}$

西有吳川—四會斷裂帶，東有西江斷裂帶與鶴城—金雞斷裂帶，北有廣三斷裂帶向西的延續段。區內主要出露元古界、寒武系、上古生界、燕山期花崗岩及白堊系等。加里東時期是為地槽褶皺帶的重要組成部份，晚古生代時期當有地台蓋層的覆蓋，強烈的燕山運動，區內普遍為花崗岩侵入吞蝕，中部強烈隆起，至今一直以剝蝕侵蝕為其主要特徵，燕山運動晚期在北部由白諸往東經新橋至白土以東一帶，及東南側—自皂幕山往西南經蒼城、開平至恩平西南一帶，分別裂陷形成白堊紀沉積盆地，後者局部繼承至古近紀。新近紀以來全區大部份以隆起為主。

(12) 貞山—雲開大山斷塊隆起區Ⅱ$_{12}$

位於吳川—四會斷裂帶及其以西地區，區域僅是其東北端部。吳川—四會斷裂隆起帶在早古生代應是一個強烈的斷陷區，沉積了活動區型的地槽型沉積建造，加里東運動，帶內北東向斷裂構造變動極為強烈，在海西、印支及燕山運動期，沿帶產生大規模的中酸性岩漿侵入活動，中生代開始已全部上升成陸，自此區域一直以持續上升為主至今。新構造時期以來，帶內斷裂差異活動較為明顯，形成多個小型古近紀斷陷盆地。在地震活動方面，斷裂帶東北段歷史上於四會及雲浮發生過中強震、西南段於電白濱海域及陽江先後發生過 6 級與 6.4 級地震。

3. 南海北部海域差異沉降區Ⅰ$_{3}$

也稱珠江口外斷陷沉降區，指以濱海斷裂與珠一坳陷斷裂帶為界，與北側的南華沿海斷塊差異隆起區相接的南海北部岸坡帶和淺海海域，屬南海北部的陸架帶。該區基底為元古界，元古代後至下古生界，區域裂陷下沉沉積了地槽型的下古生界，此後區域一直處於隆起狀態，大多缺失上古生代至中三疊世沉積，屬於相對穩定的地台隆升發展階段，晚三疊世以來，區域地殼活動加劇，斷裂斷塊差異活動強烈，火山噴發作用極為盛行。其構造線方向主要為北東東，其次是北北

西。白堊紀—始新世時期，斷陷沉降區以北處於上升狀態，隨著區域拉張活動，形成以北東東向伸展的陸相斷陷盆地，沉積了陸相含煤、含油碎屑岩岩層。新近紀至第四紀，珠江口外盆地繼續快速拗斷，普遍堆積了 1,000 - 3,000 公尺、最厚處達 4,000 公尺的海相沉積為主的屑碎岩岩層，其中第四系厚達 200 - 300 公尺。在地震活動方面，斷陷沉陷區北緣地區，地震活動強烈，是東南沿海地震區外帶地震孕育和發生的主要地段，是 7 級以上的發震構造區。

工程場地位於粵東沿海掀斜斷塊區 II_7 的西南端北側邊界附近。

2.3 區域地球物理場與地殼結構

地震一般皆發生在地表下的地殼深處，是地殼內部應力與介質相互作用的結果。就西南地區而言，地震特別是 6 級以上強震一般集中分佈於地表下約 20 - 30 公里的深度範圍內，與該深度範圍內特殊的介質結構和構造密切相關。因此，通過深部地球物理場的研究，可以揭示震源深處的介質結構和構造特徵，其目的在於為強震發生的深部構造標誌的確定和地震區（帶）及潛在震源區的合理劃分提供深部地球物理場依據。

2.3.1 重力場特徵

由布格重力異常圖（圖 2.3-1）可以看出 ，區域範圍的西北部佛山、廣州、東莞一帶存在一個醒目的重力高，異常總體走向近東西向，總體形態規則，內部起伏平緩，在該重力高內部異常強度 15×10^{-5} m/s^2 至 20×10^{-5} m/s^2（毫伽）等值線位於佛山市一帶，呈北西向。異常原因應是上地幔隆起的重力場顯示。在區域範圍的南部近海地區也存在一個顯著的北東東向重力高，這裡是南海大陸架北緣，與濱海斷裂帶位置大體一致，總體應屬南部大陸架重力高的一部分。在上述 2 個重力高帶之間—珠海、斗門、廣海灣一帶存在一個微低重力帶，最低值 -10×10^{-5} m/s^2，走向亦是北東東方向。區域範圍東部不存在線性梯度帶，廣州重力高向東緩斜，逐漸消失過渡到負重力區，大體在惠東以西。

概括地說，區域重力場自北而南有高、負、高的總體北東東向格局的特徵，區域週邊北、東、西側為負異常圍繞，南為巨大的大陸架 NEE 向重力高帶。區域週邊北、西部和區域南部邊界地區線性變化較急，構造活動應相對活躍，而東側變化平緩，構造相對應較弱。

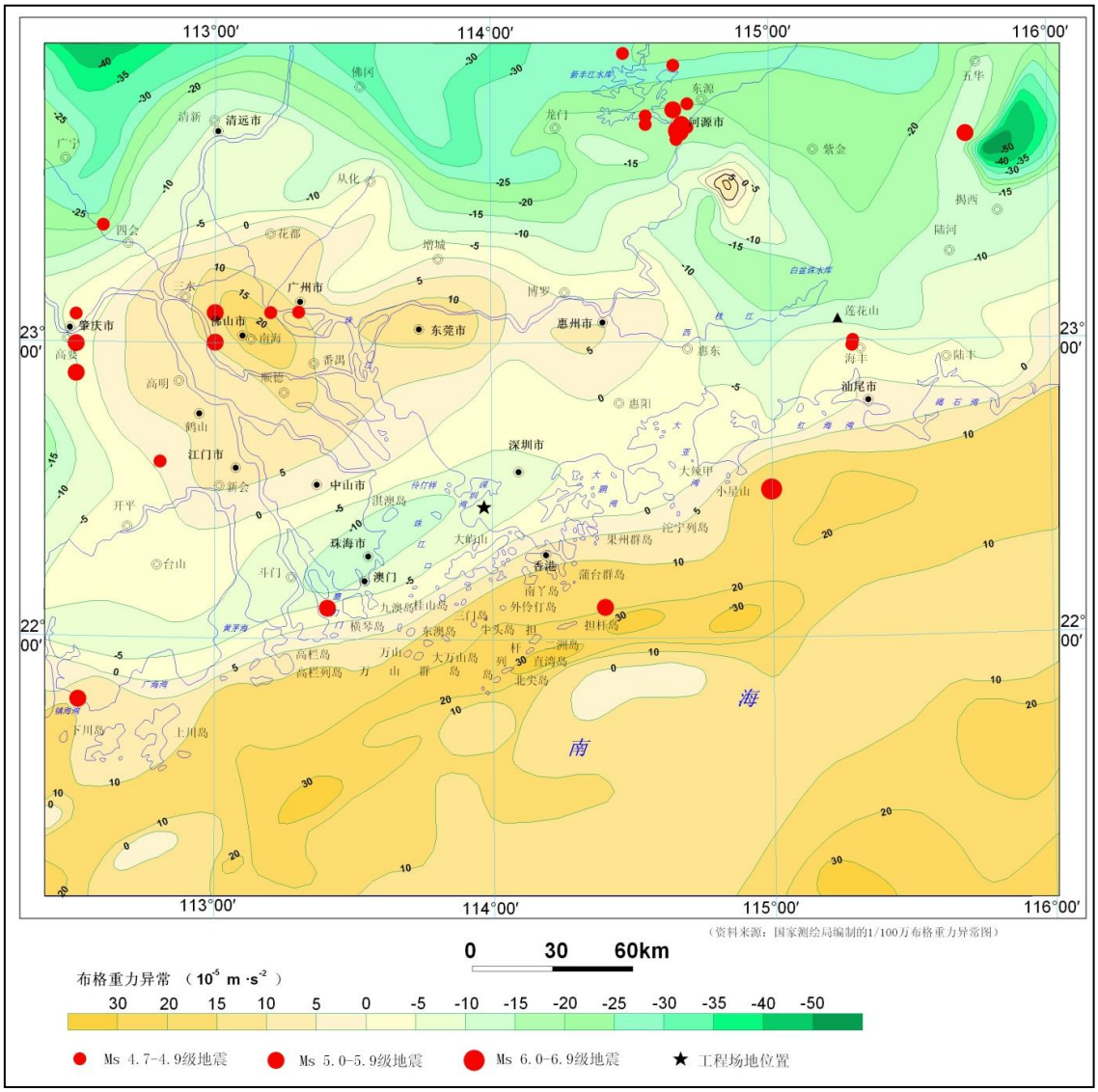

圖 2.3-1　區域布格重力異常與強震關係圖

2.3.2 航磁異常特徵

區域範圍大體上可分為 2 個磁場區（圖 2.3-2），江門—中山—深圳一線以北為第一磁場區，它屬於平緩正負磁場區，其特徵是，在正磁場的背景下，花斑狀分佈一些負磁場區。總體強度不大，約±100 - ±200 伽瑪，最大正磁場為 240 伽瑪，位於從化，岩性以花崗岩為主；最低負磁場，在惠陽潼湖一帶，最低值為 160 伽瑪，岩性以侏羅紀火山岩為主。梯度緩、磁場較寬緩、具明顯的方向性，說明磁性體埋藏較深，其發育受一定的構造方向控制。在磁場方向上，以近東西向為主體，南部更加顯著，北部的花都、從化、增城、佛山、東莞、博羅、惠東等地常表現為北東東或北西西的串珠狀磁場排列為一近東西向磁場帶。在這一磁場體的背景下，局部也發育有北東、北西向磁場體，同樣是構造控制的反映。

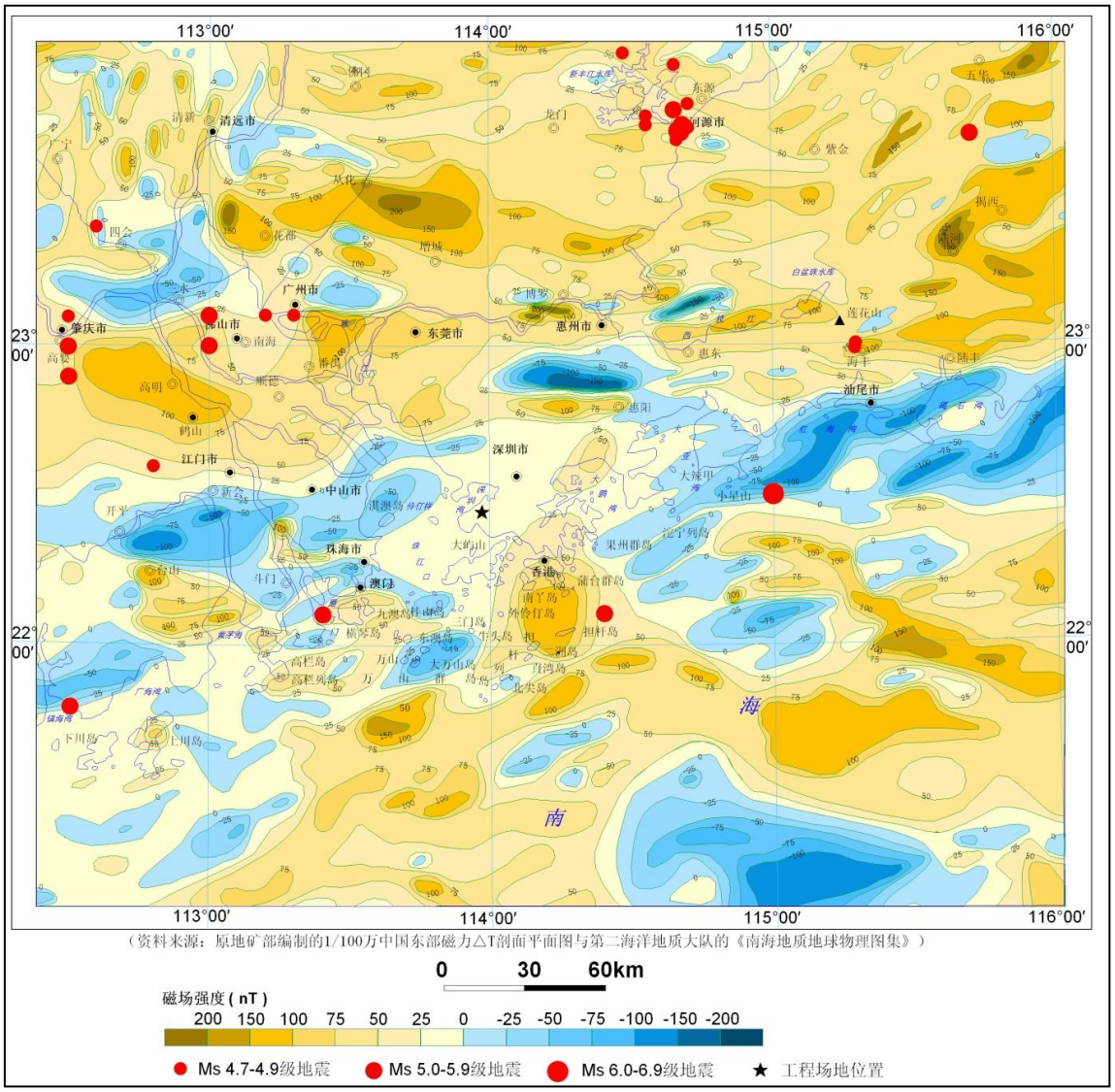

圖 2.3-2 區域磁力異常與強震關係圖

區內第二磁場區位於前一磁場區的南部，即江門—中山—深圳一線以南至海域的地區，為正負磁場變化區，其北部以負磁場為主，南部以正磁場為主。該磁場區總體仍以近東西向展布為主，同樣也存在北東和東西向局部磁場體，北部負磁場北界線呈整齊的東西向梯度帶與其北側的正磁場交界，是正負不同性質磁場的分界線。北部負磁場的南界雖然仍呈東西向，但不甚整齊，這一界限位於廣海—斗門—澳門—香港北及以東，其中介入一部分正異常場，這一界線基本上分佈在花崗岩區。磁場總體平緩，梯度不大。南區大部分為正磁場，在擔杆列島—萬山群島一線磁場梯度較大，最大磁場強度為 280 伽瑪。這一線以南海域則分佈一條巨大的負異常帶，這一正負磁性交界地區應存在深大斷裂帶，與濱海斷裂位置吻合。

2.3.3 區域地殼結構特徵

區域內沿海一帶地殼較薄，莫霍面較淺，其中香港地區的地殼厚度不足 34 公里，往北地殼厚度逐漸增厚，莫霍面逐漸加深，至佛岡、龍門一帶，地殼厚度達 34.75 公里（圖 2.3-3）。

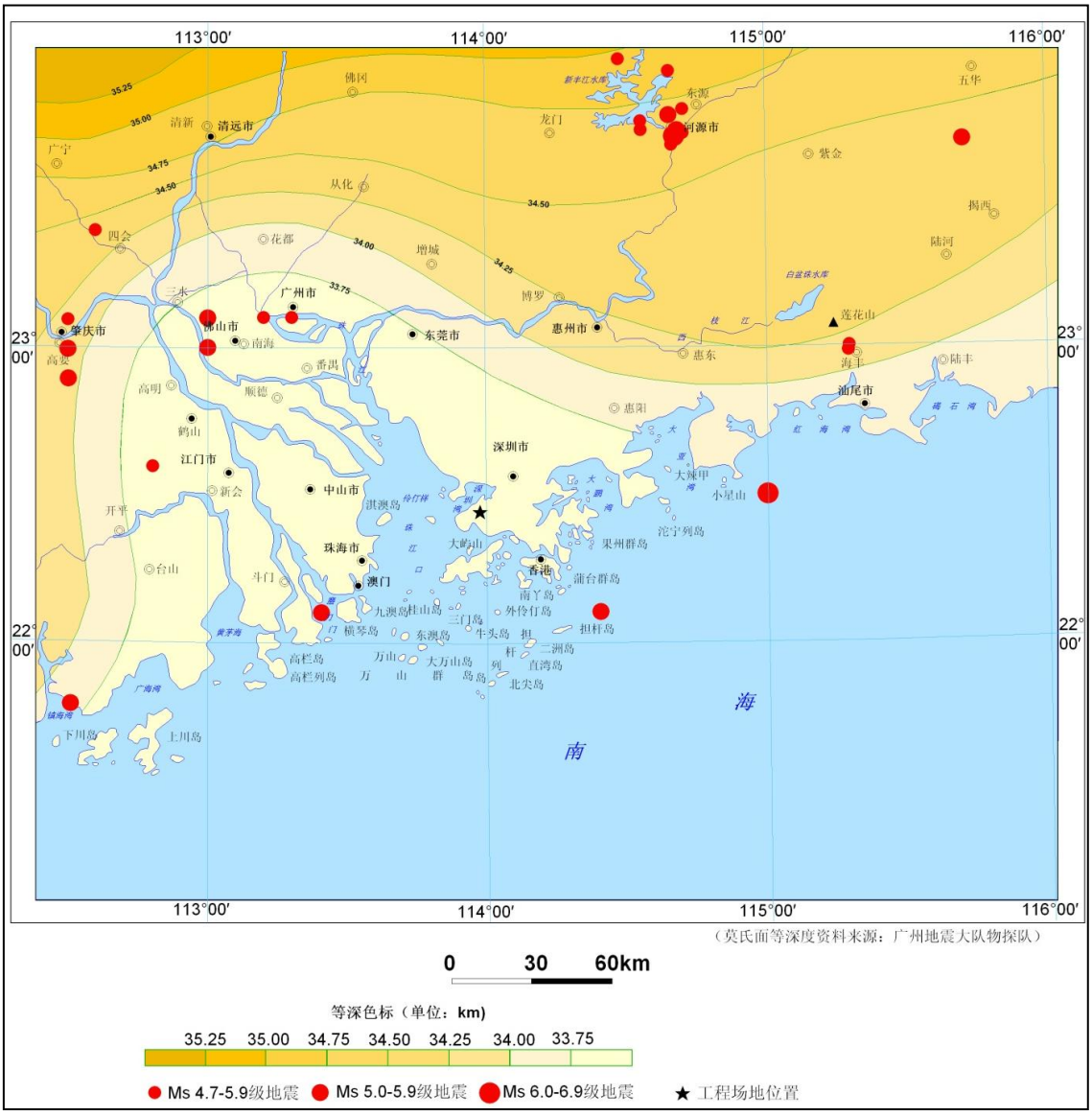

圖 2.3-3　區域地殼厚度與強震關係圖

區域西部形成莫霍面隆起區，範圍包括臺山至三水以東，惠陽以西，花都以南地區，地殼厚度不足 34 公里，是廣東省陸地地殼最薄的地段，也是莫霍面隆起

Table of Contents (Chinese)
Table of Contents (Chinese)
Table of Contents (Chinese)
Table of Contents (Chinese)

抬升之處。由圖可見，地殼等厚線在此地段形成一個舌狀形態，向北偏西方向突出。在從化—增城以北地區，地殼厚度線和莫霍面深度線方向近於東西向，地殼厚度自南向北增厚，莫霍面自南向北沉降，構成單一平緩的東西向梯級條帶。

根據重力、航磁、大地電磁測深、天然地震轉換波測深和人工地震測深等資料，本區深部構造的基本輪廓表現為莫氏介面東南淺、西北深的特點。區內莫氏面深度 33.7 - 35.3 公里。

地殼深部構造在剖面上還具有層狀結構特徵。根據岩層密度和地震波速度，地殼由上而下可分為三層（圖 2.3-4）：

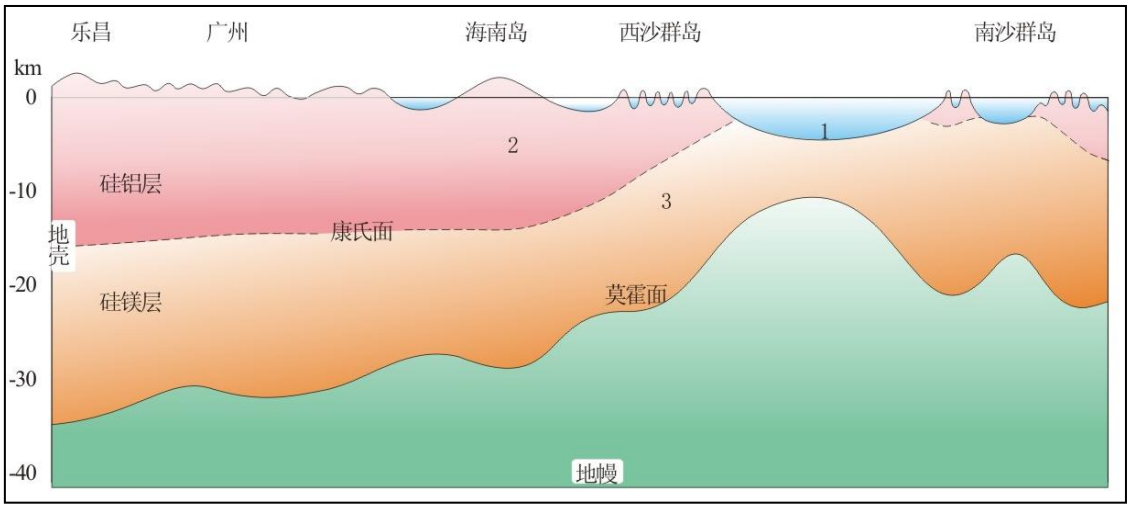

圖 2.3-4 廣東地殼結構模式示意圖

（據廣東省區域地質志資料改編）

1. 第一層：“低”密度層，為中新生代陸相沉積層，岩層平均密度值為 2.22 g/cm^3；縱波平均速度為(4.92±0.2) x 10^3 m/s，層厚約 1.4 公里，相當於地殼表層。

2. 第二層：“中”密度層，為古生代地層及其以前的變質混合岩系和花崗岩類，岩層密度值超過 2.6 g/cm^3；縱波平均速度為(6.13±0.1) x 10^3 m/s，層厚約 20 公里，相當於矽鋁層。

3. 第三層：“高”密度層，為玄武岩類岩層，岩層密度值為 2.8 - 3.3 g/cm^3；縱波平均速度為(6.83±0.1) x 10^3 m/s，層厚約 11.1 公里，相當於矽鎂層。

上地幔頂部岩層密度值大於 3.3 g/cm^3，縱波速度為 8.03 x 10^3 m/s。第二層與第三層之間的突變介面稱為康拉德面；第三層與上地幔之間的突變介面稱為莫霍面。

地球物理場、地殼結構與區域內的中強地震活動有較為密切的關係。重力異常、航磁異常反映，地震常常分佈在北東向異常與北西向及近東西向異常交匯處。在地殼深部構造平面的分帶上，地震主要位於地殼深部構造的南部隆起區，在莫霍面等深線 33.7 - 35.3 公里之間。區內的中強地震震源深度一般為 5 - 33 公里，屬於發生在地殼內的淺震。

2.4 區域主要斷裂帶特徵及其活動性

區內經歷了多期次構造運動，其中燕山運動規模最為宏偉，影響深遠，形成了一系列大小不等、方向不一、性質不同的斷裂構造，尤其是深、大斷裂，對區域構造的發展起着重要的控制作用，與地震活動有着密切的關係，北東向斷裂活動進一步加強，與此同時，形成了新生的北西向斷裂和南海北部海域的北東東向斷裂，從而奠定本區的基本構造輪廓（圖 2.4-1A、B）。茲將各組斷裂的基本特徵簡述如下。

2.4.1 北東向斷裂

北東向斷裂是區內最具規模的斷裂，遍佈全區。這些斷裂規模宏大，延伸數百公里以上，大多數生成於印支期，強烈活動於燕山期，沿斷裂分佈有中新生代斷陷盆地。控制大型山脈、水系的發育和花崗岩的侵入，斷裂的動熱變質現象顯著，沿斷裂有基性岩體和溫泉出露，屬於切割較深的斷裂帶。斷裂由西而東有：懷集—郴州斷裂帶、四會—吳川斷裂帶、廣州—從化斷裂帶、恩平—開平斷裂帶、河源—邵武斷裂帶、紫金—博羅斷裂帶、五華—深圳斷裂帶、五桂山斷裂帶、豐順—海豐斷裂帶、潮州—汕尾斷裂帶等。

F1：懷集—郴州斷裂帶

分佈在懷集、陽山、連縣，向南延入廣西蒼梧，向北入湖南茶陵，區內長度 80 公里。斷裂由兩組平行的斷裂束組成，總體走向北東 20° - 25°。斷裂帶發育在寒武、泥盆、石炭系內，普遍見強烈的擠壓破碎帶和矽化帶，寬度可達數百公尺至數公里，斷面傾向北西，傾角 50°以上，斷裂所經之處片理化帶、糜棱岩化帶廣泛發育，常常造成老地層逆掩在新地層上。沿斷裂有不同時代的岩漿岩侵入，包括加里東、印支和燕山期侵入岩。斷裂形成於加里東運動晚期，中、新生代控制白堊－第三系紅色盆地的分佈。沿帶多處溫泉湧出，但地震活動性較弱。

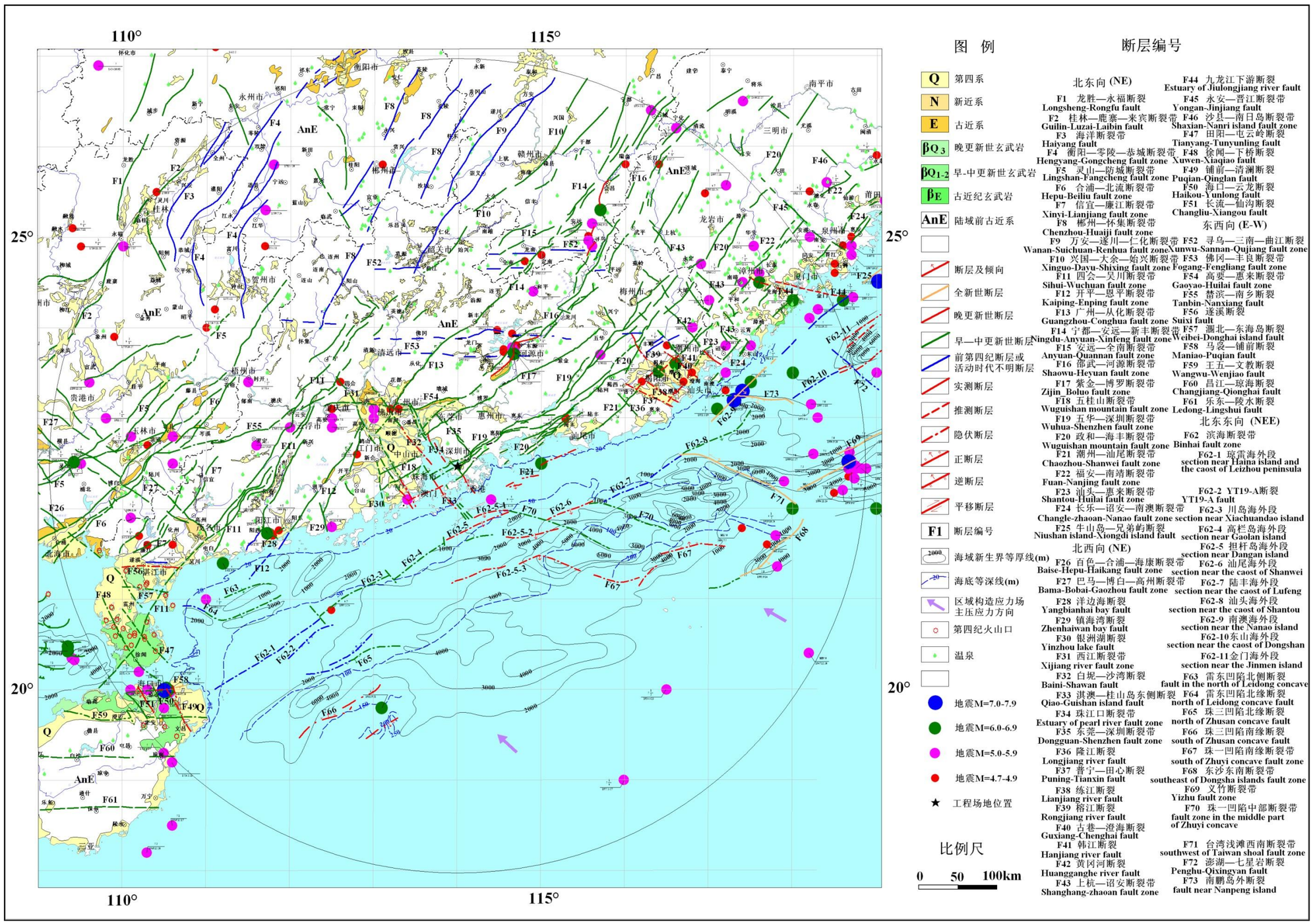

圖 2.4-1A 區域 500 公里範圍地震構造圖

Table of Contents (Chinese)
Table of Contents (Chinese)
Table of Contents (Chinese)
Table of Contents (Chinese)

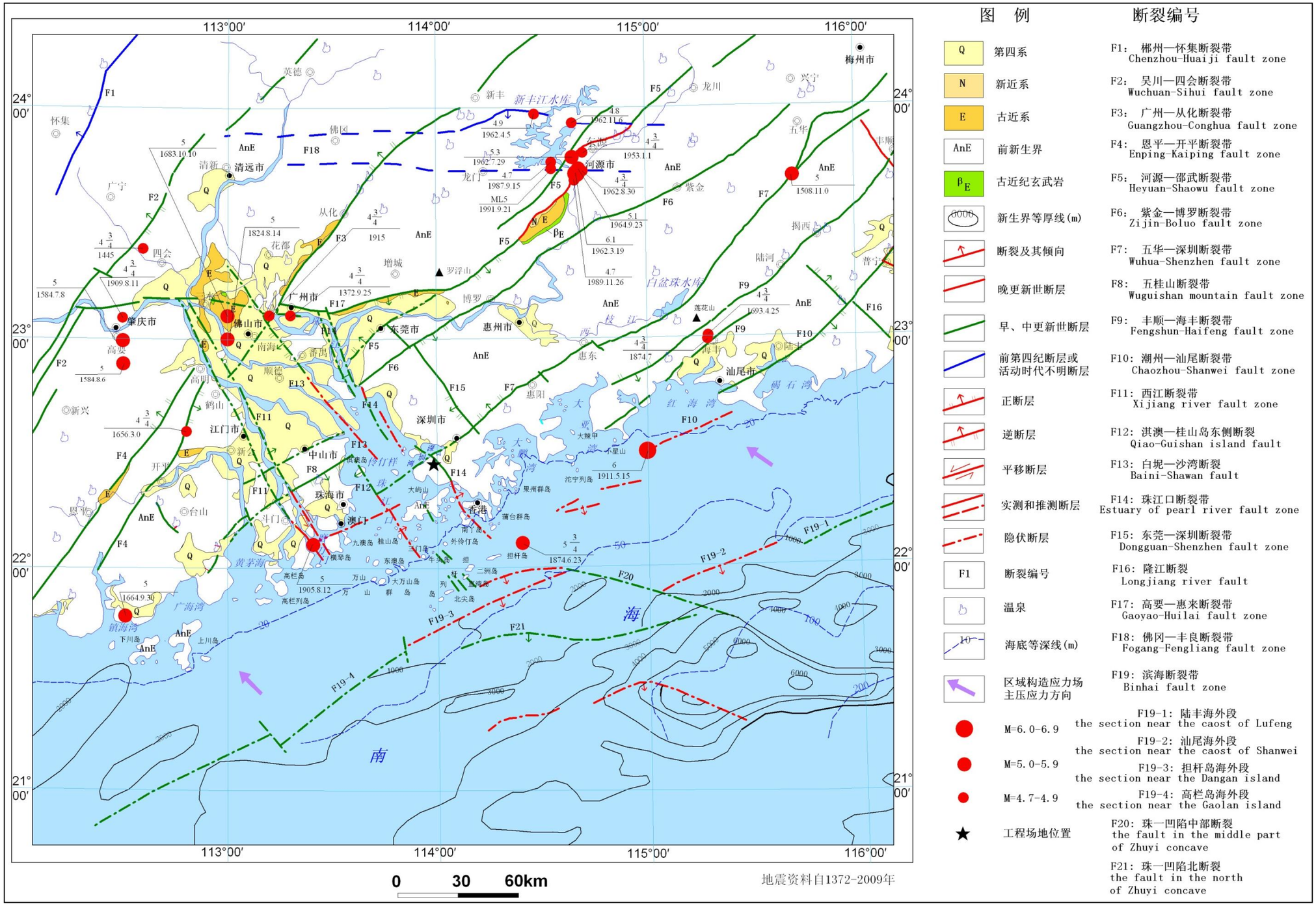

地震资料自1372-2009年

图 例

- Q 第四系
- N 新近系
- E 古近系
- AnE 前新生界
- β_E 古近纪玄武岩
- 6000 新生界等厚线(m)
- 断裂及其倾向
- 晚更新世断层
- 早、中更新世断层
- 前第四纪断层或活动时代不明断层
- 正断层
- 逆断层
- 平移断层
- 实测和推测断层
- 隐伏断层
- F1 断裂编号
- 温泉
- 10 海底等深线(m)
- 区域构造应力场主压应力方向
- M=6.0-6.9
- M=5.0-5.9
- M=4.7-4.9
- 工程场地位置

断裂编号

F1: 郴州—怀集断裂带 Chenzhou-Huaiji fault zone
F2: 吴川—四会断裂带 Wuchuan-Sihui fault zone
F3: 广州—从化断裂带 Guangzhou-Conghua fault zone
F4: 恩平—开平断裂带 Enping-Kaiping fault zone
F5: 河源—邵武断裂带 Heyuan-Shaowu fault zone
F6: 紫金—博罗断裂带 Zijin-Boluo fault zone
F7: 五华—深圳断裂带 Wuhua-Shenzhen fault zone
F8: 五桂山断裂带 Wuguishan mountain fault zone
F9: 丰顺—海丰断裂带 Fengshun-Haifeng fault zone
F10: 潮州—汕尾断裂带 Chaozhou-Shanwei fault zone
F11: 西江断裂带 Xijiang river fault zone
F12: 淇澳—桂山岛东侧断裂 Qiao-Guishan island fault
F13: 白坭—沙湾断裂 Baini-Shawan fault
F14: 珠江口断裂带 Estuary of pearl river fault zone
F15: 东莞—深圳断裂带 Dongguan-Shenzhen fault zone
F16: 隆江断裂 Longjiang river fault
F17: 高要—惠来断裂带 Gaoyao-Huilai fault zone
F18: 佛冈—丰良断裂带 Fogang-Fengliang fault zone
F19: 滨海断裂带 Binhai fault zone
F19-1: 陆丰海外段 the section near the caost of Lufeng
F19-2: 汕尾海外段 the section near the caost of Shanwei
F19-3: 担杆岛海外段 the section near the Dangan island
F19-4: 高栏岛海外段 the section near the Gaolan island
F20: 珠一凹陷中部断裂 the fault in the middle part of Zhuyi concave
F21: 珠一凹陷北断裂 the fault in the north of Zhuyi concave

圖 2.4-1B 區域 150 公里範圍地震構造圖

Table of Contents (Chinese)
Table of Contents (Chinese)
Table of Contents (Chinese)
Table of Contents (Chinese)

F2：吳川—四會斷裂帶

區內斷裂帶自西南的雲浮向東北經四會、廣寧、英德、曲江延伸至韶關。韶關以北，斷裂分為兩支，其中一支往北與江西大餘－興國－南城斷裂連接，一支與贛江斷裂相連。斷裂在雲浮以南，一支經陽春、茂名、電白、吳川，潛伏在雷瓊斷陷下，一支沿陽春、陽西織篢入南海。斷裂斜貫廣東的中、西、北部，廣東省內全長超過 500 公里，區域內長度 180 公里。

斷裂帶在衛星影像上顯示為線狀的色調變化介面。在地球物理場上是不同重力、磁場和莫霍面的分界線，布格重力場梯度帶在斷裂兩側表現為東高西低，斷裂東側為上地幔局部隆起區。航磁沿斷裂表現出一條北東向展布的局部磁場異常帶，磁場異常帶的位置與重力梯度帶相當。斷裂形成於早古生代，經歷多旋回的構造運動，沿斷裂動熱變質十分發育，形成寬數公里至近 20 公里的斷裂擠壓破碎帶和混合岩化帶，並有多期的岩漿活動，包括加里東、華力西、印支和燕山期。新構造期以來，斷裂主要以繼承性斷塊運動為特徵。

廣東省工程防震研究院、中國地震局、中山大學地質系等在粵西北多個專案的區域斷裂活動性鑒定工作中通過斷層結構面特徵、斷層樣品測年等方法推測該斷裂的最新活動時代在晚更新世以前。

沿斷裂帶歷史上於 1445 年在四會發生過 $4\frac{3}{4}$ 級地震，1611 年在電白海域發生過 6 級地震，1749 年在雲浮發生過 5 級地震。

F3：廣州—從化斷裂帶

斷裂走向北北東，北起從化良口，往南西經溫泉、從化、神崗至三元里，隱伏於平洲西等地。斷裂往北可延伸至廣東新豐一帶。區域內全長約 150 公里。

沿斷裂帶廣泛可見矽化岩、矽化岩質角礫岩與糜棱岩化岩石，破碎帶頻寬達數十公尺。斷裂控制不同構造線方向與古地理輪廓，東側為下古生代以來的隆起區，出露大面積元古界變質岩系，構造線為東西向或北東線，以西為晚古生代以來的斷陷，構造線為北北東向。第四紀早期至中期，斷裂西側的廣花平原發生向西南傾斜運動，在神崗西南的七老嶺一帶紅層明顯抬升，在神崗一帶，紅層形成較高的殘山山地。白雲山西麓與越秀山西側一帶斷裂兩側地貌反差強烈，西側為廣花平原，東側為白雲山及越秀山低山丘陵。

廣從斷裂總體上體現斷裂東側一直以繼承性上升為主，西側則相應以下降為主。古近紀時，斷裂對沉積紅盆地東界有一定的控制作用，但強度不大。

從斷裂沿線附近的地貌形態分析，在斷裂中段（廣州象崗山至從化），地形地貌反差比較明顯，東南盤為低山丘陵區，西北盤為河谷平原區，地勢平坦。主幹構造沿山前外側展佈，並被埋藏於晚更新世以來形成的沖洪積物之下，這套沉

積物在斷裂兩側厚度變化不大。斷層沿線附近未發現河涌、晚更新世以來形成的沖洪積扇、階地被錯移、扭曲等斷層新活動跡象。目標區內沿斷裂帶地表未見斷層三角面、V 字形溝谷、陡坎等新構造現象。覆蓋於斷層之上的殘積物主要形成於中更新世晚期—全新世，未見該殘積層受到擾動的跡象。南段潛伏於第四系之下，而斷裂沿線兩側第四系厚度差異不大。野外地震地質調查結果反映，廣從斷裂在晚第四紀以來處於相對穩定的狀態。

淺層地震探測結果反映，廣州—從化斷裂是一條走向北東—南西、傾向北西的正斷層，淺部可能由多條小斷層組成，這些小斷層在深部可能歸併到一條主斷層上。該斷裂向上錯斷到 T_1 地層介面，相當於第四系覆蓋層的底界。

根據廣州市活斷層探測石湖聯合排鑽對廣從斷裂的探測結果，反映古近紀時斷裂西盤下降率微弱。新近紀至晚更新世前，探測剖面及其周圍以侵蝕剝蝕為主，缺失相關沉積物。晚更新世至全新世時期，石湖一帶的斷裂為晚更新世至全新世沖積相沉積層所覆蓋，但沒有被斷裂錯動過的跡象。斷層樣品電子自旋共振（ESR）測年結果顯示，推斷斷裂在中更新世中晚期活動。

沿廣從斷裂歷史上曾發生過 2 次 $4\frac{3}{4}$ 級和多次 3 - $4\frac{1}{2}$ 級歷史地震。

F4：恩平—開平斷裂帶

南西自陽江的海陵島往北東經恩平、開平至高明一帶被北西向的西江斷裂所截，由鶴城—金雞斷裂和蒼城—海陵斷裂組成。總體走向為北東 30°左右，區域內長度 130 公里。蒼城—海陵斷裂傾向以北西為主，傾角 35° - 60°，鶴城—金雞斷裂傾向南東，傾角 50° - 70°。

兩斷裂形成對沖組合，共同控制著開（平）—恩（平）中新生代斷陷盆地的發育。斷裂帶切割了寒武系至第三系，在恩平沙湖煤礦附近，還可見到二疊系含煤地層向南東逆沖於下古近紀紅層之上，沿帶矽化、片理化、構造岩、角礫岩、糜棱岩、壓碎花崗岩和糜棱岩化花崗岩發育，寬可達 30 - 50 公尺。斷裂物質採樣進行熱釋光鑒定結果為距今 17 萬年與 35 萬年左右，即相當於中更新世中晚期。

斷裂帶控制了水系、谷地的發育，形成斷層崖和跌水。如那龍河（北貫江）、錦江、鎮海水（蒼城江）和北貫谷地、潭江谷地都是沿此斷裂帶發育。

1656 年 3 月在本斷裂帶通的鶴山發生過 $4\frac{3}{4}$ 級地震，1969 年 7 月 26 日在陽江洋邊海發生了 6.4 級地震，在這一地區，於 1986 年 1 月 28 日和 1987 年 2 月 25 日先後又發生 4.8 級和 4.6 級地震，1989 年在斷裂帶中段的恩平大槐發生過 4.0 級地震。

F5：邵武－河源斷裂帶

北起福建邵武、往南南西經江西會昌、尋烏、進入本區域，區內長度 200 公里。研究區屬於邵武－河源斷裂帶的西南段，斷裂規模大，連續性好，走向北東。在河源地區，斷裂在平面上成“S”型，傾向南東，傾角較為平緩，常在 30° - 50° 間，局部達 62°。斷裂破碎頻寬數十公尺，可分上、下構造岩，下構造岩以矽質及壓碎矽質岩為主，上構造岩以角礫岩為主，沿斷裂帶常可見斷層崖和斷層三角面。與斷裂伴生的主要北東向斷裂還有人字石斷裂、坳頭斷裂等，人字石斷裂發育在河源斷裂下盤上，距河源斷裂 3 - 8 公里，長數十公里，傾向南東，傾角 70° - 80°，發育寬約 20 - 30 公尺的矽質構造岩與矽質壓碎岩帶。

斷裂控制多個串珠狀白堊－第三系斷陷盆地的形成，包括塔下、永和圩－成塘徑、龍川、藍口、河源和楊村多個盆地等。斷陷盆地在晚白堊世時常為地塹式，晚白堊世斷陷盆地沉積完成後，其上疊的第三系盆地的沉積中心遷移至西側斷裂附近。楊村盆地在上第三系沉積前，盆地的中間地帶形成近 NNE 向長約 26 公里的裂隙式玄武岩溢流帶，形成走向北東，傾向北西，傾角 10°的玄武岩被，這是一種典型的受深部斷裂構造控制的裂隙式噴溢作用。

該斷裂河源段西側上升構成侵蝕地形。沿斷裂有斷層三角面、斷層崖、滑坡、跌水、溫泉出現，有沖穿谷、峽谷和洪積—沖積扇。對河源新豐江水庫進行了多次三角和水準複測。從 1964 - 1972 年 8 月三角測量資料顯示，河源斷裂左旋運動 8.7 毫米；1964 - 1983 年共 18 次三角測量，河源斷裂左旋錯動 21 毫米。1987 年 9 月 15 日河源 4.5 級地震前後，該斷裂左旋錯動 20 毫米。沿斷裂進行多次跨斷裂氣汞測量均顯示異常。自 1959 年河源新豐江水庫大壩建成蓄水後，不斷有地震發生。自 1962 年 3 月 19 日發生 6.1 級主震以來，餘震不斷，到 1964 年連續發生 5 次 4.8 - 5.0 級地震。近期自 1972 年以來至現在連續發生 4 級以上地震。自 1959 年至今 1 級以上地震已達上萬次之多。1962 年河源 6.1 級地震出現了寬 45 厘米的裂隙，沿北東向延長幾十公尺。

聯合剖面電法反映，該斷裂西南延伸段在石龍以東、博羅石灣、園洲一帶有多個交點，在石龍以西也有多個交點通過。同時，斷裂西南段是地下鹹、淡水分界線。在東莞樟村東江南岸，斷層樣品熱釋光測年為距今 27.69±2.08 萬年和 23.05±1.82 萬年、21.15±1.69 萬年，相對年代為中更新世。

根據以上特徵判定區域範圍內該斷裂河源段最新活動時代為晚更新世。其餘段落最新活動時代為第四紀早、中期。

F6：紫金－博羅斷裂帶

東北起自轉水圩，往西南經長布圩、紫金、博羅、龍溪至獅子洋左岸的虎門一帶，總體走向 60°，傾向南東、傾角 40° - 60°。區內全長約 180 公里。

斷裂北段對燕山期花崗岩有明顯的控制作用，並切割震旦系、寒武系、奧陶系、泥盆系、上三疊統、燕山期花崗岩、白堊系及第三系等地層，沿帶常可見斷崖、瀑布、斷層溝谷。斷裂構造岩發育，有明顯的糜棱岩化、角礫岩化、矽化與片理化帶。在湯泉一帶，可見寬達 10 - 20 公尺的矽質構造岩。據在湯泉附近採集的斷層物質的熱釋光年齡測試結果表明，斷裂在距今約 29.04±2.41 萬年曾有過活動，其相對年代為中更新世中晚期。

斷裂西南段自連平圩向西南經三馬、虎門至珠江口左岸的蛇頭灣。該段斷裂破碎帶規模不如東北段，常在 10 公尺內，在斷裂帶內可見褐鐵礦化，斷裂的活動主要表現為層間滑動。據蛇頭灣採集的斷層熱釋光樣品測年結果為距今 14.12±1.16 萬年，斷裂最新一次活動時代為中更新世晚期。

沿紫金－博羅斷裂帶歷史上未發生過破壞性地震，反映出斷裂帶現今的地震活動強度不大，自 1970 年以來，斷裂的小震活動頻度較低。

F7：五華—深圳斷裂帶

該斷裂帶展佈在蓮花山脈西側，自梅縣向南西經五華，惠東，淡水，至深圳後繼續向香港地區延伸，總長度數百公里，區域內長度約 250 公里。

五華—深圳斷裂帶生成於晚侏羅世之前，也是燕山運動以來長期發育，多期活動的斷裂帶。它控制了中、新生代安流—五華盆地、水口盆地、多祝盆地和淡水盆地，並切割了其古近紀地層。大致以多祝白堊系紅層盆地為界，斷裂東北段走向北東 30° - 50°，傾向北西，傾角 25° - 40°；斷裂南西段走向北東 50° - 70°，傾向北西，傾角 50° - 80°。該段斷裂早期呈壓扭特徵，後期具張扭性質，為走滑正斷層。

五華—深圳斷裂帶在惠陽淡水以東的主幹構造是多祝—淡水斷裂，西南段自惠陽的淡水向西逐漸撒開，到深圳地區後主要由西北的九尾嶺斷裂、中間的橫崗－羅湖斷裂和蓮塘斷裂以及西南的鹽田斷裂等組成。

第四紀以來，斷裂帶不同地段仍有活動，遂形成坪山、橫崗、深圳河谷和元朗與屯門等一系列第四紀槽地。在惠東的新庵、符圳圍等處沿斷裂有溫泉湧出，水溫 46° - 48°C。

F8：五桂山斷裂帶

斷裂帶分為南北兩支，北支稱五桂山北麓斷裂，長約 60 公里，南支稱五桂山南麓或翠亨—田頭斷裂，長約 90 公里。

北支斷裂自中山一帶往北東東向延伸，推測可至橫門一帶，屬推測隱伏斷裂，根據物探和鑽孔資料，該斷裂由多條平行斷裂組成，地貌上大體屬北部平原和南

側山地的分界線。衛星影像上呈三條互相平行的斷裂組合。穿過中心市區的斷裂影像上呈線性色調異常，隱伏於第四紀沉積之下。斷裂往南西西，跨過西江於黃布三村東北一帶發現其形跡，在該處可見走向北東 40°，傾向北西，傾角 65°，寬約 4 公尺的擠壓破碎帶，但其上為膠結較好可能屬 Q_3 以前的洪積—坡積層所覆蓋，後者完整無破壞，由此證明斷裂自晚更新世以來未有明顯活動的跡象。在小隱採集的斷層樣品電子自旋共振（ESR）測年結果為 32.2±5.0 萬年，相當於中更新世。

南支斷裂東北起自珠江口西側，往南西經翠亨、崖門、田頭而延入廣海灣。正斷層性質。斷裂在地貌上反映較明顯，北西盤五桂山山體高度一般為 300 - 400 公尺，而南東盤為谷地和平原。在五桂山南麓可見到斷層三角面，陡崖和瀑布。斷裂帶附近的花崗岩受強烈擠壓，有大量石英脈穿插，可見碎裂花崗岩、糜棱岩化花崗岩、強矽化壓碎岩等，採集的斷層樣品電子自旋共振（ESR）測年結果為 68.2±6.5 萬年。

F9：豐順—海豐斷裂帶

斷裂走向北東 30° - 60°，傾向南東，傾角 40° - 80°。自惠東平海起經海豐、陸河、揭西、豐順、豐良、大埔茶陽，至福建政和，區域內長度 160 公里。斷裂的東北段可見斷裂矽化構造頻寬 30 公尺，斷裂帶中岩石片理化和扁豆體發育，斷面呈波狀起伏。在豐順一帶，該斷裂構造帶由高排斷層、柚樹下斷層、茜坑斷層組成。每條斷層寬約 300 - 500 公尺，斷裂帶岩石強烈擠壓破碎，並見糜棱岩化，片理化和矽化現象十分發育。沿斷裂帶動力變質作用強烈，形成寬數十公尺至千餘公尺的構造岩動力變質帶，發育有糜棱岩、糜棱岩化花崗岩、壓碎花崗岩、斷層角礫岩和強烈的片理化現象。

斷裂中段在海豐—平海一帶斷層物質熱釋光測年結果為：在田心山為距今 14.69±1.20 萬年，鮨門新徑村為 51.70±3.60 萬年，南泉嶺為 51.01±6.14 萬年，雷鋒田為 17.60±1.44 萬年，相當於中更新世。歷史上 1693 年海豐 $4\frac{3}{4}$ 級地震發生在該斷裂段上，近年來小震活動頻繁。但據中國地震局地質研究所和廣東省工程防震研究院於 2007 年對海豐核電候選廠址近場區斷裂活動性的調查認為，該斷裂帶在海豐—平海的多條斷裂兩側地貌形態無明顯差異，斷裂兩側 T_1、T_2 堆積階地無錯斷現象，破碎帶無新滑動面發育，斷裂帶主要活動於侏羅紀，白堊紀以來活動強度明顯減弱，覆蓋土層無明顯的錯動跡象，該地段各斷裂無第四紀以來活動的跡象。

F10：潮州—汕尾斷裂帶

北東自饒平的三饒向西經潮州、揭陽、普寧、陸豐博美至汕尾後入海，區內長度約 170 公里。該斷裂總體走向為 30° - 50°，傾向南東（局部傾向北西），傾角 50° - 80°。斷裂形成於侏羅紀晚期燕山運動第三幕，切割了燕山晚期（晚侏羅世-晚白堊世）花崗岩和下侏羅統砂岩、上侏羅統火山岩。常見糜棱化花崗岩、壓碎花崗岩、角礫岩等，構造岩發生矽化、片理化、褐鐵礦化、葉臘石化和綠泥石化，局部還可見柔褶現象。

根據 2007 年廣東省工程防震研究院與中國地震局地球物理研究所對粵東核電候選廠址近場區斷裂活動性的調查結果，斷裂帶在普寧以西地段沒有新活動的地貌形態出現，河流階地跨越斷裂未見任何變形顯示，斷層沿線無斷層崖、斷層三角面、斷層陡坎，河流在通過斷裂地段未出現同步折拐和瀑布現象；在廣泛發育的中更新統風化殼中，斷裂沒有擾動其本身結構而總是顯示其原有的面貌；斷裂沒有切穿上覆第四紀殘坡積層。但時常會見到規模較大的斷層破碎帶由於其組成物質所具有的抗蝕力與兩盤岩性的較大差異，產生差異風化而出現特徵的線性正地形；斷層的活動表徵如褐鐵礦化、矽化膜、綠泥石蝕變、已固結的斷層角礫岩、斷層帶都沒有出現新的斷面；斷裂在該地段第四紀時期有過活動，在中更世晚期還有斷裂活動的年齡資訊，晚更新世以來沒有活動的跡象。

在區域以外的潮州一帶，沿斷裂北東段可見洪積扇、斷層崖、斷層三角面、瀑布等地貌，斷裂的活動影響到其兩側第四紀沉積物的差異，於斷裂的上升（北西盤）一側的第四系為濱海、沼澤相沉積，其厚度較小，而下降（南東盤）一側則為淺海相沉積，厚度較大。對斷裂北西側的鳳崗階地泥炭土層位及 ^{14}C 年代測定，自晚更新世晚期以來，以 0.8 毫米/年的平均速率上升，而斷裂的南東側據鑽孔中淤泥層位及 ^{14}C 年代測定，全新世以來以 2.7 - 3.8 mm/y 的速率下降。廣東省地震局地殼形變測量資料表明，潮州—揭陽段，近期呈現北東向下降條帶。在地震活動方面，歷史上在潮州、揭陽、普寧和饒平的三饒等地曾先後發生過 $4\frac{3}{4}-6\frac{3}{4}$ 級地震。

據《廣東省粵東地區核電工程初步可行性研究階段地震調查與評價工作報告》，潮州—汕尾斷裂向海域內延伸的段落—紅海灣段位於香港以東海域，成北東向延伸，是從基岩斷至表層的活動斷層（圖 2.4-2），基岩被切割成地塹、地壘，其上第四系部分錯移。該斷裂屬珠江口盆地之北的較複雜的島鏈斷裂帶（向海延伸部分）。根據地震剖面資料，該斷裂為正斷層，傾向 335°，傾角 80°，單道地震解釋剖面顯示其切錯 R_4 、R_2層位，相當於 Q_3地層，因此，應為晚更新世活動斷裂。

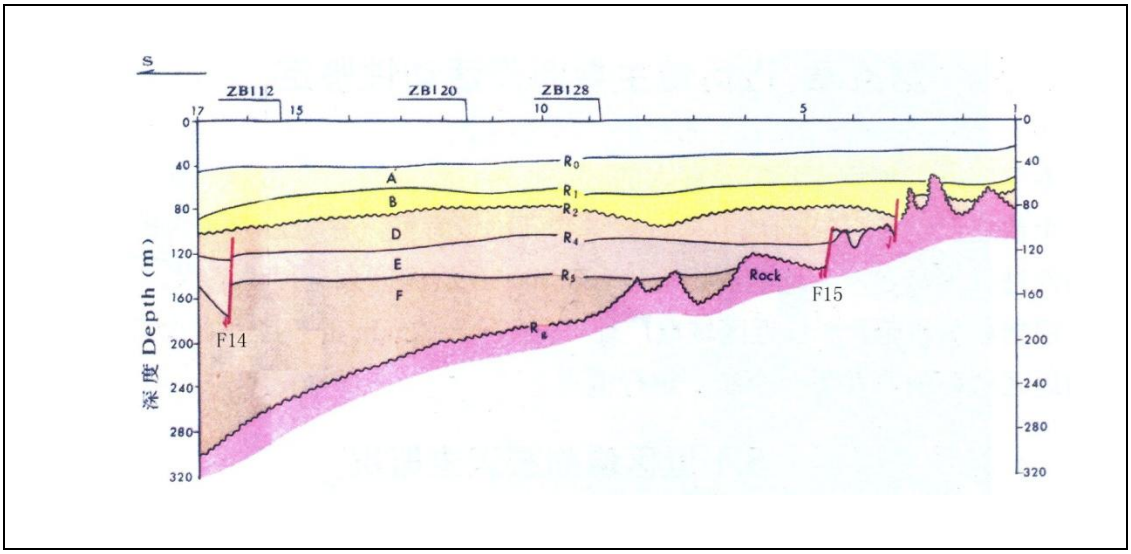

圖 2.4-2 香港幅 ZD—00 測線單道地震解譯解釋剖面

2.4.2 北西向斷裂

北西向斷裂主要分佈於沿海地區，這些斷裂規模較小，延伸一般在 100 公里以內。斷裂形成較晚，主要形成於燕山晚期和喜山期，幾乎切截了所有北東向和東西向斷裂，控制沿海水系的發育、沿海港灣的形成和發展。斷裂由西而東有：西江斷裂帶、淇澳—桂山島東側斷裂、白坭—沙灣斷裂、珠江口斷裂帶、東莞—深圳斷裂帶、隆江斷裂等。

F11：西江斷裂帶

北起於四會，往南東經肇慶蓮壙、三水河口、高要牛岷山，沿西江繼續向南東經馬口崗、龍池、潭窖山、了哥山、遠安，於磨刀門入南海。全長約 130 公里。它大體上由東西兩支平行的主幹斷裂組成，總體走向為 320º 左右。東支主幹斷裂從磨刀門往北經江門外海延至南海九江附近，走向為 330º，傾向南西或北東，傾角 60 º - 80º。西支主幹斷裂從泥灣門水道往北經江門、鶴山路延至四會。多座橫跨西江的橋樑專案在西江河道的工程地質鑽探揭露了斷裂的存在。

斷裂控制珠江三角洲斷陷盆地西緣邊界，東側為珠江三角洲盆地沉陷區，第四系最厚達 64 公尺，西側為隆起區，在鶴山沙坪一帶普遍可見由燕山期花崗岩組成的 25 - 40 公尺和 60 - 80 公尺兩級臺地。沿斷裂在青岐、白坭、太平、九江、大鼇、燈籠沙等地形成多個軸向北西的第四系沉積凹陷中心，第四系等厚線亦呈北西向長條狀分佈。根據在高要金利，南海九江，新會棠下、荷壙、睦洲，中山橫欄，斗門大赤坎，燈籠沙等 11 個鑽孔共 16 個炭化木、蠔殼、文蛤、鱷魚骨、

腐木、泥炭土、淤泥樣品的 ^{14}C 年代測定和層位高程計算，在晚更新世中期以來，斷塊運動的沉降速率平均為 1.84 mm/y，而且顯示出由北往南沉降速率逐漸增大的趨勢，北段（高要金利）沉降速率為 0.51 mm/y，中段（南海九江至新會睦洲一帶）沉降速率平均為 0.86 mm/y，南段（斗門大赤坎至燈籠沙一帶）沉降速率平均為 4.85 mm/y。

據 1989 年廣東省地震科技諮詢服務中心的“磨刀門大橋工程場地地震安全性評價報告”，從航衛片解譯到地貌、新構造特徵分析推斷該斷裂存在，在工程場地地面地質調查中也得到了西江斷裂南段存在的依據，根據物探和鑽探結果推測，斷裂東支是由 3 - 4 條斷層組成的傾向南西的斷階帶（圖 2.4-3），錯斷最新地層為 Q_3^3—Q_4^1 地層（^{14}C 年齡為 7580±520 - 20300±1300 年），西支斷裂（泥灣門斷裂）由 1-2 條斷裂組成，傾向北東，錯斷地層亦為 Q_3^3—Q_4^1 ， ZK13 號孔斷層帶物質熱釋光測年結果為距今 2.34±0.15 萬年，上述結果表明，西江斷裂最後一次活動發生在晚更新世至全新世初期。根據三角組（Q_3^3—Q_4^1）地層錯移的距離來估算斷層的活動速率，ZK8 孔和 ZK2 孔之間，由於受西江斷裂主幹的錯動，三角組錯移了 17.69 公尺，位移速率達 0.804 mm/y(176,900 毫米÷22,000 年）。從全新世中期以後，地層幾乎沒有受到什麼影響，特別是距今 2500 年以來的全新世晚期沉積—燈籠沙組（Q_4^3）在西江磨刀門一帶是相當穩定的。

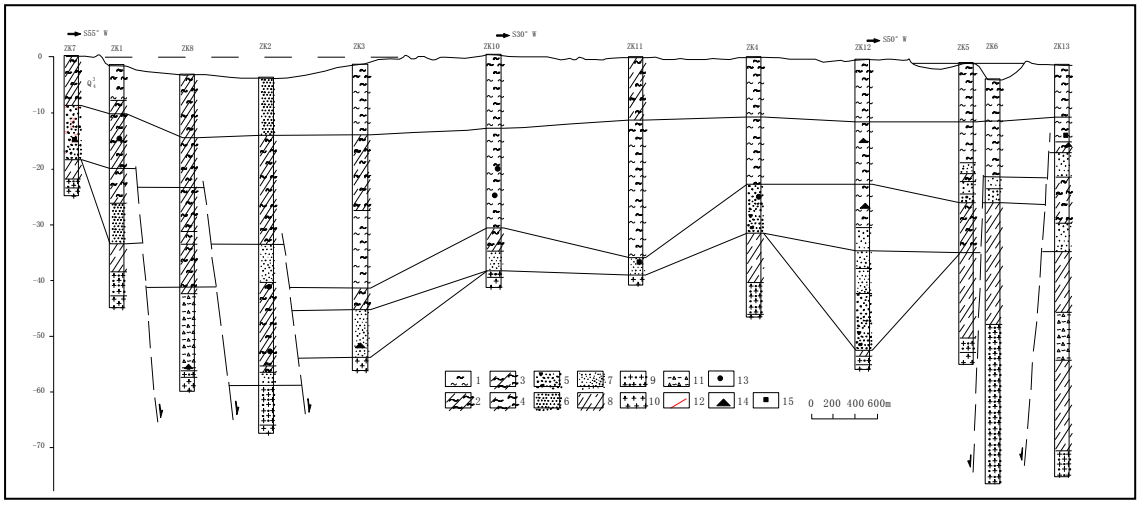

圖 2.4-3 磨刀門大橋主軸線西江斷裂剖面（據廣東省地震局）

1. 淤泥 2. 淤泥質粘土 3. 淤泥質亞粘土 4. 淤泥質輕亞粘土 5. 含礫粗砂 6. 中粗砂 7. 細砂 8. 殘積亞粘土 9. 風化花崗岩 10. 花崗岩 11. 構造破碎帶 12. 斷層 13. ^{14}C 採樣點 14. TL 採樣點 15. 電鏡掃描採樣點

由於上述鑽孔剖面中 13 個孔的三角組（Q_3^3—Q_4^1）地層厚度較穩定，13 個孔的間距為 200 - 400 公尺，按孔間該層底部高差 20 公尺計算，其坡降不到 6°，西江磨刀門一帶可能在 Q_4 以前就已經形成這種水下坡度，斷層未必切割到三角組；另外，鑽孔間距過大，沒有直接揭露到三角組被切割，僅為推測；再者，地面調查沒發現附近有 Q_4 地層被西江斷裂切割的現象。因此，本報告認為將西江斷裂南段歸為晚更新世斷裂更為合適，而“磨刀門大橋工程場地地震安全性評價報告”最終結論同樣認為西江斷裂的磨刀門段最後活動年代在 10,000 年以前，活動速率在 0.36 mm/y - 1.43 mm/y 之間，活動方式以蠕滑為主，兼少量粘滑。而斷裂北段（肇慶）和中段（六鄉）則為中更新世活動段。

在斷裂的南、北兩端磨刀門和四會分別發生過 5 和 $4\frac{3}{4}$ 級地震。

F12：淇澳—桂山島東側斷裂

斷裂展佈於淇澳島及其以南至桂山島以東水域中，總體走向北西 320°。區域內長 60 公里。

斷裂可分成北西和南東兩段，北西段稱淇澳斷裂，而南東段稱桂山島東斷裂。在淇澳斷裂北西段的淇澳島，斷裂所通過處在地貌上形成一北西向狹長形深風化谷地，兩側為海拔 100 - 150 公尺的丘陵。谷地西南側，可見斷裂的次級構造，形成寬達 2.5 公尺的壓碎花崗岩與擠壓帶。斷裂所通過的谷地第四系上更新統中段的厚度無明顯的變化，表明斷裂在晚更新世中期以來已無明顯的活動。據珠江水利委員會在珠海伶仃洋大橋橋址的淺層人工地震資料，在斷裂部位出現基岩凹槽（圖 2.4-4）凹溝相對深達 30 公尺。覆蓋在凹槽、凹溝上的第四系沉積物未見擾動，判斷為中更新世活動斷裂。斷裂南段據港珠澳大橋淺層地震揭示，最新斷錯晚更新世中期砂礫層底部，其 js 中斷點基岩頂面垂直斷距為 5 - 8 公尺，上中斷點埋深為 108 公尺；d1 中斷點基岩頂面垂直斷距為 3 - 4 公尺，上中斷點埋深 81 公尺；此外，斷裂東側 ZK3 孔岩芯破碎，碎裂結構，也證實了斷裂的存在。

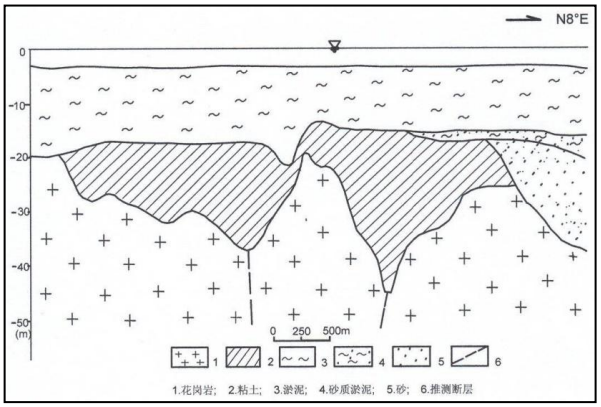

圖 2.4-4 珠海伶仃洋大橋Ⅴ-Ⅴ' 地震地質剖面（據珠委）

南支桂山島東斷裂，據港珠澳大橋淺層地震探測，在橋位段 ar 中斷點，最新斷錯晚更新世中期砂礫石層底部，垂直斷距為 3 - 4 公尺，上中斷點埋深 74 公尺。沿斷裂有第四紀基性岩溢出（圖 2.4-5）。再南的擔尾水道斷裂段，最新斷錯中更新統上部，並控制晚更新世以來沉積，再向南順斷裂方向為一條沼氣帶。表明該斷裂活動分段明顯，港珠澳大橋橋位段為晚更新世中期。

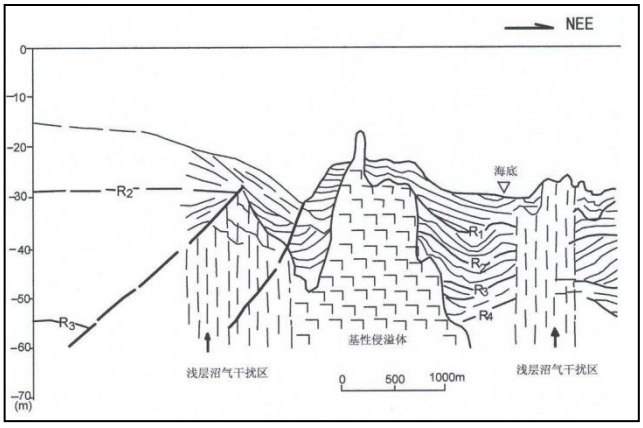

圖 2.4-5　牛頭島東淺層人工地震地質解釋剖面

F13：白坭－沙灣斷裂

該斷裂北起花都與清遠交界的國泰，經花都白坭、南海的官窯、松崗、大瀝、平洲、陳村至番禺沙灣、大崗沿蕉門進入伶仃洋，往南與香港大嶼山大澳－大浪灣斷裂相接，再向南進入南海。總體走向為北西 320° - 330°。區域內長約 150 公里。

斷裂西北段控制了三水盆地的發育，它是控制盆地東側的邊界斷裂。以廣州—三水斷裂為界，斷裂西北段大部分被第四系覆蓋，僅局部地段斷裂在地表顯露。官窯、聯表煤礦見北西向斷裂同時錯斷了北北東和近東西向斷裂。

斷裂中段在沙灣以北的大烏崗附近出露寬約 10 公尺的矽化帶。在馬腰山，斷層結構面上及其左右兩側為第四系殘坡積層所覆蓋，岩性主要為砂質粘土，粘土層內可見碎石條帶。碎石條帶連續性較好，未見明顯的錯動，表明斷裂沒有明顯的活動性。

斷裂自沙灣往東南，基本隱伏在第四系下，在沙灣至魚窩頭一帶大於 25 公尺及 40 公尺的第四系等厚線皆呈北西走向。據平洲廈教、番禺靈山、萬頃沙等鑽孔樣品 ^{14}C 年代測定，晚更新世中期以來，由斷裂控制的斷塊下降速率平均為 2.19 mm/y。據陳國能等“珠江三角洲斷裂構造最新活動性研究”，靈山大崗後山斷裂旁側發育北西向方解石脈，熱釋光測年結果為 5.09 - 7.13 萬年，相當於晚

更新世。

斷裂東南段據珠委在伶仃洋大橋淇澳島與內伶仃島之間的淺層人工地震資料顯示為基岩風化深槽，深槽比兩側相對深達 20 - 30 公尺。廣州地質勘察基礎公司經物探和鑽探後進一步證實此深槽為一古河道，堆積了較厚的河床相砂礫石層（圖 2.4-6），通過鑽探手段，於覆蓋層之下揭示出糜棱岩化花崗岩。而斷裂被覆蓋的最大 TL 年齡為 23530±1600 年的晚更新世晚期堆積物未受擾動。

在地震活動性方面，自 1970 年以來，沿白坭—沙灣斷裂帶曾發生過多次 2.0 - 3.9 級地震，地震較為集中發生在斷裂帶的東南段。

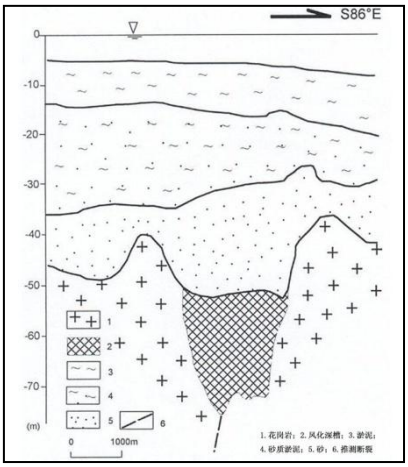

圖 2.4-6 珠海伶仃洋大橋Ⅱ-Ⅱ' 地震地質剖面（據珠委）

F14：珠江口斷裂帶

分佈在珠江口及獅子洋水道，其兩側均為北北西向斷裂所控制。它北起廣州黃埔地區，往南東經文沖船廠大塢東側潛入珠江，經獅子洋，出虎門而入內伶仃洋，抵香港大嶼山後入南海。全長 130 公里。總體走向 NW310° - 330°，傾向北東或南西，傾角 50° - 85°。主要由化龍—南沙斷裂、文沖斷裂、沙角斷裂、磡石水道東側斷裂、虎門—東博寮海峽斷裂、東涌—長沙海灘斷裂等規模較大的斷裂組成。它控制了珠江水道和磡石水道，形成一條北西向的第四系厚度陡變帶和水下地形陡變帶。衛星影像顯示為清晰粗大、平直的線性構造。

斷裂帶北段由化龍—南沙斷裂和文沖斷裂所組成，斷層物質主要為構造角礫岩、斷層碎粉岩、矽化碎裂岩和碎裂花崗岩，根據《廣州市活斷層探測與地震危險性評價初查與目標區主要活斷層鑒定》的成果，通過排鑽探測、淺層地震探測與斷層兩側地貌形態判斷，化龍—南沙斷裂晚第四紀以來斷層無活動跡象。文沖斷裂及附近覆蓋的全新統、上更新統沒有明顯的缺失現象，在構造岩中採集的斷

層樣品電子自旋共振（ESR）測年結果為：15.0±2.1 - 23.6±2.3 萬年，相當於中更新世中晚期。

斷裂中段由沙角斷裂和礬石水道東側斷裂組成，其中沙角斷裂在北面村一帶寬約 10 公尺，主幹斷裂的新活動使其上的上更新統階地形成多個 3 - 6 厘米寬的破裂面，兩側砂礫層受到明顯擾動。在階地後緣，上更新統與侏羅系為斷層接觸，斷層產狀 320°，傾向北東，傾角 60°，寬 10 厘米，上更新統頂部層位超覆於下盤侏羅系上，仍可見斷裂切割頂部上更新統地層的跡象。斷層物質的熱釋光測年結果為 5.88±0.48 萬年，相當於晚更新世。而礬石水道東側斷裂形成一條北西向的第四系厚度陡變帶和水下地形陡變帶，通過物探、斷裂對新地層切割情況、斷裂在水下顯示的深切溝槽等情況，據“珠海伶仃洋大橋工程場地地震安全性評價報告”，廣州海洋地質調查局淺層人工地震測量揭示到該斷裂切斷了水下 10 公尺的 R_1 下部層位（圖 2.4-7），判斷該斷裂為晚更新世活動斷裂。

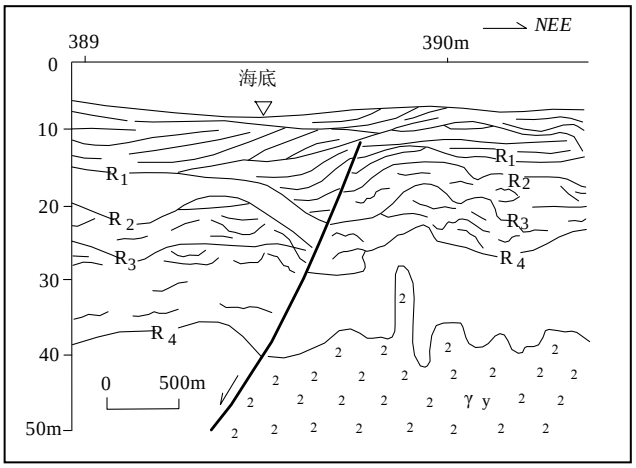

圖 2.4-7 珠江口小鏟島西北淺層人工地震解釋剖面
（據廣州海洋地質調查局）

斷裂南段由流浮山—東博寮海峽斷裂和東涌—長沙海灘斷裂組成。據香港青馬大橋鑽孔資料分析，在香港馬灣島與青衣島之間，斷裂帶附近形成明顯的直線凹槽（圖 2.4-8）全新統海相層厚度在斷層兩盤存在明顯差異，南西盤 5SW16 孔為 1.15 公尺，而北東盤的 5SW6 孔為 7.1 公尺。

斷裂南段控制馬灣－青衣海峽，東博寮海峽的發育。在流浮山附近的深圳灣岸邊可見斷層角礫岩帶。斷裂在香港深井青龍頭一帶樣品熱釋光測年為距今 9.11 ±0.75 萬年，馬灣長咀為 9.39±0.79 萬年，元朗大棠為 10.51±0.87 萬年，青衣西構造岩熱釋光測年為距今 22.6 萬年，表明該斷裂在中更新世—晚更新世有過活動。而東涌—長沙海灘斷裂線性地貌清晰，為溝谷、山垭口和海灣地貌，在伯公坳可

見寬 30 公尺的破碎帶；中國地震局地殼應力研究所在石榴埔北進行的高密度電法探測結果表明，斷層之上覆蓋的晚更新世晚期以來堆積物未受影響。

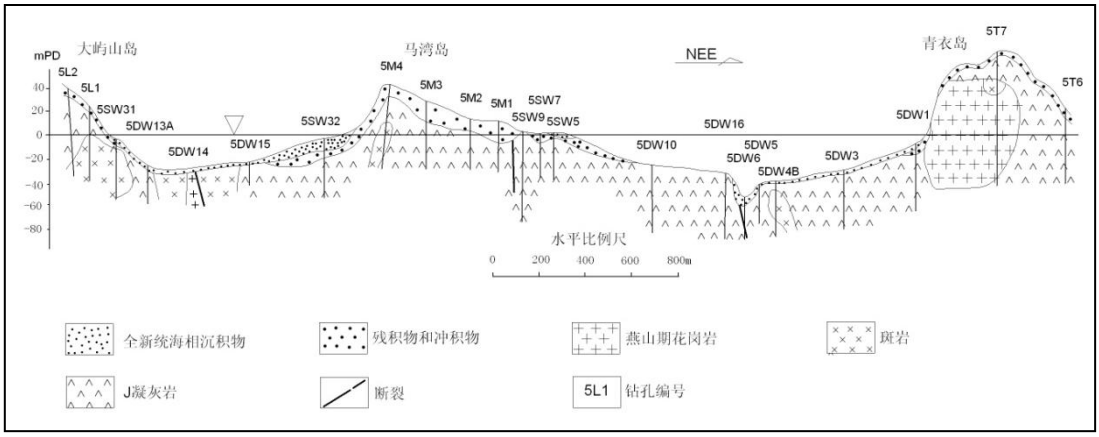

圖 2.4-8 根據鑽孔資料建立的流浮山—東博寮海峽斷裂剖面圖

F15：東莞—深圳斷裂帶

又稱溫塘—觀瀾斷裂，北西起於東莞的石龍溫塘一帶，往南東經馬蹄崗、屏山水口、雁鵝嶺進入龍和、觀瀾到深圳水庫附近，長度達 60 公里。走向西北 330°，傾向北東或南西，傾角 40° - 65°。斷裂橫切了塘夏向斜的南尾部，使下白堊統推覆於花崗岩之上，並產生片理化，花崗岩和下白堊統砂頁岩均被強烈擠壓而片理化、絹雲母化和糜棱岩化。斷裂發育寬數 10 公尺的矽化破碎帶，岩石破碎呈角礫狀，角礫呈棱角狀，成分與圍岩岩性一致，由矽質膠結，沉積岩中見褐鐵礦化，沿破碎帶常見犬牙狀石英脈穿插，石英脈寬約 1 - 2 厘米，與斷裂有一小交角，局部見花崗岩中的綠泥石化。

斷裂切割了北東至北東東向的樟木頭斷裂和大朗—三和斷裂等，使其產生水平錯移。在馬蹄崗公路收費站附近，本斷裂在地貌上形成一列走向北西的小丘，且可見 30 - 40 公尺的矽化破碎帶，帶內北西向的滑動面發育。

F16：隆江斷裂

斷裂帶沿惠來縣的峽嶺、隆江一帶發育，走向 310º，傾向北東，傾角 65º 左右，斷裂帶北西段切割了燕山晚期二長花崗岩、下侏羅統砂頁岩和上侏羅統火山岩等，沿斷裂帶可見碎裂花崗岩、斷裂破碎帶中發育的石英脈等。斷裂切割了北東向的潮安—普寧斷裂和汕頭—惠來斷裂帶。斷裂南東段被第四紀所覆蓋，其下為埋深 17.77 - 32.33 公尺的花崗岩與古紅壤型的風化殼。斷裂帶產生於燕山晚期，其與練江斷裂帶共同控制了大南山斷塊的隆起，沿斷裂帶未發生過破壞性地震。

廣東省地震局科技人員在廣東省粵東地區核電工程初可研階段地震調查工

作中對隆江斷裂的研究表明，由九福坑到北洋，斷裂控制了山形的走向，並出現一筆直延伸之谷地。中斷點人工露頭揭示的上覆殘坡積含岩石碎塊的鬆散層（厚度小於 1 公尺）並未被斷裂中的後期斷面所切穿。宏觀上，斷裂構成隆江第四紀盆地的西側邊界，同時控制了曲溪一帶局部山形的走向。斷層的後期斷面上附著的斷層物質未固結。斷裂在晚更新世以前有過活動，但未見形成斷坎和使階地變形等微地貌特徵。斷層物質的測年資訊反映出中更新世有活動。

F20：珠一坳陷中部斷裂

由珠一坳陷西部向珠二坳陷東部呈斷續延伸，走向北西西，傾向北東，屬正斷層。工作區內長度 80 公里。根據淺層人工地震資料，該斷裂最新斷至第四紀底部，為早更新世活動斷裂。

2.4.3 東西向斷裂

東西向斷裂構造分別橫貫本區北部、中部和南部地區，這些斷裂在地表斷續出露，延伸 200 - 600 公里。物探測深資料顯示，斷裂向深部延伸常達 30 公里以上，是本區深部構造的主要骨架。斷裂由北而南有：佛岡－豐良構造帶、高要—惠來斷裂帶。

F17：高要－惠來斷裂帶

這是由一系列斷續分佈的近東西向斷裂所組成的，自高要起，往東經廣利、三水到廣州北郊瘦狗嶺一帶繼續往東經仙塘、福田、長寧、湖鎮達惠來。斷裂走向近東西向，傾向南，傾角 50° - 80°。沿斷裂帶構造地貌反差明顯，如斷裂北側有羅浮山強烈隆起區，對應的南側卻是東江相對沉陷帶。沿斷裂帶出露強烈的矽化岩帶、角礫岩帶和糜棱岩帶，寬達數公尺至百餘公尺，且對白堊紀、第三紀和第四紀有明顯的控制作用，如廣州北郊出露的破碎頻寬 10 - 40 公尺，切割了古近紀紅層，紅層受擠壓後出現褶皺和片理化帶等。

瘦狗嶺斷裂和廣三斷裂是高要－惠來斷裂帶重要組成部分。據野外地震地質調查，瘦狗嶺斷裂沿線晚更新世以來沉積的沖洪積物小於 10 公尺，並將斷裂埋藏在下，未發現斷層對該沉積層產生錯斷和擾動。根據 ESR 的測年結果，斷面上方覆蓋層底部的含矽化岩碎快的殘積風化土主要形成於中更新世晚期，該層物質未受到切穿或錯動，反映斷層在晚第四紀以來是穩定的。斷裂沿線水系在斷裂附近表現寬闊平緩的“U”型寬谷，晚更新世以來沉積的沖洪積物小於 10 公尺，並將斷裂埋藏在下，未發現斷層對該沉積層產生錯斷和擾動。廣三斷裂在新滘南

路的破碎帶寬度達 50 餘公尺，糜稜岩和糜稜岩化角礫岩十分明顯，斷層帶上覆蓋的沖海積層未受到擾動，層位穩定，岩性無突變現象，斷裂熱釋光測齡結果為距今 15.65±1.09 - 20.25±1.48 萬年。可以判斷，廣三斷裂在晚更新世晚期以來無明顯活動。

F18：佛岡－豐良斷裂構造帶

兩構造帶相鄰，跨越北緯 23°30' - 24°10'之間，位於佛岡、清遠、河源、五華及豐良一帶，兩構造帶延綿 300 餘公里，主要由佛岡—豐良和清遠－安流兩條東西向平行延伸的潛伏基底斷裂組成。走向近東西向，傾向南，傾角 45°，

佛岡－豐良構造帶，顯示為一條明顯的重磁異常帶，其兩側區域背景場不一致，沿帶有成串的小岩體分佈，在佛岡高埔地區構造形跡較為清楚，發育數條近東西向斷裂。清遠－安流構造帶也是東西向重磁異常帶的一部分，對構造帶南側的北東向斷裂有強烈的阻隔作用，在北側的燕山第三期花崗岩岩體內，廣泛發育同方向的燕山四期花崗岩岩體。龍山圩西糧頭埔南側的北東走向地層在靠近構造帶處，走向急轉為東西走向，岩層傾角急劇變陡，並形成數十公尺寬的劈理化帶。

構造帶形成於加里東期，燕山運動曾發生大規模的多期次酸性岩漿噴溢和侵入。構造帶至近期仍有活動，沿帶熱泉密集。清遠－安流構造帶地震活動水準較高，河源的新豐江地區近 40 年來小震頻繁，且發生過中強地震。佛岡－豐良構造帶歷史上及近期儀器記錄的小震相對較少。

2.4.4 北東東向斷裂

F19：濱海斷裂帶

展佈於東南沿海的濱海地帶，大都沿海水等深線 30 - 40 公尺呈斷續展佈，向東經南澎列島與福建的牛山島—兄弟嶼斷裂（也稱近海斷裂）相接。在珠江口一帶，總體走向北東 60°，以傾向南東為主。該斷裂在航磁圖上表現為一條劇變的負異常帶，重力圖上表現為布格重力負異常背景上的正異常帶。斷裂衛片線性影像清晰。總長度近千公里，區內長度 320 公里。斷裂主要形成於喜山期，與南海盆地的擴張有密切關係，在橫剖面上表現出向南傾斜並往南逐級下落的階梯狀陡坎。斷裂控制了南側珠江口外盆地的形成和發展，盆地沉積了厚達 7,000 公尺的上第三系至第四系地層，其中第四系厚度就達 280 公尺。這套新地層的等厚線呈北東東向分佈。

本區域分佈的濱海斷裂主要由陸豐海外段、汕尾海外段和擔杆島海外段和高欄島海外段所組成。

陸豐海外段由一系列 NEE 走向的正斷層組成，構成傾向南東的一組斷階，傾角 50-70°。斷距變化較大，由深層向淺層逐漸減小，區內延伸長度約 50 公里。本段因缺地震剖面，故活動時代不明，但根據新構造活動背景相鄰（汕尾海外段）的活動性特徵推斷應為第四紀活動斷裂。

汕尾海外段由走向 NEE、傾向南東的一組斷階組成，斷裂兩端均為 NWW 走向的珠一凹陷中部斷裂所截，長度約 70 公里。在多道地震剖面上（圖 2.4-9），T_2層斷距為 140 公尺，向上至 T_1^3斷距為 30 公尺，顯示在第四紀早中期斷層仍有活動。在單道地震剖面上，斷裂錯斷 R_4介面，表明斷裂在中更新世晚期仍有活動。綜合多道地震剖面、單道地震剖面和本區域其它地震剖面判斷，濱海斷裂汕尾海外段的最新活動時代為中更新世晚期—晚更新世早期。

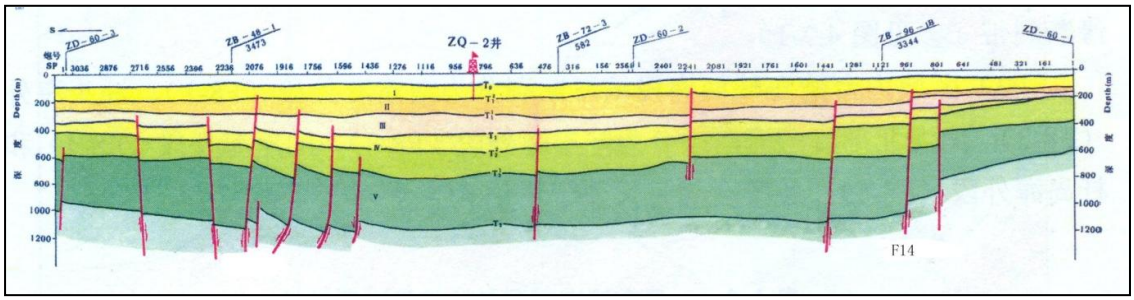

圖 2.4-9 衛灘北幅 ZD—60 測線單道、多道地震解譯解釋剖面
（據廣州海洋地質調查局）

擔杆島海外段總體上由自北向南的三組 NEE—近 EW 走向的一系列平行正斷層組成，斷裂頻寬達 30 - 60 公里。其中每組斷裂又由數條更次一級斷層組成，均為斷面南傾的正斷層。最北邊的一組斷裂分佈在區域內，位於擔杆列島東南外海，距擔杆列島約 15 公里，為單道和多道地震資料同時揭示的一條斷層，呈進東西向弧形展布，傾向南東。單道地震勘探結果顯示該斷層錯斷 R_4、R_3介面，最大斷距 16 公尺，其最新活動時代為晚更新世早期。在多道地震資料上顯示基底大斷裂性質，南盤為下降盤，北盤為上升盤見花崗岩，由深到淺斷距逐漸減小，T_2層斷距達 480 公尺，T_1^2層 15 公尺，是控制珠江口盤地新生代沉積的大斷裂（圖 2.4-10）。無論從區域構造位置或多道地震剖面實測，該斷層是珠江口北緣斷裂的一支。根據以往資料，該斷裂自燕山期形成，在古近紀、新近紀和第四紀以來長期活動，距現今海底最小埋藏深度約 50 公尺。

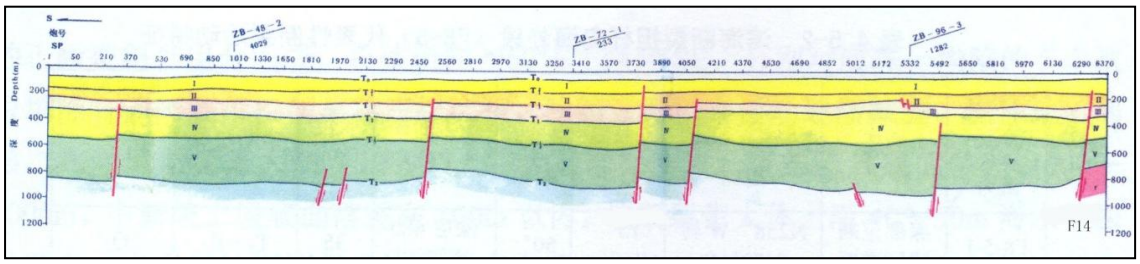

圖 2.4-10 北尖島幅 ZD—00 測線多道地震解譯解釋剖面
（據廣州海洋地質調查局）

上述 20 條區域主要斷裂的結構特徵及活動特徵見表 2.4-1。

表 2.4-1 區域主要斷裂構造活動特徵簡表

編號	斷裂名稱	區內長度（公里）	產狀			斷裂性質	最新活動時代	地震活動（區域內）
			走向	傾向	傾角			
F1	懷集—郴州斷裂帶 Huaiji-Chenzhou fault zone	80	NE20°-25°	NW	50°-60°	正斷		
F2	吳川—四會斷裂帶 Wuchuan-Sihui fault zone	180	NE30°-45°	NW	50°-60°	逆斷	Q_2	$4^3/_4$ 級以上 4 次
F3	廣州—從化斷裂帶 Guangzhou-conghua fault zone	150	NE40°-60°	NW/SE	40°-70°	正斷	Q_2	1372 年、1915 年 $4\frac{3}{4}$ 級
F4	恩平—開平斷裂帶 Enping-Kaiping fault zone	130	NE30°-35°	NW/SE	35°-70°	逆斷	Q_2	$4^3/_4$ 級地震 1 次
F5	邵武—河源斷裂帶 Heyuan-Shaowu fault zone	200	NE45°	SE	35°-70°	正斷	Q_2 , Q_3	$4^3/_4$ 級地震 9 次，最大 6.1 級
F6	紫金—博羅斷裂帶 Zijin-Boluo fault zone	180	NE60°	SE	40°-60°	正斷	Q_2	
F7	五華—深圳斷裂帶 Wuhua-Shenzhen fault zone	250	NE25°-70°	NW	40°-80°	正斷	Q_2	1508 年 5 級
F8	五桂山斷裂帶 Wuguishan mountin fault zone	90	NE40°-80°	NW/SE	50°-75°	正斷	Q_2	
F9	豐順—海豐斷裂帶 Fengshun-Haifeng fault zone	160	NE30°-60°	SE	40°-80°	逆斷	Q_2	$4^3/_4$ 級 2 次，小震群
F10	潮州—汕尾斷裂帶 Chaozhou-Shanwei fault zone	170	NE30°-50°	SE/NW	50°-80°	正斷/逆斷	Q_2 , Q_3	6 級 1 次
F11	西江斷裂帶 Xijiang river fault zone	130	320°-330°	SE/NW	60°-80°	左旋	Q_2,Q_3	1905 年 5 級
F12	淇澳－桂山島東側斷裂 Qiao-Guishan island fault	60	320°	NE/SW	陡	正斷	Q_2,Q_3	
F13	白泥－沙灣斷裂 Baini-Shawan fault	150	320°-330°	SW/NE	＞50°	正斷	Q_2,Q_3,	有小震活動

編號	斷裂名稱	區內長度（公里）	產狀			斷裂性質	最新活動時代	地震活動（區域內）
F14	珠江口斷裂帶 Estuary of pearl river fault zone	130	310°-330°	SW/NE	50°-85°	正斷	Q_2,Q_3,	
F15	東莞—深圳斷裂帶 Dongguan-Shenzhen fault zone	60	330°	SW/NE	40°-65°	正斷/逆斷	Q_2	
F16	隆江斷裂 Longjiang river fault	60	330°	NE	65°	正斷	Q_2	
F17	高要—惠來斷裂帶 Gaoyao-Huilai fault zone	200	EW	S	50°-80°	正斷	Q_2	$4^3/_4$ 級以上 5 次，最大為 5 級
F18	佛岡—豐良斷裂帶 Fogang-Fengliang fault zone	300	EW	S	45°		An Q	$4^3/_4$ 級以上多次，最大 6.1 級
F19	濱海斷裂帶 Binhai fault zone	320	NE60°-75°	SE	50°-70°	正斷	Q_2, Q_3	
F20	珠一坳陷中部斷裂 The middle part of Zhuyi concave fault	80	NWW	NE		正斷	Q_1	

2.5 區域地震構造環境評價

2.5.1 區域地震構造環境

香港屯門—元朗地震影響小區劃區域範圍處於華南加里東褶皺系的粵北、粵東北—粵中拗陷帶內。區內可進一步劃分為粵北拗陷、粵中拗陷及永梅—惠陽拗陷三個Ⅲ級構造單元。區域出露地層包括前寒武系至第四系。除了珠江三角洲盆地，其餘地區大面積分佈花崗侵入岩。第四系沖海積層主要分佈於珠江三角洲河流水網地區。

區域範圍位於華南沿海斷塊差異隆起區內，該區域北東向斷裂極為發育，但受到北西—北北西及近東西向斷裂構造的交切。北東向斷裂是地表出露規模最大，伸展最長的斷裂構造。近東西向構造主要屬基底斷裂構造，對區域重磁異常及地殼厚度的變化上起著明顯的控制作用，新構造時期以來活動強度較低。北北西—北西向斷裂構造，成生晚，切割淺，但往往是新生代斷陷盆地的重要控制構造，是區內重要的地震構造。

新構造運動以來，本區總體上是繼承了斷塊運動特徵，處於隆升狀態，但各地段的上升幅度、速度存在較大的差異，部分地段在第四紀的一定時段處於沉降狀態，接受第四紀的沉積，形成第四紀斷陷盆地。

區域範圍內地球物理場總體特徵表現出異常幅度小、變化平緩的特徵，說明本區深部構造環境的差異性不大，與地表構造活動和地震活動環境相一致，尤其

是區域及其鄰近地區的地球物理場異常變化較小。但一些主要的北東向斷裂帶，如廣州—從化斷裂、五華—深圳斷裂，在航磁異常和布格重力異常上都有較明顯的顯示。重力異常、航磁異常反映，地震常常分佈在北東向異常與北西向及近東西向異常交匯處。區域範圍內的地殼厚度接近大陸的平均值，基本處於重力均衡狀態，屬於較為穩定的地區。在地殼深部構造平面的分帶上，地震主要位於地殼深部構造的南部隆起區，在莫霍面等深線 33.7 - 34.2 公里之間。區內的中強地震震源深度一般為 5 - 33 公里，屬於發生在地殼內的淺震。

研究區內（505 公里）發生 $M \geq 4.7$ 級以上強震 151 次。歷史地震的影響主要來自區內的廣州、澳門、擔杆列島外海域、海豐外海域等地。除受區內的地震影響外，鄰近的南海、臺山、河源等地的地震對區域也造成了一定的影響。

本區現今構造應力場的方位穩定在北西西—南東東向，且以水準方向擠壓為主，在北西西—南東東向水準構造應力場的作用下，區內的北東向斷裂多表現為逆衝兼走滑性質，而北西向斷裂多表現為左旋走滑兼傾滑的活動特性。

北東向斷裂是區內最具規模的斷裂，遍佈全區，延伸長度常在數百公里以上，分別生成於海西期、印支期、燕山期，普遍強烈活動於燕山期，沿斷裂分佈有中新生代斷陷盆地。控制大型山脈、水系的發育和花崗岩的侵入，斷裂的動熱變質現象顯著，沿斷裂有基性岩體和溫泉出露，多屬於切割較深的斷裂帶。

北西向斷裂主要分佈於沿海地區，這些斷裂規模較小，延伸一般在 100 - 200 公里以內。斷裂形成較晚，主要形成於燕山晚期和喜山期，幾乎切截了所有北東向和東西向斷裂，控制沿海水系的發育、沿海港灣的形成和發展。

東西向斷裂構造橫貫本區北部，這些斷裂在地表斷續出露，延伸 200 - 600 公里。物探測深資料顯示，斷裂向深部延伸常達 30 公里以上，是本區深部構造的主要骨架。

區域的主要斷裂構造多為早更新世—中更新世活動斷層，西江斷裂西南段、白坭—沙灣斷裂南段、淇澳—桂山島斷裂南段、珠江口斷裂帶南段的石水道東側斷裂和流浮山—東博寮海峽斷裂、潮州—汕尾斷裂帶紅海灣段等屬於晚更新世活動斷裂，其中潮州—汕尾斷裂帶紅海灣段在 1911 年 5 月 15 日發生過海豐外海域 6 級地震。

2.5.2 區域強震發生的構造條件

根據前述區域新構造、第四紀活動構造、深部地球物理場及其與強震活動關係的分析，結合區域的實際情況，我們將本區的強震分為 $M \geq 7.0$ 級和 M = 6.0 -

6.9 級兩檔，分別討論它們的發生條件。

強震（*M*≥7.0）活動的發震條件共同特點有：

(1) 位於沿海地區新構造以來明顯差異活動地帶；

(2) 斷裂晚更新世以來明顯活動，明顯斷錯晚更新世晚期以來地層的幅度大，且為規模較大的區域性斷裂，長度一般大於50公里；及

(3) 發生過*M*≥7.0級地震的斷裂帶。

強震（*M* = 6.0 - 6.9）活動的發震條件共同特點有：

(1) 斷裂晚更新世以來有活動或控制晚更新世以來發育的地層的分佈；

(2) 沿斷裂有活動的線性地貌顯示，且有斷錯中更新世地層的明確證據；及

(3) 發生過6.0≤*M*≤6.9級地震的斷裂帶。

北東東向斷裂雖然在地表斷斷續續分佈，但重、磁所反映的深部線性構造卻十分清楚，是構成沿海及濱海地區的主要構造骨架，第四紀以來不僅控制了這一帶的第四紀盆地的分佈，也控制著許多*M*≥6級地震的孕育和發生，是主要的控震構造。

活動的北北西—北西向斷裂與活動的北東東—近東西向斷裂交匯處是強震發生地點的重要標誌。因為這些斷裂與區域主壓應力軸呈銳角關係，最易產生剪切滑動。而區內那些斷裂於晚更新世—全新世都有活動，對大震的發生起了決定性的作用，所以屬於晚更新世仍在活動的斷層段，應被視作未來強震的發震構造。

北東東—近東西向重、磁異常梯度帶及其局部扭曲部位，往往也是強震發生的深部構造標誌。

北東向斷裂活動性雖然較弱，但其規模大，當其與其他方向斷裂交匯時，該交匯處往往對地震的孕育有一定的控制作用。

此外，仍存在北東東向活動斷裂規模越大、北西向斷裂的新活動越強烈，則發生高震級的幾率越大；地貌反差越大，新構造運動越強烈，所發生地震的強度也會越大。

2.5.3 區域主要發震構造評價

綜合區域地質構造背景與深部構造特徵、新構造運動與現代構造活動、斷裂的基本特徵、盆地類型和沉積特徵，以及地震活動性、現代構造應力場特徵的分析認為：

區內的北東向斷裂規模最大，延伸數百公里以上，大多生成於印支期，強烈活動於燕山期，沿斷裂分佈有中新生代斷陷盆地。控制大型山脈、水系的發育和花崗岩的侵入，斷裂的動熱變質現象顯著，沿斷裂有基性岩體和溫泉出露，表明它們是切割較深的深、大斷裂，控制兩側地質發展歷史，往往是一、二級大地構造單元的分界線。地震震中分佈表明，強震沿斷裂呈條帶狀分佈，是一組控制強震震中空間分佈的控震構造。

北西向斷裂主要分佈於沿海地區，這些斷裂規模較小，延伸一般在百公里以內，主要形成於燕山晚期和喜山期，幾乎切截了所有北東向和東西向斷裂，大多數控制沿海水系的發育和沿海港灣的形成，斷裂控制了珠江三角洲的形成和發展，以及第四系等厚線和地殼垂直形變等值線的分佈。河源 6.1 級地震的極震區及餘震分佈呈北西向，陽江 6.4 級地震的餘震分佈也呈北西向，南澳 7.3 級地震和瓊山 $7\frac{1}{2}$ 級地震的極震區除呈北東東向展布外，在北西方向上也有明顯顯示，這表明北西向斷裂是中、強地震的主要發震構造。

東西向斷裂分別橫貫本區北部和中部地區，這些斷裂在地表斷續出露，延伸 200 - 600 公里。物探測深資料顯示，向深部延伸常達 30 公里以上，是本區深部構造的主要骨架。斷裂形成最早，多數形成於加里東期，以後仍有繼承性活動。

北東東向斷裂主要發育於濱海地區，以濱海斷裂帶為代表。斷裂主要形成於喜山期，與南海盆地的擴張有密切關係。斷裂在地貌上是沿海島鏈帶與陸架盆地的分界線，北側為萬山群島隆起區，南側控制珠江口外盆地的形成和發展。沿斷裂帶在東、西兩端的南澳、瓊山分別發生過 7.3 和 $7\frac{1}{2}$ 級地震，故此斷裂是 7 級以上地震的控震構造。

$M \geqslant 6$ 級地震主要分佈在東南沿海地震帶，$4\frac{3}{4}-5\frac{3}{4}$ 級地震震中的分佈則較為分散，但仍有相對集中的地區，它們是：珠江三角洲斷陷區及其鄰近地區。在沿海及濱海強震活動帶內並不是處處都具備發生 6 級以上的強震構造條件，歷史上發生 6 級以上地震大多在其東北段，如位於區外的泉州海外（曾發生 $7\frac{1}{2}$ 級地震）、南澳一帶（曾發生 7 級和 7.3 級地震）以及西南段的陽江至瓊北也發生過多次 $6-7\frac{1}{2}$ 級地震。

第三章 近場及場區地震構造

本章旨在通過對地震活動性、新構造運動特徵、主要斷裂特徵及其活動性的分析，判斷近場區域可能發生地震的地點，綜合評價近場及場區地震構造，為確定近場潛在震源區和場地地震動參數提供依據。按照中華人民共和國國家標準《工程場地地震安全性評價》（GB17741-2005）（國家技術品質監督局，2005）中對近場範圍的要求，近場區的經緯度範圍為：東經 113.62° - 114.42°，北緯 22.12° - 22.73°。

3.1 近場新構造運動基本特徵

3.1.1 地形地貌特徵

香港元朗－屯門地區近場範圍具有海灣夾持半島的地貌總體特徵。工程場地所處的九龍半島東鄰大鵬灣，西傍伶仃洋河口灣，地貌反差強烈。這種地貌特徵是粵東沿海的共同地貌特色，實質上是晚新生代斷塊升降運動的結果。

整體而言，工程場地近場範圍地勢呈現東南高西北低的特徵。近場東南部為低山丘陵地貌，西北部為丘陵谷地地貌。其特徵分述如下：

北東向的海岸山脈從深圳延伸至香港地區，構成近場東南部的主體地貌單元。自北東往西南方向，深圳梧桐山（943.7 公尺）、香港大帽山（957 公尺）、鳳凰山（934 公尺）依次為海岸山脈的主要山峰，也是場地近場範圍高海拔的地方。從岩石性質的角度來看，三個最高峰的岩石組成均為侏羅紀火山岩。由於火山岩的岩性堅硬，抗風化能力強，所以不容易受外動力作用影響，從而呈現脊尖坡陡的特徵。此外，一系列低山散佈在近場的東南部，例如青山（583 公尺）、大東山（869 公尺）、馬鞍山（702 公尺）、飛鵝山（602 公尺）、扯旗山（552 公尺）等，而一些丘陵則穿插其中，譬如流浮山、調景嶺、紫羅蘭山等。

港灣地貌是近場東南部地貌的主要特色。香港的港灣眾多，海岸曲折，著名如維多利亞港、九龍灣等。香港地區的港灣主要沿北東向和北西向斷裂帶分佈，在形態上具有向南東方向開口呈喇叭狀，向北西方向收斂的特點；另一方面，受構造作用影響，香港海岸的北西岸一般較平直，而東南岸則較曲折。

除此之外，場地近場範圍東南部還發育瀉湖平原，如西貢一帶；沖積海積平原，如元朗平原等地貌單元。

近場北西部以丘陵谷地地貌為特徵，其東部的平行嶺谷地貌和西部的環狀結構地貌是主要特色。在深圳坪山、龍崗一帶，受深圳斷裂帶的影響，坪山河谷地、

龍崗河谷地形成斷陷谷地，谷地方向均為北東向。在深圳羊臺山一帶，受花崗岩穹窿體的影響，地貌具有環狀結構特點。丘陵、臺地、階地、平原構成了近場範圍北西部的地貌單元。

3.1.2 新構造運動特徵

新構造時期以來，工程場地近場範圍地殼活動以間歇性升降運動為主要特徵，發育多級夷平面、臺地和階地，局部地形面抬升後受後期構造運動影響發生掀斜現象，例如梧桐山西北側夷平面向西北掀斜。在深圳地區，蓮花山斷裂帶以西發育四級臺地及三級夷平面，高度分別為 5—15 公尺、20—25 公尺、30—45 公尺、60—80 公尺和 100—150 公尺、200—250 公尺及 350—400 公尺；斷裂帶中發育二級臺地及四級夷平面，高度分別為 30—45 公尺、60—80 公尺和 150—200 公尺、300—350 公尺、450—500 公尺及 650—750 公尺。河流階地主要發育在布吉河以東的各主要河谷內，表現為 3—7 公尺、8—15 公尺的二級沖積階地。海積階地見於蛇口半島中部和深圳灣北岸的白石洲，為 3—5 公尺的一級海積階地（黃鎮國等，1983）。此外，深圳地區還發育多層溶洞及多級海底平臺，第四紀沖積平原下的四層溶洞標高分別為-13—-19 公尺、-23—-33 公尺、-50—-60 公尺、-90—-100 公尺，葵涌一帶第四系下溶洞最深達-80 公尺；珠江口一帶鄰近海域水下分佈五級海底平臺，分別為-15—-20 公尺、-30—-45 公尺、-50—-70 公尺、-80—-95 公尺、-100—-120 公尺。在香港地區，陸地上發育多級層狀地貌面或被抬升的古海灘，在水下則有溺谷和被埋藏在海相沉積之下的沖積－湖相堆積（張虎男，1986）。上述地質地貌現象反映了新構造時期近場範圍的地殼間歇性升降特徵。另一方面，地殼大面積的升降運動與斷裂活動相互作用一斷隆為半島，斷陷成海灣，構成了近場範圍半島相伴海灣的地貌特色。

3.2 主要斷裂特徵與活動性

香港元朗－屯門地區近場範圍斷裂以北東向和北西向最為發育（圖 3.2-0）。

北東向蓮花山斷裂帶是該地區的主體構造格架，包括九尾嶺斷裂組、橫崗－羅湖斷裂組、蓮塘斷裂組、鹽田斷裂組等主幹斷裂。北西向斷裂較北東向斷裂成生晚，但活動性較新，包括礬石水道東側斷裂、流浮山－東博寮海峽斷裂、觀瀾斷裂等主要斷裂。現將主要斷裂的特徵及其活動性分述如下：

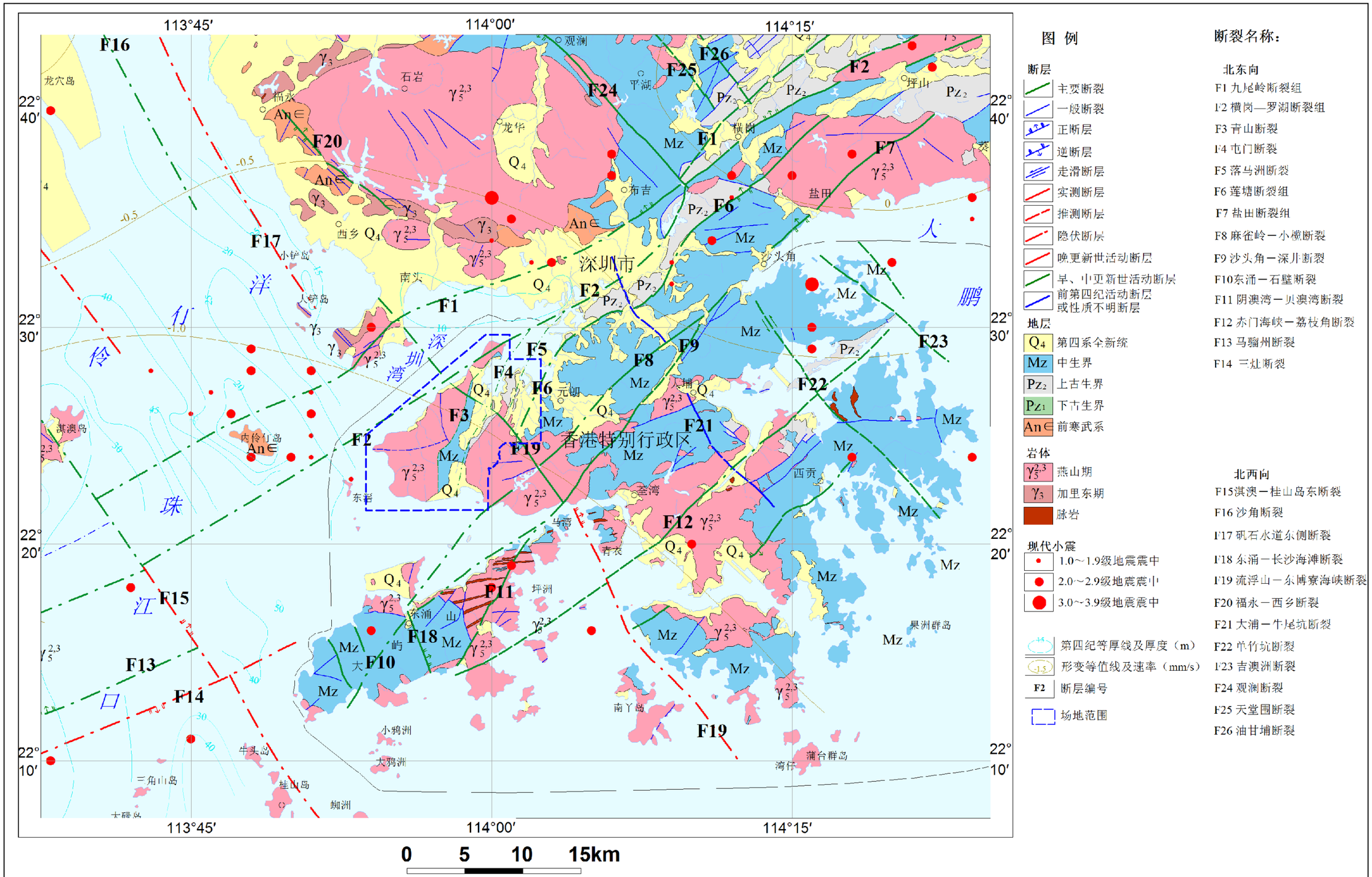

圖 3.2-0 近場區地震構造圖

Table of Contents (Chinese)
Table of Contents (Chinese)
Table of Contents (Chinese)
Table of Contents (Chinese)

九尾嶺斷裂組 F1

九尾嶺斷裂組屬於蓮花山斷裂的主幹斷裂之一，由九尾嶺斷裂及其次一級的金錢凹斷裂和望天海螺斷裂組成的一個斷裂組，從近場範圍外的惠陽淡水往西南方向延伸進近場，經荷坳、沙灣、九尾嶺、獨樹村、筆架山一帶至沙頭進入深圳灣，穿過蛇口在赤灣村一帶進入伶仃洋。斷裂總體走向 50° - 80°，傾向以北西為主，傾角為 65° - 85°。據航空紅外線攝影及側視雷達影像圖上分析，沿此斷裂顯示為平直的不同色調介面構成的線性構造組合體。在荷坳牌一帶可見陡立的斷層三角面；在九尾嶺和獨樹村一帶，斷裂破碎頻寬僅數公尺，影響頻寬也僅約十餘公尺，由破碎帶的中心向兩側依次為由斷層泥－糜棱岩－構造透鏡體－壓碎角礫岩和綠泥石化、矽化碎裂岩，在獨樹村還可見斷層泥上有清晰的斜向擦痕，該處斷層物質熱釋光測年結果為距今 26.16±1.2 萬年（圖 3.2-1），相當於中更新世。

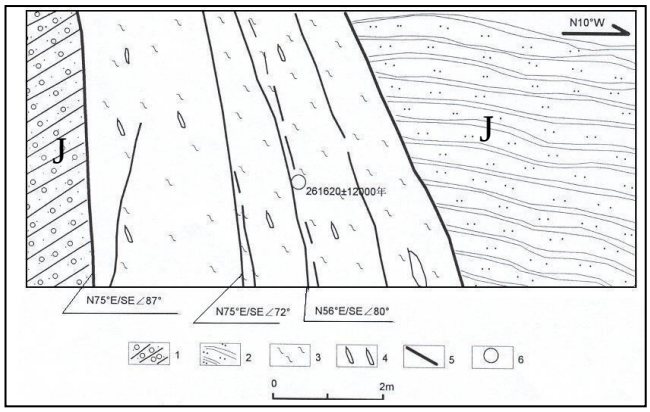

圖 3.2-1　獨樹村九尾嶺斷裂構造剖面（據中國地震局地質研究所）

1. 含礫粉砂岩；2. 變粒岩；3. 糜棱岩；4. 構造透鏡體 5. 斷裂；6. TL 採樣點

在蛇口一帶，斷層發育在燕山期花崗岩中。斷層兩側岩石強烈擠壓破碎，構造岩為角礫岩和糜棱岩，寬5公尺以上（圖3.2-2）。斷層泥電子自旋共振測年結果為距今43.9±7.9萬年。據伶仃洋大橋物探鑽探資料，在內伶仃島西側出現一條北東向相對兩側深20公尺的風化凹槽，可能同該斷裂風化有關。凹槽上覆蓋年齡大於1.43±0.3萬年的沉積物連續分佈，未見變動。由此可見，該斷裂的最新活動時代為中更新世。

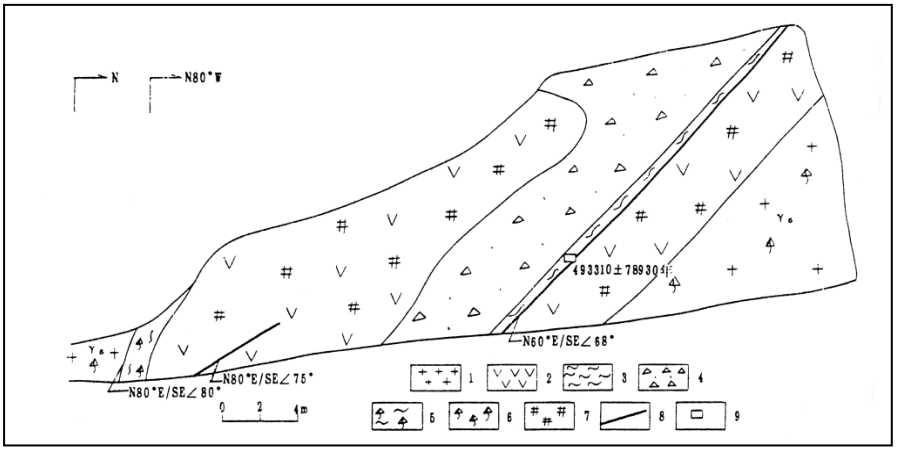

圖 3.2-2　蛇口西九尾嶺斷裂剖面（據中國地震局地殼應力所）

1.花崗岩，2.矽化層，3.糜棱岩，4.構造角礫岩，5.糜棱岩化碎裂帶，
6.碎裂岩，7.破碎帶，8.斷層，9.ESR 採樣點

橫崗—羅湖斷裂組 F2

橫崗—羅湖斷裂組屬於蓮花山斷裂的主幹斷裂之一，從近場範圍外惠陽地區往西南進入近場，經橫崗、深圳水庫至黃貝嶺，隱伏於羅湖區之下並從漁民村一帶進入香港元朗西北部地區再沒入伶仃洋。橫崗—羅湖斷裂組由橫崗－羅湖斷裂、清風嶺－爛寨頂斷裂，炮臺山－橫崗頭斷裂以及與其平行的一系列次級斷裂組成，在空間上呈舒緩波狀延伸，總體走向 30° - 70°，傾向北西，傾角 70° - 80°。

在深圳橫崗鎮北東 4 公里簡壹學校附近，斷裂發育在石炭紀中層灰白色砂岩中，寬約 15 公尺，斷裂物質由碎裂岩、角礫岩、斷層泥和矽化岩組成，可見構造透鏡體帶（圖 3.2-3）。斷裂下盤面清晰，走向 30°，傾向 NW，傾角 70°，其北西側發育 1 - 10 厘米的斷層泥和 3 公尺寬的壓碎角礫岩。斷層泥電子自旋共振年代測試結果顯示其年齡為 32.2±3.2 萬年。斷裂上覆第四紀殘積薄土層，未見其被切穿或被擾動（馬浩明，陳龐龍，2009a）。

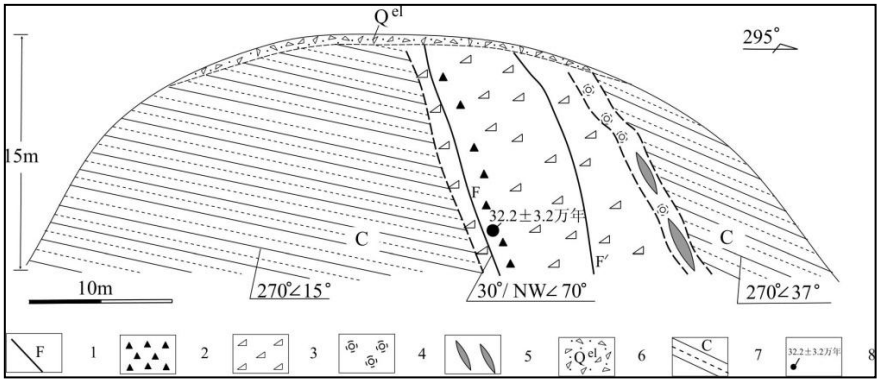

圖 3.2-3 簡壹學校北西 200 公尺處橫崗—羅湖斷裂剖面（馬浩明，陳龐龍，2009a）

1.斷裂；2.構造角礫岩；3.碎裂岩；4.矽化岩；5.構造透鏡體；6.殘積層；7.石炭紀砂岩；8.ESR 採樣年齡

在深圳市區人民橋與國貿大廈之間（圖 3.2-4），横崗－羅湖斷裂被十多公尺厚的第四系覆蓋，該底層下部為晚更新統砂礫層，上層為全新統。剖面顯示斷層兩側的 Q^3－Q^4 層位連續，埋深一致，並沒被斷裂活動錯移，表明該斷裂自晚更新世以來沒有明顯的活動（陳偉光等，2001）。此外，深圳河穿越横崗－羅湖斷裂，但尚未發現斷裂活動形成而的構造地貌。

斷裂西南段在香港境內與青山斷裂、屯門斷裂和落馬洲斷裂形成聯合弧形斷裂組。在香港爛角咀西，伶仃洋大橋 ZK4-4、ZK4-3 和 ZK4-8 孔揭示到該斷層。斷層泥熱釋光測年結果顯示斷裂最新活動時代為距今 14.43±1.3 萬年，相當於中更新世晚期。

由此可見，近場地範圍横崗－羅湖斷裂最新活動期在中更新世。

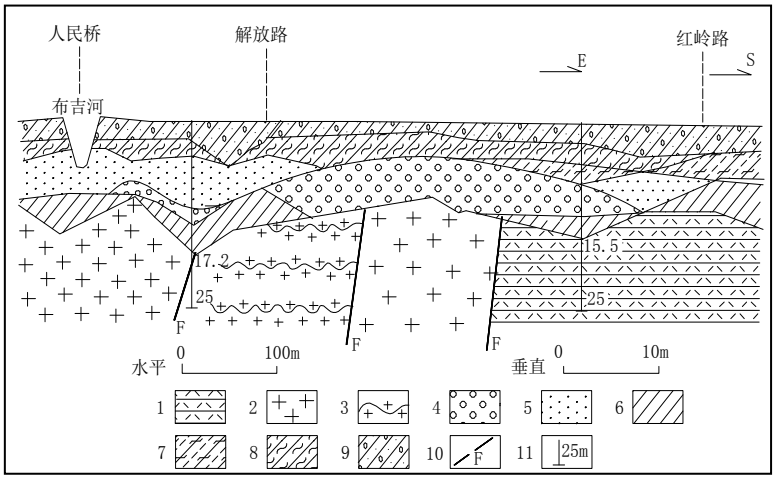

圖 3.2-4 人民橋－國貿大廈横崗－羅湖斷裂地質剖面圖（陳偉光等，2001）

1.侏羅紀凝灰岩；2.燕山期花崗岩；3.燕山期花崗片麻岩；4.礫石層；5.砂層；6.粘土層；7.夾淤泥粘土層；8.風化粘土層；9.人工堆積層；10.斷層；11.鑽孔及孔深

屯門斷裂組 F3 - F5

展佈於深圳河口至屯門一帶，總體走向從西北部的北東東向，往南逐漸偏轉為北東、北北東向。同横崗－羅湖斷裂構成聯合弧形式。該斷裂由西支青山斷裂（F3），中支屯門斷裂（F4），東支落馬洲斷裂（F5）組成。青山斷裂（F3）長 13 公里，傾向北西，斷裂西南段傾角 40° - 50°，東北段傾角 50° - 67°。燕山期花崗岩同上侏羅統火山岩層接觸，沿斷裂出現寬 10 - 150 公尺不等的韌性變質岩帶，在蝴蝶灣斷層物質採樣 TL 測定，年齡為 26.55±2.5 萬年。中支屯門斷裂（F4）為第四紀覆蓋，在屯門地區為燕山期花崗岩同上侏羅統火山岩為斷層接觸。據鑽孔揭示，沿斷裂帶基風化層厚度大，屯門地區風化深達 150 公尺。東支落馬洲斷裂（F5），長 20 公里，傾向北西，傾角 58°。該斷裂控制了元朗平原的形成和發展。

蓮塘斷裂組 F6

蓮塘斷裂由田螺坑斷裂及石井嚇－黃竹坑斷裂等組成。其北東段自樟樹南緣往西南經坪山石井嚇至三洲田水庫附近尖滅，西南段自屯洋和鹽田坳岩體西緣經梧桐山北坡的蓮塘進入香港的老鼠嶺、米埔及屯門谷地東緣。斷裂的北東段走向為 50° - 60°，西南段具明顯的舒緩波狀特徵，總體產狀為 50°/NW∠45° - 80°。

本斷裂在航空紅外線攝影及側視雷達影像圖上顯示為黑色粗線條特徵，坪山盆地邊緣為直線狀灰黑色的介面。斷裂在地貌上有明顯反映，東南盤梧桐山海拔 943.7 公尺，北西盤為階梯狀下降的丘陵臺地，航、衛片線性清楚。

石井嚇－黃竹坑斷裂的東北段切割了上泥盆統砂頁岩，西南段則切割了鹽田坳岩體、屯洋岩體和上泥盆統雙頭群。沿斷裂可見矽化帶、花崗糜棱岩化帶，密集陡直的斷層破碎帶，石英脈及花崗斑岩脈的貫入，棱角清晰的斷層角礫岩和壓扁磨圓的構造透鏡體，有的斷裂面上還可見斜衝擦痕。

田螺坑斷裂在西坑以南被北西向的永庋斷裂所切，分成南西和北東兩段，且使其呈反扭。南西段，在斷裂的東南側流紋質火山碎屑岩中發育有多條寬十餘公尺至數十公尺不等的千枚岩或超糜棱岩帶、糜棱岩帶及片理化帶，總寬可達數百公尺，在斷裂北西側的下石炭統砂頁岩內的二雲母微片岩中，有範圍較窄的滑劈理帶疊加；北東段，在燕山期花崗岩形成約 10 公尺寬的矽化構造角礫岩帶、破碎岩帶和劈理帶。

在田螺坑公路邊（圖 3.2-5）斷層泥石英顆粒表面侵蝕程度分類統計表明斷裂主要活動期為上新世中期，到上新世晚期仍有較明顯活動但強度已經減弱。對該處斷層泥分別採用熱釋光和電子自旋共振測年，結果分別為 20.27±1 萬年和 21.87±3.28 萬年（劉行松等，1993），表明斷裂最新活動期為中更新世晚期。

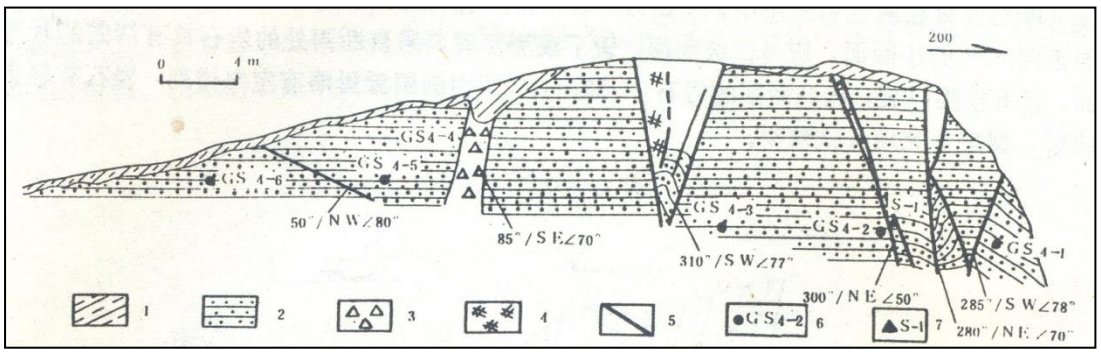

圖 3.2-5　田螺坑公路邊蓮塘斷裂地質剖面（劉行松等，1993）

1.亞沙土；2.砂岩；3.角礫岩；4.碎裂岩；5.斷層；6.定向標本採樣點；7.測年樣品採樣點

鹽田斷裂組 F7 - F11

北東段由鹽田斷裂和豆腐頭斷裂等組成，北東自澳頭往南西經葵涌、上坪、鹽田、沙頭角入香港的丹竹坑、大帽山西北麓、深井至大嶼山的灣篤－鹿地塘、貝澳後入南海。

斷裂走向北東 50° - 60°，傾向北西（或南東），傾角 40° - 70°。沿斷裂發育有 3 - 20 公尺寬不等的壓碎矽化岩、片理化碎裂岩和糜棱岩，疊加在糜棱岩化帶上的矽化岩又遭擠壓破碎，反映了斷裂的多期活動。在深圳葵涌採集該斷裂的斷層泥進行熱釋光測年，結果為距今 20.24 萬年（圖 3.2-6），石英形貌電鏡掃描結果反映本斷裂最新的一次活動發生在中更新世晚期。

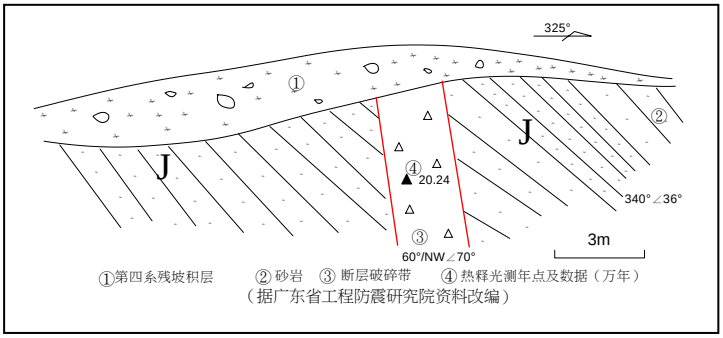

圖 3.2-6 葵涌鹽田斷裂構造剖面圖

斷裂的西南段在香港境內成掃帚狀撒開，形成由麻雀嶺－小欖斷裂 F8（粉嶺—東涌）、沙頭角－深井斷裂 F9、東涌－石壁斷裂 F10 和陰澳灣－貝澳灣斷裂 F11 組成的斷裂組。這些斷裂的線性地貌清晰，沿斷裂表現為谷地和山垭口。麻雀嶺－小欖斷裂（F8）展佈於沙頭角－深井斷裂以北，北起麻雀嶺，向西南經陳屋埔，馬鞍崗至小欖入海，總體走向北東 50°，區內長 27 公里。沿斷裂發育谷地，線性地貌清晰。沙頭角－深井斷裂（F9）總體走向北東，長 19 公里。沿斷裂形成擠壓破碎帶，控制沙頭角海和林村谷地的發育，線性地貌清晰。東涌－石壁斷裂（F10）總體走向北東東至東涌東南轉北東向，長 9 公里。沿斷裂表現谷地和山垭口線性地貌。在東涌一帶為燕山期花崗岩與上侏羅統大嶼山組晶屑凝灰岩呈斷層接觸；在黃泥屋附近可見主斷裂北旁側花崗岩中在 12 公尺寬度內出現三條與主斷裂平行的次級斷層，圖 3.2-7 為其最北的一支，斷層走向北東，傾向南東，傾角 78°，沿該斷裂發育寬 3 - 4 公尺的碎裂岩和糜棱岩，糜棱岩中出現二次小滑動面，滑動面物質 TL 年齡為 98300±6300 年，在陰澳篤南旁次級斷層物質 TL 年齡為 82000±6800 年，相當於晚更新世早期。陰澳灣－貝澳灣斷裂（F11）總體走向北東，長 13 公里。該斷裂線性地貌清晰，控制谷地和陰澳灣、貝澳灣的發育。

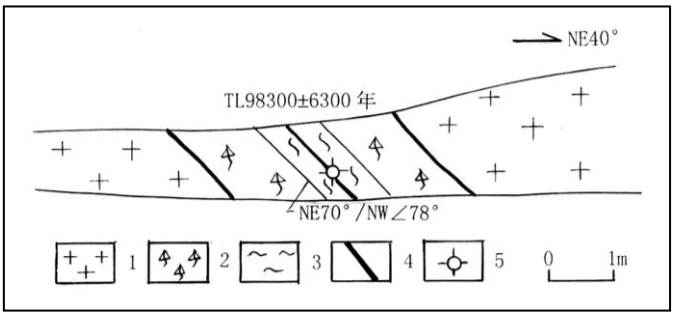

圖 3.2-7　東涌黃泥屋附近斷裂剖面（據中國地震局地殼應力研究所）

1.花崗岩，2.碎裂岩，3.糜棱岩，4.斷層和二次滑動面，5.TL 採樣點

赤門海峽－荔枝角斷裂（F12）

展佈於九龍半島的荔枝角、沙田一帶，往北東延入區外的赤門海峽，往南東被北西向東寮海峽斷裂截切後可能延至大嶼山鹹田一帶，區內長 47 公里。總體走向北東 40° - 50°，傾向南東，傾角 75° - 80°。在沙田一帶可見沿斷裂形成由碎裂岩、斷層角礫岩和斷層泥組成的破碎帶，伴隨高嶺土化和浮泥石化。斷裂地貌有明顯反映，谷地、山垭口和海灣定向分佈。

馬騮州斷裂（F13）

展佈於馬騮州水道南側，向西經大門島北緣至區外大襟島以西，向東北延伸進入伶仃洋，工作區內長 14 公里。總體走向北東 60°，傾向北西，傾角陡。

橫琴大橋工程 G69（BH5）鑽孔在第四系之下揭示到該斷層，孔深 29.73 公尺至 82.31 公尺終孔為破碎帶，綠泥石化，絹雲母化。由橫琴橋鑽孔地質剖面（圖 3.2-8）顯示，斷層之上覆蓋的晚更新世晚期（TL 年齡為 38750±880 年）的沉積物未受影響。根據中國地震局地殼應力所在橫琴大橋東旁側所做的淺層人工地震和電法探測，結果表明斷層亦未影響到晚更新世晚期地層（圖 3.2-9）。

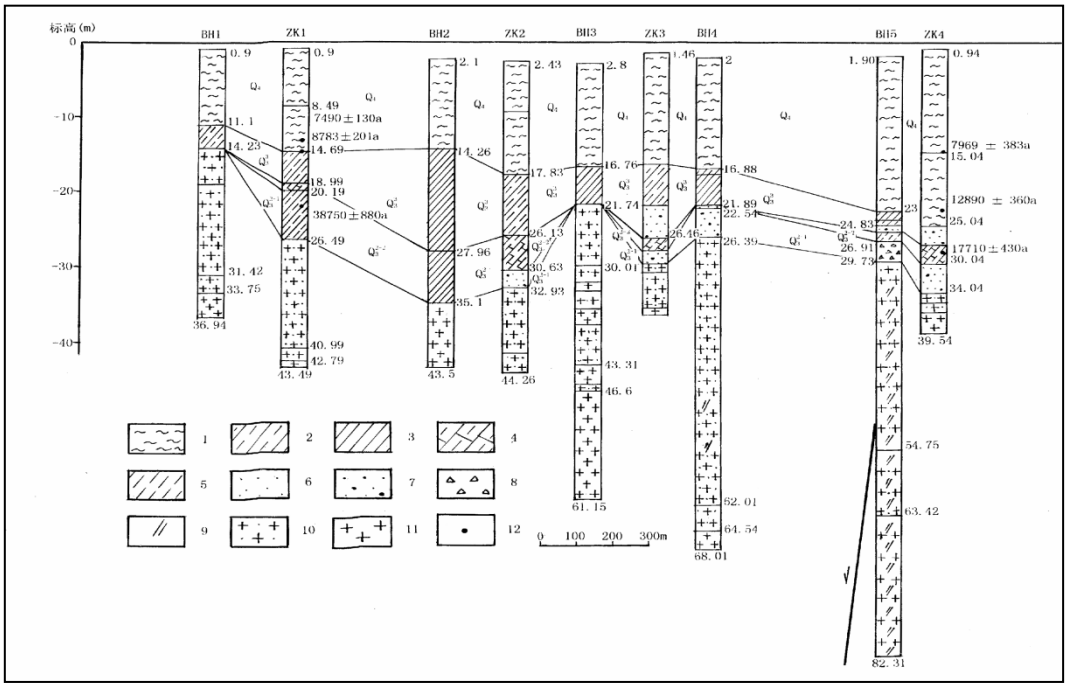

圖 3.2-8　橫琴大橋 BH1-ZK4 鑽孔地質剖面

1.淤泥，2.亞粘土，3.粘土，4.淤泥質亞粘土，5.輕亞粘土，6.細砂，
7.含礫石砂，8.碎石，9.構造破碎帶，10.風化花崗岩，11.花崗岩，12.^{14}C 採樣位置

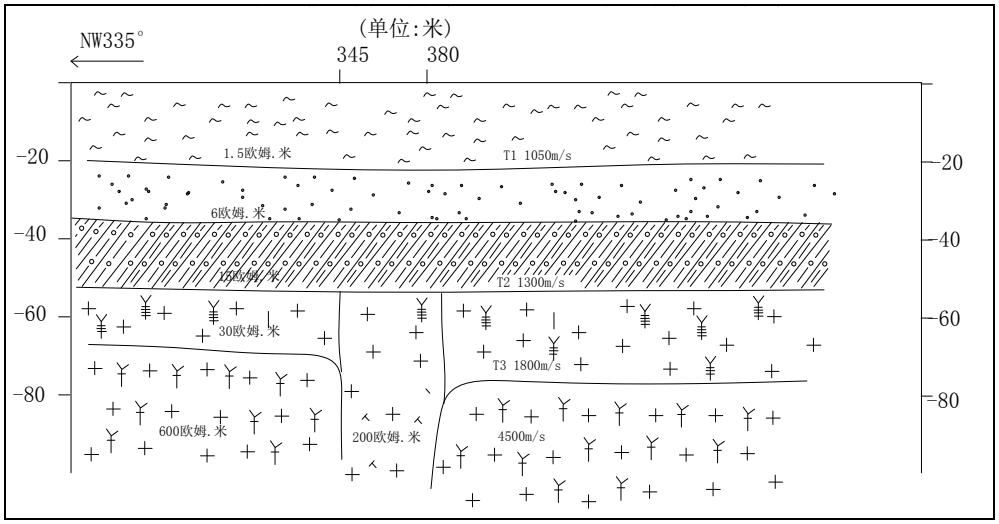

圖 3.2-9　　橫琴大橋東旁側斷裂物探地質解釋推斷剖面圖（據中國地震局地殼應力所）

大門島北側採石場中斷點，沿斷裂發育構造角礫岩和構造透鏡體，上盤泥盆系砂岩極度破碎（圖 3.2-10），並出露大的斷層滑動面和陡坎，最大者高達 20 公尺，寬 25 公尺，滑動面上擦痕，階步比比皆是。從擦痕看，至少有兩次活動，前期為擠壓兼有左旋，後期以正斷為主，兼有右旋特徵。據滑動面斷層物質 TL 測年，表明最晚一次活動發生在 16.26±1.15 萬年。該斷裂在伶仃洋水域段，港珠澳大橋 ZK10 鑽孔見及，孔深 71 公尺以下為破碎帶、碎裂岩。據斷層物質 TL 測年為 23.2±1.6 萬年。上述表明，該斷裂為一條中更新世斷裂。

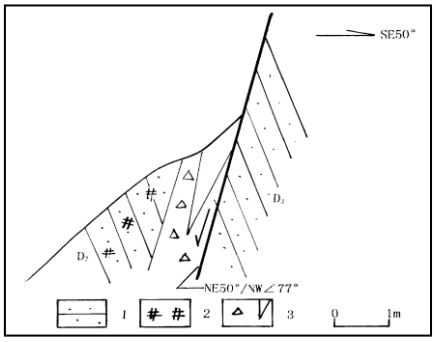

圖 3.2-10　大門島北側斷裂剖面（據中國地震局地殼應力所）

1.泥盆系砂岩，2.破碎帶，3.構造角礫岩及構造透鏡體

三灶斷裂（F14）

展佈於三灶島的三灶、斜尾村至大、小橫琴島之間，向西入海延出區外，向東入伶仃洋至香港大嶼山北，兩邊延伸入海，區內長 24 公里。總體走向為北東 60°， 傾向南東，傾角 80°。

該斷裂多隱伏於第四系之下，僅在三灶島斜尾村見出露寬達 200 多公尺的斷層帶（圖 3.2-11）。該地段岩石強烈矽化，片理化，碎裂化，見厚約 0.5 公尺的千枚岩和粉末狀糜棱岩、細脈狀矽質構造岩、片狀碎裂岩相間排列，形成許多寬約 0.9 - 4.3 公尺不等的擠壓破碎帶，並有煌斑岩脈、石英脈貫入。主斷面在公路一段通過。據斷層樣品 TL 測年，斷裂最近一次活動發生在 18.30±1.56 萬年。另據主斷裂西北旁側一小斷層樣品 TL 測定，斷裂最後一次活動距今為 5.191±0.44 萬年。

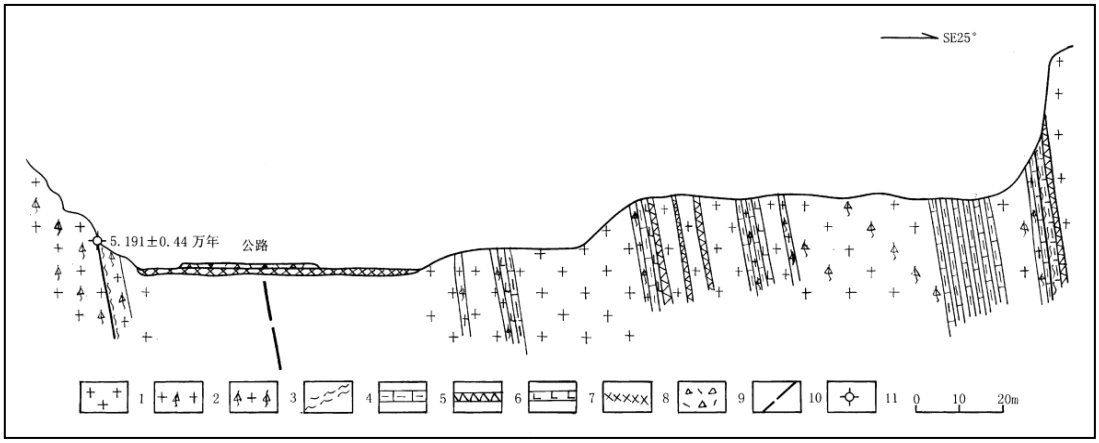

圖 3.2-11　三灶島斜尾村三灶斷裂剖面

1.花崗岩，2.碎裂岩化花崗岩，3.花崗碎裂岩，4.糜棱岩，5.脈狀矽化構造岩，6.石英脈，7.煌斑岩脈，8.人工堆積土，9.混凝土公路，10.斷層, 11.TL 採樣點

在三灶島東嘴金洋花園場地鑽孔揭露出斷層角礫岩，其中斷層泥 TL 測年，斷裂最後一次明顯活動發生在 3.23±0.2 萬年，在群星島花園附近的 ZK27 孔還發現有玄武岩噴溢活動。上述表明，三灶島斷裂最晚活動發生在晚更新世中晚期。中國地震局地殼應力研究所在大、小橫琴島間沿堤壩一線進行了淺層人工地震和電法探測，結果表明，斷層影響到上覆蓋的晚更新世沉積物（圖 3.2-12）。

在大橫琴島北側石山，斷裂走向北東 70° - 80°，傾向北北西，傾角 80° - 87°，切割黑雲母花崗岩，形成寬約 40 公尺的剪切破碎帶。

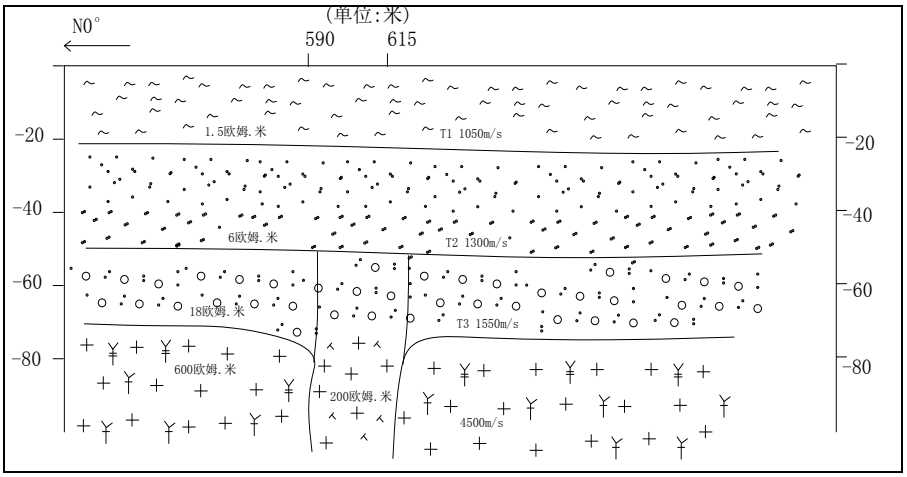

圖 3.2-12　大、小橫琴島間斷裂物探地質解釋推斷斷面圖（據中國地震局地殼應力所）

在高欄島（圖 3.2-13），斷裂走向北東 25°，傾向南東，傾角 80°，切割黑雲母花崗岩，可見寬度約 5 公尺的擠壓破碎帶。

在大襟島西北側的獅子頭灣，斷裂發育在泥盆系砂頁岩中，走向北東 40° -

60°，傾向北西，傾角 65 - 70°，斷裂頻寬約 10 - 30 公尺。採集的斷層泥的熱釋光測年結果為距今 17.28 萬年，相當於中更新世。

國家地震局所編《中國活動構造典型衛星影像集》根據島嶼和水下沙洲的線狀排列，認為下川島—氹仔島斷裂（三灶斷裂與其北東段吻合）是一條活動斷裂，它控制著近岸一系列島嶼的線狀排列。島嶼上可見到斷裂的形跡，影像清晰，線性明顯。近岸淺灘伸展至此時，常常出現陡坎，深度驟增，深淺色調的分界明顯。在地震活動方面，1905 年在該斷裂的東北端與西江斷裂交匯處或其附近曾發生 5 級地震。

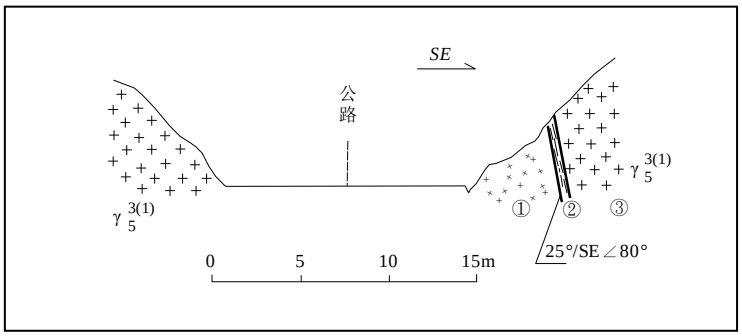

圖 3.2-13　高欄西南 500 公尺處地質構造剖面

1. 構造角礫岩　2. 擠壓片理化帶　3. 燕山四期花崗岩

淇澳島—桂山島東斷裂（F15）

斷裂展佈於淇澳島及其以南至桂山島以東水域中，總體走向北西 320°。斷裂可將其分成北西和南東兩段，北西段稱淇澳斷裂，而南東段稱桂山島東斷裂。

在斷裂北西段的淇澳島，斷裂所通過處在地貌上形成一北西向狹長形深風化谷地，兩側為海拔 100 - 150 公尺的丘陵。谷地西南側，可見斷裂的次級構造（圖 3.2-14），形成寬達 2.5 公尺的壓碎花崗岩與擠壓帶。斷裂所通過的谷地第四系上更新統中段的厚度無明顯的變化，表明斷裂在晚更新世中期以來已無明顯的活動。

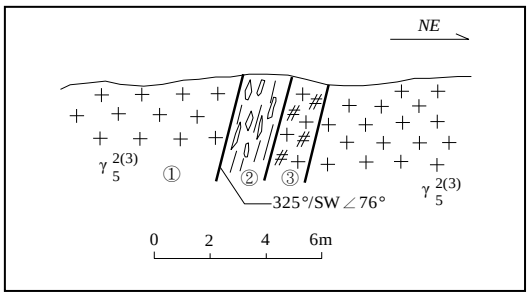

圖 3.2-14　淇澳東南地質構造剖面

1. 燕山三期花崗岩　2. 含擠壓透鏡體片理化帶　3. 壓碎花崗岩

據珠江水利委員會在珠海伶仃洋大橋橋址的淺層人工地震資料，在斷裂部位出現基岩凹槽（圖 3.2-15）凹溝相對深達 30 公尺。覆蓋在凹槽、凹溝上的第四系沉積物未見變動，判斷為中更新世活動斷裂。斷裂南段據港珠澳大橋淺層地震揭示，最新斷錯晚更新世中期砂礫層底部，其 js 中斷點基岩頂面垂直斷距為 5 - 8 公尺，上中斷點埋深為 108 公尺；d1 中斷點基岩頂面垂直斷距為 3 - 4 公尺，上中斷點埋深 81 公尺；此外，斷裂東側 ZK3 孔岩芯破碎，碎裂結構，也證實了斷裂的存在。

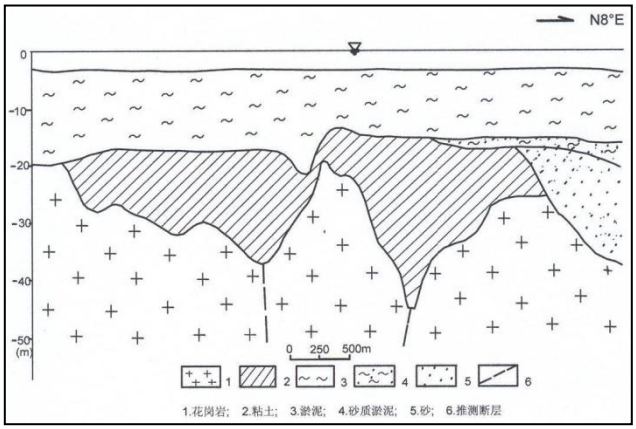

圖 3.2-15　珠海伶仃洋大橋V−V'地震地質剖面（據珠江水利委員會）

斷裂南東段，據港珠澳大橋淺層地震探測，在橋位段 ar 中斷點，最新斷錯晚更新世中期砂礫層底部，垂直斷距為 3 - 4 公尺，上中斷點埋深 74 公尺，並沿斷裂有第四紀基性岩溢出。在擔尾水道段，斷裂最新斷錯中更新統上部，並控制晚更新世以來沉積，向南順斷裂方向為一條沼氣帶。表明該斷裂活動分段明顯，港珠澳大橋橋位段為晚更新世中期。

沙角斷裂（F16）

斷裂北起虎門與威遠之間的北面村以北，往南東經沙角進入珠江口。長約 17 公里。總體走向北西 310° - 320°，傾向南西，傾角 50° - 85°。

在虎門沙角炮臺海邊，於下古生界淺變質砂岩中，見斷裂走向北西 320° - 340°，傾向南西，傾角 65° - 72°，矽質構造岩發育，地層褶皺和斷面扭曲現象十分強烈（圖 3.2-16）。

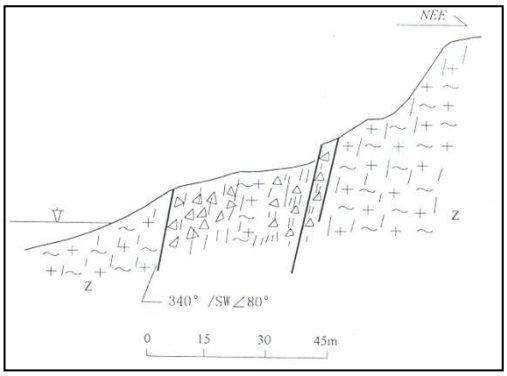

圖 3.2-16　沙角炮臺斷裂構造剖面

據虎門地震小區劃報告，在北面村一帶，斷裂頻寬約 10 公尺，由矽化岩與角礫岩組成，在主斷面上盤面約 100 公尺範圍內，還出現多條 0.1 - 1 公尺的小斷裂，走向 315° - 340°不等。斷裂下盤為前寒武系千枚岩與變質砂岩，上盤為侏羅系，斷裂被上更新統紫紅色砂礫層覆蓋，該砂礫層為高出平原面 10 - 15 公尺的堆積階地，主幹斷裂的新活動使其上的上更新統階地形成多個 3 - 6 厘米寬的破裂面，兩側砂礫層受到明顯擾動。在階地後緣，上更新統與侏羅系為斷層接觸，斷層產狀 320°，傾向北東，傾角 60°，寬 10 厘米，上更新統頂部層位超覆於下盤侏羅系上，仍可見斷裂切割頂部上更新統地層的跡象。斷層物質的熱釋光測年結果為 5.88±0.48 萬年，相當於晚更新世。

礬石水道東側斷裂（F17）

自珠江口北部沿循礬石水道東側延伸至蛇口西部。斷裂控制了礬石水道，形成一條北西向的第四系厚度陡變帶和水下地形陡變帶。通過物探、斷裂對新地層切割情況、斷裂在水下顯示的深切溝槽等情況，如在珠江口北緣小鏟島西北，據“珠海伶仃洋大橋工程場地地震安全性評價報告”，廣州海洋地質調查局淺層人工地震測量揭示到該斷裂在此處切斷了水下 10 公尺的全新統（R_1）下部層位（圖 3.2-17），判斷該斷裂在全新世仍有活動。

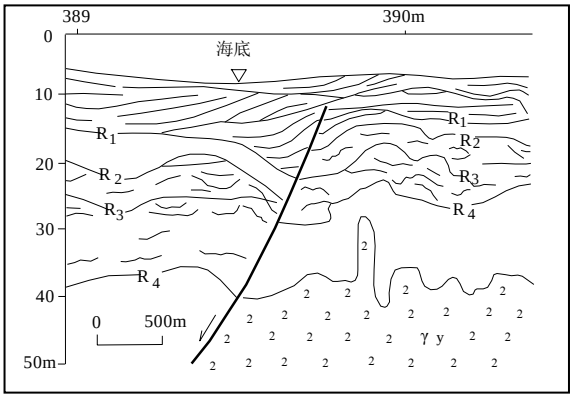

圖 3.2-17　珠江口小鏟島西北淺層人工地震解釋剖面

（據廣州海洋地質調查局）

東涌—長沙海灘斷裂（F18）

北起東涌，南至長沙海灘，往兩邊入海，陸域段長 5 公里。總體走向北北西。該斷裂線性地貌清晰，為溝谷、山垭口和海灣地貌。沿斷裂發育北北西向密集節理帶和破碎帶。在大嶼山南長沙西醫院邊溝內見中斷點（圖 3.2-18），為一組走向北西 322°的密集節理帶，節理陡立，單條寬 2 - 20 厘米，有個別沿大節理出現小滑動面，滑面斷層物質 TL 測年，為 10.1±0.8 萬年。在伯公坳可見寬 30 公尺的破碎帶。中國地震局地殼應力研究所在石榴埔北進行的高密度電法探測結果表明，斷層之上覆蓋的晚更新世晚期以來堆積物未受影響（圖 3.2-19）。

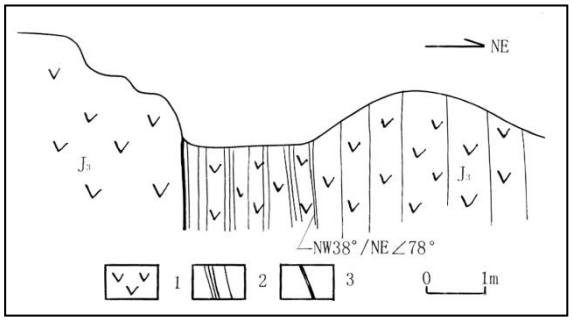

圖 3.2-18　大嶼山南長沙西醫院旁溝內大涌－長沙海灘斷裂剖面

（據中國地震局地殼應力研究所）

1.屑凝灰岩，2.節理及密集帶，3.小滑動面

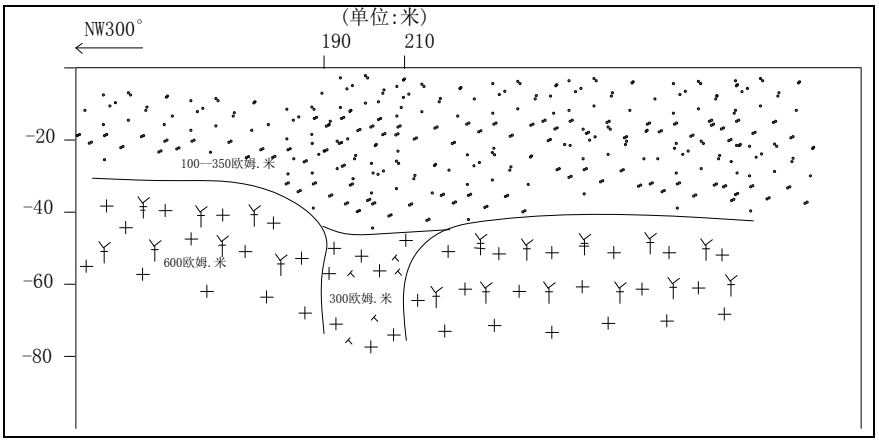

圖 3.2-19 石榴埔東涌－長沙海灘斷裂物探推斷剖面

（據中國地震局地殼應力研究所）

流浮山—東博寮海峽斷裂（F19）

本斷裂由珠江口西岸往西南延伸至蛇口，潛入深圳灣進入香港流浮山，經深井、青衣西至香港島與南丫島之間的東博寮海峽。長約 50 公里。主要由流浮山—東博寮海峽斷裂及其次級的汲水門—南丫島斷裂、打水灣—竹篙灣斷裂和陰仔灣—大白灣斷裂等組成。

斷裂總體走向北西 330°，傾向北東，傾角 53° - 75°（在雙仙灣、該斷裂產狀為 325°/NE∠53°，在深井水塘為 310°/NE∠75°）。在流浮山附近深圳灣岸邊可見斷層角礫岩帶。前人在深圳蛇口山採集的斷裂樣品熱釋光測年為距今 21.67±1.51 萬年，未切割上蓋的第四紀殘坡積層（距今 1.17±0.08 萬年，見圖 3.2-20 所表示），深圳灣大橋 ZK3 孔 54.0 公尺深構造岩滑動面為距今 11.02±0.77 萬年，未切割上蓋的第四紀沖海積層黃褐色粉細砂（距今 2.51±0.18 萬年）。

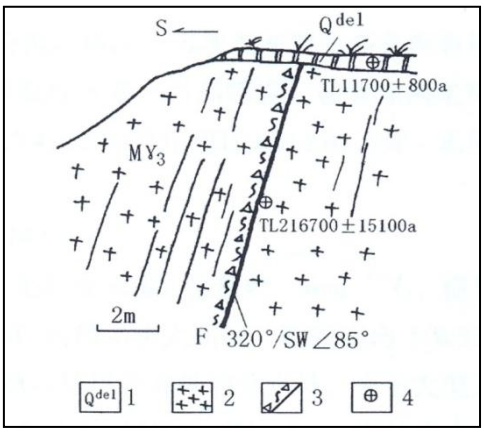

圖 3.2-20 深圳蛇口山北西向斷裂剖面圖

1.第四紀殘坡積層； 2.加里東期混合岩；3.斷層及構造岩；4 熱釋光測年點（年）

斷裂自香港馬灣往南東方向控制了馬灣－青衣海峽、東博寮海峽的發育。據香港青馬大橋鑽孔資料分析，在香港馬灣島與青衣島之間，斷裂帶附近形成明顯的直線凹槽（圖 3.2-21）：全新統海相層厚度在斷層兩盤存在明顯差異，南西盤 5DW16 孔為 1.15 公尺，而北東盤的 5DW6 孔為 7.1 公尺，表明該斷裂很可能在晚第四紀仍有一定的活動。

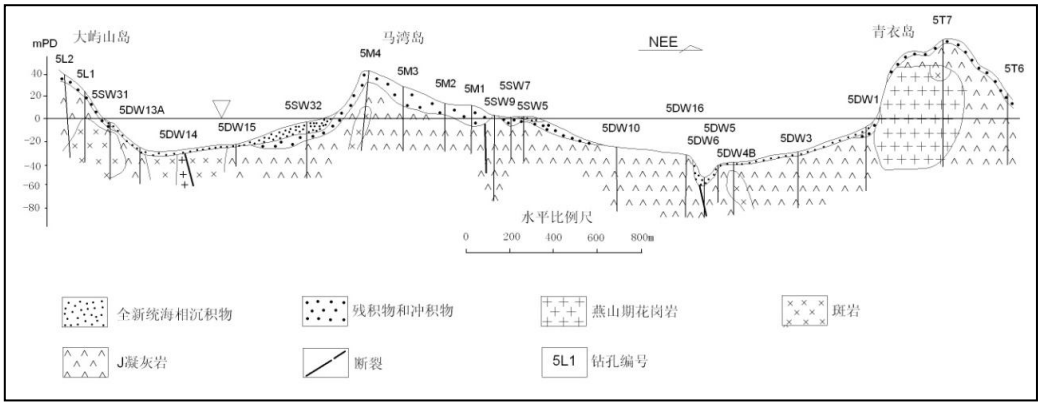

圖 3.2-21　根據鑽孔資料建立的流浮山—東博寮海峽斷裂剖面圖（丁原章，2004）

福永—西鄉斷裂（F20）

北起深圳福永鎮虎背山隧道北出口附近，往東南延伸經鐵崗水庫大壩至西鄉大坑口。長約 15 公里。由數條延伸 5 - 8 公里的規模較小的斷裂所組成，斷裂切割了前寒武系變質岩、加里東期和燕山期花崗岩，局部地段被第四系所覆蓋。斷裂總體走向 310°，傾向北東為主，傾角 45° - 70°。在地貌上，斷裂北東盤主要為丘陵區，而南東盤主要為珠江口沿岸平原和臺地殘丘。沿斷裂發育矽化構造角礫岩，寬度一般在 2 - 5 公尺。在虎背山隧道北側，據鑽孔揭露，灰白色糜棱岩化角礫岩厚度達 4 公尺，斷層物質熱釋光測年為 18.6±1.4 萬年，相當於中更新世。

大埔—牛尾坑斷裂（F21）

該斷裂南東起於香港蠔涌西南，往北西延伸香港大埔，再往西北斷續延伸至深圳羅湖漁民村、經荔枝公園、白沙嶺住宅區至筆架山。在香港境內，斷裂切割侏羅系的凝灰質砂岩和燕山期花崗岩。在深圳境內，走向西北 305° - 325°，傾向南西，傾角 65° - 75°，地表寬度 1 - 5 公尺，多個鑽孔揭露構造岩垂直厚度 5 - 23 公尺。構造岩以角礫岩和壓碎岩為主，膠結不緊密，為一富水斷裂。斷裂切割燕山晚期花崗岩及北東向斷裂，控制了上步嶺碳酸礦泉水的分佈。

單竹坑斷裂（F22）

斷裂分佈於香港船灣淡水湖—萬宜水庫之間，走向北西 310° - 320°，長約 24 公里。斷裂北段切割了白堊系紅色沙礫岩，南段切割侏羅系凝灰質砂岩。中段在赤門海峽—大埔海之間，切割了多組北東向斷裂並使其產生左旋錯移。在泥涌以

東採集的斷層物質熱釋光測年為距今 11.87±0.97 萬年（丁原章，2004），相當於中更新世。

吉澳洲斷裂（F23）

位於香港東北部吉澳洲和赤洲附近。斷裂產狀 310°/NE∠70° - 80°。在香港該斷裂有雞公頭—羊角頭斷裂和吉澳—弓洲斷裂組成。在黃泥洲採集的斷層物質熱釋光測年為距今 19.6±1.69 萬年、25.45±2.04 萬年和 19.68±1.63 萬年，相當於中更新世。

觀瀾斷裂（F24）

該斷裂北西起於東莞的石龍溫塘一帶，往南東經馬蹄崗、屏山水口、雁鵝嶺進入龍和、觀瀾到深圳水庫附近。走向西北 330°，傾向北東或南西，傾角 40° - 65°（屏山水口該斷裂產狀為 325°/NE∠40°）。它是分割虎門—樟木頭—惠州斷塊差異隆起區內大嶺—羊頭山中強隆起帶與樟木頭和緩隆起帶的分界線。斷裂橫切了塘夏向斜的南尾部，使下白堊統推覆於花崗岩之上，並產生片理化，花崗岩和下白堊統砂頁岩均被強烈擠壓而片理化、絹雲母化和糜棱岩化。斷裂發育寬數 10 公尺的矽化破碎帶，岩石破碎呈角礫狀，角礫呈棱角狀，成分與圍岩岩性一致，由矽質膠結，沉積岩中見褐鐵礦化，沿破碎帶常見犬牙狀石英脈穿插，石英脈寬約 1 - 2 厘米，與斷裂有一小交角，局部見花崗岩中的綠泥石化。

近場範圍內，觀瀾斷裂發育在低丘陵臺地地貌區，斷裂通過部位未發現有地貌差異或現代構造形變現象。據馬浩明等人對觀瀾斷裂的野外地質露頭剖面研究表明，觀瀾斷裂斷層物質由構造角礫岩、矽化岩、半固結岩屑或岩粉等組成，寬約 1 - 3 公尺，局部可見矽質被膜；斷裂沒錯動上覆殘積風化土層（圖 3.2-22）。四處斷裂樣品的電子自旋共振測年結果為 21.1±2.1 萬年、21.5±2.1 萬年、51.8±5.1 萬年和 32.0±3.2 萬年，反映斷裂活動於中更新世中、晚期（馬浩明，陳龐龍，2009b）。沿斷裂 1970 年以來極少有小震記錄。

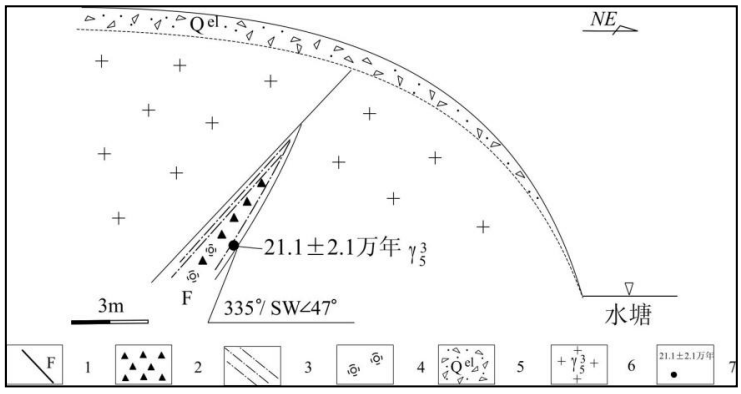

圖 3.2-22 山塘採石場觀瀾斷裂構造剖面（馬浩明，陳龐龍，2009b）

1.斷裂；2.構造角礫岩；3.糜棱岩；4.矽化岩；5.殘積層；6.燕山晚期花崗岩；7.ESR 採樣年齡

天堂圍斷裂（F25）

沿東莞伯公坳—雁田水庫一帶分佈，走向 330°，傾向北東，傾角 40° - 80°，區內長 8 公里。北段發育於侏羅系中，中段切割侏羅紀花崗岩，南東段晚古生界與侏羅系呈斷裂接觸，發育寬 20 公尺褐鐵礦化碎裂矽化岩，地貌上呈壟崗狀，岩石具先矽化，後破碎的特點，矽化岩破碎呈角礫狀，角礫棱角狀，褐鐵礦充填。

油甘埔斷裂（F26）

自深圳坳背一帶向北西經東莞油甘埔、塘廈鎮至大瀝村附近，走向 320°，傾向南西為主，局部傾向北東，傾角 60° - 80°，區內長約 7 公里。主要穿行於侏羅紀地層中，部分地段為塘廈組與晚古生代地層呈斷層接觸，局部穿切元古代變質岩，總體呈舒緩波狀延伸。發育寬 15 - 20 公尺的斷裂破碎帶，由褐鐵礦化碎裂岩、矽化碎裂岩、斷層角礫岩及矽化岩等組成。局部見斷裂構造岩的不對稱分帶現象（圖 3.2-23），由南西往北東依次為：①碎裂岩，寬約 6 公尺，岩石破碎呈碎斑狀，裂隙發育；②構造角礫岩，角礫為棱角狀—次棱角狀，有的呈透鏡狀，大小為 2 - 3 厘米，成分為砂岩，矽質膠結；③矽化岩，乳白色，緻密塊狀，石英已重結晶為微粒石英。見舒緩波狀斷面，斷面粗糙，偶見反階步。斷面附近充填幾厘米的斷層泥；地貌上為壟崗狀，尤以矽化岩出露地段明顯，突出地表約 0.5 公尺，順斷裂發育筆直的溝谷，航照上也表現明顯的線性影像特徵，兩側色調具明顯反差。

斷裂具多期活動性，早期以發育碎裂岩、斷層角礫岩為特色，發育逆衝性質的斷面；晚期形成斷層角礫岩、矽化岩，切割北東向斷裂，作右旋斜落滑移。斷裂切割了北東向的樟木頭大斷裂和大朗—三和斷裂，斷裂北西段上盤中侏羅統高基坪群推覆於下古生界深變質岩之上，中段鈉長斑岩推覆於下白堊統塘夏群之上，南東段下石炭統逆衝在下白堊統之上，但未切割第四紀殘積層。斷裂的斷層物質熱釋光測年為距今 17.75 萬年、19.06 萬年、20.18 萬年和 25.45 萬年，相當於中更新世。

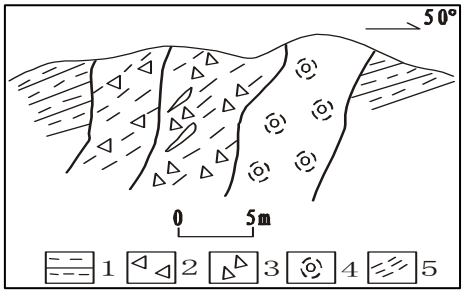

圖 3.2-23　油甘埔斷裂剖面圖（據 1/25 萬香港幅區測報告）

1.泥岩；2.碎裂岩；3.斷層角礫岩；4.矽化岩；5.劈理化帶

上述 26 條近場範圍主要斷裂的結構特徵及活動特徵見表 3.2-1。

表 3.2-1　近場範圍主要斷裂構造活動特徵簡表

編號	斷裂名稱		近場長度(公里)	產狀			斷裂性質	最新活動時代
				走向	傾向	傾角		
1	九尾嶺斷裂組 Jiuweiling Faults		75	NE50°-80°	NW/SE	65°-85°	逆斷/正斷	Q_2
2	橫崗－羅湖斷裂組 Henggang-luohu Faults		80	NE30°-70°	NW	70°-80°	正斷	Q_2
3	屯門斷裂組 Tunmen Faults	青山斷裂 Qingshan Fault	13	NE-NEE	NW	40°-67°	逆斷	Q_2
4		屯門斷裂 Tunmen Fault	16					
5		落馬州斷裂 Luomazhou Fault	10					
6	蓮塘斷裂組 Liantang Faults		40	NE50°-60°	NW	45°-80°	逆斷	Q_2
7	鹽田斷裂組 Yantian Faults	鹽田斷裂 Yantian Fault	18	NE50°-60°	NW/SE	40°-70°	逆斷	Q_2
8		麻雀嶺－小欖斷裂 Maqueling-xiaolan Fault	27	NE			逆斷	Q_2
9		沙頭角－深井斷裂 Shatoujiao-shenjing Fault	19	NE			逆斷	Q_2
10		東涌－石壁斷裂 Dongchong-shibi Fault	9	NEE	SE	78°	逆斷	Q_3 早期
11		陰澳灣－貝澳灣斷裂 Yinaowan-beiaowan Fault	13	NE			逆斷	Q_2
12	赤門海峽－荔枝角斷裂 Chimen strait-lizhijiao Fault		47	NE	SE	75°-80°	逆斷	Q_2
13	馬騮州斷裂 Maliuzhou Fault		14	NEE	NW	陡	逆斷	Q_2
14	三灶斷裂 Sanzao Fault		24	NEE	SE	80°	逆斷	Q_3
15	淇澳島－桂山島東斷裂 Qiao-guishan Fault		41	NW	NE/SW	陡	正斷	Q_2,Q_3
16	沙角斷裂 Shajiao Fault		17	320°-330°	SW	50°-80°	逆斷	Q_2
17	礬石水道東側斷裂 Eastern fanshi channel Fault		27	NW			正斷	Q_2 ,Q_3
18	東涌－長沙海灘斷裂 Dongchong-changsha beach Fault		5	NW	NE	陡	正斷	Q_2
19	流浮山－東博寮海峽斷裂 Liufushan-dongboliao strait Fault		50	NW330°	NE	53°-75°	正斷	Q_2,Q_4
20	福永－西鄉斷裂 Fuyong xixiang Fault		15	NW	NE/SW	45°-70°	逆斷	Q_2
21	大埔－牛尾坑斷裂 Dapu-niuweikeng Fault		25	305°-325°	SW	65°-75°	逆斷	
22	單竹坑斷裂 Danzhukeng Fault		24	310°-320°			左旋	Q_2
23	吉澳洲斷裂 Jiaozhou Fault		13	NW310°	NE	70°-80°	正斷	Q_2
24	觀瀾斷裂 Guanlan Fault		18	NW330°	NE/SW	40°-60°	逆斷/正斷	Q_2
25	天堂圍斷裂 Tiantangwei Fault		8	NW330°	NE	45°-60°	逆斷/正斷	Q_2
26	油甘埔斷裂 Youganpu Fault		7	NW320°	SW/NE	65°-80°	逆/右旋正	Q_2

3.3 近場及場區地震構造初步綜合評價

（1） 近場區的地貌總體特徵為海灣夾持半島，地勢東南高西北低，東南部以低山丘陵地貌為主，西北部以丘陵谷地地貌為主。新構造運動特徵是地殼間歇性升降運動與斷塊差異性升降活動。

（2） 近場區內自 1970 年以來記錄到 M_L1.0 級以上地震 53 次，最大地震是 1977 年 10 月 22 日發生在 N22.60°、E114.00°的 M_L3.1 級地震，震中距場地的最小距離約為 12 公里，表明近場區範圍內地震活動較弱。

（3） 近場區展佈的主要斷裂以北東向和北西向最為發育，其中北東向斷裂主要歸屬於蓮花山斷裂帶，即蓮花山斷裂帶是區內的主導斷裂帶。東涌－石壁斷裂（F10）、三灶斷裂（F14）、淇澳島—桂山島東斷裂(F15)、磡石水道東側斷裂（F17）、流浮山—東博寮海峽斷裂海域段（F18）等斷裂（段）在晚更新世曾有活動。考慮到斷裂的規模及活動性，這些斷裂（段）與主導斷裂帶交匯的部位在未來是最有可能發生中強地震的地方。其餘的早、中更新世斷裂，屬較穩定性斷裂，僅具備發生中、小地震的構造條件。

第四章 地震危險性分析

按照《工程場地地震安全性評價》（GB 17741-2005）的規定，本章依據前述章節關於區域及近場區域地震活動性、區域及近場區域地震構造背景的研究，確定對工程場地地震安全性有影響的地震帶及潛在震源區劃分、地震帶及潛在震源區地震活動參數，並利用所確定的適合本區的地震動衰減關係，以地震危險性的概率分析方法，進行工程場地的地震危險性分析計算。

4.1 分析方法概述

本專案採用了《工程場地地震安全性評價》（GB 17741-2005）規定的概率地震危險性分析方法，其主要特點在於考慮了地震活動的時空不均勻性。其基本思路和計算方法概述如下：

（1） 首先確定地震統計單元（地震帶），以此作為考慮地震活動時間非均

勻性、確定未來百年地震活動水準和地震危險性空間相對分佈概率的基本單元。地震帶內部地震活動在空間和時間上都是不均勻的。

地震帶內地震時間過程符合分段的泊松過程。令地震帶的震級上限為 m_{uz}，震級下限為 m_0，t 年內 m_0 - m_{uz} 之間地震年平均發生率 ν_0，ν_0 由未來的地震活動趨勢來確定，則地震帶內 t 年內發生 n 次地震的概率：

$$P(n)=\frac{(\nu_0 t)^n}{n!}e^{-\nu_0 t} \tag{4.1-1}$$

同時地震帶內地震活動性遵從修正的震級頻度關係，相應的震級概率密度函數為：

$$f(m)=\frac{\beta\exp[-\beta(m-m_0)]}{1-\exp[-\beta(m_{uz}-m_0)]} \tag{4.1-2}$$

其中，$\beta=b\ln 10$，b 為震級頻度關係的斜率。實際工作中，震級 m 分成 N_m 檔，m_j 表示震級範圍為（$m_j \pm \frac{1}{2}\Delta m$）的震級檔。則地震帶內發生 m_j 檔地震的概率：

$$P(m_j)=\frac{2}{\beta}\cdot f(m_j)\cdot Sh(\tfrac{1}{2}\beta\Delta m) \tag{4.1-3}$$

（2） 在地震帶內部劃分潛在震源區，並以潛在震源區的空間分佈函數 f_{i,m_j} 來反映各震級檔地震在各潛在震源區上分佈的空間不均勻性，而潛在震源區內部地震活動性是一致的。假定地震帶內共劃分出 N_s 個潛在震源區 $\{S_1,S_2,\cdots\cdots S_{Ns}\}$。

（3）根據分段泊松分佈模型和全概率公式，地震帶內部發生的地震，影響到場點地震動參數值 A 超越給定值 a 的年超越概率為：

$$P_k(A\ge a)=1-\exp\{-\frac{2\nu_0}{\beta}\cdot\sum_{j=1}^{N_m}\sum_{i=1}^{N_s}\iiint P(A\ge a\mid E)\cdot f(\theta)\cdot\frac{f_{i,mj}}{A(S_i)}\cdot f(m_j)\cdot Sh(\frac{1}{2}\beta\Delta m)dxdy\,d\theta\} \tag{4.1-4}$$

$A(S_i)$ 為地震帶內第 i 個潛在震源區的面積，$P(A\ge a|E)$ 為地震帶內第 i 個潛在震源區內發生某一特定地震事件（震中（x,y），震級 $m_j \pm \frac{1}{2}\Delta m$，破裂方向確定）時場點地震動超越 a 的概率，$f(\theta)$ 為破裂方向的概率密度函數。

（4）假定共有 N_z 個地震帶對場點有影響，則綜合所有地震帶的影響得：

$$P(A\ge a)=1-\prod_{k=1}^{N_z}(1-P_k(A\ge a)) \tag{4.1-5}$$

下文將就本次概率地震危險性分析各環節所需參數的確定進行論述，並根據

本次工作所得到的計算參數，給出場地概率地震危險性分析的結果。其中地震帶劃分在前面有關章節已經論述，這裡將僅就研究區域內潛在震源區劃分、地震帶及潛在震源區地震活動性參數的確定進行詳細論述。

4.2 潛在震源區的劃分

潛在震源區的劃分是工程地震危險性分析的重要步驟，它是在研究區域內確定未來潛在發生破壞性地震的區域。本項工作的潛在震源區劃分是在區域、近區域地震活動性、地震構造研究成果的基礎上，按一定的原則和方法，劃分出可能發生強震的分佈區域、潛在地震的最大強度及有關參數。

4.2.1 潛在震源區劃分的原則

潛在震源區劃分的原則可概括為歷史地震重演和構造類比兩條基本原則。

歷史地震重演原則，是認為歷史上發生過大地震的地方，將來還可能發生類似的地震。根據歷史地震的地點和強度，結合現代強震活動及中小地震活動特點和規律的研究，如強震活動空間分佈規律的研究、地震活動帶劃分、現代小震活動圖像的研究等，劃分潛在震源區。

構造類比原則，是根據已發生強震的地區發震構造條件的研究，外推到具有相同或類似構造條件的區域。需要指出，大地震並不是在深和大的構造帶上均勻發生，而只在某些具有特定發震構造條件的部位或地段發生。因此，潛在震源區劃分是在研究地震活動性、強震活動與地球物理場及深部構造的相關性、強震活動與現代構造運動的相關性以及現代構造應力場的基礎上，結合本區大地震發生的構造環境條件，進而劃分潛在震源區。

本次工作中潛在震源區的劃分原則，著重考慮了以下幾點：

（1）區內新構造特別是晚第四紀差異性活動顯著的地段，應考慮劃分潛在震源區，一般劃分為震級稍高一些的潛在震源區。

（2）對明顯斷錯早、中更新世地層的斷層，一般需考慮劃分為中等震級的潛在震源區。

（3）對於僅有斷層物質測年顯示的早更新世有活動及其以前的斷裂，地貌表現不清楚，特別是尚無斷錯相應時代地層證據的斷裂，亦無地震活動證據，則不勾劃潛在震源區。但對於斷層物質測年顯示中更新世有活動的斷裂，如果規模

較大，則應考慮劃分為震級低一些的潛在震源區。

（4）中小地震活動成帶密集發育條帶，顯示了深部有差異性活動，儘管尚未發生中強地震，也應考慮為震級上限低一些的潛在震源區。潛在震源區的範圍參考中小地震密集條帶分佈範圍劃分。

（5）確定潛在震源區的範圍和方向時主要依據斷裂延伸方向、斷裂帶的規模以及中小地震的分佈範圍。同時還考慮斷層分段和斷層交匯等因素。

4.2.2 震源區劃分震級上限的確定

根據區域地震與地質構造關係的研究和全國性各級地震發生條件的研究結果，按上述潛在震源區劃分的原則和方法，以及潛在震源區震級上限確定的依據，提出本區劃確定潛在震源區震級上限的主要判定依據：

（1） 區域地震活動的總體水準，從區域地震活動強度對潛在震源區的震級上限進行宏觀控制。

（2）各潛在震源區的震級上限應等於或大於歷史地震震級。

（3）新構造位置及活動性類似地段，如果沒有資料說明它們在晚第四紀以來構造活動存在差異，應通過構造類比劃分為相同震級上限的潛在震源區。

（4）對於在地表發現斷錯晚更新世或全新世地層的斷層，需要考慮劃分為震級上限 6.5 級或 6.5 級級以上潛在震源區的可能性。這種情況下需要考慮斷層活動幅度或活動速率的大小。

（5）對於斷錯早、中更新世斷層的斷層，需要考慮劃分為震級上限 6 級或 6 級以上潛在震源區的可能性。

（6）對於規模較大的斷層帶，如果發育較好斷層泥物質，測年結果顯示中更新世有活動，特別是有一定的線性地貌顯示，一般可劃分為低震級潛在震源區，如 5.5 級潛在震源區。

4.2.3 潛在震源區的劃分

在對本區地震活動性和地震構造研究的基礎上，依據上述潛在震源區劃分的原則和依據。在本區劃分出若干個潛在震源區， 150 公里範圍內有 23 個相關潛在震源區。其中震級上限為 7.5 級的潛在震源區 1 個，震級上限為 7 級的潛在震

源區 3 個，震級上限為 6.5 級的潛在震源區 4 個，震級上限為 6 級的潛在震源區 7 個，震級上限為 5.5 級的潛在震源區 8 個（圖 4.2-1、表 4.2-1）。

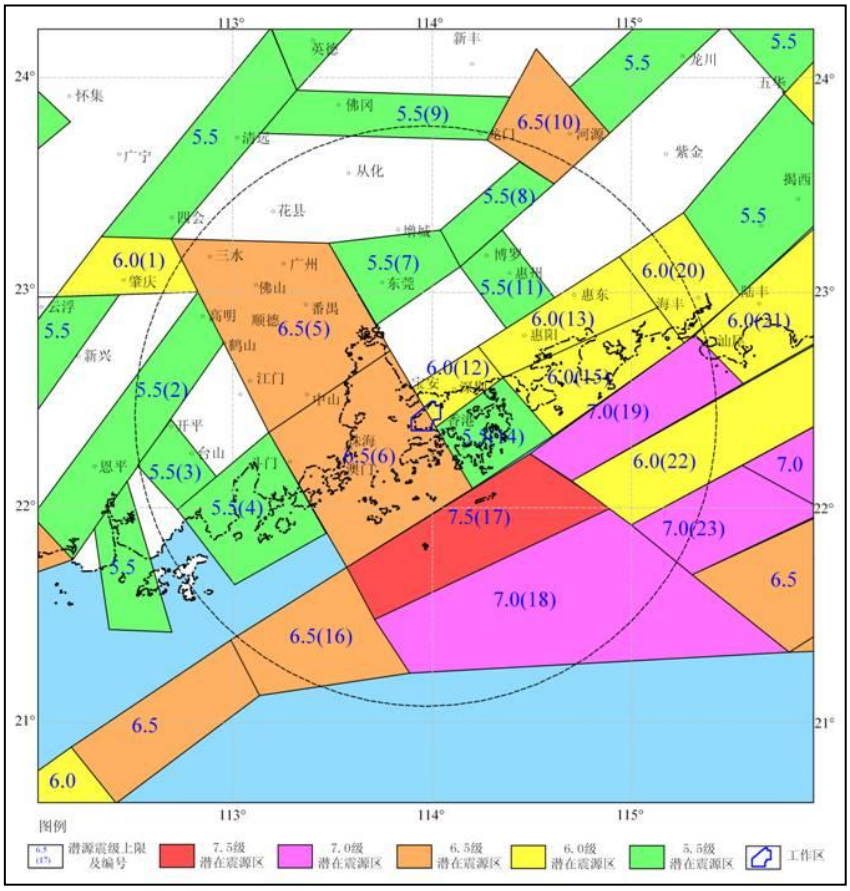

圖 4.2-1 潛在震源區劃分圖

表 4.2-1 區域主要潛在震源區表

編號	潛在震源區名稱	M_{uz}
1	肇慶潛在震源區	6.0
2	恩平潛在震源區	5.5
3	臺山潛在震源區	5.5
4	田頭－三灶潛在震源區	5.5
5、6	珠江三角洲盆地潛在震源區組 廣州：5 號；珠海：6 號	6.5
7	東莞潛在震源區	5.5
8	博羅北潛在震源區	5.5
9	佛岡潛在震源區	5.5

編號	潛在震源區名稱	M_{uz}
10	河源潛在震源區	6.5
11	惠州潛在震源區	5.5
12	深圳潛在震源區	6.0
13	惠東潛在震源區	6.0
14	香港潛在震源區	5.5
15	大亞灣潛在震源區	6.0
16	黃茅海外潛在震源區	6.5
17	擔杆島潛在震源區	7.5
18	珠一北潛在震源區	7.0
19	紅海灣潛在震源區	7.0
20	海豐潛在震源區	6.0
21	陸豐潛在震源區	6.0
22	粵東沿海潛在震源區	6.0
23	汕尾外海潛在震源區	7.0

區域主要潛在震源區描述如下：

1 肇慶潛在震源區

該潛在震源區位於肇慶和高要一帶，呈東西向梯形展布。區內分佈有新生代的白土盆地和三水盆地。新構造運動活躍，斷塊差異升降明顯，大致可以分為三個社區：西北面為雲浮強烈上升區，V 型河谷發育，有寬廣的洪沖積扇，洪沖積扇又經過兩次剝蝕，發育成為“錐中錐”，且又西南向東北轉移，至少可以看出三次上升現象；南面為新興緩慢隆起區，普遍可見 60 - 80 公尺、20 - 40 公尺二級臺地及 1 - 2.5 公尺、4.3 - 9.5 公尺和 30 公尺三級臺地；東面為三水盆地沉降區，第四紀沉積厚度達數十公尺。區內活動斷裂也比較發育，歷史上曾發生過多次中強地震，如 1584 年兩次高要 5 級地震，1909 年肇慶 4.75 級地震等，近年來小震也比較多。該潛在震源區的震級上限定為 6.0 級。

2 恩平潛在震源區

該潛在震源區沿恩平－開平斷裂帶（包括蒼城－海陵斷裂和鶴城－金雞斷裂）劃分，該斷裂帶為北東向區域性斷裂，斷層物質測年顯示早中更新世有過活動。沿斷層有小地震分佈和小震群活動，最大歷史地震震級為 $4^3/_4$ 級。該潛在震源區

的震級上限定為 5.5 級。

3 臺山潛在震源區

該潛在震源區沿北西向那金斷裂及其震群分佈範圍劃分。那金斷裂為位於廠址西北面的一條北西向斷裂，長約 25 公里。斷裂北面破碎頻寬 20 - 30 公尺，自西北向東南規模減小，南端終止於燕山期花崗岩。綜合地質、地貌和斷層泥年代測定結果，該斷裂在早更新世早期可能有過微弱的活動，但中更新世以來沒有活動過。該斷裂南段分別與 1970 年和 1997 年發生了小震震群，小地震有 300 多次，震群在空間位置上基本為原地重複，總體分佈顯示為北西方向。1970 年震群最大地震為 4 級，1997 年震群最大地震為 4.2 級，震級相近。考慮到該斷裂南段發生的上述震群，表明深部具有一定的活動性，應劃分為潛在震源區。但考慮到該斷裂僅在早更新世早期可能有過微弱的活動，中更新世以來沒有活動的顯示；震群重複的最大地震震級不大；而且斷裂長度較小，所以潛在震源區確定為 5.5 級。

4 田頭－三灶潛在震源區

該潛在震源區北部的北東翠亨－田頭斷裂是一條規模較大的向斷裂，長 110 公里，構造破碎帶達幾十公尺寬，該斷西江以東段可能中更新世以來有活動。另外，該斷裂規模較大，在第四紀早中期有微弱活動、且沿斷層零星分佈有 3 級以下的小地震。南部的三灶斷裂帶位於五華－深圳斷裂帶西南延伸部位。其規模遠小於五華－深圳斷裂帶，活動性也較前者低。根據地質調查與年代測定綜合分析，該斷裂帶僅在早更新世有過微弱的活動。根據構造類比劃分，該潛在震源區的震級上限定為 5.5 級。

5-6 珠江三角洲盆地潛在震源區組

珠江三角洲盆地潛在震源區劃分結果與《中國地震動參數區劃圖》（GB18306-2001）潛在震源區綜合方案的劃分結果基本一致該地區大部份地震安全性評價工作大多採用該劃分方案。也有相關報告提出了新的劃分方法，主要變化體現在將盆地分東西部分別劃分為 2 個北西向潛在震源區，以及震級上限提高為 7 級。根據對珠江三角洲盆地第四紀以來活動特徵分析，認為其整體活動性尚比潮汕平原的活動性低，第四紀以來斷陷幅度相對較小，歷史地震最大震級為 5 級，因此仍維持其震級上限為 6.5 級。另外，從盆地中斷層活動性分析，很難將盆地東西部之間區別開來，總體上西南部斷層活動性較北部稍高。因此，仍以中山附近為界，將該盆地劃分為南北兩個潛在震源區，即珠江盆地北部 6.5 級潛在震源區（編號 5）和珠江盆地南部 6.5 級潛在震源區（編號 6）。

7 東莞潛在震源區

該潛在震源區位於增城、東該莞一帶，呈北東東向梯形展布。區內有北西向的東莞－深圳斷裂、東西向的三水－羅浮山斷裂和北東向的河源－東莞斷裂通過，並發育有第四紀東莞斷陷盆地，第四紀沉積層厚度可達 45 公尺。近期不斷有小震活動，本潛在震源區的震級上限定為 5.5 級。

8 博羅北潛在震源區

沿北東東向東莞－河源斷裂東莞盆地與河源之間的段落劃分，該段斷裂第四紀以來活動顯示不明顯，小地震分佈很少，沒有中強地震發生，但考慮到東莞－河源斷裂為規模較大的北東向斷裂帶，且該段以南為 6 級潛在震源區，以北為河源 6.5 級潛在震源區，將其劃分為 5.5 級潛在震源區。

9 佛岡潛在震源區

該潛在震源區位於佛岡、龍門一帶，呈東西向梯形展布。區內主要發震構造有東西向的佛岡－豐良斷裂和清遠－安流斷裂，二者均屬切割較深的基底斷裂。沿斷裂有大量的溫泉出露和小震活動，在佛岡、龍門地區小震更為密集，1970 年 4 月 9 日在龍門地區發生了最大震級為 4.4 級的小震群。本潛在震源區的震級上限定為 5.5 級。

10 河源潛在震源區

該潛在震源區位於河源－邵武地震構造帶的中部，為地球物理場變異地段，同時為地殼形變幅值劇變部位。有河源－邵武斷裂、人字石斷裂、燈塔－客家水斷裂與東西向的隱伏構造及北西向斷裂在本區交匯。其中，河源－邵武斷裂規模最大，它是中強地震的控震構造。歷史上曾發生多次破壞性地震，新豐江水庫建成後誘發斷裂活動，於 1962 年 3 月 19 日發生了河源 6.1 級地震，此後小震頻繁，但呈下降趨勢，未來區內再發生 6 級以上的地震可能性不大。考慮到曾發生了 6.1 級地震，本潛在震源區的震級上限定為 6.5 級。

11 惠州潛在震源區

北東向的博羅－紫金斷裂帶通過該潛在震源區，另外，有北東向斷裂沿切割了北東向的博羅－紫金斷裂。屬於斷裂交匯部位，根據構造類比法，本潛在震源區的震級上限定為 5.5 級。

12 深圳潛在震源區

位於深圳、寶安等地，西面與珠江口 6.5 級潛在震源區相接，東面與惠東 6.0 級潛在震源區相接。區內東部有北西向大鵬灣斷裂，在中部北東向的五華—深圳斷裂橫貫全區。歷史上區內無破壞性地震記載，但 1970 年地震台網建立以來，在深圳南頭等地發生多次小地震。震級上限定為 6.0 級。

13 惠東潛在震源區

沿規模較大的五華—深圳斷裂劃分，該對中生代盆地發育起到一定的控制作用。斷裂沿線動力變質作用強烈，構造岩相當發育，寬數十公尺至數百公尺。根據構造類比劃分為 6.0 級的潛在震源區。

14 香港潛在震源區

位於香港中南等地，其東有北西向大鵬灣斷裂，西有北西向珠江口斷裂，南有北東東向擔杆列島斷裂，北有五華—深圳斷裂。這些斷裂在第四紀期間都有不同程度的活動。歷史上區內無破壞性地震記載，但1970年地震台網建立以來，在香港地區發生多次小地震。本區震級上限定為5.5級。

15 大亞灣潛在震源區

位於惠陽大亞灣地區，區內發育有中新生代淡水盆地，斷裂構造規模比較大，北東向的蓮花山斷裂帶南、北兩支均縱橫全區，另外還有北西向的大亞灣斷裂，南面近鄰濱海斷裂帶。歷史上本區雖然未記載有破壞性地震，但自地震台網建立以來，在淡水、白花、蝦涌等地出現多個小震群。根據強震標誌，震級上限為 6.0 級。

16 黃茅海外潛在震源區

濱海斷裂帶的活動性也有東強西弱的特點，濱海斷裂黃茅海外段通過本區，斷裂多數斷至距海底 30 - 100 公尺，推斷斷錯了中更新統，該區的東西兩側都有中強地震發生，根據地震活動的填充性和構造類比，確定本潛在震源區的震級上限為 6.5 級。

17 擔杆島潛在震源區

位於擔杆列島以南海域，西面為北西向的西江斷裂，活動於晚更新世晚期；北東東向的濱海斷裂橫貫全區，該斷裂也是第四紀活動斷裂。本區南緣為珠江口外盆地，沉積了7,000公尺厚的新第三系和第四系，其中第四系厚達280公尺，沉

積等厚線呈北東東向分佈。本區的地質構造環境與東部南澳和西部瓊山地區十分相似，都是在北東東向濱海斷裂帶上迭加北西向的斷陷盆地。1874年在擔杆列島東發生過5 $\frac{3}{4}$ 級地震，近期小震活動較為頻繁。本區又是濱海斷裂帶上7級地震等震距分佈的空檔地段，同時還存在一個周圍5 - 6 $\frac{3}{4}$ 級地震包圍的現象。震級上限為7.5級。

18 珠一北潛在震源區

該區內多條北東東至近東西向正斷裂斜列組合而成，總體走向北東50° - 60°，傾向南東，控制了珠一坳陷的北界。斷裂沿線第四系中發育一些北東東走向的小斷裂，大部分向上斷至距海底30 - 100公尺，達到上更新統，沿斷裂有小地震分佈。震級上限取7.0級。

19 紅海灣潛在震源區

位於大亞灣、紅海灣的外海，以南海北緣為界。處於地球物理場變異地段。現今仍強烈活動的NEE向南湖島—擔杆島斷裂貫串全區，並以NW向斷裂交匯。包含潮州—汕尾斷裂西南段，海域探測結果表明在晚更新世以來有活動，1911年紅海灣6.0級地震發生在該潛在震源區內，震級上限定為7.0級。

20 海豐潛在震源區

沿豐順—海豐斷裂西南段劃分，該斷裂規模大，斷裂在第四紀有活動，兩側有強烈的地貌反差，西北側為蓮花山，發育多級地形，東南側為丘陵和盆地，盆地中的第四系最厚可達50公尺。沿斷裂有中強地震和小地震分佈，歷史上在海豐附近發生過2次4 $\frac{3}{4}$ 級地震，1981年前後在海豐西南有過震群活動，最大地震的震級為4.2級。

21 陸豐潛在震源區

根據現有資料，普寧－陸豐段為中更新世活動段；陸豐－汕尾段前人資料表明為第四紀早期活動斷裂，本次調查的前第四段落僅很小一段，其主體部分延伸在覆蓋區和水域，靠物探推測其為前第四紀斷裂，考慮與總體構造和地震活動背景協調，將普寧到汕尾段合併劃分為震級上限6.0級的潛在震源區。

22 粵東沿海潛在震源區

該區研究資料較少，根據現有資料，沒有大規模的斷裂通過，但周圍斷裂豐富，且多為晚更新以來活動斷裂，考慮地震發生的不確定性，及與總體構造和地震活動背景協調，將潛在震源區的震級上限定為6.0級。

23 汕尾外海潛在震源區

濱海斷裂汕尾海外段通過本潛在震源區，由一組走向 NEE、傾向 SE 的斷階組成，延伸長度約 60 多公里。海域物探資料顯示斷裂在第四紀早中期仍有活動，最新活動時代為中更新世晚期－晚更新世早期，斷裂地質構造和活動性表明濱海斷裂南海北部段具有一定的規模和活動性，並且構成不同新構造區的邊界，根據構造類比方法，將汕尾海外段潛在震源區的震級上限定為 7.0 級。

4.3 地震活動性參數的確定

我國地震活動有密集成帶分佈的特點，不同地區地震活動特徵不同。在地震區劃工作中，我國地震學者對地震區、地震帶的劃分作過相當系統的研究。在概率地震危險性分析方法中，是以地震帶來反映地震活動性統計特徵的空間差異，它是分析地震時間分佈特徵、估計未來百年地震活動趨勢及地震危險性分析中地震活動性參數估算的基本單元。

4.3.1 地震帶地震活動時間分佈特徵及未來趨勢分析

地震帶地震活動時間分佈特徵和對未來地震活動趨勢的判斷，是地震帶地震活動性參數確定的主要依據。

根據前面對地震資料完整性的分析，圖 4.3-1 給出東南沿海地震帶 1600 年以來 $M_S \geq 4.7$ 級地震的應變釋放曲線。

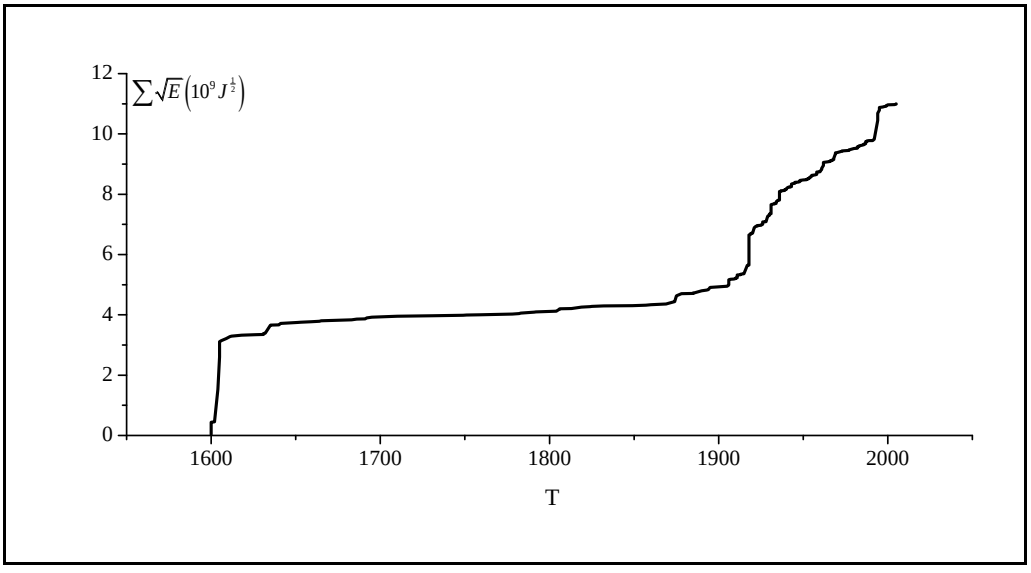

圖 4.3-1　東南沿海地震帶地震能量釋放曲線

從圖上看，現仍處於活躍期後期階段，為保守起見，未來地震活動水平仍以1900 - 2005 年 105 年的活躍水平進行估計。

4.3.2 地震帶地震活動性參數確定

地震帶活動性參數包括震級上限 M_{uz}，起算震級 M_0，震級—累計頻度關係中的係數 b 值，$Ms \geqslant 4$ 級地震年平均發生率 ν_4。

（1）震級上限 M_{uz} 和起算震級 M_0 的確定

震級上限 M_{uz} 的含義是指震級—頻度關係式中，累積頻度趨於零的震級極限值。根據《中國地震動參數區劃圖》（GB18306-2001）編制所使用的地震區帶劃分方案：東南沿海地震帶的震級上限 $M_{uz}=8.0$。

起算震級 M_0 系指對工程場地有影響的最小震級，它與震源深度、震源類型、震源應力環境等有關。由於區域範圍內地震屬淺源地震，一些 4 級地震也會產生一定程度的破壞，故在本次工作中 M_0 取 4 級。

（2）b 值的確定

震級—頻度關係中的係數 b 值決定了地震帶內大小地震頻數間的比例關係，它是確定地震帶中有效震級範圍內地震震級的分佈密度函數和各級地震年平均發生率的一個重要參數。本次工作根據歷史地震資料完整性的分析和對未來百年地震活動水準的估計，以地震帶內的地震資料擬合了震級－頻度關係，其相應係數列於表 4.3-1，震級—累積頻度關係曲線示於圖 4.3-2。

表 4.3-1 地震帶地震活動性參數

地震帶	b 值	a 值	方差 s	相關係數 r
東南沿海	0.686	5.039	0.151	0.979

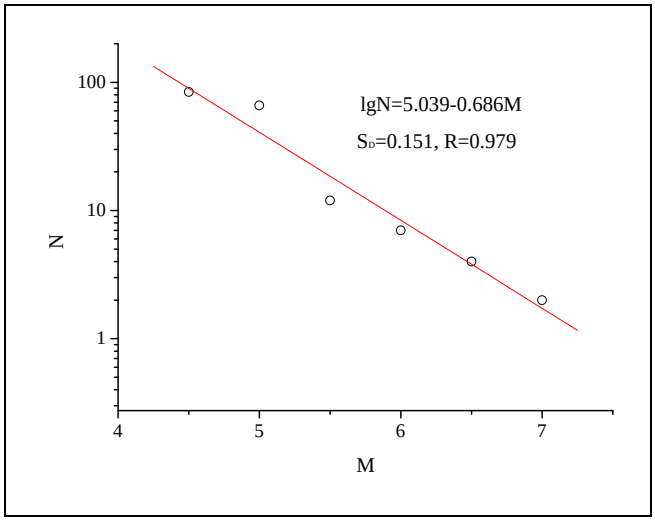

圖 4.3-2　東南沿海震級—累積頻度關係曲線

（3）地震年平均發生率ν_4的確定

地震年平均發生率ν_4代表未來時間段內地震帶地震活動的水準。由前面得出的 b 值可推算得到 4.0 級以上的地震發生頻率，進而得到東南沿海地震帶的 4.0 級以上地震的年發生率ν_4為 1.878。

4.3.3 潛在震源區活動性參數的確定

潛在震源區活動性參數包括：震級上限 M_u，空間分佈函數 f_{i,m_j}，橢圓等震線長軸取向及分佈概率。震級上限在劃分潛在震源區時，依據潛在震源區本身的地震活動性及地震構造特徵已經確定。其中，空間分佈函數 f_{i,m_j} 是一個地震帶內發生的 m_j 檔震級的一個地震落在第 i 個潛在震源區內的概率。在同一地震帶（如華南沿海地震帶）內 f_{i,m_j} 滿足歸一條件：

$$\sum_{i=1}^{n} f_{i,m_j} = 1 \qquad \text{（對不同震級檔 } m_j\text{）}$$

這裡 n 為地震帶內第 m_j 檔潛在震源區的總數。

確定影響空間分佈函數時，綜合考慮以下因素：（1）以往區劃工作潛源劃分；（2）中國大陸長期地震活動的構造背景；（3）具備發生 7 級以上地震的構造上的空段；（4）潛在震源可靠程度；（5）中小地震空間分佈密度（單位元面積的發震概率）。

中國大陸地震等震線多呈橢圓形，地震烈度在長軸和短軸方向衰減特徵不同。在計算各潛在震源區對場地的影響時，必須確定長軸方向。所以對每個潛在震源區都給出方向性因數：即給出互相垂直的兩個可能的長軸走向θ_1和θ_2和相應的概率值 P_1和 P_2。對某些具有共軛斷層的潛在震源區，依照兩個方向作用的大小，給予不同的概率值。

表 4.3-2 為華南沿海地震帶中距場地 150 公里範圍內主要潛在震源區的空間分佈函數 f_{i,m_j} 取值。

表 4.3-2　區域幾個主要潛在震源區空間分佈函數 f_{i,m_j} 取值列表

潛源編號	震級上限	4.0-5.4	5.5-5.9	6.0-6.4	6.5-6.9	7.0-7.4
5 號	6.5	0.007473	0.020076	0.044002	0.000000	0.000000
6 號	6.5	0.007019	0.039015	0.087706	0.000000	0.000000
12 號	6.0	0.007603	0.007801	0.000000	0.000000	0.000000
13 號	6.0	0.006889	0.007557	0.000000	0.000000	0.000000
15 號	6.0	0.007603	0.007801	0.000000	0.000000	0.000000
16 號	6.5	0.004874	0.006745	0.012376	0.000000	0.000000
17 號	7.5	0.006564	0.008857	0.038248	0.173749	0.160500
18 號	7.0	0.006564	0.008857	0.018248	0.040509	0.000000
19 號	7.0	0.009813	0.012920	0.021590	0.046180	0.000000
22 號	6.5	0.006044	0.008207	0.017254	0.000000	0.000000
23 號	7.0	0.009813	0.012920	0.021590	0.052661	0.000000

4.4 地震動衰減關係

由於地震地面運動要隨傳播距離增加而衰減，因此地面運動的衰減規律是場地地震危險性分析中必須考慮的又一重要因素。在地震工程問題中，地震烈度、峰值加速度以及加速度反應譜等是我們感興趣的參數。針對本項工程的實際情況，需要建立適合研究區的地震烈度和地震動衰減關係。本項工作在調研、分析比較國內外幾種常用地震動衰減關係的基礎上，選擇適合華南地區的地震烈度及地震動參數衰減關係。在此基礎上，根據地震帶和潛在震源區的地震活動性參數進行地震危險性計算。

4.4.1 地震烈度衰減關係

烈度隨震級與距離的關係，即地震烈度的衰減，通常取“橢圓型”與“圓型”兩種形式。中國大多數地區積累了豐富的歷史地震資料，其地震烈度衰減規律一般不難根據已有的歷史地震和現代強震影響場資料得到。受發震構造的控制，中國的地震烈度等震線特別是高烈度等震線一般表現為近似橢圓形，至低烈度等震線逐漸接近圓形。因此，目前中國的地震烈度衰減關係多採用橢圓模型。採用橢圓衰減模型時，一般要先確定長短軸方向，再對長短軸分別求其衰減關係，最後用橢圓連接起來。

根據華南地區的歷史地震等震線資料進行統計分析，霍俊榮、周克森、俞言祥等人先後得出了該地區的地震烈度橢圓衰減關係。90 年代初，霍俊容在採用《中國地震烈度區劃圖（1990）》編制資料的基礎上，給出了華南地區烈度橢圓衰減模型：

$$\begin{aligned} I_a &= 4.359 + 1.179M - 2.928\lg(R+15) + \varepsilon_{I_a} \qquad \sigma_{I_a} = 0.493 \\ I_b &= 3.086 + 1.179M - 2.568\lg(R+7) + \varepsilon_{I_b} \qquad \sigma_{I_b} = 0.493 \end{aligned} \tag{4.4-1}$$

其中，I_a 和 I_b 分別表示沿長軸和短軸方向的地震影響烈度。該結果在一定程度上反映了本區地震烈度的衰減特徵。

周克森等（1986）選取了自西元 1067 年以來至今 25 個歷史地震，其中包括近年來發生在臺灣海峽、北部灣以及廣東三水等地的幾個地震的等震線資料，經反復統計、對比，最終給出中國東南沿海地區如下烈度橢圓衰減關係：

$$\begin{aligned} I_a &= 4.2373 + 1.5360M - 1.7183\ln(R_a + 14) \\ I_b &= 2.8626 + 1.5360M - 1.5716\ln(R_b + 7) \\ \sigma_{Ia} &= \sigma_{Ib} = 0.604 \end{aligned} \tag{4.4-2}$$

2005 年，俞言祥根據華南地區的歷史地震等震線作了統計分析，得出該華南地區的地震烈度橢圓衰減關係如下：

$$\begin{aligned} I_a &= 4.839 + 1.506M - 3.859\lg(R+25) \qquad \sigma_{I_a} = 0.483 \\ I_b &= 2.384 + 1.506M - 2.846\lg(R+11) \qquad \sigma_{I_b} = 0.483 \end{aligned} \tag{4.4-3}$$

4.4.2 基岩峰值加速度衰減關係

對於加速度峰值和反應譜的衰減關係，由於華南地區缺乏必要數量的強震觀測記錄，一般則難以直接獲取。目前普遍採用的是胡聿賢教授提出的借助參考地區資料的地震動轉換方法，具體是先得到本區的烈度衰減關係，然後利用具有豐富強震記錄的參考區的地震烈度與強地震動觀測資料得到烈度與地震動的關係，將烈度換算為地震動，從而得到本區的地震動衰減關係。

目前，強震記錄主要集中於美國西部、日本和中國臺灣地區。美國西部是現在世界上強震記錄最多的地區之一，而且其震級與距離的覆蓋範圍較大，烈度標度也與中國相近，因此一般選用美國西部地區作為參考地區。美國西部地區的地震烈度衰減關係為（Chandra, 1979）：

$$Is = 5.876+1.500M - 2.100\ln(R+25) \qquad \sigma_I = 0.50 \tag{4.4-4}$$

其基岩加速度峰值衰減關係為（Joyner & Boore, 1981）：

$$\ln a = 8.250+0.790M - 2.167\ln(R+25) \qquad \sigma_{\ln a} = 0.649 \tag{4.4-5}$$

周克森（1992）採用地震動“映射法”轉換得到的反應近場大震飽和特徵的華南地區基岩加速度峰值衰減關係為：

$$\lg a = -1.88409+1.25428M - 0.04691M^2 - 1.45682\lg(R+0.05573e^{(0.79603M)}) \qquad \sigma_{I_a} = 0.25797 \tag{4.4-6}$$

霍俊榮等利用多元隨機變數的一致加權最小二乘回歸方法（霍俊榮等，1992），在地震動衰減模型中考慮了地震動的近場距離飽和與震級飽和特性，得到華南地區的基岩地震動峰值加速度衰減關係：

$$\begin{aligned} \lg a_{\text{長軸}} &= 1.063+0.832M - 2.295\lg(R+0.541e^{(0.641M)}) \qquad \sigma_{\lg a} = 0.247 \\ \lg a_{\text{短軸}} &= 0.207+0.808M - 2.026\lg(R+0.183e^{(0.703M)}) \qquad \sigma_{\lg a} = 0.247 \end{aligned} \tag{4.4-7}$$

Lee & Yu（1996）利用華南 76 個破壞性地震等震線資料（包括廣東、廣西、福建、湖南、江西等地區），得到華南地區基岩加速度峰值衰減關係為：

$$\ln a = 6.695+0.860M - 1.871\ln(R+22.246e^{(0.0292M)}) - 0.0028R \tag{4.4-8}$$

俞言祥等（2005）在建立美國西部參考地區衰減關係時，在霍俊榮資料的基

礎上，增加了近年來得到的部分強震記錄，採用了反映高頻地震動震級飽和與近場飽和特徵的衰減關係模型，統計得到了美國西部地區水準向基岩加速度峰值和短週期反應譜衰減關係。並與用美國南加州數位寬頻帶記錄建立的美國西部長週期加速度反應譜衰減關係結合，進而得到了美國西部週期 0.04 - 6 s 的反應譜衰減關係。得到的華南地區基岩加速度峰值衰減關係為：

$$\lg a_{\text{長軸}} = -0.150+1.257M - 0.053M^2 - 2.022\lg(R+1.192e^{(0.479M)}) \quad \sigma_{\lg a} = 0.532$$
$$\lg a_{\text{短軸}} = -0.948+1.203M - 0.050M^2 - 1.640\lg(R+0.340e^{(0.565M)}) \quad \sigma_{\lg a} = 0.532$$
(4.4-9)

4.4.3 烈度及峰值加速度衰減關係比較及選擇

圖 4.4-1、4.4-2 分別比較了周克森、霍俊榮、俞言祥等人得出的華南地區地震烈度衰減關係以及周克森華南地區和美國西部地震烈度衰減關係（*M*=5.5, 6.5, 7.5）。從中可以看出，周克森與美國西部烈度衰減關係在近場差別較大，在遠場則趨於一致；華南地區 3 種衰減關係相比，俞言祥的衰減模型處於中等水準。

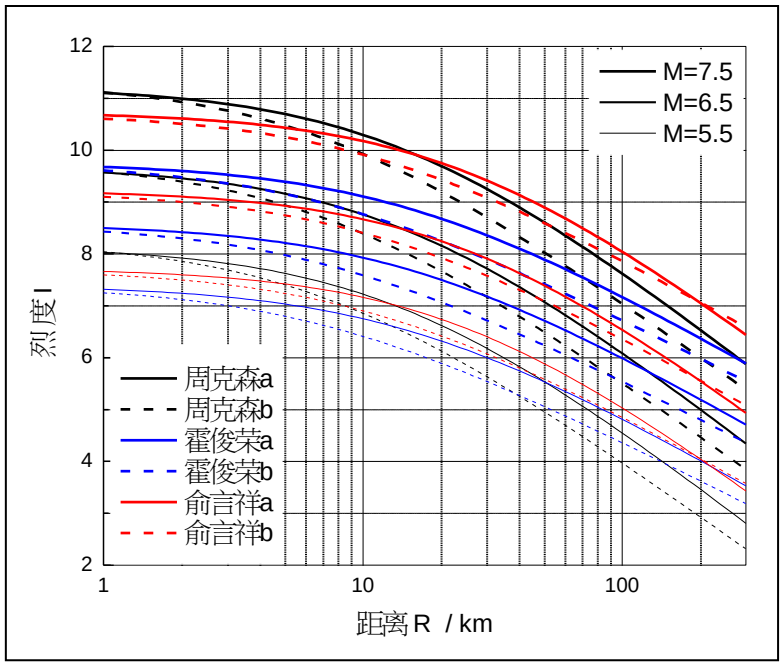

圖 4.4-1　周克森、霍俊榮、俞言祥華南地區地震烈度衰減關係比較圖（*M*=5.5, 6.5, 7.5）

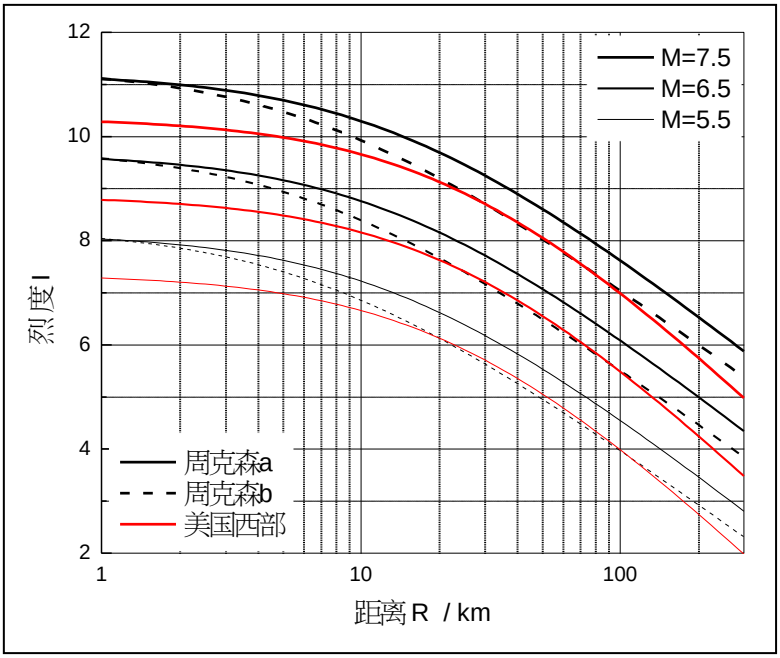

圖 4.4-2　周克森與美國西部地震烈度衰減關係比較圖（*M* = 5.5, 6.5, 7.5）

圖 4.4-3、4.4-4 分別比較了周克森、霍俊榮、俞言祥等人得出的華南地區基岩地震峰值加速度衰減關係以及周克森、美國西部和 Lee & Yu 基岩峰值加速度衰減關係（*M* = 5.5, 6.5, 7.5）。從中可以看出，在華南地區 3 種衰減關係中，俞言祥的衰減模型仍處於中等水準。

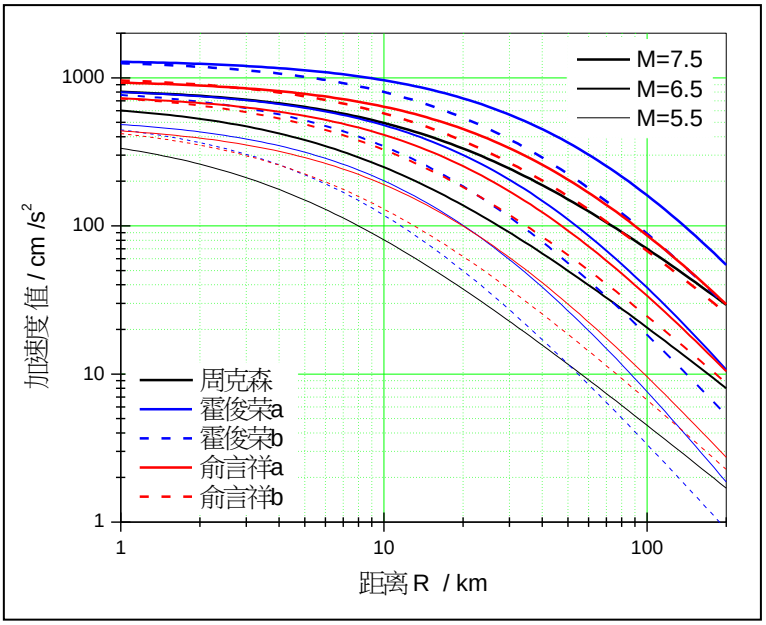

圖 4.4-3　周克森、霍俊榮、俞言祥華南地區基岩峰值加速度衰減關係比較圖（*M* = 5.5, 6.5, 7.5）

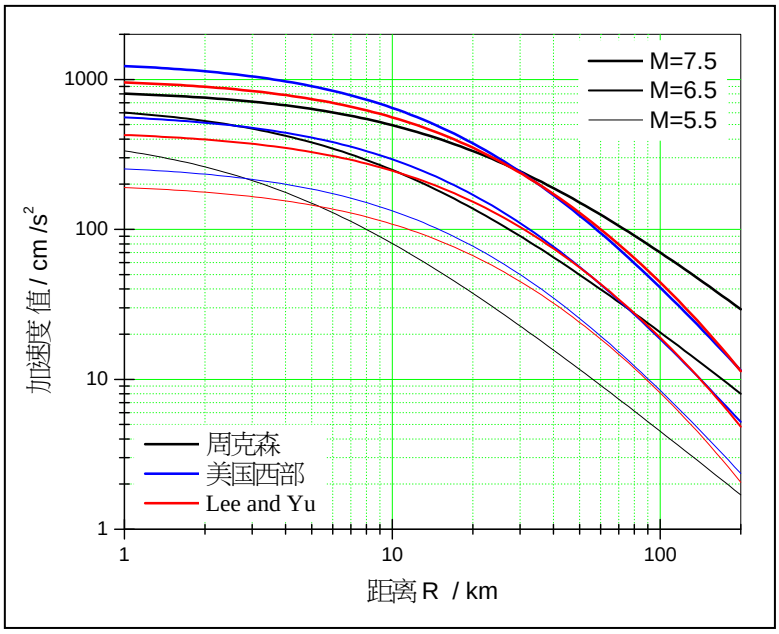

圖 4.4-4　周克森、美國西部和 Lee & Yu 基岩峰值加速度衰減關係比較圖
（*M* = 5.5, 6.5, 7.5）

在華南地區的 3 種地震動衰減關係中，最新的俞言祥的衰減關係在霍俊榮資料的基礎上，增加了近年來得到的部分強震記錄，採用了更多的強震記錄和合理的衰減關係模型，是近年來比較常用的一種華南地區衰減關係；從以上的比較也可以看出，俞言祥的衰減關係一般處於中等水準，且有配套的、衰減形式一致的基岩加速度反應譜衰減關係。因此，本項工作選用俞言祥等（2005）得到的華南地區地震烈度和加速度峰值衰減關係進行地震危險性分析計算。

4.4.4 基岩加速度反應譜衰減關係

假如華南地區的基岩加速度反應譜的衰減形式為：

$$R_0 = c_1 \exp(c_2 M) \qquad (4.4\text{-}10)$$

採用與基岩峰值加速度同樣的方法，確定出本地區的基岩加速度反應譜衰減關係。其中$a(T)$、$b(T)$、$c(T)$、$d(T)$等均為與週期有關的係數；c_1、c_2為常數。

表 4.4-1a 華南地區水準向基岩加速度反應譜衰減關係係數(長軸)

週期 $T(s)$	$a(T)$	$b(T)$	$c(T)$	$d(T)$	c_1	c_2	ε
PGA	-.150	1.257	-.053	-2.022	1.192	.479	0.232
.040	.505	1.036	-.039	-1.889	1.192	.479	0.225
.050	.513	1.018	-.038	-1.838	1.192	.479	0.226
.070	1.016	.895	-.028	-1.875	1.192	.479	0.226
.100	1.534	.801	-.020	-1.927	1.192	.479	0.231
.120	1.446	.819	-.021	-1.885	1.192	.479	0.251
.140	1.477	.813	-.020	-1.889	1.192	.479	0.258
.160	1.462	.818	-.020	-1.886	1.192	.479	0.253
.180	1.258	.868	-.022	-1.899	1.192	.479	0.259
.200	1.155	.867	-.022	-1.836	1.192	.479	0.268
.240	1.012	.875	-.022	-1.780	1.192	.479	0.269
.260	.975	.885	-.022	-1.786	1.192	.479	0.276
.300	1.025	.864	-.020	-1.800	1.192	.479	0.292
.340	.986	.864	-.020	-1.803	1.192	.479	0.308
.360	.813	.896	-.022	-1.789	1.192	.479	0.318
.400	.715	.905	-.022	-1.771	1.192	.479	0.324
.440	.475	.936	-.024	-1.737	1.192	.479	0.331
.500	.102	1.007	-.026	-1.737	1.192	.479	0.337
.600	-.337	1.061	-.029	-1.654	1.192	.479	0.339
.700	-.728	1.147	-.033	-1.708	1.192	.479	0.340
.800	-.903	1.169	-.034	-1.694	1.192	.479	0.348
1.000	-1.378	1.255	-.038	-1.706	1.192	.479	0.345
1.200	-1.597	1.286	-.039	-1.722	1.192	.479	0.338
1.500	-2.013	1.347	-.041	-1.725	1.192	.479	0.334
1.700	-2.395	1.378	-.041	-1.648	1.192	.479	0.333
2.000	-2.611	1.398	-.041	-1.646	1.192	.479	0.329
2.400	-1.326	.899	.000	-1.645	1.192	.479	0.322
3.000	-1.649	.926	.000	-1.643	1.192	.479	0.306
4.000	-1.859	.946	.000	-1.671	1.192	.479	0.307
5.000	-2.183	.958	.000	-1.619	1.192	.479	0.324
6.000	-2.450	.969	.000	-1.578	1.192	.479	0.328

表 4.4-1b 華南地區水準向基岩加速度反應譜衰減關係係數(短軸)

週期 T(s)	*a(T)*	*b(T)*	*c(T)*	*d(T)*	c_1	c_2	ε
PGA	-.948	1.203	-.050	-1.640	.340	.565	0.232
.040	-.247	.989	-.037	-1.532	.340	.565	0.225
.050	-.221	.973	-.036	-1.491	.340	.565	0.226
.070	.258	.853	-.027	-1.521	.340	.565	0.226
.100	.744	.761	-.019	-1.564	.340	.565	0.231
.120	.671	.781	-.020	-1.529	.340	.565	0.251
.140	.698	.776	-.019	-1.533	.340	.565	0.258
.160	.681	.782	-.019	-1.530	.340	.565	0.253
.180	.472	.831	-.021	-1.541	.340	.565	0.259
.200	.394	.833	-.021	-1.489	.340	.565	0.268
.240	.272	.842	-.021	-1.444	.340	.565	0.269
.260	.232	.852	-.021	-1.449	.340	.565	0.276
.300	.275	.832	-.020	-1.460	.340	.565	0.292
.340	.233	.832	-.019	-1.463	.340	.565	0.308
.360	.067	.864	-.021	-1.451	.340	.565	0.318
.400	-.023	.873	-.022	-1.436	.340	.565	0.324
.440	-.250	.904	-.023	-1.409	.340	.565	0.331
.500	-.623	.975	-.026	-1.409	.340	.565	0.337
.600	-1.028	1.032	-.029	-1.342	.340	.565	0.339
.700	-1.440	1.116	-.032	-1.385	.340	.565	0.340
.800	-1.609	1.138	-.033	-1.374	.340	.565	0.348
1.000	-2.089	1.224	-.037	-1.384	.340	.565	0.345
1.200	-2.315	1.255	-.038	-1.396	.340	.565	0.338
1.500	-2.733	1.316	-.040	-1.398	.340	.565	0.334
1.700	-3.085	1.349	-.041	-1.336	.340	.565	0.333
2.000	-3.301	1.369	-.041	-1.335	.340	.565	0.329
2.400	-2.034	.877	.000	-1.334	.340	.565	0.322
3.000	-2.357	.903	.000	-1.331	.340	.565	0.306
4.000	-2.579	.923	.000	-1.354	.340	.565	0.307
5.000	-2.880	.936	.000	-1.312	.340	.565	0.324
6.000	-3.130	.947	.000	-1.278	.340	.565	0.328

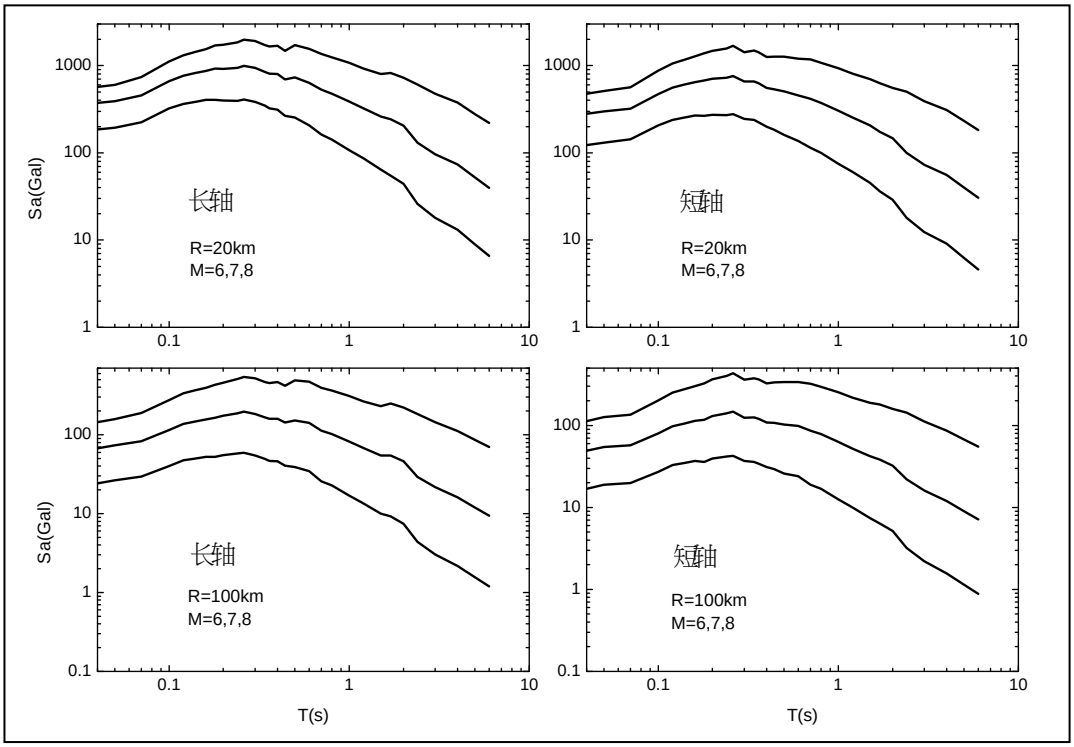

圖 4.4-5　華南地區水準向基岩加速度反應譜衰減關係圖

4.5 地震危險性計算及結果分析

根據前面所確定的地震帶、潛在震源區、地震活動性參數及地震動峰值加速度衰減關係，即可利用概率地震危險性分析方法對工作區元朗、順風圍、屯門等3個工程場地（圖 4.5-1）進行地震危險性分析。

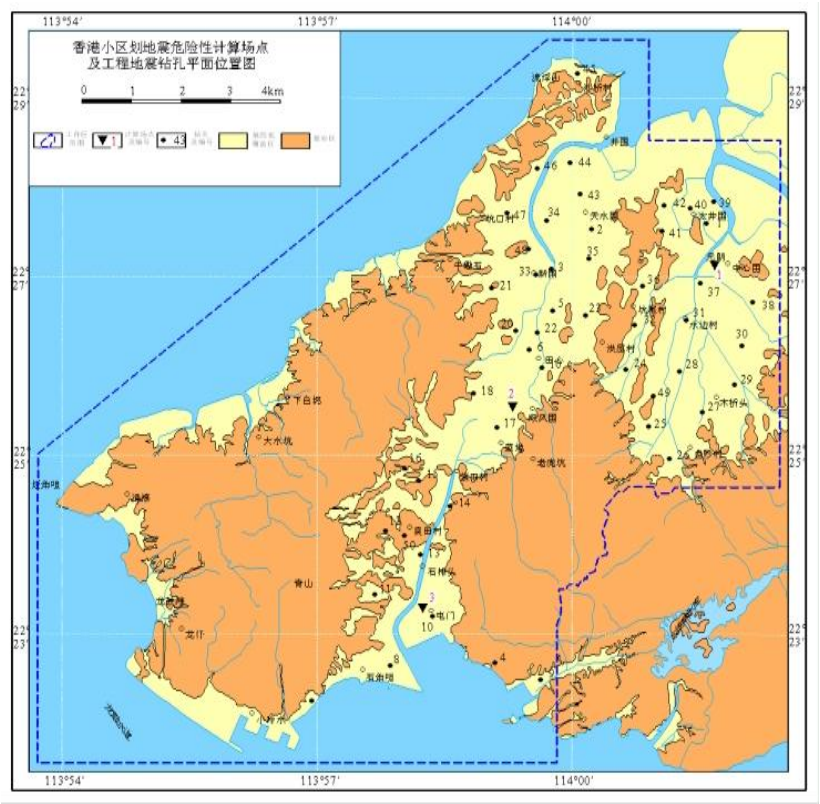

圖 4.5-1 工作區 3 個危險性計算工程場地和鑽孔位置分佈圖

4.5.1 地震危險性分析結果

通過對工作區元朗、順風圍、屯門等 3 個工程場地進行地震危險性計算，分別給出 3 個工程場地基岩水準向峰值加速度計算結果（見表 4.5-1）。

表 4.5-1 場地基岩水準向峰值加速度（*gal*）

場地	50 年 63%	50 年 50%	50 年 10%	50 年 2%
元朗	32.1	42.8	118.2	212.0
順風圍	32.5	43.5	122.5	223.1
屯門	33.2	44.8	127.9	233.9

以屯門為例，表 4.5-2a、b、c、d 分別給出了對主要潛在震源區對屯門場地的加速度峰值和反應譜年超越概率貢獻。圖 4.5-2a、b、c、d 分別給出了對主要潛在震源區對屯門場地的加速度峰值和反應譜年超越概率貢獻 3D 柱狀圖。

表 4.5-2a 區域主要潛在震源區對屯門場地的加速度峰值年超越概率貢獻表

	給定加速度值 /gal						
	1	10	50	75	100	150	200
潛源編號	加速度峰值年超越概率						
5	0.14E-1	0.38E-2	0.17E-3	0.18E-4	0.00E+00	0.00E+00	0.00E+00
6	0.20E-1	0.11E-1	0.27E-2	0.14E-2	0.74E-3	0.22E-3	0.58E-4
7	65E-2	0.76E-4	0.000	0.00E+00	0.00E+00	0.00E+00	0.00E+00
12	0.81E-2	0.56E-2	0.93E-3	0.46E-3	0.25E-3	0.61E-4	0.00E+00
13	0.11E-1	0.14E-2	0.23E-4	0.00E+00	0.00E+00	0.00E+00	0.00E+00
14	0.75E-2	0.37E-2	0.18E-3	0.39E-4	0.38E-5	0.00E+00	0.00E+00
15	.12E-1	0.15E-2	0.89E-5	0.00E+00	0.00E+00	0.00E+00	0.00E+00
17	0.19E-1	0.85E-2	0.38E-2	0.15E-2	0.47E-3	0.22E-4	0.00E+00
18	0.77E-2	0.17E-2	0.98E-5	0.00E+00	0.00E+00	0.00E+00	0.00E+00
19	0.13E-1	0.25E-2	0.98E-4	0.26E-5	0.00E+00	0.00E+00	0.00E+00
23	0.76E-2	0.15E-2	0.000	0.00E+00	0.00E+00	0.00E+00	0.00E+00

表 4.5-2b 區域主要潛在震源區對屯門場地的 0.1 s 加速度反應譜值年超越概率貢獻表

	給定加速度值 /gal						
	1	10	50	75	100	150	200
潛源編號	0.1s 加速度反應譜值年超越概率						
5	1.67E-02	7.52E-03	1.28E-03	4.62E-04	1.75E-04	1.64E-05	0.00E+00
6	2.00E-02	1.55E-02	6.46E-03	4.05E-03	2.72E-03	1.34E-03	6.66E-04
7	7.10E-03	1.59E-03	0.00E+00	0.00E+00	0.00E+00	0.00E+00	0.00E+00
12	8.13E-03	8.11E-03	3.62E-03	1.98E-03	1.17E-03	4.91E-04	2.37E-04
13	1.25E-02	5.21E-03	3.41E-04	1.02E-04	2.92E-05	0.00E+00	0.00E+00
14	7.48E-03	7.38E-03	1.70E-03	6.65E-04	2.90E-04	5.74E-05	6.97E-06
15	1.38E-02	5.93E-03	3.24E-04	7.27E-05	1.09E-05	0.00E+00	0.00E+00
16	9.39E-03	1.58E-03	9.57E-06	0.00E+00	0.00E+00	0.00E+00	0.00E+00
17	1.92E-02	1.17E-02	7.00E-03	5.47E-03	3.68E-03	1.33E-03	3.78E-04
18	1.36E-02	3.02E-03	4.53E-04	8.91E-05	7.70E-06	0.00E+00	0.00E+00
19	2.01E-02	4.79E-03	8.04E-04	2.51E-04	7.82E-05	0.00E+00	0.00E+00
22	9.32E-03	9.19E-04	8.44E-07	0.00E+00	0.00E+00	0.00E+00	0.00E+00
23	1.95E-02	2.81E-03	2.30E-05	0.00E+00	0.00E+00	0.00E+00	0.00E+00

表 4.5-2c　區域主要潛在震源區對屯門場地的 0.5 s 加速度反應譜值年超越概率貢獻表

	給定加速度值 /gal						
	1	10	50	75	100	150	200
潛源編號	0.5s 加速度反應譜值年超越概率						
5	1.65E-02	5.41E-03	9.95E-04	3.24E-04	1.08E-04	4.40E-06	0.00E+00
6	2.00E-02	1.23E-02	5.17E-03	3.13E-03	1.99E-03	8.45E-04	3.58E-04
7	7.10E-03	6.58E-04	0.00E+00	0.00E+00	0.00E+00	0.00E+00	0.00E+00
12	8.13E-03	6.58E-03	1.41E-03	7.63E-04	4.32E-04	1.80E-04	6.42E-05
13	1.25E-02	2.67E-03	1.50E-04	3.27E-05	3.20E-06	0.00E+00	0.00E+00
14	7.48E-03	4.95E-03	3.87E-04	1.05E-04	2.49E-05	0.00E+00	0.00E+00
15	1.38E-02	2.92E-03	1.37E-04	1.71E-05	0.00E+00	0.00E+00	0.00E+00
16	8.44E-03	1.23E-03	9.75E-06	0.00E+00	0.00E+00	0.00E+00	0.00E+00
17	1.92E-02	9.69E-03	6.85E-03	5.72E-03	4.22E-03	2.04E-03	9.41E-04
18	1.19E-02	2.66E-03	6.50E-04	2.16E-04	4.97E-05	0.00E+00	0.00E+00
19	1.87E-02	3.88E-03	1.05E-03	4.63E-04	1.69E-04	1.95E-05	0.00E+00
22	6.97E-03	9.02E-04	1.52E-06	0.00E+00	0.00E+00	0.00E+00	0.00E+00
23	1.34E-02	2.75E-03	2.53E-04	1.84E-06	0.00E+00	0.00E+00	0.00E+00

表 4.5-2d　區域主要潛在震源區對屯門場地的 1.0 s 加速度反應譜值年超越概率貢獻表

	給定加速度值 /gal						
	1	10	50	75	100	150	200
潛源編號	1.0s 加速度反應譜值年超越概率						
5	1.01E-02	2.96E-03	9.46E-05	3.57E-06	0.00E+00	0.00E+00	0.00E+00
6	1.71E-02	8.11E-03	1.66E-03	6.93E-04	2.91E-04	4.16E-05	0.00E+00
7	3.29E-03	0.00E+00	0.00E+00	0.00E+00	0.00E+00	0.00E+00	0.00E+00
12	8.13E-03	2.34E-03	2.54E-04	9.50E-05	2.91E-05	0.00E+00	0.00E+00
13	7.43E-03	7.20E-04	0.00E+00	0.00E+00	0.00E+00	0.00E+00	0.00E+00
14	7.46E-03	1.15E-03	0.00E+00	0.00E+00	0.00E+00	0.00E+00	0.00E+00
15	8.37E-03	7.62E-04	0.00E+00	0.00E+00	0.00E+00	0.00E+00	0.00E+00
16	3.27E-03	5.02E-04	0.00E+00	0.00E+00	0.00E+00	0.00E+00	0.00E+00
17	1.42E-02	7.92E-03	4.51E-03	2.54E-03	1.45E-03	3.98E-04	7.32E-05
18	5.33E-03	1.69E-03	1.07E-04	1.13E-06	0.00E+00	0.00E+00	0.00E+00
19	8.45E-03	2.27E-03	2.60E-04	3.85E-05	2.65E-06	0.00E+00	0.00E+00
22	2.85E-03	2.47E-04	0.00E+00	0.00E+00	0.00E+00	0.00E+00	0.00E+00
23	5.95E-03	1.71E-03	0.00E+00	0.00E+00	0.00E+00	0.00E+00	0.00E+00

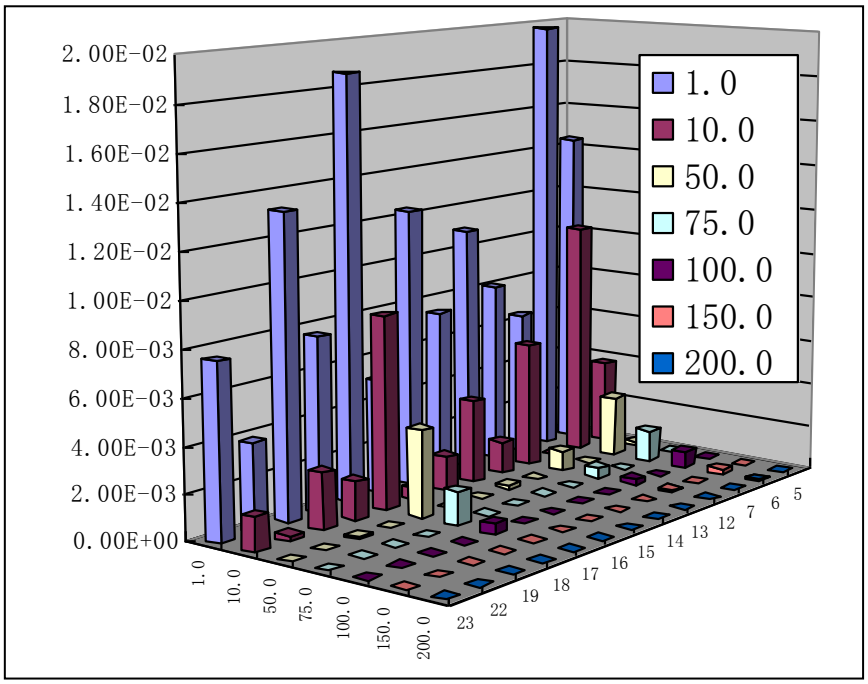

圖 4.5-2a 對屯門場地基岩加速度峰值的年超越概率貢獻 3D 柱狀圖

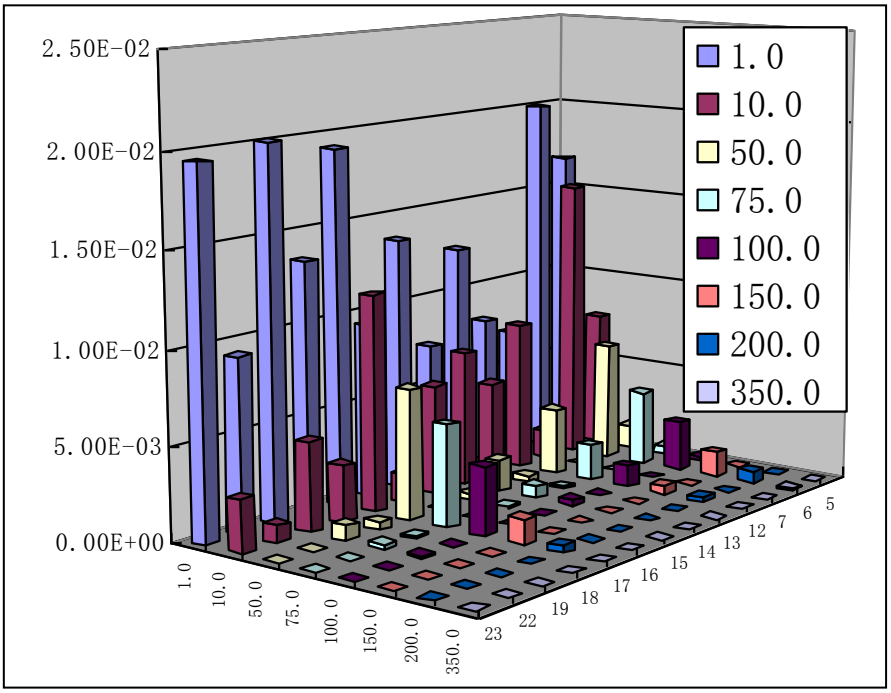

圖 4.5-2b　對屯門場地 0.1 s 基岩加速度反應譜的年超越概率貢獻 3D 柱狀圖

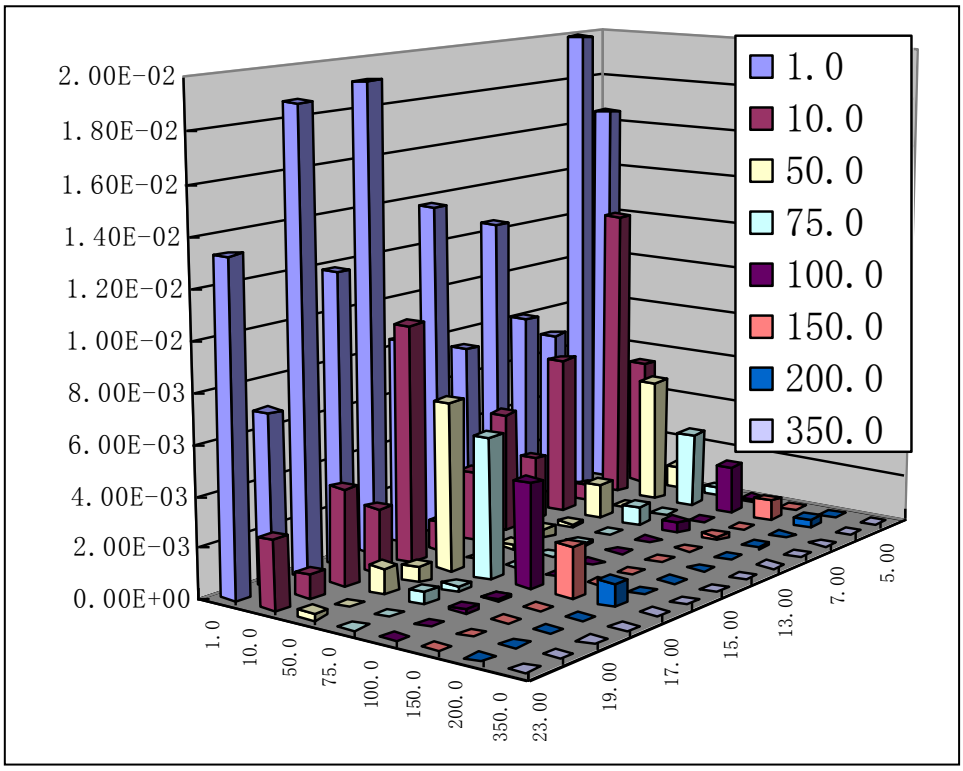

圖 4.5-2c　對屯門場地 0.5 s 基岩加速度反應譜的年超越概率貢獻 3D 柱狀圖

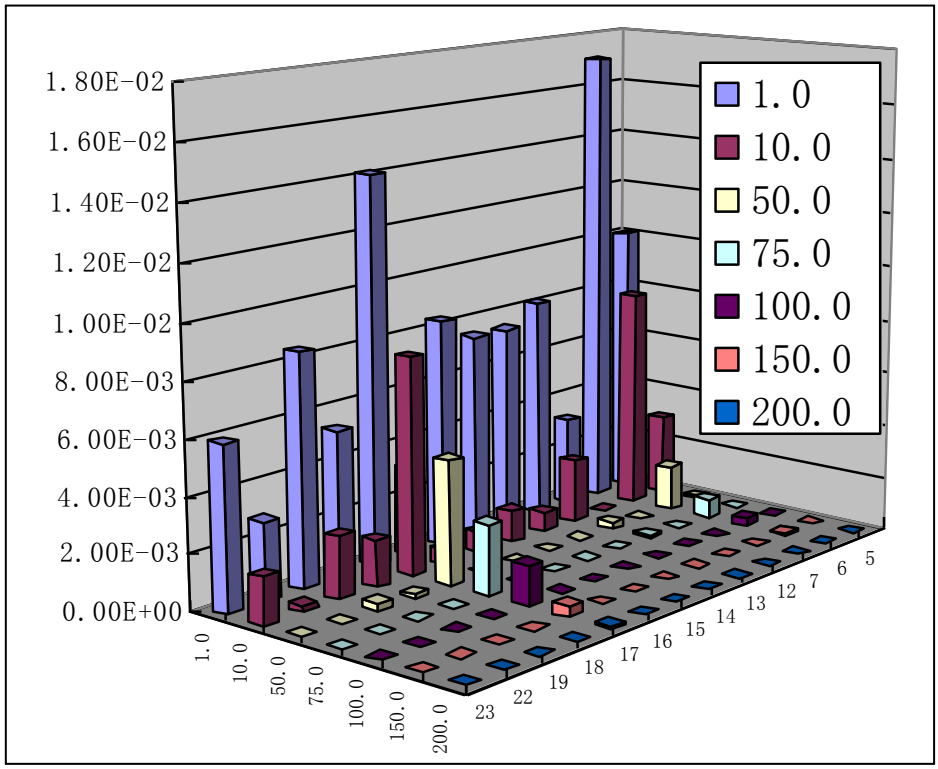

圖 4.5-2d　對屯門場地 1.0 s 基岩加速度反應譜的年超越概率貢獻 3D 柱狀圖

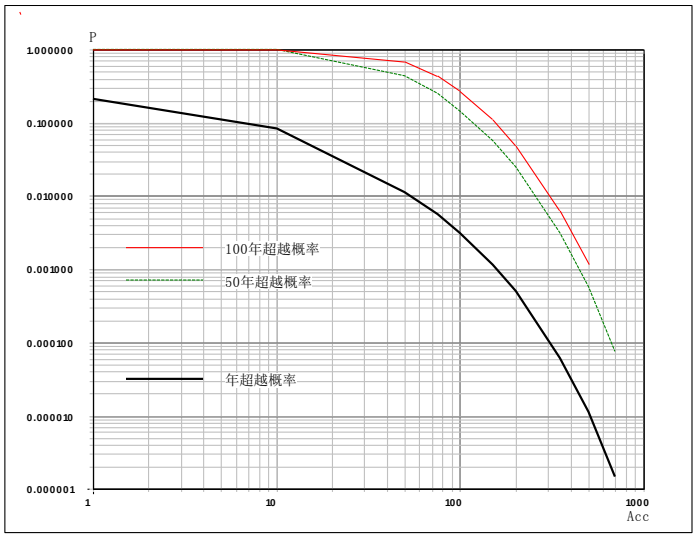

(a) 元朗

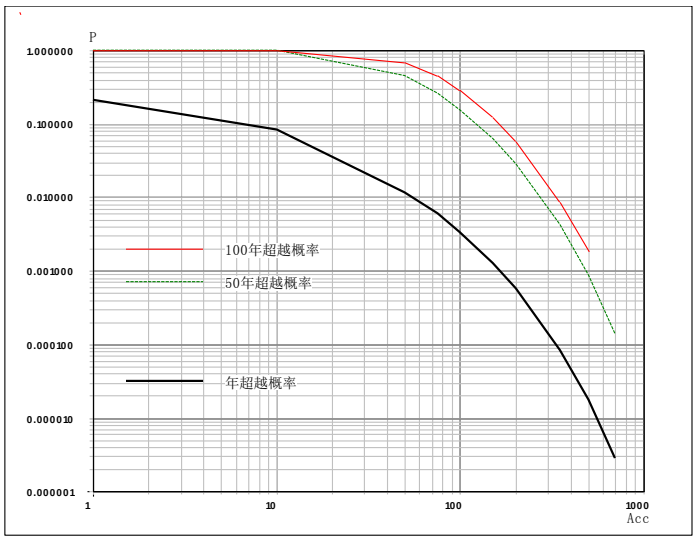

(b) 順風圍

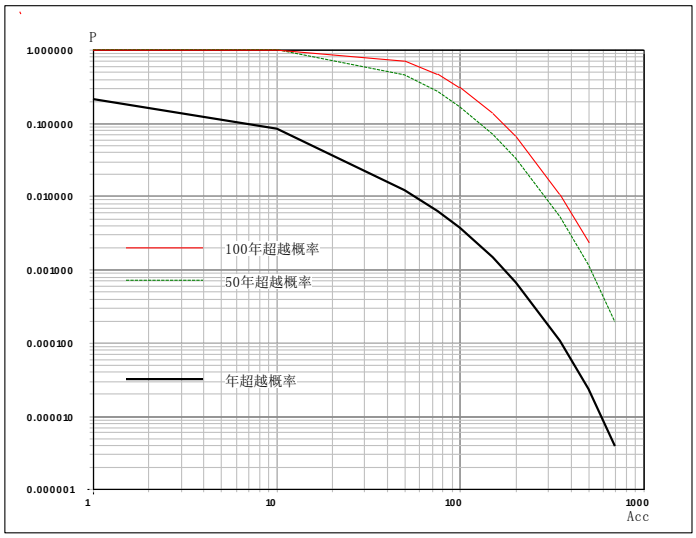

(c) 屯門

圖 4.5-3 元朗、順風圍和屯門場地的地震危險性超越概率曲線

4.5.2 場地基岩加速度反應譜

場地 50 年不同超越概率水準的基岩地震動加速度反應譜值見表 4.5-3a、b、c（h = 10 公里）。場地 50 年不同超越概率水準的基岩地震動加速度反應譜平滑曲線見圖 4.5-4 a、b、c（h = 10 公里）。

表 4.5-3a 元朗場地 50 年不同超越概率水準的基岩加速度反應譜值

	50 年超越概率			
週期 /s	63%	50%	10%	2%
0.04000	43.64	55.98	138.07	233.11
0.05000	48.89	61.10	149.96	249.07
0.07000	54.83	68.67	163.55	270.63
0.10000	83.15	103.64	239.72	408.46
0.12000	98.53	122.13	294.38	514.49
0.14000	103.73	129.23	314.68	547.44
0.16000	108.28	135.70	333.89	579.50
0.18000	108.84	137.62	353.61	626.51
0.20000	108.97	137.61	355.17	633.24
0.24000	99.70	124.51	313.39	555.31
0.26000	102.01	127.26	311.12	534.66
0.30000	93.15	116.33	284.69	498.82
0.34000	88.08	110.80	274.55	483.34
0.36000	81.79	103.61	259.09	456.07
0.40000	75.20	95.06	239.15	418.00
0.44000	65.09	82.88	213.48	369.21
0.50000	57.29	73.99	205.11	362.86
0.60000	44.13	57.82	175.22	320.68
0.70000	39.95	53.51	171.11	328.41
0.80000	34.50	46.60	151.52	292.32
1.00000	26.53	35.79	124.33	253.87
1.20000	21.10	28.18	102.00	212.63
1.50000	16.42	21.73	81.61	174.72
1.70000	13.11	17.04	63.13	135.36
2.00000	10.85	13.90	51.17	109.90
2.40000	6.39	11.07	36.52	83.33
3.00000	1.93	4.06	22.02	52.82
4.00000	1.00	1.78	15.01	31.85
5.00000	0.97	1.13	11.97	22.30
6.00000	0.91	0.99	8.76	16.45

表 4.5-3b 順風圍場地 50 年不同超越概率水準的基岩加速度反應譜值

週期 /s	50 年超越概率			
	63%	50%	10%	2%
0.04000	43.95	56.47	142.42	244.22
0.05000	49.26	61.71	153.95	260.23
0.07000	55.01	69.17	167.79	282.36
0.10000	83.16	104.04	246.02	427.21
0.12000	98.47	122.60	302.48	535.63
0.14000	103.72	129.81	324.23	572.79
0.16000	108.27	136.28	343.67	605.86
0.18000	108.90	138.33	362.60	656.03
0.20000	109.05	138.37	364.20	662.38
0.24000	99.83	125.28	323.57	580.50
0.26000	102.22	128.27	322.45	559.43
0.30000	93.37	117.19	294.11	519.23
0.34000	88.29	111.58	283.70	506.87
0.36000	82.03	104.39	267.67	479.61
0.40000	75.45	95.88	246.43	436.44
0.44000	65.49	83.73	219.78	384.89
0.50000	57.70	74.89	210.66	375.67
0.60000	44.57	58.59	180.18	331.19
0.70000	40.39	54.23	175.29	334.85
0.80000	34.94	47.41	155.71	301.16
1.00000	26.83	36.36	127.68	260.19
1.20000	21.33	28.63	104.71	218.06
1.50000	16.54	22.01	83.88	179.57
1.70000	13.19	17.20	64.59	138.11
2.00000	10.89	14.00	52.05	111.64
2.40000	6.49	11.15	37.05	84.32
3.00000	1.94	4.14	22.34	53.56
4.00000	1.00	1.80	15.20	32.33
5.00000	0.97	1.14	12.10	22.64
6.00000	0.91	0.99	8.99	16.59

表 4.5-3c 屯門場地 50 年不同超越概率水準的基岩加速度反應譜值

週期 /s	50 年超越概率			
	63%	50%	10%	2%
0.04000	44.69	57.45	147.92	254.92
0.05000	50.00	62.75	159.11	272.25
0.07000	55.53	70.19	173.19	294.74
0.10000	83.60	105.02	253.83	446.39
0.12000	99.01	123.88	312.69	557.85
0.14000	104.22	131.20	335.95	598.72
0.16000	108.83	137.74	354.79	632.61
0.18000	109.47	139.86	374.06	688.38
0.20000	109.70	139.98	376.04	695.58
0.24000	100.43	126.83	337.07	609.51
0.26000	102.87	130.06	337.46	587.56
0.30000	93.98	118.63	306.37	542.81
0.34000	88.94	113.01	295.44	529.98
0.36000	82.68	105.74	278.56	504.56
0.40000	76.03	97.27	256.04	458.62
0.44000	66.09	84.94	227.97	402.94
0.50000	58.33	76.06	218.38	392.62
0.60000	45.24	59.69	188.09	350.23
0.70000	41.04	55.27	183.62	355.68
0.80000	35.56	48.49	161.94	315.38
1.00000	27.37	37.32	133.34	272.13
1.20000	21.73	29.37	109.02	227.52
1.50000	16.79	22.50	87.59	188.21
1.70000	13.34	17.52	67.32	144.89
2.00000	10.99	14.21	53.76	115.61
2.40000	6.71	11.31	38.65	88.08
3.00000	1.98	4.34	23.42	56.57
4.00000	1.00	1.87	15.93	35.11
5.00000	0.97	1.15	12.33	23.18
6.00000	0.92	0.99	9.65	16.96

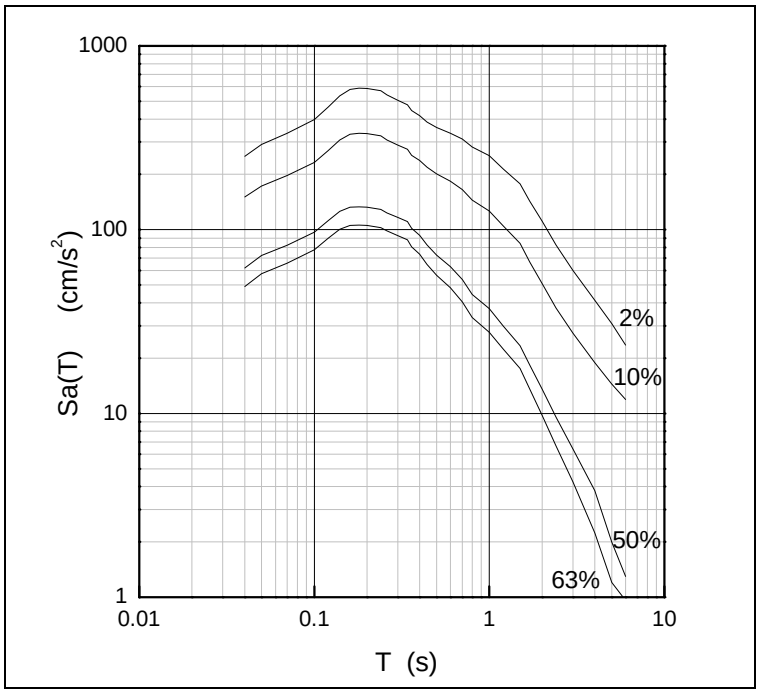

圖 4.5-4a 元朗場地不同超越概率水準的場地基岩加速度反應譜平滑曲線

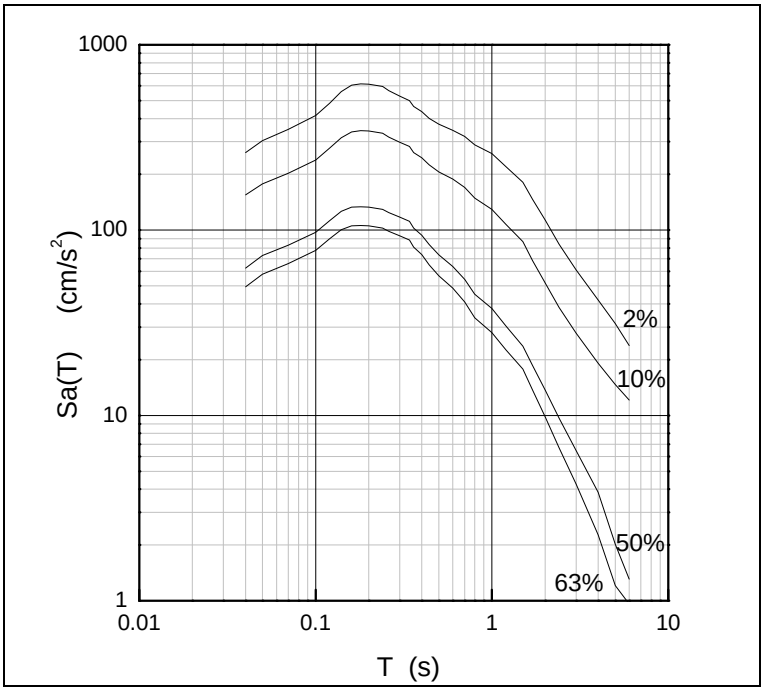

圖 4.5-4b 順風圍場地不同超越概率水準的場地基岩加速度反應譜平滑曲線

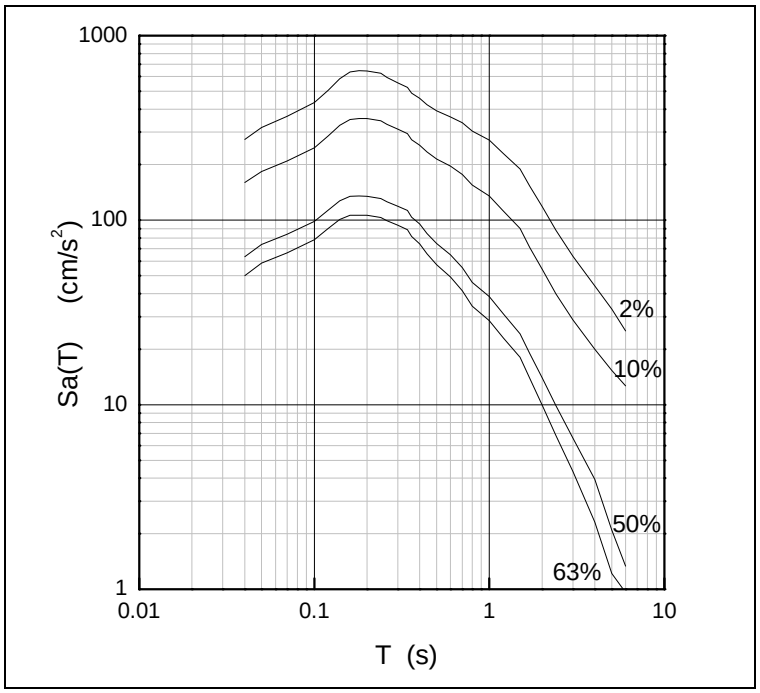

圖 4.5-4c 屯門場地不同超越概率水準的場地基岩加速度反應譜平滑曲線

主要參考文獻

丁原章. *廣東和香港地震風險概論*. 香港：商務印書館（香港）有限公司，2004。

周克森. 重要工程場地的地震小區劃問題，*第一屆兩岸地震學術討論論文集*。北京: 地震出版社，1986，300-315。

周克森. 重要工程場地的地震小區劃問題，*兩岸地震學術討論論文集*，1992，第 300-315 頁。

俞言祥，薑慧等. 地震動參數衰減關係研究. *地震安全性評價研究與結構抗震研究*，中國地震局“十五”重點科研課題研究報告，2005。

陳偉光，趙紅梅，李富光等. 深圳市斷裂構造的活動性及其對地質環境的影響. *熱帶地理*，2001，21(1):45-50。

國家技術品質監督局，2005. *工程場地地震安全性評價技術規範（GB17741-2005）*. 中國標準出版社，北京。

國家品質技術監督局，2001. *中國地震動參數區劃圖（GB18306-2001）*. 中國標準出版社，北京。

黃鎮國，李平日，張仲英等. *深圳地貌*. 廣州：廣東科技出版社，1983。

霍俊榮，胡聿賢，馮啟明，1992. 關於通過烈度資料估計地震動的研究，*地震工程與工程振動*，第 12 卷，第 3 期。

劉行松，史蘭斌，李祖信等. 高潭－深圳斷裂活動性研究. *華南地震*，1993，13(2)：15-24。

馬浩明，陳龐龍. 深圳市橫崗－羅湖斷裂第四紀活動性研究. *震災防禦技術*，2009a，4(3):266-274。

馬浩明，陳龐龍. 深圳市觀瀾斷裂第四紀活動性研究. *華南地震*，2009b，29(3)：17-24。

張虎男. 香港地區近代構造運動特徵. *國際地震動態*，1986，3:14-17。

Chandra, U. (1979). Attenuation of Intensities in the United States. 2003~2024,*BSSA*,69:6,1979.

GEO (2012). *Review of Earthquake Data for the Hong Kong Region, GEO Publication No. 1/2012*. Geotechnical Engineering Office, Hong Kong, 153 p.

Lee, C.F. & Yu, Y.B. (1996). 華南地區基岩加速度峰值衰減關係報告。

Joyner, W.B. & Boore, D.M. (1981). Peak Horizontal Acceleration and Velocity from Strong-Motion Records Including Records from the 1979 Imperial Valley,California,Earthquake. 2011~2038,*BSSA*,71:6,1981.

MAJOR GEOTECHNICAL ENGINEERING OFFICE PUBLICATIONS
土力工程處之主要刊物

Table of Contents
Table of Contents
Table of Contents
Table of Contents

GEOTECHNICAL MANUALS

Geotechnical Manual for Slopes, 2nd Edition (1984), 302 p. (English Version), (Reprinted, 2011).

斜坡岩土工程手冊(1998)，308頁(1984年英文版的中文譯本)。

Highway Slope Manual (2000), 114 p.

GEOGUIDES

Geoguide 1	Guide to Retaining Wall Design, 2nd Edition (1993), 258 p. (Reprinted, 2007).
Geoguide 2	Guide to Site Investigation (1987), 359 p. (Reprinted, 2000).
Geoguide 3	Guide to Rock and Soil Descriptions (1988), 186 p. (Reprinted, 2000).
Geoguide 4	Guide to Cavern Engineering (1992), 148 p. (Reprinted, 1998).
Geoguide 5	Guide to Slope Maintenance, 3rd Edition (2003), 132 p. (English Version).
岩土指南第五冊	斜坡維修指南，第三版(2003)，120頁(中文版)。
Geoguide 6	Guide to Reinforced Fill Structure and Slope Design (2002), 236 p.
Geoguide 7	Guide to Soil Nail Design and Construction (2008), 97 p.

GEOSPECS

Geospec 1	Model Specification for Prestressed Ground Anchors, 2nd Edition (1989), 164 p. (Reprinted, 1997).
Geospec 3	Model Specification for Soil Testing (2001), 340 p.

GEO PUBLICATIONS

GCO Publication No. 1/90	Review of Design Methods for Excavations (1990), 187 p. (Reprinted, 2002).
GEO Publication No. 1/93	Review of Granular and Geotextile Filters (1993), 141 p.
GEO Publication No. 1/2006	Foundation Design and Construction (2006), 376 p.
GEO Publication No. 1/2007	Engineering Geological Practice in Hong Kong (2007), 278 p.
GEO Publication No. 1/2009	Prescriptive Measures for Man-Made Slopes and Retaining Walls (2009), 76 p.
GEO Publication No. 1/2011	Technical Guidelines on Landscape Treatment for Slopes (2011), 217 p.

GEOLOGICAL PUBLICATIONS

The Quaternary Geology of Hong Kong, by J.A. Fyfe, R. Shaw, S.D.G. Campbell, K.W. Lai & P.A. Kirk (2000), 210 p. plus 6 maps.

The Pre-Quaternary Geology of Hong Kong, by R.J. Sewell, S.D.G. Campbell, C.J.N. Fletcher, K.W. Lai & P.A. Kirk (2000), 181 p. plus 4 maps.

TECHNICAL GUIDANCE NOTES

TGN 1	Technical Guidance Documents

GEO PUBLICATIONS AND ORDERING INFORMATION
土力工程處刊物及訂購資料

A selected list of major GEO publications is given in the next page. An up-to-date full list of GEO publications can be found at the CEDD Website http://www.cedd.gov.hk on the Internet under "Publications". Abstracts for the documents can also be found at the same website. Technical Guidance Notes are published on the CEDD Website from time to time to provide updates to GEO publications prior to their next revision.

部份土力工程處的主要刊物目錄刊載於下頁。而詳盡及最新的土力工程處刊物目錄，則登載於土木工程拓展署的互聯網網頁 http://www.cedd.gov.hk 的"刊物"版面之內。刊物的摘要及更新刊物內容的工程技術指引，亦可在這個網址找到。

Copies of GEO publications (except geological maps and other publications which are free of charge) can be purchased either by:

Writing to
Publications Sales Unit,
Information Services Department,
Room 626, 6th Floor,
North Point Government Offices,
333 Java Road, North Point, Hong Kong.

or

- Calling the Publications Sales Section of Information Services Department (ISD) at (852) 2537 1910
- Visiting the online Government Bookstore at http:// www.bookstore.gov.hk
- Downloading the order form from the ISD website at http://www.isd.gov.hk and submitting the order online or by fax to (852) 2523 7195
- Placing order with ISD by e-mail at puborder@isd.gov.hk

讀者可採用以下方法購買土力工程處刊物(地質圖及免費刊物除外):

書面訂購
香港北角渣華道333號
北角政府合署6樓626室
政府新聞處
刊物銷售組

或

- 致電政府新聞處刊物銷售小組訂購 (電話：(852) 2537 1910)
- 進入網上「政府書店」選購，網址爲 http://www.bookstore.gov.hk
- 透過政府新聞處的網站 (http://www.isd.gov.hk) 於網上遞交訂購表格，或將表格傳真至刊物銷售小組 (傳真：(852) 2523 7195)
- 以電郵方式訂購 (電郵地址：puborder@isd.gov.hk)

1:100 000, 1:20 000 and 1:5 000 geological maps can be purchased from:

Map Publications Centre/HK,
Survey & Mapping Office, Lands Department,
23th Floor, North Point Government Offices,
333 Java Road, North Point, Hong Kong.
Tel: (852) 2231 3187
Fax: (852) 2116 0774

讀者可於下列地點購買1:100 000、1:20 000及1:5 000地質圖：

香港北角渣華道333號
北角政府合署23樓
地政總署測繪處
電話: (852) 2231 3187
傳真: (852) 2116 0774

Requests for copies of Geological Survey Sheet Reports and other publications which are free of charge should be directed to:

For Geological Survey Sheet Reports which are free of charge:
Chief Geotechnical Engineer/Planning,
(Attn: Hong Kong Geological Survey Section)
Geotechnical Engineering Office,
Civil Engineering and Development Department,
Civil Engineering and Development Building,
101 Princess Margaret Road,
Homantin, Kowloon, Hong Kong.
Tel: (852) 2762 5380
Fax: (852) 2714 0247
E-mail: jsewell@cedd.gov.hk

For other publications which are free of charge:
Chief Geotechnical Engineer/Standards and Testing,
Geotechnical Engineering Office,
Civil Engineering and Development Department,
Civil Engineering and Development Building,
101 Princess Margaret Road,
Homantin, Kowloon, Hong Kong.
Tel: (852) 2762 5346
Fax: (852) 2714 0275
E-mail: florenceko@cedd.gov.hk

如欲索取地質調查報告及其他免費刊物，請致函：

免費地質調查報告:
香港九龍何文田公主道101號
土木工程拓展署大樓
土木工程拓展署
土力工程處
規劃部總土力工程師
(請交:香港地質調查組)
電話: (852) 2762 5380
傳真: (852) 2714 0247
電子郵件: jsewell@cedd.gov.hk

其他免費刊物:
香港九龍何文田公主道101號
土木工程拓展署大樓
土木工程拓展署
土力工程處
標準及測試部總土力工程師
電話: (852) 2762 5346
傳真: (852) 2714 0275
電子郵件: florenceko@cedd.gov.hk

Table of Contents
Table of Contents
Table of Contents
Table of Contents